
Science
AAAS

EDITORIAL

722 Speak Up for Science Funding
Alan I. Leshner and Mary Woolley

NEWS OF THE WEEK

726 A roundup of the week's top stories

NEWS & ANALYSIS

728 Scientists Assess Damage From Sandy's Deadly Punch

730 Did Pulses of Climate Change Drive the Rise and Fall of the Maya?
>> Report p. 788

731 Lung-on-a-Chip Breathes New Life Into Drug Discovery
>> Sci. Transl. Med. *Research Articles by D. Huh* et al. *and K. S. Thorneloe* et al. *and Perspective by D. M. Dambach and H. Uppal*

732 As Drug Pilot Wraps Up, a Lively Debate About Its Future

733 Question of Martian Methane Is Still Up in the Air

NEWS FOCUS

734 Weather Forecasts Slowly Clearing Up
One Sandy Forecast a Bigger Winner Than Others
>> Science *Podcast*

738 Poor but Smart

LETTERS

740 Limits to Religious Conservation Efforts
B. Gong et al.

Credit Due to Peter Higgs
J. Ellis

Evolution's Misleading Language
A. N. Burdett

742 TECHNICAL COMMENT ABSTRACTS

742 CORRECTIONS AND CLARIFICATIONS

BOOKS *ET AL.*

743 Visible Empire
D. Bleichmar, reviewed by P. H. Smith

744 Measurement
P. Lockhart, reviewed by B. Finegold

POLICY FORUM

745 Law and Science Collide Over Human Gene Patents
R. Cook-Deegan

PERSPECTIVES

748 A Decorated Virus Cannot Hide
R. W. Herzog and D. A. Ostrov
>> Report p. 795

749 Constraints on Sexual Selection
M. J. Wade
>> Report p. 802

750 Emerging Disease or Diagnosis?
S. K. Gire et al.

752 Driving the Formation of Molecular Knots
J. S. Siegel
>> Report p. 783

754 A Single-Molecule Engine
M. W. Bockrath
>> Report p. 779

755 Constraining Cloud Feedbacks
K. M. Shell
>> Report p. 792

756 Epigenetic Islands in a Genetic Ocean
D. Schübeler

ASSOCIATION AFFAIRS

758 Presidential Address: Transposable Elements, Epigenetics, and Genome Evolution
N. V. Fedoroff

CONTENTS continued >>



page 734



page 743



COVER

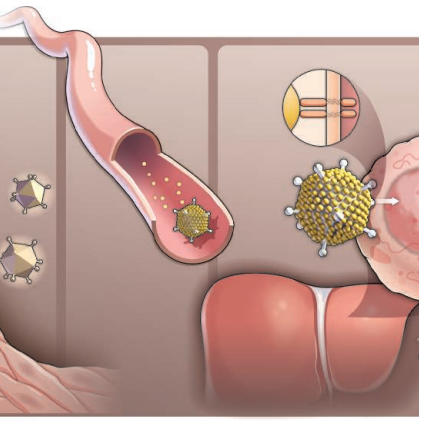
Masks on the facade of the Codz Poop Palace (Kabah site, Yucatan, Mexico). Kabah and other Maya sites in the Puuc region flourished during the Terminal Classic Period (800 to 1000 C.E.), while cities to the south collapsed as the climate became drier. Political collapse was part of a complex two-stage societal response to global climate change. See page 788.

Photo: Getty Images/DEA/G. Dagli Orti

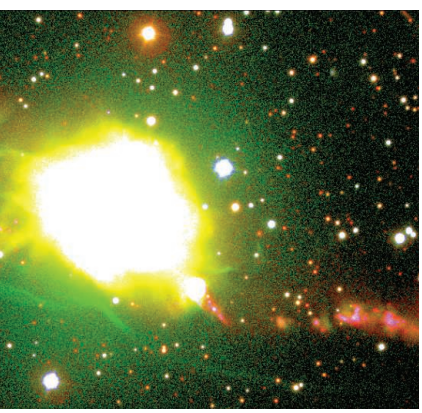
DEPARTMENTS

720 This Week in *Science*
723 Editors' Choice
724 *Science* Staff
825 New Products
826 *Science* Careers

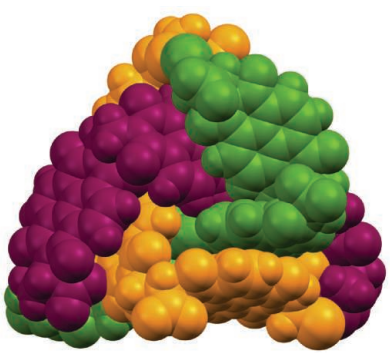
Published by AAAS



pages 748 & 795



page 773



pages 752 & 783

REVIEW

768 Hepcidin and the Iron-Infection Axis
H. Drakesmith and A. M. Prentice

REPORTS

773 An Interacting Binary System Powers Precessing Outflows of an Evolved Star
H. M. J. Boffin et al.
Spectra of a planetary nebula's central star reveal a companion star responsible for launching the system's rotating jets.

775 Polarity-Switching Top Coats Enable Orientation of Sub–10-nm Block Copolymer Domains
C. M. Bates et al.
A chemical reaction in a thin polymer film imposes orientational ordering of lamellar domains in an underlying film.

779 Driving a Macroscopic Oscillator with the Stochastic Motion of a Hydrogen Molecule
C. Lotze et al.
The random motion of an activated hydrogen molecule produces forces that drive periodic motions of a scanning probe cantilever.
>> *Perspective p. 753*

783 Discovery of an Organic Trefoil Knot
N. Ponnuswamy et al.
Hydrophobic interactions appear to steer three molecular fragments into a knot, rather than a simpler ring geometry.
>> *Perspective p. 752*

785 Tissint Martian Meteorite: A Fresh Look at the Interior, Surface, and Atmosphere of Mars
H. Chennaoui Aoudjehane et al.
A meteorite that fell in Morocco in July 2011 provides a sample to study processes that operated on Mars 700,000 years ago.

788 Development and Disintegration of Maya Political Systems in Response to Climate Change
D. J. Kennett et al.
A record of rainfall from a stalagmite in southern Belize provides a context for better understanding Maya civilization.
>> *News story p. 730*; Science *Podcast*

792 A Less Cloudy Future: The Role of Subtropical Subsidence in Climate Sensitivity
J. T. Fasullo and K. E. Trenberth
Seasonal variations in tropospheric relative humidity may provide an observational constraint on climate sensitivity.
>> *Perspective p. 755*

795 Coagulation Factor X Activates Innate Immunity to Human Species C Adenovirus
K. Doronin et al.
Tagging adenovirus with a serum protein prompts an immune response when the virus enters cells.
>> *Perspective p. 748*

798 Germ Cell Migration Across Sertoli Cell Tight Junctions
B. E. Smith and R. E. Braun
Syncytial germ cell chains span a network of transient compartments to cross the blood-testis barrier in adult mice.

802 Bateman in Nature: Predation on Offspring Reduces the Potential for Sexual Selection
J. Byers and S. Dunn
The relationship between mate number and offspring output in male pronghorn confirms Bateman's findings.
>> *Perspective p. 749*

804 Corals Chemically Cue Mutualistic Fishes to Remove Competing Seaweeds
D. L. Dixson and M. E. Hay
Goby fish remove toxic algae from their coral habitat, becoming more distasteful to predators in the process.
>> Science *Podcast*

807 A Core Metabolic Enzyme Mediates Resistance to Phosphine Gas
D. I. Schlipalius et al.
Mutations in a lipoic acid metabolism enzyme confer resistance to phosphine but also result in sensitivity to arsenite.

810 Optical Control of Protein Activity by Fluorescent Protein Domains
X. X. Zhou et al.
Shining light onto an engineered fluorescent protein controls the activity of domains fused to the protein.

815 Intramitochondrial Transport of Phosphatidic Acid in Yeast by a Lipid Transfer Protein
M. Connerth et al.
A lipid transfer protein, Ups1, controls the accumulation of cardiolipin in mitochondrial outer and inner membranes.

818 IRE1α Cleaves Select microRNAs During ER Stress to Derepress Translation of Proapoptotic Caspase-2
J.-P. Upton et al.
Protein misfolding stimulates the destruction of microRNAs and the synthesis of an enzyme that promotes cell death.

822 Mitochondrial Network Size Scaling in Budding Yeast
S. M. Rafelski et al.
Yeast cells produce buds with uniform mitochondrial content, even as the aging mother cell loses out.

Published by AAAS

SCIENCEONLINE

SCIENCEXPRESS

www.sciencexpress.org

Publication Ahead of Print

Kinetic Responses of β-Catenin Specify the Sites of Wnt Control
A. R. Hernandez et al.
10.1126/science.1228734

Acute Inflammation Initiates the Regenerative Response in the Adult Zebrafish Brain
N. Kyritsis et al.
10.1126/science.1228773

Cytoplasmic ATP Hydrolysis Powers Transport of Lipopolysaccharide Across the Periplasm in *E. coli*
S. Okuda et al.
10.1126/science.1228984

Robust Photogeneration of H_2 in Water Using Semiconductor Nanocrystals and a Nickel Catalyst
Z. Han et al.
10.1126/science.1227775

TECHNICALCOMMENTS

Comment and Response on "Glacial Survival of Boreal Trees in Northern Scandinavia"
Comment: H. H. Birks et al.
http://dx.doi.org/10.1126/science.1225345
Response: L. Parducci et al.
http://dx.doi.org/10.1126/science.1225476

SCIENCENOW

www.sciencenow.org

Highlights From Our Daily News Coverage

The Innovative Cockatoo: Figaro Invents, Makes, and Uses a Tool
Even among birds, necessity is the mother of invention.
http://scim.ag/Innovative-Cockatoo

The Eternal Youth of Asteroid Vesta
The Dawn spacecraft shows how Vesta's blemishes are removed, but why isn't space aging it?
http://scim.ag/Eternal-Youth

Many-Eyed Monsters Prove the Eyes Have It
People seek out others' eyes, even when they are not centered on the face.
http://scim.ag/Seek_Eyes

SCIENCESIGNALING

www.sciencesignaling.org

The Signal Transduction Knowledge Environment

6 November issue: http://scim.ag/ss110612

RESEARCH ARTICLE: Key Roles for the Lipid Signaling Enzyme Phospholipase D1 in the Tumor Microenvironment During Tumor Angiogenesis and Metastasis
Q. Chen et al.

PODCAST
M. A. Frohman and A. M. VanHook
Tumor growth and metastasis are attenuated in mice lacking a lipid signaling enzyme.

RESEARCH ARTICLE: Proliferative and Antiapoptotic Signaling Stimulated by Nuclear-Localized PDK1 Results in Oncogenesis
C. K. Kikani et al.
PDK1 in the nucleus drives oncogenesis in mice and correlates with human prostate tumor grade.

PERSPECTIVE: Sexy DEG/ENaC Channels Involved in Gustatory Detection of Fruit Fly Pheromones
C. W. Pikielny et al.
DEG/ENaC channels allow male fruit flies to "taste" their mates.

PERSPECTIVE: Grb2, A Double-Edged Sword of Receptor Tyrosine Kinase Signaling
A. A. Belov and M. Mohammadi
The adaptor Grb2 plays both positive and negative roles in FGF receptor signaling.

SCIENCETRANSLATIONAL MEDICINE

www.sciencetranslationalmedicine.org

Integrating Medicine and Science

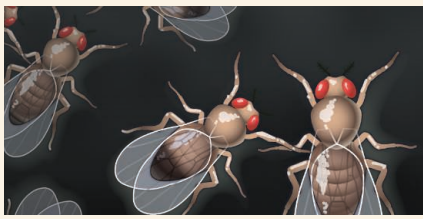
7 November issue: http://scim.ag/stm110712

RESEARCH ARTICLE: A Human Disease Model of Drug Toxicity–Induced Pulmonary Edema in a Lung-on-a-Chip Microdevice
D. Huh et al.
A human lung-on-a-chip model of human pulmonary edema predicts the efficacy of a new drug being tested in animals.

RESEARCH ARTICLE: An Orally Active TRPV4 Channel Blocker Prevents and Resolves Pulmonary Edema Induced by Heart Failure
K. S. Thorneloe et al.
Blocking TRPV4 ion channels expressed in the lung in vivo and in vitro resolves pulmonary edema induced by heart failure.

PERSPECTIVE: Improving Risk Assessment
D. M. Dambach and H. Uppal
A collaborative effort to build human organs-on-a-chip may strengthen drug-related adverse-event prediction.
>> News story p. 731

RESEARCH ARTICLE: Human Melanoma Metastasis in NSG Mice Correlates with Clinical Outcome in Patients
E. Quintana et al.
The ability of melanomas to produce circulating tumor cells and metastasize in immunocompromised mice correlates with their ability to form distant metastases in patients.



SCIENCESIGNALING
Courting fruit flies.

CREDIT: CHRIS BICKEL/AAAS

COMMENTARY: Research Results—Preserving Newborn Blood Samples
M. H. Lewis et al.
The debate about retention of dried blood samples from newborns should include their value to biomedical research.

SCIENCECAREERS

www.sciencecareers.org/career_magazine

Free Career Resources for Scientists

http://scim.ag/SciCareers9November2012

Alternative Research Metrics
L. Laursen
Researchers are seeking faster, better ways to measure research output and impact.

Content Collection: Talking to the Public
E. Pain
The benefits of public engagement justify the effort required to develop the necessary skills.

SCIENCEPODCAST

www.sciencemag.org/multimedia/podcast

Free Weekly Show for 9 November 2012

Listen to stories on coral symbiosis, climate change and the Maya, the challenges of weather forecasting, and more.

SCIENCE (ISSN 0036-8075) is published weekly on Friday, except the last week in December, by the American Association for the Advancement of Science, 1200 New York Avenue, NW, Washington, DC 20005. Periodicals Mail postage (publication No. 484460) paid at Washington, DC, and additional mailing offices. Copyright © 2012 by the American Association for the Advancement of Science. The title SCIENCE is a registered trademark of the AAAS. Domestic individual membership and subscription (51 issues): $149 ($74 allocated to subscription). Domestic institutional subscription (51 issues): $990; Foreign postage extra: Mexico, Caribbean (surface mail) $55; other countries (air assist delivery) $85. First class, airmail, student, and emeritus rates on request. Canadian rates with GST available upon request, GST #1254 88122. Publications Mail Agreement Number 1069624. **Printed in the U.S.A.**

Change of address: Allow 4 weeks, giving old and new addresses and 8-digit account number. **Postmaster:** Send change of address to AAAS, P.O. Box 96178, Washington, DC 20090–6178. **Single-copy sales:** $10.00 current issue, $15.00 back issue prepaid includes surface postage; bulk rates on request. **Authorization to photocopy** material for internal or personal use under circumstances not falling within the fair use provisions of the Copyright Act is granted by AAAS to libraries and other users registered with the Copyright Clearance Center (CCC) Transactional Reporting Service, provided that $30.00 per article is paid directly to CCC, 222 Rosewood Drive, Danvers, MA 01923. The identification code for *Science* is 0036-8075. *Science* is indexed in the *Reader's Guide to Periodical Literature* and in several specialized indexes.

AAAS
ADVANCING SCIENCE, SERVING SOCIETY

EDITED BY STELLA HURTLEY

Double-Edged Iron

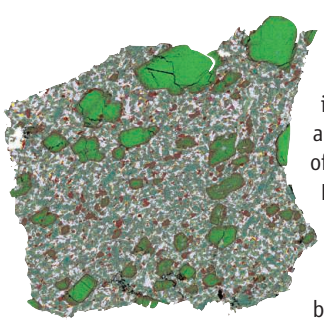
Hepcidin is a small peptide hormone discovered by three groups investigating iron-regulated liver genes and antimicrobial peptides. This new hormone turned out not only to regulate iron but also to have homology with peptides required for innate immune responses. **Drakesmith and Prentice** (p. 768) review the importance of hepcidin during infection, explaining how it is involved in withholding iron from microbial pathogens to curtail replication and how intracellular bacteria are able to thwart this host response. Recent work highlights the potential hazards of iron-supplementation in infection, particularly in malaria, whereby an overload of iron, meant to treat malaria-induced anemia, may negate the protective effects of hepcidin.

Not Single After All

Planetary nebulae form toward the end of the lives of sunlike stars. They appear after the star has shed its outer layers, and radiation from what is left of it ionizes the surrounding medium. Using the Very Large Telescope in Chile, **Boffin *et al.*** (p. 773) obtained spectra of the star at the center of Fleming 1, a point-symmetric planetary nebula with rotating bipolar jets. It has long been assumed that jets like these arose from an interacting binary system. Indeed, the data reveal that the central star in Fleming 1 has a companion in a very close orbit.

A New Rock from Mars

On 18 July 2011 a meteorite originating from Mars fell on the moroccan desert. **Chennaoui Aoudjehane *et al.*** (p. 785, published online 11 October) show that this meteorite was ejected from the surface of Mars 700,000 years ago and contains components derived from the interior, surface, and atmosphere of the red planet. Previous to this fall, only four other martian meteorites have been collected after being witnessed falling to Earth. All the other martian meteorites that are represented in collections around the world, have been found long after their arrival on Earth, and thus have suffered from exposure to the terrestrial environment.





<<Keeping Coral Clean

Seaweed overgrowth is a major problem for coral reefs and also seems to be a consequence of excessive harvesting of herbivorous fish. **Dixson and Hay** (p. 804) examined this effect on Fijian reefs. Species of small herbivorous gobies and coral-associated damselfish were compared for their effect on the toxic *Chlorodesmis* seaweed in experiments that required caging colonies of the branching coral *Acropora nasuta* and the associated fish species. Only the gobies actively removed algal fronds attached to the cages and only one species (itself toxic to predators) ate them; the damselfish simply defected from the arena when toxic algae were present. The hydrophobic toxins exuded in the algal mucus lysed coral polyps releasing cell constituents that, together with the algal toxin, attract the gobies, which then eat the algal fronds. Interestingly, the toxic goby became more toxic to predators after consumption of the seaweed, which may help to drive symbiosis with a coral colony.

Thermally Transforming Thin Films

Nanoscale features can be created by the phase separation that occurs in block copolymers that join together polymer segments with different wetting properties. For applications such as lithography, it is useful to generate small features and to orient them through simple processing steps. Top-layer coatings should be able to help drive alignment, but it is difficult to coat a layer that also has strong enough interactions to influence assembly. **Bates *et al.*** (p. 775) developed a water-soluble polymer that can top-coat lamella-forming block copolymers and that transforms during thermal annealing into a neutral wetting layer that helps drive the formation of vertically oriented lamellae.

Putting Noise to Work

Extracting energy from a noisy system (one that moves randomly) is possible if a mechanical system can induce periodicity on its motion, a phenomenon called stochastic resonance. **Lotze *et al.*** (p. 779; see the Perspective by **Bockrath**) created stochastic resonances between the cantilever attached to a scanning tunneling microscope tip and a hydrogen molecule adsorbed on a copper surface at cryogenic temperatures. The tunneling electrons at a particular bias voltage could excite the hydrogen molecules and couple their random motion to that of the cantilever, driving periodic oscillations.

Maya and Climate

Climate has affected the vitality of many different societies in the past, as shown by numerous records across the globe and throughout human history. One of the most obvious and spectacular examples of this is from the Classic Maya civilization, whose advanced culture left highly detailed records of all aspects of their existence between 300 and 1000 C.E. **Kennett *et al.*** (p. 788; see the cover) present a detailed climate record derived from a stalagmite collected from a cave in Belize, in the midst of the Classic Maya settlement. The fine resolution and precise dating of the record allows changes in precipitation to be related to the politics, war, and population fluctuations of the Mayans.

Sensitivity Training

Equilibrium climate sensitivity—the increase in global mean surface air temperature caused by the doubling of the concentration of atmospheric CO_2—is needed to predict anthropogenic climate change. For decades, models have estimated its value to be between 1.5° and 4.5°C, but with too high an uncertainty to have strong predictive value. **Fasullo and Trenberth** (p. 792; see the Perspective by **Shell**) show that

CREDITS (TOP TO BOTTOM): DANIELLE L. DIXSON/GEORGIA INSTITUTE OF TECHNOLOGY; NHM-LONDON, C. SMITH

Downloaded from www.sciencemag.org on November 9, 2012

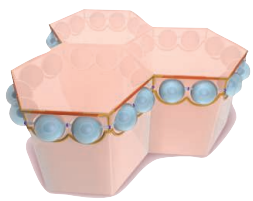
Published by AAAS

the seasonal variation of tropospheric relative humidity is related to climate sensitivity and could be used to constrain models and narrow the range of equilibrium climate sensitivity estimates, thereby allowing more accurate predictions of future warming.

Wound Healing and Immunity

Although wound healing and infection are often overlapping processes, whether the wound healing response modulates the immune response is not well understood. **Doronin *et al.*** (p. 795, published online 27 September; see the Perspective by **Herzog and Ostrov**) now show that coagulation factor X, an important component of the blood clotting cascade, helps to trigger antiviral immunity in response to adenovirus infection in mice. Factor X binds to human type C adenovirus with very high affinity. Structural analysis identified the critical binding residues between factor X and adenovirus, which, when mutated, inhibited binding. Despite being able to infect splenic macrophages in mice, transcriptional profiling of spleens from mice infected with a mutant adenovirus unable to bind to factor X revealed impaired activation of signaling cascades associated with innate immunity.

Observing Sperm Factories



The blood-testis barrier creates a permissive microenvironment for germ cell differentiation and protects meiotic germ cells from autoimmunity. To become sperm, large cysts of germline progenitors must cross the blood-testis barrier without causing damage. **Smith and Braun** (p. 798, published online 20 September) show that somatic Sertoli cells, the gatekeepers of the blood-testis barrier, manage this task by building a network of compartments bounded by old and new tight junctions. Intercellular bridges, which connect germ cells within cysts, span the transient compartments by passing through vertical strands at tricellular junctions. Only after the formation of a new blood-testis barrier are old tight junctions removed and germ cells released.

Optogenetic Control

Fluorescent proteins are widely used as optical sensors; however, optical control of protein activity remains challenging. **Zhou *et al.*** (p. 810) describe an approach that allows both sensing and control. Domains of the fluorescent protein Dronpa were designed to dimerize with one another and were fused to each of the termini of an enzyme domain. In the dark, the domains dimerized and inhibited the enzyme. However, exposure to light induced Dronpa dissociation and activated the enzyme, allowing optogenetic control.

To Die For

The unfolded protein response (UPR) adjusts the protein folding capacity of the endoplasmic reticulum (ER) to match demand. UPR signaling requires IRE1α, an ER transmembrane kinase-endoribonuclease (RNase) that becomes activated by unfolded protein accumulation within the ER and excises a segment in XBP1 messenger RNA (mRNA) to initiate production of the homeostatic transcription factor XBP1s. However, if ER stress is irremediable, sustained IRE1α RNase activity triggers cell death. Severe ER stress activates the protease Caspase-2 as an early apoptotic switch upstream of mitochondria. However, the molecular events leading from the detection of ER stress to Caspase-2 activation are unclear. **Upton *et al.*** (p. 818, published online 4 October) now report that IRE1α is the ER stress sensor that activates Caspase-2, and does so through a mechanism involving non-coding RNAs. Under irremediable ER stress, IRE1α's RNase triggers the rapid decay of select microRNAs that normally repress translation of Caspase-2 mRNA, rapidly increasing Caspase-2 levels as the first step in its activation.

Bud, This Mitochondrion's for You

How is organelle size adjusted to be appropriate for cell size? **Rafelski *et al.*** (p. 822) used a quantitative method for measuring mitochondria in living budding yeast cells and found that rather than using the apparently simplest mechanism of dividing the organelles equally among the mother and daughter cells, the cells adjusted the mitochondrial level in the bud, independent of the mother's own mitochondrial content, size, or age.

CREDIT: SMITH AND BRAUN

Published by AAAS

Downloaded from www.sciencemag.org on November 9, 2012

Speak Up for Science Funding

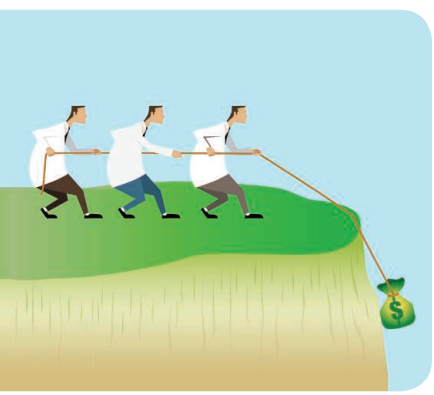


Alan I. Leshner is the chief executive officer of the American Association for the Advancement of Science and executive publisher of *Science*.



Mary Woolley is the president and chief executive officer of Research!America.

THE U.S. ELECTIONS ARE OVER, AND SITTING POLICY-MAKERS MUST TURN THEIR ATTENTION urgently to the "fiscal cliff," a perfect storm of budget landmines laid by Congress and two administrations that threaten to go into effect in early January. Congress and the president must rapidly make hugely important decisions about the debt limit, the expiration of Bush-era tax cuts, and possible draconian across-the-board budget cuts in defense and nondefense accounts known as "sequestration." Business leaders and other interests are rallying to force action, alarmed that cuts will be directed at them. Those not heard from will probably have the most to lose. It is simply not enough that scientific societies and advocacy organizations speak up. It is essential that every member of the science and engineering community personally convey to policy-makers and the U.S. public the great importance of strong science funding to the future of the country.



It is not an exaggeration to say that the nation's future is at stake and now is the time to be heard. Very likely, the first week after the election will feature both short- and long-term attempts at preventing the havoc that implementation of the fiscal cliff would cause. The alternative scenarios range from deferring the issue to a new Congress and new presidential term through some short-term fix, to enacting the bipartisan National Commission on Fiscal Responsibility and Reform's 2010 recommendations for reducing the country's budget deficit through a mix of spending cuts and tax reform. Importantly, sequestration-induced nearly double-digit reductions in the federal R&D annual budget, which has already seen a 10% decrease in constant dollars since 2010, are far from off the table. No one yet knows how individual agencies would handle budget cuts of this magnitude, but, for example, the National Institutes of Health (NIH) would lose between $2.4 billion and $5.5 billion, depending on the ultimate formula. The lesser reduction would return NIH funding to, roughly, the budget of 2002; the greater would reduce NIH funding below that of 2001. The National Science Foundation (NSF) would lose between $450 million and $1 billion of its over $6 billion annual research budget. If NSF were to absorb these cuts totally from research grants, it would mean that some 2600 grants would go unfunded next year.*

Some advocates have argued that science and engineering research funding deserves preferential treatment because of its importance to every aspect of modern life. But this argument is true for other areas, as well. There will be more listeners if scientists first acknowledge that tax and entitlement reform must go forward to ensure both new revenues and the elimination of unnecessary, duplicative programs and regulations. Economic growth is the goal shared by all, and the proven centrality of science and engineering to economic growth should be a lead argument. As former NSF Director and Assistant to the President (Clinton) for Science and Technology Neal Lane argued succinctly: "No science; no growth."† Scientists by the thousands must deliver this message during the first week of the lame-duck Congress.

The science community knows well that the United States cannot afford to be cutting science funding—the seed corn for future innovation and economic growth—precisely when its international competitors are substantially increasing their investments in R&D. The science community also knows that such drastic cuts in science funding would drive the promising young scientists who represent the nation's future into other careers, especially because their immediate predecessors already face abysmally low grant-proposal funding rates. But one cannot assume that others know and share these truths; in fact, we must assume that policy-makers are unaware. That's what we have to change through our actions, now.

– Alan I. Leshner and Mary Woolley

10.1126/science.1232218

*M. Hourihan, *Federal R&D and Sequestration in the First Five Years* (American Association for the Advancement of Science, Washington, DC, 27 September 2012); www.aaas.org/spp/rd/fy2013/SeqBrief.pdf. †N. F. Lane, "Science is the Key to Growth," *New York Times*, 28 October 2012; www.nytimes.com/2012/10/29/opinion/want-to-boost-the-economy-invest-in-science.html.

Published by AAAS

Downloaded from www.sciencemag.org on November 9, 2012

CREDITS: (TOP RIGHT) COLELLA PHOTOGRAPHY; (BOTTOM RIGHT) LOIS TEMA; (LEFT) ISTOCKPHOTO.COM

MATERIALS SCIENCE

Factoring the Growth



Many organisms, including diatoms, create very complex single-crystal mineral structures, whose shaping and patterning are regulated by a small number of proteins. It has been a challenge to decipher which proteins are fundamental to the process, and conversely, how close to the biological shapes one can get by growing the crystals in vitro using only a limited set of proteins. For sea urchins, the construction of the magnesian calcite endoskeleton is controlled by a single cell type—the primary mesenchyme cells (PMCs). Knapp *et al.* exploited this well-defined system to explore the role of recombinant vascular endothelial growth factor (rVEGF), which acts as a signaling molecule, on the shape and crystallography of the spicules that form when the PMCs are cultured in vitro. At low concentrations of rVEGF, linear spicules formed with growth parallel to the calcite *c* axis, but at much higher concentrations a triple branch point formed, with elongated arms growing parallel to the *a*-axis. Close to the branch point, the three arms were 120° apart, but these angles changed once the arms grew past 7 μm, which may explain why in sea urchins they are limited to 3 to 5 μm in size. — MSL

J. Am. Chem. Soc. 10.1021/ja309024b (2012).

CHEMISTRY

Click Your Nanoparticles

Polymer nanoparticles are frequently tailored for particular applications by the type of functional groups displayed on their surface. Often the identification of the best functional group or groups can be an iterative process that can be slowed down by inefficient synthesis processes. Zhang *et al*. streamlined nanoparticle synthesis with diblock copolymers that were made by the ultrafast ring-opening polymerization of cyclic phospholane monomers. One monomer, bearing a 2-ethylbutyl group, forms a hydrophobic core, and the other, bearing a 3-butynyl group, has an alkyne functionality that allows for subsequent derivatization with a click reaction—photomediated, radical-mediated, thiol-yne chemistry. A variety of side chains—nonionic, anionic, cationic, and zwitterionic—could be added to the diblock copolymers. Introduction into water created micelles 13 to 21 nm in diameter with a polydispersity index below 1.2. The entire synthesis could be completed for the nonionic and anionic nanoparticles in two reaction vessels in 6 hours. — PDS

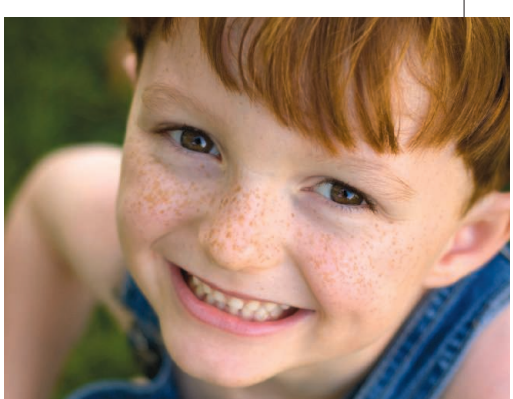
J. Am. Chem. Soc. 10.1021/ja309037m (2012).

BIOMEDICINE

Melanoma: Beyond the Light

Despite successful implementation of strategies that reduce exposure to ultraviolet radiation, the incidence of melanoma—the least common but most fatal form of skin cancer—continues to rise. This observation, together with the fact that melanomas can occur on non–sun-exposed skin, indicates that additional mechanisms independent of ultraviolet light contribute to tumorigenesis.

A new mechanistic clue has emerged from a mouse study designed to investigate why people with red hair and fair skin have the highest risk of developing melanoma. One distinguishing characteristic of these individuals is that they produce the red/yellow pigment pheomelanin.



Mitra *et al*. found that genetically manipulated mice with pigmentation mimicking the human red-hair trait developed invasive melanoma at a higher rate than did mice with pigmentation mimicking dark-skinned humans, even in the absence of exposure to ultraviolet radiation. Selective ablation of pheomelanin synthesis by introduction of an albino allele protected the mice against melanoma. This suggests that pheomelanin itself plays a causal role in melanoma development, at least in mice, possibly by inducing oxidative damage to skin cells. — PAK

Nature 10.1038/nature11624 (2012).

DEVELOPMENT

Understanding the Niche

Stem cells have the special ability to self-renew or undergo preprogrammed differentiation. The stem cell niche plays an important role in regulating this decision. If self-renewal proceeds uncontrollably, tumors can result. In the testes of *Drosophila*, a model used to understand niche–stem cell interactions, the niche is composed of the apical hub, which is important for the regulated division of its two stem cell populations: the germline stem cells (GSCs) and the cyst stem cells (CySCs). Prior studies had suggested that CySCs also serve as a niche to maintain GSCs; however, Lim and Fuller showed that after ablation of the CySCs and their progeny, early germ cells with GSC characteristics were still maintained. In particular, cells located near the apical hub were able to maintain the properties of GSCs in the absence of CySCs. Although the CySCs and cyst cells were not needed to maintain GSCs, they were necessary for their progression to the transit-amplifying stage, where the cells go through mitotic divisions before terminal differentiation. Hence, contrary to some prior conclusions, CySCs are not needed for GSC self-renewal but instead may provide signals to allow their progression through the transit-amplifying–stage divisions. This work highlights the intricate nature of the relationships between stem cells and the surrounding somatic cells. — BAP

Proc. Natl. Acad. Sci. U.S.A. 10.1073/pnas.1215516109 (2012).

CREDITS (TOP TO BOTTOM): KIRT L. ONTHANK/WIKIMEDIA COMMONS; ISTOCKPHOTO

Downloaded from www.sciencemag.org on November 9, 2012

www.sciencemag.org

Science

1200 New York Avenue, NW
Washington, DC 20005
Editorial: 202-326-6550, FAX 202-289-7562
News: 202-326-6581, FAX 202-371-9227
Bateman House, 82-88 Hills Road
Cambridge, UK CB2 1LQ
+44 (0) 1223 326500, FAX +44 (0) 1223 326501

Subscription Services For change of address, missing issues, new orders and renewals, and payment questions: 866-434-AAAS (2227) or 202-326-6417, FAX 202-842-1065. Mailing addresses: AAAS, P.O. Box 96178, Washington, DC 20090-6178 or AAAS Member Services, 1200 New York Avenue, NW, Washington, DC 20005

Institutional Site Licenses please call 202-326-6755 for any questions or information

Reprints: Author Inquiries 800-635-7181
Commercial Inquiries 803-359-4578

Permissions 202-326-7074, FAX 202-682-0816

Member Benefits AAAS Travels: Betchart Expeditions 800-252-4910; Apple Store www.store.apple.com/us/go/eppstore/aaas; NASA Federal, 1-888-NASA-FCU (1-888-627-2328) or www.nasafcu.com; Cold Spring Harbor Laboratory Press Publications www.cshlpress.com/affiliates/aaas.htm; GEICO Auto Insurance www.geico.com/landingpage/go51.htm?logo=17624; Hertz 800-654-2200 CDP#343457; Office Depot https://bsd.officedepot.com/portalLogin.do; Seabury & Smith Life Insurance 800-424-9883; Subaru VIP Program 202-326-6417; VIP Moving Services www.vipmayflower.com/domestic/index.html; Other Benefits: AAAS Member Services 202-326-6417 or www.aaasmember.org.

science_editors@aaas.org	(for general editorial queries)
science_letters@aaas.org	(for queries about letters)
science_reviews@aaas.org	(for returning manuscript reviews)
science_bookrevs@aaas.org	(for book review queries)

Published by the American Association for the Advancement of Science (AAAS), *Science* serves its readers as a forum for the presentation and discussion of important issues related to the advancement of science, including the presentation of minority or conflicting points of view, rather than by publishing only material on which a consensus has been reached. Accordingly, all articles published in *Science*—including editorials, news and comment, and book reviews—are signed and reflect the individual views of the authors and not official points of view adopted by AAAS or the institutions with which the authors are affiliated.

AAAS was founded in 1848 and incorporated in 1874. Its mission is to advance science, engineering, and innovation throughout the world for the benefit of all people. The goals of the association are to: enhance communication among scientists, engineers, and the public; promote and defend the integrity of science and its use; strengthen support for the science and technology enterprise; provide a voice for science on societal issues; promote the responsible use of science in public policy; strengthen and diversify the science and technology workforce; foster education in science and technology for everyone; increase public engagement with science and technology; and advance international cooperation in science.

Information for Authors
See pages 752 and 753 of the 10 February 2012 issue or access www.sciencemag.org/about/authors

EDITOR-IN-CHIEF **Bruce Alberts**
EXECUTIVE EDITOR **Monica M. Bradford** NEWS EDITOR **Colin Norman**
MANAGING EDITOR, RESEARCH JOURNALS **Katrina L. Kelner**
DEPUTY EDITORS **R. Brooks Hanson, Barbara R. Jasny, Andrew M. Sugden, Valda J. Vinson**

Editorial senior editors/commentary Lisa D. Chong, Brad Wible; **senior editors** Gilbert J. Chin, Pamela J. Hines, Paula A. Kiberstis (Boston), Marc S. Lavine (Toronto), Beverly A. Purnell, L. Bryan Ray, Guy Riddihough, H. Jesse Smith, Phillip D. Szuromi (Tennessee), Valda Vinson, Jake S. Yeston, Laura M. Zahn (San Diego); **associate editors** Kristen L. Mueller, Jelena Stajic, Sacha Vignieri, Nicholas S. Wigginton; **book review editor** Sherman J. Suter; **associate letters editor** Jennifer Sills; **editorial manager** Cara Tate; **senior copy editors** Jeffrey E. Cook, Cynthia Howe, Harry Jach, Lauren Kmec, Barbara P. Ordway, Trista Wagoner; **copy editor** Chris Filiatreau; **senior editorial coordinators** Carolyn Kyle, Beverly Shields; **editorial coordinators** Joi S. Granger, Anita Wynn; **publications assistants** Ramatoulaye Diop, Aneera Dobbins, Jeffrey Hearn, Lisa Johnson, Dona Mathieu, Le-Toya Mayne Flood, Shannon McMahon, Scott Miller, Jerry Richardson, Teresa R. Sakon, Brian White; **editorial assistant** Patricia M. Moore; **executive editorial assistant** Yolanda O'Bannon (San Francisco); **executive assistant** Alison Crawford; **administrative support** Maryrose Madrid; **editorial fellow** Melissa R. McCartney

Editorial director, web and new media Stewart Wills; **senior web editor** Sarah Crespi; **web editor** Kerry Klein; **web development manager** Martyn Green; **web developers** Corinna Cohn, Andrew Whitesell; **intern** Edward Hurme

News deputy news editors Robert Coontz, David Grimm (Online), Eliot Marshall, Jeffrey Mervis, Leslie Roberts, John Travis; **contributing editors** Elizabeth Culotta, Polly Shulman; **news writers** Yudhijit Bhattacharjee, Adrian Cho, Jennifer Couzin-Frankel, Carolyn Gramling, Jocelyn Kaiser, Richard A. Kerr, David Malakoff, Greg Miller, Elizabeth Pennisi, Robert F. Service (Pacific NW), Erik Stokstad; **web developer** Daniel Berger; **social media strategist** Meghna Sachdev; **intern** Emily Underwood; **contributing correspondents** John Bohannon, Jon Cohen (San Diego, CA), Ann Gibbons, Sam Kean, Eli Kintisch, Andrew Lawler, Mitch Leslie, Charles C. Mann, Virginia Morell, Gary Taubes; **copy editors** Melissa Raimondi, Kara Estelle, Linda B. Felaco; **administrative support** Scherraine Mack; **bureaus** San Diego, CA: 760-942-3252, FAX 760-942-4979; Pacific Northwest: 503-963-1940

Production director Wendy K. Shank; **assistant managers** Rebecca Doshi, Lori Murphy; **senior specialists** Steve Forrester, Christopher Redwood, Anthony Rosen; **Preflight director** David M. Tompkins; **manager** Marcus Spiegler; **specialists** Jason Hillman, Tara Kelly

Art director Yael Fitzpatrick; **associate art director** Laura Creveling; **senior illustrators** Chris Bickel, Katharine Sutliff; **illustrator** Yana Hammond; **senior art associates** Holly Bishop, Preston Huey; **art associates** Kay Engman, Garvin Grullón, Chrystal Smith; **photo editor** Leslie Blizard

***Science* International**

Europe (science@science-int.co.uk) **editorial: international managing editor** Andrew M. Sugden; **senior editor/commentary** Julia Fahrenkamp-Uppenbrink; **senior editors** Caroline Ash, Stella M. Hurtley, Ian S. Osborne, Peter Stern; **associate editor** Maria Cruz; **contributing editor** Helen Pickersgill; **editorial support** Rachel Roberts, Alice Whaley; **administrative support** Janet Clements, John Wood; **news: deputy news editor, u.k.** Daniel Clery; **contributing editor, europe** Martin Enserink; **contributing correspondents** Michael Balter (Paris), Kai Kupferschmidt (Berlin), Gretchen Vogel (Berlin)

Asia Japan Office: Asca Corporation, Tomoko Furusawa, Rustic Bldg. 7F, 77 Tenjin-cho, Shinjuku-ku, Tokyo 162-0808, Japan; +81 3 6802 4616, FAX +81 3 6802 4615, inquiry@sciencemag.jp; **asia news editor** Richard Stone (Beijing: rstone@aaas.org); **contributing correspondents** Dennis Normile [Japan: +81 (0) 3 3391 0630, FAX +81 (0) 3 5936 3531; dnormile@gol.com]; Hao Xin [China: cindyhao@gmail.com]; Mara Hvistendahl [China: mhvisten@aaas.org]; Pallava Bagla [South Asia: +91 (0) 11 2271 2896; pbagla@vsnl.com]

EXECUTIVE PUBLISHER **Alan I. Leshner**
PUBLISHER **Beth Rosner**

Fulfillment Systems and Operations (membership@aaas.org); **customer service supervisor** Pat Butler; **specialists** LaToya Casteel, Michelle Ofordire, April Marshall; **manager, data entry** Mickie Napoleoni; **data entry specialists** Tarrika Hill, JJ Regan, Eva Mae Campbell

Business Operations and Administration director Deborah Rivera-Wienhold; **business systems and financial analysis director** Randy Yi; **manager, fulfillment systems** Frits Buningh; **systems analyst** Nicole Mehmedovich; **manager, business analysis** Eric Knott; **manager, business operations** Jessica Tierney; **business analysts** Cory Lipman, Celeste Troxler; Christine Wehrli; **financial analyst** Julia Nguyen; **rights and permissions: administrator** Emilie David; **associate** Elizabeth Sandler; **marketing director** Ian King; **marketing managers** Allison Pritchard, Alison Chandler, Julianne Wielga, Samantha Smith; **marketing associates** Aimee Aponte, Mary Ellen Crowley, Elizabeth Sattler, Rebecca Riffkin; **senior marketing executive** Jennifer Reeves; **director, site licensing** Tom Ryan; **director, corporate relations** Eileen Bernadette Moran; **senior publisher relations specialist** Kiki Forsythe; **publisher relations manager** Catherine Holland; **publisher relations, eastern region** Keith Layson; **publisher relations, western region** Ryan Rexroth; **customer relations manager** Iquo Edim; **marketing manager** Christina Schlecht; **marketing associates** Paulina Curto, Mitchell Edmund; **customer relations associate:** Joe Horn; **electronic media: director** Lizabeth Harman; **assistant manager** Lisa Stanford; **production specialists** Antoinette Hodal, Thomas Jaensch, Nichele Johnston, Kimberly Oster; **web and new media: senior project manager** Trista Smith, **project leader** Luke Johnson **computer specialists** Walter Jones, Kai Zhang, **web developer** Jeremy Bates; **program director, aaas member central** Peggy Mihelich

director, global collaboration, custom publications, advertising Bill Moran
editor, custom publishing Sean Sanders: 202-326-6430
assistant editor, custom publishing Tianna Hicklin 202-326-6463
associate director, collaboration, custom publications/china/taiwan/korea/singapore Ruolei Wu +86-1367-101-5294

Product (science_advertising@aaas.org); **midwest** Rick Bongiovanni: 330-405-7080, FAX 330-405-7081; **east coast/e. canada** Laurie Faraday: 508-747-9395, FAX 617-507-8189; **west coast/w. canada** Lynne Stickrod: 415-931-9782, FAX 415-520-6940; **uk europe/asia** Roger Goncalves: TEL/FAX +41 43 243 1358; **japan**, Makiko Hara: +81 (0) 3 6802 4616, FAX +81 (0) 3 6802 4615; ads@sciencemag.jp; **china/taiwan** Ruolei Wu: +86 1367 1015 294 rwu@aaas.org

worldwide associate director of *Science* Careers Tracy Holmes: +44 (0) 1223 326525, FAX +44 (0) 1223 326532

Classified (advertise@sciencecareers.org); **u.s.: east coast/west coast/south central/south america** Tina Burks: 202-326-6577; **midwest/canada/industry** Allyson Rosen: 202-326-6578; **sales administrator** Marci Gallun; **europe/row sales** Benjamin Asfaha, Lucy Nelson; **sales assistant** Kelly Grace; **japan** Yuri Kobayashi +81 (6) 6627-9250; careerads@sciencemag.jp; **china/taiwan** Ruolei Wu: +86 1367 1015 294 rwu@aaas.org; **advertising support manager** Karen Foote: 202-326-6740; **advertising production operations manager** Deborah Tompkins; **senior production specialist/graphic designer** Amy Hardcastle; **production specialist** Yuse Lajiminmuhip; **senior traffic associate** Christine Hall; **sales coordinator** Shirley Young

AAAS Board of Directors retiring president, chair Nina V. Fedoroff; president William H. Press; president-elect Phillip A. Sharp; treasurer David E. Shaw; chief executive officer Alan I. Leshner; board May R. Berenbaum, Bonnie L. Bassler, Stephen L. Mayo, Raymond Orbach, Julia M. Phillips, Sue V. Rosser, David D. Sabatini, Inder M. Verma

AAAS
ADVANCING SCIENCE, SERVING SOCIETY

SENIOR EDITORIAL BOARD

A. Paul Alivisatos, *Lawrence Berkeley Nat'l. Laboratory*
Cori Bargmann, *The Rockefeller Univ.*
Ernst Fehr, *Univ. of Zurich*
Erin O'Shea, *Harvard Univ.*
Michael S. Turner, *University of Chicago*

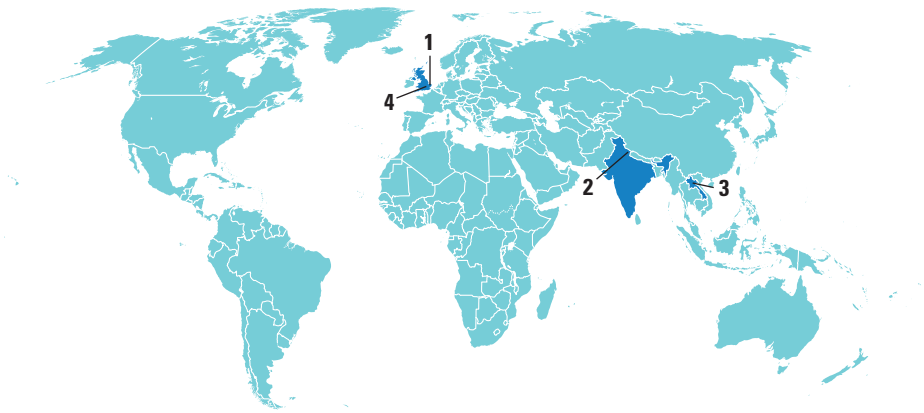
BOARD OF REVIEWING EDITORS

Adriano Aguzzi, *Univ. Hospital Zürich*
Takuzo Aida, *Univ. of Tokyo*
Sonia Altizer, *Univ. of Georgia*
Sebastian Amigorena, *Institut Curie*
Angelika Amon, *MIT*
Kathryn Anderson, *Memorial Sloan-Kettering Cancer Center*
Siv G. E. Andersson, *Uppsala Univ.*
Peter Andolfatto, *Princeton Univ.*
Meinrat O. Andreae, *Max Planck Inst., Mainz*
Johan Auwerx, *EPFL*
David Awschalom, *Univ. of California Santa Barbara*
Ben Barres, *Stanford Medical School*
Jordi Bascompte, *Estación Biológica de Doñana, CSIC*
Facundo Batista, *London Research Inst.*
Ray H. Baughman, *Univ. of Texas, Dallas*
David Baum, *Univ. of Wisconsin*
Mark Bear, *Massachusetts Inst. of Technology*
Yasmine Belkaid, *NIAID, NIH*
Philip Benfey, *Duke Univ.*
Stephen J. Benkovic, *Penn State Univ.*
Christophe Bernard, *Aix-Marseille Univ.*
Gregory C. Beroza, *Stanford Univ.*
Gabriele Bergers, *Univ. of California, San Francisco*
Peer Bork, *EMBL*
Bernard Bourdon, *Ecole Normale Superieure de Lyon*
Ian Boyd, *Univ. of St. Andrews*
Christian Büchel, *Universitätsklinikum Hamburg-Eppendorf*
Joseph A. Burns, *Cornell Univ.*
William P. Butz, *Population Reference Bureau*
Gyorgy Buzsaki, *New York Univ., School of Medicine*
Mats Carlsson, *Univ. of Oslo*
Mildred Cho, *Stanford Univ.*
David Clapham, *Children's Hospital, Boston*
David Clary, *Univ. of Oxford*
Jonathan D. Cohen, *Princeton Univ.*
Robert Cook-Deegan, *Duke Univ.*
James Collins, *Boston Univ.*
Alan Cowman, *Walter & Eliza Hall Inst.*
Robert H. Crabtree, *Yale Univ.*
Wolfgang Cramer, *Mediterranean Inst. of Biodiversity and Ecology*
F. Fleming Crim, *Univ. of Wisconsin*
Jeff L. Dangl, *Univ. of North Carolina*
Tom Daniel, *Univ. of Washington*
Frans de Waal, *Emory Univ.*
Stanislas Dehaene, *Collège de France*
Robert Desimone, *MIT*
Claude Desplan, *New York Univ.*
Ap Dijksterhuis, *Radboud Univ. of Nijmegen*
Dennis Discher, *Univ. of Pennsylvania*
Gerald W. Dorn II, *Washington Univ. School of Medicine*
Jennifer A. Doudna, *Univ. of California, Berkeley*
Julian Downward, *Cancer Research UK*
Bruce Dunn, *Univ. of California, Los Angeles*
Christopher Dye, *WHO*
David Ehrhardt, *Carnegie Inst. of Washington*
Tim Elston, *Univ. of North Carolina at Chapel Hill*
Gerhard Ertl, *Fritz-Haber-Institut, Berlin*
Barry Everitt, *Univ. of Cambridge*
Paul G. Falkowski, *Rutgers Univ.*
Ernst Fehr, *Univ. of Zurich*
Tom Fenchel, *Univ. of Copenhagen*
Michael Feuer, *The George Washington Univ.*
Alain Fischer, *INSERM*
Susan Fiske, *Princeton Univ.*
Anne C. Ferguson-Smith, *Univ. of Cambridge*
Wulfram Gerstner, *EPFL Lausanne*
Karl-Heinz Glassmeier, *TU Braunschweig*
Elizabeth Grove, *Univ. of Chicago*
Kip Guy, *St. Jude's Children's Research Hospital*
Taekjip Ha, *Univ. of Illinois at Urbana-Champaign*
Christian Haass, *Ludwig Maximilians Univ.*
Steven Hahn, *Fred Hutchinson Cancer Research Center*
Gregory J. Hannon, *Cold Spring Harbor Lab.*
Martin Heimann, *Max Planck Inst., Jena*
Isaac Held, *NOAA*
James A. Hendler, *Rensselaer Polytechnic Inst.*
Janet G. Hering, *Swiss Fed. Inst. of Aquatic Science & Technology*
Ray Hilborn, *Univ. of Washington*
Michael E. Himmel, *National Renewable Energy Lab.*
Kai-Uwe Hinrichs, *Univ. of Bremen*
Kei Hirose, *Tokyo Inst. of Technology*
David Hodell, *Univ. of Cambridge*
David Holden, *Imperial College*
Lora Hooper, *UT Southwestern Medical Ctr at Dallas*
Jeffrey A. Hubbell, *EPFL Lausanne*
Thomas Hudson, *Ontario Inst. for Cancer Research*
Steven Jacobsen, *Univ. of California, Los Angeles*
Kai Johnsson, *EPFL Lausanne*
Peter Jonas, *Universität Freiburg*
William Kaelin Jr., *Dana-Farber Cancer Inst.*
Daniel Kahne, *Harvard Univ.*
Daniel Kammen, *Univ. of California, Berkeley*
Joel Kingsolver, *Univ. of North Carolina at Chapel Hill*
Robert Kingston, *Harvard Medical School*
Roberto Kolter, *Harvard Medical School*
Alberto R. Kornblihtt, *Univ. of Buenos Aires*
Leonid Kruglyak, *Princeton Univ.*
Thomas Langer, *Univ. of Cologne*
Mitchell A. Lazar, *Univ. of Pennsylvania*
David Lazer, *Harvard Univ.*
Virginia Lee, *Univ. of Pennsylvania*
Ottoline Leyser, *Cambridge Univ.*
Olle Lindvall, *Univ. Hospital, Lund*
Marcia C. Linn, *Univ. of California, Berkeley*
John Lis, *Cornell Univ.*
Jianguo Liu, *Michigan State Univ.*
Jonathan Losos, *Harvard Univ.*
Ke Lu, *Chinese Acad. of Sciences*
Christian Lüscher, *Univ. of Geneva*
Laura Machesky, *CRUK Beatson Inst. for Cancer Research*
Anne Magurran, *Univ. of St Andrews*
Oscar Marin, *CSIC & Univ. Miguel Hernández*
Charles Marshall, *Univ. of California, Berkeley*
Martin M. Matzuk, *Baylor College of Medicine*
Graham Medley, *Univ. of Warwick*
Yasushi Miyashita, *Univ. of Tokyo*
Richard Morris, *Univ. of Edinburgh*
Edvard Moser, *Norwegian Univ. of Science and Technology*
Sean Munro, *MRC Lab. of Molecular Biology*
Thomas Murray, *The Hastings Center*
Naoto Nagaosa, *Univ. of Tokyo*
James Nelson, *Stanford Univ. School of Med.*
Timothy W. Nilsen, *Case Western Reserve Univ.*
Pär Nordlund, *Karolinska Inst.*
Helga Nowotny, *European Research Advisory Board*
Luke O'Neill, *Trinity College, Dublin*
Stuart Newman, *New York Medical College*
N. Phuan Ong, *Princeton Univ.*
Joe Orenstein, *Univ. of California, Berkeley & Lawrence Berkeley National Lab*
Stuart H. Orkin, *Dana-Farber Cancer Inst.*
Harry Orr, *Univ. of Minnesota*
Christine Ortiz, *MIT*
Andrew Oswald, *Univ. of Warwick*
Steve Palumbi, *Stanford Univ.*
Jane Parker, *Max-Planck Inst. of Plant Breeding Research*
Donald R. Paul, *Univ. of Texas at Austin*
P. David Pearson, *Univ. of California, Berkeley*
Reginald M. Penner, *Univ. of California, Irvine*
John H. J. Petrini, *Memorial Sloan-Kettering Cancer Center*
Simon Phillpot, *Univ. of Florida*
Joshua Plotkin, *Univ. of Pennsylvania*
Philippe Poulin, *CNRS*
Colin Renfrew, *Univ. of Cambridge*
Trevor Robbins, *Univ. of Cambridge*
Barbara A. Romanowicz, *Univ. of California, Berkeley*
Jens Rostrup-Nielsen, *Haldor Topsoe*
Mike Ryan, *Univ. of Texas, Austin*
Shimon Sakaguchi, *Kyoto Univ.*
Miquel Salmeron, *Lawrence Berkeley National Lab*
Jürgen Sandkühler, *Medical Univ. of Vienna*
Randy Seeley, *Univ. of Cincinnati*
Vladimir Shalaev, *Purdue Univ.*
Joseph Silk, *Institut d'Astrophysique de Paris*
Denis Simon, *Arizona State Univ.*
Alison Smith, *John Innes Centre*
Davor Solter, *Inst. of Medical Biology, Singapore*
Peter Sorger, *Harvard Medical School*
John Speakman, *Univ. of Aberdeen*
Allan C. Spradling, *Carnegie Institution of Washington*
Jonathan Sprent, *Garvan Inst. of Medical Research*
Paula Stephan, *Georgia State Univ. and National Bureau of Economic Research*
Elsbeth Stern, *ETH Zürich*
Ira Tabas, *Columbia Univ.*
Yoshiko Takahashi, *Kyoto Univ.*
Sarah Teichmann, *Cambridge Univ.*
John Thomas, *Duke Univ.*
Herbert Virgin, *Washington Univ.*
Bert Vogelstein, *Johns Hopkins Univ.*
Cynthia Volkert, *Univ. of Gottingen*
Bruce D. Walker, *Harvard Medical School*
Douglas Wallace, *Dalhousie Univ.*
Ian Walmsley, *Univ. of Oxford*
David A. Wardle, *Swedish Univ. of Agric Sciences*
David Waxman, *Fudan Univ.*
Detlef Weigel, *Max-Planck Inst., Tübingen*
Jonathan Weissman, *Univ. of California, San Francisco*
Sue Wessler, *Univ. of California, Riverside*
Kathy Willis, *Oxford Univ.*
Ian A. Wilson, *The Scripps Res. Inst.*
Timothy D. Wilson, *Univ. of Virginia*
Rosemary Wyse, *Johns Hopkins Univ.*
Jan Zaanen, *Leiden Univ.*
Kenneth Zaret, *Univ. of Penn. School of Medicine*
Mayana Zatz, *University of Sao Paolo*
Jonathan Zehr, *Univ. of California, Santa Cruz*
Maria Zuber, *MIT*

BOOK REVIEW BOARD

John Aldrich, *Duke Univ.*
David Bloom, *Harvard Univ.*
Angela Creager, *Princeton Univ.*
Richard Shweder, *Univ. of Chicago*
Ed Wasserman, *DuPont*
Lewis Wolpert, *Univ. College London*

AROUND THE WORLD



Cambridge, U.K. **1**

British Antarctic Survey Keeps Its Identity

U.K. scientists were relieved by a decision last Friday to stop a highly unpopular proposed merger between the celebrated British Antarctic Survey (BAS) and the National Oceanography Centre. The Natural Environment Research Council (NERC), which oversees both centers, proposed the merger earlier this year as a cost-cutting measure. Researchers strenuously objected, arguing that the merger was ill-conceived and might hamper BAS's mission; three BAS senior staff members left the survey earlier this year, possibly because of conflicts over the proposal. The furor prompted NERC to make its decision last week, a month sooner



than planned. On 31 October, the House of Commons Science and Technology Committee urged NERC to cancel the merger on the grounds that NERC hadn't made its case.

Despite the merger's cancellation, ongoing uncertainty about the survey's future funding and its current leadership vacuum have cast a pall over what was supposed to be a banner year for BAS, including plans to drill into a subglacial Antarctic lake in December. NERC has committed itself to funding BAS at £42 million annually through 2015. **http://scim.ag/BritAnt**

Dehradun, India **2**

Science Unclear on GM Crops

At a 29 October press conference, India's new science minister, S. Jaipal Reddy, took a skeptical stance on one of the country's hottest issues: genetically modified (GM) crops. In response to questions from *Science*, Reddy said "the science is not clear."

Reddy, a graduate in English and a career politician who is known as one of India's finest orators, took over as science minister on 29 October in a cabinet reshuffle by Prime Minister Manmohan Singh. His new job will require him to navigate the highly charged debate on GM crops. The prime minister's Scientific Advisory Council expressed support for biotechnology in an early-October report. But on 17 October, an expert panel appointed by India's Supreme Court to advise it on a GM case recommended a 10-year moratorium on GM crop field trials.


Reddy

"Not having a science background should not be a handicap for the new minister," says physicist Ajay Sood, president of the Indian Academy of Sciences in Bangalore. But he says scientists expect the influential minister to have a "positive outlook to science." **http://scim.ag/SciMinGM**

Laos **3**

Megadam Gets Green Light

Laos has given builders a green light to finish work on a controversial megadam at Xayaburi on the lower Mekong River, after a diplomatic pause this year to consult with neighboring leaders in Cambodia and Vietnam who were concerned about potential ecological impacts (*Science*, 12 August 2011, p. 814). Xayaburi, which is projected to cost more than $3.5 billion and generate 1285 megawatts of power, is primarily Thai-financed and will export most of its electricity to Thailand, although a portion of the energy will be resold to other buyers. Laos hopes the project will give its developing economy a huge boost. But opponents say this dam and 11 more now in planning could massively disrupt the lower Mekong's ecology, slowing the cyclical water movements that replenish the soil and sustain the region's migratory fish.


Go ahead. Near the site of the proposed Xayaburi dam on the Mekong River.

London **4**

Journal Pushes for Transparency

To help open up drug company data vaults, *BMJ* announced a new policy last week: Unless authors agree to share raw clinical information, their papers will not be considered for publication. In a sharply worded editorial announcing the policy, *BMJ* Editor Fiona Godlee decried the "wilful distortion" of science by scientists who "hide data, mislead doctors, and harm patients" by sitting on data useful for the study of the safety and efficacy of treatments. *BMJ* has been pushing for the past 3 years to obtain private clinical data on Roche's antiviral drug oseltamivir (Tamiflu). Starting next January, *BMJ* will require all authors to "make the relevant anonymised patient level data available on reasonable request." Pharma giant GlaxoSmithKline has already adopted a similar policy, saying it will share anonymized patient records. The trend to open up data will accelerate, said Robert Califf, research vice chancellor of Duke University in Durham, North Carolina, and an expert on clinical trials, in an e-mail. Califf believes this will benefit society, although he says the details still need to be worked out.

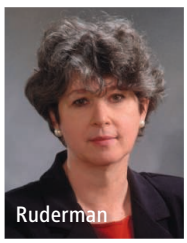
CREDITS (LEFT TO RIGHT): WIKIMEDIA COMMONS/VINCENT VAN ZEIJST; WWW.INDIA.GOV.IN; AP PHOTO/INTERNATIONAL RIVERS, PIAPORN DEETES

Downloaded from www.sciencemag.org on November 9, 2012

Published by AAAS

NEWSMAKERS

Marine Biological Laboratory Appoints New President


Ruderman

Harvard Medical School cell biologist **Joan Ruderman** is the new president and director of the Marine Biological Laboratory (MBL) in Woods Hole, Massachusetts. The announcement, made on 3 November, marks a first for MBL: Ruderman is the first woman to head the institution since its founding in 1888. She has been affiliated with MBL since 1974, when Ruderman took an embryology course that "changed my life in so many ways," she says, including introducing her to the *Spisula* organism that led to her discoveries of molecular drivers of cell division.

Although MBL has struggled financially, Ruderman says its situation is no different from that of other research institutions, and she points to a recent fundraising campaign that exceeded its $125 million goal. As director, Ruderman says she hopes to expand MBL's programs to encompass environmental research at the molecular and cellular levels, including research on the developmental origins of adult-onset diseases such as breast cancer.

FINDINGS

Rare Whales Spotted In New Zealand

Two whales stranded on a New Zealand beach in 2010 have turned out to be the first documented live specimens of a whale species previously known from only a few skeletal fragments. The 5.3-meter-long female and 3.5-meter-long juvenile male were initially mistaken for Gray's beaked whales. But a genetic analysis of tissue samples taken after the whales died determined they were spade-toothed beaked whales (*Mesoplodon traversii*).

"It was very exciting. These animals are only known from three skull fragments; we didn't know if the species was still extant," says Rochelle Constantine, a marine mammal biologist at University of Auckland in New Zealand. Once Constantine and her colleagues identified the species, they exhumed the carcasses for morphological analysis and reported their results on 6 November in *Current Biology*.


Mistaken identity. Spade-toothed beaked whales resemble this Gray's beaked whale.

Beaked whales are among the most rarely sighted and least understood. They inhabit deep waters in the South Pacific, feeding on squid and small fish and spending limited time at the surface.

"Once again we have evidence that our understanding of the biota of the deep oceans is still only (literally) scratching the surface," says marine mammal researcher Robert Harcourt of Macquarie University in Sydney, Australia. **http://scim.ag/rarewhale**

Infinitely Fast Light—Sort Of

Within a tiny device, visible light can, by one measure, travel infinitely fast, a team of researchers report. In a material such as glass, light travels slower than in empty space. The ratio of the speed of light in the vacuum to that of in the material defines the material's "index of refraction," which is usually greater than one. Not so inside the nanometer-scale "wave guide" that Albert Polman, a physicist at the FOM Institute for Atomic and Molecular Physics in Amsterdam; Nader Engheta, an electrical engineer at the University of Pennsylvania; and colleagues fashioned out of silicon dioxide and silver. In the guide, described in a paper in press at *Physical Review Letters*, light waves of one frequency zip along infinitely fast, giving the device an index of refraction of zero—a first for visible light. The gizmo doesn't violate relativity, Engheta says, because energy still flows down the channel slower than the usual speed of light.

"The demonstration of such a thing is definitely very interesting and possibly useful," says Wenshan Cai, an electrical engineer at the Georgia Institute of Technology in Atlanta. For example, such a device might serve as a collector of light in optical experiments, Cai says. **http://scim.ag/fastlight**

Science LIVE

Join us on Thursday, 15 November, at 3 p.m. EST for a live chat on a hot topic in science. **http://scim.ag/science-live**

Random Sample

Downing Biodiversity Lessons



Biodiversity has driven doctoral candidates from Trinity College Dublin to drink. Since 5 November, the students have been entertaining patrons in Dublin's bars with snappy, 3-minute talks meant to expand on information printed on beermats that they distributed to 10 local pubs in August and again in November.

"We want to capture people's interest and hope to stimulate discussion in the pub," says Trinity doctoral candidate Erin Jo Tiedeken, who studies insect pollinators and toxic compounds in nectar.

The colorful coasters invite contemplation of nuggets including the number of bees needed to produce the apples in a pint of cider, the river water in local brews, and Ireland's cold water coral reefs. Part of the "Biodiversity In Our Lives" project, the students hope to instill the message that biodiversity is valuable to everyday life, including common tipples.

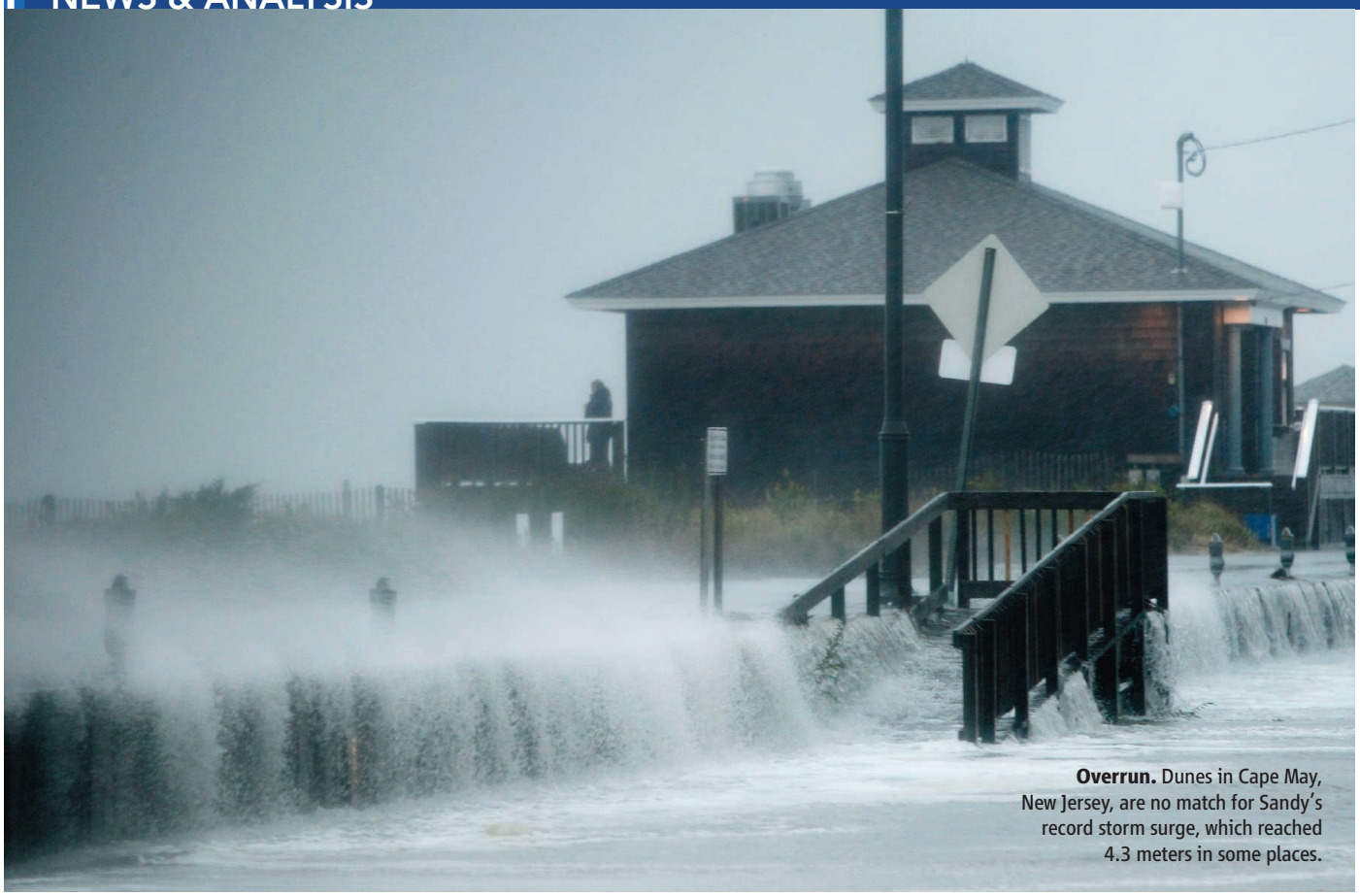
The students initially distributed their beermats to bars frequented by students and professors. But they also targeted working-class pubs. "At first they gave us the strangest looks, but one of the bartenders phoned up and said his buddy in another pub wanted some of our beermats," Tiedeken says.

By reaching out to a wider audience, Tiedeken and her colleagues hope to make the university, and their research, more accessible. They plan to further expand their project, having secured funding to print an additional 20,000 beermats. They'll distribute them, along with their flash lectures, to 20 more pubs throughout November.

CREDITS (LEFT TO RIGHT): BACHRACH STUDIOS; CROWN COPYRIGHT: NEW ZEALAND DEPARTMENT OF CONSERVATION; TE PAPA ATAWHAI (JANUARY 2011); AILEEN CROSSLEY (2)

Downloaded from www.sciencemag.org on November 9, 2012

Published by AAAS



Overrun. Dunes in Cape May, New Jersey, are no match for Sandy's record storm surge, which reached 4.3 meters in some places.

CREDIT: © ECONOMOPOULOS, ARISTIDE/STAR LEDGER/CORBIS

U.S. HURRICANE

Scientists Assess Damage From Sandy's Deadly Punch

As superstorm Sandy surged ashore in New Jersey on the night of 29 October, coastal scientists watched their computer screens with wonder as a string of 28 specialized radars collected exquisitely detailed data on the churning waves and currents far offshore. It was an opportunity to study "a storm that might come just once in a career," says physical oceanographer Josh Kohut of the Institute of Marine and Coastal Sciences at Rutgers University, New Brunswick, in New Jersey.

But that opportunity didn't last long. Sandy's pummeling winds and record floodwaters began to snuff out the signals, and in just a few hours, 17 of the 5- to 7-meter-tall radar towers were silent. "Sandy ripped right through the heart of the network," says Rutgers oceanographer Scott Glenn, adding that only sand remains where some towers once stood. "We may have lost equipment worth millions of dollars."

Glenn isn't the only scientist picking up the pieces after a storm that swept across the U.S. Atlantic Coast, submerging communities, killing more than 100 people, and leaving tens of thousands without housing and millions without power. Sandy pounded other marine science installations and flooded biomedical research facilities, killing thousands of research rodents at one New York City laboratory. The storm also disrupted countless experiments and meetings, leaving scientists wondering when they will be able to get back to work.

At the same time, Sandy presented some researchers with unprecedented opportunities. U.S. government geologists scrambled in the days before the storm to measure beaches and shorelines along its expected path for data that would improve computer models that predict coastal flooding and erosion. Other researchers rushed to launch a robotic submarine off the New Jersey coast, providing a rare look at how Sandy reshuffled conditions beneath the ocean's surface.

The storm also created some scientific heroes. Researchers at Johns Hopkins University in Baltimore, Maryland, battled dire conditions to rescue hundreds of animals from a flooded basement. And a few laboratories not only weathered the storm, but have also been helping with the recovery efforts. Their equipment is providing satellite images to disaster officials, and their emergency generators have provided electricity and hot showers to residents in nearby communities. At Cold Spring Harbor Laboratory (CSHL) on Long Island, New York, researchers posted a sign summing up that can-do attitude: "Sandy versus Science … Science Wins."

Sandy left deeper scars elsewhere. The storm dealt an especially heavy blow to New York University's (NYU's) Langone Medical Center in New York City. A loss of power forced the hospital to transfer hundreds of patients to other hospitals. Stormwater poured into the Smilow Research Center, one of several animal research facilities at the university, knocking out backup generators. "[D]ue to the speed and force of the surge," efforts to rescue more than 10,000 laboratory mice and rats housed in basement facilities were "unsuccessful," the center said in a statement. The losses included dozens of rodent variants specially bred to study neurological and physiological diseases, NYU

Downloaded from www.sciencemag.org on November 9, 2012

Published by AAAS

officials said, representing "many years of important work conducted by our researchers."

Other academic research centers quickly vowed to help NYU scientists rebuild their colonies. An online company called Science Exchange even offered to waive the fees it usually charges to arrange large-scale purchases of transgenic and other research mice. "We were obviously very upset to hear about all of the research that was lost," says Dan Knox, the company's co-founder.

Researchers at Johns Hopkins University School of Medicine in Baltimore narrowly avoided similar losses. After stormwater poured into a basement animal facility in the Koch Cancer Research Building, causing power to be turned off, "the dean and senior staff at the medical school formed a human chain, taking cages with laboratory mice to safety," says Johns Hopkins President Ronald Daniels. "It was quite an ordeal."

Sandy also hit hard at the U.S. National Oceanic and Atmospheric Administration's (NOAA's) James J. Howard Marine Sciences Laboratory in Fort Hancock, New Jersey, just north of the storm's landfall. "Word is that we are going to be closed for quite a while; there's 6 feet of sand in the road and the sewage system may be damaged," says NOAA ecologist John Manderson. Captive sea bass and flounder involved in ocean acidification studies died after generators failed, he adds. "That's a big setback."

At Cold Spring Harbor, which sits on the shore of Long Island Sound, laboratory officials were ready for Sandy. The lab had upgraded its emergency drill after Hurricane Gloria in 1985, and with Sandy approaching, staff members moved elevator cars up from basements and piled sandbags to shield against the incoming tide (which peaked at more than 2 meters above normal). With ample housing on the campus, some personnel stayed at the lab and were able to switch on eight diesel-powered generators after the power went down.

Although water seeped into one building and phone service was knocked out, staff members were able to ride out the storm. Over the next few days, they cleared away more than 100 downed trees and trucked a generator to a local gas station to fill up lab vehicles. Attracted by the lab's lights shining at night, residents queued up for meals and Internet access. (The U.S. Department of Energy's Princeton Plasma Physics Laboratory in New Jersey also offered hot showers to nearby residents.) After a 2-day delay, CSHL was even able to hold a meeting on nuclear cell receptors and disease; although some foreign scientists attended, a plenary speaker from nearby New York City couldn't make the trip.

At Rutgers, ocean researchers are upbeat despite the apparent loss of a big chunk of their high-frequency radar system. The network, which has operated since the late 1990s, stretches 1200 kilometers from Cape Hatteras in North Carolina to Cape Cod in Massachusetts and can measure ocean currents up to about 180 kilometers offshore. Poststorm surveys have revealed that at least four of the radars—which cost at least $150,000 each—"are completely gone," Glenn says, and another five are damaged. It could be weeks before the rest are fully inspected. But Glenn says the radars did "great work" before succumbing, providing a detailed look at how Sandy shifted ocean currents—potentially useful information for improving forecasting models.

The Rutgers researchers are also looking forward to crunching a mountain of data collected by the submarine "glider" that swam in the ocean beneath Sandy, about 10 nautical miles off the New Jersey coast. "We wanted to be sure we were far enough offshore that the storm didn't push it back in and wreck it," says Travis Miles, a doctoral student who helps operate the submarine.

The craft's sensors collected extensive information on how the storm stirred up bottom sediments and mixed layers of cooler and warmer waters. The temperature data are important because storms can draw energy from warm surface waters. Preliminary data suggest that Sandy's winds caused mixing that cooled surface waters by several degrees Celsius; the researchers saw a similar although more pronounced pattern last year, when a glider collected data during Hurricane Irene.

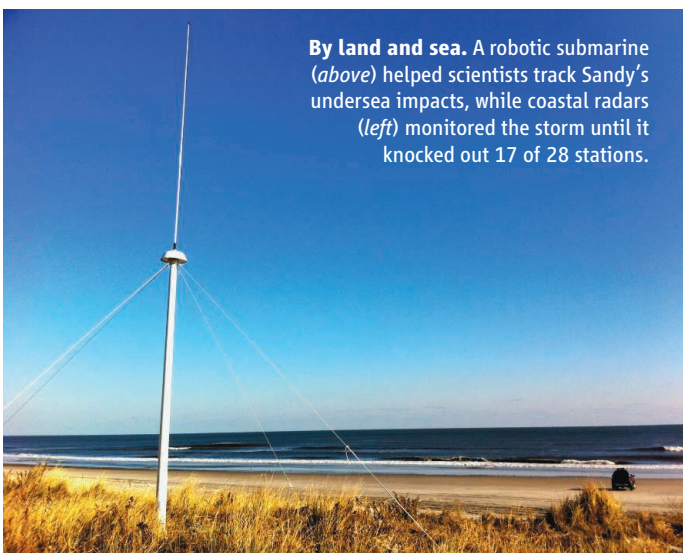
Miles, who will be using the sub's findings as part of his doctoral thesis, has mixed feelings about his good fortune. "As a scientist, you want a big storm so you can get interesting data," he says. "But you don't want it to do this much damage."

Cheryl Hapke, a geologist with the U.S. Geological Survey in St. Petersburg, Florida, jumped on a plane a few days before the storm to measure beaches and dunes at the Fire Island National Seashore in New York. Then she spent days after the storm measuring the devastation. The storm "is the biggest of my career," she says, "and it's rare to get a chance to study an event with this kind of intensity." She also hopes that her run-in with Sandy will pay off for society. Her data could improve computer models used to predict which coastal areas are likely to be flooded during the next big storm, giving people a better chance to stay out of harm's way.

–DAVID MALAKOFF

With reporting by Elizabeth Pennisi, Richard Stone, and Emily Underwood.





By land and sea. A robotic submarine (*above*) helped scientists track Sandy's undersea impacts, while coastal radars (*left*) monitored the storm until it knocked out 17 of 28 stations.

CREDITS (TOP TO BOTTOM): KAYCEE COLEMAN/RUTGERS; RUTGERS UNIVERSITY COASTAL OCEAN OBSERVATION LABORATORY (RU COOL)

Downloaded from www.sciencemag.org on November 9, 2012

Published by AAAS





Water wars. A detailed climate record from a stalagmite in a cave in Belize (*left*) links a rise in Maya warfare (*above*) to a drying trend in the 7th century C.E.

CREDITS (LEFT TO RIGHT): DOUG KENNETT; (DRAWING/PHOTOGRAPH) BY LINDA SCHELE, © DAVID SCHELE, COURTESY FOUNDATION FOR THE ADVANCEMENT OF MESOAMERICAN STUDIES, INC., WWW.FAMSI.ORG

ARCHAEOLOGY

Did Pulses of Climate Change Drive The Rise and Fall of the Maya?

For nearly 13 centuries, from 300 B.C.E. to 1000 C.E., the Classic Maya civilization flourished. Maya kings reigned as gods over dozens of city-states, Maya artists ornamented the walls of temples and palaces, and Maya scribes recorded the triumphs and defeats of their rulers in hieroglyphic inscriptions. But despite the vast ruins the Maya left behind, archaeologists have long puzzled over what fueled the ascent and downfall of this civilization—and whether climate played a starring role, a bit part, or was offstage altogether at key turning points in Maya history.

Now, an international research team led by geoarchaeologist Douglas Kennett of Pennsylvania State University, University Park, has produced the best climate record yet of Maya times: a subannual reconstruction of rainfall in the Maya heartland that extends back 2000 years. Comparing this reconstruction to records of major Maya building episodes and warfare, they conclude that an extended period of generous rainfall helped spur the growth and proliferation of Maya city-states, and a prolonged dry period played a key part in their collapse. "Climate does matter, and it matters in a very complex way," Kennett says.

The new climate record "is a really nice first cut at a high-resolution record," says paleoclimatologist Lawrence Edwards of the University of Minnesota, Twin Cities, who was not involved in the work. But many archaeologists remain reluctant to adopt climate as the chief driver of Maya society. Even so, the study's abundant new data will help clarify the role of climate in Maya history, says archaeologist Jason Yaeger of the University of Texas, San Antonio. "We can start to think of climate change as a more concrete variable, and obviously an important one, in Maya history," Yaeger says.

Paleoclimatologists and archaeologists agree that the record itself is outstanding. Previous studies have wrested paleoclimate data from sources such as marine muds off the Venezuelan coast and lake sediments from the Yucatán Peninsula (*Science*, 18 May 2001, p. 1293), building a burgeoning literature. But many archaeologists have argued that such records are too far from the Maya heartland or too broad-brush to show causal links between climate and culture.

The new record, from a 56-centimeter-long stalagmite (an upward-pointing cave-floor pillar of limestone) came from the right neighborhood: It grew from incessantly dripping water in Yok Balum Cave in southern Belize, less than 200 kilometers from many major Classic Maya city-states, including Tikal, Caracol, and Calakmul. And "the real advancement is their uranium-thorium dating," says paleoclimatologist David Hodell of the University of Cambridge in the United Kingdom. The clocklike radioactive decay of uranium-234 to thorium-230 provided geochemist Yemane Asmerom of the University of New Mexico, Albuquerque, with precise ages for mineral deposition down through the stalagmite, with strikingly small error bars of plus or minus 1 to 17 years. "Within a couple of decades, they've got [the dating] nailed," Edwards says.

The only aspect of the Yok Balum record that falls well short of ideal is the drought record preserved in the changing oxygen-isotope composition down the stalagmite. The isotopic composition of rainwater seeping down into the cave—the ratio of the rare, heavier oxygen-18 isotope to oxygen-16—reflects the amount of rainfall on the surface. But unfortunately, evaporation within the cave alters the isotopic signal of declining rainfall before it is preserved in the stalagmite, making it hard to speak quantitatively about cycles of drought on the surface. Instead, the authors write of "wet periods," "drying trends," and "dry periods."

To match the paleoclimatic data to cultural history, the team charted the rise and fall of complex Maya polities and the prevalence of warfare. Graduate student Claire Ebert of Pennsylvania State University searched an existing Maya hieroglyphic database for records of dated monuments in the heartland. She also searched for dated inscriptions containing key words or phrases related to war, such as "vassalage after defeat." Then she and Kennett charted the frequencies of these monuments and inscriptions over time, and compared them with the stalagmite data.

The team found that the Maya heartland boomed during a pronounced moist period between 400 and 640 C.E., when the number of Maya polities rose and many new royal dynasties were founded. But in the 340-year-long drying trend that followed, warfare spiked repeatedly, and many Maya rulers embarked on massive building projects, displaying their power in an increasingly fragmented and fractious political landscape. This period culminated in a major political collapse in the 9th century C.E. Then came the final blow: the driest interval in the record, a century of drought beginning in 1000 C.E., when Maya popu-

Downloaded from www.sciencemag.org on November 9, 2012

Published by AAAS

lations sharply declined. "So it's really the idea of a two-stage collapse," Kennett says.

The high-resolution paleoclimate record is "an amazing accomplishment," says archaeologist Arlen Chase of the University of Central Florida, Orlando, who was not involved in the project. But he thinks that more climate records are still needed, because the study probably underestimates the amount of microclimatic variation in the Maya heartland. Climate at the Yok Balum site could well have been different from that at, say, Caracol, on the other side of the Maya Mountains. And at the time of collapse, some Maya migrated to a much drier region, the northern Yucatán—an odd move if drought was a driver, notes archaeologist Andrew Scherer of Brown University. He adds that although the authors suggest that less rainfall meant meager harvests, that link has yet to be established. Corn, the chief crop, requires only 400 to 600 millimeters of precipitation, and a broad swath of the Maya heartland now receives between 2000 and 3000 millimeters of rainfall annually. So if precipitation dropped 40% in the 9th century—as another study has estimated—the change might not have seriously impacted food supplies in some areas, he says. "To suggest that a drop in rainfall will lead to agricultural failure is something we don't know," Scherer says.

But while archaeologists continue to puzzle over the links between climate change and Maya culture, many consider this interdisciplinary study, which puts climate variation in a societal context, to be a major step forward. "The more we engage in interdisciplinary study," Yaeger says, "the more nuanced and robust our models will be."

–HEATHER PRINGLE

With reporting by Richard A. Kerr.

BIOENGINEERING

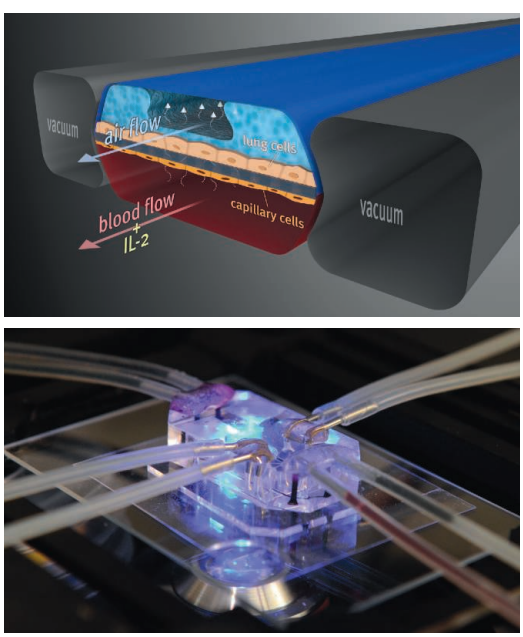
Lung-on-a-Chip Breathes New Life Into Drug Discovery

At first blush, the idea of growing facsimiles of lungs, kidneys, or other human organs in a bioreactor sounds vaguely diabolical. But researchers have been cultivating combinations of tissues for years in hopes that they would imitate working organs, and thereby serve as testing grounds for novel drugs to treat a wide variety of diseases. Now that promise has come a big step closer to reality. In this week's issue of *Science Translational Medicine* (*STM*), a team of academic and drug company researchers shows that an engineered "lung-on-a-chip" can not only faithfully model a serious respiratory ailment known as pulmonary edema, but can also accurately predict the toxicity of a compound that causes the disease and the ability of a new drug to prevent it.

"This really pushes the field to the next level," says Shuichi Takayama, a biomedical engineer at the University of Michigan, Ann Arbor, who has helped pioneer the field with his own lung-on-a-chip system. "People had been asking whether these systems could predict disease. Now it looks promising and we can ask 'How can we do this in the best way?'"

Efforts to incubate multiple cell types together to make organ mimics date back nearly 2 decades. In recent years, researchers have combined cell-culturing advances with microchip-patterning techniques to turn out artificial livers, kidneys, guts, and even brain tissue. Two years ago, a team led by Donald Ingber, a biomedical engineer at Harvard University, went so far as to make an artificial lung device complete with a layer of human capillary cells and lung cells on either side of a porous membrane, together with blood flow below the capillary layer and airflow above the lung cells. This entire assemblage was produced within a clear, flexible plastic material about the size of a computer thumb drive that could expand and contract, reproducing the mechanical motions involved in breathing (*Science*, 25 June 2010, p. 1662).

For their current study, Ingber and his colleagues used their lung-on-a-chip to model pulmonary edema. This life-threatening condition often follows heart failure, because fluid and blood-clotting proteins leak between endothelial cells in capillaries that pass through epithelial cells lining the lung and end up in alveolar pockets in the airways. It's also a common side effect among cancer patients given the chemotherapy drug interleukin-2 (IL-2). To see if their device would reproduce that effect, Ingber's team introduced IL-2 at a clinically relevant concentration into the blood flowing beneath capillary cells in their chip. Not only did the IL-2 cause the fluid leakage to occur, but this leakage increased fourfold when the chip repeatedly flexed to simulate the physical motions involved in breathing.



Disease mimic. In a lung-on-a-chip (*above*), IL-2 in the blood causes fluid to flow (*top*, white arrows) into the airway.

That success prompted Ingber's team to use this edema stand-in to screen drugs that might treat the disease. Previous work by other groups had shown that mechanical strain, such as that caused by breathing, can stimulate activity in TRPV4, a type of ion channel in capillary endothelial cells. This in turn can increase fluid leakage from capillaries into alveoli. Researchers at the pharmaceutical giant GlaxoSmithKline (GSK) had recently developed TRPV4-blocking drugs. Ingber's group partnered with Kevin Thorneloe and Allen McAlexander at GSK, and showed that the new TRPV4 blockers do in fact prevent IL-2's pulmonary edema side effects. In a separate study in the same issue of *STM*, the GSK team documented similar beneficial effects of TRPV4 inhibition in mice models of pulmonary edema caused by heart failure.

Ingber says the new results are a proof of principle that organs on chips can be a useful tool for researchers looking to screen new drugs and sort out mechanisms involved in disease. Down the road, that could limit the pharmaceutical industry's reliance on testing new drugs on animals. Of the candidate drugs that make it through animal testing, only a paltry 10% work in humans and make it to market. So any improvement could make a big impact.

–ROBERT F. SERVICE

CREDITS: WYSS INSTITUTE (2)

Downloaded from www.sciencemag.org on November 9, 2012

Published by AAAS

MALARIA

As Drug Pilot Wraps Up, a Lively Debate About Its Future

An unusual economic experiment that kicked off in 2010 has triggered one of the most impassioned debates in malaria control for years. At issue is a new funding mechanism that very few outside the field know or care much about—a "global subsidy" aimed at bringing the best malaria drugs to the patients who need them most by enlisting the private sector.

At a meeting next week, the board of the Global Fund to Fight AIDS, Tuberculosis and Malaria will decide whether to change or end the Affordable Medicines Facility-malaria (AMFm), as the program is called. The most likely outcome appears to be an integration of the program into other Global Fund activities, which AMFm supporters claim would effectively kill it. In the past few weeks, both sides have published a flurry of papers, letters, and press releases in an attempt to influence the decision.

Oxfam, a U.K. charity that opposes AMFm, says it endangers children's lives rather than saving them, a charge that public health expert Barry Bloom of the Harvard School of Public Health in Boston calls "shocking" and "outrageous." Other supporters of AMFm say the U.S. government, not a fan of AMFm, has lobbied hard to kill it, which the government denies.

AMFm was conceived to help give malaria patients access to artemisinin-based combination therapies (ACTs), a successful new generation of drugs. Many developing countries receive donor assistance to buy ACTs and distribute them through their public health systems, but up to two-thirds of patients in these countries buy their drugs in the private sector, which can be anything from licensed pharmacies to itinerant salespeople with a basketful of drugs. In these outlets, ACTs are often hard to find, and if they're sold, they're usually very expensive. With no quality guidance, poor families tend to buy cheaper, antiquated pills, or so-called artemisinin monotherapies. The World Health Organization (WHO) is seeking a worldwide ban on monotherapies because they increase the risk of drug resistance, which could make the ACT success story collapse.

The key feature of AMFm is that importers from developing countries can buy quality ACTs from approved manufacturers at a steeply discounted price; manufacturers get the rest of their money from AMFm. Then, the market's invisible hand should help the drugs find their way to even the most remote African shops at low prices, increase ACTs' market share, and "crowd out" monotherapies.

After long deliberations, a pilot was set up to test the scheme in Tanzania, Kenya, Madagascar, Uganda, Niger, Nigeria, and Ghana, backed by UNITAID, a Geneva-based health fund filled mainly through taxes on airline tickets; the Bill & Melinda Gates Foundation; and the British and Canadian governments. Together, they have contributed more than $350 million.



What's on the shelf? A pharmacist in rural Kenya, one of seven African countries where AMFm has run a pilot program.

In the seven countries, AMFm has become "a game-changer," an independent report led by Kara Hanson of the London School of Hygiene and Tropical Medicine concluded in September. (A summary of the report was published in *The Lancet* last week.) Everywhere except in Niger and Madagascar, quality ACTs became much more widely available within months after the program's introduction, their market share climbed between 16 and 40 percentage points, and prices plummeted in six pilots. In Nigeria and Zanzibar, where monotherapies were still widely sold, their market share dropped sharply.

Those numbers aren't disputed. But critics of AMFm say they tell only part of the story, in part because the malaria landscape is changing fast. Only a few years ago, it was standard practice in many countries to give antimalarial drugs to patients with high fever even without a diagnosis; it was the safest bet. But malaria rates have dropped sharply, and at the same time, fast, reliable test kits have replaced the cumbersome old way to diagnose malaria. Today, WHO recommends a diagnostic test first to avoid unnecessary treatment.

AMFm does not provide diagnostics, and shopkeepers have little incentive to sell their clients a test that might stop them from buying pills. The numbers show that most AMFm-funded pills are wasted on people who don't need them, says Oxfam's Mohga Kamal-Yanni; overall, more than 150 million doses of ACTs were ordered in the pilot, more than five times the number of estimated malaria cases in the seven countries. Moreover, she says, the evaluation hasn't shown how many drugs went to the most vulnerable group—children under 5 in poor rural areas—and how many lives were saved. The U.S. President's Malaria Initiative (PMI) raises some of the same issues in a statement on its Web site.

AMFm supporters want the scheme expanded but don't deny that changes are needed. Bloom says it should start helping shop owners provide diagnostic tests. And countries where malaria rates are low probably don't need the subsidy, he says. But asking for evidence that enough ACTs went to young children, or that AMFm has saved lives, is moving the goalposts, says Ramanan Laxminarayan, director of the Center for Disease Dynamics, Economics & Policy in Washington, D.C., and New Delhi; the evaluation wasn't set up to do so, and the pilot didn't last long enough. "AMFm needs more time to show that it has an impact," says Chioma Amajoh, a former coordinator of Nigeria's National Malaria Control Programme in Abuja.

CREDIT: © TON KEONE/VISUALS UNLIMITED/CORBIS

Downloaded from www.sciencemag.org on November 9, 2012

Published by AAAS

Over the past few months, a working group and a task force have charted a way forward. Their unpublished recommendations to the Global Fund's board include integrating AMFm into the fund's regular country activities, says Laxminarayan, who was involved in the process. That would end the core idea behind the program, the global subsidy, and the scheme would probably lose out against the more urgent priorities of African governments, he says: "It is a sure way of killing AMFm."

Laxminarayan and others say the closed-door discussions were heavily influenced by PMI; as the single biggest contributor to the Global Fund, the U.S. government carries a lot of weight, he says. Bloom, too, says PMI has been forcefully opposed to the plan from the get-go, "for reasons that I just don't understand."

PMI's deputy coordinator, Bernard Nahlen, denies that PMI has applied pressure; all it has done is ask for solid evidence that AMFm works and try to reach consensus on its future, he says. PMI isn't against subsidizing ACTs in the private sector per se, Nahlen emphasizes; it funded pediatric doses through licensed pharmacies in Rwanda and has helped Tanzanian shop owners upgrade their drug supplies and learn how to manage childhood illness. Such targeted programs are far more effective than a global subsidy, he says.

The board will make its decision during its 14 to 15 November meeting in Geneva. Whatever the outcome, donors and the Global Fund have stated that AMFm will continue through 2013 to ensure an orderly transition.

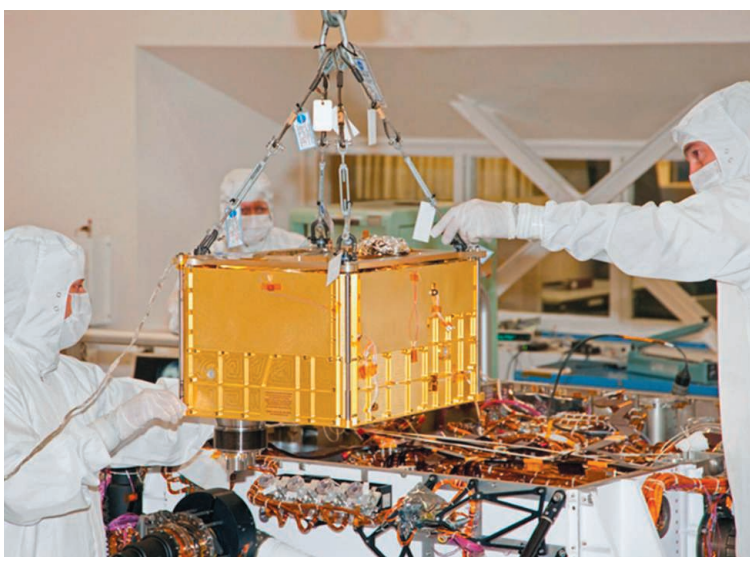
–MARTIN ENSERINK

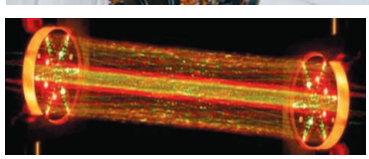
PLANETARY SCIENCE

Question of Martian Methane Is Still Up in the Air

The first groundbreaking result from the Curiosity rover will come from analyses of martian air for methane. If the rover finds even a part per billion (ppb) of methane—a possible product of microbial life—it could mean there is life on Mars today. So NASA's announcement last week that a press teleconference would "provide an update on Curiosity's studies of the Martian atmosphere" definitely piqued the media's interest.

Good luck with that. Christopher Webster of NASA's Jet Propulsion Laboratory in Pasadena, California, is the team leader for the Tunable Laser Spectrometer (TLS), Curiosity's atmospheric analyzer. In the teleconference, he reported that after two good, long analyses, he could only say that, with 95% confidence, there is between 0 and 5 ppb of martian methane. So there could be a hefty amount of methane and life on Mars, or there could be none of either.





Sniffing around. Curiosity's Tunable Laser Spectrometer (visualized, *left*)—housed in the rover's main instrument package (*above*, gold box)—has yet to definitively detect methane.

Interest in methane on Mars had been especially high because several groups of observers—using Earth-based telescopes or Mars-orbiting spacecraft—have reported spectroscopic detections of methane in the martian atmosphere (*Science*, 22 June, p. 1500). By one observing group's interpretation, Mars gushed methane from a single spot in 2003; several other groups concluded that their own observations showed repeated sudden releases and rapid destruction of atmospheric methane. Some critics eventually blasted the whole idea of methane on Mars, arguing that the observations were suspect and the supposed rapid disappearance of methane untenable.

The new upper limit on methane from Curiosity does little to settle the martian methane debate, but it does rule out one extreme possibility. Atmospheric modeler Malynda Chizek of New Mexico State University in Las Cruces and her colleagues have run an atmospheric model that calculates how fast processes like solar ultraviolet irradiation would destroy methane on Mars. In one run, she simulated the fate of a gush of methane like the one reportedly observed in 2003, assuming that the gush recurs every martian year and destruction is rapid. That scenario is what would happen if the martian spring thaw releases methane accumulated underground from bacteria. But the simulation suggested that if it were true, Curiosity would detect 20 to 35 ppb methane, far above the rover's upper limit of 5 ppb. So something else is probably going on.

Plenty of other possibilities remain, some of which would allow present-day martian life. In one scenario, rapid atmospheric reactions destroyed the 2003 gush, as observers assume. In another, destruction was slow, as most atmospheric chemists still believe, but the gush dispersed around Mars to be diluted to below Curiosity's upper limit. It's also possible that all the methane measurements have been in error, or that chemical reactions from purely lifeless processes—such as volcanic emissions or ultraviolet sunlight zapping organic-rich cosmic dust—are maintaining methane far below the current upper limit, at a few hundred parts per *trillion*.

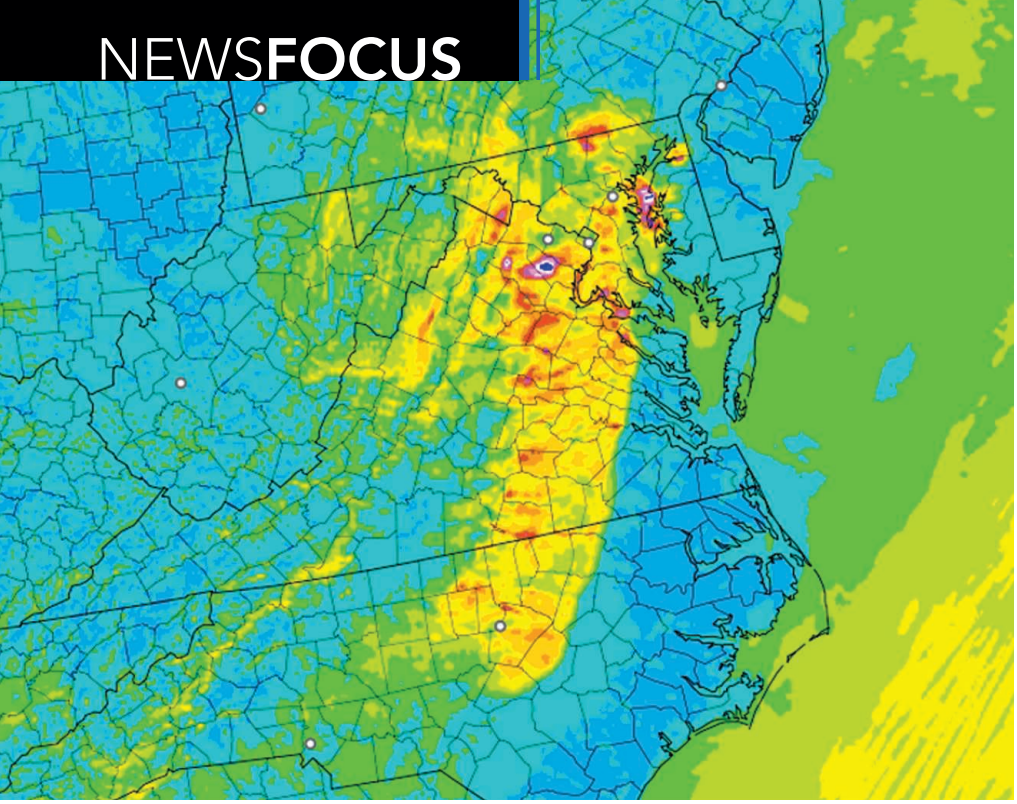
More Curiosity analyses may eliminate most of these scenarios. Webster hopes that concentrating the methane in future samples will enable TLS to detect the gas at abundances as low as 100 parts per trillion. That might pare the possibilities down to two: Either all the observations were wrong, or there really are exotic chemical reactions rapidly destroying methane on Mars. Proving either one could be difficult. In any case, it will be months, not years, before Curiosity whittles the field.

–RICHARD A. KERR

CREDITS: NASA/JPL-CALTECH (2)

Downloaded from www.sciencemag.org on November 9, 2012

Published by AAAS



Spot on. An experimental high-resolution NOAA model produced this strikingly accurate forecast of the "D.C. derecho" (higher winds are orange and white) 12 hours ahead of the storm's arrival in D.C.

Weather Forecasts Slowly Clearing Up

Ever-increasing computer power and new kinds of observations are driving weather prediction to new heights, but some kinds of weather are still not yielding

THE MACHINES AREN'T JUST CHALLENGING weather forecasters—they're taking over. Predicting tomorrow's weather, or even next week's? Computer models fed by automated observing stations on the ground and by satellites in the sky have had the upper hand for years. Predicting where a hurricane will strike land in 3 days' time? Computer models have outperformed humans since the 1990s, some by larger margins than others (see p. 736).

"People like to joke about predicting the weather," says meteorologist Kelvin Droegemeier of the University of Oklahoma, Norman, "but they have to admit that forecasting is a lot better than it used to be." And they can thank vast increases in computing power as well as technological advances, such as sharper-eyed satellites and advanced computer programming techniques.

But the machines have yet to complete their takeover. Human forecasters can usually improve, at least a bit, on numerical weather predictions by learning the machines' remaining foibles. And humans still do better than computer models at some tasks, including forecasting the fits and starts of evolving hurricanes. But that's not saying much; human forecasts of hurricane intensity are hardly more skillful today than they were 20 years ago.

Researchers working on the forecast problem say they are closing in on breakthroughs that could soon put the machines out front in even the toughest areas of forecasting. "We're not just talking," says Alexander MacDonald of the National Oceanic and Atmospheric Administration's (NOAA's) Earth System Research Laboratory (ESRL) in Boulder, Colorado, "we're building future models and seeing some spectacular results."

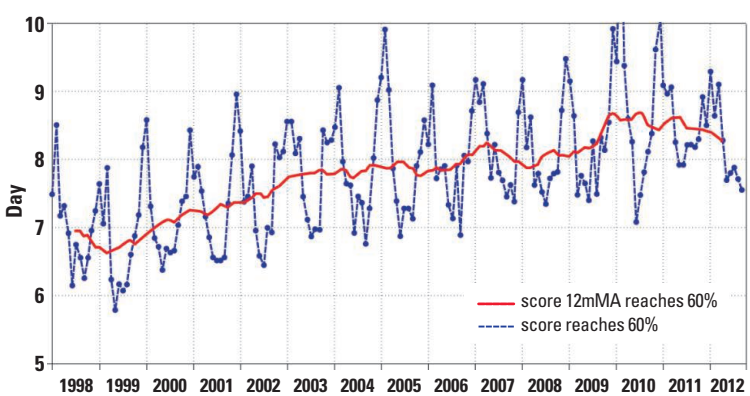
On to next week

Nothing illustrates the computer-driven rise of weather forecasting skill like the 3-decade-long track record of the European Centre for Medium-Range Weather Forecasts (ECMWF) in Reading, U.K. Since 1979, ECMWF has been feeding the couple billion weather observations made each day into the most sophisticated forecast model available and running that model on the most powerful computer in the business, all in order to predict the weather around the globe as accurately and as far into the future as possible.

From the beginning, ECMWF has been the world champ of medium-range forecasting. In 1980, its forecasts of broad weather patterns—the location and amplitude of atmospheric highs and lows—were useful out to 5.5 days ahead. Beyond then, the computer forecast became useless as the atmosphere's innate chaos swamped the model's predictive powers. Today, ECMWF forecasts remain useful into the next week, out to 8.5 days. That leaves the rest of the forecasting world, including the U.S. National Weather Service (NWS) with its less powerful computer, in the dust by a day or more.

With the help of ever-improving computer models, forecasters are also making progress on an even tougher sort of prediction: where and when heavy rain and snow will fall. NWS forecasters have nearly doubled their skill at forecasting heavy pre-

ECMWF FORECAST SKILL | Lead time at which broad pressure patterns (500 hPa) are usefully forecast



Into next week. The rising skill of the European Centre for Medium-Range Weather Forecasts' model has made forecasting the globe's weather more than 8 days ahead worthwhile.

CREDITS (TOP TO BOTTOM): EARTH SYSTEM RESEARCH LABORATORY/NOAA; ECMWF

Downloaded from www.sciencemag.org on November 9, 2012

Published by AAAS

cipitation, but it has been a long haul. They measure success on a scale of 0—complete failure—to 1, a perfect forecast. In 1961, they scored 0.18 on forecasting where 2.5 centimeters or more of rain (or 25 cm of snow) would fall a day later. Over the next 50 years, their score staggered up, never stagnating for much more than 5 years, until it stands at about 0.33 out of 1.

All hail the computer

Forecasting global weather patterns, heavy rain and snow, and any number of other sorts of weather better and further into the future has depended heavily on increasing computer power. When numerical weather prediction began in the mid-1950s, NWS's computational capacity was a meager 1 kiloflop (1000 calculations per second). It's now 10^8 megaflops, an increase of a factor of 100 billion.

Forecasters have plenty of uses for the added computing power. The most straightforward is sharpening a forecast model's view of the atmosphere. Models work by calculating changes in air pressure, wind, rain, and other properties at points on a globe-spanning grid. In principle, the more points there are in a given area, the more closely the model's weather will resemble the real weather.

In the early days of numerical weather prediction, grid spacing—or resolution—was something like 250 kilometers, far too coarse for individual thunderstorms. Today, thanks to increased computer power, grid points in global models are 15 kilometers to 25 kilometers apart. Over areas of special interest, resolution can be even greater. In the NWS global model, a grid with 4-kilometer spacing can be laid or "nested" on the lower 48 states of the United States.

So far, every increase in operational model resolution has produced more realistic simulations of the weather and thus more accurate forecasts, says William Lapenta, acting director of NWS's Environmental Modeling Center in College Park, Maryland. Now NWS's goal, he says, is to use model forecasts to warn the public about the most severe weather threats—which happen to be on the smallest scales—as soon as the models predict them. For that, the models will need to get down to 1-kilometer resolution.

Beyond increasing resolution, forecasters have used added computing power to improve a forecast model's starting point. Observations from weather stations, weather balloons, and satellites must be fed into a model to give it a jumping-off point for forecasting. But a model's intake, or "assimilation," of observations has never been optimal.

The assimilation of weather satellite observations that began in the 1970s was especially far from ideal. Satellites measure atmospheric infrared emissions at various wavelengths, and these observations were converted into temperature, pressure, and humidity values like those returned by weather balloons. "That didn't work very well," says meteorologist James Franklin of the NWS's National Hurricane Center (NHC) in Miami, Florida.

Beginning in the 1990s, instead of converting satellite observations to familiar atmospheric properties, forecasters began to assimilate the satellite observations directly into models without converting them. That improved forecasts all around, but especially forecasts of where hurricanes are headed. "A lot of the success in hurricane track forecasting is using the satellite data in a more intelligent, natural way," Franklin says.

That's because hurricanes don't propel themselves. "To first order, a hurricane is moving like a cork in a stream," notes meteorologist Russell Elsberry of the Naval Postgraduate School in Monterey, California. The better the forecast for the stream—the atmosphere's flow for thousands of kilometers around—the better the forecast for a hurricane's eventual track.

Thanks to improving models, NHC hurricane forecasters have made great strides in track forecasting. "In the 1970s, the best forecast was what human forecasters could do," says meteorologist Mark DeMaria, who works for NOAA (NWS's parent agency) at Colorado State University in Fort Collins. But by the 1990s, models forecasting hurricane tracks surpassed human performance.

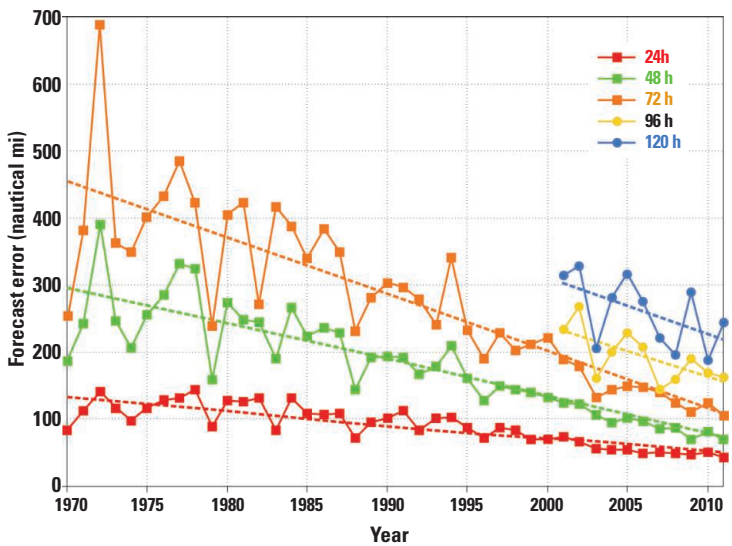
Today, NHC forecasters consult a half-dozen different models before predicting a hurricane's position 3 days into the future. Those forecasts now have an error of 185 kilometers. In the 1970s, the 3-day error was about 740 kilometers. That quartering of track error has enabled NHC forecasters to issue hurricane warnings 36 hours ahead instead of 24 hours ahead, giving coastal residents 50% more time to evacuate.

When Hurricane Sandy began brewing in October, the models consulted by NHC converged on a serious threat to the U.S. Northeast several days before landfall, though ECMWF modeling gave an inkling a whopping 10 days ahead.

Making it real

Other, less computationally demanding improvements have also brought model calculations closer to reality. For example, every weather forecast model in routine use today has a serious problem with simulating vertical air movement. In effect, their equations impose a speed limit on vertical motions. That is a particular problem in simulating the so-called supercell thunderstorms that can generate tornadoes and the

NHC OFFICIAL ANNUAL AVERAGE TRACK ERRORS | Atlantic Basin Tropical Storms and Hurricanes





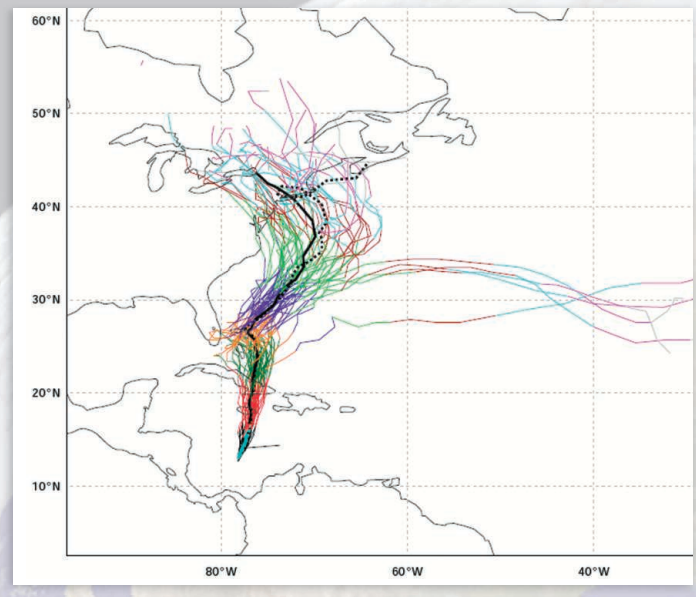
Ever lower. Errors have long been declining in NHC's official forecasting of where a hurricane will be 1 to 5 days ahead. That has allowed forecasters to warn the public earlier to flee the destruction of the coming storm.

CREDITS (TOP TO BOTTOM): NATIONAL HURRICANE CENTER/NOAA; ANDREA BOOHER/FEMA PHOTO

Downloaded from www.sciencemag.org on November 9, 2012

Published by AAAS

One Sandy Forecast a Bigger Winner Than Others



A week-ahead hit. Multiple ECMWF track forecasts (colored lines) made 7.5 days ahead had Sandy hitting the U.S. Northeast (actual track in black).

As winds swept Hurricane Sandy out of the Caribbean into the Atlantic, forecasters pored over their computer outputs to gauge its threat to land. Dramatic improvements in computing power and weather observations have steadily improved those forecasts, saving countless lives (see p. 734). In fact, official forecasts from the U.S. National Hurricane Center (NHC) in Miami, Florida, for Hurricane Sandy were even better than usual.

But among the computer forecast models that NHC forecasters consulted, the global model from the European Centre for Medium-Range Weather Forecasts (ECMWF) stood out, as it tends to do. The European edge in forecasting Sandy illustrates once again the advantages of having the greatest computing power available and a laserlike focus on a single sort of forecasting.

The ECMWF advantage was particularly evident out in the medium range 3 to 10 days ahead. Model runs made 9 to 10 days before Sandy struck New Jersey south of New York City gave "signs … of a major storm hitting somewhere in the northeast United States," says ECMWF's Tim Hewson. By 7 to 8 days ahead, ECMWF's model "had a reasonably good idea of what might happen," he says. And even at 5 days out, while the ECMWF model still had Sandy making a last-minute left turn into the Northeast, most other models showed the storm bearing right and moving harmlessly out to sea.

What the ECMWF model got right and the rest got wrong early on was an unusually complex meteorological situation. Hurricanes do not propel themselves; they drift along in the broad flows of weather systems. So forecasting where a hurricane will be in 5 days' time requires forecasting where violent winds near a hurricane's eyewall.

So researchers from the National Center for Atmospheric Research in Boulder and elsewhere spent 15 years developing the Weather Research and Forecasting Model, or WRF (pronounced "worf"). Its equations of motion allow rapid vertical acceleration of air when cold, heavy air rushes downward to become highly destructive surface winds.

In ongoing experimental forecasts, a WRF-derived forecast model being run at ESRL, called the High-Resolution Rapid Refresh model (HRRR), is having some dramatic forecast successes, ESRL's MacDonald says. On 29 June, the 3-kilometer-resolution model made a forecast over the lower 48 states, starting with a small cluster of thunderstorms in northern Illinois. The 12-hour forecast put the much-intensified system at Washington, D.C., at about 10 p.m. that night with winds to 100 kilometers per hour. That's exactly how the Indiana storm cluster actually evolved into the "D.C. derecho," the worst summer windstorm in the D.C. area in decades.



Here's hoping. Feeding radar data into models can help forecast hurricane intensity, but monitoring all the possible tornado-generating storms in Tornado Alley would be a daunting task.

Though MacDonald cautions that not every HRRR forecast is so successful, "for big, dangerous storms, we tend to do pretty well," he says. Other successes of the model include an early forecast this summer for Hurricane Isaac to head to New Orleans, Louisiana, while most other models called for it to molest the Republican convention in Tampa, Florida. For Sandy, HRRR nailed the 130-kilometer-per-hour winds that blew water into New York Harbor 15 hours ahead.

Forecasting bugaboos

Despite all the recent advances, forecasters have hit a wall when the weather plays out rapidly and on small scales. The deployment in the 1990s of NWS Doppler radars capable of mapping out the spinning winds of supercells enabled forecasters to extend average tornado warning times from 3 minutes to 13 minutes. But the new technology left the tornado false-alarm rate—how often forecasters warned of a tornado that never showed up—stuck at an uncomfortably high 75%.

The problem, says Joshua Wurman of the Center for Severe Weather Research in Boulder, is that "we don't have a good idea of what's going to make a tornado. Seventy-five to 80% of supercells don't make a tornado. Some of the meanest-looking ones don't make them. What's special about the 20% that do? We know there must be some subtle differences between supercells, but they have eluded us." And even the highest-resolution models are giving few clues to the secrets of tornadogenesis.

Hurricane forecasters trying to predict storm intensity are in much the same boat. The error in forecasting a storm's maximum sustained wind speed a few days in advance has not changed much since the NHC record began in 1990. Forecasts are particularly bad when a hurricane rapidly intensifies or weakens. In 2004, "Hurricane Charley went

CREDITS (TOP TO BOTTOM): EARTH OBSERVATORY/NASA; ECMWF; HERB STEIN, CSWR

Downloaded from www.sciencemag.org on November 9, 2012

Published by AAAS

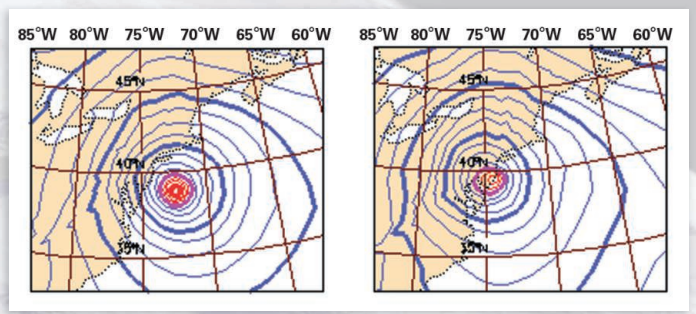
all the highs and lows and jet streams will be.

As Sandy drifted northward from the Caribbean, the track ahead was in dispute. Most models forecasted a typical fate for Sandy. The usual eastward-flowing jet would steer the storm east and north out over the Atlantic. But the ECMWF model predicted a very different situation. It had a low-pressure system moving well south over the continent while a ridge of high pressure formed over the Atlantic. With these features pushing the jet out of the picture, Sandy would continue northward until a low-pressure trough helped draw it westward across the coast. Most of the models eventually agreed on that scenario, but not until about 4 days out.

Hewson is confident about ECMWF's performance: "Our model is statistically better, a leader around the world." The reasons for that leadership—which ECMWF has held since it began forecasting in 1979—are twofold. For one, "it's a very focused organization," Hewson says. Long-range forecasting around the world is ECMWF's only business. Its analysts don't spend energy worrying about that thunderstorm spinning off tornadoes in the next county.

In addition, "you need a really good supercomputer," Hewson says. Having more computer power available for long-range forecasting than anyone else gives ECMWF's model a sharper and more detailed picture of the weather, which makes for a more realistic forecast. And the ECMWF model is run more times than other models to produce a single forecast, a practice that helps reduce the uncertainties in forecasting an inherently chaotic atmosphere.

But the ECMWF model is not always the best. In June, it had Tropical Storm Debby heading northwest into Texas. The U. S. Global Forecast System (GFS) got it right, predicting that the storm would move off to the east to hit Florida.



Pretty good. Six days ahead of landfall, the ECMWF model's forecast put Sandy (red, *in center of pressure isobars*) off the New Jersey coast (*left*), where eventually it hit (*right*, the actual storm).

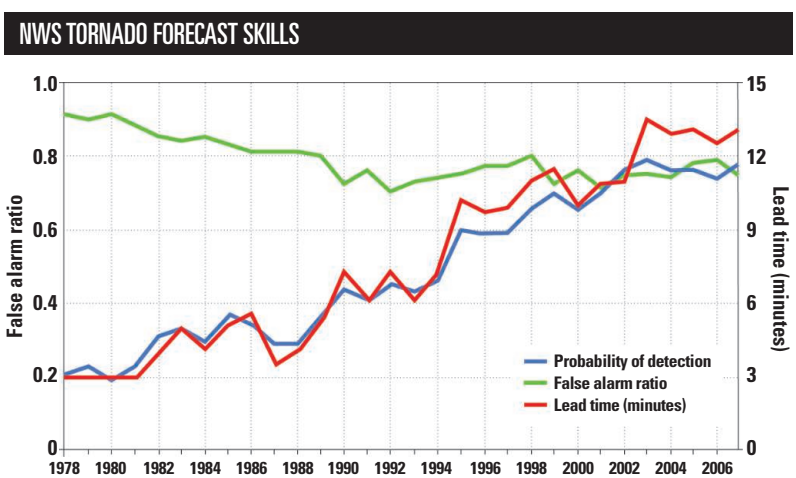
Such fallibility is why, for U.S. forecasters, "there's no single model we're always going to go with," says Joseph Sienkiewicz of the National Centers for Environmental Prediction in College Park, Maryland. The center develops and operates forecast models within the National Weather Service, including the NHC.

For Sandy, NHC forecasters combined many runs from many models, including the GFS and the ECMWF model, to create a consensus model forecast. Then they made an official forecast, taking into consideration the foibles of the various models. As Sienkiewicz notes, "forecasters still do make forecasts." And the ones they made at the NHC in the several days before Sandy's landfall served well indeed. "As the time got closer, we were able to home in on a solution," Sienkiewicz says. "It's quite a success for the science." **–R.A.K.**

from a Category 2 storm to Category 4 overnight, and nobody knows why," says tropical meteorologist Peter Webster of the Georgia Institute of Technology in Atlanta. "It's a mystery what determines intensity. Perhaps we still don't understand the basic physics of a tropical cyclone."

Help is on the way, however, at least for those predicting hurricanes. Because the mystery seems to lie at or near a tropical cyclone's eyewall, which is only a few kilometers thick, researchers have been figuring out how to usefully assimilate the detailed three-dimensional observations of airborne Doppler radar into hurricane forecast models. Meteorologist Fuqing Zhang of Pennsylvania State University, University Park, and colleagues have been doing just that using their own WRF-based forecasting system run at resolutions of 1 kilometer to 5 kilometers.

Radar input has improved the accuracy of these intensity forecasts by 30% to 40% during the past 5 years, Zhang says. In the case of Sandy, ECMWF's modeling advantages—higher resolution among them—yielded suggestions of a strong storm 8 days ahead.



Progress, or not. The U.S. National Weather Service has increased its tornado warning time (lead time, red), thanks to Doppler radar. But the false alarm ratio—how often forecasters warned of a tornado that never appeared—hasn't budged in 20 years.

Onward and upward, if ...

"The computer continues to be the big issue" in most types of weather forecasting, says James Hoke, director of NWS's Hydrometeorological Prediction Center in College Park. Researchers have long complained that they need more computing power. "It's frustrating for all of us, not being able to implement what we know," Hoke says. But "as the computer power becomes available, the current trend of improvement will hold out for at least a decade."

That is, if forecasters can afford to keep adding the needed computing power. But MacDonald sees a way ahead: so-called massively parallel, fine-grain computers such as Intel's MIC computer or NVIDIA's graphics processing units. GPUs are the specialized electronic circuits found in game consoles and other devices that require processing large blocks of data in parallel. MacDonald sees GPU-based forecast computers running at petaflop speeds at a fifth the cost of conventional central processing units.

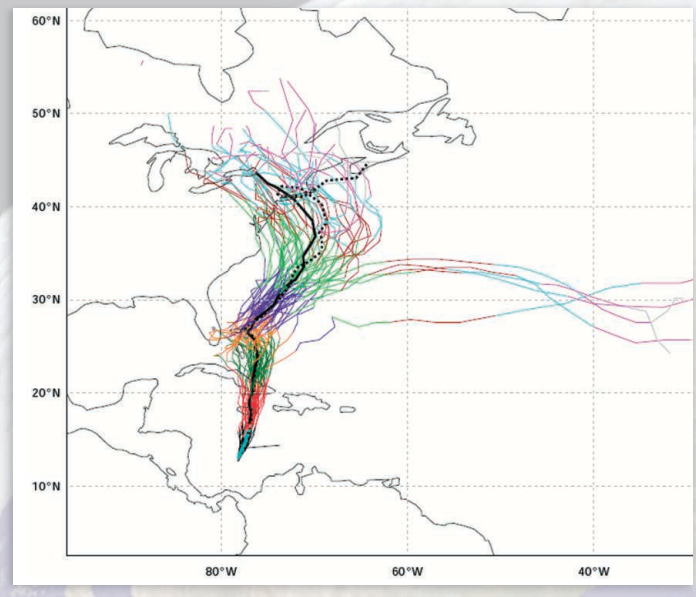
If an ongoing federal interagency program can accelerate the adoption of GPUs, MacDonald says, NWS could be producing "transformational" forecasts by fiscal year 2017. With more computer power, the assimilation of radar observations, and more physically realistic models, forecasters could be doing an even better job forecasting the next Sandy. **–RICHARD A. KERR**

CREDITS (TOP TO BOTTOM): ECMWF; J. WURMAN *ET AL.*, *BULL. AMER. METEOR. SOC.*, **93** (AUGUST 2012)

Downloaded from www.sciencemag.org on November 9, 2012

Published by AAAS

One Sandy Forecast a Bigger Winner Than Others



A week-ahead hit. Multiple ECMWF track forecasts (colored lines) made 7.5 days ahead had Sandy hitting the U.S. Northeast (actual track in black).

As winds swept Hurricane Sandy out of the Caribbean into the Atlantic, forecasters pored over their computer outputs to gauge its threat to land. Dramatic improvements in computing power and weather observations have steadily improved those forecasts, saving countless lives (see p. 734). In fact, official forecasts from the U.S. National Hurricane Center (NHC) in Miami, Florida, for Hurricane Sandy were even better than usual.

But among the computer forecast models that NHC forecasters consulted, the global model from the European Centre for Medium-Range Weather Forecasts (ECMWF) stood out, as it tends to do. The European edge in forecasting Sandy illustrates once again the advantages of having the greatest computing power available and a laserlike focus on a single sort of forecasting.

The ECMWF advantage was particularly evident out in the medium range 3 to 10 days ahead. Model runs made 9 to 10 days before Sandy struck New Jersey south of New York City gave "signs … of a major storm hitting somewhere in the northeast United States," says ECMWF's Tim Hewson. By 7 to 8 days ahead, ECMWF's model "had a reasonably good idea of what might happen," he says. And even at 5 days out, while the ECMWF model still had Sandy making a last-minute left turn into the Northeast, most other models showed the storm bearing right and moving harmlessly out to sea.

What the ECMWF model got right and the rest got wrong early on was an unusually complex meteorological situation. Hurricanes do not propel themselves; they drift along in the broad flows of weather systems. So forecasting where a hurricane will be in 5 days' time requires forecasting where violent winds near a hurricane's eyewall.

So researchers from the National Center for Atmospheric Research in Boulder and elsewhere spent 15 years developing the Weather Research and Forecasting Model, or WRF (pronounced "worf"). Its equations of motion allow rapid vertical acceleration of air when cold, heavy air rushes downward to become highly destructive surface winds.

In ongoing experimental forecasts, a WRF-derived forecast model being run at ESRL, called the High-Resolution Rapid Refresh model (HRRR), is having some dramatic forecast successes, ESRL's MacDonald says. On 29 June, the 3-kilometer-resolution model made a forecast over the lower 48 states, starting with a small cluster of thunderstorms in northern Illinois. The 12-hour forecast put the much-intensified system at Washington, D.C., at about 10 p.m. that night with winds to 100 kilometers per hour. That's exactly how the Indiana storm cluster actually evolved into the "D.C. derecho," the worst summer windstorm in the D.C. area in decades.



Here's hoping. Feeding radar data into models can help forecast hurricane intensity, but monitoring all the possible tornado-generating storms in Tornado Alley would be a daunting task.

Though MacDonald cautions that not every HRRR forecast is so successful, "for big, dangerous storms, we tend to do pretty well," he says. Other successes of the model include an early forecast this summer for Hurricane Isaac to head to New Orleans, Louisiana, while most other models called for it to molest the Republican convention in Tampa, Florida. For Sandy, HRRR nailed the 130-kilometer-per-hour winds that blew water into New York Harbor 15 hours ahead.

Forecasting bugaboos

Despite all the recent advances, forecasters have hit a wall when the weather plays out rapidly and on small scales. The deployment in the 1990s of NWS Doppler radars capable of mapping out the spinning winds of supercells enabled forecasters to extend average tornado warning times from 3 minutes to 13 minutes. But the new technology left the tornado false-alarm rate—how often forecasters warned of a tornado that never showed up—stuck at an uncomfortably high 75%.

The problem, says Joshua Wurman of the Center for Severe Weather Research in Boulder, is that "we don't have a good idea of what's going to make a tornado. Seventy-five to 80% of supercells don't make a tornado. Some of the meanest-looking ones don't make them. What's special about the 20% that do? We know there must be some subtle differences between supercells, but they have eluded us." And even the highest-resolution models are giving few clues to the secrets of tornadogenesis.

Hurricane forecasters trying to predict storm intensity are in much the same boat. The error in forecasting a storm's maximum sustained wind speed a few days in advance has not changed much since the NHC record began in 1990. Forecasts are particularly bad when a hurricane rapidly intensifies or weakens. In 2004, "Hurricane Charley went

CREDITS (TOP TO BOTTOM): EARTH OBSERVATORY/NASA; ECMWF; HERB STEIN, CSWR

Downloaded from www.sciencemag.org on November 9, 2012

Published by AAAS

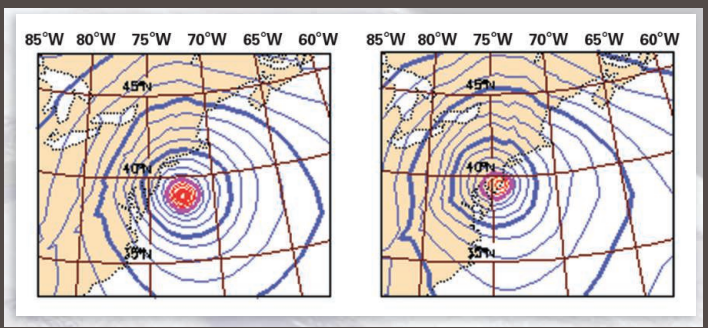
all the highs and lows and jet streams will be.

As Sandy drifted northward from the Caribbean, the track ahead was in dispute. Most models forecasted a typical fate for Sandy. The usual eastward-flowing jet would steer the storm east and north out over the Atlantic. But the ECMWF model predicted a very different situation. It had a low-pressure system moving well south over the continent while a ridge of high pressure formed over the Atlantic. With these features pushing the jet out of the picture, Sandy would continue northward until a low-pressure trough helped draw it westward across the coast. Most of the models eventually agreed on that scenario, but not until about 4 days out.

Hewson is confident about ECMWF's performance: "Our model is statistically better, a leader around the world." The reasons for that leadership—which ECMWF has held since it began forecasting in 1979—are twofold. For one, "it's a very focused organization," Hewson says. Long-range forecasting around the world is ECMWF's only business. Its analysts don't spend energy worrying about that thunderstorm spinning off tornadoes in the next county.

In addition, "you need a really good supercomputer," Hewson says. Having more computer power available for long-range forecasting than anyone else gives ECMWF's model a sharper and more detailed picture of the weather, which makes for a more realistic forecast. And the ECMWF model is run more times than other models to produce a single forecast, a practice that helps reduce the uncertainties in forecasting an inherently chaotic atmosphere.

But the ECMWF model is not always the best. In June, it had Tropical Storm Debby heading northwest into Texas. The U. S. Global Forecast System (GFS) got it right, predicting that the storm would move off to the east to hit Florida.



Pretty good. Six days ahead of landfall, the ECMWF model's forecast put Sandy (red, *in center of pressure isobars*) off the New Jersey coast (*left*), where eventually it hit (*right*, the actual storm).

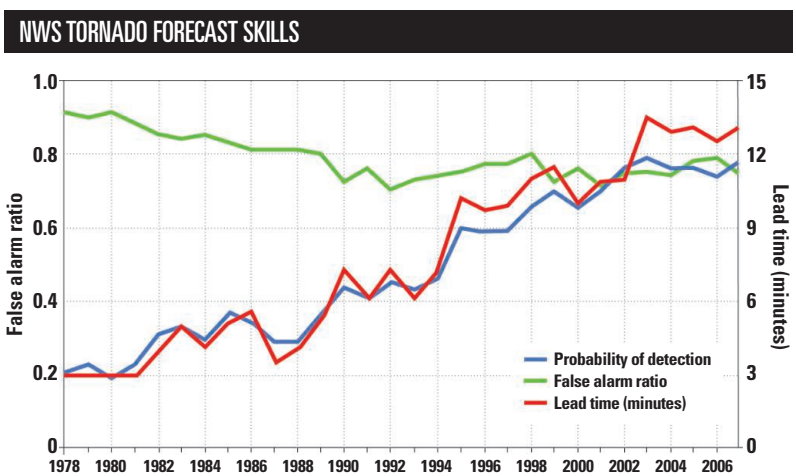
Such fallibility is why, for U.S. forecasters, "there's no single model we're always going to go with," says Joseph Sienkiewicz of the National Centers for Environmental Prediction in College Park, Maryland. The center develops and operates forecast models within the National Weather Service, including the NHC.

For Sandy, NHC forecasters combined many runs from many models, including the GFS and the ECMWF model, to create a consensus model forecast. Then they made an official forecast, taking into consideration the foibles of the various models. As Sienkiewicz notes, "forecasters still do make forecasts." And the ones they made at the NHC in the several days before Sandy's landfall served well indeed. "As the time got closer, we were able to home in on a solution," Sienkiewicz says. "It's quite a success for the science." **–R.A.K.**

from a Category 2 storm to Category 4 overnight, and nobody knows why," says tropical meteorologist Peter Webster of the Georgia Institute of Technology in Atlanta. "It's a mystery what determines intensity. Perhaps we still don't understand the basic physics of a tropical cyclone."

Help is on the way, however, at least for those predicting hurricanes. Because the mystery seems to lie at or near a tropical cyclone's eyewall, which is only a few kilometers thick, researchers have been figuring out how to usefully assimilate the detailed three-dimensional observations of airborne Doppler radar into hurricane forecast models. Meteorologist Fuqing Zhang of Pennsylvania State University, University Park, and colleagues have been doing just that using their own WRF-based forecasting system run at resolutions of 1 kilometer to 5 kilometers.

Radar input has improved the accuracy of these intensity forecasts by 30% to 40% during the past 5 years, Zhang says. In the case of Sandy, ECMWF's modeling advantages—higher resolution among them—yielded suggestions of a strong storm 8 days ahead.



Progress, or not. The U.S. National Weather Service has increased its tornado warning time (lead time, red), thanks to Doppler radar. But the false alarm ratio—how often forecasters warned of a tornado that never appeared—hasn't budged in 20 years.

Onward and upward, if ...

"The computer continues to be the big issue" in most types of weather forecasting, says James Hoke, director of NWS's Hydrometeorological Prediction Center in College Park. Researchers have long complained that they need more computing power. "It's frustrating for all of us, not being able to implement what we know," Hoke says. But "as the computer power becomes available, the current trend of improvement will hold out for at least a decade."

That is, if forecasters can afford to keep adding the needed computing power. But MacDonald sees a way ahead: so-called massively parallel, fine-grain computers such as Intel's MIC computer or NVIDIA's graphics processing units. GPUs are the specialized electronic circuits found in game consoles and other devices that require processing large blocks of data in parallel. MacDonald sees GPU-based forecast computers running at petaflop speeds at a fifth the cost of conventional central processing units.

If an ongoing federal interagency program can accelerate the adoption of GPUs, MacDonald says, NWS could be producing "transformational" forecasts by fiscal year 2017. With more computer power, the assimilation of radar observations, and more physically realistic models, forecasters could be doing an even better job forecasting the next Sandy. **–RICHARD A. KERR**

CREDITS (TOP TO BOTTOM): ECMWF; J. WURMAN *ET AL.*, *BULL. AMER. METEOR. SOC.*, **93** (AUGUST 2012)

Downloaded from www.sciencemag.org on November 9, 2012

Published by AAAS

SCIENCE IN EUROPE

Poor but Smart

It may not be an economic success. But the new, reunited Berlin has become one of Europe's hottest cities for science



The place to be. Berlin has developed a reputation as a cool, edgy city.

BERLIN—When Detlev Ganten first arrived here a year after Germany's reunification, Berlin was a giant construction site struggling to reconnect two halves. It was not exactly inviting. He and his wife moved to East Berlin to be close to Ganten's job at the newly founded Max Delbrück Center for Molecular Medicine (MDC), but taxi drivers didn't know how to find the little-known institute. Their neighborhood, which lacked supermarkets, restaurants, and even street lamps, made his wife cry. Although Germans, they felt like visitors in a foreign country.

Twenty years later, the neighborhood has undergone a transformation, and MDC is not only known to local taxi drivers but has also earned a prominent place on the world's scientific map. A 2010 Thomson Reuters ranking put it at number 14 in terms of output in molecular biology and genetics—"ahead of Stanford," as Ganten proudly proclaims.

That number tells a story—both about the institute and the ascent of Berlin as a science city. Since the Berlin Wall came down 23 years ago this week, the German capital has failed to live up to its economic expectations, but it has blossomed as a scientific hub, especially in the life sciences and mathematics. The city is now home to three respected universities and a host of nonuniversity research institutes, including MDC, one of three Helmholtz research centers residing in Berlin and neighboring Potsdam.

In May, the triannual Funding Atlas from the German Research Foundation (DFG), which covered the years 2008 to 2010, showed that Berlin had overtaken Munich, its chief rival, as the region receiving the largest amount of third-party funding in Germany. A month later, Humboldt University became the second university in Berlin to earn the title "elite university" in Germany's Excellence Initiative. (Munich is the only other city that won this accolade twice.) Later this year, a merger of MDC with the Charité, one of Europe's largest university clinics, could further boost Berlin's standing as a powerhouse for translational research.

Many institutes here now vie for top talent from around the world—and Berlin's new reputation as a hip, happening place is helping to lure them. "Poor but sexy," a term coined by Berlin Mayor Klaus Wowereit, has become Berlin's unofficial motto—but today, it might as well be "poor but smart."

Cold War fault line

Berlin has a long and glorious scientific tradition; this was, after all, the place where Robert Koch discovered the bacteria causing tuberculosis and cholera, Albert Einstein completed his theory of general relativity, and Max Planck laid the foundation of quantum theory. But National Socialism and World War II robbed the city of many of its greatest minds—and Berlin could not recover during its 44-year postwar division.

Günter Stock, the head of the Berlin-Brandenburg Academy of Sciences and Humanities, moved from Heidelberg to West Berlin in 1983 to work for pharma company Schering as a physiologist. "Berlin was not an attractive place," he recalls. West Berlin was a walled-in enclave, poised on a Cold War fault line, where cronyism thrived. "Professorships were routinely given to assistants of other professors," Stock says. It was also lacking in quality of life; to lure residents, the government gave people working in West Berlin a salary bonus. "There was a real subsidization mentality," Stock says.

In East Berlin, meanwhile, leading scientific posts were filled according to party loyalty rather than excellence, and scientific methods and equipment were often outdated. When Karl-Max Einhäupl, head of the Charité, first came to the clinic in 1993, the scene still reminded him of the set for a postwar period movie: "You wouldn't have had to add anything. And you wouldn't have had to take anything away."

Almost 2 decades later, Berlin is still struggling in many ways. The many new businesses expected in the wake of reunification never showed up, and the city's 11.8% unemployment rate is twice the national average. Commuters are exasperated by faulty brakes, jammed doors, and other problems on the city's underground, and in May, the opening of the new international airport, a multibillion-dollar prestige project, had to be pushed back by a year and a half because of planning failures and mismanagement.

The fact that science is doing so much better, most scientists agree, is based at least partly on some bold choices made after the Wall came down. While many organizations and agencies in East Germany were shut down or taken over by their Western counterparts, Berlin's science senator, Manfred Erhardt, insisted on keep-

CREDIT: ISTOCKPHOTO.COM/ANDREA ZANCHI

Downloaded from www.sciencemag.org on November 9, 2012

Published by AAAS

ing the Charité, Humboldt University, and other East German science institutions alive and independent. To be sure, they had to change: Three institutes of the East German Academy of Sciences were united to form MDC, for instance, and hundreds of university professors were suspended. But just as gene duplications allow a genome to take new evolutionary paths, the preservation of parallel structures gave Berlin science more opportunities to evolve.

The decision to base the new federal government in Berlin added scientific clout. Many scientific organizations moved their administrative offices here and started new labs or institutes. Five new Max Planck institutes opened in the Berlin area, bringing the total to eight, and the city hosts 13 Leibniz institutes. Several new government institutes opened up as well, including the Federal Institute for Risk Assessment, founded in 2002.

Perhaps most importantly, scientists wanted to come to Berlin. Really interesting scientists want an interesting environment, says Nikolaus Rajewsky, a German-born mathematical biologist who left his job at New York University in New York City to join MDC in 2006—and Berlin is such an environment. The city seems permanently in transition, even if no one is quite sure where that is leading. "Whenever I was in Berlin I had this feeling of a huge delta," Rajewsky says. "The city was changing, something was happening here."

Today, Berlin has also developed a reputation as a cool, edgy place with world-class museums, good clubs, and a huge cultural offering. It boasts three opera houses and one of the world's best symphony orchestras, artists and designers have moved into abandoned factories and warehouses, and the city has become a fertile breeding ground for Internet start-up companies. And Berlin is quite cheap. It's still possible to rent a nice three-room flat in a desirable neighborhood here for less than €800 a month—a fraction of rents in London, Paris, or San Francisco. The creative cuisine and countless bars don't break the bank either.

Competition and collaboration

Rajewsky's father, Klaus, is another prominent addition to Berlin's science scene—and a sign of larger shifts in Germany's academic world. In 2001, after 40 years of research at the University of Cologne, the noted immunologist left for Harvard Medical School in Boston, because at age 65 he was threatened with forced retirement. In 2010, he returned to his home country, where the rules had changed, and he now has an open-ended contract at MDC. "That this was possible only 10 years after I had to leave the country really shows you how much things have changed," he says.

That his son had relocated to Berlin helped nudge Klaus Rajewsky back, but he says the funding situation in the United States had also gotten worse. "Mouse genetics is expensive research, and it became more and more difficult to get grants," he says. "In Germany on the other hand, you get institutional support that U.S. researchers can only dream of." Molecular biologist Matthew Poy echoes that sentiment. The junior group leader, born and raised in the United States, came to MDC in 2008 after postdoc positions in New York and Zurich, Switzerland. His most important reason: The position came with guaranteed research funds. "The secret is out that Germany has a lot of money dedicated to science," Poy says.





Back in the *Heimat*. Klaus Rajewsky and his son Nikolaus left jobs in Boston and New York, respectively, to come to Berlin.

Indeed, Germany's deep coffers allowed Nikolaus Rajewsky to realize his dream: setting up a brand-new center, the Berlin Institute for Medical Systems Biology, which aims to study gene regulation "all the way from chromatin to protein." The nascent institute is part of MDC, but it will get a new €40 million building, currently under construction in the city center. Rajewsky has already hired researchers from Columbia, Duke, and Harvard universities.

That said, Berlin still isn't Germany's Boston—"that comparison is ridiculous," Klaus Rajewsky says. For example, it's harder to get good postdocs here, he says, and the work ethic is more relaxed. "In Boston, science is the main thing in life for most people and they work accordingly," Rajewsky says.

Berlin is also struggling to attract biotech and pharma companies, says chemist Peter Seeberger, who came to Berlin in 2009 after working as a professor at the Massachusetts Institute of Technology in Cambridge and ETH Zurich. "In Boston you can go to university, then cross the road and start working in a company," Seeberger says. "Berlin needs that to play in the first league internationally." And while nonuniversity institutes such as Max Planck can offer high salaries, Berlin's universities have missed out on some top talent because they couldn't match other universities' offers, he adds.

Healing the past

It's not just the life sciences that are booming. Mathematics has become another hot field. In 2002, mathematicians from the three Berlin universities and two institutes got together to form the research center Matheon, funded by DFG to do applications-driven research. It has made Berlin one of Germany's two top math cities, says Günter Ziegler, a scientist working at Matheon. (The other is Bonn, the former capital.) Further proof of that, he says, is the fact that the International Mathematical Union—the body that awards the Fields Medal—set up a permanent home here in 2011.

More developments are afoot. Negotiations are under way to merge MDC with the university clinic Charité. That's important because by law, German universities are paid by the states; they cannot be funded directly by the federal government. Helmholtz institutes like MDC, on the other hand, get 90% of their money from the federal government. Binding the two together in an entity would allow the federal government to give extra funding for medical research at the Charité—perhaps as much as €50 million to €80 million annually, insiders say.

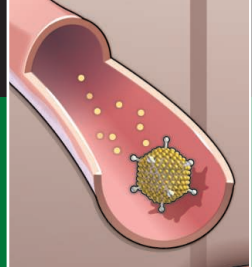
To Stock, it would be the most important event in years for Berlin's rise as a science capital. And Ganten hopes that in the long run, it will allow Berlin and the Charité to recapture some of its past glory. "Berlin has such a rich tradition," he says. "Einstein, Planck, Heisenberg. Koch, Ehrlich, Virchow. These names still mean something today." Now that the wounds of a divided city have healed, Berlin seems set to retake its place in Europe's scientific history.

–KAI KUPFERSCHMIDT

CREDITS: DAVID AUSSERHOFER/THE MAX DELBRÜCK CENTER FOR MOLECULAR MEDICINE

Downloaded from www.sciencemag.org on November 9, 2012

Published by AAAS



Bound by Factor X
748



What determines reproductive success?
749

LETTERS | BOOKS | POLICY FORUM | EDUCATION FORUM | PERSPECTIVES

LETTERS

edited by Jennifer Sills

Limits to Religious Conservation Efforts

THE LETTER "RELIGIOUSLY PROTECTING MYANMAR'S environment" (K. Y. Chong, 28 September, p. 1604) suggests that Myanmar may be able to harness the powerful influence of Buddhist monks to promote conservation efforts, particularly during predicted rapid development and industrialization after international sanctions are lifted (*1*). A growing number of development practitioners have been calling for a greater role for religious groups and consideration of local cultures in sustainable development models (*2*).



Prayer release. Fish are released in Myanmar during a Buddhist ceremony.

We agree with Chong on his basic premise but would like to offer a few words of caution. The Buddhist religion advocates that all human behavior should be in harmony with the environment (*3*) and incorporates elements of nature worship, which encourages the protection of local biodiversity and environments (*4*). However, there is little evidence that Buddhist influences have been able to limit environmental damage in other countries in the region. Laos, Cambodia, and Thailand all have large Buddhist populations, and all have suffered severe environmental degradation during the past decades of rapid industrialization and economic development (*5*). Conservation practitioners must therefore recognize the limits to which religion alone can combat the pressures of industrial and economic development needs.

In addition, a lack of ecological understanding means that some Buddhist traditions can be misinterpreted and lead to unsustainable practices. For example, a Buddhist tradition of rescuing animals from harm has given rise to the practice of "prayer animal release," during which practitioners believe they can generate good karma by releasing captive animals into the wild (*5*). Unfortunately, many animals are captured and sold specifically for religious releases, supporting the black market trade of wild animals (*6*, *7*), and many die because of overcrowding and poor husbandry, or upon release into unsuitable habitats (*6*, *8*). In addition, releasing animals into the wild may damage local ecosystems through the introduction of exotic species, novel diseases, or parasites (*9*). This example demonstrates the need for sound ecological knowledge underpinning conservation initiatives led by religious groups.

Buddhism may be a powerful resource for conservation efforts in Myanmar, but it cannot replace strong environmental governance and policy and may be limited by a lack of environmental understanding. The Myanmar government and conservation practitioners should therefore work closely with religious leaders to direct their efforts and to ensure that conservation efforts are made on the basis of sound environmental knowledge.

BAOCAO GONG, ROWENA HAMER, XIUXIANG MENG,* QINGHUI MENG, JINCHAO FENG, DAYUAN XUE

Biodiversity Studio, College of Life and Environmental Sciences, Minzu University of China, Beijing, 100081, China, and China Institute of Environment Resources, Protection for Minority Areas, Minzu University of China, Beijing, 100081, China.

*To whom correspondence should be addressed. E-mail: mengxiuxiang@muc.edu.cn

References

1. C. Schmidt, *Science* **337**, 796 (2012).
2. K. Marshall, *Peabody J. Educ.* **76**, 339 (2001).
3. W. Nan, *North-West Minorities Res.* **30**, 1001 (2001).
4. F. Wang, *J. Qingyuan Polytechnic* **5** (October, 2011).
5. P. L. Daniels, *Int. J. Soc. Econ.* **25**, 968 (1998).
6. H. Shiu, L. Stokes, *Contemporary Buddhism* **9**, 181 (2008).
7. C. R. Shepherd, J. Sukumaran, S. A. Wich, "Open Season: An analysis of the pet trade in Medan, Sumatra 1997–2001" (TRAFFIC South East Asia, 2004).
8. L. L. Severinghaus, L. Chi, *Biol. Conserv.* **89**, 301 (1999).
9. R. N. Mack *et al.*, *Ecol. Appl.* **10**, 689 (2000).

Letters to the Editor

Letters (~300 words) discuss material published in *Science* in the past 3 months or matters of general interest. Letters are not acknowledged upon receipt. Whether published in full or in part, Letters are subject to editing for clarity and space. Letters submitted, published, or posted elsewhere, in print or online, will be disqualified. To submit a Letter, go to www.submit2science.org.

Credit Due to Peter Higgs

AS A PARTICLE THEORIST WHO WAS QUOTED briefly in the News Focus story "Who invented the Higgs boson?" (A. Cho, 14 September, p. 1286), I would like to explain my point of view. The answer to the polemical question in the title of your article is simple: It was Peter Higgs. Of the "gang of six," who in 1964 postulated the spontaneous breaking of gauge symmetry in four dimensions, Higgs alone pointed out the existence of this massive scalar boson. Unlike the others, he went further 2 years later in a paper that discussed in some detail its properties (*1*), including the decays into two massive vector bosons that are among the signatures observed at the Large Hadron Collider. That is why this particle is called the Higgs boson, not because of a subsequent misprint in a paper by Steve Weinberg.

CREDIT: SOE ZEYA TUN/REUTERS

Downloaded from www.sciencemag.org on November 9, 2012

Published by AAAS

The original Higgs model was a simple prototype, but (as pointed out later by Tom Kibble) the existence of the Higgs boson is generic in more complicated theories such as the Standard Model (which relates electromagnetic, weak, and strong nuclear interactions of particles). Given that the work of Higgs and the other 1964 pioneers underpins the Standard Model, it is hardly "a fairly narrow and esoteric advance in mathematical physics" as Cho quotes some theorists (not me) as saying. Likewise, I am surprised at the remark attributed to Michael Peskin that "it's hard for me to figure out what Higgs *et al*. did that was nontrivial." They showed that two wrongs (a massless Nambu-Goldstone boson and an equally massless gauge boson) could be combined to make a right (a massive vector boson), something that Walter Gilbert had argued earlier in 1964 would be impossible in a Lorentz-invariant theory.

I agree with Chris Quigg that it would be nice if Higgs *et al*. were rewarded for something they actually did. In fact, they did solve a problem that myriad other theoretical physicists before and after 1964 tried and failed to do, namely, making consistent and calculable theories with massive vector bosons.

All the evidence from the CERN experiments indicates that the Higgs boson—the key experimental signature of this essential feature of the Standard Model—has now been discovered, opening up exciting experimental perspectives for future colliders. Peskin and Quigg have long been among the keenest American advocates of studies of the Higgs boson. We share the hope that detailed studies of this particle will lead to new insights into physics beyond the Standard Model.

JOHN ELLIS

King's College London, London, WC2R 2NS, UK. E-mail: John.Ellis@cern.ch

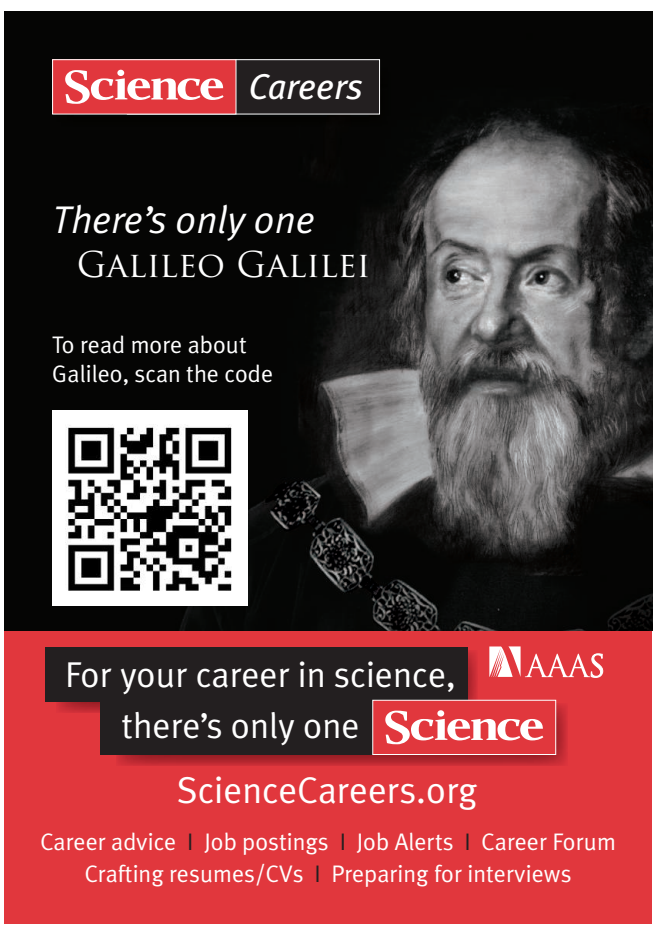
Reference

1. P. W. Higgs, *Phys. Rev.* **145**, 1156 (1966).

Evolution's Misleading Language

IN THE NEWS OF THE WEEK STORY "ALL THAT glitters" (14 September, p. 1277), Beverley Glover of the University of Cambridge describes the iridescent fruit of the African perennial herb *Pollia condensata* by saying, "The fruit's dazzling display may have evolved to capitalize on birds' attraction to sparkly objects, or to trick them into eating something that looks like a blueberry without going to the trouble of actually making juicy flesh." At a time when remarkably few people seem to understand the basic mechanism of evolution, it seems inappropriate for *Science* to publish such comments without clarifying them to ensure that no one is misled.

If our present understanding of evolution is correct, nothing has evolved to do a specific task. If birds do indeed eat or otherwise disperse the seeds of *Pollia condensata*, this phenomenon could be more accurately described by saying that the coloration of the fruit has the presumed function of attracting the attention of birds, which may then disperse the seeds. Glover's second point—that fruit has evolved to trick birds into eating something that looks like a blueberry without going to the trouble of actually making juicy flesh—combines teleology with anthropomorphism. The colloquialism "going to the trouble of" should have been stated as "at lower energetic cost," if that is what was meant.



Downloaded from www.sciencemag.org on November 9, 2012

Unfortunately, the same teleological and anthropomorphic language is used in the otherwise excellent paper on the "Pointillist structural color in *Pollia* fruit" to which the *Science* News item refers (*1*), which is indicative of how widely and unfortunately such inaccurate and misleading language is now used in the scientific literature.

ALFRED NIGEL BURDETT

Heron Publishing, 202, 3994 Shelbourne Street, Victoria, BC V8N 3E2, Canada. E-mail: alfredburdett@heronpublishing.com

Reference

1. S. Vignolinia *et al.*, *Proc. Natl. Acad. Sci. U.S.A.* **109**, 15712 (2012).

TECHNICAL COMMENT ABSTRACTS

Comment on "Glacial Survival of Boreal Trees in Northern Scandinavia"

Hilary H. Birks, Thomas Giesecke, Godfrey M. Hewitt, Polychronis C. Tzedakis, Jostein Bakke, H. John B. Birks

Parducci *et al*. (Reports, 2 March 2012, p. 1083) fail to present convincing evidence for glacial survival of *Pinus* and *Picea* in northern Scandinavia. Their methodology does not exclude contamination. Additionally, they should consider the lack of suitable habitats, the apparent extinction of both taxa after deglacial warming, and alternative hypotheses for the distribution of the *Picea* genetic marker haplotype A.

Full text at http://dx.doi.org/10.1126/science.1225345

Response to Comment on "Glacial Survival of Boreal Trees in Northern Scandinavia"

Laura Parducci, Mary E. Edwards, K. D. Bennett, Torbjørn Alm, Ellen Elverland, Mari Mette Tollefsrud, Tina Jørgensen, Michael Houmark-Nielsen, Nicolaj Krog Larsen, Kurt H. Kjær, Sonia L. Fontana, Inger Greve Alsos, Eske Willerslev

Birks *et al*. question our proposition that trees survived the Last Glacial Maximum (LGM) in northern Scandinavia. We dispute their interpretation of our modern genetic data but agree that more work is required. Our field and laboratory procedures were robust; contamination is an unlikely explanation of our results. Their description of Endletvatn as ice-covered and inundated during the LGM is inconsistent with recent geological literature.

Full text at http://dx.doi.org/10.1126/science.1225476

CORRECTIONS AND CLARIFICATIONS

Table of Contents: (5 October, p. 9). The image came from the *Science Translational Medicine* cover, not the *Science Signaling* cover as the caption indicated. The PDF version online has been corrected.

News Focus: "Roots of empire" by M. Hvistendahl (28 September, p. 1596). In a quote, paleoclimatologist Ulf Büntgen referred to the Black Death as a virus. The disease is generally thought to be caused by the bacterium *Yersinia pestis* and not by a virus.

Reports: "Fermentation, hydrogen, and sulfur metabolism in multiple uncultivated bacterial phyla" by K. C. Wrighton *et al*. (28 September, p. 1661), "Disulfide rearrangement triggered by translocon assembly controls lipopolysaccharide export" by S.-S. Chng *et al*. (28 September, p. 1665), and "Sedlin controls the ER export of procollagen by regulating the Sar1 cycle" by R. Vendetti *et al*. (28 September, p. 1668). Because of a printing error that affected some copies of the magazine, the colors were misaligned, distorting the appearance of the figures on pages 1664, 1669, and 1680. The online versions were not affected.

News & Analysis: "An enterprising time for HIV vaccine research," by J. Cohen (21 September, p. 1446). William Schief of the Scripps Research Institute elicited broadly neutralizing antibodies to respiratory synctial virus in rhesus macaques, not rabbits.

News Focus: "The new view of complement" by M. Leslie (31 August, p. 1034). The article incorrectly states that out-of-control complement activation is responsible for symptoms such as swelling of the limbs and difficulty with breathing in hereditary angioedema. The culprit in the disease is actually bradykinin, which is not considered part of the complement system.

AAAS Travels

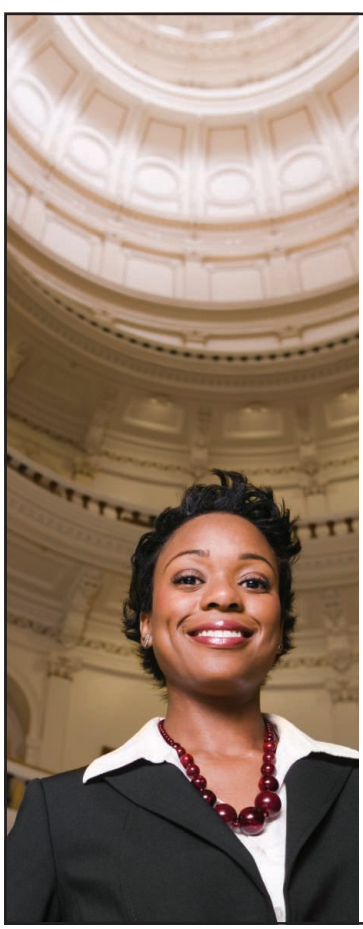


Kakadu & the Kimberley Annular Eclipse
May 2-21, 2013

Explore one of the world's greatest wilderness areas—the Kimberley in Northwest Australia—and see the Annular Solar Eclipse May 11, 2013 in Tennant Creek. Explore Darwin, Kakadu, and the Kimberley—a vast and virtually inaccessible area so remote that very few people have ever been there! End in Broome, with a dazzling sand beach, dinosaur footprints, and more! $9,550 + air

For a detailed brochure, please call (800) 252-4910
All prices are per person twin share + air

Betchart Expeditions Inc.
17050 Montebello Rd, Cupertino, CA 95014
Email: AAASInfo@betchartexpeditions.com
www.betchartexpeditions.com



AAAS is here –
bringing scientific expertise to policy making.

Good science policy is the result of politicians understanding science and scientists understanding policy. Toward this end, AAAS manages the Science & Technology Policy Fellowships program, which embeds scientists and engineers in the federal government for up to two years. From Congress to the State Department, each class of Fellows contributes to the policy-making process while getting hands-on experience at the intersection of science and policy. As a AAAS member your dues support these efforts. If you're not yet a AAAS member, join us. Together we can make a difference.

To learn more, visit
aaas.org/plusyou/fellows

AAAS + U = Δ

Downloaded from www.sciencemag.org on November 9, 2012

Comment on "Glacial Survival of Boreal Trees in Northern Scandinavia"

Hilary H. Birks,[1]* Thomas Giesecke,[2] Godfrey M. Hewitt,[3] Polychronis C. Tzedakis,[4] Jostein Bakke,[5] H. John B. Birks[1,4,6]

Parducci *et al*. (Reports, 2 March 2012, p. 1083) fail to present convincing evidence for glacial survival of *Pinus* and *Picea* in northern Scandinavia. Their methodology does not exclude contamination. Additionally, they should consider the lack of suitable habitats, the apparent extinction of both taxa after deglacial warming, and alternative hypotheses for the distribution of the *Picea* genetic marker haplotype A.

Parducci *et al*. (*1*) propose that *Picea* (spruce) and *Pinus* (pine) survived the Last Glacial Maximum (LGM) in northern Scandinavia, based on the amplification of ancient chloroplast DNA (cpDNA) in lake sediments from Endletvatn on the Andøya strandflat, northwest Norway (69°N) and genetic evidence from extant spruce populations. We comment first on their methodology and then on their interpretations.

(i) How reliable is ancient DNA (aDNA) from lake sediments? Although knowledge of aDNA, including sedimentary aDNA (sedaDNA), and environmental DNA is advancing rapidly, Hofreiter *et al*. (*2*) warn that the reliability of all aDNA sequences must be critically assessed, major concerns being contamination and the variable quality of aDNA from waterlogged sites. They urge "a critical attitude towards whether the results obtained do make sense." This new technique was apparently not validated by Parducci *et al*., who ignored the criteria and advice of Gilbert *et al*. (*3*) to minimize contamination and replicate results.

The Geonor stationary-piston sediment corer, like most piston corers, is not a contamination-free corer. A contamination-free corer (*4*) should have been used.

The core studied by Parducci *et al*. was opened in 2002, sampled, and stored at 4°C for 7 years until sampled for DNA. How certain is it that no contamination occurred during potentially unsterile sampling in 2002 from aerial pollen, dust, wood, or paper? The reported contamination by an *Urtica* plant fragment is worrying.

(ii) Was glacial survival on Andøya possible? The LGM ice sheet advanced over Andøya, including Endletvatn, reaching a 2- to 300-m altitude. Mountain glaciers left only the highest summits and plateaus as ice-free nunataks (*5*). These are mostly covered by block fields (*5*), which are not suitable habitats today for *Picea* or *Pinus*. As ice retreated at ~22 thousand years ago (ka), the extensive lowlands, including Endletvatn, were below sea level until a marine regression ~18 ka (*5*). Glacial and marine conditions prevailed at Endletvatn at the times of the cpDNA records.

(iii) Where were *Pinus* and *Picea* growing? They could not survive on exposed nunataks in the inferred polar-desert conditions (*1*, *6*). *Picea,* but not *Pinus,* may persist vegetatively for centuries in sheltered locations. To deliver DNA to the lake, they should have grown nearby, but the strandflat was glaciated or submerged (driftwood could provide aDNA) at the critical periods. Therefore, where did the cpDNA come from? Willerslev *et al*. (*7*) proposed long-distance dispersal of conifer DNA to Greenland ice. Likewise, extremely low *Pinus* values in Andøya pollen diagrams could derive from long-distance dispersal. The rather surprising absence of conifer pollen in their samples led Parducci *et al*. to exclude this source.

(iv) Does haplotype A (HapA) reflect *Picea* spreading directions? Early Holocene *Picea* mitochondrial DNA (mtDNA) from lake sediment and younger pollen in Trøndelag shows HapA (*1*), probably a single 21–base pair deletion. Western glacial survival is inferred from its modern distribution. Old cpDNA from Andøya can provide no support for this hypothesis. The distribution of other mtDNA and nuclear DNA markers (*8*)—combined with palaeoecological evidence of small scattered, perhaps palynologically silent, early *Picea* populations in Scandinavia (*9*), including a possible Late Glacial (but not LGM) occurrence on a Swedish nunatak (*10*)—suggest several immigrations along both northern and southern routes after deglaciation. This scenario would explain the observed genetic diversities from Russia to Scandinavia (*8*). Furthermore, LGM *Picea* populations south of the ice with HapA could have spread north during deglaciation, meanwhile becoming extinct in their southern refugia. Populations only expanded after ~3000 years before the present (BP) (*9*). HapA could have arisen in a pioneer southern population, increased in small populations, and spread toward the west and north, mixing with lineages sharing HapB. Multiple immigrations from western and southern directions would tend to block the spread of the northern ones (*11*). Even if HapA survived on Andøya, it would be unlikely to spread southward. Although Parducci *et al*. argue that a distinct genotype cluster in central Scandinavian populations (*8*) indicates a western origin, they should also consider the several different genotype clusters in Scandinavia that may be explained by leading-edge and surfing phenomena. Interestingly, these clusters map poorly with HapA, but the spatial resolution is coarse. To clarify colonization processes, more sampling and genetic analyses are needed to map the distribution of other individual mutations and markers. Parducci *et al*. demonstrate that *Picea*'s history in Scandinavia was probably more complex than previously thought, but they cannot claim that the lineage of the widespread HapA survived in northern Scandinavia and spread south and east.

(v) Why are *Pinus* and *Picea* absent on Andøya after 17,700 years BP? Late-Pleniglacial refugial tree populations with low palynological presence typically respond to deglacial warming with increases in pollen percentages. For example, low Pleniglacial *Picea* pollen percentages at Lake Galich, in northern Russia, increased to more than 20% during the Late Glacial interstadial (*12*). No Late Glacial expansion of *Picea* and *Pinus* is recorded on Andøya (*6*), and neither grew on Andøya during the early Holocene (*13*). *Picea*'s present northwestern limit is ~500 km to the south (*14*). Andøya's cool oceanic climate today does not support *Picea*, and *Pinus* is rare (*14*). It must have been much more inhospitable during the glacial period, with a climate resembling that of Svalbard today (*6*).

We conclude that Parducci *et al*. have not justified in sufficient detail "how their data were obtained and why they should be believed to be authentic" (*3*). Their methodology is questionable, due to the unsuitable corer, the age and storage conditions of the sediment core, and the potentially unsterile sampling. The taphonomy of DNA in lake sediment needs rigorous investigation. One cpDNA record of *Picea* and two of *Pinus* are insufficient to postulate glacial survival. No account was taken of the lack of suitable habitats on Andøya during the glacial period. Other parts of northern Scandinavia were ice-covered. The absence of *Pinus* and *Picea* during the deglacial and Holocene is contrary to all ecological expectations if small LGM populations survived near Endletvatn. The distribution of *Picea* mtDNA haplotypes can be more readily explained by postglacial colonization than by a northern

[1]Department of Biology, University of Bergen, NO-5020 Norway. [2]Department of Palynology and Climate Dynamics, Albrecht-von-Haller-Institute for Plant Sciences, University of Göttingen, 37073 Göttingen, Germany. [3]Biological Sciences, University of East Anglia, Norwich NR4 7TJ, UK. [4]Environmental Change Research Centre, Department of Geography, University College London, Gower St. London WC1E 6BT, UK. [5]Department of Earth Sciences, University of Bergen, NO-5007 Norway. [6]Department of Geography and the Environment, University of Oxford, OX1 3QY, UK.

*To whom correspondence should be addressed. E-mail: hilary.birks@bio.uib.no

Downloaded from www.sciencemag.org on November 9, 2012

LGM refuge. We consider the evidence presented by Parducci *et al*. to be unconvincing, so we reject their hypothesis that *Picea* and *Pinus* survived the last glacial period in northern Scandinavia.

References

1. L. Parducci *et al*., *Science* **335**, 1083 (2012).
2. M. Hofreiter, M. Collins, J. R. Stewart, *Quat. Sci. Rev.* **33**, 1 (2012).
3. M. T. P. Gilbert, H.-J. Bandelt, M. Hofreiter, I. Barnes, *Trends Ecol. Evol.* **20**, 541 (2005).
4. D. T. Feek, M. Horrocks, W. T. Baisden, J. Flenley, *J. Paleolimnol.* **45**, 115 (2011).
5. T. O. Vorren, L. Plassen, *Boreas* **31**, 97 (2002).
6. T. Alm, *Boreas* **22**, 171 (1993).
7. E. Willerslev, A. J. Hansen, B. Christensen, J. P. Steffensen, P. Arctander, *Proc. Natl. Acad. Sci. U.S.A.* **96**, 8017 (1999).
8. M. M. Tollefsrud *et al*., *Heredity* **102**, 549 (2009).
9. T. Giesecke, K. D. Bennett, *J. Biogeogr.* **31**, 1523 (2004).
10. L. Kullman, *J. Biogeogr.* **29**, 1117 (2002).
11. J. M. Waters, *Mol. Ecol.* **20**, 4388 (2011).
12. A. A. Velichko *et al*., *Ser. Geographiheskaya* **3**, 42 (2001) (in Russian).
13. K.-D. Vorren, E. Elverland, M. Blaauw, E. K. Ravna, C. A. H. Jensen, *Boreas* **38**, 401 (2009).
14. A. Moen, *National Atlas of Norway: Vegetation* (Norwegian Mapping Authority, Hønefoss, 1999).

29 May 2012; accepted 4 September 2012
10.1126/science.1225345

Downloaded from www.sciencemag.org on November 9, 2012

Response to Comment on "Glacial Survival of Boreal Trees in Northern Scandinavia"

Laura Parducci,[1,2] Mary E. Edwards,[3] K. D. Bennett,[4] Torbjørn Alm,[5] Ellen Elverland,[5] Mari Mette Tollefsrud,[6] Tina Jørgensen,[2,5] Michael Houmark-Nielsen,[2] Nicolaj Krog Larsen,[7] Kurt H. Kjær,[2] Sonia L. Fontana,[8] Inger Greve Alsos,[5] Eske Willerslev[2]*

Birks *et al*. question our proposition that trees survived the Last Glacial Maximum (LGM) in Northern Scandinavia. We dispute their interpretation of our modern genetic data but agree that more work is required. Our field and laboratory procedures were robust; contamination is an unlikely explanation of our results. Their description of Endletvatn as ice-covered and inundated during the LGM is inconsistent with recent geological literature.

We thank Birks *et al*. (*1*) for their comments on our paper (*2*) and continuing engagement in the long-standing debate on tree survival (or otherwise) in glacial-age Scandinavia (*3*). We know as well as any that the new field of environmental ancient DNA requires further work; however, we find their specific criticisms to be unfounded. For our results to be merely a set of errors, as might be construed from their Comment, would require contamination by independent spruce and pine genetic markers to occur in two independently obtained sediment samples, including pollen isolates, and/or in three independent ancient DNA laboratories. Additionally, for our interpretation of the genetic patterns to be erroneous, a highly complex alternative explanation of modern spruce genetic data in northern Europe must be invoked.

(i) How reliable is ancient DNA (aDNA) from lake sediments? It is a misinterpretation of Gilbert *et al*. (*4*) that a specific set of authentication criteria is needed. They recommend adding criteria of relevance to a given study rather than following a predefined list. We (i) took material from two locations with different equipment on different expeditions (minimizing cross contamination); (ii) used two independent DNA markers—chloroplast DNA (cpDNA) and mitochondrial DNA (mtDNA)—for each locality (minimizing the chance that positive findings of conifer DNA result from contamination of amplicons obtained from the other core); and (iii) undertook replication of findings in three ancient DNA laboratories (two in Uppsala and one in Copenhagen).

No piston corer is contamination-free, including that of (*5*). We followed all conventional protocols for avoiding contamination: careful core storage, cleaning of cores before sampling, and sampling from the undisturbed interior of a core in clean laboratories and with clean instruments (*5*). The lacustrine Endletvatn sediments were retrieved from a mire, so the corer was never in a lake water column; dissolved DNA from lake water is not a contaminant. Were contamination present, taxa currently abundant in the catchment (e.g., *Calluna vulgaris* and *Vaccinium* spp.) should have been found, but they were not; rather, most taxa were similar to pollen taxa.

We do not report the plant fragment retrieved from lake sediment as contamination. It was bleached to remove modern contamination (standard procedure before ancient macrofossil genotyping) and identified by DNA barcoding as *Urtica*.

(ii) Was glacial survival on Andøya possible? Our record is physically feasible. Current understanding of Last Glacial Maximum (LGM) glacial limits places northern Andøya outside those limits (*6*). The ice cover of Scandinavia was highly dynamic in space and time, even in inland areas (*7*), intermittently exposing ice-free areas. Endletvatn remained a lake above sea level during the LGM (*8*). Areas for plant growth would not have been confined to mountain peaks but would have included lower elevations and a range of topoclimates. Pollen and macrofossil records from previous Andøya studies indicate a mosaic of vegetation in space and/or time (*3*, *8*–*11*). A local temperature reconstruction (Fig. 1) shows marked fluctuations through the LGM and Late Glacial, including episodes when the mean temperature of the warmest month exceeded 10°C, compatible with the establishment and survival of tree taxa.

(iii) Where were *Pinus* and *Picea* growing? Our data, and other studies [e.g., *12*], underpin a growing case for tree survival in locations within otherwise glaciated Scandinavia, but we neither demonstrate nor claim that pine (*Pinus*) and spruce (*Picea*) survived the whole glacial period on Andøya. Indeed, we entertain alternative explanations for our findings, including redeposition, driftwood, and long-distance pollen [see supporting online material (SOM) for (*2*)] but show them to be unlikely, concluding that survival of conifers through the LGM in northern Scandinavia is the most parsimonious explanation of our results.

We do not expect aDNA results to duplicate pollen results. We do expect that, like macrofossil evidence, results will be complementary to pollen data. Understanding cases where aDNA is present but there is no corresponding pollen data (and vice versa) is an area of continuing research by our group. However, absence of pollen data is not evidence of absence.

Therefore, where did the cpDNA come from? Birks *et al*. cite (*13*) to suggest that there was long-distance dispersal of environmental DNA. Subsequent papers by the same group (e.g., *14*–*16*) find no evidence for long-distance dispersal of either animal or plant sedimentary DNA.

(iv) Does haplotype A (HapA) reflect *Picea* spreading directions? We report haplotype A as a 21–base pair deletion clearly identifiable by sequencing. The finding of this deletion at ~10,300 calibrated years before the present (BP) in more than 30% of the samples from central Norway [see SOM table S5 for (*2*)] indicates that HapA individuals were present by the early Holocene. This early abundance at high latitudes indicates that HapA populations arose at an earlier time and then expanded. Deep divergence between northern and southern European spruce populations is demonstrated by the mtDNA marker nad1, which likely predates several glacial-interglacial cycles (*17*); migration from the southern range is therefore less likely.

More genetic markers and improved population resolution are indeed needed to reveal the full history of spruce in Scandinavia. Genetic patterns revealed by other mtDNA and nuclear markers have already revealed a complex history (*17*, *18*). Elevated genetic distances in central Scandinavia and relatively high genetic diversity at nuclear loci in southern Scandinavia argue in favor of a western refugium (*18*).

(v) Why are *Pinus* and *Picea* absent on Andøya after 17,700 years BP? Interestingly, macrofossils of *Betula pubescens* at ~20,000 years BP (*3*) provide "conventional" evidence of LGM tree presence on Andøya. However, assuming "once there, always there" is a rather static vision of Quaternary biogeography. Individual populations appear locally and become extinct locally. There is no a priori reason why all populations recorded in the palaeoecological record of the LGM, particularly those in suboptimal habitats, should survive intact until today.

[1]Department of Ecology and Genetics, Evolutionary Biology Centre, Uppsala University, Norbyvägen 18D, 75236 Uppsala, Sweden. [2]Centre for GeoGenetics, Natural History Museum of Denmark, University of Copenhagen, Øster Voldgade 5-7, DK-1350 Copenhagen, Denmark. [3]Geography and Environment, University of Southampton, Highfield, Southampton SO17 1BJ, UK. [4]School of Geography, Archaeology and Palaeoecology, Queen's University Belfast, University Road, Belfast BT7 1NN, Northern Ireland. [5]Tromsø University Museum, NO-9037 Tromsø, Norway. [6]Norwegian Forest and Landscape Institute, Post Office Box 115, NO-1431 Ås, Norway. [7]Department of Geoscience, Aarhus University, Høegh-Guldbergs Gade 2, DK-8000 Aarhus C, Denmark. [8]Department of Palynology and Climate Dynamics, University of Göttingen, Untere Karspüle 2,37073 Göttingen, Germany.

*To whom correspondence should be addressed. E-mail: ewillerslev@snm.ku.dk

Downloaded from www.sciencemag.org on November 9, 2012

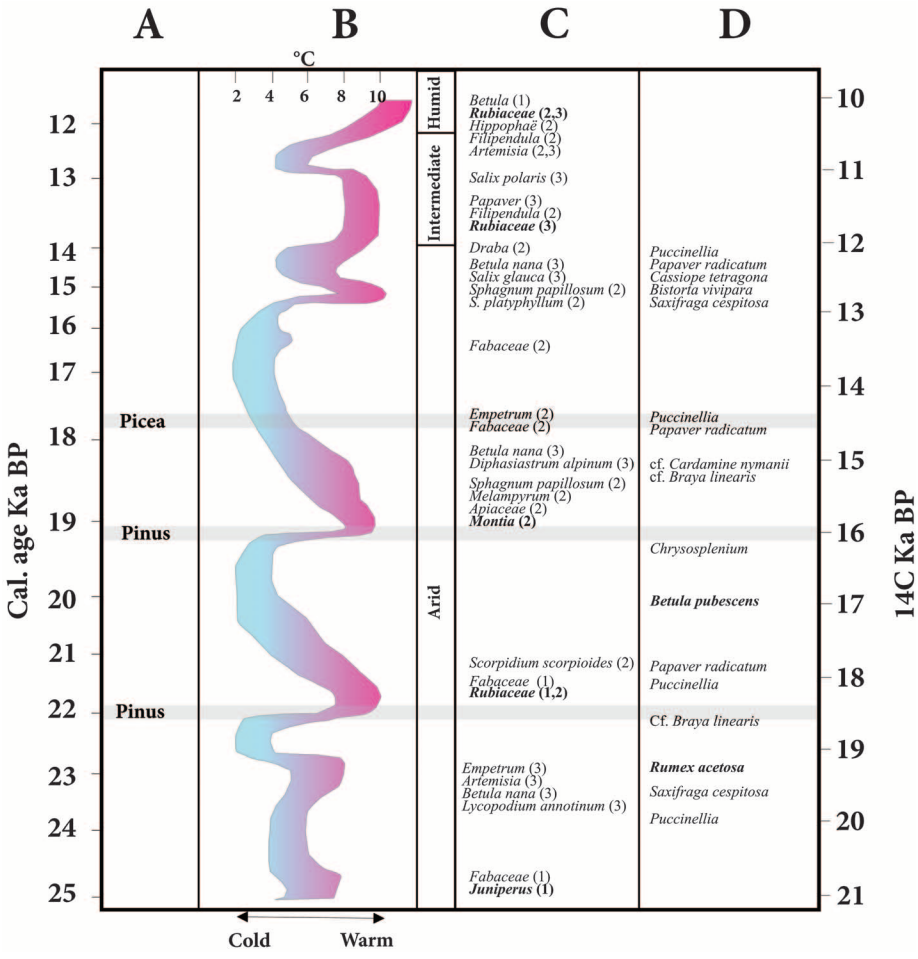


Fig. 1. Temporal occurrence of plant taxa and climate reconstruction at Andøya. (**A**) Our sedimentary aDNA (sedaDNA) findings in the Endletvatn core. (**B**) Northern Andøya mean July temperature climate curve and aridity/humidity estimates, redrawn from (*9*). (**C**) Climatic bio indicators as identified by (*9*) (no. 1), (*10*) (no. 2), and (*8*) (no. 3). (**D**) Botanical macrofossils from (*11*) and a *Betula pubescens* macrofossil from (*3*). Taxa with their current northern limit in shrub tundra (mean July temperature 10 to 12°C) are shown in bold. Radiocarbon dates have been converted into calendar years using Oxcal 4.1 with IntCal09.

References

1. H. H. Birks *et al.*, *Science* **338**, 742 (2012); www.sciencemag.org/cgi/content/full/338/6108/742-a.
2. L. Parducci *et al.*, *Science* **335**, 1083 (2012).
3. L. Kullman, *J. Biogeogr.* **33**, 377 (2006).
4. M. T. P. Gilbert, H.-J. Bandelt, M. Hofreiter, I. Barnes, *Trends Ecol. Evol.* **20**, 541 (2005).
5. D. T. Feek, M. Horrocks, W. T. Baisden, J. Flenley, *J. Paleolimnol.* **45**, 115 (2011).
6. A. Nesje *et al.*, *Boreas* **36**, 227 (2007).
7. E. Kolstrup, L. Olsen, *Norsk Geografisk Tidsskrift Norw. J. Geogr.* **66**, 30 (2012).
8. T. Vorren, K. Vorren, T. Alm, S. Gulliksen, R. Løvlie, *Boreas* **17**, 41 (1988).
9. T. Alm, *Boreas* **22**, 171 (1993).
10. K. Vorren, *Boreas* **7**, 19 (1978).
11. T. Alm, H. H. Birks, *Nord. J. Bot.* **11**, 465 (1991).
12. L. Kullman, *Quat. Sci. Rev.* **27**, 2467 (2008).
13. E. Willerslev, A. J. Hansen, B. Christensen, J. P. Steffensen, P. Arctander, *Proc. Natl. Acad. Sci. U.S.A.* **96**, 8017 (1999).
14. E. Willerslev *et al.*, *Science* **317**, 111 (2007).
15. J. Haile *et al.*, *Mol. Biol. Evol.* **24**, 982 (2007).
16. J. Haile *et al.*, *Proc. Natl. Acad. Sci. U.S.A.* **106**, 22352 (2009).
17. M. M. Tollefsrud *et al.*, *Mol. Ecol.* **17**, 4134 (2008).
18. M. M. Tollefsrud *et al.*, *Heredity* **102**, 549 (2009).

14 June 2012; accepted 4 September 2012
10.1126/science.1225476

Downloaded from www.sciencemag.org on November 9, 2012

HISTORY OF SCIENCE

Picturing Nature and Empire

Pamela H. Smith

Lavishly illustrated and lucidly written, *Visible Empire* is a book about 12,000 images, a good number of which are stunningly reproduced in it. Historian Daniela Bleichmar (University of Southern California) has tapped a treasure trove of botanical illustrations that had lain in Spanish archives mostly untouched since the early 19th century. The politics and ambitions that produced this reservoir of images eventually rendered it irrelevant, overtaken by the turbulence of the Napoleonic occupation of Spain and the wars of independence in Spain's colonies.



From New Spain. Mexican artist Atanasio Echeverría's watercolor of *Erythrina divaricata*.

CREDIT: COURTESY HUNT INSTITUTE FOR BOTANICAL DOCUMENTATION, CARNEGIE MELLON UNIVERSITY, PITTSBURGH, PA. TORNER COLLECTION OF SESSÉ AND MOCIÑO BIOLOGICAL ILLUSTRATION

Although the 18th century was a period of economic decline for the Spanish Crown in its rivalry with the British and French, if one saw only the botanical images produced between 1759 and 1808, "decline" would never come to mind. Following the accession of Charles III, nearly 60 scientific expeditions traveled through the Hispanic empire. The study of nature had become a tool of competition among the colonial powers of the Atlantic world, and the crown saw a direct link between botanical exploration and the discovery of new sources of income for state coffers. Spain and its imperial territories had previously relied on mining as the font of wealth, but the many local economic societies that formed in the 18th century called for a change of focus: "The vegetable riches of Spanish America … have over the mineral ones the advantage that they can be propagated and multiplied ad infinitum once they are possessed and naturalized." Botanical expeditions, supported by new botanical gardens, set out to possess and naturalize these riches. In the process, they created a network of naturalists and put in place impressive institutions for the study of botanical specimens and the making of images. But many of the naturalists perished on their voyages, good engravers to translate the tempera images into printable form could not be found, and in the end world events overturned the ambitions to publish these remarkable images. Today, they stand as a testament to the potential that both local and imperial governments saw in the scientific study of nature. And, as Bleichmar makes beautifully clear, they demonstrate the active scientific culture of Spain and its colonies in the 18th century as well as the intimate connection between visual culture and the pursuit of science in Enlightenment society.

Visible Empire
Botanical Expeditions and Visual Culture in the Hispanic Enlightenment
by Daniela Bleichmar
University of Chicago Press, Chicago, 2012. 298 pp. $55, £35.50. ISBN 9780226058535.

From very early on, the Spanish empire employed images for colonial administration—to visualize new lands, to demonstrate their appearance and potential, and to support arguments. Spain also sought to replace the native populations' own images, which played a central role in indigenous cultures. This it did brutally and almost completely, in an orgy of burning and destruction. Images became part of Spain's attempt to govern at a distance—one has only to think of the *relaciones geográficas* of the 1570s ordered by Philip II, which asked local governors and friars to send information about their regions. As Barbara Mundy has sensitively demonstrated (*1*), this questionnaire resulted in a collection of remarkable maps, combinations of European and indigenous cartographic traditions and cultures of representation. Making their vast lands visible—and thus knowable and governable—remained a central ambition of Spanish imperial governing into the 18th century. Bleichmar makes the intriguing point that part of Spain's (or, more correctly by the 18th century, the Creole colonial inhabitants') effort remained the erasure of the indigenous past and its bloody conquest. Naturalists heralded the scientific voyages as bringing forth knowledge that would temper the bloody battles of the past and stimulate commerce, a balm capable of healing all wounds.

In conjunction with other European men of letters, Spanish naturalists developed a "visual epistemology" that involved close looking back and forth between text and object and between known and new plants, texts, drawings, and printed images. In it, the physical act of drawing provided a form of close observation that enabled the recognition of systemic features that helped classify these unfamiliar plants. Some naturalists drew and painted, but most carefully oversaw the making of images by trained artists. These images "allowed eighteenth-century natural history to abstract information, visually embody expert observations, and mobilize across distances plants that remained in crucial ways unseen and unknown, even three centuries after Europeans had first encountered New World nature." The vast network of observers created by this circulation of images consolidated botanical methods and systems of taxonomic ordering.

Bleichmar's account provides insight into day-to-day science in the 18th century, gained primarily from the surviving correspondence of naturalists, in particular, José Celestino Mutis. Mutis gathered around him a stable of well-trained artists, at one point employing 30. His letters express pride at the enormous output of his operation—over 5000 images resulted from his expeditions. His team of plant gatherers, artists, and gar-

The reviewer is at the Department of History, Columbia University, 1180 Amsterdam Avenue, MC 2527, New York, NY 10027, USA. E-mail: ps2270@columbia.edu

Downloaded from www.sciencemag.org on November 9, 2012

Published by AAAS

deners developed means to transport plants, preserve them in a lifelike state, and render them in an innovative style.

These images were not produced solely in the service of local and European science but also in an active attempt to discover new commodities or New World versions of eastern products, such as cinnamon and pepper. Many of these economic schemes foundered on the inability to acclimatize plants or to prove that they matched species from elsewhere (hence the importance to these naturalists of taxonomic systems). But this economic agenda also illustrates one aspect of a new self-consciousness of the Creole populations of the 18th-century Spanish empire (*2*). In her final chapters, Bleichmar offers fascinating evidence of this new patriotism in an unusual set of paintings portraying the interconnectedness of local peoples, flora, fauna, history, social order, and territory.

In the past two decades, historians have fruitfully explored the relationship between the picturing of nature done by artists and that produced by practitioners of science for the periods of the Scientific Revolution and Enlightenment. Bleichmar's arresting *Visible Empire* contributes to the ongoing recovery of the formative—but hitherto little-known—role that Spain and its colonies played in this crucial period in the history of science.

References

1. B. E. Mundy, *The Mapping of New Spain: Indigenous Cartography and the Maps of the* Relaciones Geográficas (Univ. Chicago Press, Chicago, 1996).
2. J. Canizares-Esguerra, *Nature, Empire, and Nation: Explorations of the History of Science in the Iberian World* (Stanford Univ. Press, Stanford, CA, 2006).

10.1126/science.1230411

MATHEMATICS

Lifting Reality Off

Brie Finegold

Paul Lockhart makes no apologies for studying imaginary objects. On top of that, he expects the reader to help write his book about how to measure these ethereal entities. On almost every page of *Measurement* questions or demands taunt the reader: "What if time were two dimensional or circular?" "Show that a four-dimensional pyramid occupies one-quarter of its four-dimensional box." To complete reading any mathematics text without putting pen to paper would be doing oneself a great disservice, but Lockhart's questions are not numbered exercises at the end of a section of dense text. Although not always completely integral to the narrative, these questions are extremely compelling—we often yearn for a resolution enough to set out to find it.

The unassuming title and table of contents (Part One: Size and Shape; Part Two: Time and Space) truly reflect the book's focus on connecting geometric and algebraic thinking. But prospective readers should rest assured that while aimed at the nonexpert, Lockhart's writing is sophisticated and mathematically modern. Words such as "isometry," "orientation," and "invariant" are defined and incorporated into the book's conversational flow. Scientists who work with mathematicians will probably appreciate the tenor of the book, as it mimics mathematicians' everyday language and mode of discussion.

Measurement
by Paul Lockhart
Harvard University Press, Cambridge, MA, 2012. 415 pp. $29.95, £20, €27. ISBN 9780674057555.

For all his aversion to reality, researcher-turned-educator Lockhart (who teaches at Saint Ann's School, Brooklyn, New York) also exploits our real-life experiences by introducing an abstract idea such as "lines intersecting at infinity" by discussing perspective as it is used in art and architecture. Mathematicians will immediately recognize his statement that "lines are somehow like circles that pass through infinity and come back around the other side" as relating to projective space, the idea of stereographic projection, and even Moebius transformations. Reflecting on the possible novelty of this idea in the eyes of readers, Lockhart writes "Perhaps you object to these new points [points at infinity] on the grounds that they are imaginary—they're not really there. But none of the things we've been talking about are real anyway. There's no 'there' there in the first place." He goes on to relate projective geometry to a previous discussion of conic sections.

In reviewing the familiar fact that the area of a circle of radius r is πr^2, Lockhart reveals how mathematicians make formulas their own in the same way that a DJ remixes a classic. He reframes the area of a circle as one-half the product of the circumference and the radius. We then see that the area of a circle is the area of a triangle whose base is the circumference of the circle and whose height is its radius. Later, after discussing the definition of π (the ratio of circumference to diameter), Lockhart reminds us the formula for the circumference of a circle is "practically content free"—not really a discovery, but a restatement of the definition chosen by mathematicians of yore. Whereas any researcher knows that the way we choose to define terms can greatly affect our ability to perceive relationships between ideas and quantities, the public is rarely let in on this secret—that there are choices to be made when doing mathematics.

Lockhart also notes the beauty in being able to choose from the infinitely many ways to parameterize a curve (even though he avoids the term "parameterization"). He illustrates a researcher's propensity to deconstruct complex ideas into already-known components in his discussion of the parameterization of the cycloid (the curve traced out by a point on a rolling circle). First he chooses to view the location of the moving point as a vector, and then he points out how the complex periodic motion can be separated into two simple components: translational and rotational. Rather than sweeping the nuances of describing this curve under the rug and delving straight into problems of measuring velocity or arc length, Lockhart highlights the choices that he is making as he goes along—thus helping readers develop a sense of taste in mathematics just as one would develop taste in music.

In his earlier *A Mathematician's Lament* (*1*), Lockhart called for scrapping, as opposed to simply reforming, the current mathematics curriculum for primary and secondary schools. He continues to rebel against the notion that math needs a makeover; instead, he calls for a kind of makeunder. By stripping reality away, he exposes the portability, convenience, strength, and beauty of mathematical objects—objects that can be flipped, deconstructed, and reconstructed ad infinitum at the thinker's whim. In place of the usual boxed and highlighted formulas and tricks, *Measurement* offers questions to be pondered. Lockhart invites readers to trade tutorial fake problems about actual objects, which lead students to abhor school mathematics, for real problems about fantastical objects, which lead mathematicians to love math.

References

1. P. Lockhart, *A Mathematician's Lament* (Bellevue Literary, New York, 2009).

10.1126/science.1229902

The reviewer is at the Department of Mathematics, University of Arizona, 617 North Santa Rita Avenue, Tucson, AZ 85721, USA. E-mail: bfinegold@math.arizona.edu

Downloaded from www.sciencemag.org on November 9, 2012

Published by AAAS

PATENT LAW

Law and Science Collide Over Human Gene Patents

Will the Supreme Court rule that DNA sequences found in nature cannot be patented?

Robert Cook-Deegan

In 1980, the U.S. Supreme Court ruled that engineered organisms could be patented (*1*). For 30 years, genes have likewise been presumed to be eligible for patents. Recent events suggest that the Court may reverse established practice in biotechnology patents, by making DNA molecules whose sequences are found in living organisms ineligible to be patented.

The U.S. Court of Appeals for the Federal Circuit (CAFC) handed down a ruling on 26 August 2012, in the celebrated *Association of Molecular Pathology* (AMP) v. *U.S. Patent and Trademark Office* (USPTO) (*2*). That ruling is now being appealed to the U.S. Supreme Court (*3*). The lawsuit centers on patents covering the *BRCA1* and *BRCA2* genes, in which mutations can cause elevated risk of breast, ovarian, and certain other cancers.

This is not your usual patent case. It is not one company suing another over who will make money from a product that embodies patented technology. The purpose of the suit is to clarify the law about whether a gene is patentable subject matter. The lawsuit was initiated by the American Civil Liberties Union (ACLU) and the Public Patent Foundation against the USPTO, Myriad Genetics, and members of the board that oversees patents held by the University of Utah. From its start in May 2009, the case has threatened long-standing norms of patent practice in an area—diagnostic use of gene patents—with little established case law. Until this case, no lawsuits over genetic diagnostics made it as far as a decision by a judge or jury (*4*–*7*). Eleven "gene patent" cases have risen to the appellate level, but these were litigated over who would get the patents for therapeutic molecules not whether genes could be patented at all.

More than 20 plaintiffs were assembled by ACLU and the Public Patent Foundation. Plaintiffs fall into three basic categories: (i) women who wanted to get tested but believed they could not because of Myriad's business practices, (ii) laboratory physicians who want to order tests or do tests on behalf of patients at risk, and (iii) health professional and cancer advocacy organizations. The case was first heard in the U.S. Federal District Court for the Southern District of New York, Judge Robert Sweet presiding. On 29 March 2010, Judge Sweet declared that isolated genes were unpatentable products of nature and that method patents were invalid; he thus invalidated all 15 claims being challenged in seven patents held by Myriad Genetics. Myriad promptly appealed to CAFC.

CAFC Rulings

The three CAFC judges who heard the appeal were unanimous on three crucial points. They determined that only one of the plaintiffs, Harry Ostrer (who is a medical geneticist), had sufficient standing to sue. It only takes one plaintiff to bring a case, however, so they proceeded to decide the merits of the case. The CAFC judges unanimously agreed that Judge Sweet had gone too far in invalidating all DNA-based claims, which rested on his argument that DNA is unique as the physical embodiment of genetic information. The CAFC judges specifically agreed that engineered DNA molecules can be patented. This is important and indicates that complementary DNAs bereft of intronic sequences or DNAs inserted into vectors and put in cells to produce a therapeutic protein are clearly patentable. The vast majority of commercially important biotechnology patents on "genes" cover DNA molecules that have been modified in some way and would thus not be threatened by the residual disagreement in *AMP* v. *USPTO*, if one assumes that the patents meet the other criteria of novelty, nonobviousness, utility, enablement, and written description.

The disagreements among judges [and the] Solicitor General … invite the Supreme Court to decide this case.

The three CAFC judges also agreed unanimously—here upholding Judge Sweet's district court ruling—that Myriad's five broadest method claims are invalid. Those claims cover detecting a sequence difference in *BRCA1/2* between a sample sent for analysis and the reference sequence disclosed in the patent. The method claims were arguably Myriad's broadest form of protection, because the very point of a diagnostic test is to identify sequence differences, and the claims were worded in a way that was nearly impossible to circumvent. The CAFC judges invalidated these claims as being unpatentable subject matter and so never looked at other grounds. If challenged on enablement and written description, the method claims might well have been held invalid because of their breadth, but that was not addressed in this case.

The main focus of the judges' analyses—and all three CAFC judges, as well as Judge Sweet, have gone to unusual lengths in their rulings—centered on one point of disagreement: Can patent claims be drawn to DNA molecules whose sequences correspond to those found in nature? The CAFC judges split 2-1, with Judges Lourie and Moore arguing that "isolated" DNA molecules can be patented, and Judge Bryson arguing that they are not patent-eligible.



Judge Lourie argued that the molecules are deliberately cleaved from chromosomal DNA and do not exist in that form in nature. To Judge Lourie, that structural difference suffices to make isolated DNA molecules

Institute for Genome Sciences and Policy, Duke University, Durham, NC 27708, USA. E-mail: bob.cd@duke.edu

Downloaded from www.sciencemag.org on November 9, 2012

Published by AAAS

patent-eligible. Judge Moore applied a different test: different structure plus new utility. She was more skeptical of patent-eligibility with longer DNA molecules but quite concerned about removing patent rights in settled law retroactively. By isolating the molecules and showing how they can be used, the inventors have done something warranting a patent. Judges Lourie and Moore are surely right that it takes human intervention to determine a DNA sequence and that isolated DNA molecules are, more or less by definition, created when making practical use of DNA—such as determining clinically important sequence differences. DNA molecules in nature do not read out their sequence.

The question is whether DNA molecules whose sequences are found in nature are unpatentable phenomena of nature or patentable subject matter because they are isolated.



Judge Bryson, however, dissented vigorously, saying that, although the DNA molecules may be isolated, the sequences correspond to molecules in nature in every meaningful sense. The differences between isolated and natural DNA's are not material to the claimed uses. The isolated molecules are useful only to the degree that they faithfully copy the information stored and transmitted in naturally occurring DNA and, therefore, they are not "markedly" different in a way that should matter to the law. In diagnostics this is surely right in at least one sense. If the sequences in isolated molecules were not exactly the same as in a person's body, they would be diagnostically useless. One difference between a diagnostic and a patented "product of nature"—think antibiotics, adrenalin, or insulin—is that the patented therapeutics are doing something new and useful as a consequence of human intervention (being used to treat a bacterial infection or anaphylaxis or diabetes), whereas the diagnostic intervention underlying the Myriad case is to observe the *BRCA* sequence in DNA from cells in a sample. Judge Bryson's dissent is explicit that Myriad could claim probe molecules or primers, which are clearly manmade DNA molecules, but by claiming so broadly and reaching to the naturally occurring sequences, Myriad's claims go too far and cover a phenomenon of nature.

Will the U.S. Supreme Court Reverse the CAFC?

In March 2012, the Supreme Court unanimously reversed a July 2011 CAFC ruling in another case, *Mayo* v. *Prometheus* (*8*). *Mayo* v. *Prometheus* concerned patents on a method for adjusting the dose of thiopurine drugs by measuring a metabolite level. The Supreme Court was clear and unanimous that the claims covered something that simply should not be patented. The next week, it ordered CAFC to reconsider its ruling in *AMP* v. *USPTO* in light of *Mayo*. The CAFC has now done that. The CAFC panel once again ruled 2-1 that isolated DNA molecules can be patented even if they correspond to naturally occurring sequences. Judges Lourie and Moore held firm and Judge Bryson once again dissented. The question now is whether the Supreme Court will reverse the CAFC in *AMP* v. *USPTO*, this time on whether DNA molecules corresponding to those found in nature can be patented.

The Solicitor General, the U.S. government's top lawyer, entered this case twice at the CAFC. The involvement of the Solicitor General is one reason to think that the Supreme Court might agree to review the case upon appeal. After a formal multiagency process, the Solicitor General prepared an amicus curiae (friend of the court) brief arguing that engineered DNA molecules can be patented, but sequences found in nature cannot (*9*). The Surgeon General's involvement at the CAFC is unusual. It is widely known that the USPTO does not agree with the Solicitor General about *AMP* v. *USPTO*, and agrees with the 2-1 CAFC majority; the disagreement within the U.S. government came out explicitly in oral arguments on 20 July 2012 (*10*). The Solicitor General, nonetheless, speaks with the formal voice of the entire Executive Branch. The Solicitor General is sometimes called the "10th justice" of the Supreme Court. Ten cases went to the Supreme Court 1996–2011 in which the Solicitor General and the CAFC disagreed; 9 were decided in favor of the Solicitor General, and just 1 with the CAFC (*11*).

Another reason to think that the Supreme Court may reverse the CAFC is that Justice Breyer's ruling in *Mayo* v. *Prometheus* is quite clear that the Court wants "patentable subject matter" categories to do real work that other patent criteria cannot do. The Supreme Court clearly believes limits on what can be patented are important. The foremost concern argued by the Supreme Court in *Mayo* v. *Prometheus* is "how much future innovation is foreclosed relative to the contribution of the inventor" (*12*).

Judges Lourie and Moore dismiss the relevance of *Mayo* v. *Prometheus* by noting it was about methods, not molecules. The only remaining disagreement in *AMP* v. *USPTO* is about isolated *BRCA* molecules—or "compositions of matter." Judge Lourie also argues that if the concern is the breadth of a patent's scope, the proper tools to narrow claims are enablement and written description, not deciding what can be patented at all. Judge Lourie's argument flies in the face of explicit attention to the patentable subject matter doctrine in the Supreme Court's ruling in *Mayo* v. *Prometheus*. Will the Supreme Court decide that CAFC judges missed the point? Are DNA molecules with sequences the same as natural sequences, even if isolated, "basic building blocks of nature" that cannot be patented?

In contrast to Judges Lourie and Moore, Judge Bryson believes *Mayo* v. *Prometheus* is relevant to *AMP* v. *USPTO* because the granted claims to the molecules "will have broad consequences, such as preempting methods for whole-genome sequencing, even though Myriad's contribution to the field is not remotely consonant with such effects." The Solicitor General's briefs likewise center on preemptive effects and the importance of not impeding future innovation. Those arguments track more closely to *Mayo* v. *Prometheus* than Judge Lourie's and Moore's distinction between methods and molecules.

Discovery or Invention?

Justice Breyer's ruling in *Mayo* v. *Prometheus*, Judge Bryson's dissent from the CAFC majority, and the Solicitor General's arguments basically revive the distinction between invention, which is patentable, and discovery, which is not. Their line of argument: A modified DNA is an invention, but a DNA molecule corresponding to a sequence found in nature, even if isolated, is a discovery—a phenomenon of nature that cannot be the subject of a patent.

The invention-discovery distinction, however, confronts an unusual feature of U.S. patent law. The patent clause (*13*) in the U.S. Constitution says "Discoveries," and Congress deliberately blurred this very

Downloaded from www.sciencemag.org on November 9, 2012

Published by AAAS

distinction in its 1952 rewrite of the patent statute: "The term 'invention' means invention or discovery" (*14*). It does not follow, however, that the invention-discovery distinction has disappeared. As Justice Breyer notes in *Mayo* v. *Prometheus*, the Supreme Court has long found natural laws, phenomena of nature, and abstract ideas ineligible for patents. The question is whether DNA molecules whose sequences are found in nature are unpatentable phenomena of nature or patentable subject matter because they are isolated.

A determination of preemptive effect—how much exclusive rights can actually hinder the advance of science and technology—turns on a theory of how "science and the useful arts" advance. Myriad's pleadings and public statements assert that it has promoted public benefits and has not impeded research advances. Myriad notes advances to which it has contributed directly, including the nearly one million people who have been tested (*15*, *16*). It also points to more than 9000 papers on *BRCA* by 18,000 authors that have been published (*15*, *16*). The implication is that science has progressed unfettered (*17*, *18*). Myriad argues that its patents have contributed to, or at least not hindered, the accrual of knowledge about *BRCA* genes.

However, any of the research performed in jurisdictions with broad patent rights, if conducted without permission from Myriad, infringed Myriad's patents. The breadth of protection has been considerably narrowed in this case already and could be narrowed even more by the Supreme Court. But for over a decade, the presumption was that Myriad's patents were valid, and that presumption enabled a U.S. service monopoly based on vigorous enforcement once initial patents were granted. The fact that Myriad has allowed research to go forward—most of which infringes its intellectual property—is laudable, but tempered by distrust. If Myriad had a reason to go after researchers, would it do so? Indeed, it has.

Myriad restricted *BRCA* testing for clinical research by suing OncorMed and the University of Pennsylvania (*17*). All testing at the time was part of research, including trials funded by the National Cancer Institute. Myriad's definition of permissible "research" testing by others was quite narrow; its definition of appropriate testing in its own laboratory, however, was expansive, including clinical testing performed at a time when all health professional recommendations urged testing only in the context of research. OncorMed agreed to test only in research protocols, and Penn was a testing core for multi-institutional trials. It was Myriad that broke from professional standards to do clinical testing outside of research protocols in the early years (*18*–*21*). Myriad thus exercised its patent exclusivity in two ways: to establish a U.S. service monopoly and flout clinical guidelines in its own testing and to impose a narrow definition of research on others' *BRCA* testing. The Supreme Court may decide "Progress in Science and the useful Arts" is better served by clear legal limits on what can be patented at all, rather than leaving decisions about freedom to do research with patentholders.

Conclusion

The central unresolved question in *AMP* v. *USPTO* is whether isolated DNA molecules with sequences found in nature can be patented. The disagreements among judges on the CAFC—and between the CAFC majority and the Solicitor General—invite the Supreme Court to decide this case. On first blush, this may appear a large and consequential question for biotechnology, but on closer analysis, its answer has surprisingly little effect in the real world (*22*). At this point, a Supreme Court ruling that invalidates claims on DNA molecules will affect only a few companies, such as Myriad Genetics and Athena Diagnostics, that have service monopolies built on patenting naturally occurring genes and variants. It may not even affect them, given the evolution of business practices and the march of genomic technologies.

It will have little immediate practical importance beyond those few companies, because most truly valuable biotechnology patents do not claim naturally occurring DNA sequences—isolated or otherwise. A ruling against Myriad will wipe out thousands of claims on isolated DNA molecules, but most such patents include other claims that are narrower and do not depend on naturally occurring DNA sequences. Myriad itself has many claims on methods to detect specific sequences on probes, on primers, and on cDNAs that would still be intact. The exclusive rights would be narrower, and claims would have to be crafted to avoid claiming sequences found in nature. But that would actually not have a sweeping impact on biotechnology.

The larger legal significance of this case, which does carry great precedential importance, is if the Supreme Court decides to revitalize the distinction between invention and discovery long dormant in CAFC jurisprudence. Indeed, in 2011, Chief Judge Rader and CAFC Judge Pauline Newman argued vigorously against bringing cases such as *AMP* v. *USPTO* into the courts; they expressed impatience with raising patentable subject-matter challenges (*23*). A Supreme Court ruling reversing CAFC—on the very doctrine it would like to forget—would be a direct rebuke, reversing not just a case but also a line of jurisprudence. It would force a change not only in how claims are written, but further work by the federal courts. The courts would have to clarify how to draw the line between discovery and invention, that is, to develop better guidance about what kinds of things can be patented.

References and Notes

1. *Diamond* v. *Chakrabarty*, 447 U.S. 303 (1980).
2. *Association for Molecular Pathology* v. *USPTO* (The "Myriad case"), No. 2010-1406 (Fed. Cir. Aug. 16, 2012).
3. ACLU, Petition for writ of certiorari (2012), in (*2*); http://pub.bna.com/ptcj/ACLUCertPetition12Sep25.pdf.
4. C. Holman, *Kansas J. Law Pub. Pol.* **18**, 215 (2009).
5. C. M. Holman, *Science* **322**, 198 (2008).
6. In the wake of ***AMP*** v. ***USPTO***, Cancer Voices Australia brought a case against Myriad Genetics and its Australian/New Zealand licensee (Genetic Technologies Group). That case went to trial in February 2012 with a verdict still pending (*7*).
7. *Cancer Voices Australia* et al. v. *Myriad Genetics Inc.* et al., Federal Court of Australia, 8 June 2010.
8. *Mayo Collaborative Services* v. *Prometheus Laboratories, Inc.*, 566 U.S. __, 132 S.Ct. 1289 (2012).
9. Brief for the United States as Amicus Curiae in Support of Neither Party (15 June 2012), p. 2 in (*2*).
10. Oral arguments, 20 July 2012 in (*2*); www.cafc.uscourts.gov/oral-argument-recordings/2012-07-20/all.
11. A. Rai, *Yale Law J. Online* **121**, 335 (2011); http://yalelawjournal.org/2011/12/20/rai.html.
12. From (*8*), p. 1303.
13. U.S. Const. Art. I, §8.
14. 35 U.S. Code §100.
15. Myriad Genetics, Inc., Written comments on genetic diagnostic testing study, 26 March 2012 (U.S. Patent and Trademark Office, 2012), p. 20; www.uspto.gov/aia_implementation/gene-comment-myriad-gen.pdf.
16. Myriad all but claims credit for the advances embodied in those thousands of papers, although Myriad has collaborated directly with just 440 (or 2.4 percent) of those authors. And of the million tests, Myriad has provided free testing for 4000 (or 0.4 percent) (*24*).
17. *Myriad Genetics* v. *University of Pennsylvania*, Case no. 2:98-cv-829 (D. Utah 1998).
18. Contrast (*19*) with statements in (*20*, *21*).
19. M. Skolnick, *J. Clin. Oncol.* **14**, 1737 (1996).
20. F. M. Visco, *J. Clin. Oncol.* **14**, 1737 (1996).
21. F. S. Collins, *J. Clin. Oncol.* **14**, 1738 (1996).
22. J. Conley, D. Vorhaus, *Genomic Law Rep.* 17 August 2012; www.genomicslawreport.com/.
23. *Classen Immunotherapies, Inc.* v. *Biogen IDEC*, 659 F.3d 1057, 1073-1075 (Fed. Cir. 2011).
24. Myriad Genetics, Inc., Written comments on genetic diagnostic testing study, 26 March 2012 (USPTO, 2012), pp. 20–23.

Acknowledgments: Research supported by P50 HG003391 from the National Human Genome Research Institute, NIH; Fondation Brocher; and the Ewing Marion Kauffman Foundation. This Forum does not represent their views.

10.1126/science.1229854

Downloaded from www.sciencemag.org on November 9, 2012

Published by AAAS

IMMUNOLOGY

A Decorated Virus Cannot Hide

A protein that promotes blood coagulation also enables the immune system to recognize a viral pathogen.

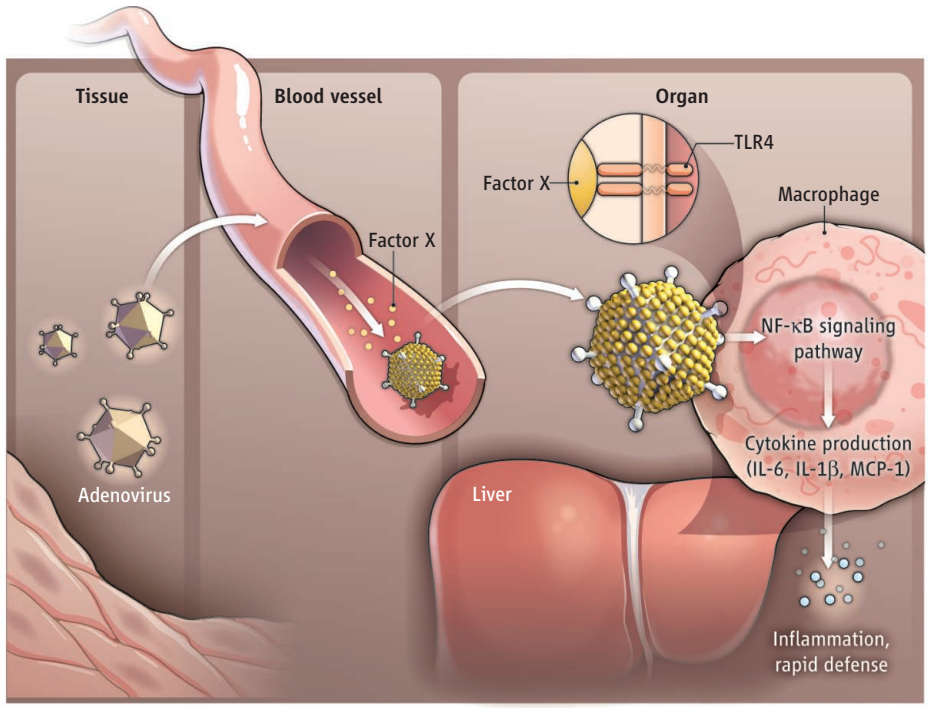
Roland W. Herzog[1] and David A. Ostrov[2]

The coagulation system protects our bodies from excessive loss of blood from a leaky or damaged vessel, whereas the immune system protects us from invading pathogens such as viruses. Unexpected links between these two systems suggest their coevolution (*1*, *2*). On page 795 in this issue, Doronin *et al*. show that an essential protein for the clotting process binds to a virus that has entered the blood stream, thereby allowing the immune system to sense the invader and mount a rapid and potent antiviral response (*3*).

The innate immune system has many sensors for pathogens. For example, toll-like receptors (TLRs) on the surface of or inside cells recognize pathogen-associated molecular patterns typical for macromolecular structures of bacteria and viruses (*4*). Pattern recognition prompts the TLR to send a "danger" signal to the immune system (*5*). One of these receptors, TLR4, binds to components of bacterial cell walls such as lipopolysaccharide (LPS), although nonbacterial structures are also ligands for TLR4 (*6*).

Doronin *et al*. investigated the innate immune response to human adenovirus (HAdv), which causes the common cold. After entry of the virus into the blood, coagulation factor X (FX) binds to the hexon structure of the adenoviral protein capsid (*3*, *7*, *8*). FX is a serine protease that circulates as an inactive zymogen and, upon activation, is a critical component of the coagulation cascade (*9*). FX interaction with the viral capsid allows the virus to infect cells, such as hepatocytes, through cell surface receptors. Doronin *et al*. now show that immune cells (macrophages) sense FX-coated virus by way of TLR4 (see the figure).

Whereas other cell surface proteins may mediate cellular entry of adenovirus, interaction of the virus with TLR4 instead elicits intracellular signaling events that switch on production of proinflammatory cytokines such as interleukin-1β (IL-1β), IL-6, and monocyte chemotactic protein–1 (MCP1). These factors attract other inflammatory cells, thereby rapidly initiating a line of defense against the viral pathogen. Doronin *et al*. show that after TLR4 (expressed by macrophages) binds to an FX-coated adenovirus particle, it activates the transcription of proinflammatory cytokine genes through a signaling pathway that involves the intracellular adaptor molecules MyD88 and Toll–IL-1 receptor domain–containing adaptor inducing interferon-β (TRIF), and the transcription factor nuclear factor κB (NF-κB). Mutated adenovirus that cannot bind FX failed to produce this response. Thus, a component of the blood coagulation cascade enables the immune system to directly recognize a viral pathogen as opposed to exerting more general effects on inflammation or responding to components that may have been shed by pathogens or infected tissues. Other cytokine responses to adenovirus (such as IL-1α) are induced when the viral particle binds to integrin 3 on the surface of macrophages. Integrin 3 binds to the virus independently of FX or TLR but fails to trigger the full immune response to the virus (*10*). Indeed, Doronin *et al*. observed that TLR4-deficient mice were much less capable of clearing adenovirus than their wild-type counterparts.



Coated for binding. Upon entry into the blood, human adenovirus serotype 5 (HAdv5) is bound by blood clotting factor X (FX). After translocation to tissues, such as liver or spleen, resident macrophages sense the FX-bound virus through TLR4, which activates the innate immune mechanism against the virus (required for a potent antiviral response).

The activation mechanism of innate immunity identified by Doronin *et al*. is similar to aspects of adaptive immune responses. FX binding to viruses is reminiscent of antibody opsonization in which a pathogen is marked for ingestion and destruction by phagocytic cells bearing Fc receptors that recognize the antibody. FX is a "self" protein that is not immunogenic, but can elicit immune responses when bound to a carrier, such as adenovirus. Doronin *et al*. suggest that TLR4 recognizes the self-protein FX and binds directly to the FX-hexon complex. There is precedent for TLR4 recognition of a self-protein. Crystal structures demonstrate that TLR4 and the self-protein MD-2 (lymphocyte antigen 96) form a heterodimer that recognizes LPS from Gram-negative bacteria (*11*). MD-2 binds to concave surfaces of the horseshoe-shaped TLR4 and to LPS moieties, thus stimulating innate proinflammatory immune responses. The findings of Doronin *et al*. suggest a model in which FX functions in a manner analogous to MD-2 in facilitating specific binding through TLR4. HAdv5 binds to a key position on the surface of FX, resulting in the formation of a pattern estab-

[1]Department of Pediatrics University of Florida, Gainesville, FL 32610, USA. [2]Department of Pathology, Immunology, and Laboratory Medicine, University of Florida, Gainesville, FL 32610, USA. E-mail: rherzog@ufl.edu; ostroda@pathology.ufl.edu

CREDIT: Y. HAMMOND/SCIENCE

Downloaded from www.sciencemag.org on November 9, 2012

Published by AAAS

lished by the symmetry of the virus. Because FX and MD-2 have similar size and shape, FX may bind the concave surface of TLR4 that MD-2 contacts when binding LPS. Similarly, hemozoin, a disposal product of blood-feeding malaria parasites, activates TLR4 signaling when bound to fibrinogen (another coagulation factor), thereby contributing to induction of tumor necrosis factor (TNF) and MCP-1 expression (*12*).

The observation that self-proteins facilitate recognition of foreign pathogens by the innate immune system has implications for understanding the evolution of the adaptive immune system. Alternative recognition mechanisms in innate immunity, such as those mediated by FX and MD-2, could have served as early precedents to the more complex mechanisms of cellular immunity whereby peptide antigens are "presented" to T cells by self–major histocompatibility complex molecules.

Development of recombinant adenoviral vectors for human gene therapy has somewhat fallen out of favor over the past decade, but has shown recent promise for vaccination and cancer therapies (*13*, *14*). Analysis of the death of a patient in a clinical trial on hepatic delivery of recombinant adenovirus in 1999, and subsequent studies, documented the very strong and multifaceted innate immune response that can occur. Activation of multiple cell types and toxicities contribute (*15*). The adenoviral capsid and genome are detected by many different receptors, such as TLR2 and TLR9, inflammasomes (multiprotein structures that activate the inflammatory responses), and cytosolic DNA sensors, among others. Doronin *et al*. specifically investigated very early steps in the innate immune response in mice, which requires FX binding to TLR4 and subsequent TLR4 signaling for effective and rapid clearance of virus. But multiple additional mechanisms direct other steps of antiviral immunity. Thus, although adenoviral vectors are excellent models to study antiviral innate immunity, their "deimmunization" for treatment of genetic disease likely remains a challenge.

References

1. D. Davalos, K. Akassoglou, *Semin. Immunopathol.* **34**, 43 (2012).
2. M. Delvaeye, E. M. Conway, *Blood* **114**, 2367 (2009).
3. K. Doronin *et al*., *Science* **338**, 795 (2012); 10.1126/science.1226625.
4. G. M. Barton, R. Medzhitov, *Science* **300**, 1524 (2003).
5. P. Matzinger, *Science* **296**, 301 (2002).
6. Y. Okamura *et al*., *J. Biol. Chem.* **276**, 10229 (2001).
7. O. Kalyuzhniy *et al*., *Proc. Natl. Acad. Sci. U.S.A.* **105**, 5483 (2008).
8. S. N. Waddington *et al*., *Cell* **132**, 397 (2008).
9. S. J. Tai *et al*., *J. Thromb. Haemost.* **6**, 339 (2008).
10. N. C. Di Paolo *et al*., *Immunity* **31**, 110 (2009).
11. B. S. Park *et al*., *Nature* **458**, 1191 (2009).
12. V. Barrera *et al*., *Blood* **117**, 5674 (2011).
13. J. Kaiser, *Science* **334**, 29 (2011).
14. S. Nayak, R. W. Herzog, *Gene Ther.* **17**, 295 (2010).
15. Y. A. Aldhamen, S. S. Seregin, A. Amalfitano, *Front. Immunol.* **2**, 40 (2011).

10.1126/science.1230342

EVOLUTION

Constraints on Sexual Selection

Sexual selection in pronghorns is determined both by variance in mate numbers among males and by viability of the young.

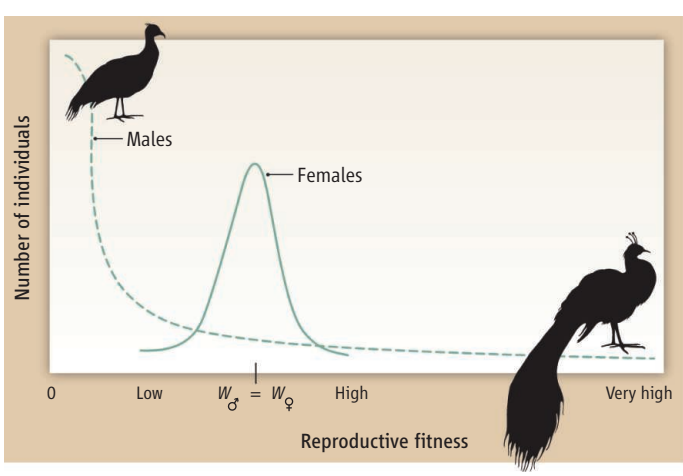
Michael J. Wade

Ever since Darwin (*1*) identified female choice of mates as a mechanism of sexual selection, it has been a challenge for evolutionary biologists to quantitatively integrate sexual selection, acting on reproductive fitness at the time of mating, with natural selection, acting on viability at other times in the life cycle. On page 802 of this issue, Byers and Dunn (*2*) report an important step toward this goal. They show how female choice of mates and offspring mortality together affect the strength of selection acting on male pronghorns, *Antilocapra americana*.

The strength of natural selection is measured by the variance in relative fitness (*3*, *4*). In sexually selected species, where males compete for reproductive access to females or females choose their mates as in the pronghorn, selection acting on males tends to be much stronger than that acting on females. Bateman (*5*) was the first to show that variation among males in mate numbers is the fundamental reason why selection acts more strongly on males. The outcome of male reproductive competition inflates the variance because, when a few males have many mates, many more males necessarily have none at all.

Bateman's insight has since been given quantitative expression (*6*, *7*). Fisher (*3*) showed that average male fitness, W_{σ}, must be related to average female fitness, W_{φ}, through the sex ratio, R, expressed as the ratio of the number of females, N_{φ}, to the number of males, N_{σ}. The variance in male fitness, V_{σ}, can also be expressed as a function of the variance in female fitness, V_{φ}, and the variance among males in mate numbers $V_{\sigma} = RV_{\varphi} + W_{\varphi}^2 V_{mates}$. It is the second term, $W_{\varphi}^2 V_{\text{mates}}$, that makes the variance of male fitness so much greater than that of females (see the first figure). The regression of mate number on offspring number is called the Bateman slope or Bateman gradient (*8*–*10*). The more steeply positive this slope, the more offspring a male gains from mating with an additional female.

In each generation, the total variance in relative fitness is a population's resource for adaptation by natural or sexual selection. Change in the average value of a trait occurs in proportion to the trait's correlation with fitness, which may change every generation. Consistency in the regression of fit-



Reproductive fitness. In this schematic, the more ornamented male (right) is chosen as a mating partner by many females, whereas the less ornamented male (left) is rejected as a mating partner. As a result, the variance in reproductive fitness of males, V_{σ}, tends to be much greater than that of females, V_{φ}, when males vary from one another in numbers of mates.

Department of Biology, Indiana University, Bloomington, IN 47405, USA. E-mail: mjwade@indiana.edu

Downloaded from www.sciencemag.org on November 9, 2012

Published by AAAS



Sexual selection in pronghorns. Byers and Dunn show that male mating success in a pronghorn population only becomes male reproductive success in years with low coyote predation on pronghorns.

ness and trait over long periods of time is necessary to allow adaptations to be exquisitely refined.

However, in evolutionary biology, most field studies of the strength of natural and sexual selection are snapshots, constructed from a portion of the life span of the species under study. Thus, few measurements of the consistency of selection exist, and for those few, it has proven difficult to separate chance variations in fitness from variations attributable to phenotypic differences between individuals (*11*). Indeed, without data across several generations or from several different populations, it is difficult to even identify the environmental factor or factors responsible for selection.

Byers and Dunn's long-term study of a closed pronghorn population (see the second figure) addresses these shortfalls in the measurement of selection. They report a positive Bateman slope in each of the 10 years of the study and convincingly rule out random variation in male mating success as its cause. Variance in mate numbers among males accounts for three-fourths of the male variance in the numbers of weaned offspring. The authors' plot of the annual distribution of individual male mating success [figure 2 in (*1*)] conforms strikingly to the very highly skewed distributions expected on theoretical grounds (*6*, *7*) to arise from strong sexual selection. Lifetime male mating success can be very high because the males that successfully mate in one season enjoy repeated mating success in subsequent breeding seasons.

The authors' repeated measurements of the Bateman slope afford the unique opportunity to use the slope itself as the dependent variable in a generalized linear model and attempt to account for its yearly variation in terms of population density, sex ratio, age structure, and fawn mortality. Byers and Dunn find a strong negative effect of fawn mortality on the Bateman slope, indicating that male mating success becomes male reproductive success only in those years when coyote predation on antelopes is low. This is an important finding because many studies of the strength of sexual selection begin and end with mating success, whereas total fitness (measured as weaned offspring) is difficult or impossible to observe in most field systems.

Furthermore, because many research programs are necessarily focused only on a portion of the life span, we rarely gain insight into the action of multiple, sequential episodes of selection. Most long-term studies have found that the strength of selection and the direction of selection vary with changes in environmental conditions. In this respect, the study of Byers and Dunn is not novel. However, unlike most studies, they discovered an interesting and opposing interaction between sexual selection and subsequent fawn viability that mitigates the former.

References

1. C. R. Darwin, *On the Origin of Species* (facsimile of 1st ed., Harvard Univ. Press, Cambridge, MA, 1964).
2. J. Byers, S. Dunn, *Science* **338**, 802 (2012).
3. R. A. Fisher, *The Genetical Theory of Natural Selection* (Dover, New York, ed. 2, 1958).
4. J. F. Crow, *Hum. Biol.* **30**, 1 (1958).
5. A. J. Bateman, *Heredity* **2**, 349 (1948).
6. M. J. Wade, *Am. Nat.* **114**, 742 (1979).
7. S. M. Shuster, M. J. Wade, *Mating Systems and Strategies* (Princeton Univ. Press, Princeton, NJ, 2003).
8. S. J. Arnold, *Am. Nat.* **144** (suppl. 1), S126 (1994).
9. A. G. Jones, G. Rosenqvist, A. Berglund, J. C. Avise, *Integr. Comp. Biol.* **45**, 874 (2005).
10. A. G. Jones, *Evolution* **63**, 1673 (2009).
11. M. D. Jennions, H. Kokko, H. Klug, *J. Evol. Biol.* **25**, 591 (2012).

10.1126/science.1230395

EPIDEMIOLOGY

Emerging Disease or Diagnosis?

Stephen K. Gire, Matthew Stremlau, Kristian G. Andersen, Stephen F. Schaffner, Zach Bjornson, Kathleen Rubins, Lisa Hensley, Joseph B. McCormick, Eric. S. Lander, Robert F. Garry, Christian Happi, Pardis C. Sabeti

Some viral infections may not represent emerging diseases, but improved detection and diagnosis of common diseases.

Outbreaks this year of the deadly and highly contagious Ebola and Marburg viruses in the Democratic Republic of Congo and Uganda and Lassa virus in Nigeria raised concerns about possible epidemic spread of these hemorrhagic fevers. These pathogens seemed to appear out of nowhere around the middle of the 20th century: Marburg virus in 1967, Lassa virus in 1969, and Ebola virus in 1976. By the early 1990s, public health concerns were crystallized in a landmark report (*1*) that was the first to popularize the concept of "emerging pathogens" (fig. S1). But could "emerging diagnosis" explain the rise in appearance of hemorrhagic fevers caused by these pathogens? Recent epidemiologic and genetic studies of Lassa and Ebola fevers suggest that these diseases may have widespread prevalence and ancient origins. They raise the possibility that some viral infections may reflect "emerging diagnoses" of diseases that are circulating more widely than thought, with an emerging character primarily a matter of improved detection of the culprit pathogens.

Emerging pathogens generally fall into two categories: microbes newly introduced to humans from other species, and existing but previously rare human pathogens that rise rapidly in prevalence or pathogenicity (*2*). Their appearance is often attributed to human encroachment on animal habitats, changing socioeconomic conditions, increased connectivity of the world, and genetic changes in the microorganisms. The concept of emerging pathogens arising through better diagnoses of disease is not commonly thought to apply to deadly viruses such as those causing Lassa and Ebola hemorrhagic fevers.

It may be that the causative pathogens of viral hemorrhagic fevers are characterized

A list of author affiliations is in the supplementary materials. E-mail: sgire@oeb.harvard.edu; psabeti@oeb.harvard.edu

Downloaded from www.sciencemag.org on November 9, 2012

CREDIT: MICHELLE GILDERS/AGE FOTOSTOCK/SUPERSTOCK

Published by AAAS

as rare because we lack the tools in the right places to routinely detect them. Contrary to popular perception, viral hemorrhagic fevers often have nonspecific symptoms such as fever, headache, and nausea, which make clinical diagnosis difficult. Without proper laboratory diagnostics, health care workers cannot accurately determine the source of fever; malaria, typhoid, or shigella is often assumed to be the culprit. Such misdiagnosis costs lives, as in a 1989 outbreak of Lassa virus in two Nigerian hospitals where 22 people died (*3*). In addition, most patients rarely present with symptoms in the hospital, and death from febrile illness is common in many developing regions of the world.

Seroprevalence surveys, which estimate the number of individuals exposed to a specific microbe (based upon the presence of antibodies for that microbe in the blood), indicate widespread exposure to Lassa and Ebola viruses in certain parts of Sub-Saharan Africa (see tables S1 and S2, and note S1). Prevalence rates for Lassa virus in surveyed regions are as high as 52% and 54.9% in parts of Sierra Leone and Guinea, respectively, with lower yet substantial rates for Nigeria (21.3%), Côte d'Ivoire (20%), Benin (9.9%), and Ghana (3.8%), suggesting that the virus is endemic in West Africa. These studies led public health officials to estimate that 100,000 to 300,000 people in West Africa become infected each year, and that Lassa infections account for as many as 15% of admissions in some regional hospitals in Sierra Leone, Guinea, and Liberia (*4*, *5*). Seroprevalence surveys of Ebola virus also indicate high exposure (table S2), with prevalence rates up to 22%, depending on the population, and 15.3% in Gabon (*6*). But the prevalence of both viruses may be higher, as assays for seroprevalence can understate actual exposure rates (because antibody concentrations in the blood wane after exposure), or lower, as they are also subject to false positives (because some assays have low specificity).

Human exposure to animal reservoirs of Lassa and Ebola viruses may underlie their widespread presence in human populations. Both viruses primarily infect nonhuman hosts, and the natural reservoirs of these hosts are abundant. Lassa virus is transmitted by the mouse *Mastomys natalensis*, which persistently maintain the infection, likely through many years of coevolution. The rodent lives in close contact with humans—in some areas, the rodents are eaten by up to 90% of the population—and a sizable fraction of the mice are infected with and shed Lassa virus. Large areas of West Africa, ranging from 10% of Ghana to 80% of Sierra Leone and Liberia, are exposed to the Lassa reservoir (*7*). The likely Ebola reservoir, the fruit bat, similarly inhabits broad swaths of Western and Central Africa (*8*).



CREDIT: S. K. GIRE

Viral discovery. Shown is a photo illustration (artistic rendition) of the Congo River in the Democratic Republic of Congo, near where Ebola virus was first discovered in 1976 (*1*). The image of the river was created to take the form of Ebola virus.

Although human outbreaks of Ebola are thought to quickly wane, a 2006 Ebola epidemic among nonhuman primates in Central Africa indicated that virus transmission can be wide-ranging and sustained. The epidemic wiped out ~95% of the exposed gorilla populations [almost 5000 animals (*9*)] and a large fraction of the chimpanzee population. Given the extreme fatality rates, it is possible that the virus was newly introduced to these populations of nonhuman primates or was a more pathogenic species or strain. In the case of a newly introduced virus, however, 12.9% of chimpanzees in Central Africa are seropositive, suggesting natural exposure and resistance (rather than the introduction of a new virus) (*10*). In 10 instances where human infection resulted from hunters handling nonhuman primate carcasses, the outbreaks had one point of origin with subsequent spread throughout Gabon, indicating that sustained transmission can occur (*11*).

Analyses of the evolutionary histories of both viruses hints at their long-time and widespread presence around the world, and possible long-standing potential for causing human disease. Lassa virus likely diverged around 500 years ago from other arenaviruses, some of which also cause hemorrhagic disease (*12*). Similarly, Ebola virus is estimated to have diverged from Marburg virus ~10,000 years ago (*13*), and itself occurs as at least five genetically distinct, stable subtypes that are dispersed geographically. Most cause disease in humans, suggesting that the virus has ancient origins and that its pathogenicity has been present for an extended period.

Multiple genomewide scans have uncovered potential evidence for human evolutionary adaptation to Lassa virus infection (*14*). Most notably, the gene *LARGE,* which encodes a protein that modifies α-dystroglycan, a cellular receptor for Lassa virus, is one of the strongest signals of natural selection in the Yoruba of Nigeria (table S3). The variants in *LARGE* (found to be under recent selection) are present only in certain West African and West African–derived populations and are estimated to have emerged between 3000 and 10,000 years ago. Establishing that the positively selected variants in *LARGE* and other identified genes confer resistance to Lassa fever would support long-term human exposure to Lassa virus.

Reports of subclinical infections suggest that natural human genetic resistance to Lassa and Ebola exists. Although fatality rates among hospital cases range from 12 to 78% for Lassa fever and 42 to 88% for Ebola fever (reference S1), the seroprevalence data and reports of asymptomatic individuals

Downloaded from www.sciencemag.org on November 9, 2012

Published by AAAS

during Ebola outbreaks indicate that there are many subclinical cases. Host immune responses may potentially restrict viral replication of both viruses (*15*). However, the degree and route of exposure to these viruses, as well as variable pathogenicity of viral species and strains, must also be considered.

How does the possibility that some "emerging diseases" are ancient and widespread affect approaches to fighting them? If exposure is indeed common, then the causative pathogens are likely already circulating—undetected—in communities and health clinics. With the right detection tools in place, we can identify where their corresponding diseases are likely to be prevalent, and begin to develop treatment, surveillance, and research capacity without waiting for the next outbreak.

Efforts to reduce the burden of Lassa fever at the Kenema Government Hospital (KGH) in Sierra Leone and the Irrua Specialist Teaching Hospital (ISTH) in Irrua, Nigeria, are informative examples. At KGH and ISTH, Lassa virus is recognized as a common cause of illness, and local and international partners work together to diagnose and treat it (*16*, *17*). These efforts have saved numerous lives and the institutions have become thriving research centers; in the process they have raised awareness nationally. In 2012, the Nigerian Federal Ministry of Health reported an increased incidence of suspected Lassa fever cases, with nearly 1000 cases reported by 41 local government agencies in 23 states, potentially due to "emergence of diagnosis."

Intriguingly, as patient outcomes for Lassa fever have improved at KGH and ISTH, the surrounding communities have become more engaged, and the sites are now referral clinics for patients with undiagnosed (or unexplained) febrile illness within hundreds of kilometers. Consequently, the sites have amassed not only numerous cases of Lassa fever but thousands of cases of unexplained fever. They provide an opportunity both to investigate Lassa virus and to identify or discover other microbes, thereby becoming sentinel sites for emerging infectious diseases.

This kind of strong and sustained partnership between local health care clinics and their communities, along with access to effective diagnostics and treatment, motivates more members of the community to seek care, resulting in a positive feedback cycle that can save lives and facilitate rapid detection of pathogens, both "emerging" ones and common pathogens whose improved detection has labeled them as emerging pathogens. Ideally, after local analysis, samples can be sent to laboratories for identification and discovery of known and new microbes through next-generation DNA sequencing. Implemented more widely, this approach could create a worldwide surveillance capacity with the ability to monitor known disease agents (including the prevalence and evolution) and to discover new disease agents. As pathogens are identified, affordable, field-deployable diagnostics could be developed to reduce the burden of disease. These efforts will thus not only have an immediate impact on affected communities, but can help detect, monitor, and characterize emerging diseases before they become global threats.

References and Notes

1. Institute of Medicine, *Emerging Infections: Microbial Threats to Health in the United States*, J. Lederberg, R. E. Shope, S. C. Oaks Jr., Eds. (National Academies Press, Washington, DC, 1992).
2. S. S. Morse, *Emerg. Infect. Dis.* **1**, 7 (1995).
3. S. P. Fisher-Hoch *et al.*, *BMJ* **311**, 857 (1995).
4. J. B. McCormick, S. P. Fisher-Hoch, *Curr. Top. Microbiol. Immunol.* **262**, 75 (2002).
5. D. G. Bausch *et al.*, *Vector Borne Zoonotic Dis.* **1**, 269 (2001).
6. P. Becquart *et al.*, *PLoS ONE* **5**, e9126 (2010).
7. E. Fichet-Calvet, D. J. Rogers, *PLoS Negl. Trop. Dis.* **3**, e388 (2009).
8. E. M. Leroy *et al.*, *Nature* **438**, 575 (2005).
9. M. Bermejo *et al.*, *Science* **314**, 1564 (2006).
10. E. M. Leroy *et al.*, *J. Infect. Dis.* **190**, 1895 (2004).
11. P. D. Walsh, R. Biek, L. A. Real, *PLoS Biol.* **3**, e371 (2005).
12. D. U. Ehichioya *et al.*, *J. Clin. Microbiol.* **49**, 1157 (2011).
13. Y. Suzuki, T. Gojobori, *Mol. Biol. Evol.* **14**, 800 (1997).
14. K. G. Andersen *et al.*, *Philos. Trans. R. Soc. Lond. B Biol. Sci.* **367**, 868 (2012).
15. S. Baize *et al.*, *Nat. Med.* **5**, 423 (1999).
16. S. H. Khan *et al.*, *Antiviral Res.* **78**, 103 (2008).
17. D. A. Asogun *et al.*, *PLoS Negl. Trop. Dis.* **6**, e1839 (2012).

Acknowledgments: The work is supported by by NIH 1DP2OD006514-01, BAA-NIAID-DAIT-NIHAI2009061, and BAA–NAID-DAIT-NIHAI2008031. We thank S. Hart, C. Edwards, J. Schieffelin, and the Sabeti Lab.

Supplementary Materials

www.sciencemag.org/cgi/content/full/338/6108/750/DC1
Figs. S1 to S2
Tables S1 to S3
Reference S1
Note S1

10.1126/science.1225893

CHEMISTRY

Driving the Formation of Molecular Knots

A molecule with a trefoil knot topology can form spontaneously through noncovalent interactions, avoiding deliberate anchoring and assembly steps.

Jay S. Siegel

Tying knots and handwriting constitute basic motor skills associated with the development of a child's conception of spatial relationships (*1*). For synthetic chemists, molecular knot tying—so-called topological stereochemistry (*2*)—often requires the slow, deliberate steps of children learning to tie their shoes. On page 783 of this issue, Ponnuswamy *et al*. report reaction conditions that appear to drive the spontaneous formation of a knotted organic molecule (*3*). Previous studies from Sanders' group under conditions known as dynamic combinatorial equilibria revealed a preference for the formation of densely packed aggregates, including topologically complex structures, such as catenanes (linked rings) (*4*). Recently, investigating the early stages of polymerization by disulfide linkage formation, they have found an unexpected product that appears to be a bona fide molecular knot.

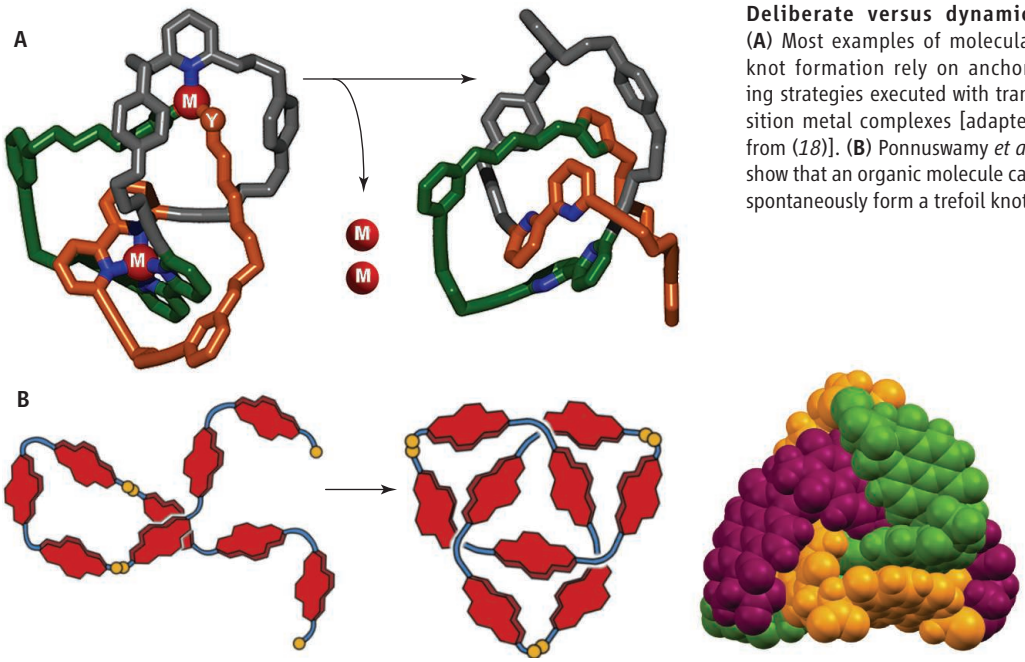
Early studies discussed the improbability of spontaneous knot formation—the accidental threading of a knot in a molecular string [see, for example, (*5*)]. Strand anchoring—holding the relative orientation of the entwined strands in place until the knot is tied off—greatly improves the chances for threading, and by using coordination bonds to transition metal complexes (*6*, *7*), one can synthesize knots in high yield and ever-increasing variety (see the figure, panel A). More elaborate anchoring scaffolds have been used to obtain trefoil-like structures, but generality is still sought (*8*).

Anchoring strategies toward the synthesis of topologically complex structures are inherently focused on kinetic control of product formation; that is, the pieces are

Organisch-Chemisches Institut, Universität Zürich, Zürich 8057, Switzerland. E-mail: jss@oci.uzh.ch

Downloaded from www.sciencemag.org on November 9, 2012

Published by AAAS



Deliberate versus dynamic. (**A**) Most examples of molecular knot formation rely on anchoring strategies executed with transition metal complexes [adapted from (*18*)]. (**B**) Ponnuswamy *et al*. show that an organic molecule can spontaneously form a trefoil knot.

held in a specific way and the new bonds are formed in a directed manner. Spontaneous assemblies such as the trefoil reported by Ponnuswamy *et al*. are rare; the Borromean linked rings reported by Stoddart and co-workers (*9*) being a signal example. In the present work, hydrophobic interactions, which favor more densely packed conformations to reduce the local disruption of water's bulk structure, drive the formation of tightly entwined knotted forms (see the figure, panel B).

From a topological perspective, molecular complexity and the emergence of new properties follows a hierarchy from linear chains through cyclic structures to links and knots. DNA can form linear or cyclic structures, and by the action of enzymes such as topoisomerases, the cyclic forms can be shuffled among various topological forms (*10*). Indeed, chemists skilled in the art of making DNA connections have led a general march toward exploiting these topologies in nanotechnology (*11*).

Although examples of knotted proteins exist, particularly among proteins with numerous disulfide linkages [see, for example, (*12*, *13*)], the majority of proteins are linearly connected. Years of investigation into the protein-folding problem attest to the rarity of robust folding or enzyme character for a random sequence (*14*). "Complex" natural products, such as terpenes and alkaloids often display cyclic and even polycyclic structures but are essentially void of any topological complexity.

Despite the successful development of small-molecule catalysts for the acceleration of reactions specific to functional group transformation, the substrate specificity, allostery, and amplification of enzymes have not been generally achieved. The field of biomimetic chemistry has attempted for years to develop highly selective enzyme-like catalysts using simple macrocycles and cyclopanes. Arguably, enzyme and complex natural product character emerges from the encoding of cooperative transstructural interactions—contacts between molecular parts disparate in linear sequence into the base structure.

In contrast to linear or simple cyclic systems, in which robust secondary structure or complex polycyclic structure are required to encode cooperative transstructural interactions, topologically entwined molecules, such as knots, links, and topologically nonplanar forms, encode such crossings at the heart of their topological taxonomy (*15*). As topological complexity increases, the number and type of transstructural interactions must also increase; thus, they offer the possibility of smaller molecules with richer properties.

Unfortunately, the synthesis of topologically complex molecules, unlike that of natural products and macrocycles, has remained a niche area (*16*). Many synthetic chemists often discount topological stereochemistry as esoteric or artistic with little chance for application. However, the synthesis of such molecules presents challenges that require new methodologies, and their properties will provide insights into complex molecule structure-function relations so far uncontemplated.

Topologically complex structures may lead to applications in pharmaceuticals and materials that go well beyond the present scope of natural products, because their structures can be highly dynamic while retaining a compact and robust manifestation of shape and functional group display (*17*). The multitude of transstructural interactions, inherent in topologically complex structures, can create cooperative networks leading to allosteric and amplification effects. Their defined but still "fuzzy" structure, combined with well-placed functional groups, offers great opportunities for obtaining protein-inspired catalysts and materials in smaller molecules.

The initial success of various anchor and spontaneous assembly strategies for the synthesis of complex molecular topologies indicates that such molecules can be obtained in a variety of forms. The spontaneous driving of the formation of molecular knots by Ponnuswamy *et al*. pushes forward this frontier. Once chemists can prepare knotted molecules with great predictability and in large quantity, the discovery of the higher-order molecular properties will follow quickly.

References

1. J. Piaget, B. Inhelder, *The Child's Conception of Space* (Routledge & Kegan Paul, London, 1956), chap. 4.
2. D. M. Walba, *Tetrahedron* **41**, 3161 (1985).
3. N. Ponnuswamy, F. B. L. Cougnon, J. M. Clough, G. D. Pantoş, J. K. M. Sanders, *Science* **338**, 783 (2012).
4. F. B. L. Cougnon, N. A. Jenkins, G. D. Pantoş, J. K. M. Sanders, *Angew. Chem. Int. Ed.* **51**, 1443 (2012).
5. H. L. Frisch, E. Wasserman, *J. Am. Chem. Soc.* **83**, 3789 (1961).
6. J.-P. Sauvage, C. Dietrich-Buchecker, Eds., *Molecular Catenanes, Rotaxanes and Knots: A Journey Through the World of Molecular Topology* (Wiley-VCH, Weinheim, Germany, 1999).
7. J.-F. Ayme *et al*., *Nat. Chem.* **4**, 15 (2012).
8. K. I. Arias, E. Zysman-Colman, J. C. Loren, A. Linden, J. S. Siegel, *Chem. Commun.* **47**, 9588 (2011).
9. K. S. Chichak *et al*., *Science* **304**, 1308 (2004).
10. J. C. Wang, *Sci. Am.* **247**, 94, 100 (1982).
11. N. C. Seeman, *Sci. Am. Rep.* **17**, 30 (2007).
12. C. Liang, K. Mislow, *J. Math. Chem.* **16**, 27 (1994).
13. L. Z. Yan, P. E. Dawson, *Angew. Chem. Int. Ed.* **40**, 3625 (2001).
14. A. L. Mallam, E. R. Morris, S. E. Jackson, *Proc. Natl. Acad. Sci. U.S.A.* **105**, 18740 (2008).
15. A. Flammini, A. Stasiak, *Proc. R. Soc. A* **463**, 569 (2007).
16. R. S. Forgan, J.-P. Sauvage, J. F. Stoddart, *Chem. Rev.* **111**, 5434 (2011).
17. X. R. Bao, H. J. Lee, S. R. Quake, *Phys. Rev. Lett.* **91**, 265506 (2003).
18. P. E. Barran *et al*., *Angew. Chem. Int. Ed.* **50**, 12280 (2011).

10.1126/science.1230319

Downloaded from www.sciencemag.org on November 9, 2012

Published by AAAS

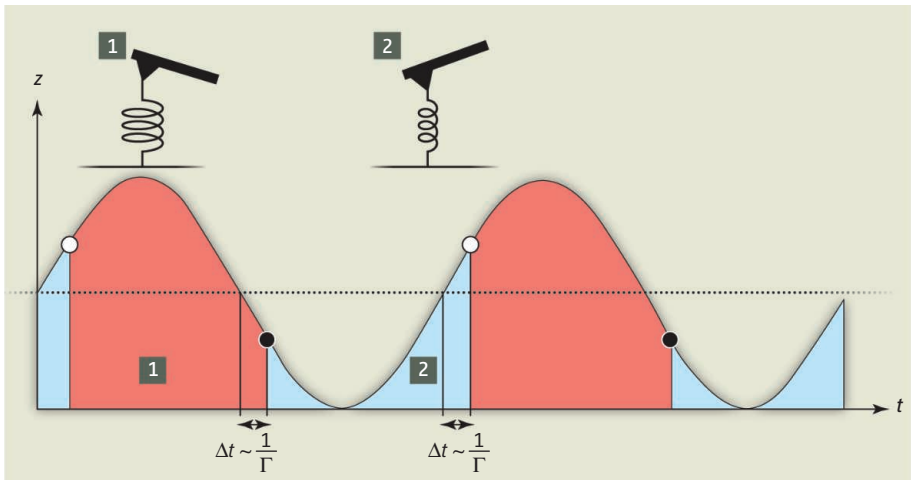
CHEMISTRY

A Single-Molecule Engine

A single hydrogen molecule can be used to drive the tip motion of a scanning tunneling microscope.

Marc W. Bockrath

In physical systems, mechanical energy usually flows from the large to the small in the form of dissipation into the random thermal motion of the molecules and atoms in the system. In biology, many natural systems have evolved to reverse this trend, enabling the flow of energy from the small to the large, with examples including photosynthesis (*1*) or motor protein motion (*2*). The desire to recreate this ability in artificial systems motivates a search for strategies and concepts that enable energy harvesting from very small subsystems. On page 779 of this issue, Lotze *et al*. (*3*) now show how the motion of a macroscopic cantilever beam can be excited using the driven motion of only a single molecule. In this case, a single hydrogen molecule is trapped between a copper surface and a scanning tunneling microscopy tip mounted on a flexible springlike cantilever. The authors find that when a particular bias voltage between the tip and copper is applied, the electric current causes the hydrogen to switch stochastically between two different positional states and the cantilever begins to oscillate spontaneously.



In the driver's seat. A simplified picture of the typical energy transfer cycle, showing the tip position above the copper surface z versus time t, plotted as the black curve. The red regions correspond to the trapped hydrogen molecule being in positional state 1, and the blue regions correspond to the hydrogen molecule being in positional state 2. In state 1, the attractive force between the hydrogen and the tip is stronger than in state 2. The horizontal dashed line marks the spatial location where the hydrogen molecule acquires a transitional lifetime between the two states, with 1 being the most probable state above the line and blue the most probable state below it. Once the threshold is crossed, a typical waiting time Δt on the order of the inverse transition rate Γ is required until the actual transitions occur, events marked by the filled ($1 \rightarrow 2$) and open ($2 \rightarrow 1$) circles. Because the force in the two hydrogen states differs, on average there is a net energy transfer to the cantilever during each cycle.

Because the hydrogen molecule and the cantilever are coupled by the molecular forces between the tip and hydrogen, which act like a spring attached to the tip, the observed oscillation results from a transfer of energy between the driven motion of the hydrogen molecule and the cantilever. Although the precise nature of the two different hydrogen positional states is not yet known, in the two states (see the figure, states 1 and 2) the effective force of the hydrogen on the cantilever differs. The electric current flowing between the tip and the substrate randomly knocks the hydrogen between the two states, producing a fluctuating force on the cantilever. To extract energy from this random motion and to transfer it to the oscillator, a vital ingredient is force hysteresis—the forces when the cantilever is approaching or receding from the surface must differ. The trick to obtaining this hysteretic force is to couple the probabilities and transition rates between the two hydrogen states to the cantilever position and motion, exploiting a phenomenon known as stochastic resonance (*4*). Lotze *et al*. accomplish this by using their finding that although the electric current randomly switches the hydrogen between the two states, the bias voltage can be tuned to a specific value so that the hydrogen positional fluctuations become highly correlated with the tip motion.

The hysteresis is then provided by the stochastic nature of the transition between the hydrogen states itself (see the figure). The tip position z is plotted as a function of time t by the sinusoidal curve. Here, starting at the arrow, the hydrogen molecule is in state 1, and when the tip crosses the spatial threshold shown by the horizontal dashed line, the probability of transition to state 2 turns on in the form of a nonzero transition rate Γ to state 2 and corresponding finite lifetime $\Delta t \sim 1/\Gamma$ for state 1. The transition typically must wait for this lifetime to happen; the event is plotted as the filled circle. The hydrogen molecule is then in state 2, corresponding to the blue region under the curve. Meanwhile, the cantilever continues its descent, finally reaching its minimum and turning around and moving upward. When the cantilever crosses the threshold again, state 2 now has a finite lifetime and again the transition takes on the order of this lifetime to occur. The hydrogen molecule makes its transition back to state 1 at the open circle. Meanwhile, the cantilever continues its upward motion, eventually turning around and continuing the cycle, corresponding to the red shaded region. In this way, although the hydrogen motion is probabilistic, on average a hysteretic force is applied to the cantilever. If it can be arranged for the force in state 2 to be less than that in state 1—as it is in the reported experiment—on average, with each cycle of motion the hydrogen will deliver a net downward impulse to the oscillator.

In reality, the spatial threshold for changing the transition probabilities between the two states is not sharp in space but smooth. Nevertheless, the detailed calculations by Lotze *et al*. show that the results are similar and account very well for their data. Another important aspect is that the energy delivered in each cycle is very small, ~10 meV. However, because it is delivered at the resonance frequency, and the intrinsic frictional losses

Department of Physics and Astronomy, University of California, Riverside, Riverside, CA 92521, USA. E-mail: marc.bockrath@ucr.edu

Downloaded from www.sciencemag.org on November 9, 2012

Published by AAAS

within the cantilever per cycle are smaller than the energy of each energy transfer, the energy from many cycles can build up enough to produce appreciable motion of the cantilever, limited ultimately by nonlinearities present in the system.

Being able to direct energy from the small to the large is an important ability if, for example, one wants to harvest chemical or other forms of energy toward powering functional nanostructures. The work of Lotze *et al*. is an intriguing demonstration of how this can work in a synthetic structure. Although the elegance and efficiency of biological systems in this regard may provide inspiration, the initial step taken by this experiment provides a strong direction for further research, toward controlling and directing large-scale motion from nanoscale or even single-molecule energy sources.

References

1. Y.-C. Cheng, G. R. Fleming, *Annu. Rev. Phys. Chem.* **60**, 241 (2009).
2. A. Gennerich, R. D. Vale, *Curr. Opin. Cell Biol.* **21**, 59 (2009).
3. C. Lotze, M. Corso, K. J. Franke, F. von Oppen, J. I. Pascual, *Science* **338**, 779 (2012).
4. L. Gammaitoni, P. Hänggi, P. Jung, F. Marchesoni, *Rev. Mod. Phys.* **70**, 223 (1998).

10.1126/science.1230530

CLIMATE CHANGE

Constraining Cloud Feedbacks

A simple diagnostic circumvents the need for measuring cloud properties, helping to improve climate sensitivity estimates.

Karen M. Shell

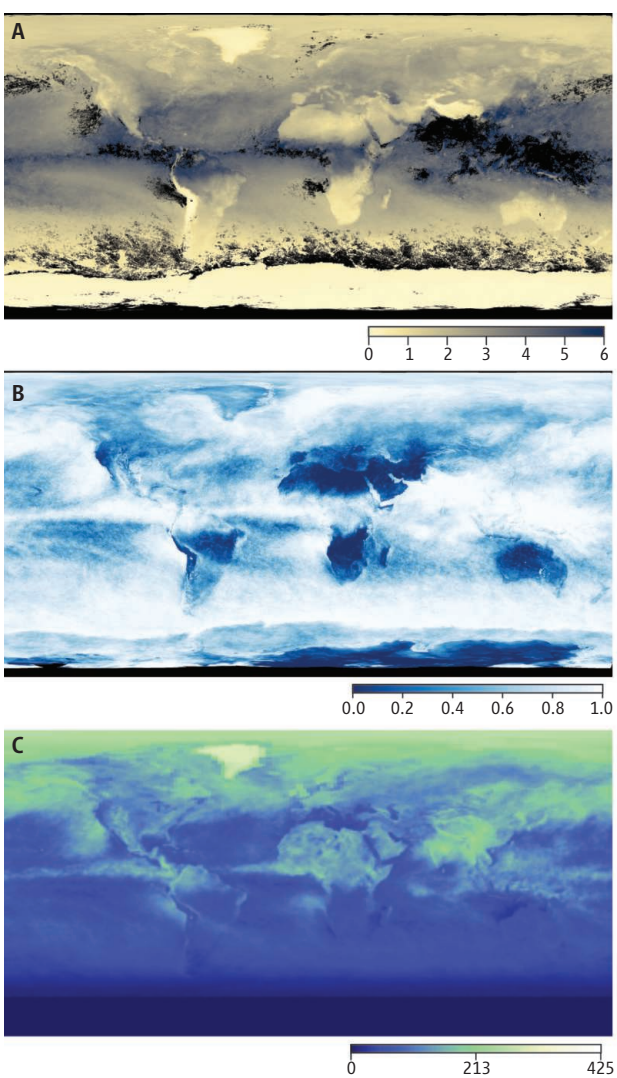
Despite decades of improvements in computer models of Earth's climate, estimates of the climate sensitivity—the change in global average surface air temperature in response to a doubling of carbon dioxide concentration—remain uncertain (*1*). Much of the uncertainty results from radiative feedbacks that amplify or dampen climate changes. Particular attention has been given to the cloud feedback. Global warming is expected to change the cloud cover, but these changes and their effects on global temperature are very difficult to predict. On page 792 of this issue, Fasullo and Trenberth (*2*) present an observational test of the cloud feedback based on satellite measurements of relative humidity (RH) in cloud-free subtropical regions. The authors focus on environmental conditions that are easier to observe than the cloud properties themselves.

Clouds cool the climate by reflecting incoming sunlight back to space, but they also warm the climate by absorbing upwelling terrestrial radiation from the surface. Their net effect is to cool the planet, but changes in clouds in response to global warming may increase or reduce this cooling. Climate models do not agree on the spatial patterns of cloud changes or their net radiative effects, and the cloud feedback is responsible for most of the uncertainty in climate sensitivity in model studies (*3*–*5*). Observational data are needed to resolve these issues.

Global, reliable satellite data are available for only a few decades, too short a time to directly observe century-scale feedbacks. Thus, determining the climate sensitivity from observations requires two nontrivial steps. First, the relation between short-term (seasonal, interannual, or decadal) and long-term feedbacks needs to be determined using models. Second, modeled short-term feedbacks must be compared to observations to test the models.

If similar processes control both short-term and long-term feedbacks—for example, cloud cover increases or decreases in a predictable manner in response to temperature increases—then these short-term observations can perhaps be used as proxies for longer-term changes. However, short-term and long-term cloud feedbacks do not appear to be correlated in models (*6*). Thus, the first step is not only difficult but may even be impossible, if short-term observations are not a guide to long-term changes.

Regarding the second step, one reason for the



Linking relative humidity to cloud feedbacks. Water vapor (in cm) (**A**), cloud fraction (**B**), and reflected solar radiation (in W/m^2) (**C**) for July 2012. Black regions in the water vapor plot indicate missing data, often due to high cloud coverage. Regions with high cloud fraction and reflected solar radiation generally coincide with high amounts of water vapor. Note in particular the subtropical regions with low reflected solar radiation. Fasullo and Trenbert use the correlations of these three fields to relate relative humidity changes to reflected solar radiation changes and, hence, cloud feedbacks.

CREDIT: (PANELS A AND B), RETO STOCKLI/NASA EARTH OBSERVATORY, DATA PROVIDED BY THE MODIS ATMOSPHERE SCIENCE TEAM/NASA GODDARD SPACE FLIGHT CENTER; (PANEL C), JESSE ALLEN/NASA EARTH OBSERVATORY, DATA PROVIDED BY THE FLASHFLUX TEAM/NASA LANGLEY RESEARCH CENTER

College of Earth, Ocean, and Atmospheric Sciences, Oregon State University, Corvallis, OR 97331, USA. E-mail: kshell@coas.oregonstate.edu

Downloaded from www.sciencemag.org on November 9, 2012

Published by AAAS

lack of success in evaluating cloud feedbacks is the difficulty of obtaining cloud properties from either satellite or surface-based observations. Assumptions of cloud droplet size or vertical distribution must go into these retrievals, and instrument error may be significant. Furthermore, due to the large temporal variability of clouds, observations at different times may result in different estimates of the cloud feedback (*7*).

Fasullo and Trenberth sidestep the difficulty in measuring cloud properties by using a quantity—the seasonal change in RH in the dry subtropics—that is easier to measure and that is strongly correlated with cloud cover. Analyzing previous model results, the authors find a strong correlation between the boreal (Northern Hemisphere) summer average of the simulated RH over the subtropical ocean (for the period 1980 to 1999) and the equilibrium climate sensitivity of climate models.

In boreal summer, the location of maximum solar heating moves north, resulting in air flow across the equator. Warm, moist air rises, loses water through rain, moves north or south, and descends in the high-pressure subtropical zones as relatively dry air (see the figure, panel A). The decreased RH makes condensation, and hence cloud formation, less likely (panel B). More sunlight is absorbed, leading to warming (panel C).

The subtropical RH does not represent merely a local process, but rather the whole subtropical atmospheric circulation. Thus, RH in these locations corresponds to cloud changes over a large region. Subtropical dry zones are expected to expand and intensify as a result of anthropogenic climate change (*8*). The strength of the annual RH cycle of the dry zones may therefore be a proxy for future changes, providing an observational constraint on models.

Fasullo and Trenberth find that only models with relatively high climate sensitivities (~4°C for a doubling of CO_2) replicate the observed seasonal RH changes. Models with large sensitivities have strong moist zones in the tropical lower troposphere and strong dry zones in the subtropical upper troposphere. An improvement of modeled subtropical dry zones may lead to better projections of future climate.

This work is but one piece of the climate sensitivity puzzle. Knowing that a modeled relative humidity is incorrect does not directly translate into the necessary model improvements, and models might not correctly simulate the dependence of cloud properties on relative humidity. Even if models capture the response of subtropical clouds to climate change, other feedbacks (including water vapor, temperature, snow and sea ice, and high-latitude cloud feedbacks) may not be related to subtropical RH or may have short-term feedbacks that differ from their long-term feedbacks. Nonetheless, the simple diagnostic reported by Fasullo and Trenberth is an encouraging step that links observations to climate sensitivity.

References

1. G. Meehl *et al.*, in *Climate Change 2007: The Physical Science Basis. Contribution of Working Group I to the Fourth Assessment Report of the Intergovernmental Panel on Climate Change*, S. Solomon *et al.*, Eds. (Cambridge Univ. Press, Cambridge, 2007), pp. 747–843.
2. J. T. Fasullo, K. E. Trenberth, *Science* **338**, 792 (2012).
3. B. J. Soden *et al.*, *J. Clim.* **21**, 3504 (2008).
4. T. Andrews, J. M. Gregory, M. J. Webb, K. E. Taylor, *Geophys. Res. Lett.* **39**, L09712 (2012).
5. A. Gettelman, J. E. Kay, K. M. Shell, *J. Clim.* **25**, 1453 (2012).
6. A. E. Dessler, *Science* **330**, 1523 (2010).
7. E.-S. Chung, B. J. Soden, A. C. Clement, *Surv. Geophys.* **33**, 733 (2012).
8. I. M. Held, B. J. Soden, *J. Clim.* **19**, 5686 (2006).

10.1126/science.1231083

MOLECULAR BIOLOGY

Epigenetic Islands in a Genetic Ocean

Mammalian methylomes reveal how DNA methylation is influenced by the underlying nucleotide sequence.

Dirk Schübeler

DNA methylation denotes the addition of a methyl group to DNA, which in eukaryotes occurs predominantly at cytosines that are adjacent to guanine (CG). Because methylation does not alter the DNA sequence, it is referred to as an epigenetic mark. The sequence symmetry of the CG dinucleotide enables propagation of the methyl mark through cell division in a process that is mechanistically well understood (*1*). This inheritability makes DNA methylation highly attractive as a potential means to store information in a form of epigenetic memory that regulates genes over developmental processes or in response to environmental conditions. However, it has proven difficult to substantiate this function because it requires showing not only that a DNA methylation pattern coincides with a particular transcriptional state, but more importantly, that it controls it.

DNA methylation appears to be obligatory in plants and vertebrates, but it is present in only a subset of fungi and insects, and its deposition pattern varies considerably among clades. Plants and lower chordates show DNA methylation primarily at genes and repetitive sequences, whereas methylation in vertebrate genomes can be almost anywhere with the exception of certain regulatory regions (*2*, *3*). A further complication is the nonuniform distribution of CG dinucleotides in mammalian genomes (*2*). CG-rich regulatory regions called CG islands are mostly unmethylated, but are efficiently repressed when methylated. Yet, CG islands make up only ~1% of our genome; for the remaining 99% that contains fewer CGs, the consequence of DNA methylation for gene regulation remains largely unclear.

Prominent examples of gene repression by DNA methylation are the CG island promoters of imprinted genes, where alleles are differentially methylated, bound by different factors, and expressed depending on the parental origin (*4*). At methylated CG islands, the sheer density of CGs could mediate repression by, for example, recruiting locally large amounts of methyl-CG–binding domain–containing proteins, which can recognize methylcytosine regardless of the surrounding sequence (*2*). Further experimental support for methylated CG islands causing gene repression comes from genetic deletions of de novo methyltransferases, which showed that a subset of genes become reactivated in the absence of methylation at linked islands (*5*, *6*).

It is also possible that certain transcription factors are sensitive to DNA methyla-

Friedrich Miescher Institute for Biomedical Research, Basel, Switzerland. E-mail: dirk@fmi.ch

Downloaded from www.sciencemag.org on November 9, 2012

Published by AAAS

tion within their binding sites (see the figure), as has been suggested for MYC and YY1 (*7*, *8*). In these cases, methylation of gene regulatory regions such as promoters and enhancers could repress gene expression by inhibiting transcription factor binding and stabilizing the off state even if these sequences are within a CG-poor region.

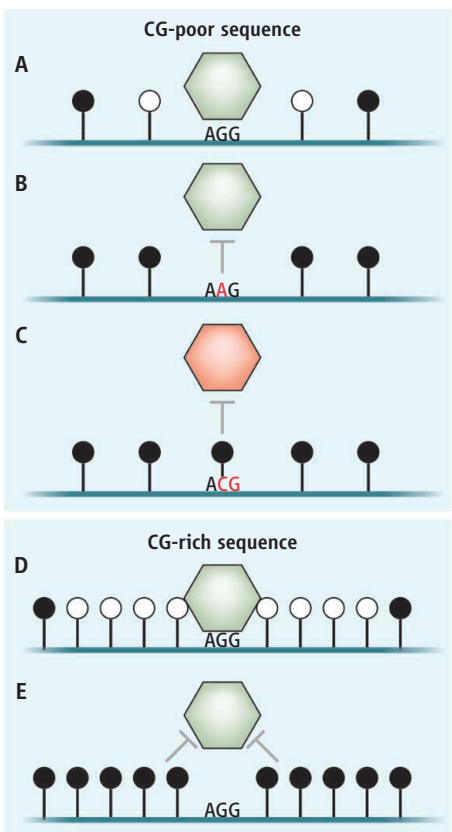
Recent advances in DNA sequencing have made it possible to measure cytosine methylation at base-pair resolution across entire genomes (*9*, *10*). The resulting methylomes of mouse and human cells have revealed new details on the genomic location of DNA methylation, particularly at CG-poor regions. Intriguingly, CG-poor distal regulatory regions show reduced amounts of DNA methylation, but only when active and occupied by transcription factors (see the figure). Although this links DNA methylation with enhancer activity, the limited experimental data available to date indicate that transcription factor binding occurs before changes in DNA methylation, thus arguing against a regulatory role for methylation in enhancer activity (*11*–*14*). While it is unclear if these findings can be generalized, it is nevertheless likely that many changes in DNA methylation at CG-poor sequences are a consequence of gene regulation rather than its cause. These observations further predict that DNA sequence variation between individuals translates into changes in methylation if they occur within regulatory regions (see the figure). Indeed, a substantial amount of the DNA methylation differences between individuals might be caused by such underlying genetic variation and thus, by definition, would not be epigenetic.

The analysis of high-resolution methylomes also exposed differences in methylation between exons and introns, suggesting that DNA methylation could be involved in regulating splicing (*15*). Although differential splicing is clearly linked to the elongation speed of the RNA polymerase (*16*), there is very little experimental evidence that methylation could modulate this (*3*). Furthermore, the observed differences in DNA methylation between exons and introns cannot readily be detected at individual genes but only become evident when the average methylation of thousands of exons and introns is calculated. It remains unclear how such subtle difference would have an effect at individual genes.

Available base-pair–resolution methylomes are limited by the static picture of DNA methylation that they provide and are uninformative with respect to the stability of the marks over time. Waves of active demethylation occur in the germ line and early embryo (*17*), and demethylation of specific loci has been reported in association with differentiation of somatic cells. However, active demethylation remains an unresolved issue because many mechanisms are theoretically possible, and because demethylation can also occur passively by lack of maintenance over cell division (*18*).

The recent discovery of the ten-eleven translocation (TET) family of enzymes (*19*, *20*) that oxidize 5-methylcytosine, however, provides a convincing mechanism for active demethylation and an opportunity to identify sites of action, because the product of the enzymatic process (5-hydroxymethylcytosine) can be detected in several ways, even at the level of individual bases (*21*, *22*). TET proteins are present in nondividing somatic cells, as is hydroxymethylcytosine, suggesting that active turnover of DNA methylation could happen in every cell. This active demethylation does not seem to occur at random. For example, TET1 localizes preferentially to unmethylated CG islands (*23*). It is unclear whether TET proteins actively generate these unmethylated states or if they safeguard them by removing any aberrantly set mark. It is further unclear whether specific proteins recognize hydroxymethylation or other demethylation products and thus if these modifications function in gene regulation. Elucidating the kinetics and sites of DNA methylation turnover is also crucial for models of epigenetic memory. Indeed, how can DNA methylation store information at a genomic site where it is constantly turned over?

Large epigenomics initiatives are currently generating base-pair methylomes in multiple tissues (*24*), which should create the needed quantitative framework to better link genotype and epigenotype. It can be expected that a large part of methylation is likely hardwired within the DNA sequence for the reasons pointed out above (*11*, *13*, *14*, *25*). Understanding this wiring will be essential to correctly interpret methylation maps and to further discriminate between sites where methylation changes are a consequence of transcription factor binding, and sites where methylation is instructive for gene regulation.



Genetics and epigenetics of transcription factor binding. (**A**) Binding of a transcription factor in CG-poor regions leads to a local unmethylated state. (**B**) Mutations in the binding site prevent binding and result in increased methylation. (**C**) Some transcription factors could be sensitive to methylation even in CG-poor regions. (**D**) Transcription factor binding in a CG-rich area (CG island) requires the region to be unmethylated, and (**E**) can be blocked if methylated. (Hexagon) Transcription factors, (black circles) methylated CG, (white circles) unmethylated CG.

References

1. J. Song, M. Teplova, S. Ishibe-Murakami, D. J. Patel, *Science* **335**, 709 (2012).
2. A. M. Deaton, A. Bird, *Genes Dev.* **25**, 1010 (2011).
3. P. A. Jones, *Nat. Rev. Genet.* **13**, 484 (2012).
4. S. Quenneville *et al.*, *Mol. Cell* **44**, 361 (2011).
5. J. Borgel *et al.*, *Nat. Genet.* **42**, 1093 (2010).
6. G. Velasco *et al.*, *Proc. Natl. Acad. Sci. U.S.A.* **107**, 9281 (2010).
7. G. Perini, D. Diolaiti, A. Porro, G. Della Valle, *Proc. Natl. Acad. Sci. U.S.A.* **102**, 12117 (2005).
8. J. Kim, A. Kollhoff, A. Bergmann, L. Stubbs,. *Hum. Mol. Genet.* **12**, 233 (2003).
9. R. Lister *et al.*, *Nature* **462**, 315 (2009).
10. S. J. Cokus *et al.*, *Nature* **452**, 215 (2008).
11. M. B. Stadler *et al.*, *Nature* **480**, 490 (2011).
12. J. Xu *et al.*, *Proc. Natl. Acad. Sci. U.S.A.* **104**, 12377 (2007).
13. M. Wiench *et al.*, *EMBO J.* **30**, 3028 (2011).
14. E. Hodges *et al.*, *Mol. Cell* **44**, 17 (2011).
15. S. Shukla *et al.*, *Nature* **479**, 74 (2011).
16. M. de la Mata *et al.*, *Mol. Cell* **12**, 525 (2003).
17. S. Feng, S. E. Jacobsen, W. Reik, *Science* **330**, 622 (2010).
18. S. K. Ooi, T. H. Bestor, *Cell* **133**, 1145 (2008).
19. S. Kriaucionis, N. Heintz, *Science* **324**, 929 (2009).
20. M. Tahiliani *et al.*, *Science* **324**, 930 (2009).
21. M. Yu *et al.*, *Cell* **149**, 1368 (2012).
22. M. J. Booth *et al.*, *Science* **336**, 934 (2012).
23. K. Williams *et al.*, *Nature* **473**, 343 (2011).
24. J. S. Satterlee, D. Schübeler, H. H. Ng, *Nat. Biotechnol.* **28**, 1039 (2010).
25. F. Lienert *et al.*, *Nat. Genet.* **43**, 1091 (2011).

10.1126/science.1227243

Downloaded from www.sciencemag.org on November 9, 2012

Published by AAAS

PRESIDENTIAL ADDRESS

Transposable Elements, Epigenetics, and Genome Evolution

Nina V. Fedoroff

Transposable genetic elements (TEs) comprise a vast array of DNA sequences, all having the ability to move to new sites in genomes either directly by a cut-and-paste mechanism (transposons) or indirectly through an RNA intermediate (retrotransposons). First discovered in maize plants by the brilliant geneticist Barbara McClintock in the mid-1940s, they were initially considered something of a genetic oddity (*1*, *2*). Several decades later, TEs acquired the anthropomorphic labels of "selfish" and "parasitic" because of their replicative autonomy and potential for genetic disruption (*3*, *4*). However, TEs generally exist in eukaryotic genomes in a reversibly inactive, genetically undetectable form we now call "epigenetically silenced," whose discovery can also be traced to McClintock's elegant genetic studies (*5*, *6*). As the underlying biochemical mechanisms emerged from obscurity and epigenetics became popular toward the end of the 20th century, it was proposed that epigenetic silencing evolved to control the proliferation of TEs and their perceived destructive potential (*5*, *6*).

Today, we know that TEs constitute more than half of the DNA in many higher eukaryotes. We know, too, that the fingerprints of TEs and transposition are everywhere in their genomes, from the coarsest features of genomic landscapes and how they change through real and evolutionary time to the finest details of gene structure and regulation. My purpose here is to challenge the current, somewhat pejorative, view of TEs as genomic parasites with the mounting evidence that TEs and transposition play a profoundly generative role in genome evolution. I contend that it is precisely the elaboration of epigenetic mechanisms from their prokaryotic origins as suppressors of genetic exchanges that underlies both the genome expansion and the proliferation of TEs characteristic of higher eukaryotes. This is the inverse of the prevailing view that epigenetic mechanisms evolved to control the disruptive potential of TEs. The evidence that TEs shape eukaryotic genomes is by now incontrovertible. My thesis, then, is that TEs and the transposases they encode underlie the evolvability of higher eukaryotes' massive, messy genomes.

I contend that it was precisely the evolution of prokaryotic epigenetic mechanisms to regulate homologous recombination within the eukaryotic genome that made it possible for genomes to grow.

Although my examples in this essay are largely from plants, I believe that the inferences drawn apply to higher eukaryotes in general, among which plants tend toward exaggeration in genome size, TE abundance, and epigenetic complexity. Perhaps because they have no recourse to behavioral responses in coping with stressful environments, plants appear to have honed genetic and epigenetic strategies for adaptation to a much greater extent than animals.

How Transposons Came to Be Called "Selfish" DNA

The invention of DNA sequencing techniques in the late 1970s and their subsequent mechanization led to an explosion of knowledge about the structure, gene content, and organization of genomes. The 1960s had seen the development of nucleic acid reassociation techniques whose application revealed the presence of much repetitive DNA in eukaryotic genomes (*7*, *8*). As DNA sequencing became a reality, a good deal of discussion arose over the value of sequencing entire genomes, particularly that of humans (*9*–*12*), in view of the calculation that only a tiny fraction of the genome consisted of genes in the then-conventional sense of protein- and structural RNA–coding sequences and their associated regulatory sequences (*13*).

A pair of papers published in *Nature* in 1980 solidified the idea that much of eukaryotic DNA, including transposons, was "junk"—a designation conferred a decade earlier by Ohno, who argued that our genomes were replete with nonfunctional DNA (*3*, *4*, *14*). The objective of the *Nature* papers was to get beyond the then

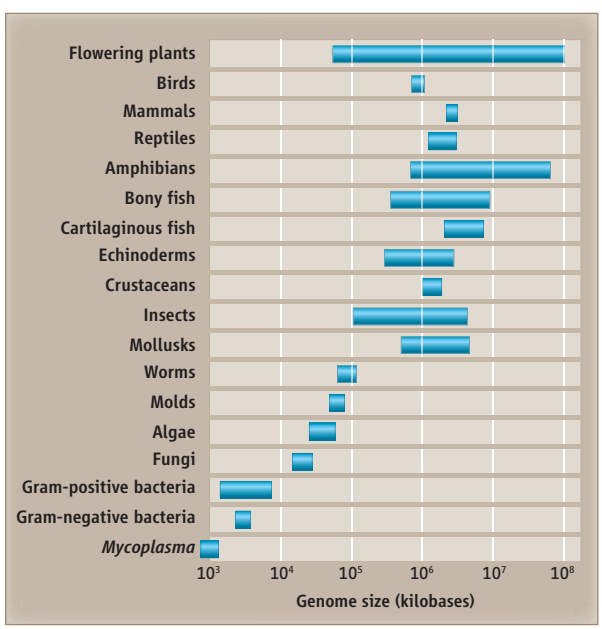


Fig. 1. The C-value paradox. The range of haploid genome sizes is shown in kilobases for the groups of organisms listed on the left. [Adapted from an image by Steven M. Carr, Memorial University of Newfoundland]

Nina V. Fedoroff is Distinguished Professor of Biosciences at the King Abdullah University of Science and Technology, Saudi Arabia, and Evan Pugh Professor in the Huck Institutes of the Life Sciences, Pennsylvania State University. She served as the Science and Technology Adviser to the Secretary of State and to the Administrator of the U.S. Agency for International Development (USAID) from 2007 to 2010. She was president of AAAS from February 2011 to February 2012. This article is based on the Presidential Address she delivered at the AAAS annual meeting in Vancouver, BC, on 16 February 2012. E-mail: nvf1@psu.edu

Downloaded from www.sciencemag.org on November 9, 2012

Published by AAAS

still-prevalent view that every bit of an organism's DNA has a specific function crafted by selection. Thus, both papers promoted Dawkins' concept of "selfish DNA"—the notion that DNA capable of proliferating within a genome, as TEs do, may need no other explanation for its survival (*15*). Orgel and Crick asserted, "The spread of selfish DNA sequences within the genome can be compared to the spread of a not-too-harmful parasite within its host" (*3*).

The selfish DNA concept was initially offered to explain the long-standing C-value paradox that organisms of similar evolutionary complexity differ vastly in their DNA content (*16*), and this it did. The C value, which is the DNA content per haploid genome, varies widely among closely related organisms of apparently comparable complexity (Fig. 1); this has for some time been attributed to the repetitive portion of the genome (*17*). Such variation is especially striking in angiosperms, whose highest and lowest C values differ by a factor of 2000 (*18*, *19*). The explanation of the C-value paradox does indeed reside largely in the profound differences among genomes in the abundance of TEs, primarily retrotransposons, even as gene numbers remain relatively constant. The *Arabidopsis* genome, for example, contains about 27,000 genes and 20 to 25 Mb of retrotransposons, whereas the maize genome contains about 40,000 genes and more than 1800 Mb of retrotransposon sequences (*20*–*22*). What the selfish DNA hypothesis does not attempt to explain, however, is how genomes can accumulate such vast amounts of repetitive sequences, given the ease of eliminating them by homologous recombination.

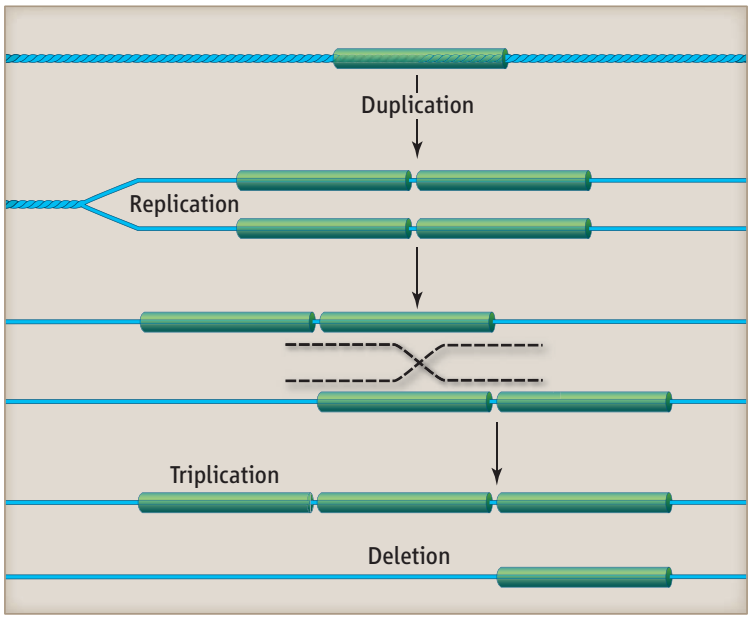


Fig. 2. Generation and elimination of duplications by unequal crossing over. Broken lines trace the recombination event.

The Selfish DNA Label Stuck

Fortunately, genome sequencing raced forward, and today we have a vastly more complex understanding of genome structure and organization than we might have had if sequencing had been restricted to protein- and RNA-coding sequences. But we find ourselves neck deep in TEs: Transposon and retrotransposon sequences constitute two-thirds of our own genome and 85% of the corn genome (*21*, *23*). Ideas about junk DNA have evolved substantially over the past two decades, with growing knowledge of the regulatory roles fulfilled by noncoding sequences and their transcripts (*24*, *25*). However, the transposon monikers from the selfish DNA papers have persisted. Having cloned the first mammalian DNA methyltransferase gene and realizing that its methyltransferase domain resembles those of prokaryotic restriction methyltransferases, Bestor proposed in 1990 that eukaryotic DNA methylation had evolved to regulate gene expression in development and chromosome structure, much along the lines of earlier proposals (*26*–*28*). But by the end of the decade, he and his colleagues had concluded that because cytosine methylation is predominantly found in TEs, methylation was more likely to represent a nuclear defense system that had evolved precisely to "control" the destructive potential of "parasitic sequences," mostly transposons and retrotransposons (*5*, *29*). This view was widely accepted, and transposons are today almost universally referred to as "invaders," "parasites," or "parasitic sequences" (*30*–*33*).

Does the notion that epigenetic mechanisms evolved to control invading "parasitic" transposons still fit the facts in the light of the many that have accumulated since this hypothesis was first advanced? Perhaps not. The difficulty starts with the question of where such parasites might have come from. It turns out that genes encoding transposases, which all have certain common structural motifs in their catalytic cores, are present throughout eukaryotes (*34*) and can be traced back into prokaryotic organisms that do not have the elaborate epigenetic regulatory superstructure of eukaryotes (*35*). That is, transposons were around long before the eukaryotic lifestyle, with its bloated genomes, appeared on the evolutionary scene. This implies that transposons coevolved with all the rest of the eukaryotic genome's inhabitants. Moreover, prokaryotic transposition is minimized and regulated by mechanisms that are similar to those in eukaryotes, including weak, enhancer-insensitive promoters, transposon-encoded regulatory proteins and regulatory RNAs, and DNA methylation (*36*–*39*). Yet prokaryotic genomes carry only modest numbers of transposons.

I argue that transposable elements accumulate in eukaryotic genomes because of, not despite, epigenetic silencing mechanisms.

It is true that the ability of eukaryotic transposons and retrotransposons to accumulate in large numbers, together with their highly generic transposition mechanisms, means that the proliferation of a transposon introduced into a genome lacking it—whether by a genetic cross or a virus—makes it resemble an "invader" (*40*, *41*). And indeed, there is growing appreciation that transposons are subject to horizontal transfer in eukaryotes, in some cases through host-parasite interactions (*42*–*46*). But the same is true of prokaryotic transposons (*37*). As well, new transposons can arise within a genome and silent transposons can be mobilized anew by a variety of physiological and genetic stresses, undergoing "bursts" of transposition to expand genomes over millennia before being silenced and decaying (*47*) or being silenced quickly within a generation (*48*).

Downloaded from www.sciencemag.org on November 9, 2012

Published by AAAS

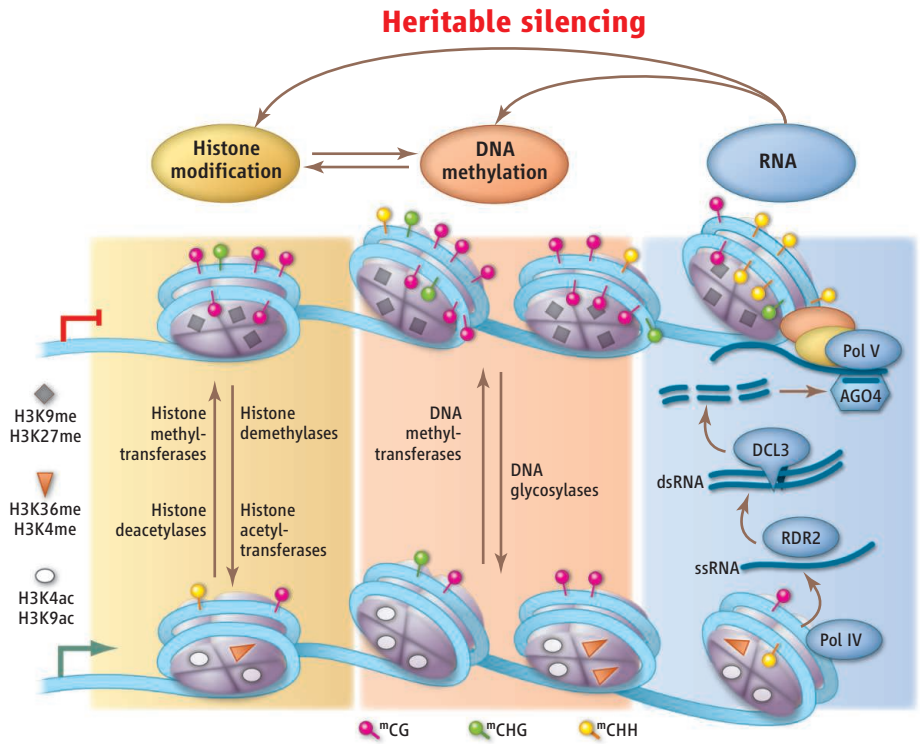


Fig. 3. Plant epigenetic mechanisms include DNA methylation, histone modification, and RNA-directed DNA methylation (RdDM). RdDM involves two plant-specific RNA polymerases (Pol IV and Pol V), an RNA-dependent RNA polymerase (RDR2), an enzyme that cleaves double-stranded RNA (DCL3), and an Argonaute-family RNA-binding protein (AGO4). [Adapted with permission from (*199*)]

How Do Genomes Get So Fat?

There's perhaps a deeper problem than the ancient origin of transposons. What distinguishes the organization of higher eukaryotic genomes from that of prokaryotes is the presence of vast amounts of duplicated DNA. It has long puzzled me that we almost universally take this for granted. But then, eukaryotes also have a markedly more complex, largely epigenetic system than do prokaryotes for managing the transcription, reproduction, and recombination of genetic material, as well as its distribution to daughter cells during mitotic and meiotic divisions. Which is cause and which is effect?

Prokaryotes can readily duplicate genome segments by virtue of small stretches of homology, but tandem duplications are rapidly lost unless retained by selection, and even then, they are generally interspersed with nonhomologous sequences (*49*–*51*). This is illustrated diagrammatically in Fig. 2. Absent either selection or a reduction in homology, tandem duplications are inevitably eliminated by homologous unequal intra- or interchromosomal crossing over between duplicated sequences, generating one-copy organisms (an absorbing state) and organisms with increasing numbers of copies that in turn throw off singletons (*50*, *52*). Organisms with many copies are quite unstable and are likely to be eliminated, either by virtue of the energetic drag of the extra DNA or by a population bottleneck. This is borne out by the observation that duplicate genes in prokaryotes are generally acquired by horizontal gene transfer rather than by duplication (*53*, *54*).

The "selfish DNA" argument rests on the assumption that there exists a category of DNA that has little or no phenotypic effect, and hence is not subject to selective pressure, but can nonetheless multiply within the genome. This is not an unreasonable inference, because we know that eukaryotic genomes are packed with repetitive DNA of all kinds. But I find it quite remarkable that it passes unremarked. How did eukaryotes tip the balance between duplication and deletion that keeps genome size small in organisms in which homology-dependent recombination mechanisms predominate? And how can transposons, whose duplicative mechanisms create dispersed repetitive sequences, build up in large numbers, given the ability of homologous recombination among them to cause major, even catastrophic, chromosomal rearrangements?

What Epigenetic Mechanisms Do and How They Came to Be

I believe that the answer to these questions lies precisely in the epigenetic mechanisms that eukaryotes have elaborated to a much greater extent than prokaryotes. Repressive protein complexes, histone methylation, RNA interference (RNAi), and RNA-directed DNA methylation, as well as recombinational regulatory complexes, are among the epigenetic mechanisms that have so far surfaced (*55*–*59*). These serve a variety of structural and regulatory functions, but perhaps the essential one for understanding the evolution of eukaryotic genomes is the minimization of illegitimate and ectopic recombination among homologous sequences during DNA replication and the DNA break-repair processes that maintain genome and chromosome stability.

Heterochromatin, the highly compacted chromosome regions rich in repetitive DNA, is recombinationally inert (*60*, *61*). Although not all eukaryotes use all of the known epigenetic mechanisms, even lower eukaryotes with relatively small genomes use RNAi to stabilize repetitive DNAs, such as ribosomal RNA genes and centromeric repeats (*61*–*63*). In fission yeast, noncoding transcripts of repetitive sequences initiate a process that generates small RNAs, which in turn target further transcripts for degradation and attract protein complexes that induce heterochromatization through histone modification (*64*, *65*). Disruption of the RNAi machinery disturbs the repair of double-strand breaks, stimulating repair by homologous recombination (*66*).

The evolutionary origins of the eukaryotic epigenetic regulatory machinery lie in bacterial systems that discriminate endogenous DNA from that acquired through horizontal gene transfer and bacteriophage infection (*67*–*69*). Although prokaryotic transposons can move both by conjugation (commonly on plasmids) and on bacteriophage, they do not appear to have been independently targeted for inactivation by either the restriction-modification system or the CRISPR (clustered regularly interspaced short palindromic repeat)–*cas* (*CRISPR-associated*) interference pathway (*70*). This recently discovered bacterial pathway confers sequence-specific immunity to phage and plasmids and exhibits parallels with eukaryotic RNAi systems, particularly the Piwi-interacting RNA

CREDIT: K. SUTLIFF/SCIENCE

Downloaded from www.sciencemag.org on November 9, 2012

Published by AAAS

system of *Drosophila* (*71*, *72*). Cytosine methylation is widespread in both prokaryotes and eukaryotes, and eukaryotic DNA methylases evolved from bacterial restriction-modification methylases by acquiring new recognition and binding modules (*69*). The evolution of DNA methylases appears to have proceeded in parallel with that of histone-modifying enzymes and RNA-based silencing mechanisms, so that today they comprise intimately interconnected systems (*68*, *69*). Some eukaryotes lack either DNA methylation or the RNAi machinery (or both), but nonetheless exhibit epigenetic silencing; hence, there is some redundancy among silencing mechanisms (*73*, *74*). Precisely how these disparate systems came together is not yet known, but the evolutionary genius of linking RNAi feedback mechanisms to the heritability of the DNA methylation mechanism means, of course, that silencing can be inducible, sequence-specific, and heritable.

My contention is that it was precisely the evolution of prokaryotic epigenetic mechanisms, originally limiting recombination among horizontally exchanged sequences, to regulate homologous recombination within the eukaryotic genome that made it possible for genomes to grow. Interference with DNA methylation, histone modification, and the small RNA pathways of contemporary genomes generally destabilizes repetitive regions, both tandem and dispersed (*48*, *61*, *62*). The ability to suppress homologous recombination might well be what tipped the balance between duplication and deletion in favor of sequence endo-reduplication in general and transposon proliferation in particular. The fact that small diffusible RNA molecules are at the heart of the silencing machinery also means that new copies of transposons cannot evade regulation by moving to new locations where the ability to cause severe chromosomal disruptions through ectopic homologous recombination might consign them to the scrap heap of evolution. What I am suggesting, then, is that TEs accumulate in eukaryotic genomes because of, not despite, epigenetic silencing mechanisms. This is exactly the inverse of the "parasite control" hypothesis, which posits that epigenetic mechanisms arose to control invading, parasitic transposons (*5*).

The ability to retain duplicated sequences is also arguably a critical step in the evolution of multicellular organisms, underpinning the ability to diversify duplicates for expression in specific cells and tissues, at different developmental moments, and in response to different environmental stimuli (*75*). Equally key is the ability to program genes for differential expression by a variety of mechanisms, among which are the relatively stable ones involving DNA and histone modification, as well as the more labile small RNA–mediated and transcriptional mechanisms. On balance, then, the likelihood that contemporary eukaryotic genomes evolved in the context of epigenetic mechanisms seems vastly greater than the likelihood that they were invented as an afterthought to combat a plague of parasitic transposons.

Plant Genomes Do It More

Plants have a more complex and redundant array of epigenetic silencing mechanisms than animals, making use of multiple DNA methylation mechanisms, chromatin protein modification, and feedback mechanisms involving small noncoding RNAs (*55*, *58*, *76*). Mammals primarily methylate the C residues in the CG dinucleotide context, whereas plants methylate C residues in nucleotides within all sequence contexts (*55*,

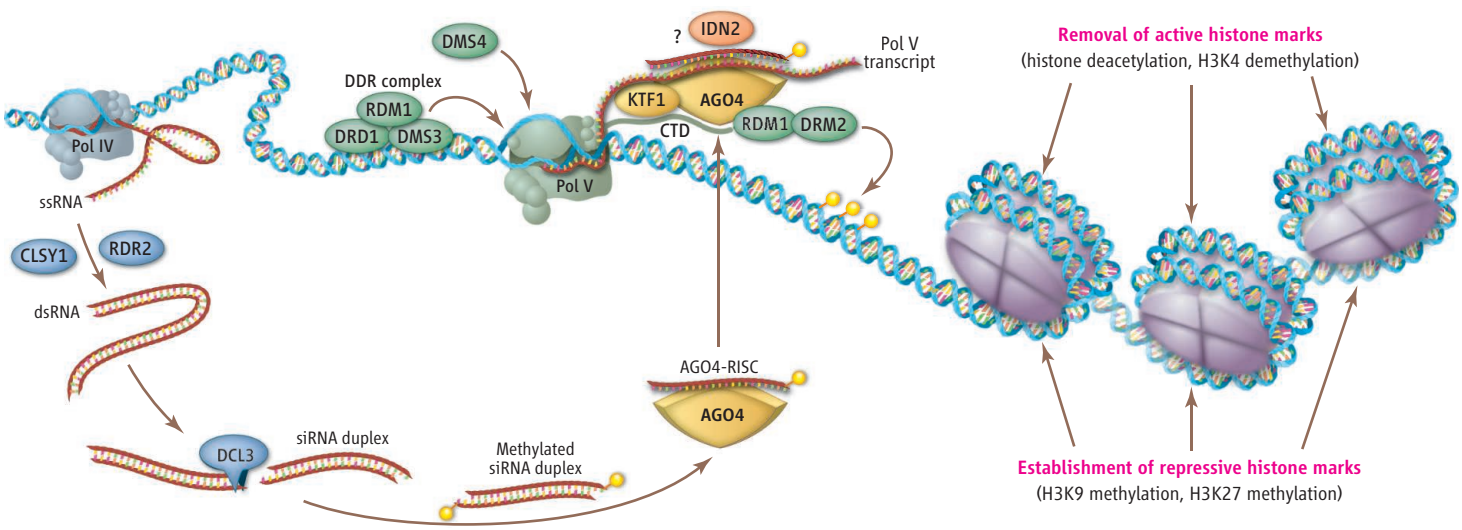


Fig. 4. The RNA-directed DNA methylation pathway. RNA polymerase IV (Pol IV) initiates RdDM, generating single-stranded RNA (ssRNA) that is then copied into double-stranded RNA (dsRNA) by RNA-DEPENDENT RNA POLYMERASE 2 (RDR2). The putative chromatin remodeler and/or helicase CLASSY 1 (CLSY1) assists in one or more of these steps. DICER-LIKE 3 (DCL3) cleaves the dsRNA into 24-nucleotide small interfering RNA (siRNA) duplexes that are then methylated at their 3′ ends by HUA-ENHANCER 1 (HEN1). A single strand of the siRNA duplex associates with ARGONAUTE 4 (AGO4) to form an RNA-induced silencing complex (RISC)–AGO4 complex. Independently of siRNA biogenesis, Pol V transcription is assisted by the DDR complex [DRD1 (DEFECTIVE IN RNA-DIRECTED DNA METHYLATION 1), DMS3 (DEFECTIVE IN MERISTEM SILENCING 3), and RDM1 (REQUIRED FOR DNA METHYLATION 1)] and DMS4. AGO4 binds Pol V transcripts through base-pairing with the siRNA and is stabilized by AGO4 interaction with the NRPE1 (the largest subunit of Pol V) C-terminal domain (CTD) and KTF1 (KOW DOMAIN-CONTAINING TRANSCRIPTION FACTOR 1), which also binds RNA. IDN2 may stabilize Pol V transcript–siRNA pairing. The RDM1 protein of the DDR complex binds AGO4 and the de novo cytosine methyltransferase DOMAINS REARRANGED METHYLTRANSFERASE 2 (DRM2), bringing them to Pol V–transcribed regions, resulting in DNA methylation. Histone modifications resulting from the RdDM pathway include the removal of activating acetylation and methylation marks [deacetylation of multiple Lys of several core histone proteins and demethylation of histone H3 Lys^4 (H3K4)] and the establishment of alternative, repressive histone methylation marks (such as the methylation of H3K9 and H3K27), thereby facilitating transcriptional silencing. [Adapted with permission from (*80*)]

CREDIT: K. SUTLIFF/*SCIENCE*

Downloaded from www.sciencemag.org on November 9, 2012

Published by AAAS

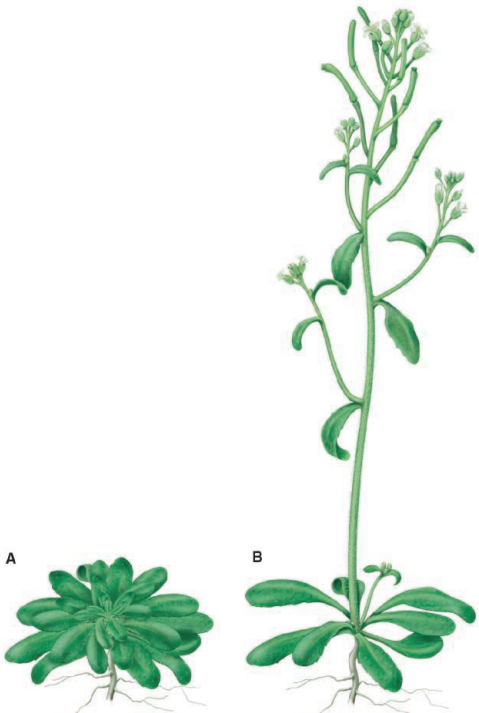


Fig. 5. Vernalization. *Arabidopsis* plants requiring vernalization grow vegetatively (**A**) unless exposed to a period of cold to induce flowering (**B**). Vernalization involves cold-induced epigenetic silencing of the *FLC* gene, a repressor of flowering.

77). DNA methylation stabilizes the silencing and inactivation of genes and other genetic elements in many eukaryotes, but is not universal; *Drosophila* and budding yeast represent well-investigated exceptions (*55*, *78*). Chromosomal protein modification, particularly histone 3 methylation, is involved in guiding DNA methylases to their correct targets in both plants and animals (*55*, *79*). In plants, unmethylated DNA is methylated by one DNA methyltransferase, whereas maintenance methylation involves two additional DNA methyltransferases (*55*). Figure 3 shows an overview of the several epigenetic mechanisms currently known to exist in plants.

Sequence specificity is imparted to DNA methylation through a mechanism called RNA-directed DNA methylation (RdDM) (*57*, *58*). RdDM involves two unique plant RNA polymerases, Pol IV and Pol V, and is mediated by 24-nucleotide small interfering RNAs (siRNAs) (*55*, *57*, *80*). As illustrated in Fig. 4, RdDM is initiated by conversion of Pol IV–generated transcripts to RNA duplexes by an RNA-dependent RNA polymerase (RDR2). The duplexes are then cleaved into 24-nucleotide siRNAs by an RNAse III–family enzyme (DCL3) and the appropriate strand associates with the Argonaute family protein AGO4 (*55*, *80*, *81*). This leads to the formation of a complex comprising the AGO4-siRNA and a number of other proteins (including a DNA methylase, DRM2), which then triggers local DNA methylation (*57*, *80*, *82*). As well, activation of RdDM promotes histone deacetylation and methylation changes that lead to the establishment of chromatin structures that repress transcription (*57*, *80*). Plant DNA demethylation is mediated by one of several DNA glycosylase activities that removes the 5-methylcytosine, after which the DNA backbone is cleaved at the abasic site and repaired (*83*).

Why and exactly how the different epigenetic systems evolved remains to be understood. But plants use epigenetic systems today in a variety of developmental contexts. Unlike higher animals, plants do not set aside a germ line early in development; this imposes more stringent requirements for maintaining genetic integrity, because differentiated genomes must eventually be reprogrammed for reproduction. So the elaboration of epigenetic mechanisms may have made possible the indeterminate lifestyle of many higher plants and their ability to reproduce in response to environmental signals. Epigenetic mechanisms, for example, regulate such environmentally responsive developmental transitions as vernalization, a cold-temperature requirement for germination or the transition to flowering, the reproductive phase. For example, *Arabidopsis* plants requiring vernalization grow vegetatively unless exposed to a period of cold to induce flowering, as illustrated in Fig. 5 (*84*, *85*). Vernalization is mediated by cold-induced epigenetic silencing of the *FLOWERING LOCUS C* (*FLC*) gene that encodes a repressor of flowering. The silencing increases with the duration of the cold period, involves production of noncoding *FLC* transcripts, and results in histone modifications that inactivate transcription of the gene (*86*).

Although transposons are primary targets for epigenetic silencing, they are far from the only targets in plants. The first plant gene silencing mechanism understood at the molecular level was that underlying the long-known ability of a viral infection to cross-protect a plant against infection by a closely related virus (*87*–*90*). Then, in 1994, it was reported that a wholly artificial gene comprising a viroid cDNA became methylated and transcriptionally inactive in the tobacco genome, but only if viroid RNA replication had occurred, suggesting a feedback mechanism initiated by transcript overabundance (*91*). It was subsequently discovered in the early days of plant molecular modification that an introduced transgene encoding an

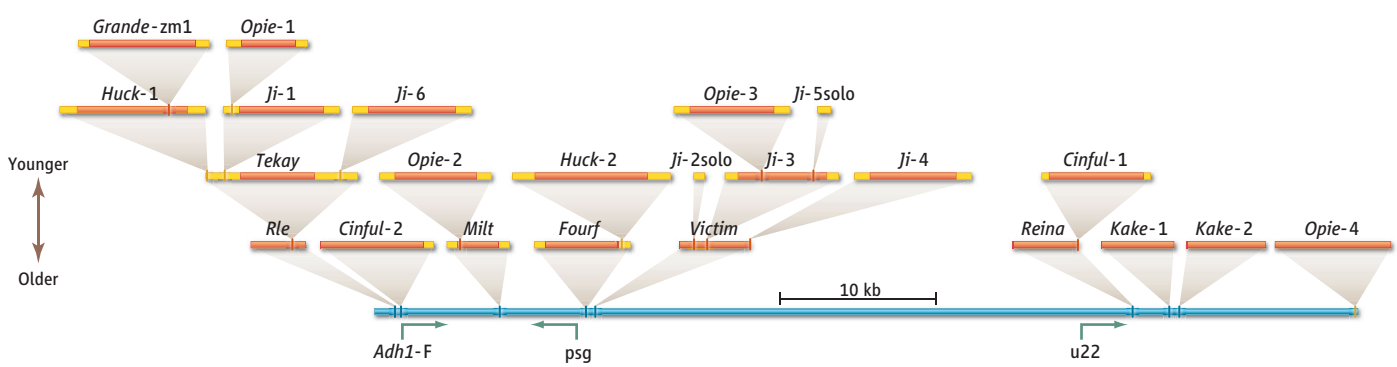


Fig. 6. The arrangement of retrotransposons in the maize *adh1*-F region. The short lines represent retrotransposons, with the internal domains represented in orange and the LTRs in yellow. Younger insertions within older insertions are represented by the successive rows from the bottom to the top of the diagram. Small arrows show the direction of transcription of the genes shown under the long blue line that represents the sequence in the vicinity of the *adh1* gene. [Adapted with permission from (*102*)]

CREDIT: K. SUTLIFF/*SCIENCE* (FIG. 5)

Downloaded from www.sciencemag.org on November 9, 2012

Published by AAAS

enzyme in the pigment biosynthetic pathway was subject to silencing (*92*–*94*). Later studies found that silencing entails both transcriptional and posttranscriptional mechanisms, and that these mechanisms share characteristics with those used by plants to control viral pathogens and are mediated by the production of siRNAs (*95*, *96*). Sequence duplication also underlies a reversible silencing phenomenon, termed "paramutation," in which an allele termed "paramutagenic" can heritably silence a susceptible allele termed "paramutable" of the same locus residing on the homolog (*97*). Paramutation involves a small RNA feedback mechanism and DNA methylation triggered by duplication of either coding or regulatory sequences (*98*, *99*). Thus, the repetitive character of the sequence is also a common trigger for siRNA-mediated gene silencing and methylation (*100*).

The Contemporary Plant Genome Landscape

Despite the multiplicity of plant epigenetic silencing mechanisms, the fingerprints of transposition and recombination are evident at every level of plant genome structure, organization, and evolution. Maize genes are clustered in small groups separated by long, uninterrupted stretches of DNA consisting of retrotransposons (*101*, *102*). Almost 85% of the contemporary 2.3-Gb maize (*Zea mays* or corn) genome comprises transposons, more than 75% of which are long terminal repeat (LTR) retrotransposons (*21*). Its roughly 40,000 genes, averaging about 3.3 kb in length, form small islands in a sea of more than a million transposons and retrotransposons belonging to almost 1300 different gene families.

In addition to forming very large blocks, retrotransposons exhibit a tendency to home to different neighborhoods. In maize, for example, *gypsy* and *copia* elements are over- and underrepresented in pericentromeric regions, respectively (*21*, *103*). Within a retrotransposon block, younger elements are progressively nested within older elements, as illustrated in Fig. 6 for a short region near the maize *adh1* gene (*21*, *102*, *103*). Such targeting can occur through the interaction of retrotransposon-specific proteins and chromatin proteins, which are themselves preferentially associated with certain types of sequences. An example is provided by the interactions of yeast Sir4p, a structural protein of heterochromatin, with a 6–amino acid motif of the Ty5 integrase protein that targets insertion into telomeric heterochromatin (*104*, *105*). An *Arabidopsis lyrata*

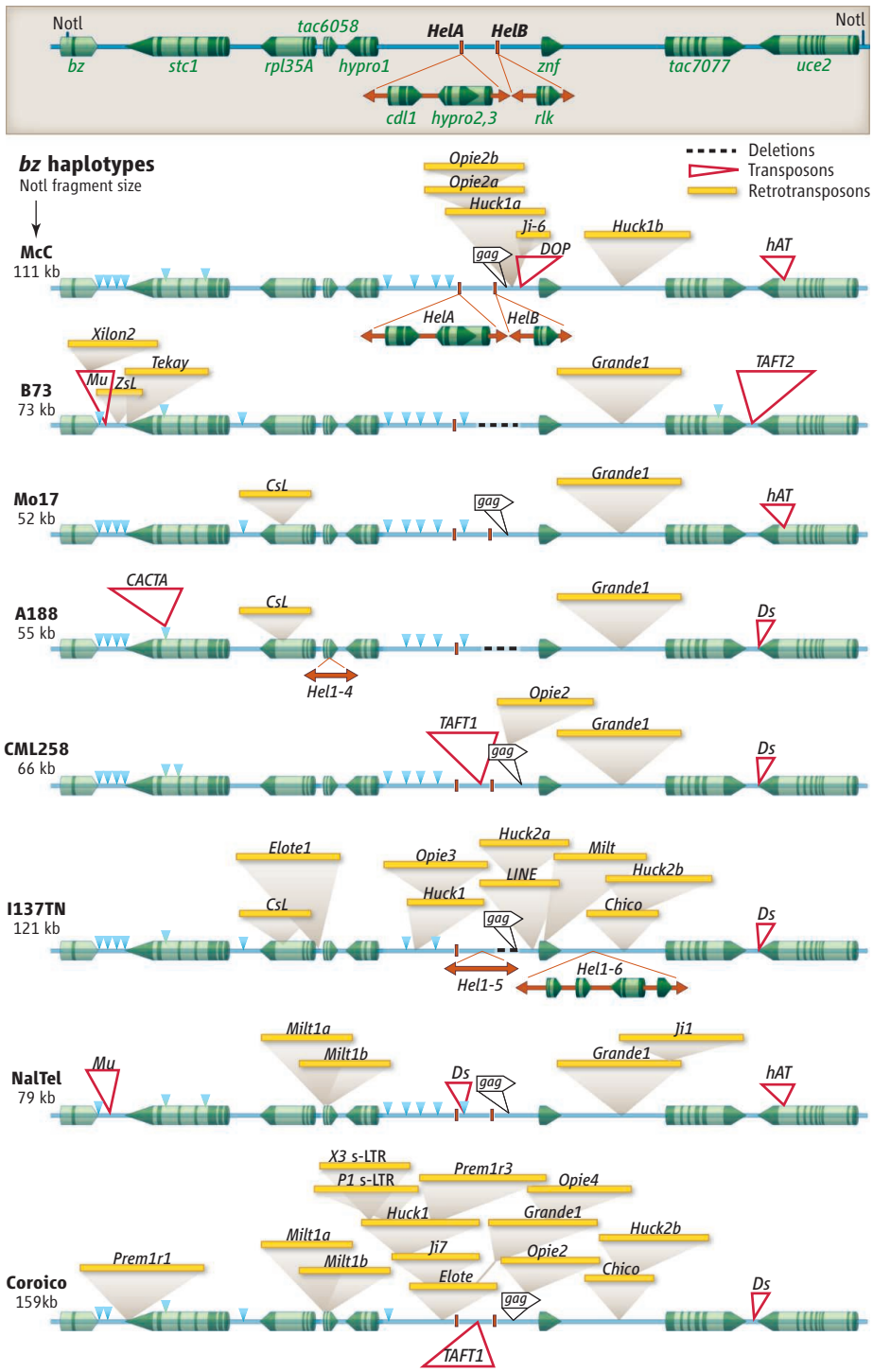


Fig. 7. The organization of the sequence adjacent to the *bronze* (*bz*) gene in eight different lines (haplotypes) of maize. The genes in this region are shown in the top diagram: *bz*, *stc1*, *rpl35A*, *tac6058*, *hypro1*, *znf*, *tac7077*, and *uce2*. The orientation of the gene is indicated by the direction of the green pentagon, pointing in the direction of transcription; exons are represented in dark green and introns in light green. Each haplotype is identified by its name and the size of the cloned NotI fragment. The same symbols are used for gene fragments carried by Helitrons (Hels), which are represented as bidirectional arrows below the line for each haplotype. Vacant sites for *HelA* and *HelB* are provided as reference points and marked by short vertical red bars. Dashed lines represent deletions. Retrotransposons are represented by yellow bars. DNA transposons and TAFTs (TA-flanked transposons), which are probably also DNA transposons, are represented by red triangles; small insertions are represented by light blue triangles. [Redrawn with permission from (*113*)]

Downloaded from www.sciencemag.org on November 9, 2012

Published by AAAS

centromeric retrotransposon was reported to insert preferentially into centromeres in *A. thaliana* (*106*). Because the centromeric sequences are quite different in the two species, targeting is likely to involve an interaction with the highly conserved centromere-specific structural proteins.

Unlike retrotransposons, which replicate through an RNA intermediate and reinsert DNA copies, DNA transposons move by a cut-and-paste mechanism, generally excising from just one newly replicated sister chromatid and reinserting into a site either nearby on the same chromosome or elsewhere in the genome (*107*). Because a copy of the transposon is retained at the donor site, such transposition events commonly give rise to additional transposon copies. DNA transposons account for a much smaller fraction of the plant genome than retrotransposons, are generally present in fewer copies, and tend to be associated with genic regions, some even inserting preferentially into genes (*108*). Mu transposons in maize favor recombinationally active regions of the genome (*109*), whereas Helitrons accumulate near but not inside each other (*110*). Such clustering may reflect the propensity of some TEs to move to nearby sites, long documented for the *Ac/Ds* (*Activator/Dissociation*) transposon family of maize (*111*).

The Rapid Pace of Plant Genome Change

Genome divergence through TE activity and recombination are ongoing processes that occur within species at surprisingly high rates. For example, a comparison among maize inbred lines revealed major differences within a region of just 150 kb surrounding the *bronze* gene in both TE abundance and composition (Fig. 7) (*112*, *113*). Speciation—the process by which subgroups of a reproductively compatible population become reproductively isolated—occurs by a variety of mechanisms, some of which involve both transposon mobilization and active genome restructuring. The genomes of newly formed plant species are necessarily similar, and the gene order is largely colinear. As the evolutionary distance increases, the colinearity declines rapidly, although the number and nature of the genes remain more or less constant (*114*, *115*). Such evolutionary scrambling of genomes is illustrated in Fig. 8, which traces orthologous sequence blocks among familiar grass genomes (*116*).

It has long been known that genes change their chromosome locations, and it has been speculated that transposons mobilize large DNA segments because they are often found at the ends of inverted or transposed sequence (*117*–*120*). McClintock's initial studies on the *Ac/Ds* transposon family showed that chromosome breaks at the site of insertion of a nonautonomous *Ds* element could be resolved with attendant duplications, deletions, inversions, and translocations of large chromosomal segments (*121*, *122*). More recent studies on *Ac/Ds*-associated rearrangements at the P locus identified transposition events that initiate at the 5′ end of one transposon and terminate at the 3′ end of a nearby transposon (*123*). Such "alternative transposition" events can generate a variety of rearrangements (depending on the relative orientation of the transposon ends) and can translocate large segments of intervening DNA.

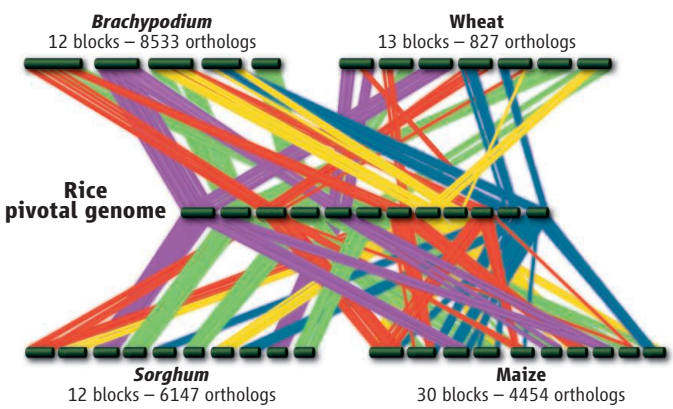


Fig. 8. Identification of orthologous sequence blocks in grass genomes. A schematic representation shows the 20,270 orthologs identified between the rice chromosomes used as a reference and the *Brachypodium*, wheat, sorghum, and maize chromosomes. Each line represents an orthologous gene. The blocks reflect the origin from ancestral protochromosomes. [Redrawn with permission from (*116*)]

The movement of genes is often mediated by a process that duplicates the gene and flanking sequences, leaving a copy at the original insertion site (*115*). Because translocated genome segments are commonly flanked by transposons, the movement of a chromosome segment is likely to be initiated by a double-strand break at the new insertion site of a transposon and may be repaired through one of several known processes that repair double-strand breaks in plants, including synthesis-dependent strand annealing, template slippage, and unequal crossing over (*114*, *124*). Such duplications can arise during mitotic chromosome replication, when transposition is known to occur, by the alternative transposition mechanism. The well-known tendency of transposons of the *Ac/Ds* family to undergo short-range transpositions from only one sister chromatid to an unreplicated site nearby gives rise to genic regions flanked by copies of the same transposon, facilitating subsequent mobilization of the intervening chromosome segment (*111*, *123*).

Genome Contraction and Divergence of Intergenic Sequences

Genomes expand by sequence duplication, transposition, and retrotransposition, and they contract by deletion mediated by a variety of homologous and illegitimate recombination events (*125*–*129*). Solo LTR generation by unequal homologous recombination between the LTRs at the ends of a single retroelement is frequent in some plant species, particularly near genes and at the kinetochore (*126*). Such unequal events can also occur between adjacent elements, leading to the deletion of the DNA between two TE copies (*125*, *126*). Not surprisingly, retrotransposon elimination by unequal and illegitimate recombination is most frequent in recombinationally active genome regions (*130*). In parts of the genome where TEs are abundant, homologous recombination is markedly suppressed; this is likely a causal factor in TE accumulation, as noted earlier (*131*, *132*).

Autonomous DNA transposons commonly decay by internal deletions that reveal the operation of double-strand break repair mechanism that duplicates genetic information, now called "filler DNA," by the invasion of a single strand into a duplex nearby and copying of a short sequence that is then inserted at the deletion breakpoint (*124*). McClintock identified and investigated a series of *Spm* derivatives that originated from an internally deleted, nonautonomous *Spm*, all of which were the result of further deletions within the same element at the same location (*133*, *134*). These arose at a high frequency, but only in the presence of an autonomous element; this finding suggests that they were initiated either directly

Downloaded from www.sciencemag.org on November 9, 2012

Published by AAAS

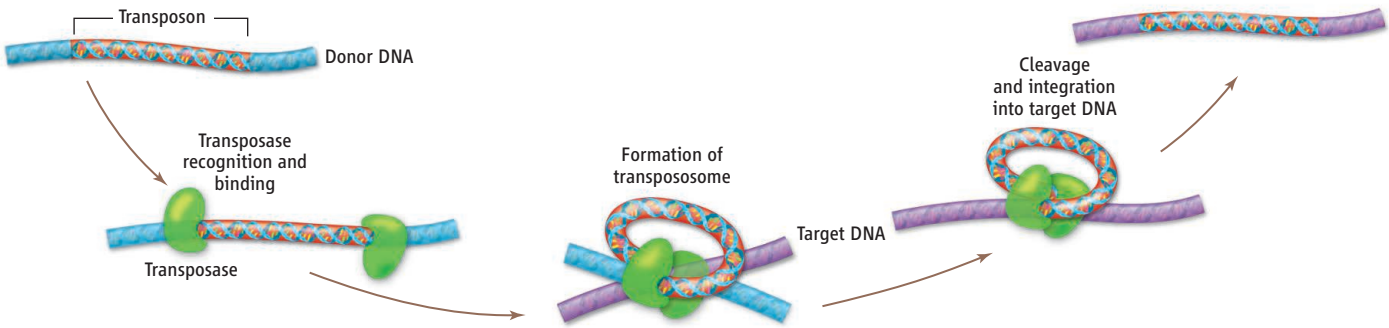


Fig. 9. DNA "cut-and-paste" transposition mechanism. Transposition is initiated by the site-specific recognition and binding of transposase to the transposon DNA ends. Dimerization of the transposase leads to formation of the transpososome, which brings together the transposon termini and a target site. Concerted cleavage at the donor and target sites is followed by integration of the excised transposon into the target site and resection of the empty donor site (*200*).

by the double-strand cleavage activity of the transposase encoded by the autonomous element or indirectly by secondary double-strand breaks incurred during the transposition reaction (*135*).

Analyses of intergenic regions in related species have revealed that they turn over very rapidly on an evolutionary time scale. Fine-grained analysis of the sequence dynamics shows that the intergenic volatility is indeed mediated by transposons, which both delete adjacent DNA sequences and insert filler DNA from elsewhere in the process of repairing the double-strand breaks in the DNA introduced by transposases (*128*). Although deletions commonly occur adjacent to a transposon end, they can remove entire transposons. Statistically significant clustering of such deletions in the vicinity of transposons suggests that they arise as a result of the double-strand breaks that initiate transposition.

Traffic in Genes and Regulatory Sequences

At a much finer level of resolution, transposons contribute to creating genes, modifying them, and programming and reprogramming them. Many transposons and retroelements contain captured gene fragments and can be part of gene regulatory regions (*136*–*142*). A classic example is provided by the maize *R* locus that encodes a transcription factor necessary for synthesis of anthocyanin pigments. The *R-r* allele comprises four tandem duplications, including a complete coding sequence and several truncated ones in direct and inverted order separated by a *Doppia* transposon. The complete coding sequence is responsible for pigment expression in the plant, whereas the several truncated copies support pigment expression in the seed (*143*).

The traffic in genes and regulatory sequences is bidirectional: Transposons pick up bits and pieces of genes that code for proteins other than transposases, and transposase genes are pressed into services other than transposition (*144*, *145*). For example, the proteins encoded by the *FAR1* and *FHY3* genes of *Arabidopsis* are both related to the MuDR family of transposases (*146*). FHY3 and FAR3 are transcription factors that regulate light-dependent chlorophyll biosynthesis in development, the former also gating phytochrome signaling to the circadian clock (*147*, *148*). A familiar example is provided by the human immune system, which uses recombinase proteins that evolved from transposases to generate sequence diversity through V(D)J recombination (*149*, *150*). Transposons provide the telomeres of some organisms and jump in to replace them in others (*151*, *152*). Centromeres contain and are often surrounded by transposons (*22*, *153*–*155*). As well, transposons are central to the epigenetic phenomenon of "imprinting" that imbues genes with different expression patterns depending on whether they were transmitted through male or female gametes; such differences arise during the major epigenetic reprogramming events of gametogenesis (*156*–*158*).

Driving Evolution

Thus, transposases hold a special place in the pantheon of genome sculptors. Arguably the products of the most abundant genes on Earth (*159*), transposases are transposon-encoded enzymes that cleave transposon ends and attach them to new sequences. The essential elements are (i) very strict sequence recognition and precise cleavage at the donor site and (ii) either a relaxed sequence specificity or no sequence specificity at the target site (*160*). The prokaryotic Mu element's transposition mechanism appears to be paradigmatic and common to many members of the transposase superfamily (*161*–*165*). Multimers of the transposase form a transpososome complex that recognizes the transposon's terminal inverted repeats and brings them together with the target insertion site (Fig. 9) (*166*, *167*). The transposon ends are brought into close juxtaposition with each other at the donor site for a coupled reaction that cleaves the transposon termini, introduces a staggered cleavage at the target site, and transfers the 3′ ends of the transposon to the overhanging 5′ ends at the target (*168*, *169*). The gapped duplexes at the two element ends are then repaired to generate the target site duplication, whose length is a TE family characteristic determined by the transposase. Subsequent excision of the transposon generally leaves behind an imperfect version of the target site duplication, generating sequence diversity (*170*, *171*).

In both bacteria and plants, recognition and cleavage of the two hemimethylated terminal inverted repeats of a single transposon ensures genome integrity and confines transposition to just one of the two newly replicated daughter strands or sister chromatids (*36*, *172*). But like other aspects of transposition, recombination, and DNA repair, this process is error-prone and can be fooled by such transposition events as the insertion of one *Ds* transposon in inverted orientation into the center of itself, giving the chromosome-breaking double *Ds* transposon that led McClintock to her momentous discoveries about how transposons move and restructure chromosomes (*173*, *174*). The bottom line for genomes is that the cleavage and resection of DNA by transposases virtually guarantees sequence variation, genome scrambling, and the appearance of transposons at rearrangement breakpoints. Simply put, transposases drive genome evolution.

CREDIT: K. SUTLIFF/*SCIENCE*

Downloaded from www.sciencemag.org on November 9, 2012

Published by AAAS

Genomic Shock and Transgenerational Epigenetic Inheritance

Both unpredictable stresses, such as irradiation, and predictable abiotic stresses, such as heat shock, elicit from genomes a highly programmed response intended to minimize the impact of the stress. McClintock coined the term "genomic shock" to refer to such a response (*175*). It is by now amply documented that plant transposons are activated in response to a variety of DNA-damaging agents and both biotic and abiotic stresses, as well as pathogen infection and the passage of plant cells through tissue culture (*176–181*). Other sources of natural chromosomal disturbance are provided by interspecific hybridization and allopolyploidization, both of which trigger the activation of transposons (*182–184*). This appears to be true as well in other eukaryotes, from yeast to flies to humans. Telomerases are relatives of retrotransposon-encoded reverse transcriptases, and transposons either comprise or can fill in for missing telomeres in flies and yeast, respectively (*152*, *185–187*).

Evidence is accumulating that both biotic and abiotic stresses induce a heritable increase in the ability of plants to withstand infection and tolerate stress (*188–191*). DNA damage, pathogen infection, and abiotic stresses also increase homologous recombination frequency and chromosomal rearrangements, both somatically and heritably (*188*, *192–195*). Thus, responses to stress—whether from pathogens, environmental extremes, or damage to the genetic apparatus—evoke not just a transcriptional response, but also a profound and to some extent heritable change in the epigenetic framework. Such changes can loosen the epigenetic constraints on transposons, allowing stress-inducible TEs to propagate stress-inducible promoters to other genes through transposition (*181*).

Just as McClintock reported that broken chromosome ends can "heal," so do transposition bursts subside, over both short and long runs (*175*). Some of the *Arabidopsis* transposons and retrotransposons demethylated in a genetic background devoid of the MET1 DNA methylase are gradually remethylated by RNA-dependent DNA methylation within several generations after reintroduction of a wild-type *MET1* gene (*196–198*). Heat-induced transcription and transposition of the *Arabidopsis ONSEN* retrotransposon is rapidly silenced, becoming transgenerational only in plants with a compromised RdDM pathway (*181*). Thus, transcriptional activation by demethylation can also trigger a feedback mechanism that restores methylation and resilences transposons. Recent years have seen progress in identifying the components of the restructuring response, but we do not yet know how cells and organisms perceive and initiate epigenetic reorganization in response to either genetic disruptions or environmental stressors.

Evolvability and Its Agents

I have argued that epigenetic mechanisms not only underpin the management of transcription and chromosome structure, but also provide the key to understanding the size and organization of eukaryotic genomes. They assure the stability of chromosomes, including vast menageries of TEs, and manage the replication and segregation of the genetic material in both mitosis and meiosis. My argument is that TEs accumulate because of, not despite, the epigenetic mechanisms that control homology-dependent recombination, whose dominance keeps the genomes of prokaryotes and many lower eukaryotes small. Absent the existence of such mechanisms, ectopic, homology-dependent recombination among dispersed TEs would rapidly eliminate them, either directly by intrachromosomal deletions or indirectly by creating nonviable chromosomes.

Plant responses to stress—whether from pathogens, environmental extremes, or damage to the genetic apparatus—evoke not just a transcriptional response, but also a profound and to some extent heritable change in the epigenetic framework.

But although epigenetic mechanisms slow the pace of genome restructuring to an evolutionary time scale, the impact of transposons and retrotransposons on genes and genomes is inescapable. Indeed, their ability to move and to move sequences has shaped higher eukaryotic genomes, from the structuring and restructuring of genes and their regulatory sequences to the shaping and reshaping of the genomic landscape. It is becoming increasingly difficult to escape the conclusion that eukaryotic genome evolution is driven from within not just by the gentle breeze of the genetic mechanisms that replicate and repair DNA, but by the stronger winds (with perhaps occasional gale-force gusts) of transposon activity. The ability to evoke rapid genome restructuring is at the heart of eukaryotic evolvability—the capacity of organisms with larger and larger genomes to maintain evolutionary flexibility.

References

1. N. V. Fedoroff, in *Discoveries in Plant Biology*, S.-D. Kung, S.-F. Yang, Eds. (World Scientific, Singapore, 1998), vol. 1, pp. 89–104.
2. N. V. Fedoroff, *Proc. Natl. Acad. Sci. U.S.A.* 0.1073/pnas.1215482109 (2012).
3. L. E. Orgel, F. H. C. Crick, *Nature* **284**, 604 (1980).
4. W. F. Doolittle, C. Sapienza, *Nature* **284**, 601 (1980).
5. J. A. Yoder, C. P. Walsh, T. H. Bestor, *Trends Genet.* **13**, 335 (1997).
6. N. V. Fedoroff, in *Plant Transposons and Genome Dynamics in Evolution*, N. V. Fedoroff, Ed. (Wiley-Blackwell, Hoboken, NJ, in press), chap. 4; www.wiley.com/WileyCDA/WileyTitle/productCd-0470959940.html.
7. M. Waring, R. J. Britten, *Science* **154**, 791 (1966).
8. R. J. Britten, D. E. Kohne, *Science* **161**, 529 (1968).
9. D. A. Smith, *Science* **233**, 1246b (1986).
10. R. L. Sinsheimer, *Science* **233**, 1246c (1986).
11. J. B. Walsh, J. Marks, *Nature* **322**, 590 (1986).
12. R. Lewin, *Science* **233**, 620 (1986).
13. J. G. Gall, *Science* **233**, 1367 (1986).
14. S. Ohno, *Brookhaven Symp. Biol.* **23**, 366 (1972).
15. R. Dawkins, *The Selfish Gene* (Oxford Univ. Press, Oxford, ed. 1, 1976).
16. J. G. Gall, *J. Cell Biol.* **91**, 3s (1981).
17. M. Rosbash, P. J. Ford, J. O. Bishop, *Proc. Natl. Acad. Sci. U.S.A.* **71**, 3746 (1974).
18. M. D. Bennett, I. J. Leitch, *Ann. Bot.* **107**, 467 (2011).
19. M. D. Bennett, J. B. Smith, *Philos. Trans. R. Soc. London Ser. B* **274**, 227 (1976).
20. R. Liu, J. L. Bennetzen, *New Phytol.* **179**, 249 (2008).
21. P. S. Schnable *et al.*, *Science* **326**, 1112 (2009).
22. R. S. Baucom *et al.*, *PLoS Genet.* **5**, e1000732 (2009).
23. A. P. J. de Koning, W. Gu, T. A. Castoe, M. A. Batzer, D. D. Pollock, *PLoS Genet.* **7**, e1002384 (2011).
24. E. Zuckerkandl, G. Cavalli, *Gene* **390**, 232 (2007).
25. *Nature* ENCODE Explorer (www.nature.com/encode/threads).
26. R. Holliday, J. E. Pugh, *Science* **187**, 226 (1975).
27. A. D. Riggs, *Cytogenet. Cell Genet.* **14**, 9 (1975).
28. T. H. Bestor, *Philos. Trans. R. Soc. London Ser. B* **326**, 179 (1990).
29. T. H. Bestor, *Novartis Found. Symp.* **214**, 187 (1998).
30. M. G. Kidwell, D. R. Lisch, *Nature* **393**, 22 (1998).
31. R. Martienssen, *Trends Genet.* **14**, 263 (1998).
32. R. K. Slotkin, R. Martienssen, *Nat. Rev. Genet.* **8**, 272 (2007).
33. D. W. Zeh, J. A. Zeh, Y. Ishida, *Bioessays* **31**, 715 (2009).
34. Y. W. Yuan, S. R. Wessler, *Proc. Natl. Acad. Sci. U.S.A.* **108**, 7884 (2011).
35. A. B. Hickman, M. Chandler, F. Dyda, *Crit. Rev. Biochem. Mol. Biol.* **45**, 50 (2010).
36. D. Roberts, B. C. Hoopes, W. R. McClure, N. Kleckner, *Cell* **43**, 117 (1985).
37. N. Kleckner, *Annu. Rev. Cell Biol.* **6**, 297 (1990).
38. R. Raina, D. Cook, N. Fedoroff, *Proc. Natl. Acad. Sci. U.S.A.* **90**, 6355 (1993).
39. J. Casadesús, D. Low, *Microbiol. Mol. Biol. Rev.* **70**, 830 (2006).
40. W. R. Engels, *Bioessays* **14**, 681 (1992).
41. M. Evgen'ev, H. Zelentsova, L. Mnjoian, H. Poluectova, M. G. Kidwell, *Chromosoma* **109**, 350 (2000).
42. M. G. Kidwell, *Genetica* **86**, 275 (1992).
43. J. C. Silva, M. G. Kidwell, *Mol. Biol. Evol.* **17**, 1542 (2000).
44. C. Gilbert, S. Schaack, J. K. Pace 2nd, P. J. Brindley, C. Feschotte, *Nature* **464**, 1347 (2010).

Downloaded from www.sciencemag.org on November 9, 2012

Published by AAAS

45. J. Thomas, S. Schaack, E. J. Pritham, *Genome Biol. Evol.* **2**, 656 (2010).
46. C. Gilbert, S. S. Hernandez, J. Flores-Benabib, E. N. Smith, C. Feschotte, *Mol. Biol. Evol.* **29**, 503 (2012).
47. R. S. Baucom, J. C. Estill, J. Leebens-Mack, J. L. Bennetzen, *Genome Res.* **19**, 243 (2009).
48. J. S. Khurana *et al.*, *Cell* **147**, 1551 (2011).
49. R. P. Anderson, J. R. Roth, *Annu. Rev. Microbiol.* **31**, 473 (1977).
50. G. Achaz, E. P. Rocha, P. Netter, E. Coissac, *Nucleic Acids Res.* **30**, 2987 (2002).
51. D. I. Andersson, D. Hughes, *Annu. Rev. Genet.* **43**, 167 (2009).
52. A. L. Koch, *J. Mol. Evol.* **14**, 273 (1979).
53. H. Isambert, R. R. Stein, *Biol. Direct* **4**, 28 (2009).
54. T. J. Treangen, E. P. Rocha, *PLoS Genet.* **7**, e1001284 (2011).
55. J. A. Law, S. E. Jacobsen, *Nat. Rev. Genet.* **11**, 204 (2010).
56. S. Feng, S. E. Jacobsen, W. Reik, *Science* **330**, 622 (2010).
57. H. Zhang, J. K. Zhu, *Curr. Opin. Plant Biol.* **14**, 142 (2011).
58. S. A. Simon, B. C. Meyers, *Curr. Opin. Plant Biol.* **14**, 148 (2011).
59. G. L. Moldovan *et al.*, *Mol. Cell* **45**, 75 (2012).
60. L. Vanderlyn, *Bot. Rev.* **15**, 507 (1949).
61. J. C. Peng, G. H. Karpen, *Curr. Opin. Genet. Dev.* **18**, 204 (2008).
62. J. C. Peng, G. H. Karpen, *Nat. Cell Biol.* **9**, 25 (2007).
63. J. Torres-Rosell *et al.*, *Nat. Cell Biol.* **9**, 923 (2007).
64. A. Verdel *et al.*, *Science* **303**, 672 (2004).
65. E. H. Bayne *et al.*, *Cell* **140**, 666 (2010).
66. M. Zaratiegui *et al.*, *Nature* **479**, 135 (2011).
67. S. A. Shabalina, E. V. Koonin, *Trends Ecol. Evol.* **23**, 578 (2008).
68. L. Aravind, S. Abhiman, L. M. Iyer, *Prog. Mol. Biol. Transl. Sci.* **101**, 105 (2011).
69. L. M. Iyer, S. Abhiman, L. Aravind, *Prog. Mol. Biol. Transl. Sci.* **101**, 25 (2011).
70. J. van der Oost, M. M. Jore, E. R. Westra, M. Lundgren, S. J. Brouns, *Trends Biochem. Sci.* **34**, 401 (2009).
71. R. Barrangou *et al.*, *Science* **315**, 1709 (2007).
72. A. Szczepankowska, *Adv. Virus Res.* **82**, 289 (2012).
73. T. J. Young, A. L. Kirchmaier, *Biochim. Biophys. Acta* **1819**, 303 (2012).
74. J. H. Brickner, *Curr. Opin. Cell Biol.* **21**, 127 (2009).
75. K. L. Adams, *J. Hered.* **98**, 136 (2007).
76. M. Zaratiegui, D. V. Irvine, R. A. Martienssen, *Cell* **128**, 763 (2007).
77. A. Bird, *Genes Dev.* **16**, 6 (2002).
78. P. Meyer, *FEBS Lett.* **585**, 2008 (2011).
79. H. Cedar, Y. Bergman, *Nat. Rev. Genet.* **10**, 295 (2009).
80. J. R. Haag, C. S. Pikaard, *Nat. Rev. Mol. Cell Biol.* **12**, 483 (2011).
81. E. R. Havecker *et al.*, *Plant Cell* **22**, 321 (2010).
82. J. A. Law, A. A. Vashisht, J. A. Wohlschlegel, S. E. Jacobsen, *PLoS Genet.* **7**, e1002195 (2011).
83. J. K. Zhu, *Annu. Rev. Genet.* **43**, 143 (2009).
84. M. Groszmann *et al.*, *Biochim. Biophys. Acta* **1809**, 427 (2011).
85. M. W. Yaish, J. Colasanti, S. J. Rothstein, *J. Exp. Bot.* **62**, 3727 (2011).
86. J. Song, A. Angel, M. Howard, C. Dean, *J. Cell Sci.* **125**, 3723 (2012).
87. A. C. Cassells, C. C. Herrick, *Virology* **78**, 253 (1977).
88. P. P. Abel *et al.*, *Science* **232**, 738 (1986).
89. D. C. Baulcombe, *Plant Cell* **8**, 1833 (1996).
90. F. Ratcliff, B. D. Harrison, D. C. Baulcombe, *Science* **276**, 1558 (1997).
91. M. Wassenegger, S. Heimes, L. Riedel, H. L. Sänger, *Cell* **76**, 567 (1994).
92. R. Jorgensen, *Trends Biotechnol.* **8**, 340 (1990).
93. R. Jorgensen, *Dev. Genet.* **15**, 523 (1994).
94. Q. Que, R. A. Jorgensen, *Dev. Genet.* **22**, 100 (1998).
95. J. M. Kooter, M. A. Matzke, P. Meyer, *Trends Plant Sci.* **4**, 340 (1999).
96. X. Chen, *Plant J.* **61**, 941 (2010).
97. R. A. Brink, *Cold Spring Harb. Symp. Quant. Biol.* **23**, 379 (1958).
98. V. L. Chandler, *Cell* **128**, 641 (2007).
99. M. A. Arteaga-Vazquez, V. L. Chandler, *Curr. Opin. Genet. Dev.* **20**, 156 (2010).
100. S. W. Chan, X. Zhang, Y. V. Bernatavichute, S. E. Jacobsen, *PLoS Biol.* **4**, e363 (2006).
101. P. SanMiguel *et al.*, *Science* **274**, 765 (1996).
102. P. SanMiguel, B. S. Gaut, A. Tikhonov, Y. Nakajima, J. L. Bennetzen, *Nat. Genet.* **20**, 43 (1998).
103. A. H. Paterson *et al.*, *Nature* **457**, 551 (2009).
104. X. Gai, D. F. Voytas, *Mol. Cell* **1**, 1051 (1998).
105. P. G. Fuerst, D. F. Voytas, *Chromosoma* **112**, 58 (2003).
106. S. Tsukahara *et al.*, *Genes Dev.* **26**, 705 (2012).
107. T. Wicker *et al.*, *Nat. Rev. Genet.* **8**, 973 (2007).
108. F. Wei *et al.*, *PLoS Genet.* **5**, e1000728 (2009).
109. S. Liu *et al.*, *PLoS Genet.* **5**, e1000733 (2009).
110. L. Yang, J. L. Bennetzen, *Proc. Natl. Acad. Sci. U.S.A.* **106**, 19922 (2009).
111. I. M. Greenblatt, R. A. Brink, *Genetics* **47**, 489 (1962).
112. H. Fu, H. K. Dooner, *Proc. Natl. Acad. Sci. U.S.A.* **99**, 9573 (2002).
113. Q. Wang, H. K. Dooner, *Proc. Natl. Acad. Sci. U.S.A.* **103**, 17644 (2006).
114. T. Wicker, J. P. Buchmann, B. Keller, *Genome Res.* **20**, 1229 (2010).
115. T. Wicker *et al.*, *Plant Cell* **23**, 1706 (2011).
116. M. Abrouk *et al.*, *Trends Plant Sci.* **15**, 479 (2010).
117. J. L. Bennetzen, M. Freeling, *Genome Res.* **7**, 301 (1997).
118. A. P. Tikhonov *et al.*, *Proc. Natl. Acad. Sci. U.S.A.* **96**, 7409 (1999).
119. J. L. Bennetzen, *Plant Cell* **12**, 1021 (2000).
120. T. Wicker *et al.*, *Plant J.* **41**, 184 (2005).
121. B. McClintock, *Carnegie Inst. Wash. Yearb.* **49**, 157 (1950).
122. B. McClintock, *Proc. Natl. Acad. Sci. U.S.A.* **36**, 344 (1950).
123. C. Yu, J. Zhang, T. Peterson, *Genetics* **188**, 59 (2011).
124. H. Puchta, *J. Exp. Bot.* **56**, 1 (2005).
125. K. M. Devos, J. K. Brown, J. L. Bennetzen, *Genome Res.* **12**, 1075 (2002).
126. J. Ma, K. M. Devos, J. L. Bennetzen, *Genome Res.* **14**, 860 (2004).
127. C. Vitte, J. L. Bennetzen, *Proc. Natl. Acad. Sci. U.S.A.* **103**, 17638 (2006).
128. J. P. Buchmann, T. Matsumoto, N. Stein, B. Keller, T. Wicker, *Plant J.* **71**, 550 (2012).
129. J. H. Xu, J. L. Bennetzen, J. Messing, *Mol. Biol. Evol.* **29**, 861 (2012).
130. Z. Tian *et al.*, *Genome Res.* **19**, 2221 (2009).
131. H. Fu *et al.*, *Proc. Natl. Acad. Sci. U.S.A.* **98**, 8903 (2001).
132. H. Fu, Z. Zheng, H. K. Dooner, *Proc. Natl. Acad. Sci. U.S.A.* **99**, 1082 (2002).
133. Z. Schwarz-Sommer, A. Gierl, R. Berndtgen, H. Saedler, *EMBO J.* **4**, 2439 (1985).
134. P. Masson, R. Surosky, J. A. Kingsbury, N. V. Fedoroff, *Genetics* **117**, 117 (1987).
135. B. McClintock, *Carnegie Inst. Wash. Yearb.* **66**, 20 (1968).
136. L. E. Talbert, V. L. Chandler, *Mol. Biol. Evol.* **5**, 519 (1988).
137. N. Jiang, Z. Bao, X. Zhang, S. R. Eddy, S. R. Wessler, *Nature* **431**, 569 (2004).
138. N. Jiang, A. A. Ferguson, R. K. Slotkin, D. Lisch, *Proc. Natl. Acad. Sci. U.S.A.* **108**, 1537 (2011).
139. C. Du, N. Fefelova, J. Caronna, L. He, H. K. Dooner, *Proc. Natl. Acad. Sci. U.S.A.* **106**, 19916 (2009).
140. N. Elrouby, T. E. Bureau, *Mol. Genet. Genomics* **287**, 143 (2012).
141. K. Naito *et al.*, *Nature* **461**, 1130 (2009).
142. S. R. Ludwig, L. F. Habera, S. L. Dellaporta, S. R. Wessler, *Proc. Natl. Acad. Sci. U.S.A.* **86**, 7092 (1989).
143. E. L. Walker, T. P. Robbins, T. E. Bureau, J. Kermicle, S. L. Dellaporta, *EMBO J.* **14**, 2350 (1995).
144. D. Lisch, J. L. Bennetzen, *Curr. Opin. Plant Biol.* **14**, 156 (2011).
145. D. Lisch, *Annu. Rev. Plant Biol.* **60**, 43 (2009).
146. M. E. Hudson, D. R. Lisch, P. H. Quail, *Plant J.* **34**, 453 (2003).
147. T. Allen *et al.*, *Plant Cell* **18**, 2506 (2006).
148. W. Tang *et al.*, *Plant Cell* **24**, 1984 (2012).
149. V. V. Kapitonov, J. Jurka, *PLoS Biol.* **3**, e181 (2005).
150. K. Hiom, M. Melek, M. Gellert, *Cell* **94**, 463 (1998).
151. M. J. McEachern, J. E. Haber, *Annu. Rev. Biochem.* **75**, 111 (2006).
152. M. Belfort, M. J. Curcio, N. F. Lue, *Proc. Natl. Acad. Sci. U.S.A.* **108**, 20304 (2011).
153. J. Ma, J. L. Bennetzen, *Proc. Natl. Acad. Sci. U.S.A.* **103**, 383 (2006).
154. L. Kanizay, R. K. Dawe, *Funct. Integr. Genomics* **9**, 287 (2009).
155. R. K. Slotkin, *Epigenetics* **5**, 483 (2010).
156. M. Gehring, Y. Choi, R. L. Fischer, *Plant Cell* **16** (suppl.), S203 (2004).
157. T. Kinoshita, Y. Ikeda, R. Ishikawa, *Semin. Cell Dev. Biol.* **19**, 574 (2008).
158. M. Gehring, K. L. Bubb, S. Henikoff, *Science* **324**, 1447 (2009).
159. R. K. Aziz, M. Breitbart, R. A. Edwards, *Nucleic Acids Res.* **38**, 4207 (2010).
160. N. L. Craig, *Annu. Rev. Biochem.* **66**, 437 (1997).
161. P. D. Kaufman, D. C. Rio, *Cell* **69**, 27 (1992).
162. D. H. Dreyfus, *Ann. Allergy Asthma Immunol.* **97**, 567 (2006).
163. S. P. Montaño, P. A. Rice, *Curr. Opin. Struct. Biol.* **21**, 370 (2011).
164. I. V. Nesmelova, P. B. Hackett, *Adv. Drug Deliv. Rev.* **62**, 1187 (2010).
165. J. H. Keith, C. A. Schaeper, T. S. Fraser, M. J. Fraser Jr., *BMC Mol. Biol.* **9**, 73 (2008).
166. K. Mizuuchi, R. Craigie, *Annu. Rev. Genet.* **20**, 385 (1986).
167. S. Haapa-Paananen, H. Rita, H. Savilahti, *J. Biol. Chem.* **277**, 2843 (2002).
168. H. Savilahti, P. A. Rice, K. Mizuuchi, *EMBO J.* **14**, 4893 (1995).
169. T. L. Williams, E. L. Jackson, A. Carritte, T. A. Baker, *Genes Dev.* **13**, 2725 (1999).
170. L. Scott, D. LaFoe, C. F. Weil, *Genetics* **142**, 237 (1996).
171. H. Kim, K. Kim, J. Kim, S. H. Kim, J. Yim, *Biochem. Biophys. Res. Commun.* **417**, 335 (2012).
172. F. Ros, R. Kunze, *Genetics* **157**, 1723 (2001).
173. H. P. Döring, I. Pahl, M. Durany, *Mol. Gen. Genet.* **224**, 40 (1990).
174. J. J. English, K. Harrison, J. D. G. Jones, *Plant Cell* **7**, 1235 (1995).
175. B. McClintock, *Science* **226**, 792 (1984).
176. M. A. Grandbastien *et al.*, *Genetica* **100**, 241 (1997).
177. K. Sugimoto, S. Takeda, H. Hirochika, *Plant Cell* **12**, 2511 (2000).
178. C. Mhiri *et al.*, *Plant Mol. Biol.* **33**, 257 (1997).
179. C. M. Ki *et al.*, *Mol. Cells* **14**, 231 (2002).
180. H. Hirochika, K. Sugimoto, Y. Otsuki, H. Tsugawa, M. Kanda, *Proc. Natl. Acad. Sci. U.S.A.* **93**, 7783 (1996).
181. H. Ito *et al.*, *Nature* **472**, 115 (2011).
182. A. Madlung *et al.*, *Plant J.* **41**, 221 (2005).
183. K. Kashkush, M. Feldman, A. A. Levy, *Nat. Genet.* **33**, 102 (2003).
184. M. Kenan-Eichler *et al.*, *Genetics* **188**, 263 (2011).
185. T. H. Eickbush, *Science* **277**, 911 (1997).
186. M. L. Pardue, O. N. Danilevskaya, K. L. Traverse, K. Lowenhaupt, *Genetica* **100**, 73 (1997).
187. M. J. Curcio, M. Belfort, *Proc. Natl. Acad. Sci. U.S.A.* **104**, 9107 (2007).
188. P. Kathiria *et al.*, *Plant Physiol.* **153**, 1859 (2010).
189. A. Slaughter *et al.*, *Plant Physiol.* **158**, 835 (2012).
190. E. Luna, T. J. A. Bruce, M. R. Roberts, V. Flors, J. Ton, *Plant Physiol.* **158**, 844 (2012).
191. M. Jaskiewicz, U. Conrath, C. Peterhänsel, *EMBO Rep.* **12**, 50 (2011).
192. A. Bilichak, Y. Ilnystkyy, J. Hollunder, I. Kovalchuk, *PLoS ONE* **7**, e30515 (2012).
193. Y. Yao, I. Kovalchuk, *Mutat. Res.* **707**, 61 (2011).
194. Y. Yao, A. Bilichak, A. Golubov, I. Kovalchuk, *Mutat. Res.* **709–710**, 7 (2011).
195. A. Boyko *et al.*, *PLoS ONE* **5**, e9514 (2010).
196. F. K. Teixeira *et al.*, *Science* **323**, 1600 (2009).
197. H. Saze, T. Kakutani, *Curr. Opin. Plant Biol.* **14**, 81 (2011).
198. J. Paszkowski, U. Grossniklaus, *Curr. Opin. Plant Biol.* **14**, 195 (2011).
199. C. Miguel, L. Marum, *J. Exp. Bot.* **62**, 3713 (2011).
200. A. Changela, K. Perry, B. Taneja, A. Mondragon, *Curr. Opin. Struct. Biol.* **13**, 15 (2003).

Downloaded from www.sciencemag.org on November 9, 2012

Published by AAAS

Hepcidin and the Iron-Infection Axis

Hal Drakesmith[1]* and Andrew M. Prentice[2]*

Iron lies at the center of a battle for nutritional resource between higher organisms and their microbial pathogens. The iron status of the human host affects the pathogenicity of numerous infections including malaria, HIV-1, and tuberculosis. Hepcidin, an antimicrobial-like peptide hormone, has emerged as the master regulator of iron metabolism. Hepcidin controls the absorption of dietary iron and the distribution of iron among cell types in the body, and its synthesis is regulated by both iron and innate immunity. We describe how hepcidin integrates signals from diverse physiological inputs, forming a key molecular bridge between iron trafficking and response to infection.

Of the 30 or so essential micronutrients, iron has a very particular role in mediating host-pathogen interactions. It has been the focus of an ongoing evolutionary battle for nutritional resource because its valency states endow it with useful oxidoreductive properties that have been adopted by numerous enzyme and oxygen transport systems across most life forms, and because it is extremely insoluble at neutral pH. Iron is the only micronutrient known to have a regulatory hormone that responds to both nutrient status and infection: The recently discovered hepcidin (Box 1) integrates diverse signals from iron status and infectious threat and orchestrates a series of host-protective responses.

It has long been established in animal models that a host's iron status can influence infection, and there is parallel evidence in humans. For example, a study of iron-deficient Somali refugees recorded five times the number of infections (including reactivation of preexisting malaria, brucellosis, and tuberculosis) in those receiving iron supplements relative to a placebo group (*1*). However, the subsequent evidence for associations between host iron status and infectious diseases in humans has been mixed, reflecting several issues: (i) The evolutionary battle is finely balanced; (ii) most studies of therapeutic iron supplementation assess hematological rather than infectious outcomes, and a physician may be satisfied if the presenting condition of anemia or iron deficiency abates; (iii) iron status is often poorly defined, and hemoglobin represents an imperfect proxy, particularly when infections are prevalent; and (iv) the effects are likely to be context-specific, depending on the patient's preexisting iron status, exposure to potential infections and co-infections, and genetic background (*2*) (Fig. 1). A large iron supplementation trial of young children in Pemba Island, which was prematurely terminated as a result of an excess of serious adverse events (including deaths) in those receiving iron, illustrates these complexities (*3*).

Host Mechanisms for Withholding Iron from Microorganisms

Unbound iron or heme (released during constitutive or infectious hemolytic conditions), as well as providing the most critical growth-limiting nutrient to potential pathogens, can generate toxic free radicals that would cause host tissue damage if not contained. Systems have therefore evolved to ensure that iron and heme are tightly chaperoned. In humans, the dominant chaperone proteins are transferrin, lactoferrin, and ferritin for iron; haptoglobin for hemoglobin; and hemopexin for heme. These are regulated according to need and participate in receptor-mediated uptake by target cells. The fact that all are acute-phase proteins whose levels are modulated by infection (negatively in the case of transferrin, positively for the others) is an important clue concerning the centrality of iron in host defense against potential pathogens. The abundance of lactoferrin in breast milk and other epithelium-protecting secretory fluids, together with its release by neutrophils at foci of infection, is further compelling evidence.

The bacteriostatic effects of iron-binding proteins were first reported by Schade and Caroline (*4*), who noted that specific iron-binding proteins in egg white (ovotransferrin) and blood (transferrin) inhibited the growth of certain bacteria—an effect easily reversed by adding iron. Under normal physiological circumstances, although there is abundant iron in body fluids, these iron-binding proteins are only partially saturated and the amount of free iron in equilibrium is about 10^{-18} M, far too low to sustain bacterial growth (*5*). When an infectious threat is recognized by the host, these very low levels of iron are reduced still further by the "hypoferremia of infection," a host-defense mechanism also recognized in the 1940s and now known to be largely mediated by hepcidin (see below). In several genetic conditions (e.g., hemochromatosis), transferrin saturation rises and free iron (so-called non–transferrin-bound iron, NTBI) may become available, enhancing the threat of infection (*6*). Iatrogenic causes of NTBI include transfusional iron overload and, less recognized, simple oral iron supplementation. Oral iron supplementation provides a nonphysiological bolus dose of highly absorbable iron that can temporarily overwhelm the regulatory and chaperone mechanisms that normally mediate the safe passage of iron from enterocytes to the target tissues.

During the relatively unhygienic conditions of our evolutionary history (conditions that remain prevalent in many regions of the world), humans were under constant and simultaneous threat from a range of potentially fatal microorganisms and, like an overstretched general fighting a war on many fronts, would have been forced to select which battles to fight first. The hypoferremia of infection is only one of numerous innate and adaptive defenses. It is targeted against iron-dependent extracellular organisms that could otherwise cause a rapidly fatal septicemia. But in choosing to divert iron toward macrophages, the host provides an opportunity for intracellular organisms. The niche selection of such pathogens may have evolved to capitalize on the rich source of the growth-critical nutrient iron in the macrophages of a host that is busy protecting itself from other pathogens.

Mechanisms for Iron Acquisition by Microorganisms

Almost all microorganisms are dependent on iron to a greater or lesser extent. This appears to be true for most human pathogens, and, in competition with the host's evolution of iron-withholding strategies, they have evolved an array of mechanisms for scavenging iron. There are more than 500 known bacterial siderophores (small, high-affinity iron-chelating compounds), some with iron binding constants that would challenge the skills of the best synthetic chemists. Further confirmation of the centrality of iron for pathogen vigor is provided by the high level of genomic investment in iron-acquiring mechanisms and by the frequent concentration of such genes in high-pathogenicity islands. For example, highly pathogenic strains of *Yersinia enterolytica*, *Y. pseudotuberculosis*, and *Y. pestis* possess a common high-pathogenicity island (apparently acquired by horizontal capture from another organism) that encodes proteins necessary for the synthesis, transport, and regulation of the siderophore yersiniabactin (*7*). Genetic detective work based on the full sequence of *Y. pestis* suggests that acquisition of these improved iron-acquiring capabilities allowed the organism to make a niche transition from being an enteric to a systemic pathogen (*8*). Niche specificity is determined by the source from which bacteria obtain iron and by the efficiency with which they can do so (Fig. 2).

Hepcidin: Master Regulator of Iron Metabolism

In the 1930s, a consensus developed that iron homeostasis in humans is maintained by regulating intestinal absorption (*9*). About 1 mg of iron

[1]Molecular Immunology Group and Medical Research Council (MRC) Human Immunology Unit, MRC Weatherall Institute of Molecular Medicine, University of Oxford, John Radcliffe Hospital, Oxford OX3 9DS, UK. [2]MRC International Nutrition Group, London School of Hygiene and Tropical Medicine, London WC1E 7HT, UK, and MRC Keneba, The Gambia.

*To whom correspondence should be addressed. E-mail: alexander.drakesmith@ndm.ox.ac.uk (H.D.); andrew.prentice@lshtm.ac.uk (A.M.P.)

Downloaded from www.sciencemag.org on November 9, 2012

is typically absorbed per day from the diet, with the majority destined to be incorporated into heme during erythropoiesis in the bone marrow. Senescent red blood cells are phagocytosed and degraded by macrophages, with about 25 mg of iron per day recycled back into serum via this route (fig. S1A). How is this iron cycle controlled?

Although many molecular pathways are involved, the current thinking is that the circulating peptide hormone hepcidin, produced predominantly by hepatocytes, is hierarchically the master regulator (see Box 1). The final step of transfer of iron from the lumen of the gut into serum, as well as the return of recycled iron to the circulation from macrophages, are both mediated by the multitransmembrane protein ferroportin (fig. S1B). Hepcidin's mode of action is to bind ferroportin and induce its degradation, thus inhibiting cellular iron efflux (*10*). Hepcidin exerts control over systemic iron trafficking by regulating the transfer of dietary, recycled, and stored iron from intracellular compartments to extracellular fluid (see Box 1 and fig. S1B). The mature bioactive hepcidin peptide consists of 25 amino acids, eight of which are cysteines, and like the *Drosophila* antifungal peptide drosomycin, hepcidin has four internal disulfide bonds. Hepcidin sequences are found in fish, mammals, reptiles, and amphibians, but not in birds or invertebrates.

An abundance of genetic evidence in humans and experimental animals indicates that the ferroportin-hepcidin interaction is the dominant and nonredundant regulator of iron homeostasis in vertebrates. For example, hepcidin knockout mice rapidly become iron-loaded (*11*), as do humans with ferroportin variants that resist hepcidin control (*12*), and genetic defects that cause hepcidin overproduction lead to severe iron-deficiency anemia (*13*). The regulation of hepcidin expression is complex, influenced by diverse physiological inputs, and incompletely understood at a molecular level (see fig. S2). Increases in iron induce hepcidin transcription through the bone morphogenetic protein (BMP) signaling pathway, forming a feedback mechanism that prevents iron overload. Defects in genes that disrupt the BMP pathway cause abnormalities in iron balance, ranging from early-onset severe iron accumulation (e.g., BMP6 deficiency in mice) to development of iron overload in later life in individuals with HFE-linked hemochromatosis, which leads to mildly suppressed hepcidin levels. Hepcidin synthesis is greatly reduced by iron deficiency, hypoxia, and increased erythropoietic drive (including that associated with β-thalassemia), causing higher levels of iron to be absorbed from the diet. The molecular mechanisms that mediate hepcidin suppression under these conditions are still not completely clear.

Hepcidin expression is upregulated during inflammation. For example, turpentine-induced inflammation is associated with elevated hepcidin in mice, and

Box 1. The Emergence of Hepcidin

Hepcidin was discovered by three laboratories working independently (*42*–*44*); two of these groups were looking for new antimicrobial peptides, and the third was searching for iron-regulated liver-expressed genes. In retrospect, this underscores the nature of hepcidin as being an iron hormone of innate immune ancestry. The laboratory of Tomas Ganz invented the name hepcidin, because the gene is highly expressed in the liver (hep-) and was found to possess some microbicidal activity (-cidin). Hepcidin gene expression was observed to be induced by inflammation in mice, and peptide levels were highly increased in the urine of one human donor with a systemic infection. The degree to which hepcidin can be directly antimicrobial is uncertain, but it is thought to be weak relative to specialized microbicidal peptides such as defensins. In addition, the high degree of conservation of hepcidin genes (relative to defensins) among vertebrate species that have evolved during exposure to different pathogen types is more consistent with hepcidin having a nonmicrobicidal role. The link of hepcidin to iron regulation, suggested by its up-regulation in iron-loaded mice, was further strengthened when mice that were engineered to lack the transcription factor Usf2 and also lacked the neighboring hepcidin-encoding gene *Hamp1* were found to be iron-overloaded (*11*). Follow-up studies confirmed that mice lacking *Hamp1* alone recapitulated this phenotype, whereas mice overexpressing hepcidin were severely (usually mortally) anemic at birth. The molecular mode of action of hepcidin was then elucidated by Nemeth *et al.*, who found that hepcidin binds and causes the intracellular degradation of ferroportin, a well-conserved (among vertebrates) iron exporter (*10*). The nonredundant nature of the hepcidin-ferroportin interaction for controlling systemic iron levels and iron partitioning has since been confirmed by a large number of human and mouse studies.

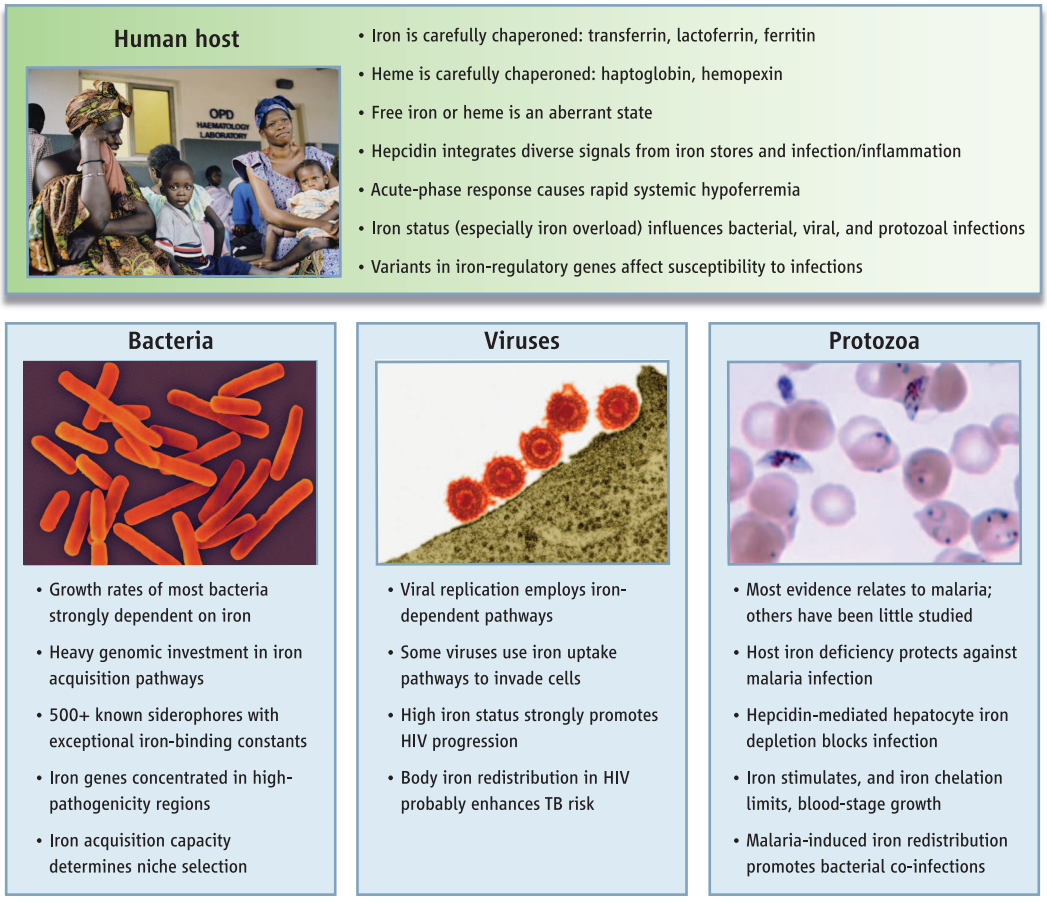


Fig. 1. The host-pathogen battle for iron. Exemplar organisms illustrated: hemorrhagic *E. coli* (O157:H7), herpes simplex virus, and *Plasmodium falciparum* blood-stage infection. [Image credits: people by Felicia Webb; bacteria images copyright Dennis Kunkel Microscopy Inc.]

Downloaded from www.sciencemag.org on November 9, 2012

hypoferremia after turpentine treatment does not occur in mice lacking hepcidin (*14*). Experiments in which hepcidin peptide was injected into mice showed a dose-dependent suppression of serum iron of 80% within 1 hour, which was sustained for up to 2 days, although the majority of hepcidin had been cleared in 24 hours (*15*). This profound systemic effect is likely due to the blockade of macrophage iron recycling while bone marrow consumption of iron continues unabated. In mice that constitutively overexpress hepcidin, a decrease in hepatocyte iron is observed (*16*), whereas hepatic iron deposition, high serum iron, and a relative paucity in macrophage iron are associated with hepcidin deficiency (for example, in hemochromatosis).

The aggregate of the above findings is that hepcidin integrates signals from iron in serum and the liver, from bone marrow iron requirements, and from inflammation, thus acting as a useful biomarker reflecting iron status. However, hepcidin also determines iron availability and distribution. Because of the importance of iron for pathogen proliferation, and because infectious agents tend to have distinct tropisms for particular cell types or anatomical niches (for example, *Plasmodium* has hepatocyte and erythrocyte life stages, whereas *Mycobacterium tuberculosis* inhabits macrophages), how hepcidin is controlled during infections affects iron-dependent pathogen growth and pathogenesis (Fig. 3).

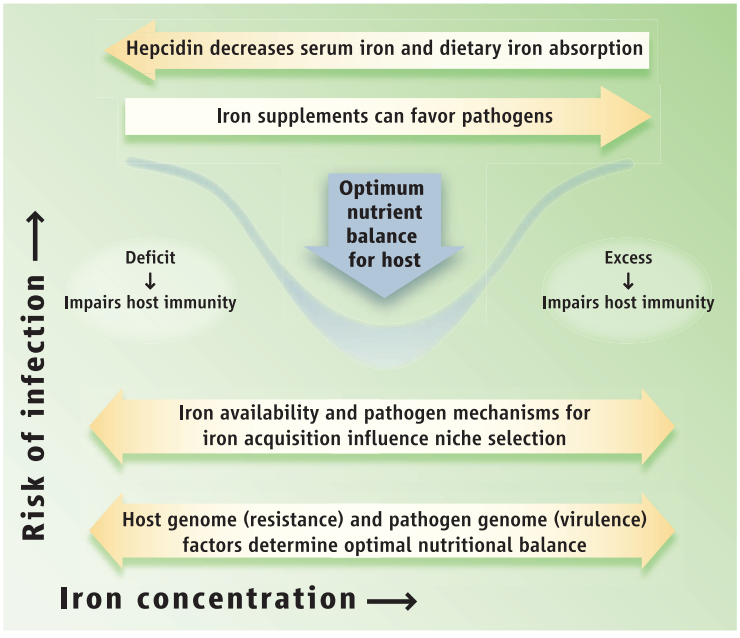


Fig. 2. Iron—a delicate balancing act. Risk of infection (represented by the curved line) is increased by iron deficiency and iron overload. In animal models, iron deficiency impairs various aspects of cellular immunity. The extent to which this holds at the levels of deficiency commonly seen in humans is less certain. An excess of iron or heme arising from genetic or iatrogenic causes and/or hemolytic conditions can overload normal chaperone pathways, thereby making iron more easily available for pathogen growth. The optimum level of host iron status may differ for different pathogens and in different organs and cell types. Host redistribution of iron as a defense against extracellular organisms may increase susceptibility to intracellular organisms. Pathogens also manipulate cellular iron supply. For example, an initial liver-stage *Plasmodium* infection down-regulates ferroportin and up-regulates DMT-1 in hepatocytes to enrich its iron supply, but blood-stage infection stimulates host hepcidin and thereby depletes hepatocyte iron, thus starving new sporozoites from a competing *Plasmodium* strain attempting to establish a secondary infection—an example of "interkingdom signaling." Note that this figure represents a dynamic situation in which, within highly infectious environments, the terrain and focus of the battle is constantly changing as the host combats multiple foes, each of which has a rapid capacity to adapt its strategy and avoid immune surveillance.

Innate Immune Signaling Regulates Hepcidin

Specific host mediators causing hepcidin up-regulation in the context of infection and inflammation have been investigated (see fig. S2 for details and references). Interleukin (IL)–6, IL-22, and type I interferon stimulate hepcidin transcription through STAT3 signaling, and several microbial-derived Toll-like receptor (TLR) ligands can induce hepcidin expression, likely via induction of IL-6. In particular, agonists that bind plasma membrane–expressed TLRs seem to induce hepcidin, consistent with a role for hepcidin in innate immunity against extracellular pathogens. However, mechanisms that sense internal cellular status can also regulate hepcidin. Endoplasmic reticulum (ER) stress and the accumulation of misfolded proteins, which may occur during infections, can trigger hepcidin synthesis. Through IL-6, IL-22, type I interferon, TLR ligands, and the ER stress response, molecular control of hepcidin is linked to innate responses to pathogens.

The development of innate immune responses influences the polarity and magnitude of subsequent adaptive immunity. Activation of hepcidin transcription is positively regulated by SMAD and STAT3 signaling, which together also play a role in T helper cell 17 (T_H17) responses. The proliferation of T and B lymphocytes is iron-dependent, and expression of the iron acquiring transferrin receptor (CD71) is associated with their activation. The possibility exists that by controlling the availability of transferrin-chaperoned iron in serum, and through linkage with T cell differentiation programs, hepcidin may influence and be associated with particular types of adaptive immune responses.

The first demonstration of hepcidin stimulation during an in vivo infection with live pathogens was made in fish, where up-regulation of liver expression by a factor of 4500 was observed after sea bass were infected with *Streptococcus iniae* (*17*). Although hepatocytes are the main source of hepcidin, early reports in mammalian infection systems analyzed hepcidin production by leukocytes. Experiments in a granulomatous pouch model of *Escherichia coli* in mice revealed hepcidin up-regulation in immune cells at the site of infection (*18*). Later work confirmed that neutrophils and macrophages synthesized hepcidin in response to Gram-positive (group A *Streptococcus*) and Gram-negative (*Pseudomonas aeruginosa*, *Salmonella typhimurium*) bacteria in a TLR4-dependent fashion, both in vitro and in skin, after subcutaneous infection (*19*). This work suggests that local production of hepcidin may alter iron availability to pathogens at foci of infection, without necessarily altering systemic iron balance.

Lower serum iron levels and anemia are common in malaria. Increased systemic hepcidin levels are observed during the blood stage of *Plasmodium* infection; upon antimalarial treatment, hepcidin levels and serum iron return to normal (*20*), but the mechanism of hepcidin up-regulation during malaria in humans is unclear. Other pathogens shown to increase liver hepcidin in mice with concomitant reduction of transferrin saturation are influenza virus A and *Candida albicans*, and both pathogens likely increase hepcidin via an inflammatory STAT3-mediated response (*21*). Likewise, after intraperitoneal injection of *P. aeruginosa*, liver hepcidin mRNA levels also increase (*19*). In general, infections or stimuli that invoke a systemic inflammatory response are likely to induce liver hepcidin expression, reduce serum iron, and increase iron accumulation in reticuloendothelial cells.

Hepcidin and the Pathogenesis of Infections

An exception to infection stimulating hepcidin expression is chronic hepatitis C virus (HCV) infection. Hepatic iron accumulation occurs in 30 to 40% of HCV patients and is a morbidity factor for disease pathogenesis; excess iron damages the liver through generation of free radicals, and iron removal may be beneficial. Reduced levels of hepcidin occur in untreated chronic HCV patients despite ongoing inflammation, likely causing the predisposition to hepatic iron loading (*22*). Hepcidin induction occurs rapidly after commencement of antiviral therapy with pegylated type I interferon and ribavirin, and the degree of hypoferremia resulting from this treatment corre-

Downloaded from www.sciencemag.org on November 9, 2012

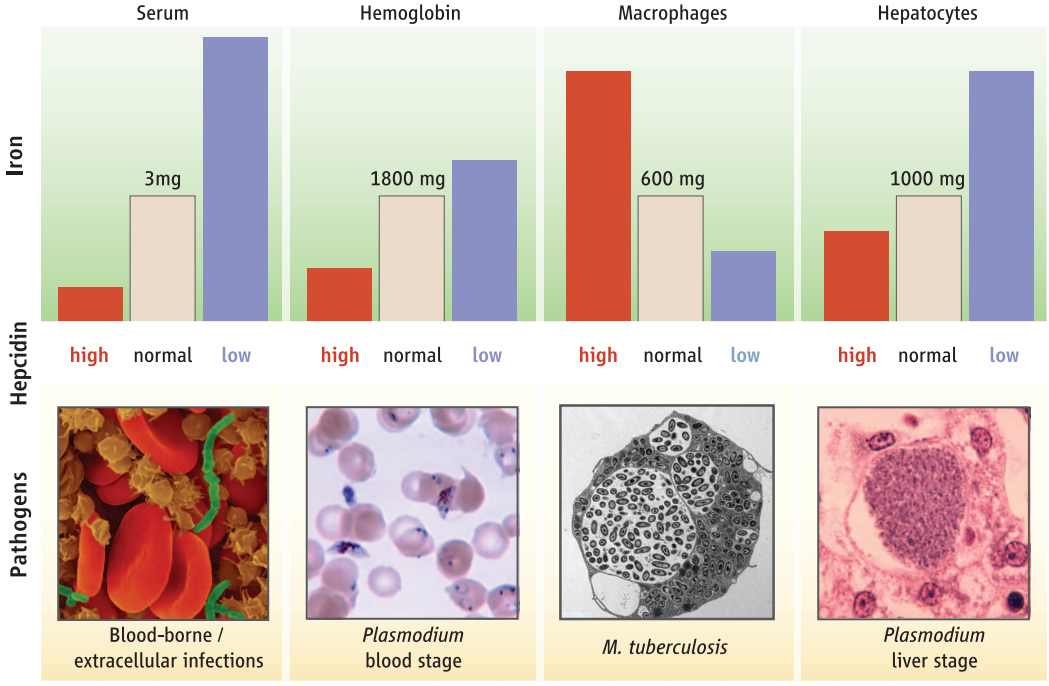


Fig. 3. Hepcidin, iron partitioning, and infectious pathogens. By inhibiting ferroportin, hepcidin controls the total amount of iron entering the circulation as well as the compartments and cell types to which the iron is directed. The usual amounts of iron in serum (bound to transferrin), hemoglobin, macrophages, and hepatocytes are given (represented by beige columns). In conditions of high hepcidin (red columns), iron recycling through macrophages is inhibited while consumption of iron by the bone marrow continues, leading to a rapid decline in serum iron levels. Over time, persistently high hepcidin reduces iron absorption and locks iron in the reticuloendothelial system, so that hemoglobin iron levels wane, causing anemia. Iron redistribution also leads to less iron in hepatocytes, which express low levels of ferroportin. Conversely, when hepcidin is low (blue columns), iron is highly absorbed and readily released from macrophages, leading to elevated levels in serum and moderately increased hemoglobin. The excess iron in the system accumulates in parenchymal tissues, most frequently in hepatocytes. Note that the changes in iron levels represented by the columns are intended to represent trends rather than quantitative measures. Iron-requiring pathogens often inhabit specific anatomical compartments or target particular cell types. Examples include some types of bacteria that thrive and become pathogenic in the bloodstream; others, such as *M. tuberculosis*, are macrophage-tropic. *Plasmodium* replication in hepatocytes and erythrocytes is highly iron-dependent (many other pathogen types also target hepatocytes because they are energy- and nutrient-rich). Fluctuations in hepcidin—directly consequent to infection as part of the innate immune response, or due to the underlying iron status of the infected individual, or caused by experimental or therapeutic intervention—alter iron availability to the infectious organism, with likely downstream effects on pathogenesis. Iron is required for host immune mechanisms to generate microbicidal effectors (reactive oxygen species, nitric oxide) and for antigen-specific lymphocyte proliferation. [Image credits: Wikimedia, CDC, NIH; bacteria images copyright Dennis Kunkel Microscopy Inc.]

lates with later viral clearance, suggesting an interaction between iron regulation and antiviral immunity (*23*). Iron accumulation also occurs in other noninfectious disorders of the liver, indicating that inflammation or oxidative tissue damage within this organ (for example, induced by alcohol) may predispose to reduced levels of hepcidin, whereas the liver responds to inflammatory signals originating extrahepatically by increasing hepcidin.

Elevated iron levels as a result of low hepcidin in hemochromatosis enhance vulnerability to certain pathogens, such as *Vibrio* species, that are not usually able to scavenge iron from the human host. A striking example of this effect is the enhanced virulence of an attenuated *Yersinia pestis* strain, within which high-affinity iron acquisition genes had been deleted, that occurred in a researcher with undiagnosed hemochromatosis who was working with this organism (*6*). This single case shows that altered iron availability, caused by altered hepcidin expression, can play a major role in the outcome of host-pathogen interactions.

The impact of hepcidin on an infectious disease has been best studied in malaria. Increased erythrophagocytosis and dyserythropoiesis during malaria contribute to malaria-associated anemia. However, hepcidin likely plays an important role as well; for example, children with post-malarial anemia and elevated hepcidin show poor incorporation of oral iron into erythrocytes (*24*). The restricted iron flow to the bone marrow caused by hepcidin may add to the development of anemia and predispose to functional iron deficiency, but could also be protective if parasitemia is limited by the reduced number of red blood cells. *Plasmodium* proliferation within red blood cells and in hepatocytes is iron-dependent. Mice overexpressing hepcidin have less liver iron and a reduced level of parasite growth in the liver; administration of hepcidin peptide has a similar inhibitory effect (*25*). This effect of hepcidin may offer defense against superinfection, whereby an ongoing blood-stage infection prevents the establishment of a second *Plasmodium* infection by stunting the growth of the liver stage (*25*). These experimentally determined interrelationships among hepcidin, iron, and parasite growth may underlie some important observations of human *Plasmodium* infection—for example, that iron deficiency protects against severe malaria in children (*26*) and that iron administration is linked to increased incidence of infection (*3*).

Nontyphoidal *Salmonella* (NTS) is a common cause of bacteremia in the developing world, and NTS is often particularly severe in individuals co-infected with *Plasmodium*. Hemolysis during malaria can increase susceptibility to NTS through recruitment of immature neutrophils from the bone marrow that have increased levels of hemeoxygenase-1 (HO-1), resulting in a reduced capacity for the microbicidal oxidative burst (*27*). Furthermore, the higher iron levels produced by HO-1 may favor proliferation of NTS within infected granulocytes. However, hemolysis alone does not entirely explain the enhanced virulence of NTS in the presence of *Plasmodium*, because hemolytic anemia, equivalent to that induced by malaria but induced by injection of antibodies to red blood cells, does not fully recapitulate the severe NTS dissemination seen in malaria (*28*). The growth of NTS within macrophages is iron-dependent and is reduced by higher levels of ferroportin that exports iron, an effect counteracted by hepcidin (*29*). Therefore, the increased levels of hepcidin that are observed in malaria [but not in hemolytic anemia, in which hepcidin is suppressed (*14*)] may exacerbate the virulence of NTS.

Macrophages facilitate a rapid throughput of iron and strongly express ferroportin, so the growth of pathogens that target and infect this cell type may be particularly influenced by hepcidin. *M. tuberculosis* infection is more severe in iron-loaded mice, and increased dietary iron uptake can be associated with a higher risk of developing tuberculosis in humans (*30*, *31*). A role for the hepcidin-ferroportin axis in the pathogenesis of *M. tuberculosis* infection, as well as being likely on theoretical grounds, is also supported by the finding that single-nucleotide polymorphisms in

Downloaded from www.sciencemag.org on November 9, 2012

ferroportin associate with different levels of susceptibility to tuberculosis (*32*). How hepcidin and ferroportin might influence iron acquisition by *M. tuberculosis* is not yet clear; although high levels of hepcidin would increase iron storage within macrophages, the iron is mostly caged within ferritin shells, and it is not known whether *M. tuberculosis* can scavenge iron sequestered in this way. On the other hand, in conditions of high iron export, although the steady-state level of iron in macrophages may be low, the throughput of loosely chelated "labile" iron may be higher, and *M. tuberculosis* synthesizes siderophores that could access iron in this form. An additional factor is that the generation of microbicidal molecules (including reactive oxygen species and nitric oxide) by macrophages is iron-dependent. Up-regulation of ferroportin (and consequent loss of cellular iron) in macrophages reduces the synthesis of nitric oxide and allows intracellular growth of *M. tuberculosis* (*33*). This double-edged nature of iron—as a nutrient needed for pathogen growth and for host antimicrobial defenses—may be particularly important for macrophage-tropic organisms, and how this balance is regulated by hepcidin requires careful exploration.

The Future of Hepcidin

The discovery of hepcidin as the master hormonal regulator of iron metabolism has revitalized research into iron and infection. The ancestry, structure, and regulation of hepcidin reflect the underlying link between iron regulation and immunity. Because we understand that hepcidin controls both the overall level of iron and its location, the question is no longer only how much iron influences infectious diseases, but also where the iron is located. From this perspective, associations of altered iron status and infectious disease progression need to be reinvestigated. For example, tuberculosis severity is enhanced by HIV-1 co-infection, which is a particular problem in sub-Saharan Africa and elsewhere. HIV-1 replication is also iron-dependent, and in vitro the hepcidin-ferroportin interaction influences viral growth (*34*). Furthermore, increased iron status in HIV-1–infected individuals, and higher macrophage iron in particular, correlates with poor prognosis (*35*, *36*). However, there is currently a dearth of information on hepcidin levels and regulation during acute and chronic HIV-1 infection and how this affects susceptibility to secondary infections, co-infections, and progression to AIDS. There is a similar lack of information on hepcidin regulation during two other infections that are major causes of iron deficiency worldwide: bilharzia (schistosomiasis) and hookworm infection.

In general, understanding whether altered hepcidin regulation contributes to the development of an iron-deficient state will be important for formulating the best way to counteract iron deficiency at the individual and population level. Dietary iron supplementation in the context of high infectious disease burden has been controversial since the Pemba trial found that iron increases the incidence of malaria in infants (*3*). Iron supplementation may also be futile (or even detrimental) in individuals with increased hepcidin, as the blockade on ferroportin likely prevents iron absorption and transport to the bone marrow. In these nutritional contexts, diagnostic hepcidin measurement in target populations could be crucial.

A major future direction for the field is deliberate therapeutic manipulation of hepcidin activity. Advances are being made in this area through the development of small-molecule modulators of hepcidin regulation pathways, neutralizing antibodies to hepcidin, and supra-active mini-hepcidins, among others (*37*–*39*). The ability to determine hepcidin activity theoretically allows control of the level of iron absorption from the diet, as well as partitioning of iron among serum, liver, bone marrow, and the reticuloendothelial system. Such interventions would have potential clinical utility. For example, hepcidin antagonists may enhance recovery from anemia and treatment of iron deficiency in infants, in pregnancy, and in the elderly, whereas therapies that safely increase hepcidin activity may benefit people with iron-loading disorders (*16*).

Deprivation of iron from invading pathogens is in theory a useful strategy for decreasing virulence. Infectious organisms may acquire the ability to both evade immune surveillance and resist antibiotics, but they cannot escape their basic iron requirement for growth. If the properties of hepcidin can be exploited to divert iron away from pathogens that scavenge the nutrient from particular niches, the resulting inhibition of pathogen replication may allow time for immunity to develop and control infections before rapid microbial growth overwhelms the infected individual.

Another concept recently proposed is that of tolerance to microbial burden (*40*), such that infection is not met with catastrophic immunopathology, and higher levels of pathogens are harbored. Interestingly, intracellular iron levels affect innate immune TLR signaling in response to infection, and hepcidin antagonists can be used to attenuate inflammation (*41*). Thus, as well as controlling iron availability to pathogens, hepcidin regulation has the potential to allow manipulation of the host response, and hence could be exploited to augment other therapeutic and preventive interventions, including vaccination.

References and Notes

1. M. J. Murray, A. B. Murray, M. B. Murray, C. J. Murray, *BMJ* **2**, 1113 (1978).
2. J. M. McDermid, A. M. Prentice, *Clin. Sci.* **110**, 503 (2006).
3. S. Sazawal *et al.*, *Lancet* **367**, 133 (2006).
4. A. L. Schade, L. Caroline, *Science* **100**, 14 (1944).
5. J. J. Bullen, H. J. Rogers, E. Griffiths, *Curr. Top. Microbiol. Immunol.* **80**, 1 (1978).
6. K. M. Frank, O. Schneewind, W. J. Shieh, *N. Engl. J. Med.* **364**, 2563 (2011).
7. E. Carniel, *Int. Microbiol.* **2**, 161 (1999).
8. J. Parkhill *et al.*, *Nature* **413**, 523 (2001).
9. R. A. McCance, E. M. Widdowson, *Lancet* **230**, 680 (1937).
10. E. Nemeth *et al.*, *Science* **306**, 2090 (2004).
11. G. Nicolas *et al.*, *Proc. Natl. Acad. Sci. U.S.A.* **98**, 8780 (2001).
12. H. Drakesmith *et al.*, *Blood* **106**, 1092 (2005).
13. K. E. Finberg *et al.*, *Nat. Genet.* **40**, 569 (2008).
14. G. Nicolas *et al.*, *J. Clin. Invest.* **110**, 1037 (2002).
15. S. Rivera *et al.*, *Blood* **106**, 2196 (2005).
16. S. Gardenghi *et al.*, *J. Clin. Invest.* **120**, 4466 (2010).
17. H. Shike *et al.*, *Eur. J. Biochem.* **269**, 2232 (2002).
18. S. T. Motley *et al.*, *Cell. Microbiol.* **6**, 849 (2004).
19. C. Peyssonnaux *et al.*, *Blood* **107**, 3727 (2006).
20. Q. de Mast *et al.*, *J. Infect. Dis.* **199**, 253 (2009).
21. A. E. Armitage *et al.*, *Blood* **118**, 4129 (2011).
22. D. Girelli *et al.*, *J. Hepatol.* **51**, 845 (2009).
23. J. D. Ryan *et al.*, *Hepatology* **56**, 492 (2012).
24. A. M. Prentice *et al.*, *Blood* **119**, 1922 (2012).
25. S. Portugal *et al.*, *Nat. Med.* **17**, 732 (2011).
26. M. Gwamaka *et al.*, *Clin. Infect. Dis.* **54**, 1137 (2012).
27. A. J. Cunnington, J. B. de Souza, M. Walther, E. M. Riley, *Nat. Med.* **18**, 120 (2012).
28. C. M. Roux *et al.*, *Infect. Immun.* **78**, 1520 (2010).
29. S. Chlosta *et al.*, *Infect. Immun.* **74**, 3065 (2006).
30. I. T. Gangaidzo *et al.*, *J. Infect. Dis.* **184**, 936 (2001).
31. U. E. Schaible, H. L. Collins, F. Priem, S. H. Kaufmann, *J. Exp. Med.* **196**, 1507 (2002).
32. M. A. Baker *et al.*, *J. Infect. Dis.* **205**, 1043 (2012).
33. E. E. Johnson, A. Sandgren, B. J. Cherayil, M. Murray, M. Wessling-Resnick, *Infect. Immun.* **78**, 5099 (2010).
34. M. Xu *et al.*, *Retrovirology* **7**, 104 (2010).
35. C. de Monyé, D. S. Karcher, J. R. Boelaert, V. R. Gordeuk, *AIDS* **13**, 375 (1999).
36. J. M. McDermid *et al.*, *Am. J. Clin. Nutr.* **90**, 225 (2009).
37. G. C. Preza *et al.*, *J. Clin. Invest.* **121**, 4880 (2011).
38. B. J. Sasu *et al.*, *Blood* **115**, 3616 (2010).
39. P. B. Yu *et al.*, *Nat. Chem. Biol.* **4**, 33 (2008).
40. R. Medzhitov, D. S. Schneider, M. P. Soares, *Science* **335**, 936 (2012).
41. L. Wang *et al.*, *J. Clin. Invest.* **119**, 3322 (2009).
42. A. Krause *et al.*, *FEBS Lett.* **480**, 147 (2000).
43. C. H. Park, E. V. Valore, A. J. Waring, T. Ganz, *J. Biol. Chem.* **276**, 7806 (2001).
44. C. Pigeon *et al.*, *J. Biol. Chem.* **276**, 7811 (2001).

Acknowledgments: Supported by the Medical Research Council UK (MC-A760-5QX00) and the Beit Memorial Fellowship for Medical Research. We thank R. Moxon, L. Eddowes, and A. Armitage for critical reading of the manuscript.

Supplementary Materials

www.sciencemag.org/cgi/content/full/338/6108/768/DC1
Figs. S1 and S2
References (*45*–*58*)

10.1126/science.1224577

Downloaded from www.sciencemag.org on November 9, 2012

An Interacting Binary System Powers Precessing Outflows of an Evolved Star

Henri M. J. Boffin,[1]* Brent Miszalski,[2,3] Thomas Rauch,[4] David Jones,[1] Romano L. M. Corradi,[5,6] Ralf Napiwotzki,[7] Avril C. Day-Jones,[8] Joachim Köppen[9]

Stars are generally spherical, yet their gaseous envelopes often appear nonspherical when ejected near the end of their lives. This quirk is most notable during the planetary nebula phase, when these envelopes become ionized. Interactions among stars in a binary system are suspected to cause the asymmetry. In particular, a precessing accretion disk around a companion is believed to launch point-symmetric jets, as seen in the prototype Fleming 1. Our finding of a post–common-envelope binary nucleus in Fleming 1 confirms that this scenario is highly favorable. Similar binary interactions are therefore likely to explain these kinds of outflows in a large variety of systems.

Planetary nebulae (PNe) are thought to represent the transitory phase of the end of the lives of solarlike stars. The mass-loss mechanisms at play during the late stages of stellar evolution that produce the observed shapes of PNe have been a matter of debate in the past two decades (*1*). The leading paradigm to produce the most extreme nebular morphologies is evolution in an interacting binary system (*2*–*4*), in particular common-envelope (CE) evolution: the dramatic outcome of unstable mass transfer resulting in a binary system with a greatly reduced orbital period ($P < \sim$1 day for PNe). Despite recent detections of multiple post-CE binary central stars (*5*–*7*), there are as yet no clear-cut examples of binaries actively shaping their surrounding PNe. A handful of post-CE nebulae are known to be oriented in agreement with the orbital inclination of the binaries that ejected them (*8*), as would be expected. However, we do not yet have any inkling how a particular binary configuration gives rise to a specific fundamental nebula shape. An alternative approach to tackle this difficult problem is to focus instead on nebular features that are impossible to explain without binaries. These are the low-ionization microstructures that include filaments, knots, and collimated fast outflows (hereafter jets). Theory prescribes that jets are launched and collimated by accretion, rotation, and/or magnetic mechanisms (*9*), but in the case of PNe only the binary explanation is feasible (*10*). In fact, the idea of precessing jets from a binary to explain the point-symmetric structures observed in PNe is at least 30 years old (*11*).

Fleming 1 (PN G290.5+07.9, hereafter Fg 1; Table 1) is a southern PN renowned for its spectacular set of bipolar jets delineated by a symmetric configuration of high-speed knots (*12*, *13*). At an assumed distance of 2.4 kpc (*14*) they span about 2.8 pc from tip to tip. The knots in the jets around Fg 1 follow a curved path distinguished by opposing pairs whose connecting lines intersect precisely with the position of the central star. The outermost knots are elongated and, because of their measured radial velocities of roughly 75 km/s with respect to the bulk motion of the nebula, were probably ejected about 16,000 years ago, whereas the innermost ones were possibly ejected some 9000 or 10,000 years later (*12*). On the basis of its reported expansion velocity, one can also estimate the innermost nebula to be about 5000 years old, assuming a constant expansion rate. Because of their appearance suggestive of episodic ejections produced by a precessing source, Fg 1 became the archetype of a morphological subclass of PNe named after their bipolar, rotating, episodic jets.

In 2011, we obtained a series of medium-resolution spectra of the central star of Fg 1 with FORS2 on ESO's Very Large Telescope (*15*) (table S1). The velocities, measured from an average of the C IV lines at 581.1 and 581.2 nm, show a periodic behavior (Fig. 1) that we attribute to the presence of a close companion. By using a Levenberg-Marquardt minimization method, we fitted a circular orbit with an orbital period of 1.1953 ± 0.0002 days (the error bar indicates one standard deviation uncertainty) and semi-amplitude of 87.65 ± 1.68 km/s, where the errors were estimated via a bootstrap method. Treating the eccentricity as a free parameter, we find no evidence for a noncircular orbit (e = 0.015 ± 0.017).

A nonlocal thermodynamic equilibrium analysis of the spectra shows that they can be fitted with a pure solar abundance hydrogen and helium atmosphere having an effective temperature, $T_{\rm eff}$ = 80,000 ± 15,000 K, and a surface gravity, log g = 5.00 ± 0.25 cm/s^2 (*15*). A comparison with post–asymptotic giant branch (post-AGB) evolutionary tracks (*16*) implies an approximate mass of the primary star: $0.56^{+0.3}_{-0.04}$ solar masses.

The morphology of Fg 1 can be represented by a PN core that has the shape of a butterfly with its axis tilted at about 50° to the line of sight (*17*). This is most likely also the orientation of the orbital plane (the main jet axis being perpendicular to it), and we can thus make use of this fact to estimate the mass of the secondary star by using our measured orbital parameters. By assuming an inclination of 45° ± 5° and using our value

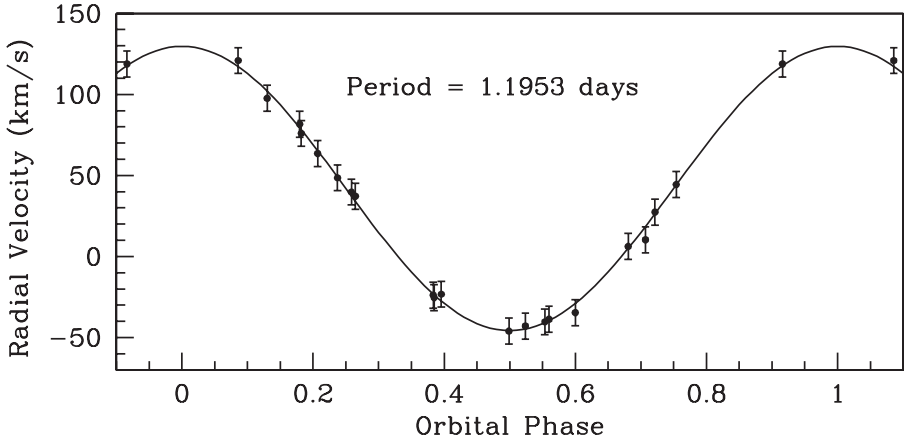


Fig. 1. Radial velocity curve of the central star of Fg 1. The measured radial velocities are folded on the orbital period of 1.1953 days, and a sinusoidal curve is indicated for comparison. Error bars indicate the one standard deviation uncertainty, conservatively taken as 3 km/s.

[1]European Southern Observatory (ESO), Alonso de Cordova 3107, Vitacura, Casilla 19001, Santiago, Chile. [2]South African Astronomical Observatory (SAAO), Post Office Box 9, Observatory 7935, South Africa. [3]Southern African Large Telescope Foundation, Post Office Box 9, Observatory 7935, South Africa. [4]Institute for Astronomy and Astrophysics, Kepler Center for Astro and Particle Physics, Eberhard Karls University, Sand 1, 72076 Tübingen, Germany. [5]Instituto de Astrofísica de Canarias, E-38200 La Laguna, Tenerife, Spain. [6]Departamento de Astrofísica, Universidad de La Laguna, E-38206 La Laguna, Tenerife, Spain. [7]Physics, Astronomy and Mathematics, University of Hertfordshire, Hatfield AL10 9AB, UK. [8]Universidad de Chile, Santiago, Casilla 36-D, Chile. [9]Observatoire de Strasbourg, 11 rue de l'université, F-67000 Strasbourg, France.

*To whom correspondence should be addressed. E-mail: hboffin@eso.org

Downloaded from www.sciencemag.org on November 9, 2012

of the binary mass function, we derive a mass of the secondary between 0.7 and 1 solar masses. The companion must therefore be either an early K or G dwarf or a more massive white dwarf. A main-sequence companion would, however, be irradiated by the hot primary, as seen for example in the 1.16-day binary system inside the Necklace nebula (*6*). We are able to discard any photometric variability above 0.05 mag (*15*), much smaller than would be expected for a 1.2-day orbital period and the range of effective temperature we consider (*18*). Moreover, the absence of any irradiated emission lines at all orbital phases that would indicate the presence of a main-sequence companion (*15*) provides additional proof that the system must be a double degenerate, that is, that the companion is a slightly more massive white dwarf that has either become too faint or whose spectral energy distribution peaks in the ultraviolet and is no longer detectable in the visible wavelength domain. For such a companion to provide the required number of ionizing photons above 54 eV to explain the observed ionization level of the nebula (which the observed central star cannot supply), its temperature needs to be greater than 120 kK. Such a high temperature would also make it undetectable in the visual spectrum. A more detailed analysis (*15*) shows that stars on post-AGB tracks with masses of 0.63 to 0.7 solar masses would meet these conditions. Thus, Fg 1 is most likely the latest addition to the very few examples of double-degenerate systems found in PNe. For the two stars to be still inside a nebula and with the secondary being so hot, either the initial mass ratio was very close to unity and the two stars evolved toward the PN phase almost simultaneously or the secondary has been reheated by accretion, just before the CE.

Our deep images of Fg 1, obtained with FORS2 in Hα+[N II], [O III], and [O II] filters, show both an envelope of shocked gas around the jets (Fig. 2) and a ring of low-ionization knots (Fig. 3). The characteristics of the fragmented jets in Fg 1 resemble the ballistic model predictions for jets from time-dependent sources. Three-dimensional gas-dynamical simulations show that the clumps are ejected in a bipolar outflow from a source in a circular orbit that has a precessing outflow axis (*19*, *20*). At later times a mostly point-symmetric structure remains, in which the flow has developed flat-topped ends, very similar to what is seen in Fg 1. Another characteristic of these models is the presence of an envelope around the jets, similar to that seen in our images (Fig. 2). This envelope adds further weight to the argument that the precessing jets do in fact originate from a time-dependent source as prescribed by the models. Such precession is best explained by an accretion disk around a companion star and has been invoked to explain point-symmetric jets in other PNe (*21*). The presence of polar ejections older than the main body of the nebula, as recently found in a few systems (*6*, *7*, *22*), indicates that mass transfer before the CE is most likely

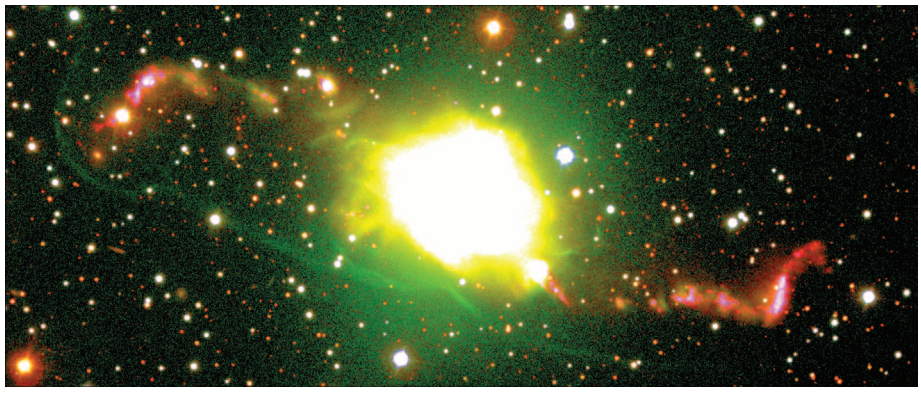


Fig. 2. FORS2 color-composite image of Fg 1 showing the [O III] envelope around the bipolar jets. The 5.5′-by-2.3′ image is based on individual images obtained through Hα+[N II] (red), [O III] (green), and [O II] (blue) filters. The orientation is the same as in Fig. 3.

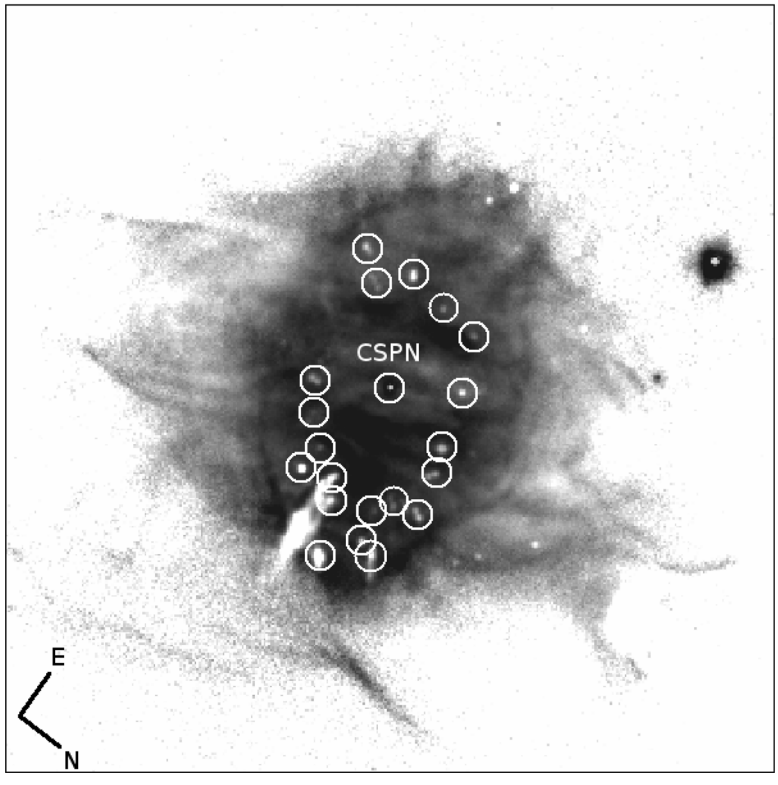


Fig. 3. The central nebula of Fg 1. This 90″-by-90″ image shows the ratio between the [O III] and Hα+[N II] FORS2 images. Black corresponds to high ratios ([OIII] bright), whereas white corresponds to small ratios (Hα+[NII] bright). The central star (CSPN) and the low-ionization knots (forming an approximate ring roughly 35″ by 64″ in size) are highlighted.

responsible for the jets. The extent of its S-shaped jets, a strong signature of precession, distinguishes Fg 1 from these other systems, and the reason may lie in the fact that it contains two degenerate objects.

The necessary accretion disc is likely to have formed around the secondary (*10*), most probably from material lost by the stellar wind (*23*). We conjecture that such a disc could have formed through "wind Roche-lobe overflow" (*24*), when the wind material fills the giant's Roche lobe and is transferred to the companion through the inner Lagrangian point. This can dramatically increase the accretion rate with respect to normal wind accretion and has also been invoked to explain the current state of the symbiotic star SS Lep (*25*). Once the AGB star filled its Roche lobe, the mass transfer became unstable, and a CE formed, shutting off the accretion disc and its associated jets, meanwhile forming the 5000-year-old inner nebula and shrinking the orbit of the binary system to the current observed value.

A double-degenerate central star would imply that Fg 1 must have gone through two suc-

Downloaded from www.sciencemag.org on November 9, 2012

Table 1. Characteristics of Fg 1.

	Value
Right ascension	11 28 36.2
Declination	–52 56 03
Orbital period, *P*	1.1953 ± 0.0002 days
T° (modified Julian date)	55671.556 ± 0.018 days
Eccentricity, *e*	0 (fixed)
Radial velocity semi-amplitude, *K*	87.65 ± 1.68 km/s
Mass function, *f*(*m*)	0.084 ± 0.005 solar mass

cessive mass-transfer episodes. In the first one, the system avoided the CE, because the remaining system must have been still wide enough to leave space for the secondary to expand to the AGB phase. In the second mass transfer event, described above, this was not the case. The existence of symbiotic and other peculiar red giant systems composed of a red giant and a white dwarf with orbital periods of several hundreds or thousands of days (*26*) shows that such stable episode of mass transfer is not uncommon, even though the details are still far from understood (*27*).

As with the jets in Fg1, its inner ring of knots (Fig. 3) is also thought to result from a binary interaction (*28*, *29*). Such knotty rings are found in a variety of stars at the end of their evolution, one of the most spectacular cases being SN1987A (*30*). These rings are a distinctive feature of many PNe around close binaries (*31*), most notably in the Necklace (*7*). However, similar torus structures are observed in much wider binaries like symbiotic stars [e.g., (*32*)], as well as in several evolved massive stars (*33*). The examples provided by Fg 1, the Necklace, the other PNe with close binary central stars, and symbiotic Miras point to a common mechanism linked to binary evolution for the formation of ring nebulae around many kinds of stars.

References and Notes

1. B. Balick, A. Frank, *Annu. Rev. Astron. Astrophys.* **40**, 439 (2002).
2. N. Soker, *Publ. Astron. Soc. Pac.* **118**, 260 (2006).
3. J. Nordhaus, E. G. Blackman, *Mon. Not. R. Astron. Soc.* **370**, 2004 (2006).
4. O. De Marco, *Publ. Astron. Soc. Pac.* **121**, 316 (2009).
5. B. Miszalski, A. Acker, A. F. J. Moffat, Q. A. Parker, A. Udalski, *Astron. Astrophys.* **496**, 813 (2009).
6. B. Miszalski *et al.*, *Mon. Not. R. Astron. Soc.* **413**, 1264 (2011).
7. R. L. M. Corradi *et al.*, *Mon. Not. R. Astron. Soc.* **410**, 1349 (2011).
8. D. Jones *et al.*, in *Evolution of Compact Binaries*, vol. 447 of *Astronomical Society of the Pacific Conference Series*, L. Schmidtobreick, M. Schreiber, C. Tappert, Eds. (Astronomical Society of the Pacific, San Francisco, 2011), pp. 165–170.
9. R. E. Pudritz *et al.*, in *Protostars and Planets V*, B. Reipurth, D. Jewitt, K. Keil, Eds. (Univ. of Arizon Press, Tucson, AZ, 2007), pp. 277–294.
10. N. Soker, M. Livio, *Astrophys. J.* **421**, 219 (1994).
11. J. P. Phillips, N. K. Reay, *Astron. Astrophys.* **117**, 33 (1983).
12. J. A. Lopez, J. Meaburn, J. W. Palmer, *Astrophys. J.* **415**, L135 (1993).
13. J. A. Lopez, M. Roth, M. Tapia, *Astron. Astrophys.* **267**, 194 (1993).
14. W. J. Maciel, *Astron. Astrophys.* **55** (suppl.), 253 (1984).
15. Additional information is available in the supplementary materials on *Science* Online.
16. D. Schoenberner, *Astrophys. J.* **272**, 708 (1983).
17. J. W. Palmer *et al.*, *Astron. Astrophys.* **307**, 225 (1996).
18. O. De Marco, T. C. Hillwig, A. J. Smith, *Astron. J.* **136**, 323 (2008).
19. J. A. Cliffe, A. Frank, M. Livio, T. W. Jones, *Astrophys. J.* **447**, L49 (1995).
20. A. C. Raga *et al.*, *Astrophys. J.* **707**, L6 (2009).
21. L. F. Miranda, J. M. Torrelles, M. A. Guerrero, R. Vazquez, Y. Gomez, *Mon. Not. R. Astron. Soc.* **321**, 487 (2001).
22. D. L. Mitchell *et al.*, *Mon. Not. R. Astron. Soc.* **374**, 1404 (2007).
23. T. Theuns, H. M. J. Boffin, A. Jorissen, *Mon. Not. R. Astron. Soc.* **280**, 1264 (1996).
24. S. Mohamed, P. Podsiadlowski, in *International Conference on Binaries: In Celebration of Ron Webbink's 65th Birthday*, V. Kologera, M. van der Sluys, Eds. (American Institute of Physics Conference Proceedings 1314, Melville, NY, 2010), pp. 51–52.
25. N. Blind *et al.*, *Astron. Astrophys.* **536**, A55 (2011).
26. J. Mikolajewska, *Balt. Astron.* **21**, 1 (2012).
27. T. E. Woods, N. Ivanova, M. V. van der Sluys, S. Chaichenets, *Astrophys. J.* **744**, 12 (2012).
28. L. Sandquist, R. E. Taam, X. Chen, P. Bodenheimer, A. Burkert, *Astrophys. J.* **500**, 909 (1998).
29. A. C. Raga, A. Riera, G. Mellema, A. Esquivel, P. F. Velázquez, *Astron. Astrophys.* **489**, 1141 (2008).
30. S. Mattila *et al.*, *Astrophys. J.* **717**, 1140 (2010).
31. B. Miszalski, A. Acker, Q. A. Parker, A. F. J. Moffat, *Astron. Astrophys.* **505**, 249 (2009).
32. M. Santander-García *et al.*, *Astron. Astrophys.* **465**, 481 (2007).
33. N. Smith, J. Bally, J. Walawender, *Astron. J.* **134**, 846 (2007).

Acknowledgments: This paper uses data from ESO programs 084.C-0508(A), 085.D-0629(A), and 087.D-0446(B) and includes observations made at the SAAO. The measured radial velocities and observed spectrum are provided in the supplementary materials. Observations obtained with ESO telescopes can also be obtained from the ESO science archive at http://archive.eso.org, using the above-mentioned program numbers. The SAAO photometric data are available from www.eso.org/~hboffin/Fg1/. B.M. thanks ESO for its hospitality and the opportunity to participate in its visitor program during January 2012. T.R. is supported by the German Aerospace Center (DLR) grant 05 OR 0806. This work was cofunded under the Marie Curie Actions of the European Commission (FP7-COFUND). The work of R.L.M.C. has been supported by the Spanish Ministry of Science and Innovation (MICINN) under grant AYA2007-66804. A.C.D.-J. is supported by a FONDECYT (Fondo Nacional de Desarrollo Científico y Tecnológico) "postdoctorado" fellowship under project number 3100098 and partially supported by the Joint Committee ESO–Government of Chile.

Supplementary Materials

www.sciencemag.org/cgi/content/full/338/6108/773/DC1
Supplementary Text
Figs. S1 to S4
Table S1
References

30 May 2012; accepted 2 October 2012
10.1126/science.1225386

Polarity-Switching Top Coats Enable Orientation of Sub–10-nm Block Copolymer Domains

Christopher M. Bates,[1] Takehiro Seshimo,[1] Michael J. Maher,[1] William J. Durand,[2] Julia D. Cushen,[2] Leon M. Dean,[2] Gregory Blachut,[2] Christopher J. Ellison,[2] C. Grant Willson[1,2]*

Block copolymers (BCPs) must necessarily have high interaction parameters (χ), a fundamental measure of block incompatibility, to self-assemble into sub–10-nanometer features. Unfortunately, a high χ often results from blocks that have disparate interfacial energies, which makes the formation of useful thin-film domain orientations challenging. To mitigate interfacial forces, polymers composed of maleic anhydride and two other components have been designed as top coats that can be spin-coated from basic aqueous solution in the ring-opened, acid salt form. When baked, the anhydride reforms and switches polarity to create a neutral layer enabling BCP feature alignment not possible by thermal annealing alone. Top coats were applied to the lamella-forming block copolymers poly(styrene-*block*-trimethylsilylstyrene-*block*-styrene) and poly(trimethylsilylstyrene-*block*-lactide), which were thermally annealed to produce perpendicular features with linewidths of 15 and 9 nanometers, respectively.

The self-assembly of block copolymers (BCPs) into domains on the length scale of ~1 to 100 nm (*1*) is attractive for many applications, including organic optoelectronics (*2*), nanoporous membranes (*3*), and next-generation lithography (*4*). Molecular-level BCP ordering into morphologies such as cylinders and lamellae is well understood in bulk (*5*), but most en-

Downloaded from www.sciencemag.org on November 9, 2012

gineering applications demand thin films in which the orientation of the structures is perpendicular to the substrate. Variations in film thickness, substrate interfacial energy, and substrate topography have been exploited to orient and direct the assembly of BCP features for high-resolution patterning applications (*6*). In order to self-assemble into features smaller than 10 nm, BCPs must have high interaction parameters (χ), which are a fundamental measure of block incompatibility. Orienting such materials is challenging, because the blocks generally have disparate polarities. Solvent annealing can induce perpendicular orientation of high-χ BCPs (*7*), but this process has important shortcomings, including dewetting, long annealing times, deformation of the structures (*8*), and incompatibility with processes commonly used in nanomanufacturing. Unfortunately, inducing perpendicular orientations of high-χ BCPs by thermal treatment alone requires control of both the substrate (bottom) and top interfaces of the film, which is a challenge.

The orientation challenge stems from the fact that, in the absence of solvent or other components, there exist three possible equilibrium arrangements of a lamella-forming AB diblock copolymer thin film (Fig. 1A). When thermally annealed, the minimum energy state is largely determined by interfacial interactions (*9*). Thus, achieving desirable orientations demands control of the interfacial interactions. There are as many as four pairs of interfacial energies to be considered: $\gamma_{A\text{-}Top}$, $\gamma_{A\text{-}Bot}$, $\gamma_{B\text{-}Top}$, $\gamma_{B\text{-}Bot}$, where γ is the interfacial interaction energy; the subscripts A and B refer to the two blocks of a two-component BCP; and "Bot" and "Top" refer to the bottom and the top surface, respectively. Orientations of lamella perpendicular to the substrate occur when the difference between the individual block interfacial energies with each surface is minimized; that is, $\Delta\gamma_{Top} \sim \Delta\gamma_{Bot} \sim 0$, where $\Delta\gamma_{Top} \equiv |\gamma_{B\text{-}Top} - \gamma_{A\text{-}Top}|$ and $\Delta\gamma_{Bot} \equiv |\gamma_{B\text{-}Bot} - \gamma_{A\text{-}Bot}|$. Surfaces that have this characteristic are referred to as neutral. As these differences deviate from near 0, lamellae form in an orientation that creates planes of blocks parallel to the substrate that have a single block in contact with each surface.

Substrate interfacial interactions can be controlled through a variety of methods, including grafting a polymer or monolayer to functional groups on a surface (*10*), cross-linking a spin-coated polymer film on a surface (*11*), and directly changing substrate composition (*12*). By tailoring the interfacial energy to be between those of the individual blocks, the bottom surface can be neutralized ($\Delta\gamma_{Bot} \sim 0$). In high-$\chi$ BCPs, the strong interaction of the nonpolar block with air, which has a low dielectric constant, drives domain orientation to be parallel to the substrate. Several attempts have been made to circumvent this parallel orientation. Physical confinement of a BCP between two solid surfaces (*13*, *14*) and the application of neutral polymeric top coats by floating (*15*) both provide top surface control but suffer from scalability issues and the introduction of defects. Blending surfactants with BCPs introduces swelling and has been demonstrated only with poly(styrene-*block*-methyl methacrylate) (PS-PMMA) (*16*), which does not require such processing to achieve alignment and cannot achieve sub–10-nm feature sizes. The application of polymeric top coats by spin-coating from water has been reported (*17*), but materials deposited in this way are very polar and again, the process was demonstrated only with PS-PMMA. BCPs that decouple bulk and thin-film thermodynamics appear promising, but require precise post-polymerization modifications that could be difficult to control on a large scale (*18*).

PS-PMMA has been the standard material for thin-film studies, because several neutral bottom-layer treatments are known, and in air, $\Delta\gamma_{Top}$ becomes zero at ~210°C ($\gamma_{PS\text{-}Air} \approx \gamma_{PMMA\text{-}Air}$) (*19*). Thus, PS-PMMA can be readily oriented perpendicular to a substrate. Unfortunately, its low χ (~0.039 at 150°C) (*20*) limits the minimum feature size to ~13 nm. Higher-χ BCPs that can form smaller features, such as poly(styrene-*block*-2-vinylpyridine) (PS-P2VP, $\chi \sim 0.12$ at 150°C) (*21*) and poly(styrene-*block*-dimethylsiloxane) (PS-PDMS, $\chi \sim 0.12$ at 150°C) (*22*), unfortunately have $\Delta\gamma_{Top} >> 0$ with air, which drives the orientation of domains at the top interface parallel to the substrate. Even in the presence of neutral substrate surface treatments (*23*, *24*), they cannot be aligned by thermal annealing alone.

An ideal solution to the high-χ BCP orientation challenge would be to confine the BCP between bottom and top interfaces that are rendered neutral. A top coat that can be applied by spin-coating has several advantages: (i) it employs the same coating equipment used to apply the BCP film, (ii) it ensures uniform coverage across large substrates, and (iii) is compatible with thermal annealing processes. Unfortunately, neutral polymers that can be spin-coated onto a BCP will necessarily only be soluble in a solvent that dissolves or is sorbed by at least one of the blocks of the BCP. Polymers that can be coated from a solvent that does not interact with the BCP will have interfacial energies that are not intermediate between those of the two blocks. Hydrophobic organic BCPs require a top coat that can be spin-coated out of a very polar solvent such as water, but water-soluble top coats are far too polar to have an interfacial energy between that of the hydrophobic blocks.

Our approach to solving the dilemma is to use a top coat that switches polarity after spin-coating over a BCP film via a subsequent chemical reaction. In its polar form, the top coat is soluble in aqueous ammonium hydroxide, which permits its application onto a water-insoluble organic BCP thin film by spin-coating. Upon baking, the top coat quickly loses ammonia and undergoes a chemical transformation into a less polar state, which modulates the top-coat inter-

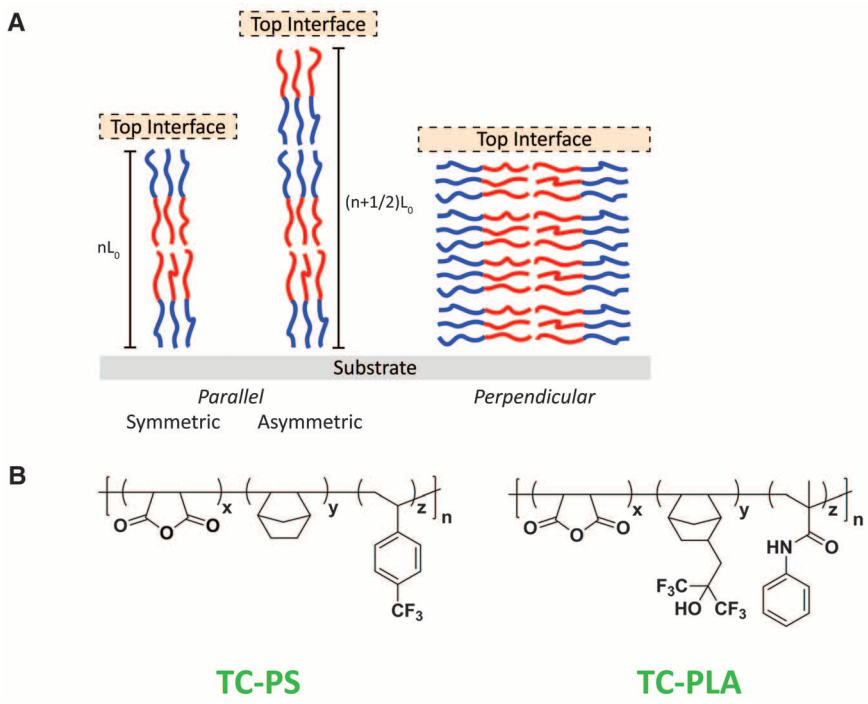


Fig. 1. (**A**) Three thin-film orientations of a lamella-forming AB diblock copolymer. (**B**) The chemical structures of the two top coats tested here. TC-PS was applied to PS-PTMSS-PS and TC-PLA was applied to PTMSS-PLA. Experimental details can be found in the supplementary materials.

[1]Department of Chemistry, University of Texas at Austin, 1 University Station A5300, Austin, TX 78712, USA. [2]Department of Chemical Engineering, University of Texas at Austin, 1 University Station C0400, Austin, TX 78712, USA.

*To whom correspondence should be addressed. E-mail: willson@che.utexas.edu

Downloaded from www.sciencemag.org on November 9, 2012

facial energy and effectively neutralizes the top interface, enabling perpendicular orientation of the BCP when it is annealed above the glass transition temperature (T_g) of the blocks. The top coat can then be stripped by washing with an aqueous base.

A successful top coat must be soluble in a solvent that does not interact with either block of the BCP, undergo a change in interfacial energy upon baking that renders it nearly neutral, and ideally can be stripped by solvent after BCP alignment. The top coat must also have a T_g above that of all blocks, and preferably a relatively high molecular weight. These latter requirements stem from a need to preclude intermixing of the top coat with any block during annealing. This mixing requires polymer interdiffusion, and interdiffusion coefficients are very low below T_g (*25*) and scale strongly and inversely with molar mass (*26*).

The top coat process was successfully demonstrated with two different lamella-forming, silicon-containing BCPs: poly(styrene-*block*-trimethylsilylstyrene-*block*-styrene) (PS-PTMSS-PS) and poly(trimethylsilylstyrene-*block*-D,L-lactide) (PTMSS-PLA) (figs. S1 to S3). The two BCPs used in this study were chosen for several reasons. Both incorporate a silicon-containing block, because the silicon-containing block has a lower O_2 reactive ion etch rate relative to the other block, which is helpful in subsequent pattern transfer steps (*27*). In general, silicon-containing BCPs are notoriously difficult to orient in thin films. Neither perpendicular cylinders nor lamellae have ever been reported at the top interface of thin films of silicon-containing BCPs when subjected only to thermal annealing (*24*, *28*). The triblock copolymer was chosen because previous studies (*29*, *30*) suggest that ABA triblock copolymers with relative interfacial energies $\gamma_B < \gamma_A$ adopt a perpendicular orientation more readily than AB diblocks. PTMSS-PLA has a very high χ and self-assembles into sub–10-nm features (*31*). All attempts to align either PS-PTMSS-PS or PTMSS-PLA by thermal annealing alone in air, nitrogen, or under vacuum were unsuccessful. Both architectures oriented exclusively parallel to the substrate in the absence of a top coat.

The structures of two spin-coated top coats are shown in Fig. 1B (for full characterization data, see schemes S1 to S3 and figs. S2 to S4). The polarity-switching mechanism exploits the ring-opening and -closing reaction of the maleic anhydride moiety (Fig. 2A), which has been reported previously (*32*). Norbornene was introduced as a co-monomer because it produces high T_g, alternating copolymers with maleic anhydride by free-radical polymerization (*33*). A third co-monomer, the proportion of which can be varied, was introduced to further tune the interfacial characteristics of the top-coat material. The introduction of pendant substituents on the norbornene and the third co-monomer allow tuning of the interaction energy of the top coat. The annealing temperature must be above the T_g of each block to allow for BCP reorganization (fig. S2, PS-PTMSS-PS: $T_{g\text{-PS}}$ = 106°C, $T_{g\text{-PTMSS}}$ = 131°C; PTMSS-PLA: $T_{g\text{-PTMSS}}$ = 102°C, $T_{g\text{-PLA}}$ = 54°C) but below that of the top coats ($T_{g\text{-TC-PS}}$ = 214°C, $T_{g\text{-TC-PLA}}$ = 180°C) to prevent interdiffusion. The ring-opening and -closing reactions were verified with a model polymer containing maleic anhydride, norbornene, and a fluorinated methacrylate (TC-IR, figs. S5 and S6) using infrared (IR) spectroscopy (Fig. 2B). The anhydride carbonyl out-of-plane and in-plane stretching bands $\nu_{op}(C{=}O)_2$ = 1775 cm^{-1} (strong) and $\nu_{ip}(C{=}O)_2$ = 1850 cm^{-1} (weak) are in good agreement with reported values (*34*). Upon coating from aqueous NH_4OH, there was complete disappearance of the anhydride carbonyl bands at 1775 and 1850 cm^{-1} and the appearance of symmetric and asymmetric carboxylate COO^- stretching bands at ν_{sym} = 1400 cm^{-1} and ν_{asym} = 1560 cm^{-1}, and a band attributed to the asymmetric C=O stretch of the free carboxylic acid at ν_{asym} = 1660 cm^{-1} (*35*). Subsequent heating at 210°C for 1 min caused reappearance of the anhydride carbonyl bands at 1775 and 1850 cm^{-1} and a corresponding decrease in the intensity of the ring-opened carboxylate and carbonyl stretching bands.

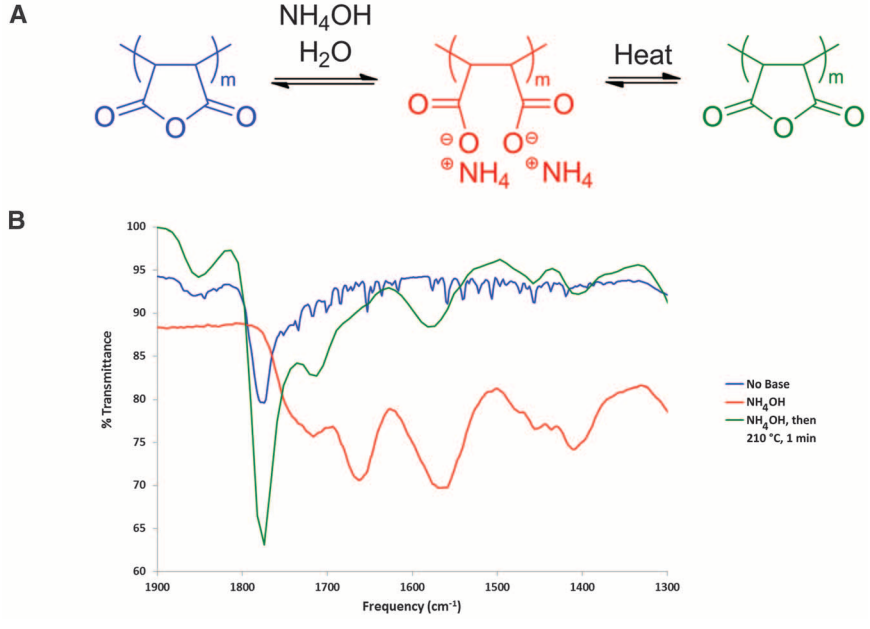


Fig. 2. (**A**) Ring-opening and -closing reactions that modulate the polarity of the top coats. (**B**) IR data from a model top coat (TC-IR, see supplementary materials) that demonstrate the ring-opening and -closing reactions of the poly(maleic anhydride) component. Blue curve, cast from 2-butanone; red curve, cast from 30 weight % (wt %) aqueous (aq.) NH_4OH; green curve, aqueous NH_4OH-cast sample subsequently annealed at 210°C for 1 min.

PS-PTMSS-PS triblock copolymer samples confined between a substrate surface treated with poly(4-methoxystyrene-*random*-4-vinylbenzylazide) (XST-OMe, see the supplementary materials) and the TC-PS top coat, annealed at 210°C for 1 min on a hot plate in an air environment, showed well-formed perpendicular lamellae over the entire film (Fig. 3A). The figure shows scanning electron microscope (SEM) data after the top coat was stripped with aqueous ammonium hydroxide and the oriented film was subjected to development by O_2 reactive ion etching. In contrast, samples annealed in the absence of a top coat (Fig. 3A, inset) but subjected to identical annealing, stripping, and O_2 reactive ion etch conditions show absolutely no signs of perpendicular self-assembly in any region of the film. They have parallel-oriented lamellae. The top coat very efficiently induces perpendicular orientation of the silicon-containing BCP, which otherwise orients parallel to the substrate. Tilted SEM images of samples etched with O_2 are consistent with perpendicular lamellae penetrating the entire thickness of the film (fig. S7). Furthermore, the O_2-etched pattern was successfully transferred into single-crystal silicon (fig. S8).

One-minute thermal annealing for PS-PTMSS-PS with the top coat matches the fastest self-assembly processes reported even for PS-PMMA, which are on the order of 1 min at 250°C (*36*). The bulk periodicity (L_0) value as calculated from Fig. 3A (29 nm) is in good agreement with the bulk value calculated from small-angle x-ray scattering (SAXS) data (30 nm) (*37*). Similar thin-film orientation behavior was observed with the high-χ lamella-forming PTMSS-PLA annealed with top-coat TC-PLA (Fig. 3B). Well-formed perpendicular lamellae were observed after the top coat was stripped, with measured L_0 values ~19 nm, corresponding to linewidths of <10 nm. In this case, the SAXS data for the bulk sample shows an even smaller L_0 (15 nm). We believe that the lack of perfect agreement between these measurements is probably the result of imprecise SEM metrology at a resolution near

Downloaded from www.sciencemag.org on November 9, 2012

the limit of our instrument. Samples annealed and stripped in the absence of a top coat produced only slight surface roughness, with no perpendicular lamella in any region (Fig. 3B, inset).

The difference in orientation between a film with and without a top coat can be understood in terms of the differences in the thin-film free energies of the orientations that the block copolymer can adopt. For simplicity, a symmetric AB diblock copolymer is modeled using PS and PTMSS constituents, which have bulk free energy (*38*) and interfacial interactions similar to those of the ABA triblock copolymer. The bulk free energy of the BCP must be modified in the case of thin films because of the addition of substantial interfacial free energies. Three orientations of the lamella-forming BCP were considered: horizontal symmetric, horizontal asymmetric, and vertical (Fig. 1A). Turner (*39*) and Walton (*40*) introduced a thin-film free-energy model that evaluates the free energy of each of the three lamellar orientations F_V (vertical), $F_{H\text{-}sym}$ (horizontal symmetric), and $F_{H\text{-}asym}$ (horizontal asymmetric) relative to the bulk free energy of the BCP (F_0). These relationships are expressed as follows (Eqs. 1 to 3)

$$\frac{F_V}{F_0} = \frac{1}{3}\left[3 + \frac{1}{d}\left(\frac{(\gamma_{B\text{-}Bot} - \gamma_{A\text{-}Bot}) + (\gamma_{B\text{-}Top} - \gamma_{A\text{-}Top})}{2\gamma_{AB}} + \frac{\gamma_{A\text{-}Top} + \gamma_{A\text{-}Bot}}{\gamma_{AB}}\right)\right] \quad \text{Eq. 1}$$

$$\frac{F_{H\text{-}sym}}{F_0} = \frac{1}{3}\left[\left(\frac{d}{n}\right)^2 + \frac{2n}{d} + \frac{1}{d}\left(\frac{\gamma_{A\text{-}Top} + \gamma_{A\text{-}Bot}}{\gamma_{AB}}\right)\right] \quad \text{Eq. 2}$$

$$\frac{F_{H\text{-}asym}}{F_0} = \frac{1}{3}\left[\left(\frac{d}{n+\frac{1}{2}}\right)^2 + \frac{2\left(n+\frac{1}{2}\right)}{d} + \frac{1}{d}\left(\frac{\gamma_{A\text{-}Top} + \gamma_{B\text{-}Bot}}{\gamma_{AB}}\right)\right] \quad \text{Eq. 3}$$

where the normalized film thickness $d = D/L_0$ (D is the actual BCP film thickness); n is a series of positive integers; and $\gamma_{A\text{-}Top}$, $\gamma_{A\text{-}Bot}$, $\gamma_{B\text{-}Top}$, and $\gamma_{B\text{-}Bot}$ represent the interfacial energies of PTMSS (subscript A) and PS (subscript B) with either the bottom or top interface, with $\gamma_{A\text{-}Top} \leq \gamma_{B\text{-}Top}$ by definition. The block-block interfacial energy $\gamma_{AB} = (k_B T \chi^{1/2})/(6^{1/2}\alpha^2)$ is dependent on the segment-segment interaction parameter χ and the statistical segment length α (*41*); k_B, the Boltzmann constant.

The smaller of the three normalized free-energy ratios (F_V/F_0, $F_{H\text{-}sym}/F_0$, and $F_{H\text{-}asym}/F_0$) will determine the energetically preferred orientation of the BCP at a given normalized film thickness d. The free-energy equations have been rewritten below in terms of the differences between the horizontal and vertical orientations, $(F_H - F_V)/F_0$, which depend on the difference in the interfacial energy of each block with both the top and bottom interfaces ($\Delta\gamma_{Top} \equiv |\gamma_{B\text{-}Top} - \gamma_{A\text{-}Top}|$ and $\Delta\gamma_{Bot} \equiv |\gamma_{B\text{-}Bot} - \gamma_{A\text{-}Bot}|$), not on the absolute values of $\gamma_{A\text{-}Top}$, $\gamma_{A\text{-}Bot}$, $\gamma_{B\text{-}Top}$, and $\gamma_{B\text{-}Bot}$ (Eqs. 4 to 6).

$$\frac{F_{H\text{-}sym} - F_V}{F_0} = c - \frac{\Delta\gamma_{Bot} + \Delta\gamma_{Top}}{6d\gamma_{AB}} \quad \text{Eq. 4}$$

$$\frac{F_{H\text{-}asym} - F_V}{F_0} = c + \frac{\Delta\gamma_{Bot} - \Delta\gamma_{Top}}{6d\gamma_{AB}} \quad \text{Eq. 5}$$

$$c = \frac{d^3 + 2m^3}{3dm^2} - 1 \quad \text{Eq. 6}$$

where $m = n$ for $F_{H\text{-}sym}$ and $m = n + ½$ for $F_{H\text{-}asym}$.

We calculated the effects of $\Delta\gamma_{Top}$ on the orientation of a lamella-forming BCP using these equations. The segment-segment interfacial energy is estimated to be $\gamma_{AB} = 0.80$ mN/m,

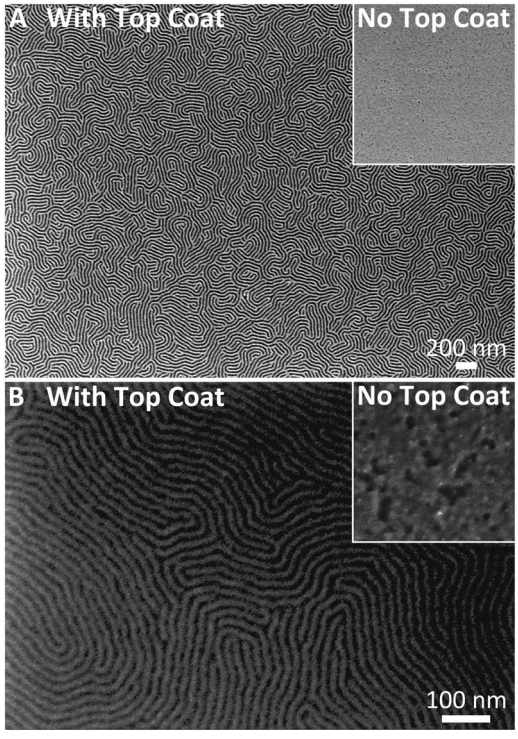


Fig. 3. (**A**) Scanning electron micrographs of PS-PTMSS-PS (L_0 = 29 nm as measured, 30 nm bulk), annealed at 210°C for 1 min on a hot plate open to air with a top coat TC-PS (main figure) and without a top coat (inset). The BCP film thickness was 43 nm (1.4 × L_0). After thermal annealing, both samples were stripped with 3:1 by weight MeOH:aq. 30 wt % NH_4OH and subjected to O_2 reactive ion etching for 30 s. The scale bar is valid for both the image and the inset. (**B**) Scanning electron micrographs of PTMSS-PLA (L_0 = 19 nm as measured, 15 nm in bulk), annealed at 170°C for 20 hours with a top coat TC-PLA (main figure) and without a top coat (inset). The BCP film thickness was 10 nm (0.66 × L_0). After thermal annealing, both samples were stripped with 3:1 by weight MeOH:30 wt % aq. NH_4OH. The scale bar is valid for both the image and the inset. For both (A) and (B), the bottom surface treatment was an XST-OMe cross-linkable copolymer (see supplementary materials).

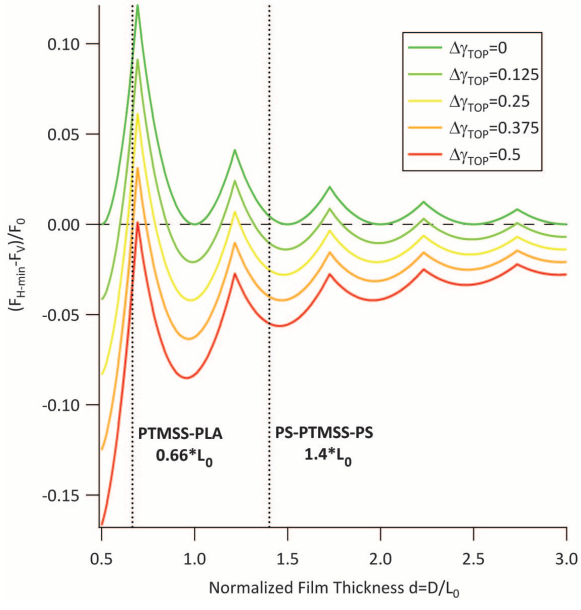


Fig. 4. Differences in BCP thin-film free energies between the horizontal and vertical orientations ($F_{H\text{-}min} - F_V$)/F_0 as a function of reduced film thickness d. For a given d, if the value of ($F_{H\text{-}min} - F_V$)/F_0 is negative, a horizontal orientation is preferred; if it is positive, a vertical orientation is preferred. Different curves represent different values of $\Delta\gamma_{Top}$ measured in mN/m. $\Delta\gamma_{Top}$ = 0 mN/m represents a perfectly neutralizing top coat. For $\Delta\gamma_{Top} \geq 0.5$ mN/m, a horizontal orientation is realized for all d. The dashed line at D = 1.4 × L_0 corresponds with the 43-nm PS-PTMSS-PS film used to produce the scanning electron micrographs shown in Fig. 3A; the dashed line at D = 0.66 × L_0 corresponds with the 10-nm PTMSS-PLA film used to produce the scanning electron micrographs shown in Fig. 3B.

Downloaded from www.sciencemag.org on November 9, 2012

using a statistical segment length $\alpha = 0.68$ nm for PS (*42*) and $\chi_{PS\text{-}PTMSS} = 0.024$, as calculated for PS-PTMSS-PS at 150°C based on absolute intensity SAXS measurements (*37*). The results are virtually identical using the values for PTMSS-PLA, $\chi_{PTMSS\text{-}PLA} = 0.34$ at 150°C (*31*) and $\gamma_{AB} = 1.39$ mN/m. To minimize the effect of the substrate interface on the BCP orientation, a neutral bottom interface was modeled such that $\gamma_{B\text{-}Bot} = \gamma_{A\text{-}Bot} = \frac{1}{2}\gamma_{AB}$, implying that $\Delta\gamma_{Bot} = 0$, analogous to Walton *et al*. (*40*). The value of $\Delta\gamma_{Top}$ was then varied to isolate the role of the top surface on BCP orientation. A perfectly neutralizing top coat has $\Delta\gamma_{Top} = 0$. For comparison, in the case of a BCP composed of a silicon-containing block and a relatively nonpolar organic block (such as PTMSS and PS), an air top interface results in $\Delta\gamma_{Top} \approx 20$ mN/m (*43*).

A free-energy curve was generated from the superposition of the parabolic expressions at incremental values of n for both of the horizontal orientations, horizontal symmetric ($F_{H\text{-}sym}/F_0$) and horizontal asymmetric ($F_{H\text{-}asym}/F_0$). For each horizontal orientation, the minimum value of the collection of parabolas at a given $d = D/L_0$ resulted in a function for $F_{H\text{-}sym}/F_0$ or $F_{H\text{-}asym}/F_0$. The vertical orientation free energy did not depend on n and did not require the superposition of multiple curves; so the free energy F_V/F_0 could be calculated directly. To evaluate the energetically favorable orientation, the difference between the minimum horizontal orientation free energy, $F_{H\text{-}min} \equiv$ minimum $[F_{H\text{-}sym}, F_{H\text{-}asym}]$, and the vertical orientation free energy F_V/F_0 was plotted as a function of $d = D/L_0$ (Fig. 4). The value $(F_{H\text{-}min} - F_V)/F_0$ should be negative if a horizontal orientation is energetically favorable and positive if a vertical or perpendicular orientation is favored. A plot of $(F_{H\text{-}min} - F_V)/F_0$ as a function of d for different values of $\Delta\gamma_{Top}$ ranging from 0 to 0.5 mN/m is also shown in Fig. 4; the general trends are in good agreement with the efficacy of the top coats described here. With $\Delta\gamma_{Top} \geq 0.5$ mN/m, a relatively modest difference in interfacial energies $\gamma_{B\text{-}Top}$ and $\gamma_{A\text{-}Top}$, $(F_{H\text{-}min} - F_V)/F_0$ is always negative and thus favors a horizontal orientation of BCP domains at all film thicknesses. This situation models silicon-organic BCPs in contact with air, which often have $\Delta\gamma_{Top} \approx 20$ mN/m and experimentally always produce horizontal orientations at the top interface in the absence of top coats. As the $\Delta\gamma_{Top}$ value decreases ($\Delta\gamma_{Top} < 0.5$ mN/m), $(F_{H\text{-}min} - F_V)/F_0$ becomes positive at some values of d, implying that vertical features can be obtained at certain film thicknesses, as was observed in Fig. 3. In the limit of a perfectly neutral top surface ($\Delta\gamma_{Top} = 0$), vertical orientation is favored over all film thicknesses.

The surface energy of the less polar form of the top coat should therefore be tuned to achieve neutrality for the specific BCP for which it was designed. The top coat for the triblock copolymer described here seems to be nearly optimized, based on its performance. We do not believe that the top coat for the high-χ diblock material is fully optimized. A top coat with a nonpolar state that is nearer to neutrality could provide a wider process window and enable shorter annealing times for this BCP. Ultimately, top coats of this general polarity-switching design should find application in a wide variety of technologies where control of interfacial energy is required.

References and Notes

1. F. S. Bates, G. H. Fredrickson, *Annu. Rev. Phys. Chem.* **41**, 525 (1990).
2. R. A. Segalman, B. McCulloch, S. Kirmayer, J. J. Urban, *Macromolecules* **42**, 9205 (2009).
3. M. A. Hillmyer, *Adv. Polym. Sci.* **190**, 137 (2005).
4. D. J. C. Herr, *J. Mater. Res.* **26**, 122 (2011).
5. F. S. Bates *et al*., *Science* **336**, 434 (2012).
6. H.-C. Kim, S.-M. Park, W. D. Hinsberg, *Chem. Rev.* **110**, 146 (2010).
7. Y. S. Jung, J. B. Chang, E. Verploegen, K. K. Berggren, C. A. Ross, *Nano Lett.* **10**, 1000 (2010).
8. M. Y. Paik *et al*., *Macromolecules* **43**, 4253 (2010).
9. J. N. L. Albert, T. Epps III, *Mater. Today* **13**, 24 (2010).
10. P. Mansky, Y. Liu, E. Huang, T. P. Russell, C. Hawker, *Science* **275**, 1458 (1997).
11. D. Y. Ryu, K. Shin, E. Drockenmuller, C. J. Hawker, T. P. Russell, *Science* **308**, 236 (2005).
12. H.-S. Suh, H. Kang, C.-C. Liu, P. F. Nealey, K. Char, *Macromolecules* **43**, 461 (2010).
13. S.-X. Ji, C.-C. Liu, G.-L. Liu, P. F. Nealey, *ACS Nano* **4**, 599 (2010).
14. G. Liu *et al*., *Phys. Rev. Lett.* **108**, 065502 (2012).
15. E. Huang *et al*., *Macromolecules* **31**, 7641 (1998).
16. J. G. Son, X. Bulliard, H. Kang, P. F. Nealey, K. Char, *Adv. Mater. (Deerfield Beach Fla.)* **20**, 3643 (2008).
17. Panasonic, Patent JP 2011-78978 (2011).
18. S. Kim, P. F. Nealey, F. S. Bates, *ACS Macro Letters* **1**, 11 (2012).
19. P. Mansky *et al*., *Phys. Rev. Lett.* **79**, 237 (1997).
20. Y. Zhao, E. Sivaniah, T. Hashimoto, *Macromolecules* **41**, 9948 (2008).
21. H. Yokoyama, E. J. Kramer, *Macromolecules* **31**, 7871 (1998).
22. C. M. Hardy, F. S. Bates, M.-H. Kim, G. D. Wignall, *Macromolecules* **35**, 3189 (2002).
23. L. Wan, X. Yang, *Langmuir* **25**, 12408 (2009).
24. S. Ji *et al*., *Macromolecules* **41**, 9098 (2008).
25. J. L. Duda, *Pure Appl. Chem.* **57**, 1681 (1985).
26. P. T. Gilmore, R. Falabella, R. L. Laurence, *Macromolecules* **13**, 880 (1980).
27. J. D. Cushen *et al*., *ACS Nano* **6**, 3424 (2012).
28. C. A. Ross *et al*., *J. Vac. Sci. Technol. B* **26**, 2489 (2008).
29. T. Vu, N. Mahadevapuram, G. M. Perera, G. E. Stein, *Macromolecules* **44**, 6121 (2011).
30. M. W. Matsen, *Macromolecules* **43**, 1671 (2010).
31. J. D. Cushen *et al*., *Macromolecules* 10.1021/ma301238j (2012).
32. T. Higuchi, L. Eberson, J. D. McRae, *J. Am. Chem. Soc.* **89**, 3001 (1967).
33. F. M. Houlihan, T. I. Wallow, O. Nalamasu, E. Reichmanis, *Macromolecules* **30**, 6517 (1997).
34. R. A. Nyquist, *Interpreting Infrared, Raman, and Nuclear Magnetic Resonance Spectra: Variables in Data Interpretation of Infrared and Raman Spectra* (Academic Press, San Diego, CA, 2001), vol. 1.
35. R. M. Silverstein, F. X. Webster, D. J. Kiemle, Eds., *Spectrometric Identification of Organic Compounds* (Wiley, Hoboken, NJ, ed. 7, 2005).
36. A. M. Welander *et al*., *Macromolecules* **41**, 2759 (2008).
37. T. Seshimo *et al*., *J. Photopolym. Sci. Technol.* **25**, 125 (2012).
38. E. Helfand, Z. R. Wasserman, *Macromolecules* **9**, 879 (1976).
39. M. S. Turner, *Phys. Rev. Lett.* **69**, 1788 (1992).
40. D. G. Walton, G. J. Kellogg, A. M. Mayes, P. Lambooy, T. P. Russell, *Macromolecules* **27**, 6225 (1994).
41. F. S. Bates, G. H. Fredrickson, *Phys. Today* **52**, 32 (1999).
42. G. E. Stein, J. A. Liddle, A. L. Aquila, E. M. Gullikson, *Macromolecules* **43**, 433 (2010).
43. C. M. Bates *et al*., *Langmuir* **27**, 2000 (2011).

Acknowledgments: The authors gratefully thank Nissan Chemical Company and the Rashid Engineering Regents Chair for financial support. This material is based on work supported by the NSF Scalable Nanomanufacturing Program under grant no. 1120823. C.J.E. thanks the Welch Foundation (grant F-1709) for partial financial support. T.S. thanks Tokyo Ohka Kogyo Co. for financial support. W.J.D. thanks the Virginia and Ernest Cockrell, Jr. Fellowships in Engineering for partial support. J.D.C. thanks NSF for a Graduate Research Fellowship. L.M.D. thanks the National Merit Scholarship and the Arrington Endowed Scholarship for support. G.B. thanks the Paul D. Meek Endowed Graduate Fellowship in Engineering for support. The authors also thank D. Romanovicz for SEM assistance. The University of Texas has submitted a provisional patent application covering aspects of the work described in this paper to the U.S. Patent Office.

Supplementary Materials

www.sciencemag.org/cgi/content/full/338/6108/775/DC1
Materials and Methods
Figs. S1 to S8
References

13 June 2012; accepted 26 September 2012
10.1126/science.1226046

Downloaded from www.sciencemag.org on November 9, 2012

Driving a Macroscopic Oscillator with the Stochastic Motion of a Hydrogen Molecule

Christian Lotze,[1] Martina Corso,[1] Katharina J. Franke,[1] Felix von Oppen,[1,2] Jose Ignacio Pascual[1,3,4]*

Energy harvesting from noise is a paradigm proposed by the theory of stochastic resonances. We demonstrate that the random switching of a hydrogen (H_2) molecule can drive the oscillation of a macroscopic mechanical resonator. The H_2 motion was activated by tunneling electrons and caused fluctuations of the forces sensed by the tip of a noncontact atomic force microscope. The stochastic molecular noise and the periodic oscillation of the tip were coupled in a concerted dynamic that drives the system into self-oscillation. This phenomenon could be a way for enhancing the transfer of energy from incoherent sources into coherent dynamics of a molecular engine.

Nature widely uses processes that extract energy and coherence from random and noisy sources of energy. Examples of these span from mechanisms for pumping energy in cellular activity (*1*) to the amplification and transduction of signals (*2*–*4*). An oscillator coupled to

a noisy environment can self-oscillate when the dynamics of the noise is modulated by the oscillator and vice versa. This phenomenon, named stochastic resonance (SR) (*5*), predicts the enhancement of energy transfer from the noisy to the periodic subsystem. Noise at the molecular scale is ubiquitous. Stochastic molecular motion is caused by temperature or by stimuli such as electrons or photons. Here, we report that the stochastic motion of H_2 out of thermal equilibrium induced by tunneling electrons can drive the oscillation of a mechanical oscillator of macroscopic dimensions, demonstrating the concept of energy harvesting through SRs at the molecular scale.

We investigated a molecular tunnel junction formed by H_2 enclosed between two metal electrodes, those of a copper surface and the tip of a scanning tunneling microscope (STM) at low temperatures (5 K). The H_2 molecule can lie in different adsorption states. Fluctuations between these states are triggered by the inelastic tunneling of electrons when they excite certain vibrational modes of the molecule in the cavity. The electron-driven fluctuations of the H_2 molecule are stochastic (*6*–*8*) and involve displacements of tens of picometers, as well as energies of tens of millielectronvolts. They are expected to exert forces on the electrodes of hundreds of piconewtons.

The crucial question treated here is the detection of mechanical forces exerted by the electron-induced molecular motion on the electrodes. To do so, we fixed one of the electrodes (the tip of the STM) to the prong of a quartz tuning fork, acting here as a mechanical oscillator with high quality factor Q. We show that this force sensor [named qPlus after (*9*)] self-oscillates in response to the fluctuating forces caused by the stochastic switching of a hydrogen molecule. The self-oscillation reveals an efficient energy transfer from the random molecular bistability to the periodic motion of the resonator. By theoretical modeling, we determined that the key feature is the concerted dynamics of molecular switching and oscillator motion, coupled to each other through the fluctuating electric field and forces in the junction.

To form the molecular junction, we exposed an atomically clean Cu(111) surface to a flux of H_2 molecules, at low temperature (5 K) and in ultra-high vacuum [section 1.1 in (*10*)]. Adsorbed H_2 can be too mobile for imaging by STM at low surface coverages; only after high gas exposures could a H_2 monolayer be imaged as a compact hexagonal lattice (Fig. 1A). Nevertheless, the presence of H_2 molecules condensed on the metal surface became evident from sharp nonlinearities in the current-bias (I_t-V_s) spectra of the junction (Fig. 1B) (*7*, *8*, *11*–*14*). These features arise from the activation of fast, bistable motion of a H_2 molecule between two molecular configurations with different conductances. These fluctuations led to sharp dips of negative differential conductance dI_t/dV_s at the threshold bias $\pm V_{th}$ (Fig. 1C), which indicate the point where the stability of the two states was reversed (*7*). The symmetric alignment of V_{th} with respect to zero bias is a fingerprint of a vibrationally activated process (*15*, *16*). In fact, the strong spectral nonlinearities of a H_2 junction can be well modeled by vibrationally activated two-level fluctuations (TLFs) of the molecule between two adsorption configurations (*8*, *11*, *12*).

The qPlus sensor allows us to measure its resonance frequency ν_0 simultaneously with a differential conductance spectrum. Forces in the tunneling junction shift the resonance frequency by an amount $\Delta\nu_0$. In the limit of small tip oscillation amplitudes A_{osc} (sub-Ångstrom in our experiments) and conservative forces, $\Delta\nu_0$ is proportional to the gradient of the vertical forces in the tunnel junction (*17*), that is, the stiffness of the junction. Figure 1D shows the $\Delta\nu_0$ spectrum measured simultaneously with the spectra of Fig. 1, B and C. The presence of H_2 induced a steplike anomaly at the threshold values $\pm V_{th}$. The steps of $\Delta\nu_0$ revealed that there are two bias regimes of different junction stiffness (labeled 1 and 2 in Fig. 1D), each associated with a different molecular configuration in the junction. Assuming that forces are conservative far from V_{th}, the larger negative value of the frequency shift (e.g., for the low bias state 1) is symptomatic of a larger attractive force. We estimated the difference in force between the two states $\Delta f = f_2 - f_1$ by integrating their corresponding $\Delta\nu_0$ difference along the vertical direction X [section 2.1 in (*10*)]. We found that Δf increased as the tip approached the sample and reached a maximum value of more than 150 pN. At the transition bias $\pm V_{th}$, stochastic fluctuations between the two molecular states (*7*) would inevitably result in fluctuations of the force sensed by the tip. Because the amplitude of the fluctuations is Δf, their effect on the tip motion becomes more important as the tip approaches.

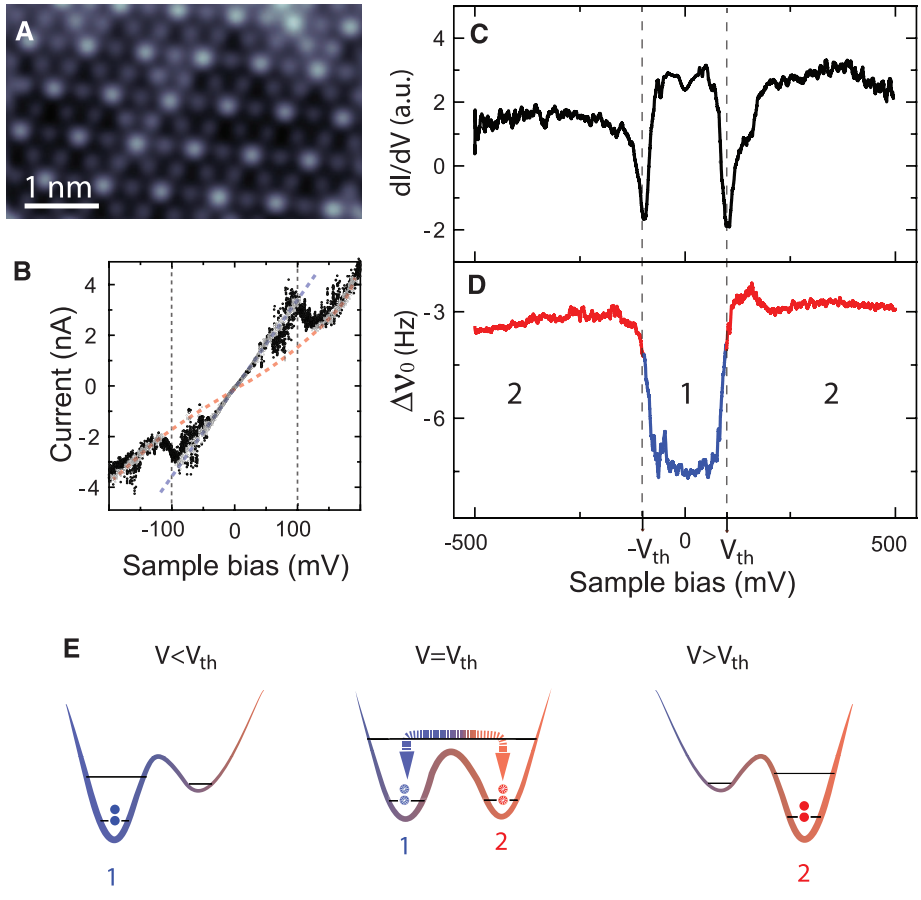


Fig. 1. (**A**) STM image of a hexagonal H_2 layer on Cu(111) (V_s = –37 mV, I_t = 200 pA) (*25*). (**B**) Tunneling current and (**C**) differential conductance spectra of a Cu(111) surface with submonolayer H_2 coverage. The current spectrum shows two conductance regimes (marked with dashed lines) and an increased noise in the transition biases between them, at $V_{th} \sim \pm 100$ mV. The dI_t/dV_s spectrum shows dips with negative differential conductance at $\pm V_{th}$, caused by vibrationally induced fluctuations of a H_2 molecule between two configurations in the junction. (**D**) Simultaneously acquired plots of the frequency shift of the qPlus force sensor (A_{osc} = 50 pm, ν_0 = 20.609 kHz) reveal that the two states interact differently with the STM tip above and below V_{th}. (**E**) Model of the bistable potential and vibrational TLFs of a H_2 molecule in the tunnel junction.

[1]Fachbereich Physik, Freie Universität Berlin, 14195 Berlin, Germany. [2]Dahlem Center for Complex Quantum Systems, Freie Universität Berlin, 14195 Berlin, Germany. [3]CIC nanoGUNE, 20018 Donostia-San Sebastián, Spain. [4]IKERBASQUE, Basque Foundation for Science, 48011 Bilbao, Spain.

*To whom correspondence should be addressed. E-mail: ji.pascual@nanogune.eu

Downloaded from www.sciencemag.org on November 9, 2012

Figure 2 shows the evolution of conductance and $\Delta\nu_0$ spectra as the STM tip approached ΔX = 1.5 Å toward the surface, with respect to an initial position with junction conductance of 5 nS. The set of spectra shows a monotonous decrease of the bias V_{th} with tip approach (*7*). This provides evidence that the narrowing of the junction and the increase of the electric field reduce the energy required for driving the TLFs (*18*). This effect turned out to be crucial because it caused the periodic motion of the tip at $V_s \sim V_{th}$ to change the relative stability of the two H_2 states. At approach distances $\Delta X > 0.75$ Å, the negative dI_t/dV_s dips became more pronounced (Fig. 2, A and B) and the $\Delta\nu_0$ signal exhibited sharp peaks at the same bias value (Fig. 2, C and D). The stochastic switching of H_2 in the vicinity of the threshold voltage makes the forces nonconservative and nonlinear. To resolve their effect on the tip oscillation, we analyzed the mechanical energy dissipated during the tip oscillation. This magnitude captures the effect of nonconservative dynamics by tracking changes of the energy per cycle required to maintain a constant oscillating amplitude A_{osc}. In our experiment, this was quantified through the amplitude of the external signal required to drive the motion, A_D [(*17*); details in section 1.2 in (*10*)].

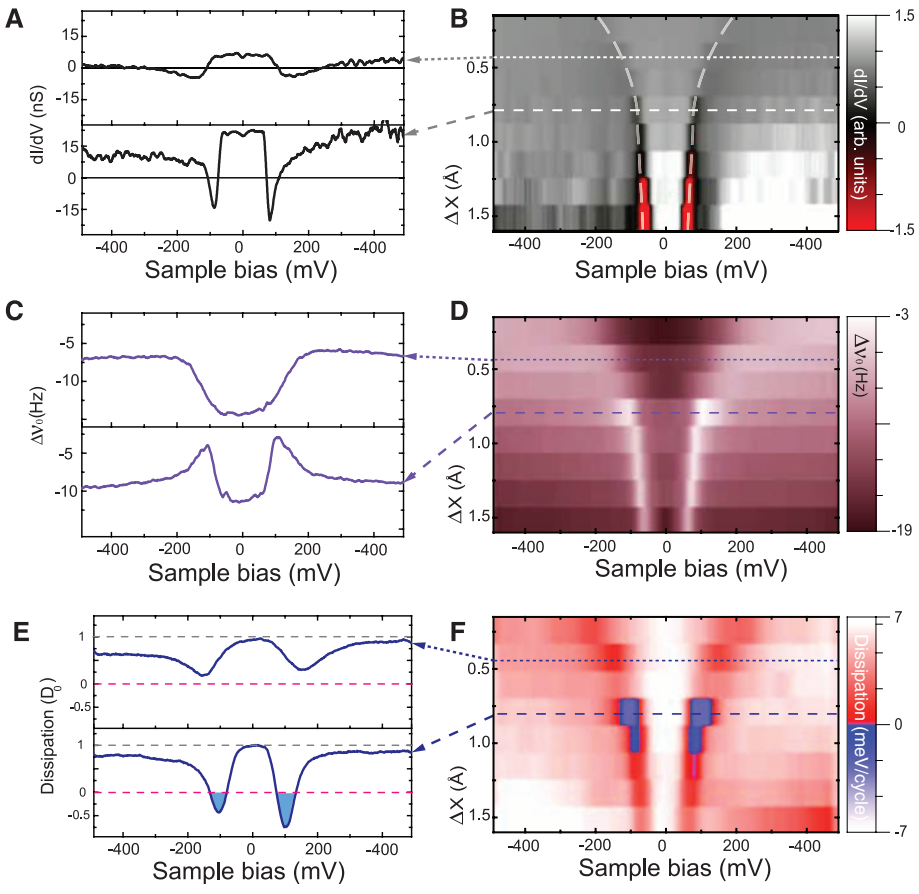


Fig. 2. Simultaneously acquired spectra of the (**A** and **B**) differential conductance, (**C** and **D**) frequency shift, and (**E** and **F**) dissipation signal of a H_2 molecular junction at eight different tip-sample distances (A_{osc} = 50 pm, ν_0 = 20.609 kHz). The color maps picture the corresponding magnitude versus bias and approaching distance ΔX with respect to an initial position with tunneling conductance 5 nS. The curved dashed lines in Fig. 2B indicate the reduction in the bias V_{th} with the tip-sample distance. The energy dissipation is plotted in units of D_0, the intrinsic dissipation of the free tip oscillating with A_{osc} = 50 pm (here, D_0 = 7 meV/cycle) [section 1.2 in (*10*)].

The dissipation-bias spectrum of a H_2 junction shows pronounced minima at the bias $\pm V_{th}$ (Fig. 2), which were absent on clean surfaces. The minima revealed that the H_2 fluctuations contributed to driving the motion of the tuning fork and diminished the demand for external driving. Most strikingly, the dips in the dissipation signal became gradually sharper as the tip approached the sample and reached negative values, as shown in Fig. 2, E and F, at $\Delta X >$ 0.75 Å. A negative dissipation signal is a fingerprint of the system entering into a regime of self-oscillation (SO). Here, the phase of the external driving signal is inverted with respect to the tip oscillation to counteract the growing amplitude of the tip motion. In this situation, the fluctuating H_2 molecule drives the motion of the tip-oscillator against the external load.

Further proof that the tip SO was driven by fluctuations of a H_2 molecule could be obtained by measuring the bias dependence of the amplitude of tip oscillation A_{osc} in the absence of any external driving force (A_D = 0 mV). Figure 3 shows that A_{osc} was zero for most bias voltages, except near the threshold bias V_{th}, where the tip started to self-oscillate with A_{osc} ~1 Å. As in Fig. 2, the value of V_{th} decreased with the tip approach, and the SO regime appeared for junction conductances on the order of 10 nS. In certain cases, the SO amplitude could reach several Ångstroms—i.e., greater than the size of H_2. These results demonstrate that the local forces associated with the electron-induced fluctuations of the H_2 molecule were remarkably efficient in driving the motion of the macroscopic oscillator. These forces compensated the intrinsic energy dissipation of the tuning fork (for the case of Fig. 2, ~ 7 meV/cycle) by providing mechanical energy of tens of millielectronvolts per cycle [section 2.2 in (*10*)].

Current-induced TLFs are stochastic in nature, so that the corresponding force fluctuations acting on the cantilever have a broad power spectrum in the frequency domain. When the power spectrum has appreciable weight near the resonance frequency of the cantilever, the force fluctuations can resonantly excite the oscillator to reach a stationary state. Under optimal conditions, this mechanism could cause an oscillation

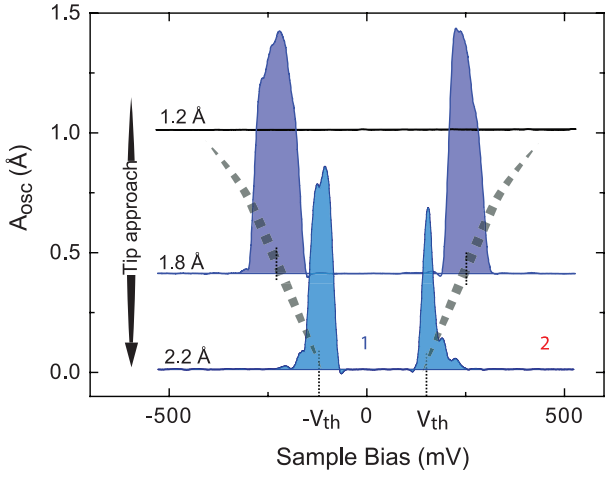


Fig. 3. Oscillation amplitude A_{osc} versus sample bias in the absence of external driving forces (A_D = 0 mV). Each spectrum is measured at the indicated approach distances with respect to an initial position at junction conductance of 0.22 nS and shifted to lower values for clarity. The tip oscillates driven by electron-induced fluctuations of the H_2 molecule at $\pm V_{th}$. The dashed lines indicate the gradual decrease of V_{th} with the tip-sample distance.

Downloaded from www.sciencemag.org on November 9, 2012

amplitude on the order of $\langle (X(t))^2 \rangle^{1/2} \cong |\Delta f|/(4\sqrt{2}\omega_0^{3/2}\gamma^{1/2}M)$ [section 3.2 in (*10*)]. Using the values of our experimental set-up ($\Delta f = f_2 - f_1 \sim 100$ pN, $\gamma \sim 10 s^{-1}$, $\omega_0 = 2\pi\nu_0 \sim 10^5 s^{-1}$, and M ~ 0.1 mg for the intrinsic damping coefficient, resonance frequency and mass of the cantilever, respectively), we obtained oscillation amplitudes on the order of 1 pm, far smaller than the values observed in our experiment.

To explain the experimental results, a crucial aspect must be considered: The switching rates between the two molecular states depended on the distance between tip and surface; that is, they were tuned by the periodic oscillation of the tip. There are two possible causes for this: (i) the tunneling current and, with it, the switching rates varied with tip-substrate distance; and (ii) at fixed bias, the tip displacement $X(t)$ shifted the threshold bias V_{th} and, hence, the relative stability of the two states (*7*). This last effect turned out to be crucial because it changed the switching rates Γ_1 and Γ_2 in opposite directions (described in Fig. 4B) and caused an appreciable modulation of the occupations $n_1(t)$ and $n_2(t)$ of the two switching states of H_2 with the periodic motion of the tip. This modulation of the populations fed back into the oscillator motion by generating a corresponding modulation of the force $f(t) = f_1\langle n_1(t)\rangle + f_2\langle n_2(t)\rangle$ sensed by the tip. The result was coherent coupling of the dynamics of noise and oscillation as described in the theory of stochastic resonances (*5*).

The effect of the force modulation $f(t)$ could be described analytically when assuming a linear variation of the switching rates Γ_i with cantilever displacement $X(t)$ (valid for small displacements). Remarkably, we found that by this mechanism the average force $f(t)$ acquired components proportional to the tip's displacement $X(t)$ and to its velocity $\dot{X}(t)$, which yield renormalizations of both the restoring force and the friction coefficient of the cantilever [section 3.3 in (*10*)]. The former merely caused a shift in the resonance frequency of the tip's oscillation, thus accounting for the $\Delta\nu_0$ peaks observed in our experiments at V_{th}. The most interesting prediction of this feedback model is that the renormalization of the friction coefficient could be negative and reduce the overall friction of the cantilever. In fact, we estimated that the switching-induced renormalization of the damping coefficient was on the order of $\Delta\gamma_{eff} \sim -|\Delta f|\frac{|\Gamma_1'|}{M\omega_0^2} \sim -10\ s^{-1}$, which could overcompensate the intrinsic friction $\Delta\gamma \sim 10\ s^{-1}$ of the high-Q cantilever and cause overall negative friction. In this case, the equilibrium position of the oscillator would become unstable, entering into SOs. The conditions for reaching the regime of negative friction are a set of switching rates Γ_i not too different from ω_0, and a modulated force $f(t)$ that becomes less attractive (or more repulsive) at the closest tip position $X(t)$ [section 3.3 in (*10*)]. This condition was fulfilled in the H_2 molecular junction for bias values near V_{th} (Fig. 4): Because of the monotonous reduction of V_{th} with the tip-surface distance, the state with a less attractive force (regime 2) became more frequent in the part of the cycle with smaller tip-sample distances (Fig. 4).

In the regime of SOs, the oscillation amplitude was ultimately controlled by nonlinearities of the restoring forces. These nonlinearities are dominated by the tip-substrate forces rather than the intrinsic nonlinearities of the oscillator. Modeling the nonlinearity of the tip-substrate force through a cubic Duffing force of strength α, we estimated the amplitude of the self-oscillations to be on the order of $\left(\frac{4\gamma_{eff}\omega_0}{3\alpha}\right)^{\frac{1}{2}} \sim 1$ nm [section 3.4 in (*10*)], consistent with our experimental observations.

Despite the large difference in mass and size, the motion of H_2 molecule and tuning fork require similar energies due to the high quality factor of the qPlus sensor. Therefore, the tens of millielectronvolts involved in the H_2 switching were sufficient to feed an oscillation cycle of the tip with amplitudes of Ångstroms. However, the incoherent character of the random energy source usually would inhibit an efficient energy transfer to the oscillator. Here, the stochastic resonance played a crucial role. The concerted dynamics of molecular bistability and tip oscillation created a coherent pathway for transferring energy from the noisy source into the periodic motion. In this case, the harvested energy originated from inelastic tunneling of electrons. Such a mechanism might also generalize to other energy sources or more complex molecular junctions (*19*–*24*). We envision that appropriately designed intrinsic mechanisms of SR feedback could be a way for enhancing the energy transfer in molecular motors transforming stochastic motion into directional motion.

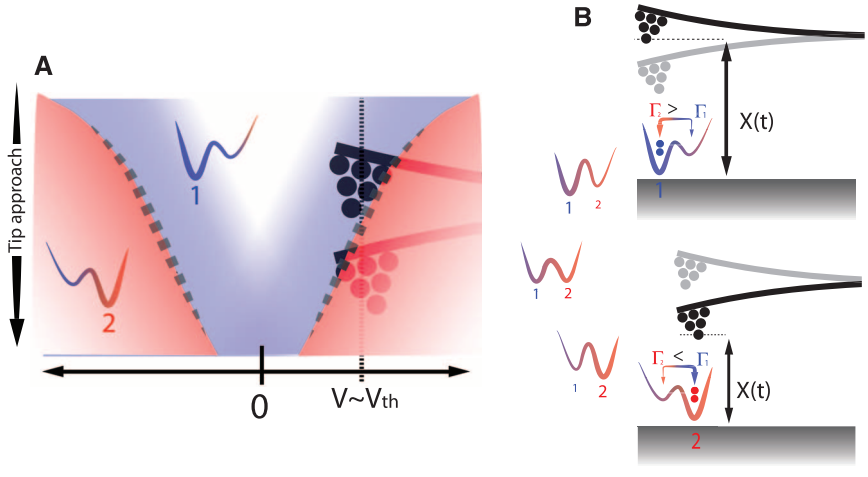


Fig. 4. Sketch of the concerted dynamics of H_2 molecule fluctuations and tip periodic motion. (**A**) Bias-distance diagram of the population of the two states of H_2, summarizing the behavior depicted in Fig. 2. The tip oscillation at a bias V_{th} drives the system from the more attractive state 1 to the more repulsive state 2. (**B**) Diagram illustrating the tuning of the bistable potential of the H_2 molecule by the tip oscillation. When the tip is close (far) the state 2 (state 1) is more stable, and the rate Γ_2 (Γ_1) describing the switching out of state 2 (state 1) is smaller. The switching rates Γ_2 and Γ_1 have the opposite behavior with tip distance $X(t)$. The molecular conformation of the two states is unknown, albeit the vibration connecting them behaves as a frustrated H_2 rotation (*18*).

References and Notes

1. R. D. Astumian, M. Bier, *Biophys. J.* **70**, 637 (1996).
2. J. K. Douglass, L. Wilkens, E. Pantazelou, F. Moss, *Nature* **365**, 337 (1993).
3. K. Wiesenfeld, F. Moss, *Nature* **373**, 33 (1995).
4. S. I. Kiselev *et al.*, *Nature* **425**, 380 (2003).
5. L. Gammaitoni, P. Hänggi, P. Jung, F. Marchesoni, *Rev. Mod. Phys.* **70**, 223 (1998).
6. B. C. Stipe, M. A. Rezaei, W. Ho, *Science* **279**, 1907 (1998).
7. J. Gupta, C. Lutz, A. Heinrich, D. Eigler, *Phys. Rev. B* **71**, 115416 (2005).
8. W. H. Thijssen, D. Djukic, A. F. Otte, R. H. Bremmer, J. M. van Ruitenbeek, *Phys. Rev. Lett.* **97**, 226806 (2006).
9. F. J. Giessibl, *Appl. Phys. Lett.* **76**, 1470 (2000).
10. Materials and methods are available as suppplementary materials on *Science* online.
11. A. Halbritter, P. Makk, S. Csonka, G. Mihaly, *Phys. Rev. B* **77**, 075402 (2008).
12. M. Trouwborst, E. Huisman, S. van der Molen, B. van Wees, *Phys. Rev. B* **80**, 081407 (2009).
13. R. Temirov, S. Soubatch, O. Neucheva, A. C. Lassise, F. S. Tautz, *New J. Phys.* **10**, 053012 (2008).
14. C. Weiss *et al.*, *Phys. Rev. Lett.* **105**, 086103 (2010).
15. B. C. Stipe, M. A. Rezaei, W. Ho, *Science* **280**, 1732 (1998).
16. R. H. Smit *et al.*, *Nature* **419**, 906 (2002).
17. F. J. Giessibl, *Rev. Mod. Phys.* **75**, 949 (2003).
18. D. Djukic *et al.*, *Phys. Rev. B* **71**, 161402 (2005).
19. T. Brumme *et al.*, *Phys. Rev. B* **84**, 115449 (2011).
20. T. Kudernac *et al.*, *Nature* **479**, 208 (2011).
21. H. L. Tierney *et al.*, *Nat. Nanotechnol.* **6**, 625 (2011).
22. G. A. Steele *et al.*, *Science* **325**, 1103 (2009).
23. B. Lassagne, Y. Tarakanov, J. Kinaret, D. García-Sanchez, A. Bachtold, *Science* **325**, 1107 (2009).
24. S. P. Fletcher, F. Dumur, M. M. Pollard, B. L. Feringa, *Science* **310**, 80 (2005).
25. I. Horcas *et al.*, *Rev. Sci. Instrum.* **78**, 013705 (2007).

Acknowledgments: We gratefully acknowledge the Alexander von Humboldt Foundation for the research grant of M.C. and the Deutsche Forschungsgemeinschaft for financial support through the collaborative projects Sfb 658 and SPP 1243.

Supplementary Materials

www.sciencemag.org/cgi/content/full/338/6108/779/DC1
Materials and Methods
Supplementary Text
Figs. S1 to S3
References (*26*–*31*)

18 July 2012; accepted 13 September 2012
10.1126/science.1227621

Downloaded from www.sciencemag.org on November 9, 2012

Discovery of an Organic Trefoil Knot

Nandhini Ponnuswamy,[1] Fabien B. L. Cougnon,[1] Jessica M. Clough,[1] G. Dan Pantoş,[2] Jeremy K. M. Sanders[1]*

Molecular knots remain difficult to produce using the current synthetic methods of chemistry because of their topological complexity. We report here the near-quantitative self-assembly of a trefoil knot from a naphthalenediimide-based aqueous disulfide dynamic combinatorial library. The formation of the knot appears to be driven by the hydrophobic effect and leads to a structure in which the aromatic components are buried while the hydrophilic carboxylate groups remain exposed to the solvent. Moreover, the building block chirality constrains the topological conformation of the knot and results in its stereoselective synthesis. This work demonstrates that the hydrophobic effect provides a powerful strategy to direct the synthesis of entwined architectures.

Molecular knots first observed in DNA (*1*) and then in proteins (*2*) have been associated with increased thermal and mechanical robustness. The protein knots are highly conserved throughout evolution and appear to protect active regions by providing resistance against degradation, but the mechanisms involved in the spontaneous threading of a polypeptide chain through a loop to form a knot are not well understood (*3*).

Chemists are well acquainted with this problem: The synthesis of molecular knots is particularly difficult because it requires precisely defined pathways and transition states that are entropically much more demanding than topologically simpler macrocyclization or catenation processes. Over the past two decades, the only strategy that has provided the necessary well-defined geometry relies on metal coordination (*4*–*10*). Only two examples of knot syntheses based on weaker interactions, such as hydrogen bonding (*11*, *12*), have been reported: These knots were formed unexpectedly and in low yields during the process of macrocyclization, and the forces underlying the knotting process remain difficult to rationalize, which limits the scope of the discovery. Trefoil knots are inherently chiral structures, and the previously published syntheses produce, with two notable exceptions (*10*, *12*), only racemic mixtures.

We now report the stereoselective synthesis of a purely organic molecular trefoil knot in water. The knot was assembled almost quantitatively from a readily accessible amino acid–derived dithiol building block, following a dynamic combinatorial approach (*13*). The knot appears to be the smallest structure that minimizes the solvent-exposed hydrophobic surface. Hydrophobicity has been suggested to be involved in the formation of certain knotted proteins (*14*), and we propose that our system may offer a simple model of the relation between the chemical structure of an oligomer and its potential to fold into a knot.

The building block is composed of three hydrophobic electron-deficient π-systems (1,4,5,8-naphthalenediimide, NDI) connected by flexible hydrophilic amino acids (L-β-amino-alanine). It is terminated at both ends by L-cysteine, which provides a thiol for disulfide exchange and additional carboxylate anions for water solubility. The building block was readily synthesized in five steps with a 62% overall yield.

A first dynamic combinatorial library was generated by dissolving the building block at a concentration of 1 mM in water in the presence of two equivalents of NaOH (Fig. 1A). The pH was adjusted to pH 8 using a concentrated stock solution of NaOH (100 mM). The library was stirred for 1 day under air in capped vials to allow slow oxidation of the building block. After full oxidation of the library, liquid chromatography–mass spectrometry (LC-MS) analysis (Fig. 1A) revealed a distribution composed predominantly of the closed monomer (eluted at 12 min) and dimer (at 16 min). A trace amount of a trimeric macrocycle (at 13 min) was also identified, which was amplified, in accordance with Le Chatelier's principle, when the library was rerun at higher concentrations (5 mM) (Fig. 1B).

Although the formation of a trimer was not completely unexpected, its exceptionally short retention time caught our attention. Hydrophobicity and size effects usually give a closed monomer the lowest retention time, followed in succession by dimer and trimer. This irregularity is characteristic of an interlocked macrocycle, such as a catenane (*15*). However, tandem mass spectrometry MS/MS analyses disclosed a fragmentation pattern characteristic of a noncatenated macrocycle, which suggested that the trimer could be folded into another well-organized and compact structure: the trefoil knot, depicted in Figs. 1 and 2, in which the hydrophobic surfaces are efficiently buried and the hydrophilic side chains are exposed to the solvent.

This hypothesis was reinforced by the observation that addition of high concentrations of salt ($NaNO_3$) (Fig. 1, C and D), which enhances the hydrophobic effect, resulted in further amplification to a nearly quantitative assembly (94%) of the knotted trimer. The use of other mineral salts led to an identical library distribution (fig. S3), which confirmed that the assembly is independent of the salt chosen and is mainly driven by the increased polarity of the medium. Conversely, addition of acetone reduced both the medium polarity and the yield of the knot (fig. S4). Among the salts used, only tetrabutylammonium nitrate (Bu_4NNO_3) (Fig. 1E), which can solvate the NDI surface (*16*), led to a different library distribution, as it amplifed the dimer at the expense of the other macrocycles and thus acted as a negative template for the knot (*17*). Addition of the Bu_4NNO_3 also resulted in the amplification, albeit to a lesser extent, of a new peak identified by MS as another trimeric macrocycle, likely to be the trivial trimer, with a retention time of 22 min. The presence of two trimers at different retention times in similar libraries strongly suggests that these two macrocycles are topologically inequivalent.

To confirm that the trimeric macrocycle eluting at 13 min was a knot, we isolated it by preparative high-performance liquid chromatography (HPLC) (isolated yield: 92%) (fig. S2) and analyzed the redissolved sample by nuclear magnetic resonance (NMR) and circular dichroism (CD). The trimeric macrocycle exhibits sharp NMR signals in water (500 MHz, 298 K): This suggests that it is not a flexible macrocycle, as these usually exhibit broad NMR signals that sharpen with increase in temperature (*15*). In D_2O at 358 K and in 1:1 water/acetone mixture

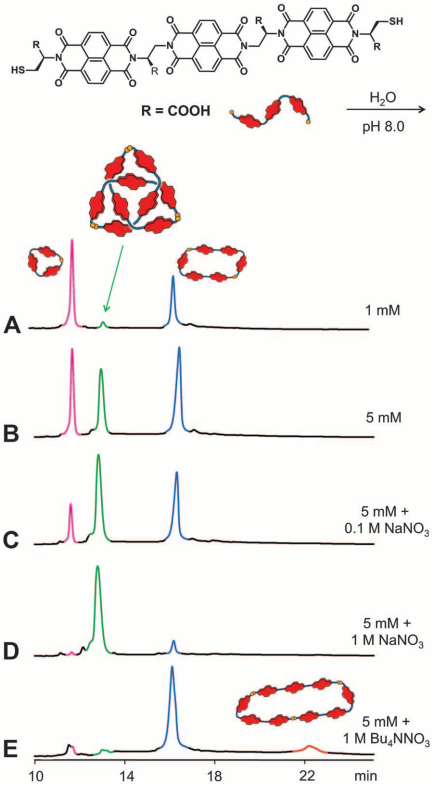


Fig. 1. Reversed-phase HPLC analysis of libraries at 1 mM (**A**) and 5 mM of building block, in the absence (**B**) and presence (**C** to **E**) of salts. Absorbance was recorded at 383 nm.

[1]Department of Chemistry, University of Cambridge, Lensfield Road, Cambridge CB2 1EW, UK. [2]Department of Chemistry, University of Bath, Bath BA2 7AY, UK.

*To whom correspondence should be addressed. E-mail: jkms@cam.ac.uk

Downloaded from www.sciencemag.org on November 9, 2012

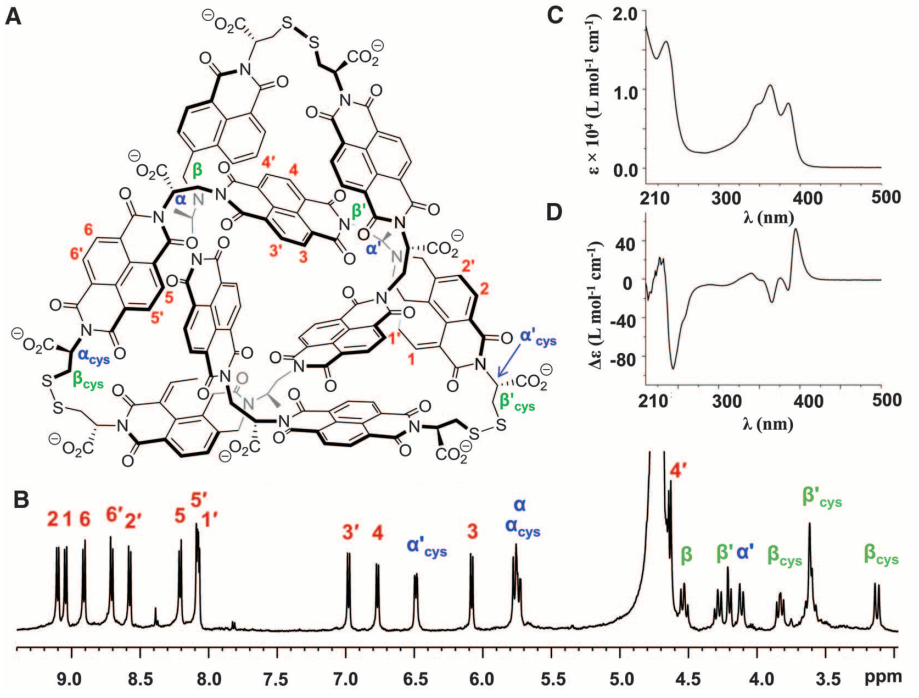


Fig. 2. (**A**) Chemical structure of the right-handed knot. (**B**) ^{1}H-NMR spectrum of the knot (500 MHz, D_2O, 298 K). The protons are labeled according to the scheme shown above. (**C**) UV-Vis and (**D**) CD spectra of the knot in water at 298 K.

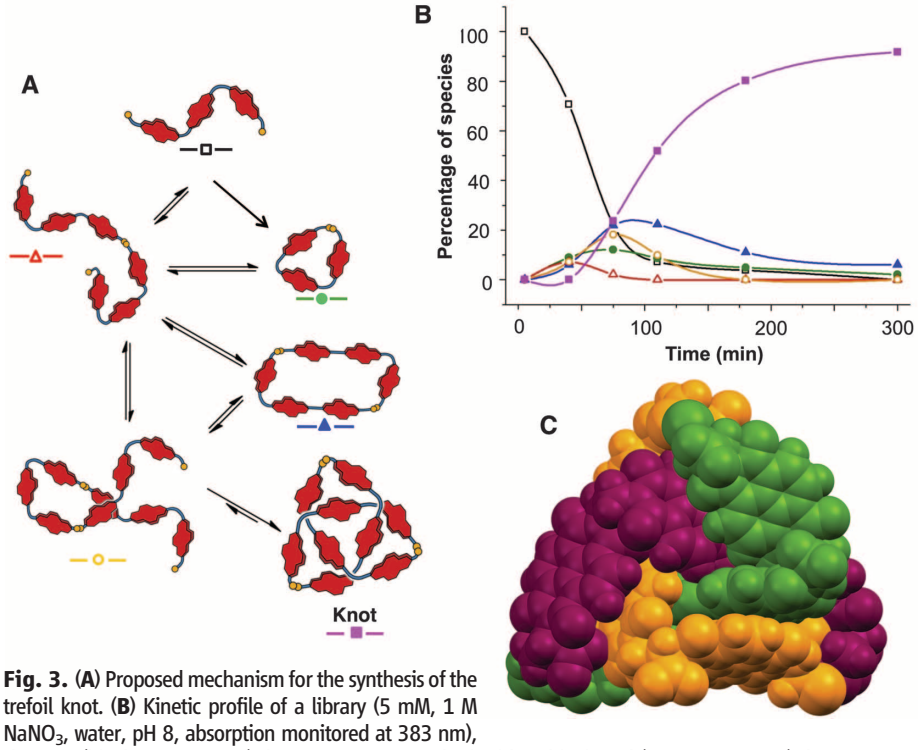


Fig. 3. (**A**) Proposed mechanism for the synthesis of the trefoil knot. (**B**) Kinetic profile of a library (5 mM, 1 M $NaNO_3$, water, pH 8, absorption monitored at 383 nm), showing (black open square) the consumption of the building block and (magenta square) the formation of the knot. The formation and disappearance of the macrocyclic intermediates can also be traced: (green filled circle) closed monomer, (red open triangle) open dimer, (blue triangle) closed dimer, (yellow open circle) open trimer. The percentages were evaluated from the HPLC peak areas. (**C**) Energy-minimized model of the knot from molecular modeling at a semiempirical level using PM6-DH+ (*20*, *21*) force field with COSMO (*22*) parameters for expressing the dielectric medium.

at 298 K, the ^{1}H-NMR spectrum remained essentially unchanged, which indicates the absence of flexibility or gross conformational change (figs. S5 and S6).

The ^{1}H-NMR spectrum at 298 K (Fig. 2B) is entirely consistent with the suggested trefoil knot drawn in Fig. 2: a structure that exhibits C_3 symmetry, with an inequivalent environment for each proton of an individual building block but overall equivalence of the three building blocks composing the knotted macrocycle. The NDI protons span a wide range of chemical shifts from $\delta = 9.2$ to 4.6 ppm. The occurrence of an NDI proton signal (4′ in Fig. 2) at 4.6 ppm fortifies the hypothesis of a knot structure where at least one hydrophobic NDI aromatic core is deeply buried within the molecule and so experiences shielding from neighboring NDIs. The ^{1}H-NMR could be fully rationalized by matching the structure of the proposed knot and the observed nuclear Overhauser effect (NOE) crosspeaks, which allows the assignment of each proton of the molecule as labeled in Fig. 2A (figs. S7 to S11).

A trefoil knot is topologically chiral, and in this case, the right- and left-handed knots would be diastereomers, because the building block is chiral. However, only one diastereomer of the knot was observed by LC-MS and NMR, which implies that the building block, composed of all L-amino acids, is dictating the chirality of the knot. The enantiomeric building block derived from all D-amino acids leads to the formation of the enantiomeric knot. The racemic mixture of all-L- and all-D building blocks mainly self sorts to give the single diasteromer of the knot in racemic form (figs. S19 and S20), which further demonstrates that this structure is exceptionally efficient in its packing and, therefore, thermodynamically stable. By contrast, the diastereomeric building block containing L-cysteine and D-β-amino-alanine does not form the knot but instead gives mainly the dimer (fig. S18).

The CD signal of the knot (Fig. 2D) consists of an intense positive band in the NDI absorption region (385 nm) and a strong negative band in the imide region (245 nm); this matched a Zerner's intermediate neglect of differential overlap–random phase approximation (ZINDO/RPA)–predicted CD spectrum (fig. S17) based on the right-handed knot depicted in Fig. 2A. This induced CD signal is orders of magnitude stronger than that in related catenanes and macrocycles reported in earlier publications by our group (fig. S15), which indicates rigid geometrical relations between the NDI units.

The library is fully oxidized after only 4 hours and may not reach thermodynamic equilibrium; therefore, kinetics plays an important role in the knot formation and allows us to explore possible mechanistic pathways. The oxidation of a 5 mM library containing 1 M $NaNO_3$ was monitored by LC-MS every 35 min (Fig. 3B). The formation and disappearance of intermediate species (macrocycles and open oligomers) highlight the reversibility of the system in the early

Downloaded from www.sciencemag.org on November 9, 2012

stages of oxidation and show the conversion of the less stable macrocycles into the knot, which is presumably the smallest oligomer that can maximize hydrophobic stabilization. Although other pathways may be involved, the kinetic profile shown in Fig. 3 suggests that knot formation predominantly occurs via the formation and folding of the open trimer. Once formed, the open trimer folds into condensed structures that bury the hydrophobic NDI surfaces. Presumably only one of the structures places the terminal thiols in sufficiently close proximity to allow the ring closure that results in a knot. If the ring were opened by cleavage of a disulfide link, closure would be rapid, whereas unfolding would require unfavorable and slow reexposure of hydrophobic surfaces. The formation of the trefoil knot is, therefore, kinetically and thermodynamically favored and closely mimics the mechanism of knot formation in naturally occurring α/β methyl transferases (*18*).

The conclusions drawn from the experimental results were corroborated by molecular modeling calculations, which showed that the knot was relatively more stable and has a smaller surface area and volume than its topological isomers (the closed trimer and the [2]catenane) (*19*).

Although the cyclic monomer and dimer are transiently formed in the library, the reversible nature of the disulfide bond allows their reorganization into the more ordered, but more stable, trimeric knot, highlighting the dual conflicting role of entropy at the different stages of the folding process: On one hand, the formation of small molecules is preferred, whereas the formation and stability of the larger knot result from the necessity of burying hydrophobic surfaces. Overall, the design of the building block offers an efficient way to access purely organic knotted macrocycles in aqueous media. First, the alternation of rigid hydrophobic NDIs, which can stack and form the core of the knot and bury most hydrophobic surfaces, and flexible hydrophilic loops supplies an ideal scaffold for the knitting of organic oligomers into complex knots. Second, the choice of the amino acid chirality is crucial: The all-L and all-D building blocks induce the directionality of the knot; whereas in the D/L building block, the mismatch of chiralities prevents knot formation. The folding of a linear species into a knot, driven by the hydrophobic effect, may provide a simple model for the formation of knots in proteins.

References and Notes

1. L. F. Liu, L. Perkocha, R. Calendar, J. C. Wang, *Proc. Natl. Acad. Sci. U.S.A.* **78**, 5498 (1981).
2. C. Z. Liang, K. Mislow, *J. Am. Chem. Soc.* **116**, 11189 (1994).
3. P. Virnau, A. L. Mallam, S. E. Jackson, *J. Phys. Condens. Matter* **23**, 033101 (2011).
4. J.-P. Sauvage, D. B. Amabilino, *Supramol. Chem.* (2012).
5. J. Guo, P. C. Mayers, G. A. Breault, C. A. Hunter, *Nat. Chem.* **2**, 218 (2010).
6. C. O. Dietrich-Buchecker, J.-P. Sauvage, *Angew. Chem. Int. Ed. Engl.* **28**, 189 (1989).
7. J.-F. Ayme *et al.*, *Nat. Chem.* **4**, 15 (2012).
8. P. E. Barran *et al.*, *Angew. Chem. Int. Ed. Engl.* **50**, 12280 (2011).
9. K. I. Arias, E. Zysman-Colman, J. C. Loren, A. Linden, J. S. Siegel, *Chem. Commun. (Camb.)* **47**, 9588 (2011).
10. L.-E. Perret-Aebi, A. von Zelewsky, C. Dietrich-Buchecker, J.-P. Sauvage, *Angew. Chem. Int. Ed.* **43**, 4482 (2004).
11. O. Safarowsky, M. Nieger, R. Fröhlich, F. Vögtle, *Angew. Chem. Int. Ed. Engl.* **39**, 1616 (2000).
12. M. Feigel, R. Ladberg, S. Engels, R. Herbst-Irmer, R. Fröhlich, *Angew. Chem. Int. Ed.* **45**, 5698 (2006).
13. P. T. Corbett *et al.*, *Chem. Rev.* **106**, 3652 (2006).
14. S. Wallin, K. B. Zeldovich, E. I. Shakhnovich, *J. Mol. Biol.* **368**, 884 (2007).
15. F. B. L. Cougnon, N. A. Jenkins, G. D. Pantoş, J. K. M. Sanders, *Angew. Chem. Int. Ed. Engl.* **51**, 1443 (2012).
16. N. Ponnuswamy, G. D. Pantoş, M. M. J. Smulders, J. K. M. Sanders, *J. Am. Chem. Soc.* **134**, 566 (2012).
17. S. Anderson, H. L. Anderson, J. K. M. Sanders, *Acc. Chem. Res.* **26**, 469 (1993).
18. A. L. Mallam, E. R. Morris, S. E. Jackson, *Proc. Natl. Acad. Sci. U.S.A.* **105**, 18740 (2008).
19. The lower stability of the cyclic monomer and dimer was apparent when, during our attempt to isolate these macrocycles, they rapidly reequilibrated into a library dominated by the knot.
20. J. J. P. Stewart, *J. Mol. Model.* **13**, 1173 (2007).
21. M. Korth, *J. Chem. Theory Comput.* **6**, 3808 (2010).
22. A. Klamt, G. Schüürmann, *J. Chem. Soc., Perkin Trans. 2* **2**, 799 (1993).

Acknowledgments: We are grateful to Gates Cambridge (N.P.), Engineering and Physical Sciences Research Council (F.B.L.C., J.K.M.S.), and the University of Bath (G.D.P.) for financial support. We thank S. Jackson for helpful discussions, N. Jenkins for his contribution in the early stage on the project, and A. Belenguer for maintaining the LC-MS facility.

Supplementary Materials

www.sciencemag.org/cgi/content/full/338/6108/783/DC1
Materials and Methods
Figs. S1 to S22
Tables S1 to S4
References

5 July 2012; accepted 11 September 2012
10.1126/science.1227032

Tissint Martian Meteorite: A Fresh Look at the Interior, Surface, and Atmosphere of Mars

H. Chennaoui Aoudjehane,[1,2]* G. Avice,[3] J.-A. Barrat,[4] O. Boudouma,[2] G. Chen,[5] M. J .M. Duke,[6] I. A. Franchi,[7] J. Gattacceca,[8] M. M Grady,[7,9] R. C. Greenwood,[7] C. D. K. Herd,[5] R. Hewins,[10] A. Jambon,[2] B. Marty,[3] P. Rochette,[8] C. L Smith,[9,11,12] V. Sautter,[10] A. Verchovsky,[7] P. Weber,[13] B. Zanda[10]

Tissint (Morocco) is the fifth martian meteorite collected after it was witnessed falling to Earth. Our integrated mineralogical, petrological, and geochemical study shows that it is a depleted picritic shergottite similar to EETA79001A. Highly magnesian olivine and abundant glass containing martian atmosphere are present in Tissint. Refractory trace element, sulfur, and fluorine data for the matrix and glass veins in the meteorite indicate the presence of a martian surface component. Thus, the influence of in situ martian weathering can be unambiguously distinguished from terrestrial contamination in this meteorite. Martian weathering features in Tissint are compatible with the results of spacecraft observations of Mars. Tissint has a cosmic-ray exposure age of 0.7 ± 0.3 million years, consistent with those of many other shergottites, notably EETA79001, suggesting that they were ejected from Mars during the same event.

Demonstration in the early 1980s that an important group of meteorites was of martian origin represented a breakthrough in attempts to understand the geological evolution of Mars (*1*–*3*). Unfortunately, most of the samples were collected long after their arrival on Earth and thus have experienced variable degrees of terrestrial weathering (*4*). Even the few martian meteorites that were collected shortly after their observed fall to Earth have been exposed to organic and other potential contaminants during storage. Here, we report on the Tissint martian meteorite, which fell on 18 July 2011 in Morocco (figs. S1 and S2). This is only the fifth witnessed fall of a meteorite from Mars and therefore provides an opportunity to improve our understanding of processes that operated on that planet at the time the meteorite was ejected from its surface.

The largest recovered stones from the Tissint fall are almost fully covered with a shiny black fusion crust (Fig. 1). Internally the meteorite consists of olivine macrocrysts set in a fine-grained matrix of pyroxene and feldspathic glass (maskelynite) (*5*) (figs. S3 to S6 and tables S1 to S6). The matrix is highly fractured and penetrated by numerous dark shock veins and patches filled with black glassy material enclosing bubbles (fig. S7). The petrology of Tissint shows similarities to that of other picritic shergottites (an important group of olivine-rich martian basaltic rocks), in particular, lithologies A and C of EETA79001 (*2*). The grain density and magnetic properties of Tissint (fig. S8) also match previous results from basaltic and picritic shergottites (*6*).

Tissint is an Al-poor ferroan basaltic rock, rich in MgO and other compatible elements (Ni,

Downloaded from www.sciencemag.org on November 9, 2012

Cr, Co). Its major element abundances are similar to those of the other picritic shergottites, especially EETA79001. Furthermore, key element weight (wt) ratios (wt %/wt %) such as FeO/MnO (39.7), Al/Ti (7.2), Na/Ti (1.41), Ga/Al (3.9 10^{-3}), Na/Al (0.20) (*3*, *4*, *7*), and $\Delta^{17}O$ [+0.301 per mil (‰)] (fig. S9) (*8*) are also typical of martian meteorites. The average composition of the black glass (tables S7 and S8) is identical to a mixture of the major phases of the rock (augite, maskelynite, and olivine: 50:20:30) with compositional variations reflecting incomplete dissolution of one phase or another (fig. S7). Among minor elements in the black glass, chlorine is always below the detection level of electron microprobe analysis [100 parts per million (ppm)], whereas fluorine and sulfur exhibit variations in the range 0 to 4000 ppm and 0 to 6000 ppm, respectively (*5*).

Like most other picritic shergottites, bulk Tissint displays a marked depletion in light rare earth elements (LREEs) and other highly incompatible elements, such as Rb, Li, Be, Nb, Ta, Th, and U (Fig. 2). Its Lu/Hf ratio (0.2) is in the range of values measured for EETA79001 and other basaltic shergottites [0.1 to 0.2; e.g., (*9*)], and lower than those of the picritic shergottites DaG 476/489, SaU 005, and Dhofar 019 [about 0.3 (*10*–*12*)]. Although the sizes of the two samples analyzed here are somewhat limited (0.49 and 1.25 g), their trace-element abundances are very similar and so are likely to be representative of the whole rock composition, despite the irregular distribution of olivine megacrysts.

To evaluate the possible heterogeneity of this stone, we analyzed two additional samples: a groundmass-rich sample (devoid of large olivine crystals and weighing 181 mg) and a fragment of the same glassy pocket selected for volatile analysis (40 mg). Both samples display markedly higher LREE abundances, with REE patterns generally similar to those of the enriched shergottites, as exemplified by Zagami. However, there is a minor, but analytically valid, positive Ce anomaly (Ce/Ce* = 1.1) (Fig. 2), and the La/Nd, La/Nb, and Th/La ratios are higher than those of other enriched shergottites (fig. S10). These two samples indicate that an LREE-enriched component, different from those previously recorded in other shergottites, is heterogeneously dispersed throughout the matrix of Tissint.

The presence of short-lived ^{48}V (half-life = 16 days), among other cosmogenic isotopes, demonstrates that the stones we analyzed are from the fall of 18 July (table S10). We measured stable cosmogenic isotopes of He, Ne, and Ar in three aliquots, consisting of matrix-rich, glass-matrix mixed, and glass-rich separates (table S11). The cosmic-ray exposure (CRE) ages computed for $^{3}He_c$, $^{21}Ne_c$, and $^{38}Ar_c$ are 1.2 ± 0.4, 0.6 ± 0.2, and 0.9 ± 0.4 million years (My), respectively, resulting in an average CRE age of 0.7 ± 0.3 My for Tissint. This age is in the range of CRE ages of other shergottites, notably that of EETA79001 [0.73 ± 0.15 My (*2*)], suggesting that Tissint and other shergottites were ejected during a single event. Nitrogen isotopes were analyzed together with the noble gases. The glass aliquot displayed a well-defined excess of ^{15}N, which persisted after correction for contribution of cosmogenic $^{15}N_c$ (assuming a production rate of 6.7 ± 2.6 × 10^{-13} mol ^{15}N/gMa) (*13*). This excess ^{15}N is best explained by trapping of a martian atmospheric component (*2*). Using a $\delta^{15}N$ versus $^{40}Ar/N$ correlation and taking a martian atmospheric value from the Viking measurements of 0.33 ± 0.03 (*14*), we obtain a $\delta^{15}N$ value of 634 ± 60‰ (1σ), which agrees well with the Viking measurement of 620 ± 160‰ (*7*) (Fig. 3).

Simultaneous measurement of carbon and nitrogen was carried out by stepped combustion–mass spectrometry on a small chip (21 mg) from the same sample that we used for oxygen isotopic analysis (*5*). The sample had a total carbon abundance of 173 ppm and $\delta^{13}C$ of –26.6 ‰ and contained 12.7 ppm nitrogen with total $\delta^{15}N$ of –4.5‰. At temperatures above 600°C, both carbon and nitrogen were distributed among three discrete martian components (fig. S11 and table S12). Below 600°C, readily resolvable components of organic material combusted; although these may have been introduced during postfall collection and sample storage and are an unavoidable consequence of sample handling procedures, we cannot yet rule out the presence of small quantities of indigenous martian organic matter (*5*). At the highest temperatures of the extraction, there was a clear indication of the presence of trapped martian atmosphere, with elevated $\delta^{13}C$ and $\delta^{15}N$ (even allowing for a cosmogenic component, blank-corrected $\delta^{13}C$ reaches +16‰ and $\delta^{15}N$ reaches +298 ± 25‰). At intermediate temperatures (600° to 800°C), there were maxima in both $\delta^{13}C$ (–14‰) and $\delta^{15}N$ (+110‰), suggesting that the component bears some relationship to the martian atmosphere. In addition, there was clear analytical evidence for a simultaneous release of sulfur (~19 ppm), presumably from either sulfide or sulfate decomposition. This intermediate component probably corresponds to a surface-derived weathering component, as identified in Tissint glass on the basis of REE, S, and



Fig. 1. The Natural History Museum (London) stone. This 1.1-kg stone (BM.2012,M1) exhibits a black fusion crust with glossy olivines. The olivine macrocrysts (pale green) and the numerous black glass pockets and veins are characteristics of this shergottite. The scale is in centimeters.

[1]Hassan II University Casablanca, Faculty of Sciences, Géosciences Appliquées à l'Ingénierie et l'Aménagement (GAIA) Laboratory, BP 5366 Maârif, Casablanca Morocco. [2]Université Pierre et Marie Curie Paris 6, Institut de la Terre de Paris (UMR 7193) 4 Place Jussieu, 75005 Paris France. [3]Centre de Recherches Pétrographiques et Géochimiques-CNRS, Université de Lorraine, 15 rue Notre Dame des Pauvres, BP 20, F-54501 Vandoeuvre-lès-Nancy, France. [4]Université de Bretagne Occidentale–Institut Universitaire Européen de la Mer, UMR 6538, Place Nicolas Copernic, 29280 Plouzané Cedex, France. [5]Department of Earth and Atmospheric Sciences, University of Alberta, Edmonton, AB, T6G 2E3, Canada. [6]SLOWPOKE Nuclear Reactor Facility, 1-20 University Hall, University of Alberta, Edmonton, AB, T6G 2J9, Canada. [7]Planetary and Space Sciences, The Open University, Walton Hall, Milton Keynes, MK7 6AA, UK. [8]Centre Européen de Recherche et d'Enseignement des Géosciences de l'Environnement, CNRS Aix-Marseille University, BP80 13545 Aix en Provence, Cedex 4, France. [9]Department of Mineralogy, Natural History Museum, Cromwell Road London SW7 5BD, UK. [10]Laboratoire d'Etudes de la Matière Extraterrestre, Muséum National d'Histoire Naturelle and CNRS-UMS2679, 61 rue Buffon, 75005 Paris, France. [11]ESA (European Space Agency) European Space Research and Technology Center, Keplerlaan 1, 2200 AG Noordwijk, Netherlands. [12]UK Space Agency, ESA Harwell Centre, Atlas Building, Harwell Oxford, Didcot, Oxfordshire OX11 0QX, UK. [13]University of Bern, Albert Einstein Center for Fundamental Physics, Sidlerstrasse 5, CH-3012 Bern, Switzerland.

*To whom correspondence should be addressed. E-mail: chennaoui_h@yahoo.fr, h.chennaoui@fsac.ac.ma

Downloaded from www.sciencemag.org on November 9, 2012

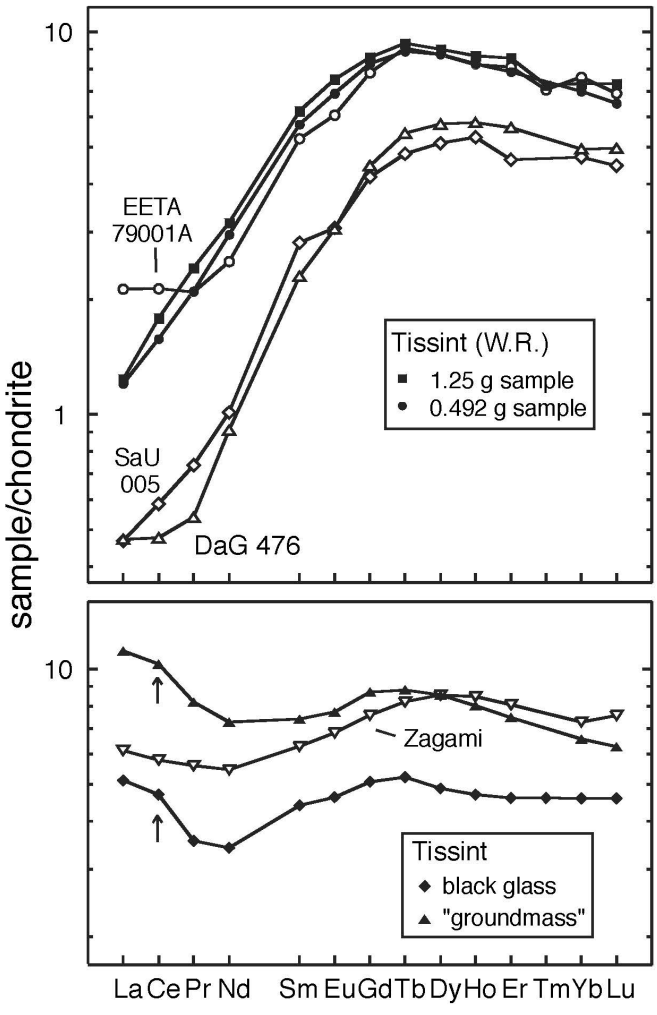


Fig. 2. REE patterns. (**Top**) Tissint in comparison with other depleted picritic shergottites. (**Bottom**) Black glass and groundmass-rich fraction in comparison with enriched shergottite Zagami. Data from (*10*–*12*). CI chondrite normalization values are from (*24*).

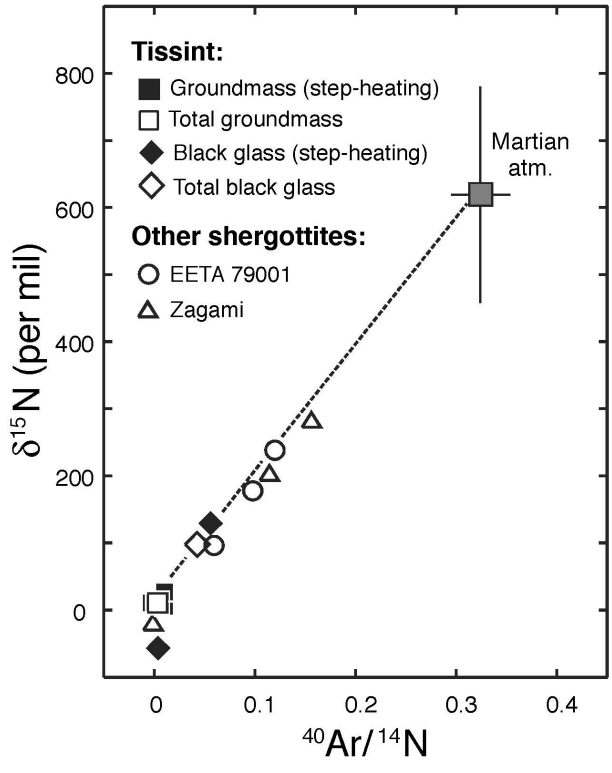


Fig. 3. Gas analyses of the black glass. Both bulk analyses and step-heating analyses plot on a single mixing line between terrestrial atmospheric gas (at left) and Mars atmospheric gas (*14*). Zagami data from (*25*).

F data (see below). The third martian component represents magmatic carbon, which is present in low abundance (1.4 ppm with $\delta^{13}C$ of –26.3‰) and is associated with isotopically light nitrogen ($\delta^{15}N < +10‰$).

Our study demonstrates that Tissint is a picritic shergottite comparable in many respects to EETA79001. The black shock glass resembles lithology C of EETA79001, as well as shock melt pockets commonly found in other shergottites (*15*). Major elements and oxygen isotope data indicate that this glass represents a melted mixture of the surrounding bulk rock, composed of olivine, maskelynite, and clinopyroxene (*5*). However, this glass is substantially different from the bulk meteorite and igneous groundmass in that it has a variable but generally high S and F content; a distinct LREE-enriched composition; and a high $\delta^{15}N$ value indicative of trapped martian atmosphere.

The LREE-enriched composition of the glass is somewhat enigmatic. Phosphates are often invoked as a carrier of REE. However, the P content of the black glass relative to bulk rock is not consistent with enrichment in phosphates. One possibility to explain the LREE composition of the glass might be selective crustal contamination before final emplacement of the Tissint magma. Although LREE-enriched magmatic rocks have been generated on Mars, as exemplified by the Nakhlites and Chassignites, these do not exhibit anomalous Ce abundances (*16*, *17*). In addition, crustal contamination of magma is unlikely to result in REE ratio variations at the subcentimeter scale, as observed here. Decoupling of Ce from the other REE indicates partial oxidation to Ce^{4+}, a process that requires oxidizing conditions, such as those that prevail in the near-surface environment of Mars. Surface weathering caused by leaching of phosphates by acid aqueous fluids, the process that is responsible for terrestrial alteration of eucritic meteorites in Antarctica (*18*), would also explain the LREE-enriched composition of the Tissint glass. The high $\delta^{15}N$ value of the Tissint glass, as well as its enrichment in S and F, demonstrates that it has been contaminated by martian surface components. In view of this evidence, the most likely explanation for the relatively LREE-enriched composition of the glass, and the origin of the Ce anomaly, is that these features also reflect the presence of a near-surface martian component in Tissint. A martian soil component was previously suggested for EETA79001 lithology C, which also contains martian atmospheric gases (*19*). However, because this meteorite is a find, rather than a fresh fall like Tissint, there's the possibility of terrestrial contamination, which complicates the interpretation (*20*).

We propose the following scenario to explain the composite nature of Tissint. A picritic basalt was emplaced at or near the surface of Mars. After some period, the rock was weathered by fluids, which had leached elements from the martian regolith. Subsequently, these fluids

Downloaded from www.sciencemag.org on November 9, 2012

deposited mineral phases within fissures and cracks. The martian weathering products are the most likely source of the required LREE, incompatible, and volatile elements. Upon impact, preferential, shock-induced melting occurred in the target rock along fractures where weathering products were concentrated. This melting produced the black glass and retained in it chemical signatures characteristic of the martian surface. Shock melting also trapped a component derived from the martian atmosphere, as revealed by stepped combustion–mass spectrometry. About 0.7 My ago, the sample was ejected from Mars and eventually landed on Earth in July 2011. The martian weathering features in Tissint described here are compatible with spacecraft observations on Mars, including those made by the NASA Viking landers, MER Spirit rover, and ESA's Mars Express orbiter (*5*, *21*–*23*).

References and Notes

1. D. D. Bogard, P. Johnson, *Science* **221**, 651 (1983).
2. R. H. Becker, R. O. Pepin, *Earth Planet. Sci. Lett.* **69**, 225 (1984).
3. A. H. Treiman, J. D. Gleason, D. D. Bogard, *Planet. Space Sci.* **48**, 1213 (2000).
4. G. Crozaz, M. Wadhwa, *Geochim. Cosmochim. Acta* **65**, 971 (2001).
5. Supplementary materials are available on *Science* Online.
6. P. Rochette *et al.*, *Meteorit. Planet. Sci.* **40**, 529 (2005).
7. A. O. Nier, M. B. McElroy, *J. Geophys. Res.* **82**, 4341 (1977).
8. I. A. Franchi, I. P. Wright, A. S. Sexton, C. T. Pillinger, *Meteorit. Planet. Sci.* **34**, 657 (1999).
9. J. Blichert-Toft, J. D. Gleason, P. Télouk, F. Albarède, *Earth Planet. Sci. Lett.* **173**, 25 (1999).
10. G. Dreibus *et al.*, *Meteorit. Planet. Sci.* **35**, A49 (2000).
11. J. A. Barrat, J. Blichert-Toft, R. W. Nesbitt, F. Keller, *Meteorit. Planet. Sci.* **36**, 23 (2001).
12. C. R. Neal, L. A. Taylor, J. C. Ely, J. C. Jain, M. A. Nazarov, *Lunar Planet. Sci.* **32**, 1671 (2001).
13. B. Marty, K. Hashizume, M. Chaussidon, R. Wieler, *Space Sci. Rev.* **106**, 175 (2003).
14. T. Owen *et al.*, *J. Geophys. Res.* **82**, 4635 (1977).
15. J.-A. Barrat *et al.*, *Geochim. Cosmochim. Acta* **66**, 3505 (2002).
16. V. Sautter *et al.*, *Earth Planet. Sci. Lett.* **195**, 223 (2002).
17. P. Beck *et al.*, *Geochim. Cosmochim. Acta* **70**, 2127 (2006).
18. D. W. Mittlefehldt, M. M. Lindstrom, *Geochim. Cosmochim. Acta* **67**, 1911 (2003).
19. M. N. Rao, L. E. Borg, D. S. McKay, S. J. Wentworth, *Geophys. Res. Lett.* **26**, 3265 (1999).
20. E. L. Walton, P. J. Jugo, C. D. K. Herd, M. Wilke, *Geochim. Cosmochim. Acta* **74**, 4829 (2010).
21. R. E. Arvidson, J. L. Gooding, H. J. Moore, *Rev. Geophys.* **27**, 39 (1989).
22. L. A. Haskin *et al.*, *Nature* **436**, 66 (2005).
23. A. Gendrin *et al.*, *Science* **307**, 1587 (2005).
24. J. A. Barrat *et al.*, *Geochim. Cosmochim. Acta* **83**, 79 (2012).
25. K. Marti, J. S. Kim, A. N. Thakur, T. J. McCoy, K. Keil, *Science* **267**, 1981 (1995).

Acknowledgments: We acknowledge D. N. Menegas and family for their generous donation enabling the acquisition of Tissint (BM.2012,M1), M. Aoudjehane for fieldwork, A. Aaranson for field information, J. Gibson for assistance with oxygen isotope analysis, L. Labenne for loan of a sample, and A. Irving for 400 mg of powdered sample. This study was funded at Hassan II University Casablanca, Faculté des Sciences Ain Chock, by Centre de Recherches Scientifiques et Techniques Morocco and CNRS France (Projet International de Coopération Scientifique, Sciences de l'Univers 01/10), and by Comité Mixte Inter Universitaire Franco-Marocain Volubilis (MA/11/252); CRPG Nancy, France, by the CNES, CNRS, and European Research Council under the European Community's Seventh Framework Programme (FP7/2007-2013 no. 267255); Université de Bretagne Occidentale–Institut Universitaire Européen de la Mer, Plouzané, France, by the Programme National de Planétologie, Institut National des Sciences de l'Univers; Open University, by Science and Technology Facilities Council grant to the Planetary and Space Sciences Discipline; and University of Alberta, by the Natural Sciences and Engineering Research Council of Canada (grant 261740-03).

Supplementary Materials

www.sciencemag.org/cgi/content/full/science.1224514/DC1
Materials and Methods
Supplementary Text
Figs. S1 to S11
Tables S1 to S13
References (*26*–*35*)

9 May 2012; accepted 25 September 2012
Published online 11 October 2012;
10.1126/science.1224514

Development and Disintegration of Maya Political Systems in Response to Climate Change

Douglas J. Kennett,[1]*† Sebastian F. M. Breitenbach,[2]* Valorie V. Aquino,[3] Yemane Asmerom,[4] Jaime Awe,[5] James U.L. Baldini,[6] Patrick Bartlein,[7] Brendan J. Culleton,[1] Claire Ebert,[1] Christopher Jazwa,[1] Martha J. Macri,[8] Norbert Marwan,[9] Victor Polyak,[4] Keith M. Prufer,[3] Harriet E. Ridley,[6] Harald Sodemann,[10] Bruce Winterhalder,[11] Gerald H. Haug[2]

The role of climate change in the development and demise of Classic Maya civilization (300 to 1000 C.E.) remains controversial because of the absence of well-dated climate and archaeological sequences. We present a precisely dated subannual climate record for the past 2000 years from Yok Balum Cave, Belize. From comparison of this record with historical events compiled from well-dated stone monuments, we propose that anomalously high rainfall favored unprecedented population expansion and the proliferation of political centers between 440 and 660 C.E. This was followed by a drying trend between 660 and 1000 C.E. that triggered the balkanization of polities, increased warfare, and the asynchronous disintegration of polities, followed by population collapse in the context of an extended drought between 1020 and 1100 C.E.

The Classic Maya (300 to 1000 C.E.) left a remarkable historical record inscribed on well-dated stone monuments. Wars, marriages, and accessions of kings and queens are tied to long count calendar dates and correlate with specific days in the Christian calendar (Goodman-Thompson-Martinez correlation). The termination of this tradition between 800 and 1000 C.E. marks the widespread collapse of Classic Maya political systems. Multidecadal drought has been implicated, but remains controversial because of dating uncertainties and insufficient temporal resolution in paleoclimatic records. Lake sediments from the Yucatan Peninsula provided the first evidence of substantial drying in the Terminal Classic (*1*). However, disturbances to lake sediment sequences caused by prehistoric deforestation and agricultural expansion during the Classic Period complicate reproducing these results near the largest and most politically important Maya centers (such as Tikal and Caracol). Several studies more distant from the Maya lowlands (ML) support either relatively dry conditions or a series of droughts during the Terminal Classic (*2*–*5*), but the relevance of these records for the ML remains unclear (*6*).

Cave deposits in the ML show great promise for paleoclimatic reconstruction (*7*–*9*). The challenge lies in developing long, continuous records from rapidly growing stalagmites that can be dated precisely by using ^{234}U-^{230}Th (U-Th). Here, we present a subannually resolved rainfall record from an exceptionally well-dated stalagmite collected from Yok Balum (YB) Cave in Belize (16°12'30.780" N, 89°4'24.420" W, 366 m above sea level) (*10*). YB cave is located 1.5 km from the Classic Period Maya site of Uxbenká. Three other important Maya centers (Pusilha, Lubaantun, Nim Li Punit) are within 30 km (fig. S1); Tikal and other major Classic Period population centers (such as Caracol, Copan, and Calakmul) are

[1]Department of Anthropology, Pennsylvania State University, University Park, PA 16802, USA. [2]Department of Earth Science, Eidgenössische Technische Hochschule (ETH), CH-8092 Zürich, Switzerland. [3]Department of Anthropology, University of New Mexico, Albuquerque, NM 87131, USA. [4]Department of Earth and Planetary Sciences, University of New Mexico, Albuquerque, NM 87131, USA. [5]Institute of Archaeology, National Institute of Culture and History, Belmopan, Belize. [6]Department of Earth Sciences, University of Durham, Durham DH1 3LE, UK. [7]Department of Geography, University of Oregon, Eugene, OR 97403, USA. [8]Department of Native American Studies, University of California, Davis, Davis, CA 95616, USA. [9]Potsdam Institute for Climate Impact Research, Post Office Box 60 12 03, 14412 Potsdam, Germany. [10]Institute for Atmospheric and Climate Science, ETH, CH-8092 Zürich, Switzerland. [11]Department of Anthropology, University of California, Davis, Davis, CA 95616, USA.

*These authors contributed equally to this work.
†To whom correspondence should be addressed. E-mail: djk23@psu.edu

Downloaded from www.sciencemag.org on November 9, 2012

within 200 km and are influenced by the same climate systems (fig. S8). Age control of our climate reconstruction is comparable in precision with the historical record, providing a foundation for examining the complex nature of political dynamics in response to climate change.

In 2006, we collected a 56-cm-long stalagmite (YOK-I) from 50 m inside the western entrance of the cave (figs. S2 and S3). Forty U-Th dates indicate that the upper 415 mm of the stalagmite grew continuously between 40 B.C.E. and 2006 C.E. (table S2 and fig. S4). Analytical precision for the U-Th dates ranges from ±1 to ±17 years, and time averaging related to sample drilling is ~20 years (table S3 and fig. S5). The climate record is based on >4200 oxygen isotope ($\delta^{18}O$) measurements taken continuously in 0.1-mm increments, representing a mean temporal resolution of 0.5 years (table S4 and fig. S6). Monitoring data from YB cave combined with Hendy tests on stalagmite and glass drip plate carbonate indicate that $\delta^{18}O$ values reflect rainfall amount above the cave and that minor kinetic effects exist that increase $\delta^{18}O$ values, possibly enhancing the signal when climate conditions are dry (figs. S9 to S14). The $\delta^{18}O$ record ranges from –5.2 to –2.5 per mil (‰) and oscillates on decadal to multicentennial scales (Fig. 1). Multidecadal droughts occur between ~200 to 300, 820 to 870, 1020 to 1100, and 1530 to 1580 C.E., and the high-resolution YOK-I record permits the identification of other shorter and occasionally very severe droughts, particularly centered on AD 420, 930, and 1800. The $\delta^{18}O$ record is considered unreliable in the 20th century and not a reflection of drought conditions (fig. S7) (*10*).

We argue that climate variability was predominantly driven by Intertropical Convergence Zone (ITCZ) migration and changes in El Niño frequency, the linkage being a general perturbation of tropical climate (Walker Circulation) accompanying El Niño–Southern Oscillation (ENSO)–time scale variability. During El Niño years, the ITCZ is positioned over the eastern equatorial Pacific, and boreal summer moisture delivery to the ML decreases (*11*). Strengthened vertical wind shear linked to ITCZ position during El Niño years reduces the number of tropical depressions, storms, and hurricanes crossing the ML. Power spectral analyses of the YOK-I $\delta^{18}O$ record shows statistically significant periodicities centered on 3 to 8 years, which is consistent with a strong ENSO signal (fig. S15). Previous research used titanium concentrations in marine sediments from the Cariaco Basin to reconstruct ITCZ-related rainfall changes over the ML (*2*, *11*). We tuned the past 2000 years of the Cariaco Ti chronology within that record's errors using our high-precision U-Th chronology (Fig. 1B and fig. S16). A correlation may exist between the YOK-I $\delta^{18}O$ record and other lower-resolution records from the ML, including Lake Chichancanab sediment density record (Fig. 1C) (*12*), Lake Punta Laguna ostracod $\delta^{18}O$ record (Fig. 1D) (*13*), and the Macal Chasm speleothem luminescence record (Fig. 1E) (*8*). However, statistically significant correlations between these records are difficult to demonstrate because the chronological uncertainties of older records allow for a range of correlation coefficients. Given these uncertainties, we cannot definitively link these regional records, but visually similar trends are evident on multidecadal time scales (fig. S17).

We hypothesize that precipitation-induced changes in agricultural productivity mediated the tendency toward political integration or disintegration in the ML. Droughts recorded in the Yucatan between 1535 and 1575 C.E. (*14*) correspond to one of four multidecadal droughts evident in the YOK-I record (Fig. 2). The interval from 1535 to 1542 C.E. was particularly dry. Historical accounts link this drought to reduced agricultural productivity, famine, disease, death, and population relocation. Some estimates suggest that drought-related agricultural disaster caused nearly a million deaths in Mexico in 1535 C.E. (*15*), illustrating how meteorologically dry conditions presage agricultural drought with severe effects scaled to population density and level of agricultural intensification.

A dry period comparable with the historical drought of 1535 C.E. is evident in the YOK-I record

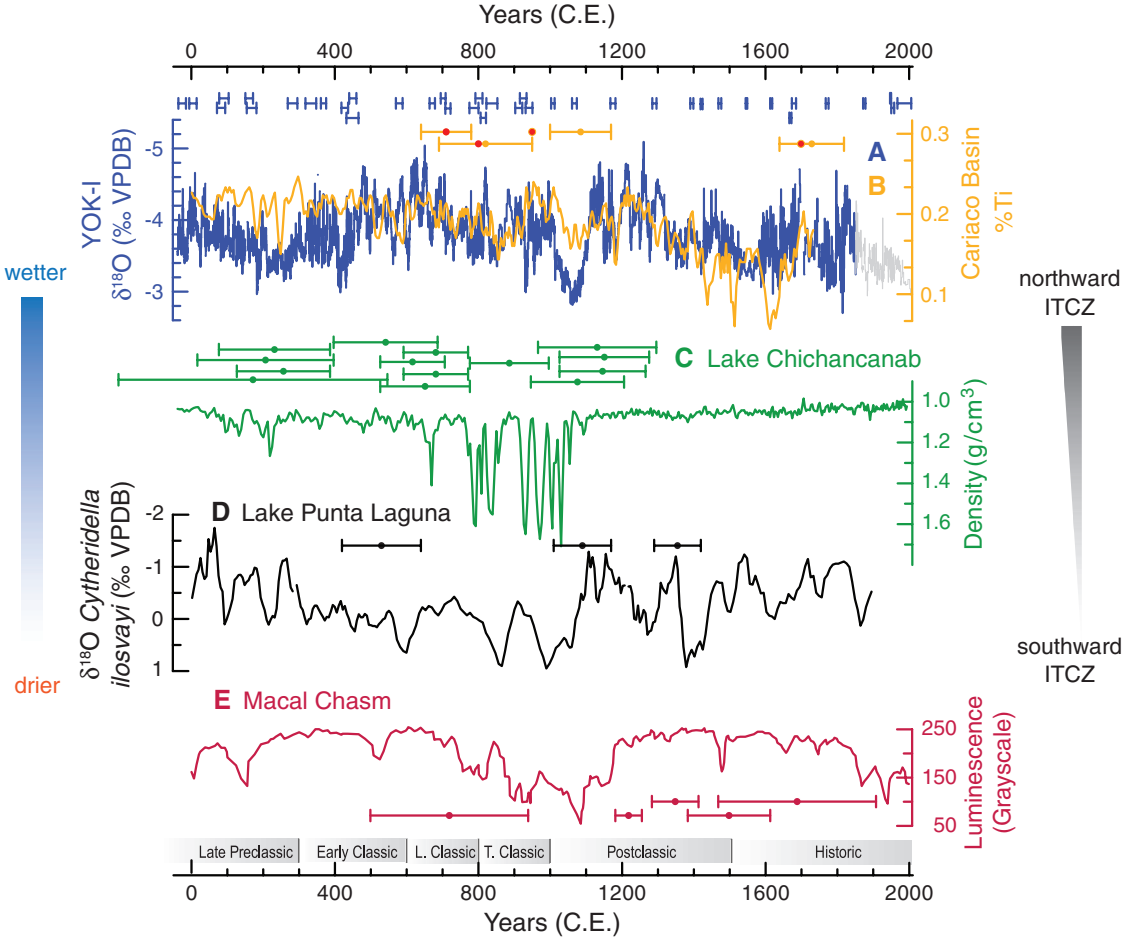


Fig. 1. Comparison of (**A**) stalagmite YOK-I $\delta^{18}O$ with (**B**) Tuned (red dots) (*10*) bulk sediment titanium record from the Cariaco Basin, Venezuela (*11*). (**C**) Lake Chichancanab sediment density record (*12*). (**D**) Lake Punta Laguna ostracod (*Cytheridella ilosvayi*) $\delta^{18}O$ record (*13*). (**E**) Macal Chasm speleothem luminescence record (*8*). Similarities in the YOK-I and Cariaco records suggest that rainfall variability was strongly modulated by ITCZ migration. Age models for each record are based on calibrated ^{14}C or U-Th, with error bars showing the relative chronological precision of each record. Smoothed records that emphasize multidecadal trends are shown in fig. S17. The light gray line denotes uncertainties in the 20th- century $\delta^{18}O$ record (details and climate archive locations are available in the supplementary materials).

Downloaded from www.sciencemag.org on November 9, 2012

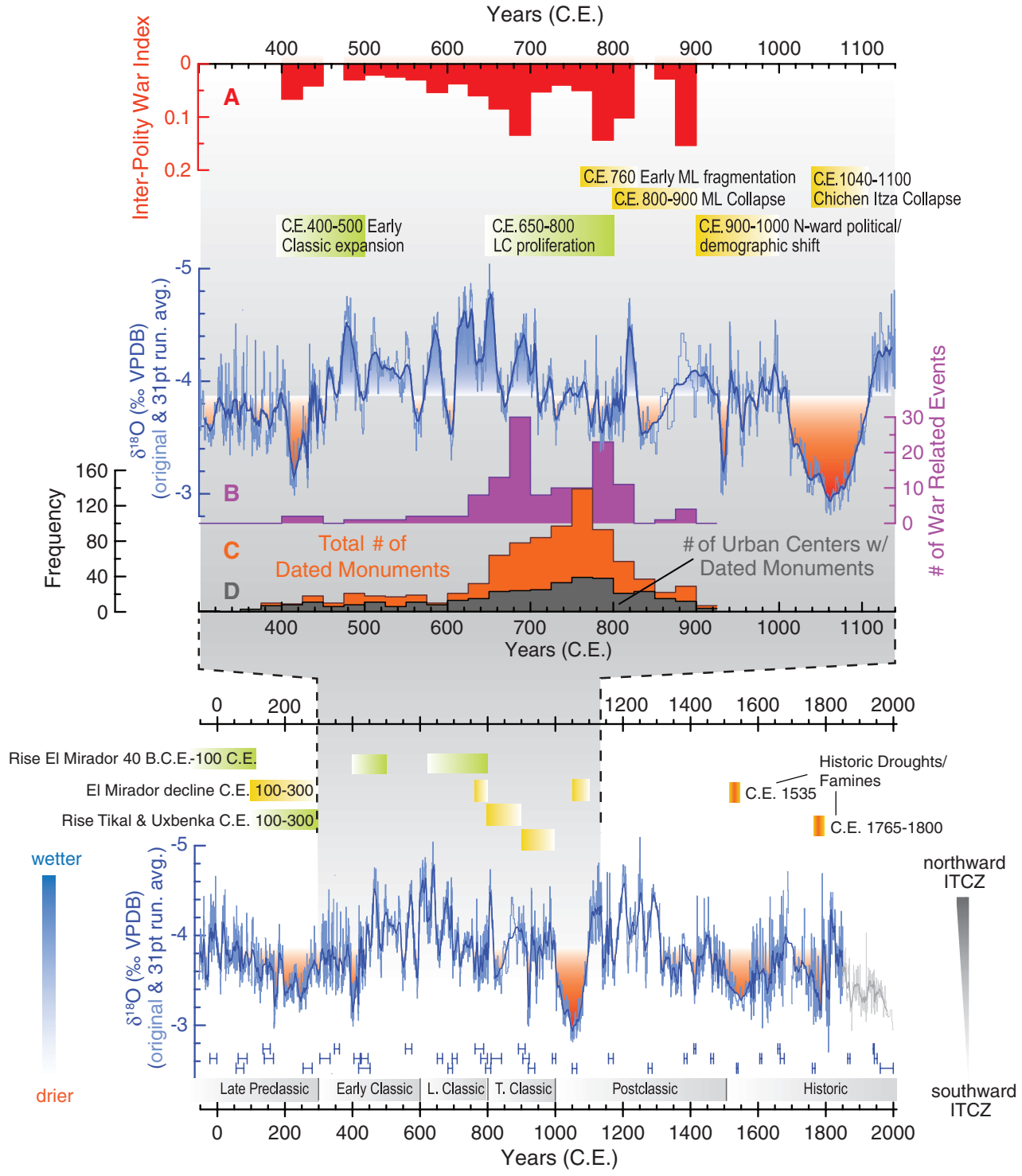


Fig. 2. (Bottom) YOK-I $\delta^{18}O$ climate record spanning the past 2000 years (40 B.C.E. to 2006 C.E.) shown relative to Maya chronology and major historical events. Blue bars just below the $\delta^{18}O$ curve indicate the small error for each of the 40 U-Th dates used to constrain the chronology of the $\delta^{18}O$ climate record (*10*). Drier-than-average conditions during this interval are shown in orange. Two historically recorded droughts in the 16th- and 18th-century C.E. accord well with the YOK-I record, and the earliest multidecadal drought in the record (200 to 300 C.E.) corresponds with decline of the large center of El Mirador and a major sociopolitical reorganization in the ML. (Top) The YOK-I $\delta^{18}O$ climate record between 300 and 1140 C.E. shown relative to major historic events along with (**A**) An interpolity warfare index based on the number of war-related events between Maya sites or rulers relative to the total number of events recorded during each interval. (**B**) Raw number of war-related events. (**C**) Frequency distribution of long-count dated monuments in the ML. (**D**) Total number of urban centers with dated monuments through time as a proxy for the development and disintegration of complex polities in the ML. All hieroglyphic data are from the Maya Hieroglyphic database (raw data is available in the supplementary materials) (*28*) and are binned in 25-year intervals. The light gray line denotes uncertainties in the 20th-century $\delta^{18}O$ record (*10*).

Downloaded from www.sciencemag.org on November 9, 2012

at the end of the Preclassic Period (200 to 300 C.E.). Maya populations had expanded across the ML during the Middle and Late Preclassic Periods (1000 B.C.E. to 100 C.E.), exploiting productive agricultural soils and seasonal wetlands (*16, 17*). Multiple fully developed polities emerged in the ML (*18*), including the large center of El Mirador in northern Guatemala (*19*). The drying trend evident in the YOK-I record starting at 100 C.E. culminated in a century-long dry interval (200 to 300 C.E.) that corresponds to the demise of El Mirador, which is consistent with the hypothesis that drought played a role in the political realignment and reorganization of ML population centers between 150 to 300 C.E. (*12*). Several ML polities persisted, however, and became more integrated and grew in size, including Uxbenká (*20*).

Tikal, already established in the central Peten (Guatemala) as an important regional center during the Middle and Late Preclassic (1000 B.C.E. to 300 C.E.), emerged as a dominant sociopolitical force in the wake of the climatic and social instability of the 3rd and 4th centuries C.E. (*21*). Tikal, Calakmul, and other important sites in the central Peten were positioned near seasonal wetlands under intensive use (*22*). High rainfall during the Early Classic evident in the YOK-I record (Fig. 2) maintained these wetlands and seasonally recharged constructed water storage systems (reservoirs and tanks) (*23*). This helps to explain the growing geopolitical influence of polities like Tikal, Calakmul, Caracol, and Naranjo. Many of the best-recorded ruling Maya lineages were founded around 440 to 500 C.E. (*24*) during this interval of anomalously high rainfall. The overall number of monument-bearing political centers and indications of war among them also increased throughout the Early Classic (300 to 650 C.E.) (Fig. 2).

Terminal Classic Period droughts have been cited as causes of societal collapse in the Maya lowlands (*1*). The YOK-I record is consistent with this hypothesis, showing a multidecadal drought at this time (820 to 870 C.E.). This finding is consistent with arguments for a ~40% reduction in summer rainfall during the Terminal Classic Period (*9*). Multidecadal drought between 820 and 870 C.E. was part of a broader regional drying trend starting 640 C.E., culminating at 1020 C.E. in a century-long dry period that is the most pronounced in our record. The early stages of this drying trend correspond with an increase in interpolity warfare (Fig. 2, A and B) and expansion in the number of competing political centers, enumerated here from long count-dated historical texts (Fig. 2, C and D, and tables S7 and S8). War-related events increased during a dry interval between 640 and 660 C.E., but then peaked after a lag during a wetter interval between 660 and 700 C.E. Climate drying after 640 C.E. may have exacerbated environmental degradation that occurred with 5th- and 6th-century C.E. population expansion under a wetter climatic regime. Drying constrained agricultural productivity, stimulated inter-polity warfare (*25*), and promoted political competition and fissioning that was ultimately unsustainable.

The first evidence for political fragmentation occurred in the Petexbatun region between 760 and 800 C.E. (*26*), corresponding with a dry interval in the YOK-I record, peak population densities throughout the region (145 people per km^2) (*27*), and the maximum spatial extent of monument-bearing urban centers (Fig. 2, C and D). Historical texts on stone monuments were dedicated in at least 39 centers from 750 to 775 C.E., with rulers commissioning monuments at several large centers at unprecedented rates. These texts point to a dynamic and unstable geopolitical landscape centered on status rivalry, war, and strategic alliances (*28*). A precipitous drop in the number of texts at key centers (such as Tikal) between 775 and 800 C.E. was the precursor to a 50% drop in the number of centers with text-dated monuments between 800 and 825 C.E., which is evidence for widespread failure of these political systems. Increasing interpolity warfare (Fig. 2A) is most evident in the historical record between 780 and 800 C.E. Political power became decentralized as the institution of divine kingship collapsed between 780 and 900 C.E. Less is known about the fate of the people integrated into these polities, but depopulation took centuries and entailed migration, reorganization (*29*, *30*), and persistence in the environs surrounding abandoned cities (such as Mopan Valley, Guatemala) (*21*). Centers of political importance shifted to the northern parts of the Yucatan Peninsula as carved stone monuments were commissioned less frequently in the central Peten; the tradition ended at Chichen Itza sometime between 1000 and 1100 C.E. during the longest and driest interval of the past 2000 years.

ITCZ migration–influenced climate variability in the ML as recorded in YOK-I aids in understanding the complex socio-natural processes associated with Maya political dynamics during the past 2000 years. Population increases and the expansion of Classic Maya polities were favored by anomalously high rainfall and increased agricultural productivity between 440 and 660 C.E. High-density Maya populations were increasingly susceptible to the agricultural consequences of climate drying. We propose that a two-stage collapse commenced with the 660 C.E. drying trend. It triggered the balkanization of polities, increased warfare, and abetted overall sociopolitical destabilization. Political disintegration in the Petexbatun region foreshadows two multidecadal dry intervals that further reduced agricultural yields and caused more widespread political disintegration between 800 and 900 C.E. This was followed by a second stage of more gradual population decline and then punctuated population reductions during the most extreme dry interval in the YOK-I record between 1020 and 1100 C.E. The linkage between extended 16th-century drought, crop failures, death, famine, and migration in Mexico provides a historic analog evident in the YOK-I record for the sociopolitical tragedy and human suffering experienced by the 11th-century Maya. It also helps explain why the cultural elaboration evident during the Classic Period never fully redeveloped.

References and Notes

1. D. A. Hodell, J. H. Curtis, M. Brenner, *Nature* **375**, 391 (1995).
2. G. H. Haug *et al.*, *Science* **299**, 1731 (2003).
3. S. E. Metcalfe, M. D. Jones, S. J. Davies, A. Noren, A. MacKenzie, *Holocene* **20**, 1195 (2010).
4. D. W. Stahle *et al.*, *Geophys. Res. Lett.* **38**, L05703 (2011).
5. M. S. Lachniet, J. P. Bernal, Y. Asmerom, V. Polyak, D. Piperno, *Geology* **40**, 259 (2012).
6. J. Aimers, D. Hodell, *Nature* **479**, 44 (2011).
7. A. B. Frappier, D. Sahagian, S. J. Carpenter, L. A. González, B. R. Frappier, *Geology* **35**, 111 (2007).
8. J. W. Webster *et al.*, *Palaeogeogr. Palaeoclimatol. Palaeoecol.* **250**, 1 (2007).
9. M. Medina-Elizalde, E. J. Rohling, *Science* **335**, 956 (2012).
10. Materials and methods are available as supplementary material on *Science* Online.
11. G. H. Haug, K. A. Hughen, D. M. Sigman, L. C. Peterson, U. Röhl, *Science* **293**, 1304 (2001).
12. D. A. Hodell, M. Brenner, J. H. Curtis, *Quat. Sci. Rev.* **24**, 1413 (2005).
13. J. H. Curtis, D. A. Hodell, M. Brenner, *Quat. Res.* **46**, 37 (1996).
14. B. Mendoza, V. García-Acosta, V. Velasco, E. Jáuregui, R. Díaz-Sandoval, *Clim. Change* **83**, 151 (2007).
15. V. García-Acosta, J. M. Pérez-Zevallos, A. Molina del Villar, *Desastres Agrícolas en México. Catálogo Histórico. Tomo I: Épocas Prehispánica y Colonial* (Fondo de Cultura Económica and CIESAS, México, 2003), pp. 958–1822.
16. N. P. Dunning *et al.*, *Ann. Assoc. Am. Geogr.* **92**, 267 (2002).
17. S. Luzzadder-Beach, T. P. Beach, N. P. Dunning, *Proc. Natl. Acad. Sci. U.S.A.* **109**, 3646 (2012).
18. F. Estrada-Belli, *The First Maya Civilization: Ritual and Power Before the Classic Period* (Routledge, London, 2011).
19. R. D. Hansen, S. Bozarth, J. Jacob, D. Wahl, T. Schreiner, *Ancient Mesoamerica* **13**, 273 (2002).
20. B. J. Culleton, K. M. Prufer, D. J. Kennett, *J. Archeologic. Sci.* **39**, 1572 (2012).
21. J. P. Laporte, V. Fialko, *Ancient Mesoamerica* **6**, 41 (1995).
22. T. Beach *et al.*, *Quat. Sci. Rev.* **28**, 1710 (2009).
23. V. L. Scarborough *et al.*, *Proc. Natl. Acad. Sci. U.S.A.* **109**, 12408 (2012).
24. S. Martin, N. Grube, *Chronicle of the Maya Kings and Queens* (Thames & Hudson, London, 2008).
25. D. Webster, *The Fall of the Ancient Maya: Solving the Mystery of the Maya Collapse* (Thames and Hudson, London, 2002).
26. A. Demarest, *Ancient Maya: The Rise and Fall of a Rainforest Civilization* (Cambridge Univ. Press, Cambridge, 2004).
27. T. P. Culbert, D. S. Rice, Eds., *Precolumbian Population History in the Maya Lowlands* (Univ. of New Mexico Press, Albuquerque, 1990).
28. J. L. Munson, M. J. Macri, *J. Anthropol. Archaeol.* **28**, 424 (2009).
29. J. A. Sabloff, *Proc. Am. Philos. Soc.* **151**, 11 (2007).
30. P. M. Rice, D. S. Rice, in *The Terminal Classic in the Maya Lowlands: Collapse, Transition, and Transformation*, A. A. Demarest, P. M. Rice, D. S. Rice, Eds. (Univ. Press of Colorado, Boulder, CO, 2004), pp. 125–139.

Acknowledgments: We thank D. Hodell, M. Brenner, J. Yaeger, J. Lohse, J. Kennett, D. Webster, and three anonymous reviewers for their useful comments. Thanks to H. Meyer (AWI Potsdam for isotope analysis of rain and drip water. This research was supported by NSF (HSD-0827305, BCS-0940744, and EAR-0326902), European Research Council (240167), Swiss National Foundation (CRSI22-132646/1), the German Science Foundation (DFG FOR1380 "HIMPAC"), and the Alphawood Foundation.

Supplementary Materials

www.sciencemag.org/cgi/content/full/338/6108/788/DC1
Materials and Methods
Figs. S1 to S17
Tables S1 to S8
References (*31–211*)

19 June 2012; accepted 26 September 2012
10.1126/science.1226299

Downloaded from www.sciencemag.org on November 9, 2012

A Less Cloudy Future: The Role of Subtropical Subsidence in Climate Sensitivity

John T. Fasullo* and Kevin E. Trenberth

An observable constraint on climate sensitivity, based on variations in mid-tropospheric relative humidity (RH) and their impact on clouds, is proposed. We show that the tropics and subtropics are linked by teleconnections that induce seasonal RH variations that relate strongly to albedo (via clouds), and that this covariability is mimicked in a warming climate. A present-day analog for future trends is thus identified whereby the intensity of subtropical dry zones in models associated with the boreal monsoon is strongly linked to projected cloud trends, reflected solar radiation, and model sensitivity. Many models, particularly those with low climate sensitivity, fail to adequately resolve these teleconnections and hence are identifiably biased. Improving model fidelity in matching observed variations provides a viable path forward for better predicting future climate.

Estimates of how much Earth's global surface temperature would increase if the concentration of atmospheric carbon dioxide were double its pre-industrial concentration vary across climate models by a factor of about 2 (*1*). This metric, termed equilibrium climate sensitivity (ECS), serves as a canonical measure of climate model sensitivity to external changes. Differences across models cause considerable uncertainty in projected future climate. Despite substantial model improvements, the simulated range of ECS has changed little over the past several decades (*2*). This study therefore addresses the questions of what physical processes govern the spread of ECS among models, and whether model development efforts can be better directed at the goal of reducing this uncertainty.

Changes in clouds exert a primary influence on Earth's energy budget and ECS. Clouds apparently act as a modest net positive feedback (*3*, *4*), thereby amplifying changes due to anthropogenic influences, and most models capture this behavior (*5*–*7*). Constraining simulated clouds is a challenge, however, as clouds are complex and difficult to observe. The historical record is plagued by errors associated with the drift and failure of satellites, inconsistencies in the detection of clouds, and instrument biases (*8*). Moreover, clouds can vary not just in their bulk characteristics but also in their microphysical properties, for which global observations are lacking generally, and considerable uncertainty persists regarding the feedbacks of various cloud types that may occur in a changing climate (*9*). Hence, owing to the wide range of scales involved, cloud processes in models are often not represented explicitly but instead are parameterized and tuned. Although there is some anticipation that new satellite programs may begin to address observational issues, and model resolution is improving, it is likely to be several decades before observations provide an adequate constraint on models.

We propose an approach for circumventing many of these issues that emphasizes constraints on the environment in which clouds occur, rather than on the clouds themselves. Doing so provides a robust and physically based framework for reducing uncertainty about future climate through the use of readily available observations. Variations in clouds and relative humidity (RH) are inherently linked in nature, and the approach here is motivated by the fact that models generally use RH to parameterize clouds (e.g., fig. S1). Tropospheric RH is proposed as a particularly useful diagnostic because it also is strongly linked to the dynamics of the overturning circulation, for which observable constraints are weak (*9*). Although it is known that biases exist in the simulated mean state of RH and that a modest relationship exists between its biases and model sensitivity (*10*), the reasons for the simulated variability of RH remain poorly understood, and constraints linking present-day variations to future climate have not yet been thoroughly explored. Whereas some model fields, such as clouds and the planetary energy budget, are generally tuned (*11*) to observations, the vertical structure of the troposphere is not. However, observations of RH through the full depth of the troposphere are readily available, including those from microwave observations from operational NOAA satellites and the AIRS (Atmospheric Infrared Sounder) instrument aboard NASA's Aqua satellite since July 2002. Along with balloon-borne measurements, they provide a solid baseline of both the mean state and variability across a range of time scales.

As shown here, the annual cycle provides a useful framework for exploring cloud-RH relationships, given its large variability relative to noise and observational uncertainty. Satellite retrievals from NASA's AIRS and CERES (Clouds and the Earth's Radiant Energy System) instruments are used to examine covariability between the seasonal extremes in RH and albedo, and hence clouds (Fig. 1). In the tropics and subtropics, the annual cycle of the Hadley circulation is intimately linked with that of the monsoon circulations, which lift moist air from the near-surface boundary layer in regions of tropical deep convection (e.g., north equatorial Africa, southeast Asia) into the upper troposphere, resulting in strong precipitation and drying of the ascending air. There it is advected meridionally to subside in the subtropics, where a deep zone of remarkably low RH exists across much of the depth of the free troposphere.

Seasonal increases in RH in the deep convective zones are thus dynamically coupled with

National Center for Atmospheric Research, Boulder, CO 80305, USA.

*To whom correspondence should be addressed. E-mail: fasullo@ucar.edu

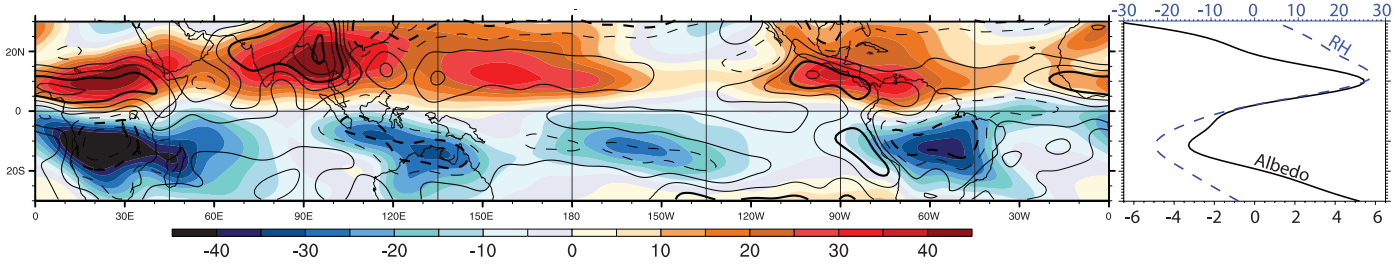


Fig. 1. Seasonal differences in observed RH at 500 hPa (color scale) and albedo (lines, 2% intervals, dashed for negative values) as estimated from the difference between June-to-August and December-to-February climatologies from 2002 to 2007, using NASA AIRS estimates of RH and CERES estimates of top-of-atmosphere radiative fluxes. Zonal mean differences are at right.

Downloaded from www.sciencemag.org on November 9, 2012

subtropical RH minima (*12*), and a marked spatial coherence between RH variations and albedo therefore exists, particularly from a zonal mean perspective. It is notable that RH at a single level (500 hPa) is strongly related with albedo, which is largely determined by clouds throughout the vertical extent of the troposphere. The coherence underscores the utility of RH in diagnosing clouds both locally and throughout the depth of the vertical column through its association with monsoon teleconnections.

In the annual average, the zonal mean structure of the dry zones exhibits a broad vertical extent and exceptional aridity (Fig. 2), but how well do models capture this observed feature? This question is explored using the CMIP3 model archive, a compilation of present-day simulations and future projections used in the most recent Intergovernmental Panel on Climate Change (IPCC) AR4 climate assessment (*1*). Comparison of the RH structure with the zonal height structure of projected future cloud loss (dashed lines in Fig. 2) further suggests direct relevance to cloud feedback. A canonical character of future projections under warming is the poleward expansion of the dry zones (arrows in Fig. 2) (*13*–*16*), although the lateral extent of projected RH and cloud reductions varies widely across models. It is evident that the regions of strongest future cloud loss also coincide with the poleward fringe of these dry zones (*17*). The strong spatial coherence between dry zone expansion and cloud loss suggests a direct role for these zones in influencing both the cloud feedback under warming and climate sensitivity. These strong relationships therefore motivate questions regarding model fidelity in resolving the dry zones and whether it exhibits a relationship to climate sensitivity.

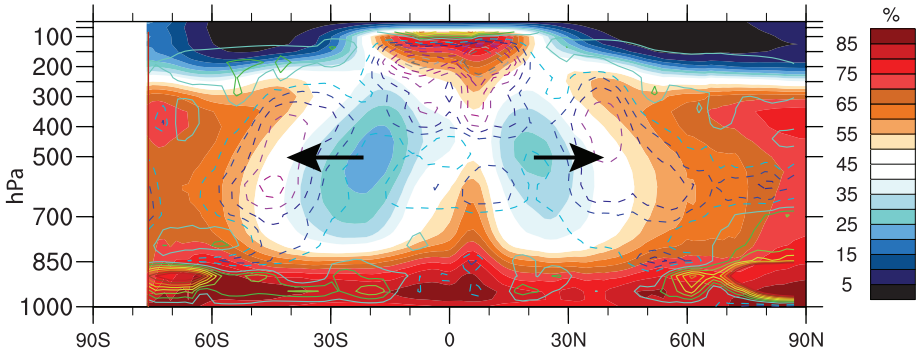


Fig. 2. The zonal height structure over ocean of observed climatological annual mean RH from AIRS (2002–2007) (color scale), with model mean projected changes in cloud amount from the CMIP3 model archive (contour lines, 0.5% intervals, dashed for cloud loss). The cloud loss in a warming climate at about 40°N/S coincides with broadening of the dry zones, as indicated by the arrows.

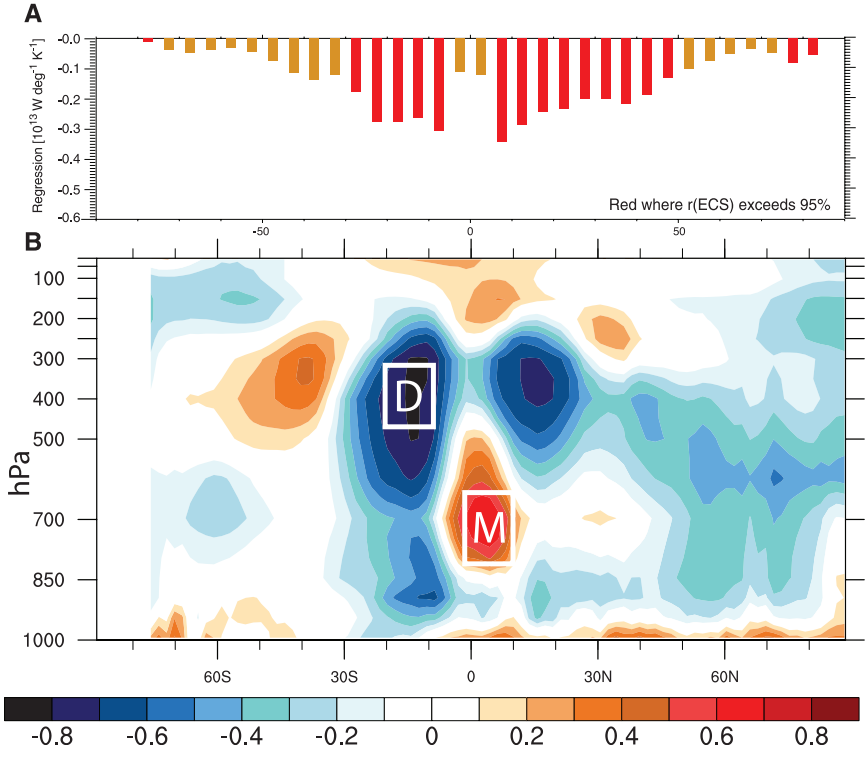


Fig. 3. (**A**) Median change in simulated top-of-atmosphere net shortwave flux as a function of latitude under 21st-century warming in CMIP3 SRES A1B projections. Red bars denote latitudes at which the change in net shortwave flux correlates with ECS at the 5% confidence limit. (**B**) Zonal mean vertical structure of the correlation between present-day (1980–1999) simulated RH over ocean from May to August in CMIP3 models and ECS. Boxed regions highlight peak positive and negative correlations in the moist (M) and dry (D) zones, respectively, where the statistical significance of the relationships exceeds the 1% confidence limit.

Indeed, the present-day RH climatology (Fig. 2) may be ideal for evaluating interactions among RH, clouds, and dynamics in models, as the season coincides with a substantial northward shift of the Hadley cell and a broadening and intensification of the southern subtropical dry zone, similar to that projected under climate change (*14*).

The vertical structure of the relationship in boreal summer between simulated present-day RH and ECS (Fig. 3) reveals robust and highly statistically significant negative correlations in the dry zones bounding a region of significant positive correlation in regions of monsoonal deep convection. Because the boreal summer encompasses the strong Asian monsoon, the spatial contrast between moist and dry zones is greater, whereas during the austral summer, deep convection is located closer to the equator and subsidence is relatively symmetric about the equator.

The structure (Fig. 3) suggests that the depth and intensity of the Hadley circulation and its embedded monsoon circulations links the dry and moist regions; indeed, a strong relationship with the circulation consistent with this interpretation is evident (fig. S2), with a zonal structure that suggests direct monsoonal connections (fig. S3). The correlations with RH are not only statistically significant but of sufficient magnitude to explain a considerable fraction of the variance in ECS across models, with highly significant negative (< -0.8) and positive (>0.5) correlations in the subsident dry and ascending moist domains, respectively. Similar relationships between present-day RH and sensitivity are evident in the newer, though currently incomplete, CMIP5 model archive (fig. S4). A strong spatial coherence between regions where RH and ECS are correlated is also evident in the atmospheric energy budget, with albedo trends (normalized by 21st-century warming) at latitudes

Downloaded from www.sciencemag.org on November 9, 2012

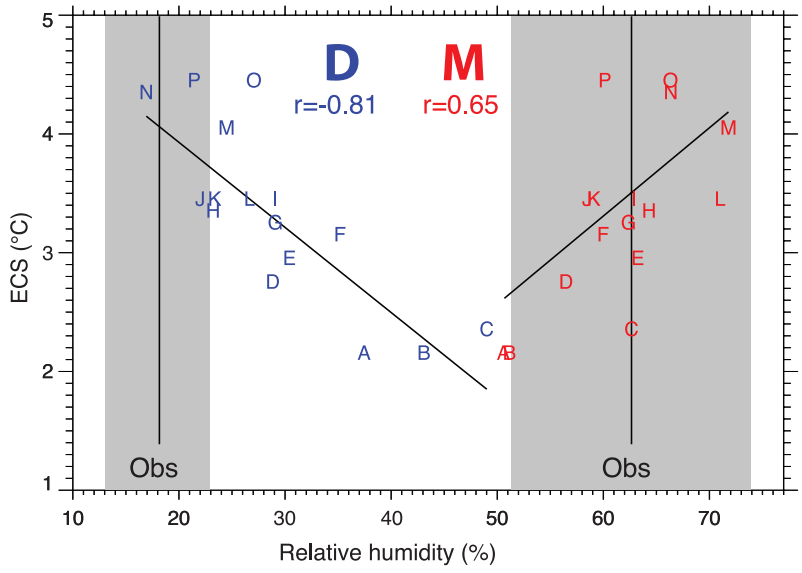


Fig. 4. Scatterplot of present-day simulated zonal mean RH over ocean from May to August in the dry (D) and moist (M) zones (Fig. 3) versus equilibrium climate sensitivity. Mean observed values (vertical black lines) and their range (gray) are based on values from AIRS retrievals and the MERRA and ERA Interim reanalyses. Letters denote individual model runs from coupled 20th-century runs (table S1). The correlations with ECS for each region are shown and indicated by the least-squares regression line. Observations and model values are based on climatologies from 1980 to 1999, except for AIRS, which is based on 2002–2007 data.

from 5° to 30°S and 5° to 50°N also exhibiting strong correlations with ECS (Fig. 3, upper panel).

Observed RH fields from satellite and reanalysis data sets can be used to evaluate the model distributions (Fig. 4) in the regions of peak positive and negative correlations in the moist ascending and dry descending domains (regions labeled M and D in Fig. 3, respectively). The strength of these relationships is robust to details in the choice of domain (fig. S5). The range of uncertainty in observations in Fig. 4 is gauged from the full range of climatologies from existing estimates of the mean state combined with the uncertainty arising from their temporal variability. The observations show that models are generally systematically too moist in the subsident domain, with only three models falling within the observed range. Although the correlation with climate sensitivity in the deep convective regime (M) is also strong, the range of uncertainty in observations is greater than for the dry zone; only a few models, generally of lower sensitivity, are identifiably biased. Because the meridional extent of subsident regimes greatly exceeds that of deep convective regimes (e.g., Fig. 2), their relative influence on the area-integrated energy budget is also disproportionately greater. The ability of observations to constrain the value of RH in the subsident domain is also greater, as there are fewer complicating factors involving clouds and precipitation.

These results suggest a systematic deficiency in the drying effect of either subsident circulations or spurious mixing of moister air into the region in low-sensitivity models (figs. S2 and S3) that directly relate to their projected changes in cloud amount and albedo. Although the lower-sensitivity models are clearly at odds with observations, extrapolating the consequences of these model biases to climate sensitivity is nontrivial, as the net feedback in terms of energy depends on the interaction of RH trends with the cloud field, whose vertical distribution in models is known to be biased (*18*). Thus, even if the RH response is well represented in models, its projection onto biased cloud fields may result in an incorrect estimation of the net cloud feedback. The results thus underscore the need to correctly represent the seasonally varying vertical structures of both RH and clouds in order to correctly project future climate.

Given the challenges involved in resolving the forced component of climate change in observed trends, process-based constraints on feedbacks such as the one proposed here are likely to be a key to reducing the uncertainty in future projections. The physically based perspective relates RH to ECS while explaining substantial variance across models, using fields in which observational uncertainty is small relative to model spread. In addition to providing a focus for improving models, the results strongly suggest that the more sensitive models perform better, and indeed the less sensitive models are not adequate in replicating vital aspects of today's climate. The correct simulation of the vertical structure of RH and clouds should be a prerequisite for developing confidence in projections for the future.

Major questions persist. These include the relative contributions of various cloud types to the overall cloud feedback (*19*) and the sources of biases in the vertical RH and cloud distributions, and these are the focus of ongoing research. In a broader context, improved representation of regions of strong subsidence, particularly at low latitudes, is of fundamental importance. Such an improvement is essential not only for correctly simulating climate sensitivity, but also for characterizing changes in climate extremes and related impacts. Their scrutiny is therefore likely to be beneficial in understanding the broad range of uncertainties that currently exist in our future climate.

References and Notes

1. G. A. Meehl *et al.*, in *Climate Change 2007: The Physical Science Basis. Contribution of Working Group I to the Fourth Assessment Report of the Intergovernmental Panel on Climate Change*, S. Solomon *et al.*, Eds. (Cambridge Univ. Press, Cambridge, 2007), pp. 747–845.
2. R. Knutti, G. C. Hegerl, *Nat. Geosci.* **1**, 735 (2008).
3. A. E. Dessler, *Science* **330**, 1523 (2010).
4. A. C. Clement, R. Burgman, J. R. Norris, *Science* **325**, 460 (2009).
5. J.-L. Dufresne, S. Bony, *J. Clim.* **21**, 5135 (2008).
6. B. J. Soden, I. M. Held, *J. Clim.* **19**, 3354 (2006).
7. K. E. Trenberth, J. T. Fasullo, *Geophys. Res. Lett.* **36**, L07706 (2009).
8. K. E. Trenberth, *Science* **296**, 2095a (2002).
9. S. Bony *et al.*, *Clim. Dyn.* **22**, 71 (2004).
10. E. M. Volodin, *Izv. Atmos. Ocean. Phys.* **44**, 288 (2008).
11. F. Bender, *Environ. Res. Lett.* **3**, 014001 (2008).
12. M. J. Rodwell, B. J. Hoskins, *J. Clim.* **14**, 3192 (2001).
13. I. Richter, S.-P. Xie, *J. Geophys. Res.* **113**, D24118 (2008).
14. D. J. Posselt, S. Van den Heever, G. Stephens, M. Igel, *J. Clim.* **25**, 557 (2012).
15. J. Lu, G. A. Vecchi, T. Reichler, *Geophys. Res. Lett.* **34**, L06805 (2007).
16. I. M. Held, B. J. Soden, *J. Clim.* **19**, 5686 (2006).
17. J. Scheff, D. Frierson, *J. Clim.* **25**, 4330 (2012).
18. M. H. Zhang *et al.*, *J. Geophys. Res.* **110**, D15S02 (2005).
19. M. D. Zelinka, S. A. Klein, D. L. Hartmann, *J. Clim.* **25**, 3736 (2012).

Acknowledgments: NCAR is sponsored by the National Science Foundation. This work was supported by NASA award NNX09AH89G. Support of the CMIP data sets is provided by the Office of Science, U.S. Department of Energy. We acknowledge the World Climate Research Programme's Working Group on Coupled Modelling, which is responsible for CMIP, and we thank the climate modeling groups for producing and making available their model output.

Supplementary Materials

www.sciencemag.org/cgi/content/full/338/6108/792/DC1
Figs. S1 to S5
Table S1

16 July 2012; accepted 28 September 2012
10.1126/science.1227465

Downloaded from www.sciencemag.org on November 9, 2012

Coagulation Factor X Activates Innate Immunity to Human Species C Adenovirus

Konstantin Doronin,[1]* Justin W. Flatt,[2]* Nelson C. Di Paolo,[1]* Reeti Khare,[1] Oleksandr Kalyuzhniy,[3]† Mauro Acchione,[4] John P. Sumida,[4] Umeharu Ohto,[5,6] Toshiyuki Shimizu,[5,6] Sachiko Akashi-Takamura,[7] Kensuke Miyake,[7,8] James W. MacDonald,[9] Theo K. Bammler,[9] Richard P. Beyer,[9] Frederico M. Farin,[9] Phoebe L. Stewart,[2] Dmitry M. Shayakhmetov[1]‡

Although coagulation factors play a role in host defense for "living fossils" such as horseshoe crabs, the role of the coagulation system in immunity in higher organisms remains unclear. We modeled the interface of human species C adenovirus (HAdv) interaction with coagulation factor X (FX) and introduced a mutation that abrogated formation of the HAdv-FX complex. In vivo genome-wide transcriptional profiling revealed that FX-binding–ablated virus failed to activate a distinct network of nuclear factor κB–dependent early-response genes that are activated by HAdv-FX complex downstream of TLR4/MyD88/TRIF/TRAF6 signaling. Our study implicates host factor "decoration" of the virus as a mechanism to trigger an innate immune sensor that responds to a misplacement of coagulation FX from the blood into intracellular macrophage compartments upon virus entry into the cell.

Upon infection with microbial and viral pathogens, specialized innate immune sensors recognize specific pathogen-associated chemical moieties [pathogen-associated molecular patterns (PAMPs)] (*1*). This triggers the activation of effector mechanisms aimed at restricting spread and facilitating pathogen elimination from the host. In the context of sterile inflammation, the innate immune receptors can also recognize host moieties released from damaged cells as an intrinsic danger signal [danger-associated molecular patterns (DAMPs)] (*2*) to initiate tissue repair. Often, innate immune recognition of pathogens leads to a severe inflammatory host response that may be solely responsible for the morbidity and mortality associated with the infection (*3*–*6*).

Human species C adenovirus (HAdv) induces potent innate immune and inflammatory responses (*7*). For immunocompromised individuals, HAdv infections can be lethal (*8*–*10*). Disseminated HAdv infections are frequently associated with liver and kidney failure and a high virus burden in the blood (*11*). When HAdv-based vectors are injected intravenously in preclinical and clinical gene therapy trials, they induce an acute inflammatory response that may lead to morbidity and mortality (*12*, *13*). The molecular basis for innate immune activation by HAdv remains poorly characterized. While in the blood, species C HAdv2 and HAdv5 bind coagulation factor X (FX) with high affinity (*14*, *15*). Because coagulation factor activation may trigger systemic inflammation, we hypothesized that FX

[1]Department of Medicine, University of Washington, Seattle, WA 98195, USA. [2]Department of Pharmacology and Cleveland Center for Membrane and Structural Biology, Case Western Reserve University, Cleveland, OH 44106, USA. [3]Department of Biochemistry, University of Washington, Seattle, WA 98195, USA. [4]Department of Medicinal Chemistry, University of Washington, Seattle, WA 98195, USA. [5]Graduate School of Pharmaceutical Sciences, University of Tokyo, Hongo, Bunkyo-ku, Tokyo 113-0033, Japan. [6]RIKEN SPring-8 Center, Kouto 1-1-1, Sayo, Hyogo 679-5148, Japan. [7]Division of Innate Immunity, Department of Microbiology and Immunology, University of Tokyo, 4-6-1 Shirokanedai, Minatoku, Tokyo 108-8639, Japan. [8]Laboratory of Innate Immunity, Center for Experimental Medicine and Systems Biology, Institute of Medical Science, University of Tokyo, 4-6-1 Shirokanedai, Minatoku, Tokyo 108-8639, Japan. [9]Functional Genomics and Proteomics Core Facility, Department of Environmental and Occupational Health Sciences, University of Washington, Seattle, WA 98195, USA.

*These authors contributed equally to this work.
†Present address: Neutralizing Antibody Center, International AIDS Vaccine Initiative, Scripps Research Institute, La Jolla, CA 92037, USA.
‡To whom correspondence should be addressed. E-mail: dshax@uw.edu

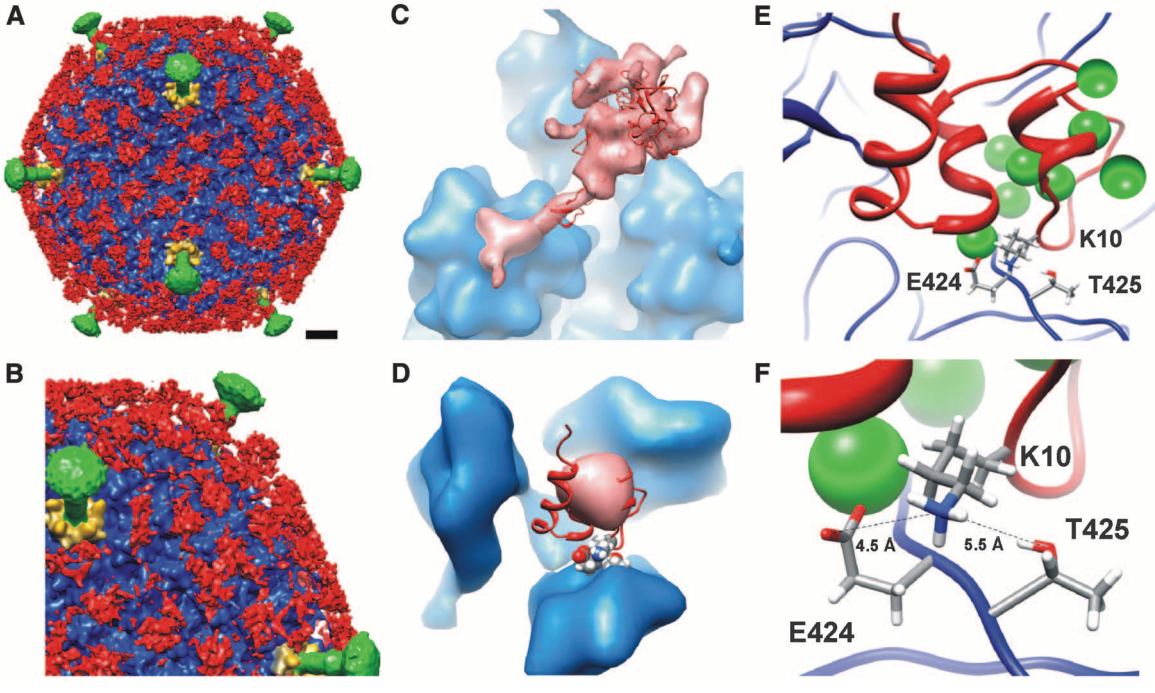


Fig. 1. Cryo-EM structure of the FX-HAdv5 complex and simulation of the FX-hexon interface using MDFF. (**A**) The cryo-EM structure of HAdv5 in complex with FX. The density is shown with the hexon capsid in blue, penton base in gold, fiber in green, and FX in red. Scale bar, 100 Å. (**B**) An enlarged view of the FX-HAdv5 complex showing the network of the FX density above the hexon capsid. (**C**) The best rigid-body fit orientation of the zymogenic FX model (red ribbon) within FX cryo-EM density (transparent pink). This FX density is selected from above a hexon near the icosahedral threefold axis of the capsid. (**D**) Coordinates from a frame in the MDFF simulation that show hexon residues E424 and T425 surround residue K10 of the FX-GLA domain. The side chains of these three residues are shown in space-filling representation and colored by element. (**E**) FX-GLA domain and associated Ca_2^+ ions (green) in the central depression of the hexon trimer. (**F**) Residue K10 in the FX-GLA domain is in close enough proximity to E424 and T425 of hexon to engage in electrostatic interactions.

Downloaded from www.sciencemag.org on November 9, 2012

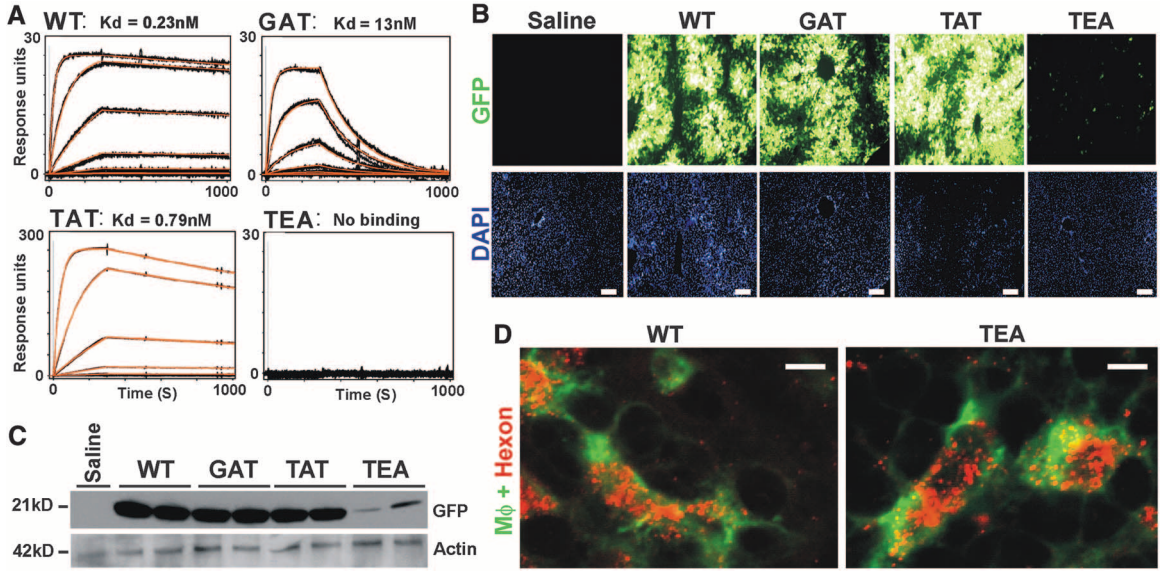


Fig. 2. A single amino acid substitution (T425A) abrogates FX biding to HAdv5. (**A**) Kinetic response data and dissociation constant (K_d) for FX binding to the indicated mutant viruses obtained by using surface plasmon resonance analysis (Biacore, GE Healthcare Biosciences, Pittsburgh, PA). Black indicates experimentally obtained data. Orange indicates global fits of these data to 1:1 single-site interaction model. Representative data obtained from four independent experiments are shown. (**B** to **D**) In vivo analysis of hexon-mutated viruses. (B) Histological analysis of virus-encoded GFP expression in mouse hepatocytes 48 hours after intravenous infection of mice with WT HAdv5 (WT) or mutated viruses. Representative fields are shown (n = 5 biological replicates). GFP expression is observed as green fluorescence on fixed liver sections. Corresponding fields in 4′,6-diamidino-2-phenylindole channel (blue, nuclei-specific staining) are shown. Scale bar, 100 μm. (C) Western blotting analysis of GFP expression in the livers of mice shown in (B). The biological duplicate samples for each virus are shown. (D) Colocalization of virus particles (red) with splenic CD169$^+$ and MARCO$^+$ marginal zone macrophages (green) observed 1 hour after infection for indicated viruses analyzed by means of confocal microscopy. Scale bar, 10 μm. Representative fields are shown. n = 5 biological replicates.

binding to HAdv may trigger virus recognition by the innate immune system and activation of an antiviral inflammatory response. As a first step in testing this hypothesis, we analyzed the interaction interface between FX and HAdv by determining a high-resolution cryogenic electron microscopy (cryo-EM) structure followed by molecular dynamics flexible fitting (MDFF) simulations (*16*).

In the cryo-EM structure, FX density protrudes from the top of each hexon in the HAdv5 capsid (Fig. 1, A to C, and movie S1). FX interacts with the capsid by attaching to threefold symmetric central depressions in each hexon trimer, as seen in earlier moderate resolution cryo-EM structures (*14*, *15*). Atomic models for hexon and FX were docked into cryo-EM density (9 Å resolution for the capsid and 11 Å resolution for the capsid plus FX). MDFF simulations revealed an electrostatic interaction between FX–γ-carboxyglutamic acid (GLA) domain residue K10 and HAdv5 hexon residues E424 and T425 (Fig. 1, D to F; table S1; and movie S2). [Single-letter abbreviations for the amino acid residues are as follows: A, Ala; C, Cys; D, Asp; E, Glu; F, Phe; G, Gly; H, His; I, Ile; K, Lys; L, Leu; M, Met; N, Asn; P, Pro; Q, Gln; R, Arg; S, Ser; T, Thr; V, Val; W, Trp; and Y, Tyr.] To test the robustness of the MDFF simulated protein-protein interface, we performed a series of simulations with the FX starting orientation rotated by ±10 or ±20° about the threefold molecular axis of hexon (figs. S1 and S2 and table S1). Despite these adjustments, the FX-GLA/HAdv5 hexon interface snaps back to form the same packing arrangement.

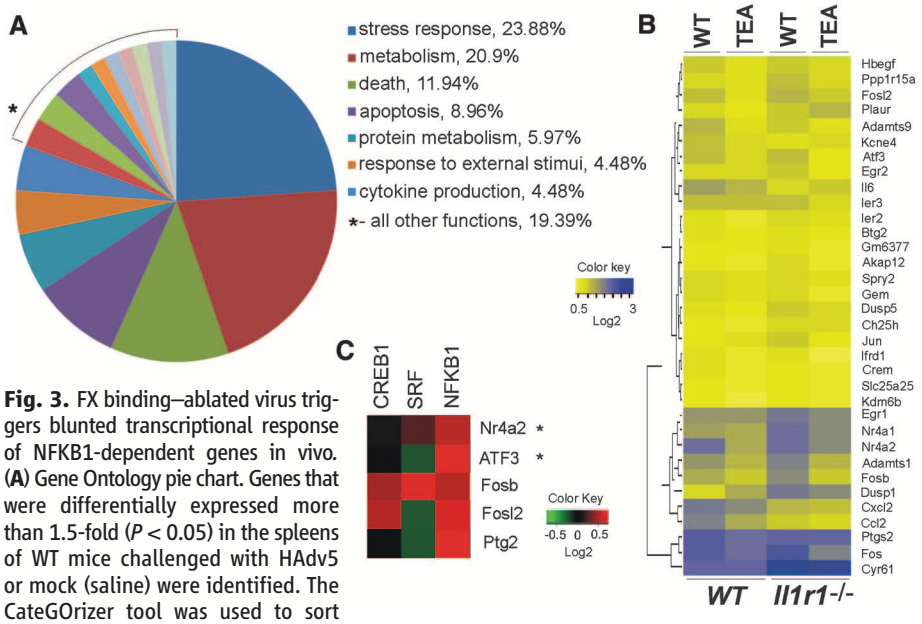


Fig. 3. FX binding–ablated virus triggers blunted transcriptional response of NFKB1-dependent genes in vivo. (**A**) Gene Ontology pie chart. Genes that were differentially expressed more than 1.5-fold ($P < 0.05$) in the spleens of WT mice challenged with HAdv5 or mock (saline) were identified. The CateGOrizer tool was used to sort these genes in Gene Ontology categories and determine percentages of differentially expressed genes for each category. (**B**) Heatmap representation of the averaged gene expression levels for 34-gene set (coactivated in WT and *Il1r1*$^{-/-}$ mice with $P < 0.0002$) when WT and *Il1r1*$^{-/-}$ mice were infected with either HAdv5 or TEA mutant virus. In each experimental group, n = 3 biological replicates. The yellow and blue color legend shows $\log_2$-transformed fold changes. Heatmap was generated by using the Bioconductor gplots package (Seattle, WA). (**C**) z-score map of the transcription factor binding site frequencies in proximal promoters of indicated genes was generated by means of P-scan from the analysis of binding sites for 116 transcription factors (Transfac database). The five-gene set represents a subset of genes from (B) that are the most differentially inducted by HAdv5 and TEA mutant virus (1.5-fold cut off). Nr4a2, $^*P = 9.61 \times 10^{-7}$; ATF3, $^*P = 6.77 \times 10^{-6}$. The green and red color legend shows $\log_2$-transformed fold z-score changes.

Downloaded from www.sciencemag.org on November 9, 2012

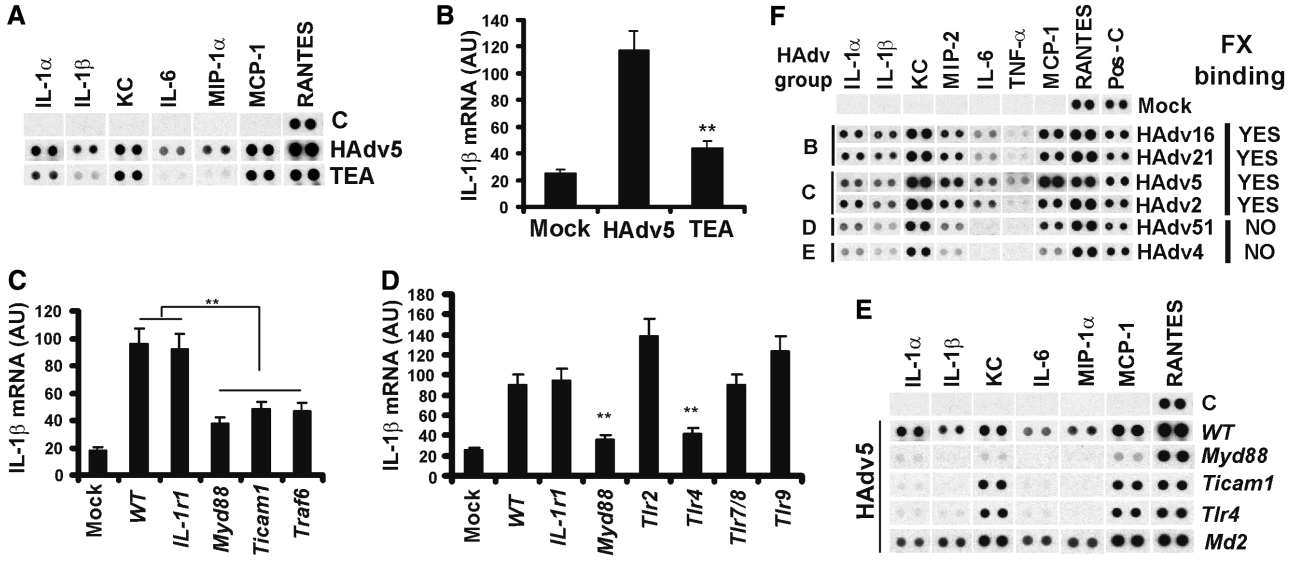


Fig. 4. HAdv5 binding to FX induces NFκ-B1–dependent inflammatory cytokines and chemokines downstream of the TLR4-TRIF/MyD88-TRAF6 signaling axis in vivo. (**A**) Mouse cytokine array panel showing differences in inflammatory cytokines and chemokines in the spleens of WT mice 1 hour after infection with HAdv5 or TEA mutant, determined by means of proteome profiler antibody array. Representative blot from four independent experiments is shown. C, mouse was challenged with saline. (**B**) mRNA expression of IL-1β in the spleen of WT mice 30 min after challenge with indicated viruses. Graphs show mean ± SD, $n = 4$ biological replicates, $^{**}P < 0.01$. AU, arbitrary units reflecting IL-1β to glyceraldehyde-3-phosphate dehydrogenase (GAPDH) mRNA ratios. (**C** and **D**) mRNA expression of IL-1β in the spleen of WT mice and mice deficient for indicated genes 30 min after challenge with HAdv5. Graphs show mean ± SD, $n = 4$ biological replicates, $^{**}P < 0.01$. AU, arbitrary units reflecting IL-1β to GAPDH mRNA ratios. (**E**) Mouse cytokine array panel showing differences in inflammatory cytokines and chemokines in the spleens of WT and *Myd88*$^{-/-}$, *Ticam1*$^{-/-}$, *Tlr4*$^{-/-}$, and *Md2*$^{-/-}$ mice 1 hour after challenge with HAdv5, determined by means of proteome profiler antibody array. Representative blot from four independent experiments is shown. C, mouse was challenged with saline. (**F**) Mouse cytokine array panel showing differences in inflammatory cytokines and chemokines in the spleens of WT mice 1 hour after challenge with WT human adenoviruses of indicated species, determined by means of proteome profiler antibody array. Representative blot from four independent experiments is shown. C, mouse was mock infected with saline.

To test whether glutamic acid E424 and threonine T425 are essential for formation of the FX-HAdv5 complex, we introduced single–amino acid substitutions in this region of the hexon by substituting the wild-type (WT) amino acid sequence TET at positions 423 to 425 for GAT, TAT, or TEA (fig. S3A). Surface plasmon resonance analysis revealed that the affinity of GAT and TAT mutants for FX remained in the low nanomolar range, whereas TEA mutant was unable to bind FX (Fig. 2A). The in vitro infection of CHO-K1 cells (which can only be infected in the presence of FX) showed that unlike all other viruses, the TEA mutant failed to infect these cells in the presence of FX (fig. S3B). In contrast, all of the mutant viruses were able to infect susceptible lung carcinoma A549 cells with equal efficacy (fig. S3). Because FX-binding–ablation abrogates HAdv5 infection of hepatocytes in vivo (*14*, *15*, *17*), we injected mice intravenously with virus mutants expressing green fluorescent protein (GFP) and analyzed GFP expression 48 hours later. This analysis confirmed that all the mutants, except for TEA, infected hepatocytes efficiently (Fig. 2, B and C, and fig. S3F). Analysis of virus interaction with tissue macrophages showed that both liver and spleen macrophages trapped all of the viruses with comparable efficacy (Fig. 2D and figs. S4 to S6).

Because tissue macrophages are the principal inducers of inflammation in response to adenovirus (*18*, *19*), we next compared the innate immune response to TEA virus versus control WT HAdv5. The analysis of transcripts for >28,000 genes revealed that expression of 519 genes was changed more than 1.5-fold ($P < 0.001$) in the spleen of WT mice 30 min after HAdv injection. Gene ontology analysis with the CateGOrizer tool (Iowa State University, Ames, IA) (materials and methods are available as supplementary materials on *Science* Online) showed that over 60% of genes transcriptionally up-regulated in response to HAdv5 were divided between four categories: stress response (23.88%), metabolism (20.90%), death pathways (11.94%), and apoptosis (8.96%) (Fig. 3A). To define the signaling pathway (or pathways) specifically activated by HAdv sensors, we identified only those genes that were coactivated after HAdv injection in both WT and *Il1r1*$^{-/-}$ mice. This is because signaling downstream of HAdv sensors occurs independently of interleukin-1 receptor 1 (IL-1R1), and IL-1R1 triggers feed-forward amplification loops (*19*). We found that after applying a strict cut off criteria ($P < 0.0002$), there were 34 genes coactivated after HAdv injection in both WT and *Il1r1*$^{-/-}$ mice (table S2). We next injected WT and *Il1r1*$^{-/-}$ mice with TEA mutant virus and compared the transcriptional signatures induced by HAdv5 and TEA on this 34-coactivated-gene set. This analysis showed that there were numerous genes differentially activated by HAdv and TEA viruses (Fig. 3B and table S3). For *Nr4a2* ($P = 9.61 \times 10^{-7}$), *Atf3* ($P = 6.77 \times 10^{-6}$), *Fosb*, *Fosl2*, and *Ptgs2* genes, differential activation ranged between 2.2- and 5.8-fold. The P-scan analysis also demonstrated that there was enrichment for cyclic adenosine monophosphate (cAMP) response element–binding protein 1 (CREB1), nuclear factor–κB 1 (NFKB1), and serum response factor (SRF) transcription factor binding sites within the promoters of the 34-gene set (fig. S7). However, only NFKB1 transcription factor binding sites were overrepresented in proximal promoters of the gene set differentially activated by HAdv and TEA (Fig. 3C). Using Pathway Analysis software (Ingenuity Systems, Redwood City, CA), we further confirmed that NFKB1, CREB1, and SRF are at the center of a signaling network that responds to HAdv entry into macrophages in vivo (figs. S8 and S9).

Because nuclear factor–κB (NF-κB) is a transcription factor that activates numerous early response genes, including genes encoding for inflammatory cytokines and chemokines, we next analyzed whether WT HAdv5 and TEA viruses trigger differential expression of proteins associated with innate immunity. Indeed, TEA mutant failed to activate several NF-κB–dependent cytokines and chemokines, including IL-1β, IL-6, and MIP-1α (macrophage inflammatory protein-1α) (Fig. 4A). A ribonuclease (RNase) protection assay further confirmed that TEA virus failed to activate IL-1β transcription in vivo in WT mice

Downloaded from www.sciencemag.org on November 9, 2012

(Fig. 4B and fig. S10A). Deconvolution of the signaling pathway that leads to NF-κB activation in gene-deficient mice revealed that IL-1β transcriptional activation required TRAF6, MyD88, and TRIF (encoded by *Ticam1*) (Fig. 4C and fig. S10B). Because MyD88 and TRIF are the signaling adapters for Toll-like receptors (TLRs), we analyzed IL-1β expression in response to HAdv challenge in mice deficient in TLR2, -4, -7 and -8, or -9. This analysis showed that transcriptional activation of IL-1β was impaired only in *Tlr4*$^{-/-}$ mice (Fig. 4D and fig. S10C). Analysis of inflammatory cytokines and chemokines in *Tlr4*$^{-/-}$, *Myd88*$^{-/-}$, and *Ticam1*$^{-/-}$ mice confirmed reduced amounts of cytokines and chemokines that depend on NF-κB (Fig. 4E). Collectively, these data demonstrate that a full-scale inflammatory response to HAdv requires TLR4/TRAF6/NF-κB signaling, and FX binding–ablated TEA virus failed to activate this pathway in vivo. In vitro infection of primary macrophages from WT and *Tlr4*$^{-/-}$ mice with WT HAdv5 confirmed that full cytokine and chemokine activation is dependent on the presence of FX (figs. S11 to S13). Surface plasmon resonance analysis revealed differential binding of the HAdv5-FX complex to human and mouse TLR4/MD2 complexes that were immobilized on a sensor chip in vitro (fig. S14). The impeded cytokine and chemokine activation in *Tlr4*$^{-/-}$ mice resulted in significantly lower recruitment and retention of polymorphonuclear leukocytes (PMNs) in the splenic marginal zone as compared with that of WT mice (figs. S15 and S16A). Furthermore, WT mice or mice deficient in inflammasome components Caspase-1 and ASC (encoded by *Pycard*) (*20*) effectively cleared the WT HAdv5 virus from the spleen and liver, whereas *Tlr4*$^{-/-}$ mice failed to clear the virus. The failure to clear the virus allowed for the extensive virus replication, and the amount of viral genomes in the liver 24 hours after the infection in *Tlr4*$^{-/-}$ mice was two orders of magnitude higher, as compared with that of WT mice (fig. S16, B to D).

We next analyzed activation of a panel of cytokines and chemokines in response to a number of WT HAdv species and found that those viruses that bind FX activated a broader spectrum of cytokines and chemokines as compared with those of WT HAdv species that do not bind FX (*14*) (Fig. 4F). Analysis of PMN distribution in the spleen showed lack of retention of PMNs in the splenic marginal zone after infection of mice with HAdv4 and HAdv51 (do not bind FX) and efficient retention of PMNs in marginal zone after infection with HAdv2 and HAdv5 (bind FX) (fig. S17).

Thus, our results suggest that FX, a noninflammatory humoral factor of the coagulation cascade, binds to the surface of the virus and becomes a pathogen-associated molecular pattern that, upon viral entry into the cell, triggers activation of innate immunity via the TLR/NF-κB pathway (fig. S18). Direct binding of coagulation factors FVII and FX was recently reported for human herpes virus HSV-1 (*21*). The data presented here provide evidence for an evolutionary conserved link between the coagulation system and innate immunity in higher organisms, in which the coagulation system functions to facilitate direct recognition of a pathogen and activation of innate immune defenses.

References and Notes

1. C. A. Janeway Jr., R. Medzhitov, *Annu. Rev. Immunol.* **20**, 197 (2002).
2. P. Matzinger, *Science* **296**, 301 (2002).
3. J. C. Kash *et al.*, *Nature* **443**, 578 (2006).
4. Y. Imai *et al.*, *Nature* **436**, 112 (2005).
5. J. Chen, K. Subbarao, *Annu. Rev. Immunol.* **25**, 443 (2007).
6. H. T. Wen, Y. Lei, S. Y. Eun, J. P. Y. Ting, *J. Exp. Med.* **207**, 2943 (2010).
7. C. E. Thomas, G. Schiedner, S. Kochanek, M. G. Castro, P. R. Löwenstein, *Proc. Natl. Acad. Sci. U.S.A.* **97**, 7482 (2000).
8. H. Ardehali, K. Volmar, C. Roberts, M. Forman, L. C. Becker, *Transplantation* **71**, 998 (2001).
9. A. M. Leen, C. M. Rooney, *Br. J. Haematol.* **128**, 135 (2005).
10. Y. J. Kim, M. Boeckh, J. A. Englund, *Semin. Respir. Crit. Care Med.* **28**, 222 (2007).
11. J. P. Lynch 3rd, M. Fishbein, M. Echavarria, *Semin. Respir. Crit. Care Med.* **32**, 494 (2011).
12. N. Morral *et al.*, *Hum. Gene Ther.* **13**, 143 (2002).
13. S. E. Raper *et al.*, *Mol. Genet. Metab.* **80**, 148 (2003).
14. O. Kalyuzhniy *et al.*, *Proc. Natl. Acad. Sci. U.S.A.* **105**, 5483 (2008).
15. S. N. Waddington *et al.*, *Cell* **132**, 397 (2008).
16. L. G. Trabuco, E. Villa, K. Mitra, J. Frank, K. Schulten, *Structure* **16**, 673 (2008).
17. R. Alba *et al.*, *Blood* **114**, 965 (2009).
18. Y. Zhang *et al.*, *Mol. Ther.* **3**, 697 (2001).
19. N. C. Di Paolo *et al.*, *Immunity* **31**, 110 (2009).
20. D. A. Muruve *et al.*, *Nature* **452**, 103 (2008).
21. J. R. Livingston, M. R. Sutherland, H. M. Friedman, E. L. G. Pryzdial, *Biochem. J.* **393**, 529 (2006).

Acknowledgments: We thank S. Akira (Osaka University, Japan) for providing mice deficient in MyD88, MD2, TLR4, TLR7/8, and TLR9; J.-I. Inoue (University of Tokyo, Japan) for TRAF6-deficient mice; R.A. Flavell (Yale University, CT) for Caspase-1–deficient mice; and V. Dixit (Roche, CA) for ASC-deficient mice. We acknowledge the assistance of D. R. Williams during cryo-EM data acquisition. The cryo-EM data was collected while J.W.F. and P.L.S. were at Vanderbilt University. We thank M. D. Hollenberg (University of Calgary, Canada), A. Aderem, and D. Zak (SeattleBioMed, USA) for helpful discussion and L. K. Baldwin for manuscript editing. This study was supported by U.S. NIH grants AI065429 and CA141439 to D.M.S., the University of Washington National Institute of Environmental Health Sciences–sponsored Center for Ecogenetics & Environmental Health (P30ES07033), and Center for Intracellular Delivery of Biologics Analytical Biopharmacy Core facility, which is funded by the Washington State Life Sciences Discovery Fund. D.M.S. and P.L.S. designed the research; K.D., J.W.F., N.C.D.P., R.K., M.A., J.P.S., and O.K. conducted experiments and collected and analyzed the data; U.O, T.S., S.A.-T., and K.M. expressed, purified, and provided critical reagents; J.W.M., T.K.B., R.P.B., and F.M.F. collected and processed all the microarray data; and P.S. and D.S. wrote the paper. The data are tabulated in the main paper and supplementary materials. The cryo-EM structure has been deposited in the Electron Microscopy Data Bank with accession no. EMD-5494. The microarray data have been submitted in Minimum Information About a Microarray Experiment (MIAME)–compliant format to the Gene Expression Omnibus database (accession no. GSE36078).

Supplementary Materials

www.sciencemag.org/cgi/content/full/science.1226625/DC1
Materials and Methods
Figs. S1 to S18
Tables S1 to S3
References (*22*–*29*)
Movies S1 and S2

27 June 2012; accepted 11 September 2012
Published online 27 September 2012;
10.1126/science.1226625

Germ Cell Migration Across Sertoli Cell Tight Junctions

Benjamin E. Smith[1] and Robert E. Braun[1,2]*

The blood-testis barrier includes strands of tight junctions between somatic Sertoli cells that restricts solutes from crossing the paracellular space, creating a microenvironment within seminiferous tubules and providing immune privilege to meiotic and postmeiotic cells. Large cysts of germ cells transit the Sertoli cell tight junctions (SCTJs) without compromising their integrity. We used confocal microscopy to visualize SCTJ components during germ cell cyst migration across the SCTJs. Cysts become enclosed within a network of transient compartments fully bounded by old and new tight junctions. Dissolution of the old tight junctions releases the germ cells into the adluminal compartment, thus completing transit across the blood-testis barrier. Claudin 3, a tight junction protein, is transiently incorporated into new tight junctions and then replaced by claudin 11.

Tight junctions are specialized anchoring connections between cells and are composed of several integral and peripheral membrane proteins (*1*, *2*). The elaborate fibrils formed by the tight junction components play a critical role in multicellular organisms by sealing off the space between neighboring epithelial cells, thereby partitioning compartments within an organism (*3*).

Spermatogenesis takes place within seminiferous tubules of the testis. Extensive tight junctions between somatic Sertoli cells, referred to ultrastructurally as basal ectoplasmic specializations, create one of the body's tightest epithelial barriers and in doing so create separate functional compartments for diploid spermatogonia in the basal compartment and differentiating spermatocytes and haploid spermatids in the adluminal compartment (Fig. 1A). To prevent autoimmunity and maintain a conducive microenvironment for differentiation, differentiating germ cells must cross this barrier without disrupting its functional integrity (*4*). To compound the challenge, germ cells are contained

[1]Department of Genome Sciences, University of Washington School of Medicine, Seattle, WA 98195, USA. [2]The Jackson Laboratory, 600 Main Street, Bar Harbor, ME 04609, USA.

*To whom correspondence should be addressed. E-mail: bob.braun@jax.org

Downloaded from www.sciencemag.org on November 9, 2012

within cysts, which can be composed of hundreds of cells connected by intercellular bridges formed as a result of incomplete cytokinesis during transit amplification of differentiating spermatogonia (*5*). The mechanism by which large syncytial chains of preleptotene spermatocytes move from the basal to the adluminal compartment without causing damage to the SCTJs is unknown.

To visualize the three-dimensional (3D) organization of the SCTJs, we stained whole seminiferous tubules dissected from adult mice for claudin 11 (CLDN11) and F-actin, both of which are known constituents of the SCTJs (*6*, *7*). The tubules were then imaged by confocal microscopy from the basal surface into the tubule in ~200 optical sections, which were rendered into a single image with a depth of approximately 15 μm (Fig. 1A).

First, we imaged regions of the seminiferous tubules where no germ cells were migrating across the SCTJs. CLDN11 and bundles of filamentous-actin, labeled with phalloidin, both marked the SCTJs. In these regions, CLDN11 circumscribed each Sertoli cell near the basement membrane (Fig. 1, B and C) and delineated the basal and adluminal compartments by passing between the spermatogonia and pachytene spermatocytes (fig. S1, A and B).

We then imaged regions of the seminiferous tubules where preleptotene spermatocytes were migrating across the SCTJs, using spermiation (release of spermatids into the lumen) as a marker for this transit (*8*). During preleptotene spermatocyte translocation across the SCTJs, CLDN11 tight junctions were observed on both the basal and apical sides of the migrating spermatocytes (Fig. 2, A and B). Additionally, we observed vertical cross-linked connections between the basal and apical tight junction fibrils, enclosing the spermatocytes in small compartments. These vertical tight junctions were found only at the tricellular junctions of three Sertoli cells (Fig. 2A, arrowhead), possibly suggesting a role of these specialized tight junction structures in the formation of the compartments (*9*). These tight junction–demarcated compartments were observed only enclosing leptotene spermatocytes. Therefore, as initially suggested more than three decades ago (*10*), leptotene spermatocytes are temporarily enclosed in an intermediate compartment (Fig. 2B).

Because leptotene spermatocytes are syncytial, forming long chains of cells joined by cytoplasmic bridges (*5*), and the compartments we observed generally contained only two or three leptotene spermatocytes, we hypothesized that the cytoplasmic bridges must pass between the enclosed compartments at the regions of the tricellular junctions. To image cysts of leptotene spermatocytes in the context of the SCTJ compartments, seminiferous tubules were stained with both CLDN11 and testis-expressed gene 14 (TEX14), which localizes to a portion of each cytoplasmic bridge (*11*). As expected, TEX14 was observed between cells within individual compartments and, as hypothesized, we observed intercellular bridges, marked by TEX14, within tricellular junctions (Fig. 2A, arrowhead), suggesting that cells within a common syncytia span compartments (Fig. 2B). In no cases did we observe costaining of TEX14 with either the apical (old) or basal (new) tight junction fibrils, suggesting that intercellular bridges connecting germ cells within a cyst pass between the smaller compartments, linking them to ultimately comprise a single large network of compartments enclosing the entire cyst.

Our observation that migrating spermatocytes are bounded both apically and basally by SCTJs suggests that the basal surface of the Sertoli cells form new Sertoli-Sertoli cell contacts to accommodate the formation of the new tight junctions. To visualize the 3D structure of the Sertoli cells, we generated mice that express enhanced green

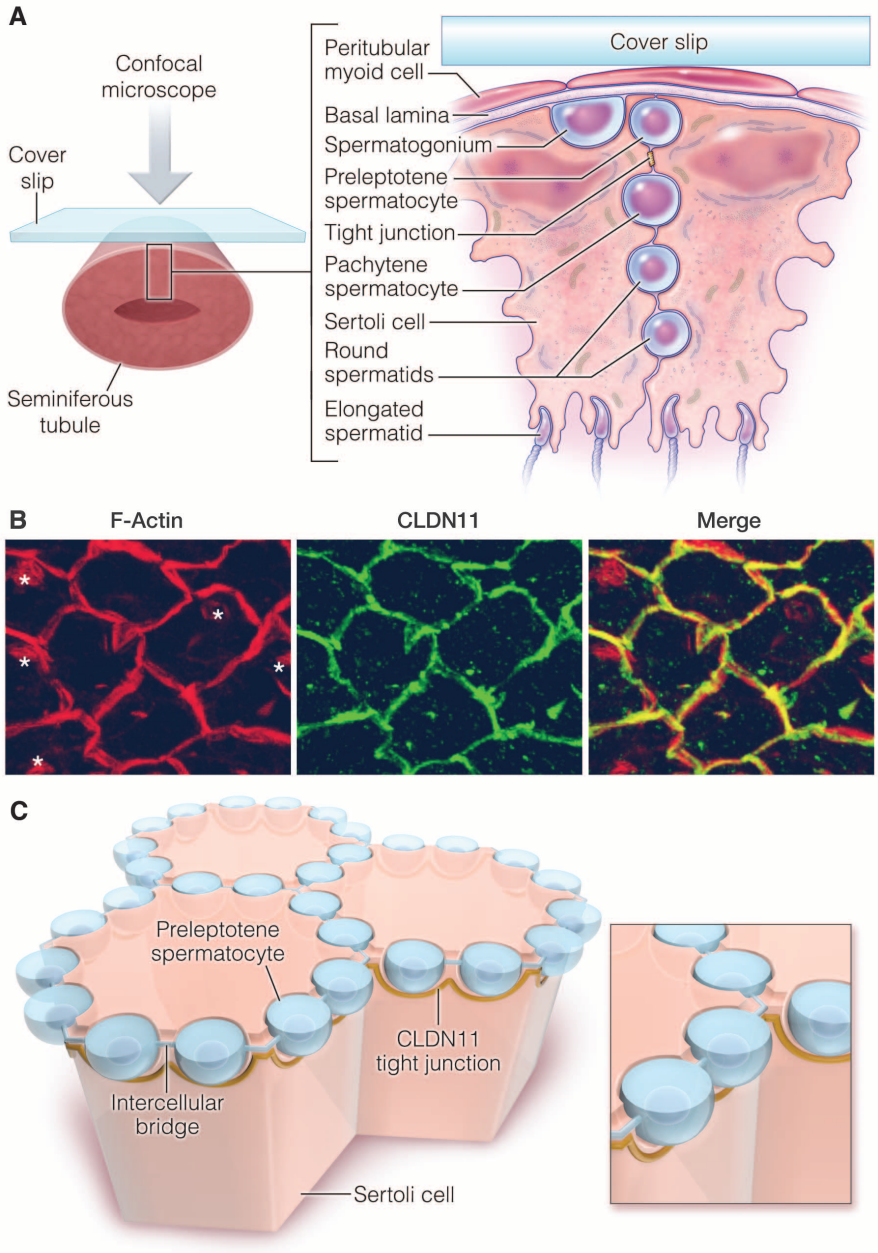


Fig. 1. Imaging tight junction fibrils between Sertoli cells. (**A**) The schematic on the left illustrates the orientation of the confocal microscope with respect to the seminiferous tubule. The area imaged is demarcated with a rectangle. The schematic on the right depicts a region of the epithelium before preleptotene migration, showing germ cells at different steps of differentiation along with supporting Sertoli and peritubular myoid cells. (**B**) Confocal image of SCTJs visualized during stage IV, a stage in which germ cells are not transiting the SCTJs, using two different markers, F-actin and CLDN11. Bundles of F-actin, labeled with phalloidin, were detected at both the SCTJs and the apical ectoplasmic specializations surrounding the heads of elongating spermatids (*). CLDN11 localized to just the SCTJs. The merged image shows that both markers label the SCTJs. (**C**) An artist's rendition of the confocal images shown in (B), fig. S2, and movie S1, illustrating three Sertoli cells, the CLDN11-containing tight junctions circumscribing each Sertoli cell, and chains of preleptotene spermatocytes connected by intercellular bridges.

Downloaded from www.sciencemag.org on November 9, 2012

fluorescent protein (EGFP) only within the cytoplasm of Sertoli cells. The seminiferous tubules from the resulting mice were then stained for EGFP to visualize the Sertoli cell body, and CLDN11 and F-actin, to visualize the SCTJs. Before leptotene migration across the SCTJs, we observed the basal surfaces of Sertoli cells adhered to the basement membrane, except where spermatogonia were present (fig. S2A). To accommodate spermatogonia that were also bound to the basement membrane, the basal surfaces of neighboring Sertoli cells were displaced away from the

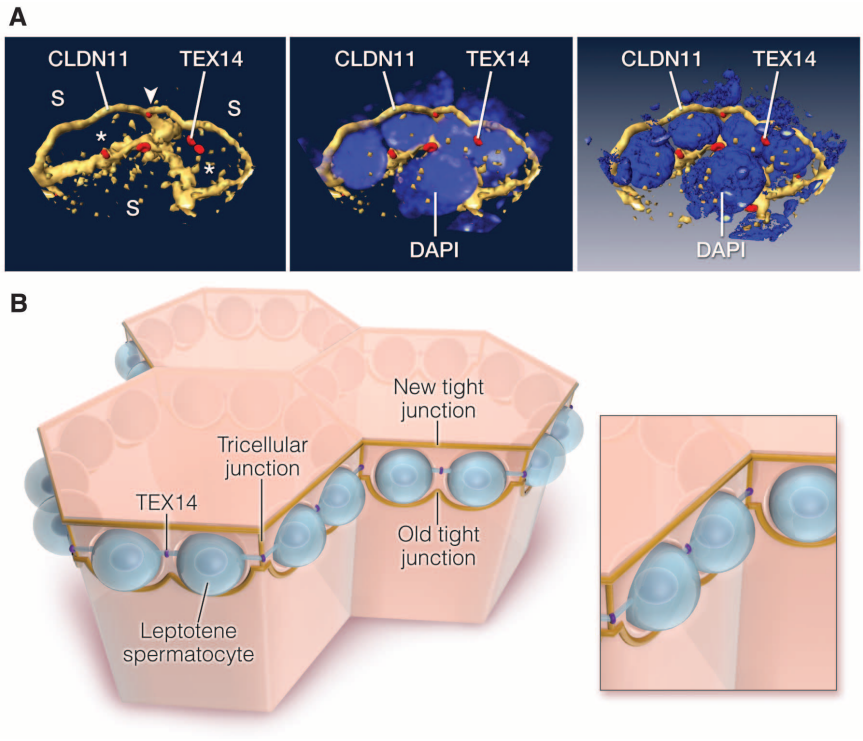


Fig. 2. Formation of transient compartments bounded by tight junctions during migration of preleptotene spermatocytes across Sertoli cell tight junctions. (**A**) During germ cell migration across the SCTJs, stage IX of the seminiferous epithelium cycle, the leptotene spermatocytes are enclosed within compartments (*) bounded by SCTJs. A double-layer tight junction that sandwiches the leptotene spermatocytes forms the compartments. The arrowhead shows connections between tight junction layers formed at the tricellular junction of three Sertoli cells (S). TEX14 (red) marks the cytoplasmic bridges between the leptotene spermatocytes. TEX14 localization to the tricellular junctions (arrowhead) reveals that the cytoplasmic bridges between spermatocytes pass through the tricellular junctions. (**B**) A schematic of (A) illustrating germ cell migration across the SCTJs showing that the leptotene spermatocytes are transiently enclosed within a network of compartments bounded by tight junctions both apically and basally.

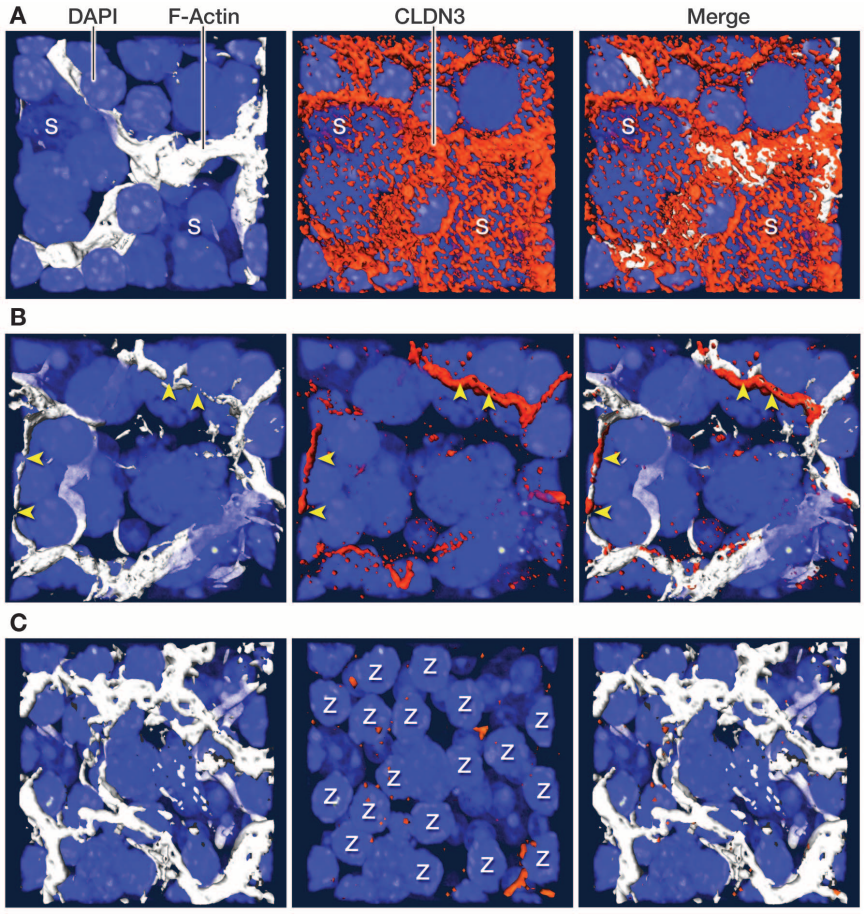


Fig. 3. CLDN3 localizes to the newly forming SCTJs. (**A**) Just before the migration of preleptotene spermatocytes across the SCTJs, in stage VII of the seminiferous epithelium cycle, CLDN3 (orange) is initially localized to the basal surface of the Sertoli cells (S) rather than the SCTJs (white), labeled with phalloidin. (**B**) In stage IX of the seminiferous epithelium cycle, when the leptotene spermatocytes migrate across the SCTJs, the spermatocytes are enclosed within the SCTJs (white). However, in this image, the basal side of these compartments is incomplete, as visualized as breaks in the tight junctions (yellow arrowheads). CLDN3 (orange) localizes to these breaks in the incomplete tight junction fibrils. (**C**) During stage XI of the seminiferous epithelium cycle, after the zygotene spermatocytes (Z) have emerged into the adluminal compartment, CLDN3 (orange) has been almost completely removed from the SCTJs (white). By stage XI, much of the old (apical) tight junctions have been removed.

Downloaded from www.sciencemag.org on November 9, 2012

basement membrane, cradling the spermatogonia in trough-like structures (fig. S2A). The SCTJs were present at the Sertoli-Sertoli cell contacts just below the spermatogonia (movie S1). As spermatogonia continue to proliferate and differentiate, the chains of cells expand between the Sertoli cells, such that by stage VII of spermatogenesis, just before the leptonema migration, the basal surfaces of the Sertoli cells no longer contact one another (fig. S2B). As the preleptotene spermatocytes lose contact with the basement membrane, the basal surface of the Sertoli cells intercalate between the preleptotene spermatocytes (now leptotene spermatocytes) and the basement membrane (fig. S2C), enclosing the migrating spermatocytes in a tunnel-like structure (fig. S2D). This change in Sertoli cell shape also allows for the formation of new Sertoli-Sertoli cell contacts and new tight junctions on the basal side of the leptotene spermatocytes, while still maintaining the old SCTJs.

We have previously shown that CLDN3 is transiently expressed at the time of SCTJ remodeling and translocation of leptotene spermatocytes from the basal to the adluminal compartment (*12*). To determine whether CLDN3 localizes to new or old tight junctions, we stained adult seminiferous tubules for CLDN3 and with phalloidin, which stains bundles of F-actin anchored at CLDN11-delineated tight junction fibrils (Fig. 1B). We first observed CLDN3 staining in stage VII, just before the leptonema migration. Rather than localizing to the SCTJs as expected, CLDN3 was distributed across the basal surface of the Sertoli cells (Fig. 3A), consistent with the observation that there are no Sertoli-Sertoli cell contacts on the basal surface of Sertoli cells at this stage to allow for tight junction formation.

At stages VIII-IX of spermatogenesis, when the leptotene spermatocytes are crossing the SCTJs, CLDN3 was integrated into SCTJs and no longer distributed on the basal surface (Fig. 3B). Specifically, CLDN3 was localized to the newly forming tight junction at the new Sertoli-Sertoli cell contacts near the basement membrane, bridging gaps in the SCTJs where migrating preleptotene spermatocytes were being enclosed in the SCTJs. By stage XI, when the leptotene spermatocytes emerge into the adluminal compartment, CLDN3 was almost completely absent from the seminiferous tubule (Fig. 3C).

Based on these findings, we propose a model for spermatocyte translocation across the SCTJs. In this model, as the preleptotene spermatocytes lose contact with the basement membrane, the basal membrane of the Sertoli cells is loaded with CLDN3 (Fig. 4A). The Sertoli cells then intercalate between the basement membrane and the preleptotene spermatocytes, and new CLDN3-containing tight junctions form at regions of new Sertoli-Sertoli cell contact (Fig. 4B). CLDN11 then replaces CLDN3, enclosing the chains of leptotene spermatocytes within the SCTJs. Once the chain is fully enclosed within the SCTJs, the "old" tight junctions are removed, releasing zygotene spermatocytes into the adluminal compartment (Fig. 4C).

We have shown that portions of syncytial chains of preleptotene spermatocytes become enclosed within a network of transient compartments, bounded by apical and basal tight junction fibrils and sealed by vertical tight junction strands that form at tricellular junctions. By visualizing a portion of the cytoplasmic bridges using TEX14, we were able to conclude that the intercellular bridges that connect germ cells within a syncytium span neighboring compartments by crossing the tricellular junctions, thereby allowing a complete syncytium to remain intact while also being enclosed within the SCTJs. Our studies resolve the long-standing question of movement of an entire syncytium across the blood-testis barrier and provide insight into the molecular and cellular mechanism of new tight junction formation.

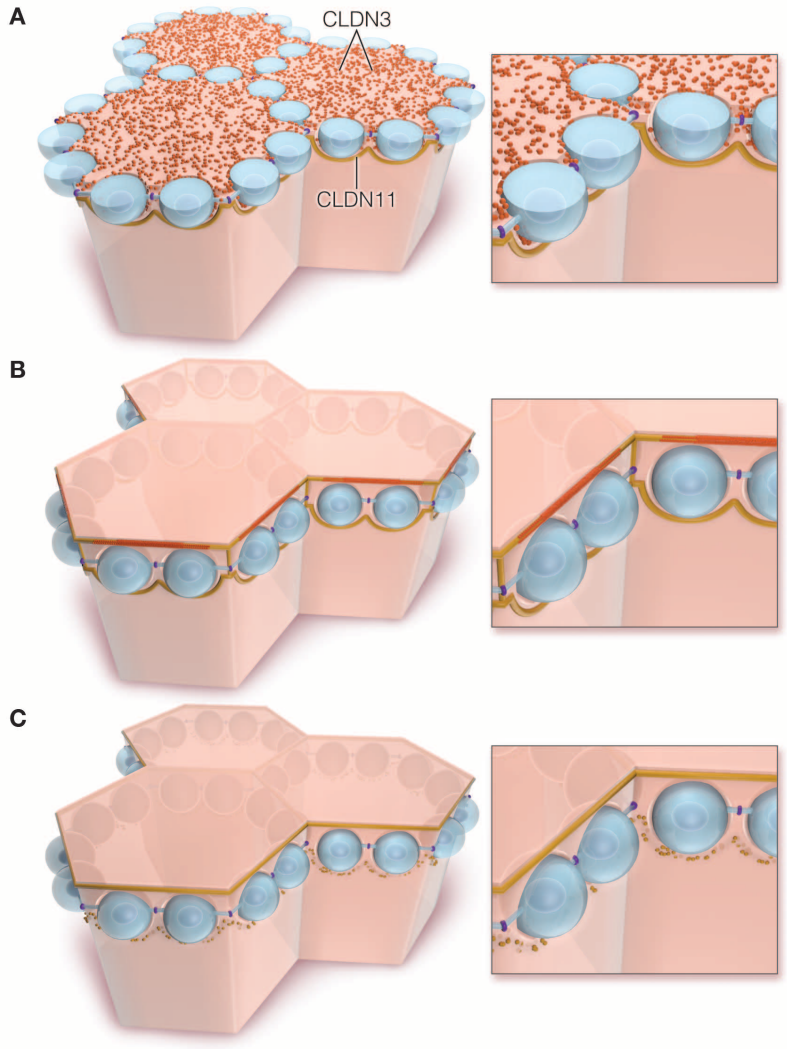


Fig. 4. Model for tight junction remodeling during germ cell cyst transit across the blood-testis barrier. (**A**) Schematic illustration of the confocal image in Fig. 3A. (**B**) Drawing representing the confocal image in Fig. 3B showing segmental localization of CLDN3 (red) and CLDN11 (brown) in areas of new tight junction formation. CLDN11 is usually found in and near tricellular junctions. Once the preleptotene spermatocyte leaves the basement membrane, stage VIII, the basal surface of the Sertoli cells intercalates between the basement membrane and the preleptotene spermatocyte, forming new Sertoli-Sertoli cell contacts. CLDN3 (red) then localizes to this new contact and forms a new tight junction that encloses the preleptotene spermatocytes. (Inset) Passage of an intercellular bridge, marked by TEX14 (purple) through a tricellular junction connecting two compartments. (**C**) Illustration of confocal image in Fig. 3C showing replacement of CLDN3 with CLDN11 in the new tight junction and removal of the old tight junction.

References and Notes

1. S. Tsukita, M. Furuse, M. Itoh, *Nat. Rev. Mol. Cell Biol.* **2**, 285 (2001).
2. E. E. Schneeberger, R. D. Lynch, *Am. J. Physiol. Cell Physiol.* **286**, C1213 (2004).
3. S. Tsukita, Y. Yamazaki, T. Katsuno, A. Tamura, S. Tsukita, *Oncogene* **27**, 6930 (2008).
4. M. Dym, J. C. Cavicchia, *Biol. Reprod.* **17**, 390 (1977).
5. J. E. Weber, L. D. Russell, *Am. J. Anat.* **180**, 1 (1987).
6. K. Morita, H. Sasaki, K. Fujimoto, M. Furuse, S. Tsukita, *J. Cell Biol.* **145**, 579 (1999).
7. L. D. Russell, A. Bartke, J. C. Goh, *Am. J. Anat.* **184**, 179 (1989).
8. E. F. Oakberg, *Am. J. Anat.* **99**, 507 (1956).
9. S. Masuda *et al.*, *J. Cell Sci.* **124**, 548 (2011).
10. L. Russell, *Am. J. Anat.* **148**, 313 (1977).
11. M. P. Greenbaum *et al.*, *Proc. Natl. Acad. Sci. U.S.A.* **103**, 4982 (2006).

Downloaded from www.sciencemag.org on November 9, 2012

12. J. Meng, R. W. Holdcraft, J. E. Shima, M. D. Griswold, R. E. Braun, *Proc. Natl. Acad. Sci. U.S.A.* **102**, 16696 (2005).

Acknowledgments: We thank M. Lessard and J. Denegre for ssistance with confocal imaging and S. Leighton for artistic rendering of the images. This research was supported by a grant to R.E.B. from the National Institute of Child Health and Human Development/NIH (HD12629) as part of the Specialized Cooperative Centers Program in Reproduction Research and from the National Cancer Institute (CA34196) in support of The Jackson Laboratories shared services.

Supplementary Materials
www.sciencemag.org/cgi/content/full/science.1219969/DC1
Materials and Methods
Figs. S1 and S2
Movie S1

2 February 2012; accepted 5 September 2012
Published online 20 September 2012;
10.1126/science.1219969

Bateman in Nature: Predation on Offspring Reduces the Potential for Sexual Selection

John Byers* and Stacey Dunn

Sexual selection is driven by competition for mates, and the advantage of a competitor is determined by the number of offspring it produces. Early experiments by Angus Bateman characterized this interaction, and the quantitative relationship between a male's number of mates and number of offspring is known as the Bateman slope. Sexual dimorphism, one of the most obvious results of sexual selection, largely requires a positive Bateman relationship, and the slope provides an estimate of the potential for sexual selection. However, natural selection from the environment can also influence male success, as can random effects, and some have argued for inclusion of the latter in calculations of mate success. Data from pronghorn (*Antilocapra americana*) reveal the presence of a positive Bateman slope in each year of a 10-year study. We found no evidence that random effects skewed male mating success; however, substantial yearly variation in the Bateman slope due to predation on fawns was evident. These results support the validity of the Bateman relationship, yet they also demonstrate that environmental or extrinsic influences can limit the potential for sexual selection.

Angus Bateman's laboratory experiments on *Drosophila melanogaster* provided the first experimental support for Darwin's sexual selection hypothesis (*1*). The results of these experiments described the relationship between male mating success and male number of offspring, and the findings are now codified as the three Bateman principles (*2*): (i) Male variance in number of offspring exceeds that of females; (ii) male variance in number of mates exceeds that of females; and (iii) males show a significant correlation between number of mates and number of offspring, whereas females do not. These conditions, and especially the third, are considered necessary to support the evolution of sexual dimorphism.

Following from these principles, the slope of the linear regression of male number of mates on male number of offspring (called the Bateman slope) indicates the magnitude of the potential for sexual selection. Over time, several comparative studies have investigated whether the Bateman slope predicts the degree of sexual dimorphism, and a recent comprehensive review (*3*) called for a much better understanding of the forces that affect the slope. Two main factors, independent of male competitive success, could influence the Bateman slope and thus potential for sexual selection. First, factors that reduce offspring survival (and recruitment) could reduce the contribution of a male to subsequent populations, independent of his quality; thus, environmental conditions could possibly modulate the potential for sexual selection. Additionally, variance in male success (i.e., number of offspring produced) can become greater than female variance solely by random effects when the sexes differ in the latency to remate (*4*, *5*). If random processes such as this drive differential male success, traits from the highest-quality males will not necessarily be passed on to subsequent generations, and selection for reproductively advantageous traits could be swamped.

Here, we used a long-term data set, collected from every individual within the pronghorn (*Antilocapra americana*) population of the National Bison Range (NBR; Northwestern Montana, USA) between 1999 and 2010, to test the random effects hypothesis, ascertain the temporal stability of the Bateman relationship, and determine whether, and to what extent, population and environmental effects altered the magnitude of the Bateman slope. For each year of the study, we knew the number and ages of potentially breeding males and females, the sire and dam of each fawn born, and each fawn's birth mass, foot length, and survival to

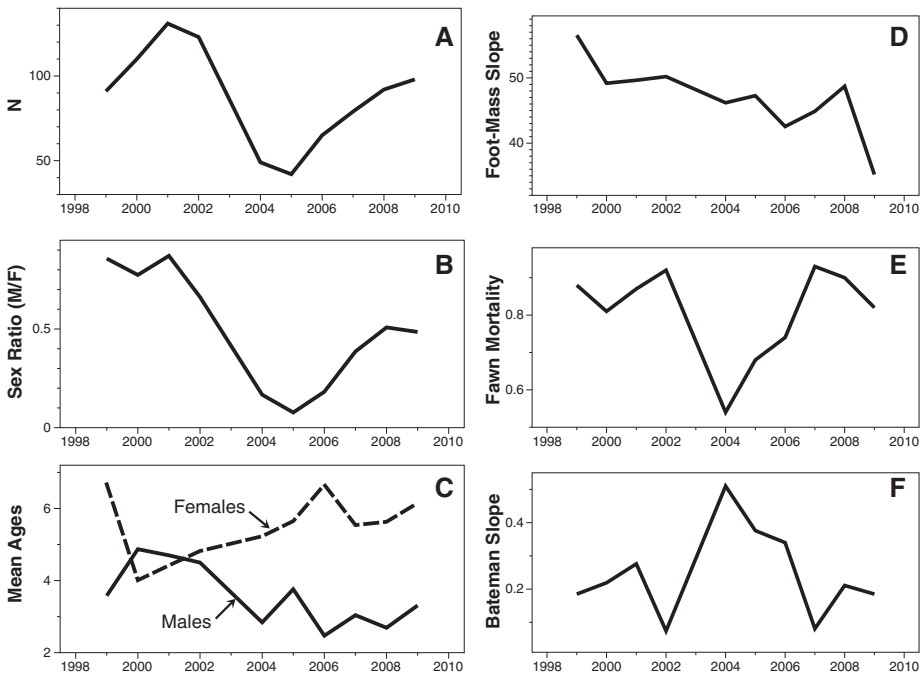


Fig. 1. Variation in population characteristics. (**A**) Number of breeding-age adults. (**B**) Sex ratio of breeding-age adults. (**C**) Mean ages of males and females. (**D**) Slope of the linear regression of fawn birth mass on foot length. (**E**) Proportion of fawns that died before weaning. (**F**) Slope of the linear regression of male offspring recruited against male number of mates in the previous rut.

Department of Biological Sciences, University of Idaho, Moscow, ID 83844–3051, USA.

*To whom correspondence should be addressed. E-mail: jbyers@uidaho.edu

Downloaded from www.sciencemag.org on November 9, 2012

weaning (at 12 weeks). An individual that survives to weaning is recruited and is likely to reach breeding age (*6*). Therefore, for all reproductive-age individuals, we quantified the number of mates (including all males that had no mates) and the number of offspring recruited to the population. These data allowed us to calculate yearly Bateman slopes (from offspring recruited rather than from offspring produced), male and female *I* (where *I* is the opportunity for selection, defined as σ^2/mean^2), the breeder sex ratio, the average ages of males and females, yearly fawn condition (least-squares slope of foot length against birth mass), and mortality (Fig. 1).

In an iteroparous species such as pronghorn, the random effects hypothesis can be evaluated by a distribution test. If, in each mating season, random effects cause the skew in male mating success, then, across several seasons, the mating success of all males will approach a Gaussian distribution (see supplementary materials). If, in contrast, random effects are not important and mating success is caused by male phenotype (i.e., a population subset of males always performs well), then the distribution of mating success across multiple years will remain skewed. Across all years of our study, the frequency distribution of the number of offspring produced by breeding-age males was highly skewed (Fig. 2), significantly different from Gaussian (Doornik-Hansen test for univariate normality $\chi^2 = 1749$, $P < 0.00001$), and significantly different from a Poisson distribution with the same mean [Levene's robust test for the equality of variances W0 = 51.54, df (1, 653), $P < 0.0001$]. The empirical distribution of male mating success also differed from the expected distribution generated by the random effects hypothesis [empirical median = 0, expected median = 1.5, Levene's robust test W0 = 58.177, df (1, 653), $P < 0.0001$]. Thus, we found no support for the presence of random effects and rather conclude that a population subset of individual males sired most of the offspring. The results also support the three Bateman principles (Table 1). The variance in male number of offspring recruited exceeded the variance in female number of offspring recruited (paired $t = 3.41$, df = 9, $P = 0.008$). Variance in number of mates for males exceeded variance for females by more than two orders of magnitude, and number of recruited offspring produced by males was largely explained by male number of mates (331 male rut years, slope = 0.36, $r^2 = 0.73$). Females usually mated once, but when they mated twice or more so that two males were sires of the two fawn litter, their rates of offspring recruitment did not differ from those of females that mated once ($\chi^2 = 0.24$, $P = 0.89$).

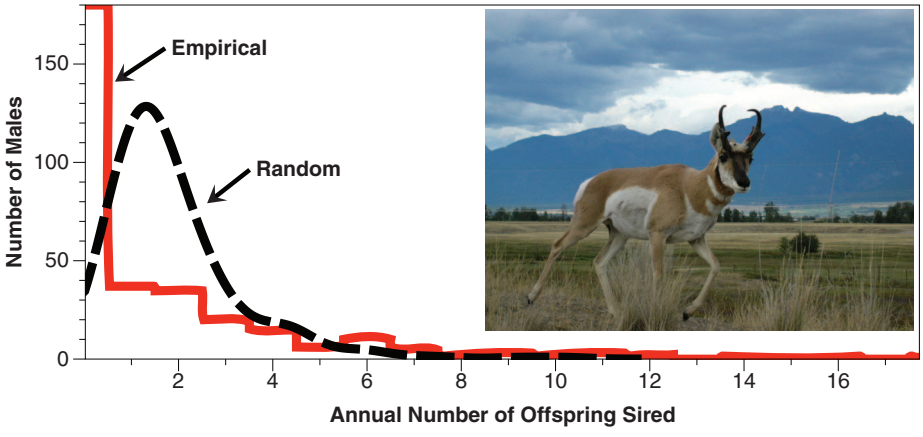


Fig. 2. The red line shows the annual distribution of individual male mating success summed across all years of the study. The dashed black line shows the expected distribution generated by simulations that followed the assumptions of the random effects hypothesis (see supplementary materials).

Table 1. Bateman principle statistics. *I*, the opportunity for selection, is the standardized variance.

Bateman principle	Males	Females
Offspring recruited: male σ^2 > female σ^2	$I = 4.84$	$I = 2.29$
Number of mates: male σ^2 > female σ^2	$I = 3.73$	$I = 0.09$
Correlation between number of mates and number of offspring recruited: male > female	$r = 0.85$	One mate: $I = 1.80$ Two mates: $I = 2.06$

Although we rejected the random effects hypothesis and confirmed the Bateman principles in a species with obvious sexual dimorphism in weapon size, pugnacity, and behavioral focus on copulation, the Bateman slope varied more than fivefold during the decade (Fig. 1F). Thus, our study offered the opportunity to evaluate the environmental and population elements that may affect the maximum intensity of sexual selection and specifically to test the hypothesis that environmentally induced offspring mortality would affect the Bateman slope.

We evaluated the magnitude of possible effects using a generalized linear model (GLM), in which the yearly Bateman slope was the dependent variable and the independent variables were population size, sex ratio, average ages of both sexes, fawn mortality, and condition slope (slope of the yearly least-squares regression of foot length on fawn mass). Density, sex ratio, and age structure are commonly predicted to be population characteristics that could alter the Bateman slope (*7*), and fawn condition is potentially important as a yearly indicator of the overall probability of survival to recruitment. The result (Table 2) showed clearly that one variable, fawn mortality, affected the Bateman slope. The effect of fawn mortality on the Bateman

Table 2. Results of a GLM analysis in which the yearly Bateman slope was the dependent variable.

Independent variable	Coefficient	SE	*z*	*P*
Population size	0.0013	0.0030	0.43	0.66
Breeding adult sex ratio	−0.015	0.2770	−0.06	0.95
Mean male age	−0.035	0.0531	−0.67	0.50
Mean female age	−0.991	0.0477	−0.03	0.97
Fawn mortality	−1.201	0.3418	−3.51	>0.001
Fawn foot-mass regression slope	0.004	0.0068	0.69	0.49
Constant	1.023	0.5601	0.68	0.07

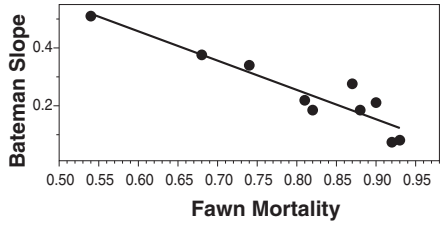


Fig. 3. Yearly proportion of fawns that died before weaning plotted against the Bateman slope for that year. Each point represents a year.

Downloaded from www.sciencemag.org on November 9, 2012

slope was negative, linear, and very strong (Fig. 3, $r^2 = 0.87$).

The interpretation of this finding rests upon understanding the causes of fawn mortality. If fawn mortality has a largely environmental cause, then our hypothesis that environmental mortality can affect the Bateman gradient is supported. In our population and across western North America, evidence points to coyotes (*Canis latrans*) as the primary cause. On the NBR and elsewhere, rates of fawn survival are directly related to rates of coyote removal practiced by state and federal agency personnel (*8*). Additionally, fawn survival in Yellowstone National Park is predicted by local wolf density and winter snowpack, two factors that reduce local coyote density (*9*). Finally, in the NBR population, fawn survival increases with maternal age, although the magnitude of maternal expenditure does not (*6*). With age, females appear to gradually improve the complex behavior of the hiding strategy, the mechanism to conceal fawns from predators during the first 3 to 4 weeks of life (*10*). Environmental characteristics that may affect the rate of coyote predation on pronghorn fawns include the density and litter sizes of territorial coyote pairs; the density of floaters; the densities of alternative prey, such as rodents of the genus *Microtus*; and the magnitude of spring precipitation, which can influence rodent densities as well as the quality of pronghorn milk and the concomitant change in fawn growth rates (*11*).

In all years of our study, the result of the fall rut was substantial variance in male mating success. However, mating success translated directly into reproductive success only when the rate of coyote predation was relatively low. When the rate was higher, fawn mortality eliminated most incipient variation in male reproductive success. Long-term studies show that the intensity and the direction of natural selection fluctuate with environmental conditions (*12*) and that the target of sexual selection varies with the nature of female mate choice (*13*). We now show that the maximum possible rate of evolutionary change under sexual selection varies with predator-driven offspring mortality. Bateman was a pioneer in the study of sexual selection (*14*) who established important principles that continue to guide empirical work. However, our study shows that single point estimators of the Bateman principles may be misleading and that ecological forces can modulate the potential for sexual selection. Sexual selection and natural selection are entangled.

References and Notes

1. A. J. Bateman, *Heredity* **2**, 349 (1948).
2. S. J. Arnold, *Am. Nat.* **144**, S126 (1994).
3. A. G. Jones, N. L. Ratterman, *Proc. Natl. Acad. Sci. U.S.A.* **106** (suppl. 1), 10001 (2009).
4. W. J. Sutherland, *Anim. Behav.* **33**, 1349 (1985).
5. S. P. Hubbell, L. K. Johnson, *Am. Nat.* **130**, 91 (1987).
6. J. A. Byers, *American Pronghorn. Social Adaptations and the Ghosts of Predators Past* (Univ. of Chicago Press, Chicago, 1997).
7. A. G. Jones, *Evolution* **63**, 1673 (2009).
8. J. A. Byers, *J. Mammal.* **78**, 894 (1997).
9. K. K. Barnowe-Meyer *et al.*, *J. Mammal.* **91**, 712 (2010).
10. J. A. Byers, K. Z. Byers, *Behav. Ecol. Sociobiol.* **13**, 147 (1983).
11. J. A. Byers, *Proceedings of the 22nd Biennial Pronghorn Workshop* **22**, 27 (2006).
12. P. R. Grant, B. R. Grant, *Science* **296**, 707 (2002).
13. A. S. Chaine, B. E. Lyon, *Science* **319**, 459 (2008).
14. M. J. Wade, S. M. Shuster, *Heredity* **105**, 507 (2010).

Acknowledgments: We thank the dozens of field volunteers who helped build our data set, L. Waits for laboratory guidance, S. Nuismer for statistical consultation, and the U.S. Fish and Wildlife Service for access permits and support. Supported by NSF grants 9808377, 0097115, and 0738012 to J.B. Data location: Dryad Digital Repository (http://datadryad.org/handle/10255/dryad.34974).

Supplementary Materials

www.sciencemag.org/cgi/content/full/338/6108/802/DC1
Materials and Methods
References (*15*–*20*)

14 May 2012; accepted 11 September 2012
10.1126/science.1224660

Corals Chemically Cue Mutualistic Fishes to Remove Competing Seaweeds

Danielle L. Dixson and Mark E. Hay*

Corals in the genus *Acropora* generate much of the structural complexity upon which coral reefs depend, but they are susceptible to damage from toxic seaweeds. *Acropora nasuta* minimizes this damage by chemically cuing symbiotic goby fishes (*Gobidon histrio* or *Paragobidon enchinocephalus*) to remove the toxic seaweed *Chlorodesmis fastigiata*. Within minutes of seaweed contact, or contact from only seaweed chemical extract, the coral releases an odor that recruits gobies to trim the seaweed and dramatically reduce coral damage that would otherwise occur. In turn, chemically defended gobies become more toxic after consumption of this noxious alga. Mutualistic gobies and corals appear to represent a marine parallel to terrestrial ant-plants, in that the host provides shelter and food in return for protection from natural enemies.

Coral reefs are in global decline, with seaweeds commonly replacing corals. Coral cover has decreased by ~80% in the Caribbean (*1*) and by ~50% along the Great Barrier Reef (*2*). Drivers of decline are debated, but all major stresses—including overfishing of herbivores, pollution, ocean heating, acidification, and disease (*3*, *4*)—suppress corals, enhance seaweeds, and result in greater seaweed-coral competition.

School of Biology and Aquatic Chemical Ecology Center, Georgia Institute of Technology, 310 Ferst Drive, Atlanta, GA 30332, USA.

*To whom correspondence should be addressed. E-mail: mark.hay@biology.gatech.edu

For reefs to flourish, rapidly growing, branching corals such as Acroporids are critical because they create much of the topographic complexity upon which other species depend (*4*, *5*). Other species, such as herbivorous fishes, then enhance reef resilience by grazing on competing algae and facilitating the colonization and growth of corals after disturbances (*3*, *4*, *6*). In the Caribbean, when two dominant *Acropora* species declined, structural complexity was lost across the entire region with likely effects on fishes, fisheries, biodiversity, coastal protection from wave damage, and ecosystem function in general (*7*, *8*).

Reef-scale herbivory facilitates coral growth and maintenance by removing competitively superior seaweeds (*3*, *4*, *9*, *10*), as exemplified by herbivore-rich reefs and marine protected areas that are higher in coral and lower in macrophyte cover, whereas overfished reefs with fewer herbivores have fewer corals and more macroalgae (*3*, *9*, *10*). However, individual corals are damaged only by adjacent seaweeds. Thus, critical aspects of competition occur at coral edges, a spatial scale over which corals might exert influence. Recent studies of seaweed-coral competition emphasize effects of seaweed allelopathy (*11*, *12*) (chemical suppression of competitors), seaweeds vectoring coral diseases (*13*, *14*), and near-contact creating anoxic zones or enhancing detrimental microbes on corals (*14*, *15*). These mechanisms all require close contact for seaweeds to damage corals. Thus, millimeter- to centimeter-scale differences in proximity may cause large differences in coral health (*11*, *12*, *15*). Just as mutualist ants on *Acacia* trees protect their host by removing nearby competitors (*16*), we reasoned that the goby or pomacentrid fishes that shelter in many Acroporid corals (*17*) might play a similar function and remove seaweed competitors from coral edges.

We therefore focused on the common coral *Acropora nasuta* and asked the following: (i) whether commensal fishes sheltering in *Acropora* suppressed an allelopathic seaweed competitor, (ii) whether different commensal fish species varied in the protection they provided the coral, (iii) whether the interaction was affected by a specialist crab that lives only in the allelopathic sea-

Downloaded from www.sciencemag.org on November 9, 2012

weed (*18*), (iv) if the coral chemically cued the fishes to remove toxic seaweed at sites of contact, and (v) whether mutualistic fish that consume the toxic seaweed become more toxic to generalist predatory fishes.

We assessed how coral-dwelling fishes affected seaweed-coral interactions in the field (*19*) by placing the allelopathic seaweed (*12*) *Chlorodesmis fastigiata* versus a control for shading and abrasion (an algal mimic made of nylon line) in contact with *A. nasuta* colonies occupied by four different commensal fishes ($n = 20$ corals per fish species). We then evaluated coral health at the coral-algal or coral-control area of contact using pulse-amplitude modulated (PAM) fluorometry to assess coral photophysiology as a proxy for coral health (*12*, *20*). In corals occupied by the gobies *Gobiodon histrio* or *Paragobiodon echinocephalus*, *C. fastigiata* abundance declined by 30% over 3 days and the damaging effect of *C. fastigiata* on *A. nasuta* declined by 70 to 80% compared with *A. nasuta* colonies lacking gobies (Table 1 and Fig. 1). In contrast, the control had minimal effect (Fig. 1). The alga's specialist crab (*18*), *Cyphyra rotundifrons*, had no effect on these interactions. *C. fastigiata* was found in the gut of 17 of 20 *G. histrio* and 0 of 20 *P. echinocephalus* from corals that were contacting *C. fastigiata* ($\chi^2 = 29.57$, df = 1, $P < 0.001$); thus, *G. histrio* consumed *C. fastigiata*, whereas *P. echinocephalus* removed the seaweed but did not consume it. Guts of *G. histrio* or *P. echinocephalus* occupying corals not contacting *C. fastigiata* ($n = 20$ each) were devoid of *C. fastigiata*. Given that the allelopathic compounds from *C. fastigiata* are hydrophobic and the alga must contact the coral for these to be transferred (*11*, *12*), gobiid removal of *C. fastigiata* filaments contacting the coral should lessen or prevent coral damage, which is what we found in our field experiments (Fig. 1). For this interaction to be broadly important, goby occupancy of *A. nasuta* would need to be frequent. We assessed this by running eight haphazardly placed 30- × 2-m transects across the reef and evaluating goby occupancy of all *A. nasuta* located in these transects. Gobies occurred in 81 ± 16% (mean ± 1 SD) of the 207 colonies assessed. An assessment in Australia also indicated common co-occurrence, with 1593 *Gobiodon* individuals occurring in the 1373 colonies of 11 Acropora species evaluated (*17*).

Table 1. Effects of coral-associated gobies and an alga-associated crab on abundance (volumetric displacement) of the alga *C. fastigiata* after 3 days of exposure (± SEM) ($N = 20$).

	Algal abundance (ml) before and after exposure to			
	G. histrio		*P. echinocephalus*	
Treatment	Initial	Post	Initial	Post
Empty	1.49 ± 0.03	1.48 ± 0.03	1.48 ± 0.07	1.48 ± 0.04
Crabs only	1.41 ± 0.04	1.39 ± 0.04	1.42 ± 0.03	1.39 ± 0.03
Gobies only	1.50 ± 0.04	0.99 ± 0.05*	1.45 ± 0.03	1.04 ± 0.02*
Crabs and gobies	1.40 ± 0.03	0.97 ± 0.06*	1.41 ± 0.04	0.99 ± 0.03*

*Significant ($P < 0.05$) loss of the alga.

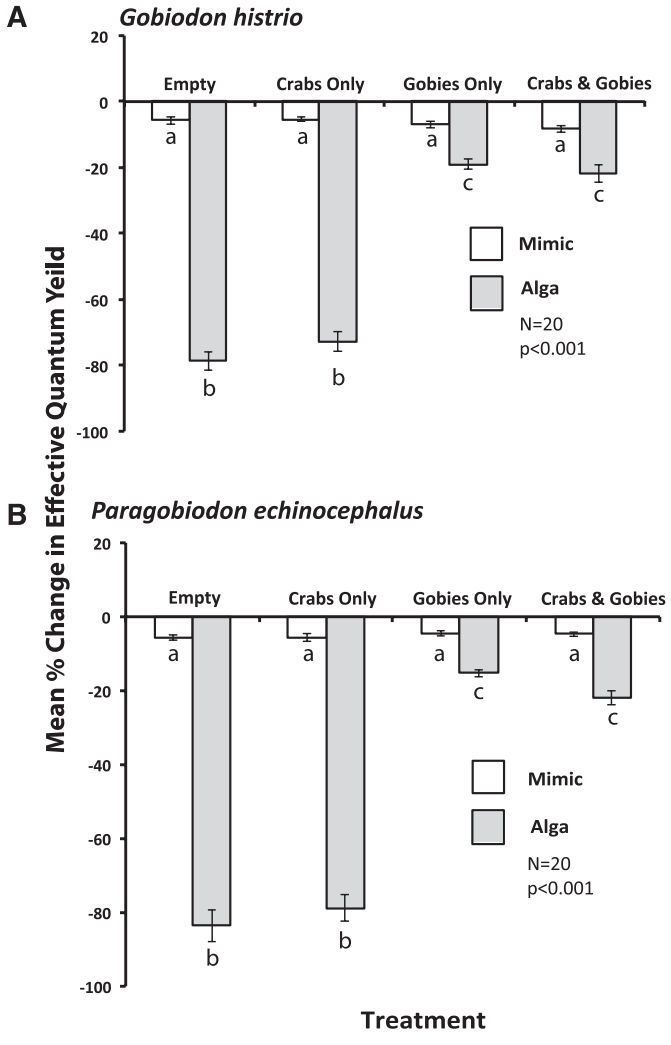


Fig. 1. Effects of gobies (**A**) *G. histrio* and (**B**) *P. echinocephalus* on algal-coral interactions. Mean (± 1 SE) percent difference in effective quantum yield of the coral holobiont when exposed to the seaweed *C. fastigiata* or an inert mimic compared to the control location on the coral that was exposed to no treatment. *P* value is from a split-plot analysis of variance (ANOVA) (arcsine-transformed data). Letters designate significant groupings.

Because G. histrio produces a toxic skin secretion, whereas *P. echinocephalus* does not (*21*), we tested the effect (*22*) of *G. histro* mucus on two model predators that consume a variety of invertebrates and small fishes to see if potency of *G. histro* secretions increased after consumption of *C. fastigiata*. We placed mucus from one disturbed *G. histrio* into 300 ml of seawater with the cardinal fishes *Ostorhinchus nigrofasciatus* ($n = 20$) and *Nectamia similis* ($n = 10$). The mucus of both control and *C. fastigiata*–exposed *G. histrio* produced significant effects; however, secretions of *G. histrio* from coral heads contacting *C. fastigiata* caused predators to lose equilibrium (falling forward or sideways) more than twice as fast (66 ± 4 and 65 ± 8 s, respectively) as mucus of *G. histrio* from corals without *C. fastigiata* (143 ± 9 and 162 ± 11 s, respectively; $P < 0.001$ for each species, *t* test). The toxins producing the effects are unknown, but thin-layer chromatograms of extracts from *C. fastigiata* and from *G. histrio* mucus did not show secondary metabolites from *C. fastigiata* in *G. histrio* mucus.

In contrast to the advantage that both gobies provide coral by removing *C. fastigiata*, the coral-sheltering damselfishes *Dascyllus aruanus* or *Chromis viridis* provided no advantage (fig. S1). All *D. aruanus* and *C. viridis* abandoned *C. fastigiata*–treated *A. nasuta* within 24 to 48 hours; none abandoned colonies treated with the mimic alone ($P < 0.001$ for each species, $n = 20$, Fisher's exact test). Initial presence or absence of fish had no effect on photosynthesis of the coral holobiont when in contact with *C. fastigiata* (*D. aruanus* $F_{1,38} = 2.221$, $P = 0.144$; *C. viridis* $F_{1,38} = 2.234$, $P = 0.147$). By day 3 of the experiment, contact with *C. fastigiata* had damaged corals and suppressed effective quantum yield by ~80%, whether or not damselfishes had been

Downloaded from www.sciencemag.org on November 9, 2012

present. In contrast, algal mimics suppressed photosynthesis by only ~5% ($F_{1,38}$ = 2280.66, P < 0.001 for both fish species), which indicated the primacy of chemical, as opposed to physical, effects.

To determine whether fish were responding to chemical cues from the seaweed or the coral, we used 60-ml syringes to pull in situ seawater from: among the filaments of *C. fastigiata* alone, the *C. fastigiata–A. nasuta* contact area with *C. fastigiata* still present, the *C. fastigiata–A. nasuta* contact area after removing *C. fastigiata* 20 min earlier (allowing loss of algal odor but retention of odor from the damaged coral), and the water column well away from the benthos (as a control) and then slowly released these odors into corals containing *G. histrio*. Olfactory cues from *C. fastigiata* alone generated no response by the goby. In contrast, odors from the coral-algal contact point or from the stressed coral alone caused 17 and 19, respectively, of the goby pairs in 20 separate *A. nasuta* colonies to move toward the odor source. Thus, the goby responds to chemical cues from the host coral, not to cues from the seaweed (Fig. 2, Υ = 559.12, df = 2, P < 0.001; G test,).

The same experiment conducted with odors from *Acropora millepora* produced no responses from *G. histrio* living in *A. nasuta* (Fig. 2). Thus, gobies responded to cues from their host species, but not to odors from a closely related coral, even one that *G. histrio* sometimes occupies.

Because *G. histrio* effectively defended its host and was the most common goby in *A. nasuta*, we conducted assays evaluating how rapidly *A. nasuta* cued its goby symbionts and whether the coral would signal in response to the seaweed's chemistry alone. *C. fastigiata* damages *Acropora* species via hydrophobic compounds including acetylated diterpenes (*12*). We obtained the hydrophobic crude extract from *C. fastigiata* via extraction in methanol followed by partitioning between water and ethyl acetate, removed the solvent in vacuo, redissolved the ethyl acetate partition in ether, coated this lipid-soluble extract onto algal mimics at natural volumetric concentration (*12*), and placed extract-treated mimics against *A. nasuta*–harboring *G. histrio*. Control mimics treated with the same solvent but without the algal extract also were placed against the coral. Gobies rapidly moved to the site of contact between the extract-treated mimic and the coral (Fig. 3). Fifteen minutes after contact, 70% of the 20 goby pairs were beneath the treated mimics, this increased to 95% by 30 min; movement to the control ranged from 0 to 10% (P = 0.001 at 30 min; Kolmogorov-Smirnov test). Patterns in Fig. 3 indicate that the coral signaled in response to *C. fastigiata* compounds alone and that the signal was produced within 5 to 15 min of coral exposure.

Thus, the gobies serve as bodyguards for host corals, and the coral chemically cues gobies to attract them to the site of coral-algal contact where they begin removing the alga within minutes of seaweed contact (or contact by the seaweed's hydrophobic extract alone). Gobies are not attracted to cues from *C. fastigiata* alone nor to cues from related corals in contact with *C. fastigiata*; they respond only to odors from their host species. Symbiotic gobies that spend their adult life in a single coral played this protective role; damselfishes did not. Just as terrestrial plants release volatile signals that attract predators of herbivores (*23*), *A. nasuta* releases chemicals that cue symbiotic gobies to remove a competing, allelopathic seaweed. We could find no previous example of a species chemically cuing consumers to remove its competitors.

As corals have declined and seaweed cover has increased on reefs over recent decades, understanding seaweed-coral competition has become more important (*3*, *24*). Because Acroporid corals are major builders of topographic complexity on coral reefs, they play critical roles as foundation species (*5*, *7*), creating critical habitat that is associated with the diversification of numerous lineages of reef fishes (*25*). Coral-dwelling gobies facilitate persistence of these corals despite increased competition from seaweeds. These small, inconspicuous fishes may have effects considerably larger than their mass would predict.

The coral-goby relation appears similar to terrestrial ant-plant symbioses as exemplified by ants and *Acacia* trees (*16*). Ants receive food and shelter from their host *Acacia* and protect the host from competitors and consumers. Symbiotic gobies have a similar relationship with Acropid corals. Several gobies consume coral tissue (5 of the 19 species of *Gobiodon* are corallivores), but no species feeds exclusively on coral (*26*, *27*). Most Acroporid coral colonies host at least one pair of gobiids (*17*), these fish remain in the same coral colony for most of their adult life, and death of host corals is commonly correlated with goby population decline (*17*). Gobies consume coral

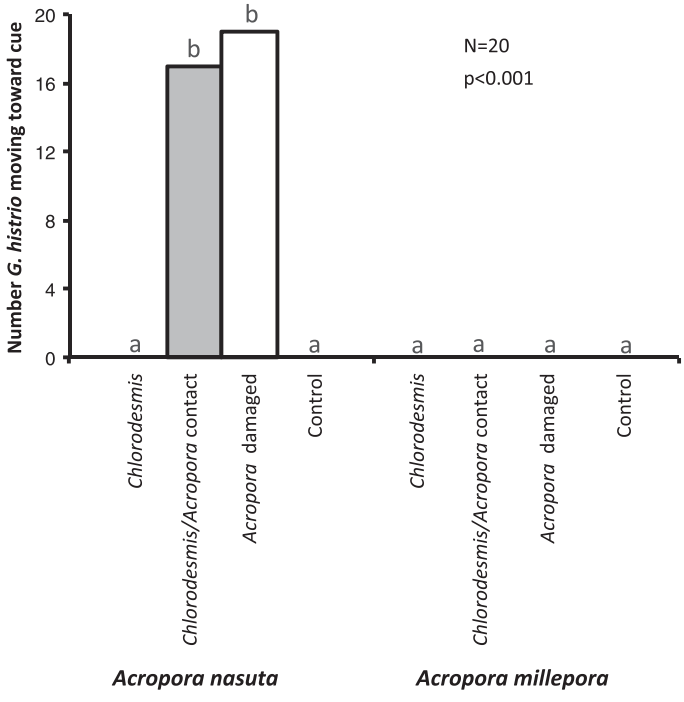


Fig. 2. Response of the goby *G. histrio* to chemical cues from: the alga *C. fastigiata* alone, *C. fastigiata* in contact with the coral *A. nasuta*, or the damaged coral that had been in contact with *C. fastigiata* but with the *C. fastigiata* removed 20 min before the odor was collected. Right side of graph is the same experiment with the same types of cues from *Acropora millepora* introduced to gobies living in *A. nasuta*. *P* value from a *G* test. Letters indicate significant groupings.

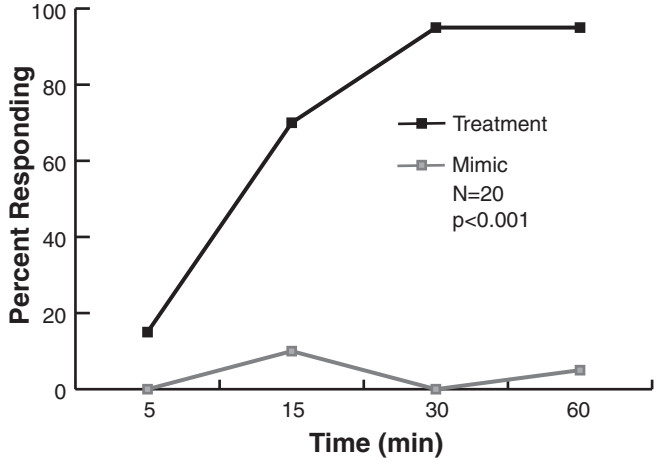


Fig. 3. Response of *G. histrio* to *A. nasuta* in contact with algal mimics treated with natural concentrations of the lipid-soluble extract from *C. fastigiata* (treatment) versus control algal mimics treated with solvent only and placed against the coral host. *P* value from a Kolmogorov-Smirnov test of the 30-min data.

Downloaded from www.sciencemag.org on November 9, 2012

tissue [they also consume copepods (*26*) and algae growing against the coral base (*27*)]. Thus, like ants on *Acacia*, they receive shelter and food from their host, which they protect from a damaging competitor.

Both gobies we investigated protected their host by removing *C. fastigiata*; however, only *G. histrio* consumed the alga, which contains metabolites that deter feeding by numerous reef herbivores (*18*, *28*). These findings may explain why *P. echinocephalus* removes, but does not consume, algal tissue in contact with its host coral. Consumption of this chemically noxious alga may benefit *G. histrio* by making its skin secretions more noxious to predators. However, metabolites from *C. fastigiata* are unlikely to be a primary source of skin toxins because *G. histrio* not exposed to *C. fastigiata* were also toxic, just less so.

As reefs continue to convert from coral to macroalgal dominance, there is increasing need to understand interactions that enhance coral resilience or suppress seaweed impacts on corals. Symbiotic gobies play a key role in defending Acroporid corals from an allelopathic alga, with chemical signals and cues mediating responses of both the coral (Fig. 3) and fish (Figs. 2 and 3). A worrisome recent discovery is that chemically mediated behaviors, such as these, that often are critical to reef function can be disrupted or even reversed (i.e., attraction to predator odors) by changes in ocean pH (*29*, *30*). With ocean acidification (*24*), critical aspects of chemical communication in the sea may be destabilized, with the attendant loss of key processes underlying reef resilience.

References and Notes

1. T. A. Gardner, I. M. Côté, J. A. Gill, A. Grant, A. R. Watkinson, *Science* **301**, 958 (2003).
2. D. R. Bellwood, T. P. Hughes, C. Folke, M. Nyström, *Nature* **429**, 827 (2004).
3. T. P. Hughes, N. A. J. Graham, J. B. C. Jackson, P. J. Mumby, R. S. Steneck, *Trends Ecol. Evol.* **25**, 633 (2010).
4. P. J. Mumby, R. S. Steneck, *Trends Ecol. Evol.* **23**, 555 (2008).
5. G. P. Jones, M. I. McCormick, M. Srinivasan, J. V. Eagle, *Proc. Natl. Acad. Sci. U.S.A.* **101**, 8251 (2004).
6. A. C. Baker, P. W. Glynn, B. Riegl, *Coast Shelf Sci* **80**, 435 (2008).
7. L. Alvarez-Filip, N. K. Dulvy, J. A. Gill, I. M. Cote, A. R. Watkinson, *Proc. Biol. Sci.* **276**, 3019 (2009).
8. D. E. Williams, M. W. Miller, *Coral Reefs* **31**, 369 (2012).
9. C. L. Birrell, L. J. McCook, B. L. Willis, G. Diaz-Pulido, *Oceanogr. Mar. Biol. Annu. Rev.* **46**, 25 (2008).
10. J. B. C. Jackson *et al.*, *Science* **293**, 629 (2001).
11. D. B. Rasher, M. E. Hay, *Proc. Natl. Acad. Sci. U.S.A.* **107**, 9683 (2010).
12. D. B. Rasher, E. P. Stout, S. Engel, J. Kubanek, M. E. Hay, *Proc. Natl. Acad. Sci. U.S.A.* **108**, 17726 (2011).
13. M. M. Nugues, G. W. Smith, R. J. Hooidonk, M. I. Seabra, R. P. M. Bak, *Ecol. Lett.* **7**, 919 (2004).
14. J. E. Smith *et al.*, *Ecol. Lett.* **9**, 835 (2006).
15. K. L. Barott *et al.*, *Proc. Biol. Sci.* **279**, 1655 (2012).
16. D. H. Janzen, *Evolution* **20**, 249 (1966).
17. P. L. Munday, G. P. Jones, M. J. Caley, *Mar. Ecol. Prog. Ser.* **152**, 227 (1997).
18. M. E. Hay, J. R. Pawlik, J. E. Duffy, W. Fenical, *Oecologia* **81**, 418 (1989).
19. Materials and methods are available as supplementary materials on *Science* Online.
20. W. K. Fitt, B. E. Brown, M. E. Warner, R. P. Dunne, *Coral Reefs* **20**, 51 (2001).
21. Y. Hashimoto, K. Shiomi, K. Aida, *Toxicon* **12**, 523 (1974).
22. M. Schubert, P. L. Munday, M. J. Caley, G. P. Jones, E. Llewellyn, *Environ. Biol. Fishes* **67**, 359 (2003).
23. M. Dicke, *Plant Cell Environ.* **32**, 654 (2009).
24. O. Hoegh-Guldberg *et al.*, *Science* **318**, 1737 (2007).
25. P. F. Cowman, D. R. Bellwood, *J. Evol. Biol.* **24**, 2543 (2011).
26. E. Riedlecker, J. Herler, *J. Zool. Sys. Evol Res.* **47**, 160 (2009).
27. R. M. Brooker, P. L. Munday, T. D. Ainsworth, *J. Fish Biol.* **76**, 2578 (2010).
28. K. D. Meyer, V. J. Paul, H. R. Sanger, S. G. Nelson, *Coral Reefs* **13**, 105 (1994).
29. P. L. Munday *et al.*, *Proc. Natl. Acad. Sci. U.S.A.* **106**, 1848 (2009).
30. D. L. Dixson, P. L. Munday, G. P. Jones, *Ecol. Lett.* **13**, 68 (2010).

Acknowledgments: Support provided by NSF grant OCE-0929119, NIH grant U01-TW007401, and the Teasley Endowment to the Georgia Institute of Technology. We thank the Fijian government and the Korolevu-i-wai district elders for collection and research permissions; B. Devine, J. White, G. Longo, R. Bonaldo, and D. Rasher for field, lab, or statistical assistance; J. Kubanek, D. Rasher, P. Munday, J. P. Hobbs, and anonymous reviewers for comments on the manuscript; and V. Bonito for assisting scientifically and culturally. The data reported in this manuscript are presented in the main paper and supplementary materials.

Supplementary Materials

www.sciencemag.org/cgi/content/full/338/6108/804/DC1
Materials and Methods
Fig. S1
References (*31*–*33*)

7 June 2012; accepted 24 September 2012
10.1126/science.1225748

A Core Metabolic Enzyme Mediates Resistance to Phosphine Gas

David I. Schlipalius,[1,2,3]* Nicholas Valmas,[4,5]* Andrew G. Tuck,[1,2,3] Rajeswaran Jagadeesan,[2] Li Ma,[2] Ramandeep Kaur,[2] Anita Goldinger,[4] Cameron Anderson,[4] Jujiao Kuang,[2] Steven Zuryn,[4] Yosep S. Mau,[4,6] Qiang Cheng,[4] Patrick J. Collins,[1,3] Manoj K. Nayak,[1,3] Horst Joachim Schirra,[4,7]† Massimo A. Hilliard,[5]†‡ Paul R. Ebert[2,4]†‡

Phosphine is a small redox-active gas that is used to protect global grain reserves, which are threatened by the emergence of phosphine resistance in pest insects. We find that polymorphisms responsible for genetic resistance cluster around the redox-active catalytic disulfide or the dimerization interface of dihydrolipoamide dehydrogenase (DLD) in insects (*Rhyzopertha dominica* and *Tribolium castaneum*) and nematodes (*Caenorhabditis elegans*). DLD is a core metabolic enzyme representing a new class of resistance factor for a redox-active metabolic toxin. It participates in four key steps of core metabolism, and metabolite profiles indicate that phosphine exposure in mutant and wild-type animals affects these steps differently. Mutation of DLD in *C. elegans* increases arsenite sensitivity. This specific vulnerability may be exploited to control phosphine-resistant insects and safeguard food security.

Extensive use of phosphine has selected for pest insects that are highly resistant (*1*–*3*), but a suitable replacement fumigant does not exist. The nematode *Caenorhabditis elegans* is also vulnerable to phosphine. We previously isolated *phosphine-resistant* (*pre*) *C. elegans* strains by ethylmethane sulfonate mutagenesis (*4*). Four independent mutants were found to survive a phosphine dose that killed 100% of wild-type N2 nematodes (Fig. 1A) and to have resistance factors >4 based on median lethal concentration (LC_{50}) values at 20°C (Fig. 1B and fig. S1) (*5*–*10*). Complementation analysis revealed that the four alleles define two complementation groups (fig. S2): *pre-7* (alleles *wr1, wr2*, and *wr3*) and *pre-33* (allele *wr4*). We localized the *C. elegans pre-7* locus to a 96-kb region on chromosome II (*10*, *11*) (fig. S3A). Genomic DNA rescue experiments revealed that a wild-type, but not a *wr3* mutant copy of one of the genes in the interval, *alh-6*, restored phosphine sensitivity to *wr3* mutants (Fig. 2A and fig. S4A). *C. elegans* subjected to RNA interference (RNAi) of *alh-6* acquired phosphine resistance (Fig. 2A and fig. S5A). Sequence analysis revealed a unique point mutation in the coding sequence of the *alh-6* gene in each of the three *pre-7* alleles (Fig. 2A and table S1).

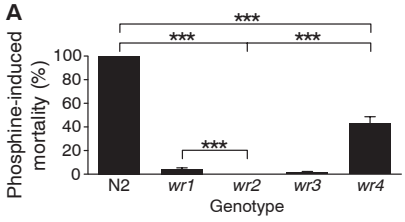
For the *pre-33(wr4)* mutant, crossing with the strain CB4856 and mapping of phosphine-resistant F_5 *C. elegans* (*10*) confined the resistance locus to a 2-Mb interval on chromosome IV (fig. S3B), and then a 475-kb region, revealing it to be a C to T transition in the *dld-1* gene (table

[1]Agri-Science Queensland, Department of Agriculture, Fisheries and Forestry, Ecosciences Precinct, Level 3C-West, GPO Box 267, Brisbane, QLD 4001, Australia. [2]School of Biological Sciences, The University of Queensland, Brisbane, QLD 4072, Australia. [3]Cooperative Research Centre for National Plant Biosecurity, LPO Box 5012, Bruce, ACT 2617, Australia. [4]School of Chemistry and Molecular Biosciences, The University of Queensland, Brisbane, QLD 4072, Australia. [5]Queensland Brain Institute, The University of Queensland, Brisbane, QLD 4072, Australia. [6]Faculty of Agriculture, The University of Nusa Cendana, Kupang, NTT 85001, Indonesia. [7]Centre for Advanced Imaging, The University of Queensland, Brisbane, QLD 4072, Australia.

*These authors contributed equally to this work.
†These authors contributed equally to this work.
‡To whom correspondence should be addressed. E-mail: p.ebert@uq.edu.au (P.R.E.); m.hilliard@uq.edu.au (M.A.H.)

Downloaded from www.sciencemag.org on November 9, 2012

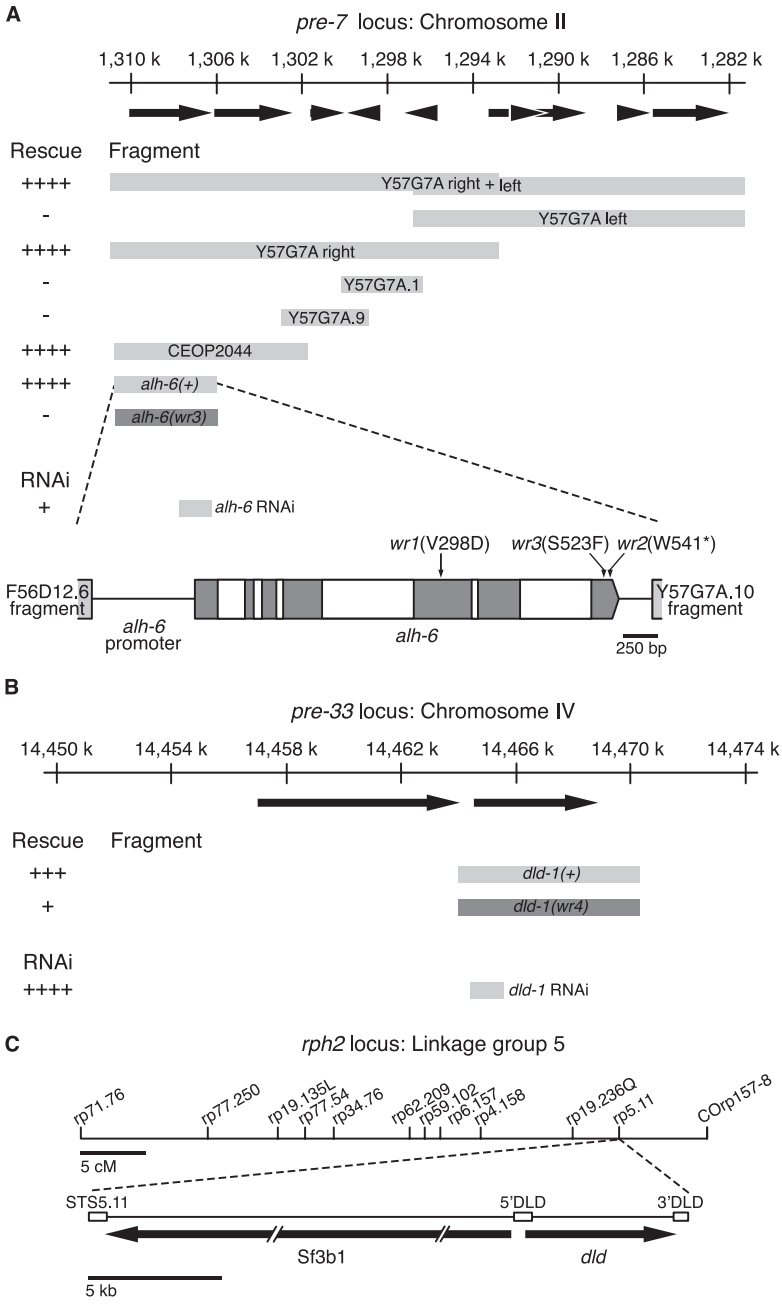
Fig. 1. Phosphine-resistant nematodes and insects. (**A**) Phosphine toxicity of the wild-type N2 *C. elegans* strain and four phosphine-resistant mutants at 2000 ppm. ***P < 0.001 (t test for proportions with Yates correction). Error bars, SEM; n = 3 population replicates. (**B**) Phosphine resistance factors of *C. elegans*, *R. dominica*, and *T. castaneum* strains relative to the LC_{50} of respective wild-type lines. *Minimum LC_{50} based on survival of discriminating dose. Superscript numbers indicate references, and S1 refers to fig. S1.



B

Species	Strain	LC_{50} resistance factor
C. elegans	N2	-[5]
C. elegans	*wr1*	>4x*
C. elegans	*wr2*	>4x*
C. elegans	*wr3*	>4x[S1]
C. elegans	*wr4*	4x[6]
R. dominica	QRD14	-[7]
R. dominica	QRD369	23.4x[7]
R. dominica	QRD569	600x[7]
R. dominica	NNRD2864	225x[8]
R. dominica	NSRD3075	100x[8]
R. dominica	QNRD345	>60x*
R. dominica	QNRD378	>60x*
R. dominica	QQRD1722	>60x*
T. castaneum	QTC4	-[9]
T. castaneum	QTC931	431x[9]

Fig. 2. Phosphine-resistance genes in *C. elegans* and *R. dominica*. (**A** and **B**) Genomic regions of the phosphine-resistance loci *pre-7* and *pre-33*, respectively. DNA fragments injected to assess rescue of the wild-type phenotype (phosphine-induced mortality) are shown; each + corresponds to ~25% increase over wild-type mortality. RNAi targets that cause resistance in N2; each + corresponds to ~25% reduction in phosphine-induced mortality. An expanded view of the *alh-6* gene is included in (A) showing the identities of the *wr1, wr2*, and *wr3* alleles. (**C**) *rph2* linkage to the marker rp5.11 on *R. dominica* linkage group 5, and the resistance-flanking markers STS5.11, 5′ DLD, and 3′DLD, and the neighboring gene, splicing factor 3b subunit 1 (Sf3b1) (*13*).



Downloaded from www.sciencemag.org on November 9, 2012

S1), which generates an A460V missense mutation in the corresponding protein (Fig. 3A and table S2). DNA rescue experiments demonstrated that a wild-type copy of *dld-1* fully restored phosphine sensitivity to *wr4* mutants (Fig. 2B and fig. S4B), and RNAi was sufficient to induce phosphine resistance in wild-type nematodes and enhance the resistance phenotype of *wr4* (Fig. 2B and fig. S5B). Both *pre* genes encode evolutionarily conserved mitochondrial enzymes: *alh-6/pre-7* encodes the *C. elegans* delta-1-pyrroline-5-carboxylate dehydrogenase (P5CDH), and *dld-1/pre-33* encodes dihydrolipoamide dehydrogenase (DLD).

Although we have not yet found direct evidence for *alh-6* orthologs being polymorphic or genetically linked to resistance in insects (12 strains analyzed), we have discovered that *dld-1* orthologs are responsible for phosphine resistance in the most common phosphine-resistant grain pests: *Rhyzopertha dominica* and *Tribolium castaneum*. We collected seven strains of *R. dominica* and one strain of *T. castaneum* from geographically independent resistance outbreaks (fig. S6) (*7*–*9*, *12*), each of which survives phosphine exposure that is 100% lethal to wild-type strains (Fig. 1B). The genetic basis of resistance is shared between the seven strains, with two major loci, *rph1* and *rph2*, responsible for strong resistance in combination (*8*, *13*) but only weak resistance when alone (*12*, *13*). Previous work identified a genetic marker, STS5.11, within ~11 kb of *rph2* (*13*). We sequenced genomic DNA of *R. dominica* and assembled the sequence around the STS5.11 locus, revealing that it included the ortholog of *dld-1* (Fig. 2C). We also identified a single base change causing a K142E substitution in DLD (Fig. 3A and fig. S7) in the highly resistant QRD569 strain of *R. dominica* compared with the sensitive QRD14 strain (table S2). The association of this polymorphism with resistance was then validated using a population of 10,000 individuals from the 90th generation (F_{90}) of a single parent cross between QRD569 and QRD14 strains. From this population, genetically heterogeneous with respect to *rph1* and *rph2*, 72 individuals survived selection for phosphine resistance. All survivors were monomorphic for the DLD K142E substitution. Two highly resistant field-collected strains (NNRD2864 and NSRD3075) (Fig. 1B and fig. S6) failed to complement QRD569 resistance (*8*). DNA sequencing of the *dld* gene from these strains, and a further three highly resistant strains of *R. dominica* (QNRD345, QNRD378, and QQRD1722) (Fig. 1B and fig. S6), revealed that each carried a unique amino acid substitution in DLD (Fig. 3A, fig. S7, and table S2).

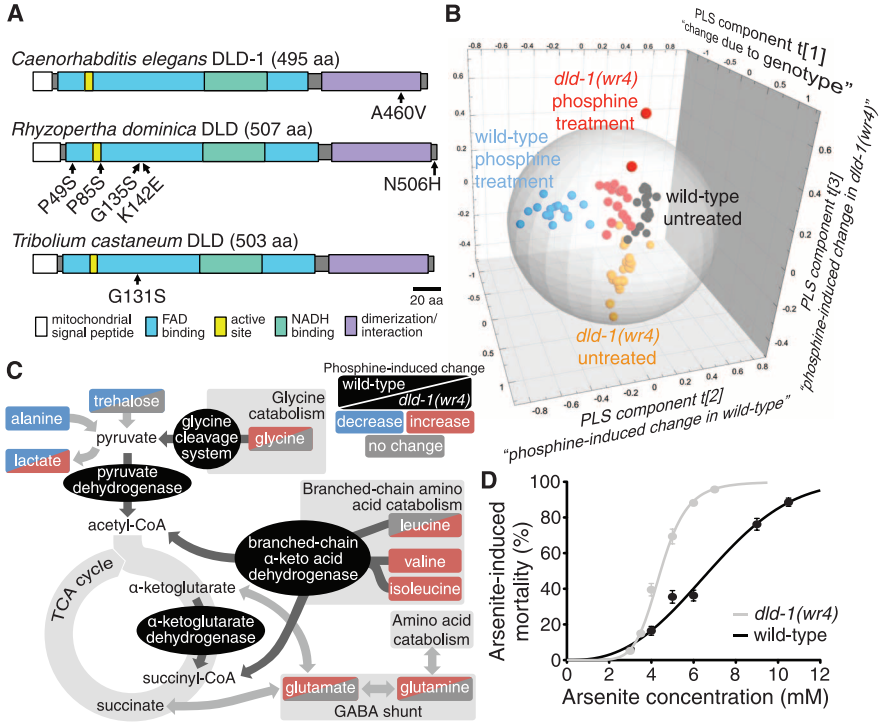


Fig. 3. Effect of *dld-1* mutations. (**A**) Representations of DLD annotated with polymorphisms found in resistant strains and predicted domains. (**B**) Partial least-squares discriminant analysis of NMR spectra from wild-type and *dld-1(wr4)* in air and after phosphine exposure. Axes are subtitled with the biological relevance of each dimension. (**C**) Pathways involving metabolites identified in (B). Colors indicate decreasing (blue) or increasing (red) metabolite levels in response to phosphine in N2 (upper left), or *dld-1(wr4)* (lower right). DLD-containing enzyme complexes are shown as black ovals, and dark arrows represent associated pathways. (**D**) Mortality of wild-type, *dld-1(wr4)*, *alh-6(wr3)*, and *dld-1(wr4)* carrying wild-type *dld*-1 transgene and nontransgenic siblings after 24 hours exposure to arsenite. Data points are weighted means from three replicates. Error bars, SEM.

In the case of *T. castaneum,* we sequenced the ortholog of DLD from cDNA of a susceptible strain (QTC4) and a highly resistant strain (QTC931) (Fig. 1B and fig. S6) (*14*). Two missense mutations were found within the *dld* coding region of the QTC931 strain, one of which was identical to the amino acid change previously identified in the *R. dominica* QQRD1722 strain (Fig. 3A and table S2). We validated the association of these polymorphisms with resistance using a population of 1552 F_{19} progeny of a single-pair intercross (QTC4×QTC931) selected for strong resistance, which requires homozygosity at both *rph1* and *rph2*. In survivors ($n = 16$ individuals), we saw absolute cosegregation of *dld* with resistance at the *rph2* locus.

The DLD protein is an obligate homodimer and an essential component of four major metabolic multienzyme complexes in mitochondria: pyruvate dehydrogenase (PDH), α-ketoglutarate dehydrogenase (KGDH), branched-chain ketoacid dehydrogenase (BCKDH), and the glycine cleavage system (GCS). DLD has a highly conserved primary sequence across phyla (table S3) (*15*). We generated homology models of the nematode and insect proteins based on human DLD (figs. S7 and S8, and table S2). The amino acid substitutions responsible for phosphine resistance in insects cluster around the disulfide catalytic center and the cavity leading to it, both of which are formed by dimerization of DLD monomers (Fig. 3A and fig. S8). The nematode mutation is located in a protein region that functions as both the DLD homodimerization interface and the interaction interface between DLD and the core proteins of the four enzyme complexes (Fig. 3A and fig. S8). Although we do not know the mode of action of phosphine, it can reduce disulfide bonds and has been suggested to react with "critically placed" disulfide bonds at vulnerable sites (*15*). The location of the resistance mutations suggests that phosphine might react with the disulfide active site of DLD.

To investigate how the *C. elegans* mutation affects the response to phosphine, we measured the metabolite profiles of wild-type and *dld-1(wr4)* nematodes in response to phosphine using nuclear magnetic resonance (NMR) spectroscopy and analyzed the profile differences with partial least-squares discriminant analysis (PLS-DA) (Fig. 3B, fig. S9, and tables S4 and S5). Exposure of wild-type and *dld-1(wr4) C. elegans* to 216 parts per million (ppm) phosphine caused changes in the metabolite profile equivalent to 12 and 6% of the total variance, respectively, indicating that the *dld-1(wr4)* mutant was less severely affected (fig. S9 and table S4). The changes in the NMR spectra caused by phosphine treatment of the wild type were almost precisely orthogonal to the same treatment in *dld-1(wr4)*, indicating that the metabolites of these two strains changed in different ways in response to phosphine (Fig. 3B and fig. S9). Metabolite changes in wild-type *C. elegans* in response to phosphine (visible in dimension t[2]) included accumulation of branched-

Downloaded from www.sciencemag.org on November 9, 2012

chain amino acids, glutamate, and glycine (Fig. 3C, fig. S9, and table S5). Accumulation of these metabolites would be expected if the KGDH, BCKDH, and GCS enzyme complexes, which contain DLD, were inhibited (Fig. 3C, fig. S9, and table S5). In agreement with the orthogonality observed in the PLS-DA (Fig. 3B and fig. S9), in *dld-1(wr4)* nematodes the metabolite changes in response to phosphine (in dimension t[3]) were different for most metabolites feeding into the KGDH, GCS, and PDH enzyme complexes, but not for BCKDH (Fig. 3C, fig. S9, and table S5).

The DLD-1 substitution in *C. elegans* is located at the interface with the E2 subunits, which are unique to each complex and have nonidentical interactions with DLD (fig. S8F), producing complex-specific effects similar to those observed in human DLD deficiencies. (*16*). In addition, extra-mitochondrial activities of DLD could further contribute to the metabolic effects of the mutation. Interestingly, resistance alleles of DLD in insects do not cause a deficiency in the metabolic activity of the enzyme (fig. S10), indicating that resistance in the field is confined to variants with low fitness effects.

It is known that mutations that perturb the *dld* gene in plants generate sensitivity to arsenic (*17*) and that an oxidized toxic form of arsenic, arsenite (AsO_2^-), interacts with the dihydro form of the lipoamide cofactor that is reoxidized by the active disulfide of DLD (*18*). Furthermore, phosphine resistance in a genetically uncharacterized insect isolate coincided with increased sensitivity to arsine (AsH_3), a reduced form of arsenic (*19*). We tested the arsenite and arsine sensitivity of *C. elegans dld-1(wr4)* mutants and found that they had an increased sensitivity to both compounds (Fig. 3D and fig. S11A). In contrast, *dld-1(wr4)* transgenic animals expressing wild-type *dld-1*, together with *alh-6(wr3)* mutants, did not show increased sensitivity to either compound (Fig. 3D and fig. S11A). Furthermore, five out of six insect strains carrying phosphine resistance substitutions also presented increased sensitivity to arsine (fig. S11, B and C).

The attribution of phosphine resistance to a *dld-1* mutation suggests a specific model to explain sensitivity to arsenic compounds: Mutations in *dld-1* that decrease electron transfer from lipoamide increase the amount of the cofactor in the reduced state, a condition that makes it susceptible to arsenite attack, resulting in termination of tricarboxylic acid cycle activity. This insight suggests that chemicals that mimic the reactivity of arsenic compounds with dihydrolipoamide will be potent phosphine synergists, and that the mutated proteins we have characterized will provide the tools to identify such compounds. Indeed, one of the most intriguing outcomes of this study is that resistance to a small redox-active gas can exhibit such metabolic specificity, despite its potentially diverse reactivity within cells.

References and Notes

1. H. Benhalima, M. Q. Chaudhry, K. A. Mills, N. R. Price, *J. Stored Prod. Res.* **40**, 241 (2004).
2. P. J. Collins, G. J. Daglish, H. Pavic, R. A. Kopittke, *J. Stored Prod. Res.* **41**, 373 (2005).
3. I. Lorini, P. J. Collins, G. J. Daglish, M. K. Nayak, H. Pavic, *Pest Manag. Sci.* **63**, 358 (2007).
4. Q. Cheng *et al.*, *Toxicol. Sci.* **73**, 60 (2003).
5. N. Valmas, P. R. Ebert, *PLoS ONE* **1**, e130 (2006).
6. S. Zuryn, J. Kuang, P. Ebert, *Toxicol. Sci.* **102**, 179 (2008).
7. P. J. Collins, G. J. Daglish, M. Bengston, T. M. Lambkin, H. Pavic, *J. Econ. Entomol.* **95**, 862 (2002).
8. Y. S. Mau, P. J. Collins, G. J. Daglish, M. K. Nayak, P. R. Ebert, *PLoS ONE* **7**, e34027 (2012).
9. R. Jagadeesan, P. J. Collins, G. J. Daglish, P. R. Ebert, D. I. Schlipalius, *PLoS ONE* **7**, e31582 (2012).
10. Materials and methods are available as supplementary materials on *Science* Online.
11. S. R. Wicks, R. T. Yeh, W. R. Gish, R. H. Waterston, R. H. A. Plasterk, *Nat. Genet.* **28**, 160 (2001).
12. Y. S. Mau *et al.*, *PLoS ONE* **7**, e31541 (2012).
13. D. I. Schlipalius *et al.*, *Heredity* **100**, 506 (2008).
14. S. Richards *et al.*; Tribolium Genome Sequencing Consortium, *Nature* **452**, 949 (2008).
15. J. Robinson, E. Bond, *J. Stored Prod. Res.* **6**, 133 (1970).
16. C. A. Brautigam, J. L. Chuang, D. R. Tomchick, M. Machius, D. T. Chuang, *J. Mol. Biol.* **350**, 543 (2005).
17. W. H. Chen, Y. J. Chi, N. L. Taylor, H. Lambers, P. M. Finnegan, *Plant Physiol.* **153**, 1385 (2010).
18. E. R. Bergquist, R. J. Fischer, K. D. Sugden, B. D. Martin, *J. Organomet. Chem.* **694**, 973 (2009).
19. M. Q. Chaudhry, N. R. Price, *Comp. Biochem. Phys. C* **99**, 41 (1991).

Acknowledgments: This work was supported by the Cooperative Research Centre for National Plant Biosecurity (CRC20080 and CRC50150) (D.I.S.); Australian Research Council (ARC) (DP0558507) and Grains Research and Development Corporation (UQ00010) (P.R.E.); National Institutes of Health (R01NS060129), National Health and Medical Research Council (PG# 569500), and ARC Future Fellowship (M.A.H.); Queensland Smart State Fellowship (H.J.S.); Australian Postgraduate Award scholarships (N.V., S.Z., and J.K.); University of Queensland Research Scholarship (Q.C., R.J., and R.K.); and AusAid scholarship (Y.S.M.). Sequence accession numbers (JX434596 to JX434608). We thank R. Tweedale, P. Bazzicalupo, and R. Tellam for comments and R. Barrero, H. Pavic, L. Bond, L. Kirszenblat, P. Mugno-Ramirez, A. Johnston, N. Mathew, and M. Mathew for technical assistance. Nematode strains provided by the *Caenorhabditis* Genetics Center, funded by the NIH National Center for Research Resources. NMR data acquired at the Queensland NMR Network and University of Queensland-Institute of Molecular Bioscience NMR facilities. Author contribution statement: N.V., L.M., A.G.T., S.Z, J.K., Q.C., M.A.H., and P.R.E. provided data and analysis for *C. elegans*. R.J., R.K., A.G.T., and D.I.S. provided data and analysis for *R. dominica* and *T. castaneum*. H.J.S., A.G., and C.A. provided metabolomics data and analysis. H.J.S. performed homology modeling. P.J.C. and M.K.N. provided insect strains and phenotype data. D.I.S., N.V., H.J.S., M.A.H., and P.R.E. drafted the manuscript.

Supplementary Materials

www.sciencemag.org/cgi/content/full/338/6108/807/DC1
Materials and Methods
Figs. S1 to S11
Tables S1 to S7
References (*20*–*29*)

21 May 2012; accepted 7 September 2012
10.1126/science.1224951

Downloaded from www.sciencemag.org on November 9, 2012

Optical Control of Protein Activity by Fluorescent Protein Domains

Xin X. Zhou,[1] Hokyung K. Chung,[1] Amy J. Lam,[1] Michael Z. Lin[1,2]*

Fluorescent proteins (FPs) are widely used as optical sensors, whereas other light-absorbing domains have been used for optical control of protein localization or activity. Here, we describe light-dependent dissociation and association in a mutant of the photochromic FP Dronpa, and we used it to control protein activities with light. We created a fluorescent light-inducible protein design in which Dronpa domains are fused to both termini of an enzyme domain. In the dark, the Dronpa domains associate and cage the protein, but light induces Dronpa dissociation and activates the protein. This method enabled optical control over guanine nucleotide exchange factor and protease domains without extensive screening. Our findings extend the applications of FPs from exclusively sensing functions to also encompass optogenetic control.

The ability to control protein activity by light is enormously beneficial for studying protein function within physiological contexts and for controlling synthetic biological systems with spatial or temporal specificity (*1*, *2*). Protein domains that naturally exhibit light-dependent conformational changes or interactions have been adapted to control other proteins (*3*–*10*). However, existing methods require exogenous cofactors (*3*) or endogenous cofactors that might vary between cells and physiological states (*11*), exhibit slow kinetics (*10*), force homodimerization (*6*, *7*), or use toxic blue light (*7*–*10*). Furthermore, strategies for optical control of a particular polypeptide require extensive screening and optimization (*7*, *9*, *12*, *13*). Here, we describe the discovery of an engineered protein interaction that is controlled by less energetic cyan light and requires no cofactors. We use this light-controlled association to develop a simple generalizable design for light-inducible proteins.

Dronpa is a monomeric fluorescent protein (FP) derived from a tetrameric parent (*14*). Fluorescence of Dronpa switches off under cyan light

[1]Department of Bioengineering, Stanford University, Stanford, CA 94305, USA. [2]Department of Pediatrics, Stanford University, Stanford, CA 94305, USA.

*To whom correspondence should be addressed. E-mail: mzlin@stanford.edu

(~500 nm) and switches on under violet light (~400 nm) (*14*). With off-photoswitching, β strand 7 near the chromophore becomes flexible (*15*); this strand forms part of the cross-dimer interface in the tetrameric parent (*15*). A Dronpa mutant with Lys^{145} on β strand 7 changed to Asn (Dronpa145N) is tetrameric at low micromolar concentrations, but dilution promotes monomerization and facilitates off-photoswitching (*16*). This suggests that multimerization inhibits conformation changes associated with off-photoswitching. We hypothesized, conversely, that conformation changes occurring during off-photoswitching might promote monomerization, whereas on-photoswitching might promote multimerization (Fig. 1A).

To determine if light could control Dronpa145N multimerization, we performed native polyacrylamide gel electrophoresis (PAGE) (see supplementary materials and methods). Dronpa145N was tetrameric at concentrations from 10 to 100 μM in the initial bright state, whereas wild-type Dronpa (Dronpa145K for clarity; K, Lys) was monomeric (fig. S1A). Cyan illumination of 100 μM Dronpa145N induced a shift from cyan-absorbing to violet-absorbing species (Fig. 1C) and a loss of green fluorescence (fig. S1B), as previously described (*14*). Simultaneously, Dronpa145N redistributed from tetrameric toward monomeric species (Fig. 1B, lane 2), implying that off-photoswitched Dronpa145N has a dissociation constant exceeding 100 μM. Violet light restored cyan absorbance (Fig. 1C) and green fluorescence (fig. S1B) and also induced retetramerization (Fig. 1B, lane 3), indicating that monomerization was not due to irreversible protein damage. These results show that Dronpa145N interactions can be controlled by light.

A dimer-to-monomer conversion might be more easily harnessed to control protein activity than a tetramer-to-monomer conversion. Given the lack of multimerization of Dronpa 145K, we explored whether oligomerization of Dronpa145K and Dronpa145N could be limited to dimerization. To achieve high effective concentrations of Dronpa145K and Dronpa145N without driving Dronpa145N tetramerization, we fused Dronpa145K in tandem to Dronpa145N via a linker (K-N tandem dimer) (Fig. 1D). The effective concentration of one domain relative to another on the same polypeptide has been estimated at ~70 μM (*17*). The K-N construct migrated in native PAGE primarily as expected for a tandem dimer (Fig. 1E). If the Dronpa domains were engaged in light-sensitive intramolecular interaction, illumination should induce dissociation, resulting in a more elongated faster-migrating conformation. Indeed, the tandem dimer migrated faster after cyan illumination, and this process was reversed after violet light–induced recovery (Fig. 1E). Expected transitions between cyan- and violet-absorbing forms were again observed (Fig. 1F and fig. S1C). Thus, the K-N tandem dimer undergoes reversible light-induced conformational changes consistent with dissociation and reassociation of Dronpa domains.

To determine whether light-induced Dronpa145N dissociation could occur in mammalian cells, we created two fusions: N-CAAX, a fusion of Dronpa145N to the membrane-anchoring K-Ras C-terminal farnesylation motif (CAAX box), and mNeptune-N, a fusion of the far-red FP mNeptune to Dronpa145N (Fig. 2A) (*18*). Upon 10-fold relative overexpression of N-CAAX to insure an excess of membrane-localized Dronpa, some mNeptune-N was membrane-bound through Dronpa145N oligomerization (Fig. 2, C and D). Cyan light switched off Dronpa fluorescence (Fig. 2B) and resulted in the release of mNeptune from the membrane (Fig. 2, C and D). Release required prolonged exposures (2 min, metal halide lamp at 100% neutral density through a 40× 1.2–numerical aperture lens) and was only partial, but nevertheless indicated that light could induce Dronpa domain dissociation in cells.

To find conditions for Dronpa domain dissociation that require less light, we explored Dronpa145K-Dronpa145N heterodimerization (Fig. 2E). Dronpa145K-CAAX (K-CAAX) was able to recruit mNeptune-N to the membrane (Fig. 2G). Off-photoswitching of membrane fluorescence was faster than with N-CAAX (Fig. 2F), and release of mNeptune required only 20 s of illumination (Fig. 2, G and H). On-photoswitching

Downloaded from www.sciencemag.org on November 9, 2012

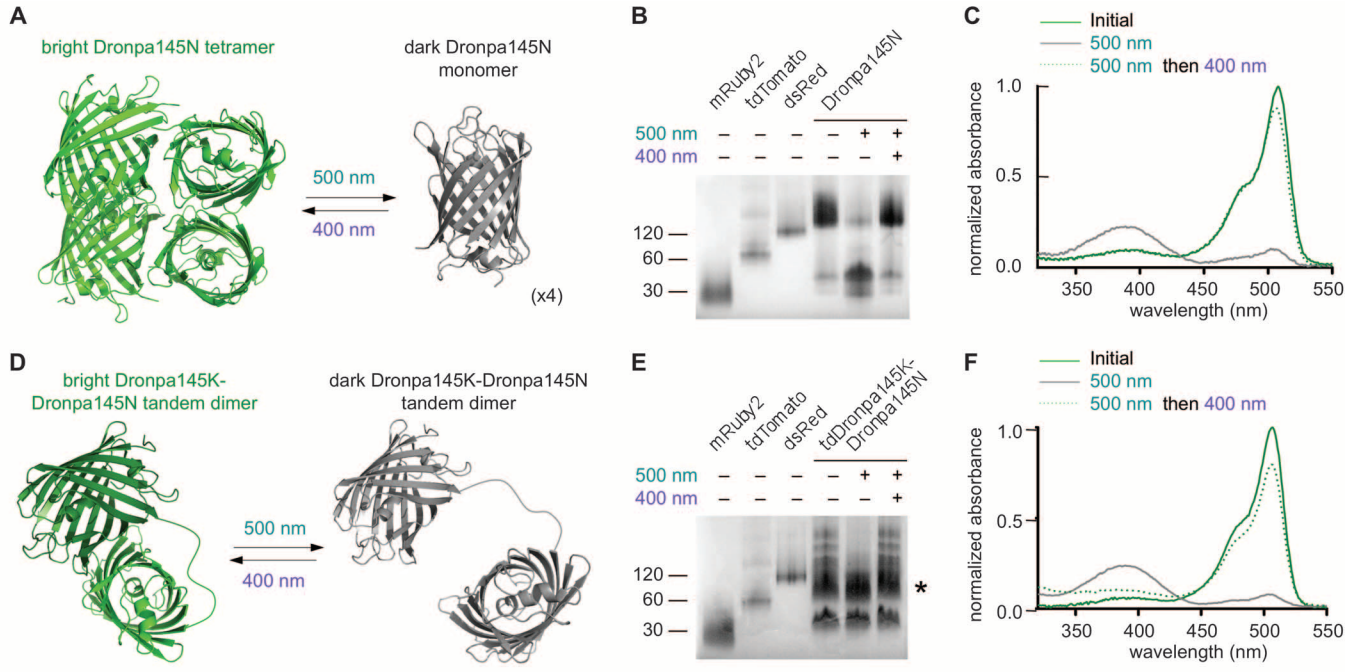


Fig. 1. Control of photochromic FP domain association by light. (**A**) Hypothesized bidirectional control of Dronpa145N oligomerization state by 500-nm cyan and 400-nm violet light. (**B**) Native PAGE of Dronpa145N (100 μM) demonstrated 500-nm–induced dissociation and 400-nm–induced retetramerization. mRuby2 (*31*), tdTomato, and dsRed2 (20 μM) served as monomeric, dimeric, and tetrameric standards, respectively. All proteins were polyhistidine-tagged at the NT. (**C**) Absorbance spectra confirm reversible photoswitching. (**D**) Hypothesized bidirectional conformational switching by light in a Dronpa145K-Dronpa145N (K-N) tandem dimer. (**E**) Native PAGE of the K-N tandem dimer demonstrated faster migration by the K-N tandem dimer (100 μM) after 500-nm light, an effect reversed by 400-nm light. The asterisk marks the location expected for tandem dimer migration, similar to tdTomato. Some cleavage of the tandem dimer to a monomer in this protein preparation was apparent. (**F**) Absorbance spectra of K-N tandem dimers confirm reversible photoswitching.

of Dronpa by violet light induced membrane relocalization of mNeptune-N (Fig. 2, G and H). Reversing the positions of Dronpa domains by expressing N-CAAX and mNeptune-Dronpa145K (mNeptune-K) did not result in membrane mNeptune signal (fig. S2A), perhaps because tetramerization between concentrated N-CAAX molecules outcompeted weaker heterodimerization with mNeptune-K. Use of only monomeric Dronpa domains (K-CAAX and mNeptune-K) also resulted in no membrane mNeptune (fig. S2B), as expected.

We hypothesized that we could use Dronpa to build light-controllable single-chain proteins. Specifically, we hypothesized that protein functions could be blocked by fusing Dronpa domains to the amino terminus (NT) and the carboxyl terminus (CT) (fig. S3A). Binding of the two Dronpa domains would "cage" the protein in an inactive state by masking surfaces required for binding interaction partners or substrates, similarly to autoinhibition of many kinases (*19*), transcription factors (*20*), and guanine nucleotide exchange factors (GEFs) for monomeric guanosine triphosphatases (GTPases) (*21*). Protein function could then be induced by light-mediated dissociation of the Dronpa domains (fig. S3A).

We first controlled the Cdc42 GEF intersectin, which can be inactivated by terminal circularization (*22*). We fused Dronpa145K or Dronpa145N at the NT of the intersectin Dbl homology (DH) domain and Dronpa145N at the CT followed by the CAAX sequence, creating K-I-N-CAAX and N-I-N-CAAX (fig. S3B). As catalytically active controls, we fused Dronpa145K to either side of intersectin (K-I-CAAX and I-K-CAAX) (fig. S3B). We coexpressed these constructs in fibroblasts with a mNeptune-fascin reporter to mark filopodia and lamellipodia (*23*). I-K-CAAX or K-I-CAAX robustly induced filopodia and lamellipodia (fig. S3, C and D), as expected for Cdc42 activation, which induces filopodia directly and lamellipodia directly via the formin-family protein FMNL2 (*24*) and indirectly via Rac (*25*). Cells expressing N-I-N-CAAX and K-I-N-CAAX produced filopodia or lamellipodia at much lower frequencies than I-K-CAAX or K-I-CAAX (fig. S3, C and D). These experiments were performed by transient transfection, which results in variable expression levels. When designated as low, medium, or high expressers by Dronpa fluorescence (fig. S4, A and C), low expressers, which included the majority of cells, exhibited basal filopodia or lamellipodia infrequently (0% for N-I-N-CAAX and 8% for K-I-N-CAAX) (fig. S4, B and D). Thus, fusion of flanking Dronpa domains cages intersectin activity effectively as long as higher expression levels are avoided, similar to phototropin-based photoactivable Rac (PA-Rac) (*26*).

We next asked whether caged intersectins could mediate filopodia or lamellipodia induction by light (Fig. 3, A and E). Illumination with 490/20-nm light for 30 s switched off more than 50% of the fluorescence in both N-I-N-CAAX– and K-I-N-CAAX–transfected fibroblasts (Fig. 3, B and F). This light dose induced abundant filopodia formation within 30 min in 78% of cells expressing N-I-N-CAAX (Fig. 3C and fig. S5D). This response was light-dependent, as only 10% of cells expressing N-I-N-CAAX formed filopodia in the same time interval without illumination ($P < 0.0001$ by Pearson χ^2 test) (fig. S5, A and D). Cells continued to exhibit filopodial mobility throughout 1 hour of observation and did not show blebbing that might indicate phototoxicity

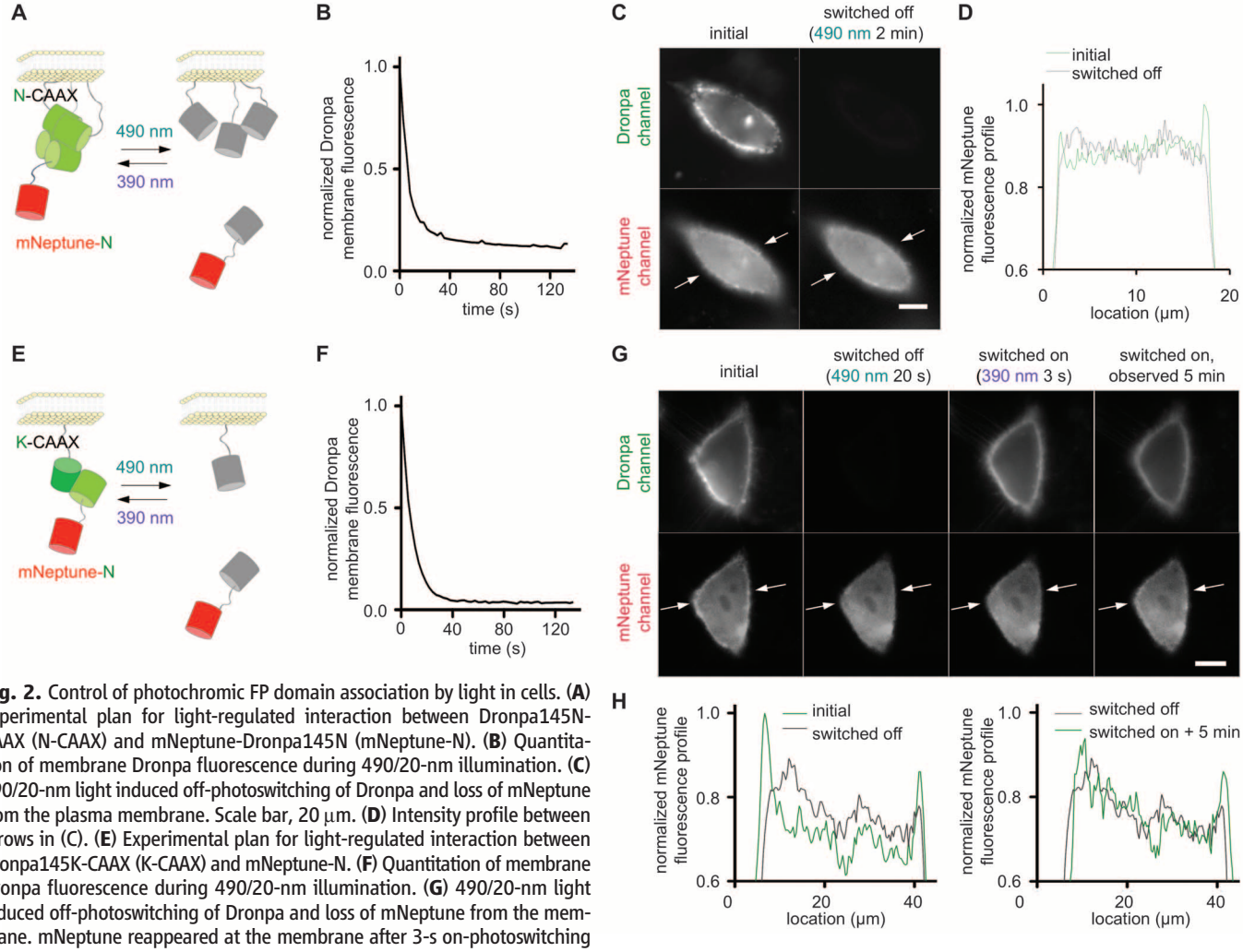


Fig. 2. Control of photochromic FP domain association by light in cells. (**A**) Experimental plan for light-regulated interaction between Dronpa145N-CAAX (N-CAAX) and mNeptune-Dronpa145N (mNeptune-N). (**B**) Quantitation of membrane Dronpa fluorescence during 490/20-nm illumination. (**C**) 490/20-nm light induced off-photoswitching of Dronpa and loss of mNeptune from the plasma membrane. Scale bar, 20 μm. (**D**) Intensity profile between arrows in (C). (**E**) Experimental plan for light-regulated interaction between Dronpa145K-CAAX (K-CAAX) and mNeptune-N. (**F**) Quantitation of membrane Dronpa fluorescence during 490/20-nm illumination. (**G**) 490/20-nm light induced off-photoswitching of Dronpa and loss of mNeptune from the membrane. mNeptune reappeared at the membrane after 3-s on-photoswitching with 390/15-nm light. Scale bar, 20 μm. (**H**) Intensity profiles between arrows in (G).

Downloaded from www.sciencemag.org on November 9, 2012

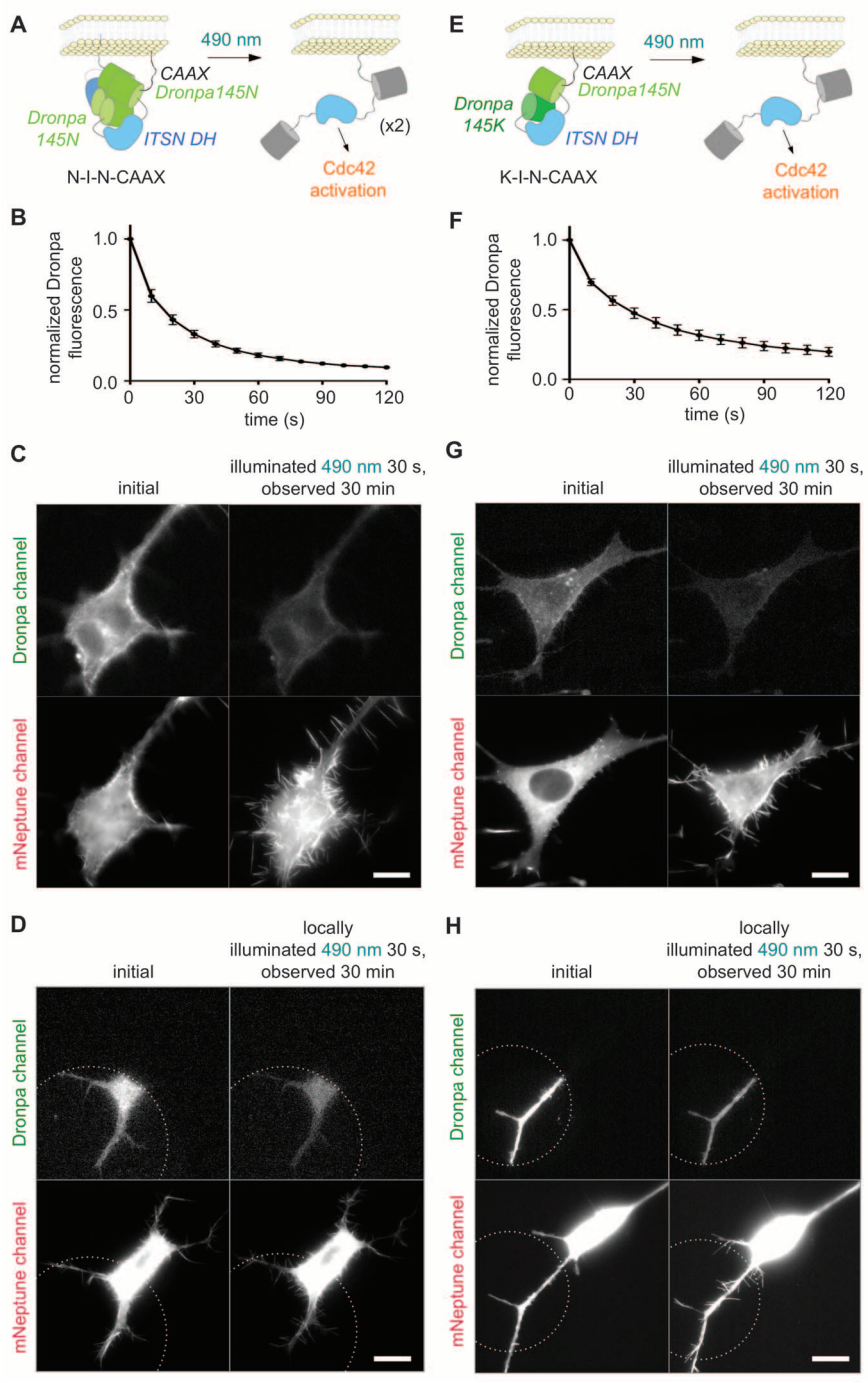


Fig. 3. A light-inducible single-chain GEF. (**A**) Proposed mechanism for photo-uncaging of N-I-N-CAAX activity. ITSN, intersectin. (**B**) Off-photoswitching of Dronpa fluorescence in N-I-N-CAAX versus 490/20-nm light dosage during microscopy. Whole-cell fluorescence results from five cells were quantified and normalized to the initial value. Error bars represent SD. (**C**) In NIH 3T3 cells expressing N-I-N-CAAX, 490/20-nm illumination for 30 s (off-switching) followed by incubation at 37°C for 30 min resulted in robust induction of filopodia, as revealed by mNeptune-Fascin. (**D**) Local illumination by 490/20-nm light locally induced filopodia, marked by mNeptune-fascin, in NIH 3T3 cells expressing N-I-N-CAAX. The dotted curves indicate the area of illumination. (**E**) Proposed mechanism for photo-uncaging of K-I-N-CAAX activity. (**F**) Off-photoswitching of Dronpa fluorescence in K-I-N-CAAX versus 490/20-nm light dosage during microscopy. The experiment was performed as in (B). (**G**) In NIH 3T3 cells expressing K-I-N-CAAX, exposure to 490/20-nm light for 30 s (off-switching) followed by incubation at 37°C for 30 min resulted in robust induction of filopodia. (**H**) Local illumination by 490/20-nm light locally induced filopodia, marked by mNeptune-fascin, in NIH 3T3 cells expressing K-I-N-CAAX. The dotted curves indicate the area of illumination. Scale bars in (C), (D), (G), and (H), 20 μm.

(movie S1). Similarly, 90% of cells expressing K-I-N-CAAX formed abundant filopodia within 30 min after illumination (Fig. 3G, fig. S5D, and movie S2), compared with 25% not exposed to light ($P < 0.0001$ by Pearson χ^2 test) (fig. S5, B and D). Illumination of K-CAAX–expressing cells did not induce filopodia (fig. S5, C and D), confirming that the effect is not due to light alone. These results demonstrate that a protein caged by Dronpa fusion can be uncaged by light.

We investigated whether caged intersectin constructs could control filopodia formation with spatial or temporal specificity. First, we performed local illumination (490/20-nm light for 30 s) to portions of cells expressing N-I-N-CAAX or K-I-N-CAAX and observed that filopodia appeared specifically in the illuminated regions (Fig. 3, D and H). We next tested whether light could induce filopodia in different locations at different times in one cell. We applied a 30-s uncaging pulse of cyan light at one subcellular region, a 3-s global recaging pulse of violet light, and finally another 30-s uncaging pulse at a different subcellular region. After the first uncaging pulse, filopodia appeared in the first region, whereas after the global recaging and second uncaging pulse, filopodia appeared in the second region simultaneous with retraction in the first region (fig. S6).

Whether Cdc42 activation can lengthen existing filopodia has been unclear, as Cdc42 effectors that promote filopodia extension rather than initiation have not been found. Rapid induction of intersectin activity by light allowed us to address this question. We observed that photo-uncaging of intersectin caused lengthening of many preexisting filopodia (fig. S7). This suggests that models in which Cdc42 governs only filopodia initiation are incomplete (*27*) and that effectors may exist that promote filopodia extension analogous to how FMNL2 promotes lamellipodia extension downstream of Cdc42 (*24*),

An attractive feature of our design is potential generalizability. Other methods for optical control of single polypeptides, such as fusion to xanthopsin or phototropin, require extensive screening to achieve coupling of light-induced conformational changes to protein activation and, thus, have been applied to only a few targets (*7*, *9*, *13*). Our caged protein design does not require precise linkages; therefore, it should be more easily generalizable. Proteases are a class of enzymes for which light activation has not yet been achieved. Unlike GTPases or kinases, proteases are not naturally regulated by membrane recruitment, preventing the use of reversible membrane targeting methods to control them. Hence, we investigated whether we could create a light-inducible protease by fusion to Dronpa domains. We chose to regulate the hepatitis C virus (HCV) NS3-4A protease because its high sequence specificity and lack of overt toxicity allows assessment of function in mammalian cells (*28*). Furthermore, it is composed predominantly of β strands and loops (*29*), providing a structural contrast to the completely α-helical DH domain (*30*).

Downloaded from www.sciencemag.org on November 9, 2012

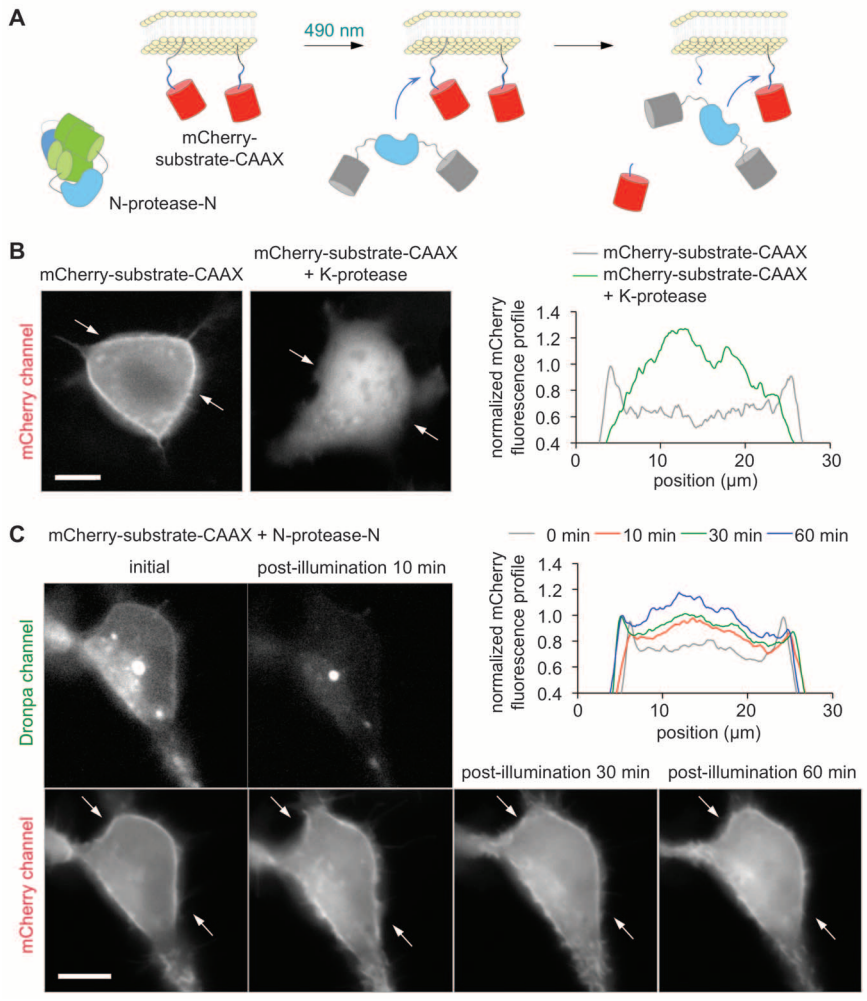


Fig. 4. A light-inducible single-chain protease. (**A**) Strategy for sensing activity of the N-protease-N protein with mCherry-substrate-CAAX. (**B**) Distribution of mCherry in cells expressing mCherry-substrate-CAAX in the absence (left) or presence (middle) of cotransfected K-protease. The chart at right shows the fluorescence intensity profile along the line between the arrows in the images. (**C**) As expected from its size (81 kD), N-protease-N was excluded from the nucleus (left). 490/20-nm light for 15 s induced off-photoswitching of Dronpa fluorescence (Dronpa channel) and induced release of mCherry from the membrane (mCherry channel). The chart at right shows the intensity profile along the line between the arrows in the images, which confirmed that mCherry fluorescence decreases from the membrane and increases in the cytosol and nucleus after illumination. Scale bars in (B) and (C), 20 μm.

We constructed a Dronpa145N-protease-Dronpa145N fusion (N-protease-N) and, as a protease reporter, a fusion of mCherry, the NS4A/NS4B cleavage site of HCV polypeptide, and the CAAX-box farnesylation signal (mCherry-substrate-CAAX) (Fig. 4A). We expected that mCherry fluorescence would be released from the membrane into the cytosol by protease activity. Indeed, mCherry signal was membrane-bound in cells expressing mCherry-substrate-CAAX alone and cytoplasmic in cells coexpressing a positive control Dronpa145K-protease (Fig. 4B). We then used mCherry-substrate-CAAX to report light induction of N-protease-N. After off-switching of Dronpa fluorescence, cells showed an increase in cytosolic mCherry within 10 min, which continued to increase over 60 min (Fig. 4C). This response required illumination (fig. S8A) and protease (fig. S8B). Thus, the caged protein design can be used to control an enzyme domain that is not easily regulated by relocalization within the cell.

Since their discovery, FPs have seen widespread use exclusively as sensing tools. We discovered that photochromic FPs can have dual identities as optical sensors and light-controlled actuators. We have translated this discovery into a simple design for optically controllable proteins, which we propose to call FLIPs, for fluorescent light-inducible proteins. FLIPs also serve as their own reporters, as the photochromic FP domains report both protein localization and activity state. Thus, our results place photochromic FPs in a distinct central location in the optogenetic toolbox, integrating both sensing and controlling functions in a single protein class.

References and Notes

1. U. Krauss, T. Drepper, K. E. Jaeger, *Chemistry* **17**, 2552 (2011).
2. C. W. Riggsbee, A. Deiters, *Trends Biotechnol.* **28**, 468 (2010).
3. A. Levskaya, O. D. Weiner, W. A. Lim, C. A. Voigt, *Nature* **461**, 997 (2009).
4. S. Shimizu-Sato, E. Huq, J. M. Tepperman, P. H. Quail, *Nat. Biotechnol.* **20**, 1041 (2002).
5. A. B. Tyszkiewicz, T. W. Muir, *Nat. Methods* **5**, 303 (2008).
6. M. J. Kennedy *et al.*, *Nat. Methods* **7**, 973 (2010).
7. H. Y. Fan *et al.*, *Biochemistry* **50**, 1226 (2011).
8. D. Strickland, K. Moffat, T. R. Sosnick, *Proc. Natl. Acad. Sci. U.S.A.* **105**, 10709 (2008).
9. Y. I. Wu *et al.*, *Nature* **461**, 104 (2009).
10. M. Yazawa, A. M. Sadaghiani, B. Hsueh, R. E. Dolmetsch, *Nat. Biotechnol.* **27**, 941 (2009).
11. H. J. Powers, B. M. Corfe, E. Nakano, *Subcell. Biochem.* **56**, 229 (2012).
12. A. Möglich, K. Moffat, *Photochem. Photobiol. Sci.* **9**, 1286 (2010).
13. D. Strickland *et al.*, *Nat. Methods* **7**, 623 (2010).
14. R. Ando, H. Mizuno, A. Miyawaki, *Science* **306**, 1370 (2004).
15. H. Mizuno *et al.*, *Proc. Natl. Acad. Sci. U.S.A.* **105**, 9227 (2008).
16. H. Mizuno *et al.*, *Photochem. Photobiol. Sci.* **9**, 239 (2010).
17. J. Müller, N. Johnsson, *ChemBioChem* **9**, 2029 (2008).
18. M. Z. Lin *et al.*, *Chem. Biol.* **16**, 1169 (2009).
19. T. A. Leonard, J. H. Hurley, *Cell* **129**, 1037 (2007).
20. M. A. Pufall, B. J. Graves, *Annu. Rev. Cell Dev. Biol.* **18**, 421 (2002).
21. B. Yu *et al.*, *Cell* **140**, 246 (2010).
22. B. J. Yeh, R. J. Rutigliano, A. Deb, D. Bar-Sagi, W. A. Lim, *Nature* **447**, 596 (2007).
23. J. C. Adams, *Curr. Opin. Cell Biol.* **16**, 590 (2004).
24. J. Block *et al.*, *Curr. Biol.* **22**, 1005 (2012).
25. T. Nishimura *et al.*, *Nat. Cell Biol.* **7**, 270 (2005).
26. Y. I. Wu, X. Wang, L. He, D. Montell, K. M. Hahn, *Methods Enzymol.* **497**, 393 (2011).
27. J. Faix, D. Breitsprecher, T. E. Stradal, K. Rottner, *Int. J. Biochem. Cell Biol.* **41**, 1656 (2009).
28. M. Z. Lin, J. S. Glenn, R. Y. Tsien, *Proc. Natl. Acad. Sci. U.S.A.* **105**, 7744 (2008).
29. K. P. Romano, A. Ali, W. E. Royer, C. A. Schiffer, *Proc. Natl. Acad. Sci. U.S.A.* **107**, 20986 (2010).
30. J. T. Snyder *et al.*, *Nat. Struct. Biol.* **9**, 468 (2002).
31. A. J. Lam *et al.*, *Nat. Methods* **9**, 1005 (2012).

Acknowledgments: We thank M. Davidson (Florida State University) for pcDNA3-mNeptune-Fascin, N. Shaner and R. Tsien (University of California San Diego) for pBAD-tdTomato, M. Yazawa and R. Dolmetsch (Stanford University) for cell lines and advice, Y. Geng in the Lin laboratory for assistance with plasmid design, and other members of the Lin laboratory. This work was funded by the Stanford School of Engineering and a Stanford Graduate Fellowship (X.X.Z.); a Siebel Foundation Scholarship (A.J.L.); and the Lucille Packard Children's Health Initiative, a Burroughs Wellcome Career Award for Medical Scientists, and NIH grant R01NS076860 (M.Z.L.). M.Z.L. is a Rita Allen Foundation Scholar. X.X.Z. and M.Z.L. are inventors on a patent application filed by Stanford University covering the construct design described in the paper. X.X.Z. designed, executed, and analyzed experiments and cowrote the manuscript. H.K.C. designed, executed, and analyzed experiments. A.J.L. assisted with experimental design. M.Z.L. conceived of the study, directed the project, provided advice, analyzed experiments, and cowrote the manuscript.

Supplementary Materials

www.sciencemag.org/cgi/content/full/338/6108/810/DC1
Materials and Methods
Figs. S1 to S8
References
Movies S1 and S2

2 July 2012; accepted 18 September 2012
10.1126/science.1226854

Downloaded from www.sciencemag.org on November 9, 2012

Intramitochondrial Transport of Phosphatidic Acid in Yeast by a Lipid Transfer Protein

Melanie Connerth,[1]* Takashi Tatsuta,[1]* Mathias Haag,[1]* Till Klecker,[2] Benedikt Westermann,[2] Thomas Langer[1,3]†

Mitochondria are dynamic organelles whose function depends on intramitochondrial phospholipid synthesis and the supply of membrane lipids from the endoplasmic reticulum. How phospholipids are transported to and in-between mitochondrial membranes remained unclear. We identified Ups1, a yeast member of a conserved family of intermembrane space proteins, as a lipid transfer protein that can shuttle phosphatidic acid between mitochondrial membranes. Lipid transfer required the dynamic assembly of Ups1 with Mdm35 and allowed conversion of phosphatidic acid to cardiolipin in the inner membrane. High cardiolipin concentrations prevented membrane dissociation of Ups1, leading to its proteolysis and inhibiting transport of phosphatidic acid and cardiolipin synthesis. Thus, intramitochondrial lipid trafficking may involve a regulatory feedback mechanism that limits the accumulation of cardiolipin in mitochondria.

Each cellular membrane has a characteristic lipid composition that is required for its function (*1*, *2*). Phospholipids are synthesized predominantly in the endoplasmic reticulum (ER) and must be redistributed to all cellular membranes (*3*). Extensive exchange of phospholipids between the ER and mitochondria is important in the synthesis of specific lipids (*4*, *5*). These include cardiolipin (CL), a signature phospholipid of mitochondrial membranes, which is required for mitochondrial function and morphogenesis (*5*). CL is synthesized along an enzymatic cascade in the mitochondrial inner membrane (IM) from phosphatidic acid (PA) that is imported from the ER (Fig. 1A). However, how phospholipids shuttle from the ER to mitochondria, across the outer membrane (OM) to the IM and back, is not understood.

In yeast, Ups1 and Ups2, members of the conserved MSF1′/PRELI protein family localized in the mitochondrial intermembrane space (IMS),

[1]Institute for Genetics, Cologne Excellence Cluster on Cellular Stress Responses in Aging-Associated Diseases (CECAD), Center for Molecular Medicine (CMMC), University of Cologne, 50674 Cologne, Germany. [2]Institute for Cell Biology and Electron Microscopy Laboratory, University of Bayreuth, 95440 Bayreuth, Germany. [3]Max-Planck-Institute for Biology of Aging, 50931 Cologne, Germany.

*These authors contributed equally to this work.
†To whom correspondence should be addressed. E-mail: thomas.langer@uni-koeln.de

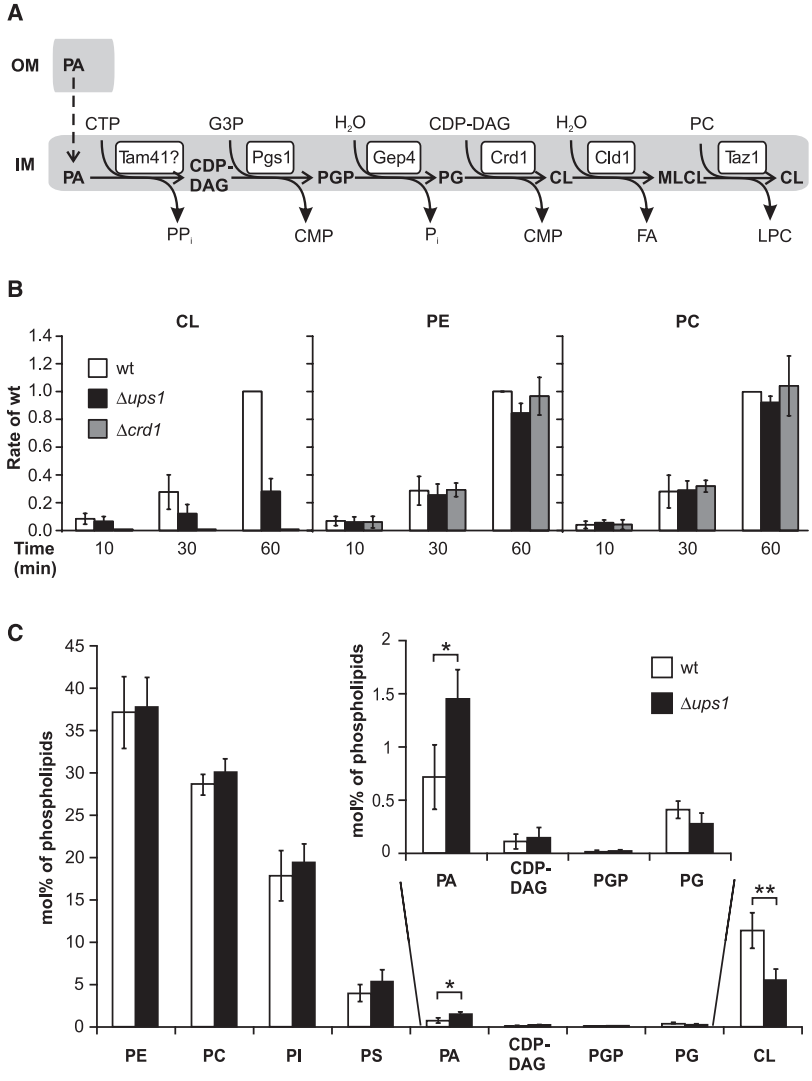


Fig. 1. CL synthesis in Δ*ups1* mitochondria. (**A**) Enzymatic cascade mediating CL synthesis. The function of Tam41 at early stages of CL synthesis is unclear. MLCL, monolysocardiolipin; LPC, lysophosphatidylcholine; G3P, glycerol-3-phosphate; FA, fatty acid; CMP, cytidine 5′-monophosphate; CTP, cytidine 5′-triphosphate; P_i, inorganic phosphate; PP_i, inorganic pyrophosphate. Other abbreviations are used as in the text. (**B**) Impaired CL synthesis in Δ*ups1* mitochondria. Incorporation of ^{32}P into CL, PE, or PC was monitored at the indicated times in wild-type (wt), Δ*ups1*, and Δ*crd1* cells. ^{32}P incorporation in wt was set to 1. (**C**) Phospholipidome of sucrose gradient–purified wt and Δ*ups1* mitochondria determined by MS. Data represent mean values ± SD, $n = 4$: $^*P < 0.05$, $^{**}P < 0.005$ (unpaired *t* test, two-tailed).

Downloaded from www.sciencemag.org on November 9, 2012

are required for the mitochondrial accumulation of CL and phosphatidylethanolamine (PE), respectively (*6*, *7*). Incorporation of ^{32}P into CL was impaired in Δ*ups1* mitochondria and completely inhibited in the absence of the cardiolipin synthase Crd1 (Fig. 1B). To define the role of Ups1 in CL synthesis, we determined the phospholipidome of Δ*ups1* mitochondria by quantitative mass spectrometry (MS) (Fig. 1C). CL was reduced in Δ*ups1* mitochondria, whereas other main phospholipids remained unaffected (Fig. 1C and fig. S1) (*6*, *8*). The low-abundance precursor phospholipid PA accumulated in these mitochondria (Fig. 1C), suggesting that Ups1 acts early during CL synthesis.

To substantiate this conclusion, we performed a genetic epistasis analysis of *UPS1* with genes affecting early steps of CL synthesis such as *PGS1* and *TAM41*. Pgs1 catalyzes the formation of phosphatidylglycerolphosphate (PGP) (*9*, *10*), whereas Tam41 acts before Pgs1, exerting an unknown function (*11*–*13*). Cell growth was severely impaired upon deletion of *PGS1*, *TAM41*, or both, but restored upon deletion of *UPS1* (Fig. 2A and fig. S2). Ultrastructurally, mitochondria lacking Pgs1 contained extremely elongated cristae sheets, which remained connected to the inner boundary membrane and frequently formed IM septae or onionlike structures (Fig. 2B). Deletion of *UPS1* did not affect the mitochondrial ultrastructure but restored mitochondrial cristae morphology in Δ*pgs1* cells (Fig. 2B).

We further determined by MS the mitochondrial phospholipidome of cells lacking Ups1 in combination with Pgs1 or Tam41 (Fig. 2C and fig. S3). CL was reduced or absent in mitochondria lacking either protein, but PA, phosphatidylinositol (PI), and cytidine 5′-diphosphate-diacylglycerol (CDP-DAG) accumulated in mitochondria lacking Pgs1 (Fig. 2C and fig. S3). Thus, the different membrane lipid composition rather than merely the absence of CL affects cristae morphology in Δ*pgs1* mitochondria. Deletion of *TAM41* resulted in accumulation of PA but not CDP-DAG, suggesting that Tam41 affects CDP-DAG synthesis (Fig. 2C). The phospholipid composition of Pgs1- and Tam41-deficient mitochondria lacking Ups1 was similar to that of Δ*ups1* mitochondria. Thus, Ups1 is epistatic to Pgs1 and Tam41.

The requirement of Ups1 in the IM for early steps of CL synthesis suggests that Ups1 may facilitate the transport of PA to the IM (Fig. 1A). To define the molecular function of Ups1, we carried out in vitro experiments with purified Ups1. Ups1 assembles with Mdm35, which ensures its accumulation in the IMS and protects Ups1 against degradation by Yme1 (*14*). Consistently, Ups1 was prone to aggregation upon expression in *Escherichia coli* and recovered in the soluble fraction only when coexpressed with Mdm35 (fig. S4). This allowed purification of heterodimeric Ups1-Mdm35 complexes to homogeneity (fig. S5).

To examine whether Ups1-Mdm35 binds phospholipids, we performed flotation experiments using liposomes composed of phosphatidylcholine (PC) (80%) and another phospholipid (20%) (Fig. 3A). Ups1 exclusively bound to liposomes containing negatively charged phospholipids such as CL, PA, phosphatidylglycerol (PG), phosphatidylserine (PS), PI, or CDP-DAG but did not interact with PE or PC (Fig. 3, A and B). Purified Mdm35 did not bind any phospholipid tested (fig. S6), suggesting liposome binding via Ups1. The low amount of Mdm35 recovered with floated membranes in the presence of Ups1 indicated that liposome binding destabilizes Ups1-Mdm35 complexes (Fig. 3B).

Next, we investigated whether the Ups1-Mdm35 complex transfers phospholipids between liposomes in vitro. Donor liposomes, whose lipid composition resembles that of the OM, were

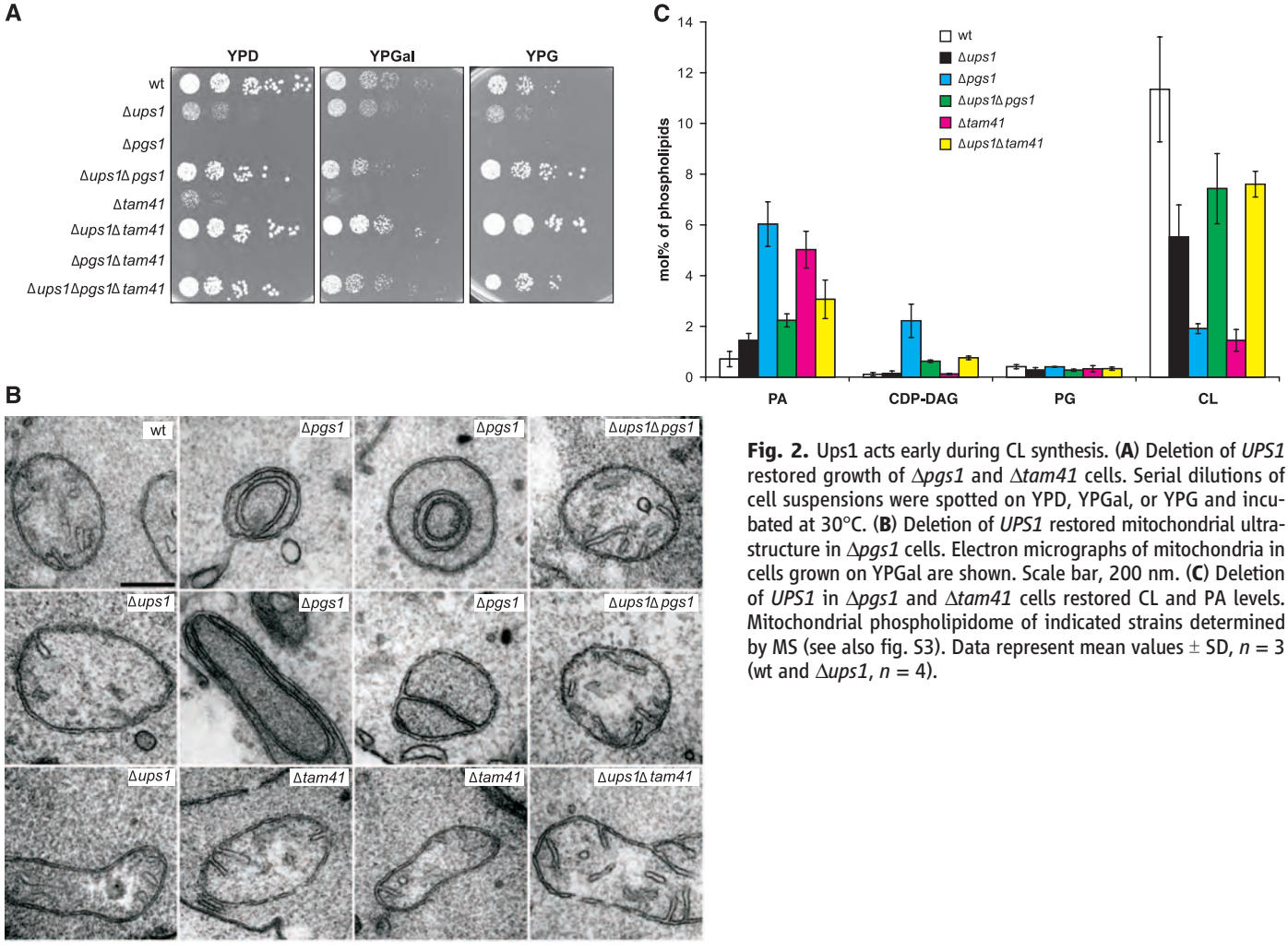


Fig. 2. Ups1 acts early during CL synthesis. (**A**) Deletion of *UPS1* restored growth of Δ*pgs1* and Δ*tam41* cells. Serial dilutions of cell suspensions were spotted on YPD, YPGal, or YPG and incubated at 30°C. (**B**) Deletion of *UPS1* restored mitochondrial ultrastructure in Δ*pgs1* cells. Electron micrographs of mitochondria in cells grown on YPGal are shown. Scale bar, 200 nm. (**C**) Deletion of *UPS1* in Δ*pgs1* and Δ*tam41* cells restored CL and PA levels. Mitochondrial phospholipidome of indicated strains determined by MS (see also fig. S3). Data represent mean values ± SD, $n = 3$ (wt and Δ*ups1*, $n = 4$).

Downloaded from www.sciencemag.org on November 9, 2012

incubated with Ups1-Mdm35 complexes and acceptor liposomes resembling the IM but lacking PA, PS, PG, or CDP-DAG. We isolated acceptor membranes after flotation and determined their phospholipid composition by MS (Fig. 3C and fig. S7). Ups1-Mdm35 complexes, but not Mdm35, facilitated PA transfer (Fig. 3C). To further define the transport specificity, we used PC-PE donor liposomes containing one negatively charged phospholipid only (Fig. 3D). Transfer of PA but not of PI, CDP-DAG, CL, PS, or PG occurred, substantiating the high selectivity of Ups1. Lipid transfer assays using ^{14}C-PA and ^{14}C-PC confirmed the protein-dependent and lipid-specific transport of PA by Ups1-Mdm35 complexes (Fig. 3E).

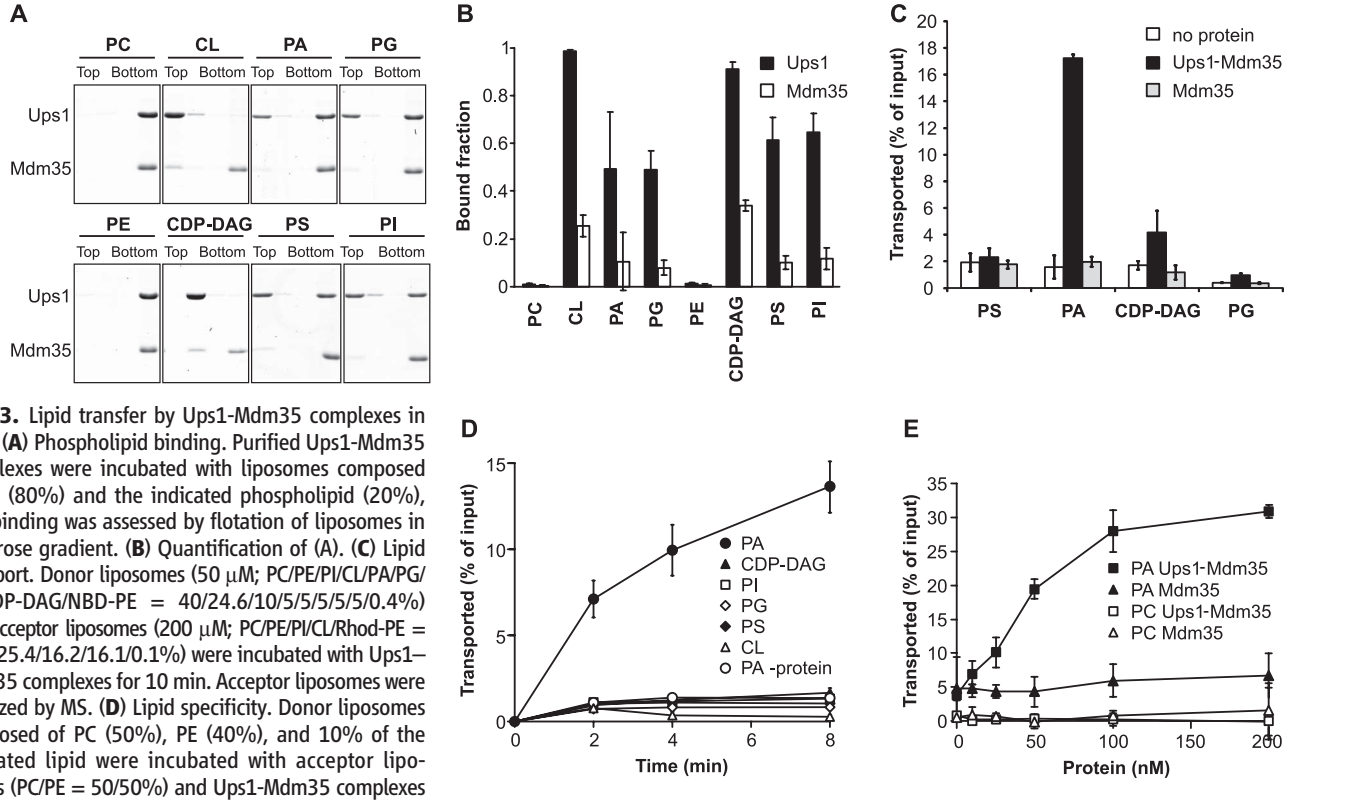


Fig. 3. Lipid transfer by Ups1-Mdm35 complexes in vitro. (**A**) Phospholipid binding. Purified Ups1-Mdm35 complexes were incubated with liposomes composed of PC (80%) and the indicated phospholipid (20%), and binding was assessed by flotation of liposomes in a sucrose gradient. (**B**) Quantification of (A). (**C**) Lipid transport. Donor liposomes (50 μM; PC/PE/PI/CL/PA/PG/PS/CDP-DAG/NBD-PE = 40/24.6/10/5/5/5/5/5/0.4%) and acceptor liposomes (200 μM; PC/PE/PI/CL/Rhod-PE = 42.2/25.4/16.2/16.1/0.1%) were incubated with Ups1–Mdm35 complexes for 10 min. Acceptor liposomes were analyzed by MS. (**D**) Lipid specificity. Donor liposomes composed of PC (50%), PE (40%), and 10% of the indicated lipid were incubated with acceptor liposomes (PC/PE = 50/50%) and Ups1-Mdm35 complexes (66.7 nM). Acceptor liposomes were analyzed by MS. (**E**) PA transport. Donor liposomes (50 μM; PC/PE/PI/lactosyl-PE/PS/CL/PA/NBD-PE = 40/17.1/15/10/5/5/5/0.4%) containing ^{14}C-PA or ^{14}C-PC and acceptor liposomes (200 μM; PC/PE/PI/CL/Rhod-PE = 42.2/25.4/16.2/16.1/0.1%) were incubated for 10 min with the indicated proteins. Data represent mean values ± SD, $n = 3$.

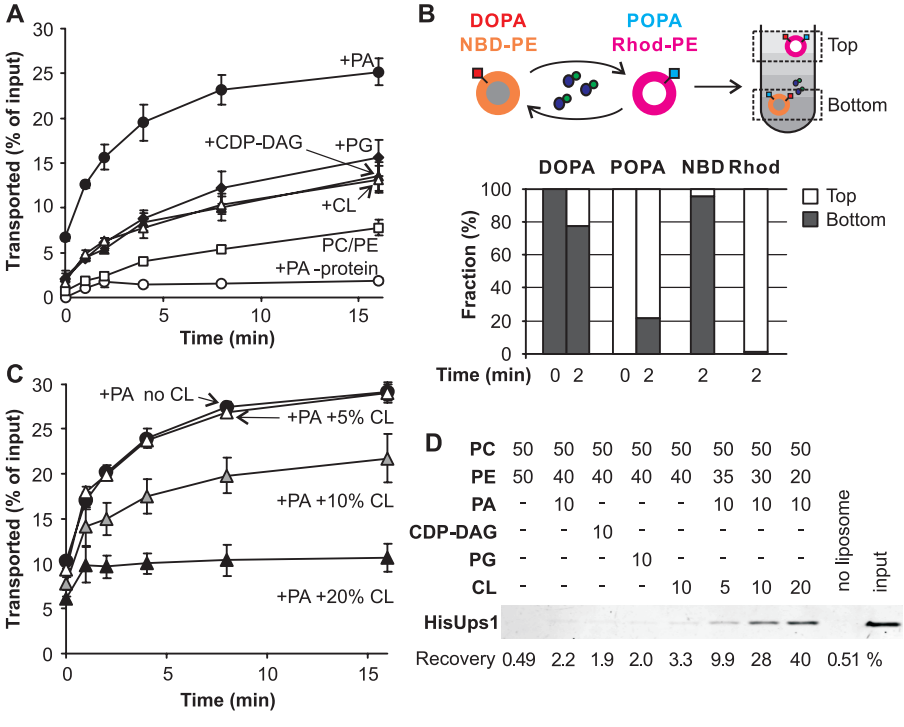


Fig. 4. Characteristics of PA transfer by Ups1-Mdm35 complexes. (**A**) Negatively charged phospholipids in the acceptor membrane facilitated PA transport. Ups1-Mdm35 complexes (20 nM) were incubated with donor liposomes (25 μM; PC/PE/PA/lactosyl-PE/NBD-PE = 50/29.6/10/10/0.4%) containing ^{14}C-PA and acceptor liposomes (100 μM) composed of PC and PE (50/40%) and the indicated phospholipid (10%). Data represent mean values ± SEM, $n = 3$. (**B**) Bidirectional transport of PA. Ups1-Mdm35 complexes (20 nM) were incubated with heavy liposomes [(50 μM; PC/PE/DOPA(*di*-18:1PA)/NBD-PE = 50/39.9/10/0.1%] and light liposomes [(50 μM; PC/PE/POPA(16:1/18:1PA)/Rhod-PE = 50/39.9/10/0.1%]. Liposomes were separated by flotation and lipids analyzed by MS. (**C**) CL in the acceptor membrane inhibits PA transport. Donor liposomes (25 μM; PC/PE/PA/lactosyl-PE/NBD-PE = 50/29.6/10/10/0.4%) containing ^{14}C-PA and acceptor liposomes (100 μM; PC/PE/PA/Rhod-PE = 50/39.9/10/0.1%) containing increasing concentrations of CL (replacing PE) were incubated with Ups1-Mdm35 complexes (20 nM). Data represent mean values ± SEM, $n = 3$. (**D**) Ups1 remains bound to CL-rich liposomes. Ups1-Mdm35 complexes (20 nM) were incubated with liposomes (100 μM) of the indicated composition. Liposome-associated proteins were analyzed by SDS–polyacrylamide gel electrophoresis and immunoblotting.

Downloaded from www.sciencemag.org on November 9, 2012

Because negatively charged phospholipids like CL, PG, or CDP-DAG were bound by Ups1 but not efficiently transported, we tested whether they influence PA transport when present in acceptor membranes (Fig. 4A). We observed slow PA transport in the absence of any negatively charged phospholipid. However, transport was accelerated when CL, PG, or CDP-DAG was present in the acceptor membrane (10%) (Fig. 4A), indicating that Ups1 binding is rate-limiting for transport under these conditions. Although binding to Ups1 with similar efficiency (Fig. 3A), the presence of PA in acceptor membranes stimulated the transport more than other negatively charged phospholipids (Fig. 4A).

We reasoned that Ups1-Mdm35 complexes mediated PA transport in a bidirectional manner, similar to that of other lipid transfer proteins (*15*, *16*). Accordingly, PA in acceptor liposomes could facilitate membrane dissociation of Ups1 after PA delivery. To obtain evidence for bidirectional transport, we included PA with different acyl chains in donor 1,2-dioleoyl-*sn*-glycero-3-phosphate (DOPA) and acceptor 1-palmitoyl-2-oleoyl-*sn*-glycero-3-phosphate (POPA) liposomes and monitored the redistribution of PA in the presence of Ups1-Mdm35 complexes by MS (Fig. 4B). DOPA accumulated in acceptor membranes at levels similar to those of POPA in donor membranes, suggesting that PA transport can occur bidirectionally and independent of its acyl chain composition (Fig. 4B).

The IM contains higher concentrations of CL than the OM (*17*). We thus performed lipid transfer assays at optimal PA and increasing CL concentrations in acceptor membranes (Fig. 4C). CL inhibited PA transfer when present in acceptor membranes at concentrations that mimic the IM (10 to 20%). Similarly, PG exerted an inhibitory effect on PA transport (fig. S8). At high CL concentrations, Ups1 remained associated with liposomes (Fig. 4D), indicating that CL impairs the dissociation of Ups1 from the membrane. Similarly, Ups1 accumulated at the IM in mitochondria that contain similar concentrations of CL but lack Yme1, which is responsible for its rapid turnover (*14*) (fig. S9). Thus, CL present at physiological concentrations traps Ups1 irreversibly at membranes, where it is degraded by Yme1, rendering PA transport irreversible.

Here, we identify Ups1 as a lipid transfer protein in the IMS that acts early during CL biosynthesis. Our in vitro results suggest that Ups1 mediates PA transport between mitochondrial membranes in distinct steps (fig. S10): Upon PA binding to Ups1 and PA extraction from the membrane, Ups1 assembles with Mdm35, which stabilizes Ups1 in a transfer-competent conformation. Negatively charged phospholipids facilitate the interaction of Ups1-Mdm35 complexes with the acceptor membrane, which is accompanied by the dissociation of Mdm35 and the release of PA. The enzymatic conversion of PA into CL in the IM provides directionality to the transport reaction.

Ups1 binds but does not transfer negatively charged phospholipids like CL, which is enriched at contact sites between the IM and OM (*18*). PA accumulates at these sites in Δ*ups1* mitochondria (fig. S11). CL binding may thus recruit Ups1 to contact sites and facilitate PA transfer at sites of close membrane apposition in vivo, although direct membrane contacts are not required for Ups1-mediated PA transport in vitro (figs. S12 and S13). Moreover, high CL concentrations impair the dissociation of Ups1 from the IM and inhibit PA transfer, offering an intriguing possibility to limit CL accumulation in the IM.

Our epistasis analysis revealed an alternative route for CL synthesis that is activated in the absence of Ups1 and does not depend on PGP synthesis by Pgs1. These observations indicate that CL precursor lipids other than PA can reach the IM by other means. Although this pathway remains to be defined, the positive genetic interaction of Ups1 with Pgs1 and Tam41 suggests deleterious effects of PA accumulating in the IM in Δ*pgs1* and Δ*tam41* mitochondria.

The mechanism of PA transport by Ups1 is reminiscent of other known lipid transfer proteins that shuttle lipids between cellular membranes (*2*, *19*). Although not related at the sequence level, structural modeling using template-based comparative modeling [i-TASSER (*20*)] suggests a fold for Ups1 similar to that of phosphatidylinositol transfer proteins (fig. S14). Ups1 is functionally conserved from yeast to human and a member of a conserved family of mitochondrial proteins (*21*). Other family members may serve as lipid transfer proteins with different lipid specificity within mitochondria.

References and Notes

1. G. van Meer, D. R. Voelker, G. W. Feigenson, *Nat. Rev. Mol. Cell Biol.* **9**, 112 (2008).
2. W. A. Prinz, *Cell* **143**, 870 (2010).
3. G. Daum, N. D. Lees, M. Bard, R. Dickson, *Yeast* **14**, 1471 (1998).
4. B. Kornmann, P. Walter, *J. Cell Sci.* **123**, 1389 (2010).
5. C. Osman, D. R. Voelker, T. Langer, *J. Cell Biol.* **192**, 7 (2011).
6. C. Osman *et al.*, *J. Cell Biol.* **184**, 583 (2009).
7. Y. Tamura, T. Endo, M. Iijima, H. Sesaki, *J. Cell Biol.* **185**, 1029 (2009).
8. Y. Tamura *et al.*, *J. Biol. Chem.* **287**, 15205 (2012).
9. S. C. Chang, P. N. Heacock, C. J. Clancey, W. Dowhan, *J. Biol. Chem.* **273**, 9829 (1998).
10. M. Janitor, M. Obernauerová, S. D. Kohlwein, J. Subík, *FEMS Microbiol. Lett.* **140**, 43 (1996).
11. S. Kutik *et al.*, *J. Cell Biol.* **183**, 1213 (2008).
12. C. Osman, M. Haag, F. T. Wieland, B. Brügger, T. Langer, *EMBO J.* **29**, 1976 (2010).
13. Y. Harada, Y. Tamura, T. Endo, *Biochem. Biophys. Res. Commun.* **392**, 228 (2010).
14. C. Potting, C. Wilmes, T. Engmann, C. Osman, T. Langer, *EMBO J.* **29**, 2888 (2010).
15. M. de Saint-Jean *et al.*, *J. Cell Biol.* **195**, 965 (2011).
16. A. M. Kasper, G. M. Helmkamp Jr., *Biochim. Biophys. Acta* **664**, 22 (1981).
17. E. Zinser *et al.*, *J. Bacteriol.* **173**, 2026 (1991).
18. R. Simbeni, L. Pon, E. Zinser, F. Paltauf, G. Daum, *J. Biol. Chem.* **266**, 10047 (1991).
19. K. Hanada, K. Kumagai, N. Tomishige, T. Yamaji, *Biochim. Biophys. Acta* **1791**, 684 (2009).
20. A. Roy, A. Kucukural, Y. Zhang, *Nat. Protoc.* **5**, 725 (2010).
21. H. Sesaki *et al.*, *J. Cell Biol.* **173**, 651 (2006).

Acknowledgments: We thank G. Zimmer for technical assistance, S. Geimer for advice on electron microscopy, T. Endo for sharing unpublished results, and J. Nunnari for yeast strains. This work was supported by grants from the Deutsche Forschungsgemeinschaft (SFB635, FOR885) and the European Research Council (AdG No. 233078) to T.L.

Supplementary Materials

www.sciencemag.org/cgi/content/full/science.1225625/DC1
Materials and Methods
Figs. S1 to S16
Table S1
References (*22*–*31*)

4 June 2012; accepted 17 September 2012
Published online 4 October 2012;
10.1126/science.1225625

IRE1α Cleaves Select microRNAs During ER Stress to Derepress Translation of Proapoptotic Caspase-2

John-Paul Upton,[1,7]* Likun Wang,[2,6,8]* Dan Han,[2,6,8] Eric S. Wang,[1] Noelle E. Huskey,[2,7] Lionel Lim,[2,7] Morgan Truitt,[3,7] Michael T. McManus,[4,5,6] Davide Ruggero,[3,8] Andrei Goga,[2,8] Feroz R. Papa,[2,5,7,9]† Scott A. Oakes[1,8]†

The endoplasmic reticulum (ER) is the primary organelle for folding and maturation of secretory and transmembrane proteins. Inability to meet protein-folding demand leads to "ER stress," and activates IRE1α, an ER transmembrane kinase-endoribonuclease (RNase). IRE1α promotes adaptation through splicing *Xbp1* mRNA or apoptosis through incompletely understood mechanisms. Here, we found that sustained IRE1α RNase activation caused rapid decay of select microRNAs (miRs -17, -34a, -96, and -125b) that normally repress translation of *Caspase-2* mRNA, and thus sharply elevates protein levels of this initiator protease of the mitochondrial apoptotic pathway. In cell-free systems, recombinant IRE1α endonucleolytically cleaved microRNA precursors at sites distinct from DICER. Thus, IRE1α regulates translation of a proapoptotic protein through terminating microRNA biogenesis, and noncoding RNAs are part of the ER stress response.

Various physiological events (e.g., secretory cell differentiation or polypeptide hormone production) and pathological insults (e.g., hypoxia, ischemia, or changes in intracellular pH) increase protein-folding demand on the secretory pathway, which, in turn, triggers ER stress

Downloaded from www.sciencemag.org on November 9, 2012

[1]Department of Pathology, University of California, San Francisco, San Francisco, CA 94143, USA. [2]Department of Medicine, University of California, San Francisco, San Francisco, CA 94143, USA. [3]Department of Urology, University of California, San Francisco, San Francisco, CA 94143, USA. [4]Department of Microbiology and Immunology, University of California, San Francisco, San Francisco, CA 94143, USA. [5]Diabetes Center, University of California, San Francisco, San Francisco, CA 94143, USA. [6]Keck Center for Noncoding RNAs, University of California, San Francisco, San Francisco, CA 94143, USA. [7]Lung Biology Center, University of California, San Francisco, San Francisco, CA 94143, USA. [8]Helen Diller Comprehensive Cancer Center, University of California, San Francisco, San Francisco, CA 94143, USA. [9]California Institute for Quantitative Biosciences, University of California, San Francisco, San Francisco, CA 94143, USA.

*These authors contributed equally to this work.
†To whom correspondence should be addressed. E-mail: frpapa@medicine.ucsf.edu (F.R.P.) and scott.oakes@ucsf.edu (S.A.O.)

(*1*). The tripartite unfolded protein response (UPR)–signaling arms of IRE1α, PERK, and ATF6α attempt to resolve ER stress through complementary homeostatic mechanisms, which include inhibiting cap-dependent protein translation, increasing ER chaperones, and enhancing ER-associated protein degradation (ERAD) (*2*). However, if ER stress cannot be remedied through these mechanisms, the UPR induces apoptosis through the mitochondrial BAX/BAK–dependent pathway (*1*). Excessive ER stress–induced cell loss contributes to numerous human degenerative diseases, including diabetes, neurodegeneration, and cardiovascular disease (*1*, *3*, *4*).

Severe ER stress activates the protease Caspase-2 (CASP2) as an early apoptotic switch upstream of mitochondria (*3*–*7*). Once activated, CASP2 cleaves the BH3-only protein BID, which then localizes to mitochondria to induce BAX/BAK–dependent apoptosis (*8*, *9*). However, the molecular events leading from the detection of upstream ER stress to CASP2 activation remain unknown. To address this question, we challenged wild-type (WT) and apoptosis-resistant $Bax^{-/-}Bak^{-/-}$ (DKO) mouse embryonic fibroblasts (MEFs) with brefeldin A (BFA), a drug that retards protein trafficking in the secretory pathway to cause ER stress (*10*). CASP2 protein, which is normally expressed at low levels in these cells, increased dramatically within 2 hours of BFA treatment and rose steadily over the next 12 to 18 hours (Fig. 1, A and B, and fig. S1). CASP2 then underwent internal cleavage at ~18 hours,

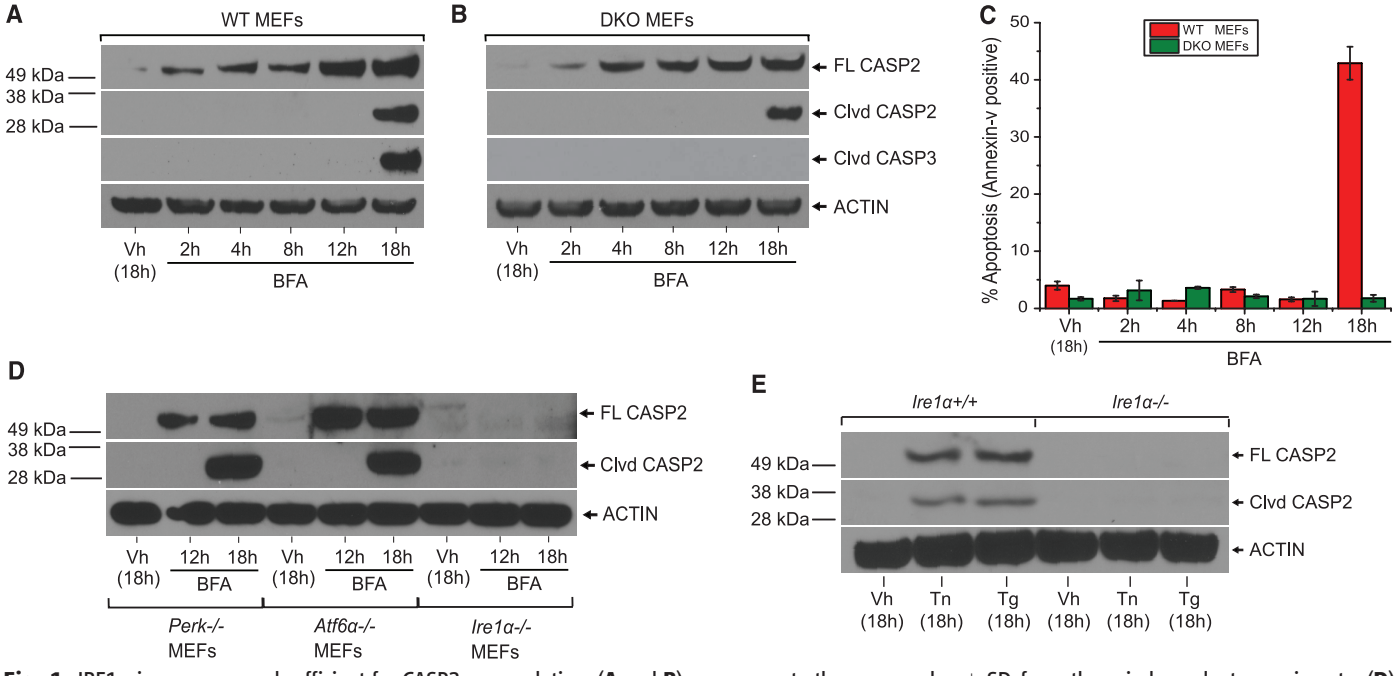


Fig. 1. IRE1α is necessary and sufficient for CASP2 up-regulation. (**A** and **B**) Immunoblot for full-length (FL) CASP2 and cleaved (Clvd) CASP2 in WT and DKO MEFs after BFA treatment. (**C**) Annexin V–directed fluorescence-activated cell sorting analysis of WT and DKO MEFs treated with BFA. Each data point represents the mean value ± SD from three independent experiments. (**D**) CASP2 immunoblot in UPR sensor–deficient MEFs treated with BFA. (**E**) CASP2 immunoblot of $Ire1\alpha^{+/+}$ and $Ire1\alpha^{-/-}$ MEFs treated with tunicamycin (Tn) or thapsigargin (Tg).

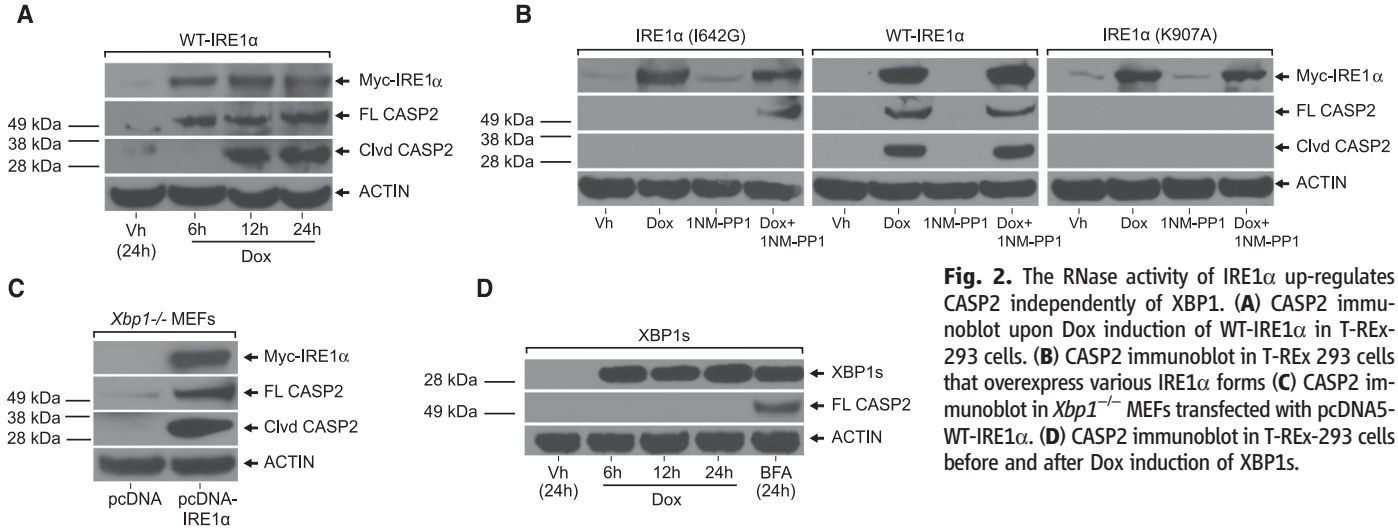


Fig. 2. The RNase activity of IRE1α up-regulates CASP2 independently of XBP1. (**A**) CASP2 immunoblot upon Dox induction of WT-IRE1α in T-REx-293 cells. (**B**) CASP2 immunoblot in T-REx 293 cells that overexpress various IRE1α forms (**C**) CASP2 immunoblot in $Xbp1^{-/-}$ MEFs transfected with pcDNA5-WT-IRE1α. (**D**) CASP2 immunoblot in T-REx-293 cells before and after Dox induction of XBP1s.

Downloaded from www.sciencemag.org on November 9, 2012

concomitant with entry of WT—but not DKO—MEFs into the apoptotic pathway, as evidenced by activation of the downstream executioner CASP3 and annexin V staining (Fig. 1, A to C). CASP2 up-regulation and activation were preserved in DKO MEFs, which suggests that they occur upstream of the mitochondrial apoptotic pathway (Fig. 1, B and C). Furthermore, CASP2 was efficiently induced by ER stress in *Atf6α*$^{-/-}$ and *Perk*$^{-/-}$, but not in *Ire1α*$^{-/-}$, MEFs (Fig. 1, D and E), and CASP2-dependent proteolytic activation of BID in response to ER stress was absent in *Ire1α*$^{-/-}$ MEFs (fig. S2). Thus, IRE1α may represent the upstream ER sensor used by cells to up-regulate CASP2 protein. Consistent with this notion, *Ire1α*$^{-/-}$ MEFs were resistant to BFA-induced apoptosis, and provision of IRE1α reconstituted apoptosis in a BAX/BAK–dependent manner (figs. S3 and S4).

IRE1α consists of an N-terminal sensor domain within the ER that detects misfolded proteins, a transmembrane region, and a cytosolic tail containing two distinct catalytic activities—a serine-threonine kinase and an endoribonuclease (RNase) (*11*, *12*) (fig. S7). Accumulation of misfolded proteins within the ER leads to IRE1α oligomerization and subsequent trans-autophosphorylation, which allosterically activates its RNase. Isogenic T-REx-293 cell lines have been generated that express either WT or various mutant forms of IRE1α under doxycycline (Dox) control (*13*). Because activation of IRE1α requires oligomerization in the ER membrane, this process can be driven by mass action in the absence of ER stress (*13*). Activation of WT-IRE1α was sufficient for both robust up-regulation of CASP2 and its subsequent cleavage, similar to what occurs under irremediable ER stress (Fig. 2A and figs. S5 and S6).

To determine the contribution of the kinase and/or RNase activity of IRE1α in CASP2 up-regulation, we tested various IRE1α mutants (fig. S7). A kinase-active and RNase-dead variant of IRE1α (K907A) was unable to up-regulate CASP2 (Fig. 2B). We used a chemical-genetic tool that can selectively activate IRE1α's RNase, IRE1α (I642G) (*13*). The IRE1α (I642G) mutant is deficient in phosphotransfer activity (*13*, *14*), but, in the presence of the adenosine triphosphate analog 1NM-PP1, it undergoes a conformational change that activates its RNase (*13*, *14*). Dox-induced expression of IRE1α (I642G) alone (RNase "OFF") did not increase CASP2, but the addition of 1NM-PP1 (RNase "ON") increased CASP2 as efficiently as WT-IRE1α (Fig. 2B). Unlike under WT-IRE1α activation, there was no CASP2 cleavage after 1NM-PP1 activation of IRE1α (I642G). Thus, CASP2 is subject to multistep regulation downstream of IRE1α, and activating the RNase of IRE1α (I642G) with 1NM-PP1 selectively activates the initial step in the process. Consistent with this notion, forcible activation of IRE1α (I642G) does not cause apoptosis (*13*). IRE1α-mediated CASP2 up-regulation occurred independently of its classical target, XBP1 (Fig. 2, C and D, and fig. S8).

Although *Casp2* mRNA levels remained stable in response to BFA or WT-IRE1α (fig. S9), polyribosome-associated *Casp2* mRNA significantly increased within 1 hour of BFA in *Ire1α*$^{+/+}$, but not *Ire1α*$^{-/-}$, MEFs (Fig. 3A and fig. S10). Moreover, CASP2 increased in response to BFA even when transcription was blocked with actinomycin D (Fig. 3B) but not when translation was blocked with cycloheximide (fig. S11). Thus, IRE1α's RNase appears to up-regulate CASP2 expression posttranscriptionally. A bioinformatic analysis of *Casp2* mRNA revealed several high-confidence matches for binding sequences of known miRNAs within its 3′ untranslated region (3′UTR), including miR-17, miR-34a, miR-96, and miR-125b (fig. S12). These four miRNAs rapidly and significantly decreased in *Ire1α*$^{+/+}$, but not *Ire1α*$^{-/-}$, MEFs upon BFA treatment (Fig. 3C); an unrelated miRNA, let-7a, did not. We could mimic this regulation using our chemical-genetic tools: WT-IRE1α or 1NM-PP1 activation of IRE1α (I642G) also caused rapid decreases in miR-17, -34a, -96, and -125b (Fig. 3D).

To test whether IRE1α-mediated reduction of select miRNAs can increase translation of a target mRNA, we devised a reporter system with an mCherry gene construct containing defined miRNA binding sites within its 3′UTR. As such,

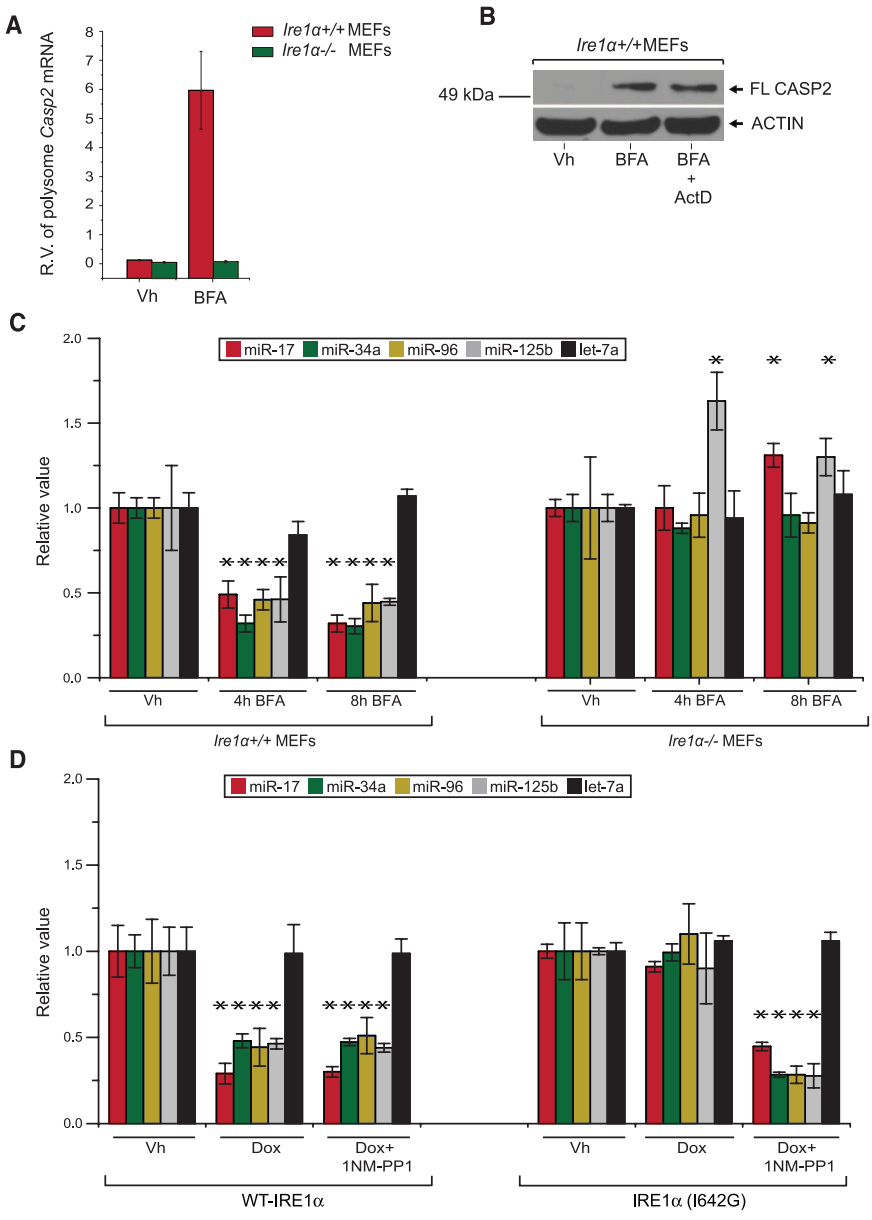


Fig. 3. Anti-*Casp2* miRNAs decrease in IRE1α-dependent manner. (**A**) Quantitative polymerase chain reaction (QPCR) on polyribosome-associated *Casp2* mRNA derived from *Ire1α*$^{+/+}$ and *Ire1α*$^{-/-}$ MEFs before and after BFA treatment. (**B**) CASP2 Immunoblot of *Ire1α*$^{+/+}$ MEFs treated with BFA plus or minus pretreatment with actinomycin A (ActD). QPCR of select miRNAs forms. (**C**) *Ire1α*$^{+/+}$ and *Ire1α*$^{-/-}$ MEFs after BFA treatment and (**D**) T-REx-293 cells after overexpression of WT-IRE1α or 1NM-PP1 activation of IRE1α (I642G). Each data point represents the mean value ± SD from three independent experiments. Asterisks indicate a statistically significant change from the vehicle-treated controls ($P < 0.05$).

Downloaded from www.sciencemag.org on November 9, 2012

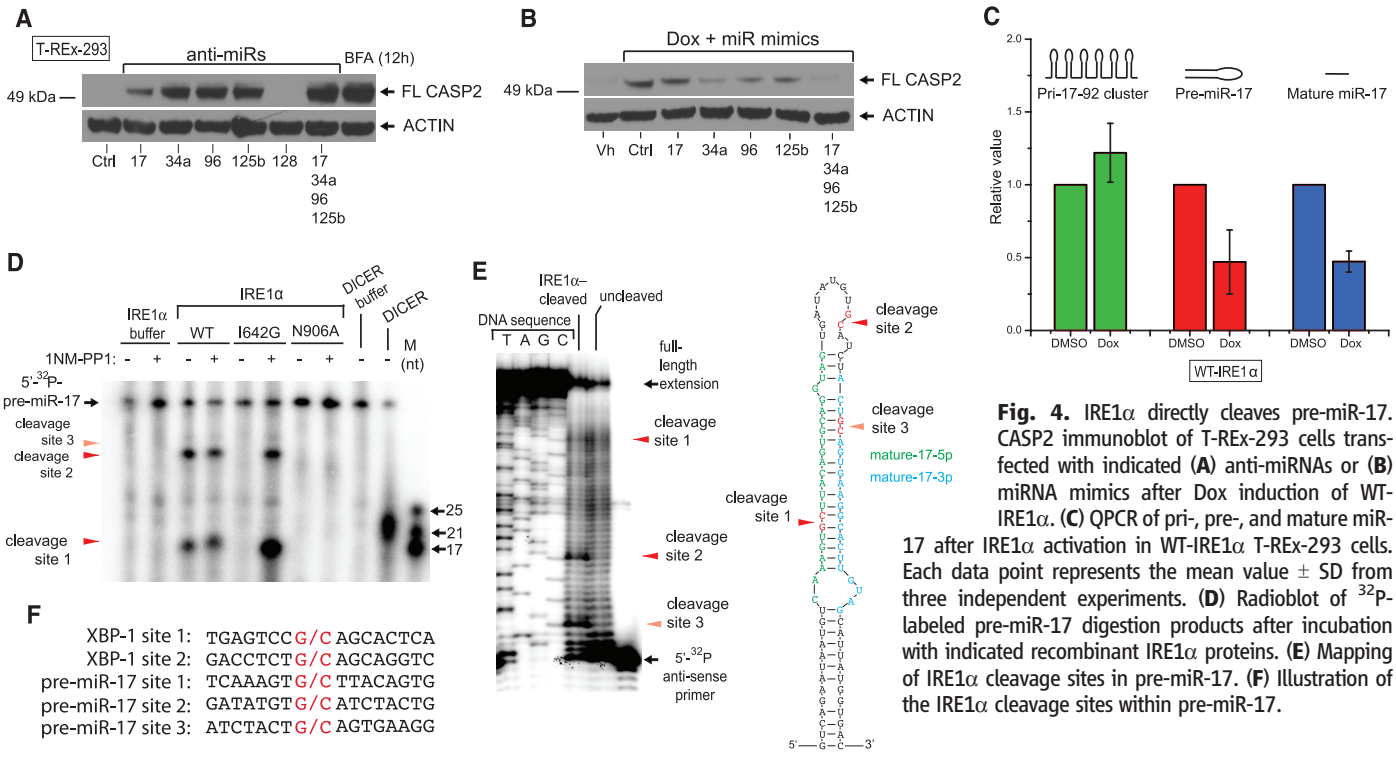


Fig. 4. IRE1α directly cleaves pre-miR-17. CASP2 immunoblot of T-REx-293 cells transfected with indicated (**A**) anti-miRNAs or (**B**) miRNA mimics after Dox induction of WT-IRE1α. (**C**) QPCR of pri-, pre-, and mature miR-17 after IRE1α activation in WT-IRE1α T-REx-293 cells. Each data point represents the mean value ± SD from three independent experiments. (**D**) Radioblot of ^{32}P-labeled pre-miR-17 digestion products after incubation with indicated recombinant IRE1α proteins. (**E**) Mapping of IRE1α cleavage sites in pre-miR-17. (**F**) Illustration of the IRE1α cleavage sites within pre-miR-17.

mCherry expression is low in the presence of the matching miRNA, but becomes up-regulated if the specific miRNA decreases sufficiently. The mCherry reporters for miR-17, -34a, -96, and -125b (but not let-7a) in T-REx-293 cells were all up-regulated after Dox induction of WT-IRE1α or IRE1α (I642G) plus 1NM-PP1 (fig. S13, A, B, G, and H). BFA caused similar increases in these miRNA reporters in *Ire1α*$^{+/+}$, but not *Ire1α*$^{-/-}$, MEFs (fig. S13, C to F). To examine the role of these miRNAs in regulating *Casp2* translation, we transfected T-REx-293 cells with specific anti-miRNA oligonucleotides (*15*–*17*). Anti–miR-17, -34a, -96, or -125b each modestly increased CASP2, but all four together led to CASP2 levels similar to those seen with BFA (Fig. 4A). Conversely, single anti-*Casp2* miRs (-17, -34a, -96, and -125b) partially reduced, and the combination of all four effectively prevented, CASP2 up-regulation by IRE1α (Fig. 4B). To determine whether the binding sequences for miR-17, -34a, -96 and -125b within the 3′UTR of *Casp2* mRNA are critical for translational control, we introduced the complete 3′UTR sequence into a dual Firefly (FLuc) and *Renilla* (RLuc) luciferase reporter system in the T-REx-293 cells (*18*). Similar to the endogenous *Casp2* mRNA, Dox induction of WT-IRE1α or I642G-IRE1α plus 1NM-PP1 activated 3′UTR-dependent translation as indicated by increases in the RLuc/FLuc ratio, but not when the binding sequences for the anti-*Casp2* miRNAs were mutated (fig. S14). Thus, IRE1α controls *Casp2* translation via down-regulating these select anti-*Casp2* miRNAs.

To explore the mechanism through which IRE1α down-regulates these miRNAs, we examined the biogenesis of miR-17. IRE1α activation did not affect pri-miR-17, but it significantly reduced both pre-miR-17 and mature miR-17 (Fig. 4C), which suggested that IRE1α regulates its biogenesis at the precursor step. Indeed, incubation of radiolabeled pre-miR-17 with recombinant human WT-IRE1α or 1NM-PP1–activated IRE1α (I642G) (but not the K907A RNase mutant) resulted in two prominent fragments [of ~40 nucleotides (nt) and ~17 nt], as well as a slightly less abundant ~49-nt fragment (Fig. 4D). These IRE1α cleavage products all mapped to positions distinct from DICER sites but with some similarity to IRE1α's scission sites in *Xbp1* (Fig. 4, E and F). Thus, IRE1α appears to cleave select pre-miRNAs directly to prevent proper DICER processing of their mature forms, a mechanism recently described for how another ribonuclease, MCPIP1, terminates miRNA biogenesis (*19*).

Hyperactivated WT-IRE1α—but not 1NM-PP1 activated IRE1α (I642G)—endonucleolytically degrades hundreds of ER-localized mRNAs, which further compromises ER protein-folding capacity and hastens cell demise (*13*). Although activated WT-IRE1α and IRE1α (I642G) both decreased anti-*Casp2* miRNAs to induce expression of pro-CASP2, only the former triggered its subsequent proteolytic processing, which suggested that ER-localized mRNA decay may be a critical "second signal" for full CASP2 activation and apoptosis. Unlike mRNAs directed to the ER membrane through a signal peptide leader sequence, it is currently unclear how pre-miRNAs gain proximity to IRE1α under conditions of ER stress. Possibilities include alterations in miRNA localization structures (e.g., P-bodies or stress granules), the involvement of miRNA-binding proteins, or the loss of other miRNA protective factors (*20*–*22*). Alternatively, because the outer nuclear membrane is continuous with the ER, IRE1α may become exposed to pre-miRNAs as they transit through the nuclear pore.

There have been previous hints of a connection between miRNAs and ER stress signaling. For instance, the apoptotic proteins BIM, BAK, and PUMA are known to increase during ER stress-induced apoptosis (*7*, *23*, *24*) and to contain putative miRNA binding sites within their 3′UTRs. Furthermore, we recently found that IRE1α posttranscriptionally stabilizes the mRNA encoding the pro-oxidant thioredoxin-interacting protein (TXNIP), in part, through reducing miR-17 to activate the NLRP3 inflammasome in pancreatic beta cells under ER stress (*25*). Here, we provide evidence that the action of IRE1α on miRNA biogenesis is direct and that it antagonizes classical processing by DICER to derepress a translational block to entry into apoptosis. Thus, endonucleolytic cleavage of miRNA precursors by IRE1α adds to a growing list of extra-*Xbp1* mRNA splicing functions controlled by this UPR sensor. Given their potential to alter expression of multiple mRNA targets simultaneously, noncoding RNAs are well-suited to govern complex cellular remodeling in response to ER stress signaling.

References and Notes

1. G. C. Shore, F. R. Papa, S. A. Oakes, *Curr. Opin. Cell Biol.* **23**, 143 (2011).
2. D. Ron, P. Walter, *Nat. Rev. Mol. Cell Biol.* **8**, 519 (2007).
3. H. Yoshida, *FEBS J.* **274**, 630 (2007).
4. N. A. Reyes *et al.*, *J. Clin. Invest.* **120**, 3673 (2010).
5. J. P. Upton *et al.*, *Mol. Cell. Biol.* **28**, 3943 (2008).

Downloaded from www.sciencemag.org on November 9, 2012

6. L. K. Nutt *et al.*, *Dev. Cell* **16**, 856 (2009).
7. L. K. Nutt *et al.*, *Cell* **123**, 89 (2005).
8. C. Bonzon, L. Bouchier-Hayes, L. J. Pagliari, D. R. Green, D. D. Newmeyer, *Mol. Biol. Cell* **17**, 2150 (2006).
9. M. C. Wei *et al.*, *Science* **292**, 727 (2001).
10. Materials and methods are available as supplementary materials on *Science* Online.
11. W. Tirasophon, A. A. Welihinda, R. J. Kaufman, *Genes Dev.* **12**, 1812 (1998).
12. X.-Z. Wang *et al.*, *EMBO J.* **17**, 5708 (1998).
13. D. Han *et al.*, *Cell* **138**, 562 (2009).
14. F. R. Papa, C. Zhang, K. Shokat, P. Walter, *Science* **302**, 1533 (2003).
15. J. Krützfeldt *et al.*, *Nature* **438**, 685 (2005).
16. A. Vermeulen *et al.*, *RNA* **13**, 723 (2007).
17. D. P. Bartel, *Cell* **136**, 215 (2009).
18. S. Yekta, I. H. Shih, D. P. Bartel, *Science* **304**, 594 (2004).
19. H. I. Suzuki *et al.*, *Mol. Cell* **44**, 424 (2011).
20. M. I. Almeida, R. M. Reis, G. A. Calin, *Mutat. Res.* **717**, 1 (2011).
21. D. Long *et al.*, *Nat. Struct. Mol. Biol.* **14**, 287 (2007).
22. A. K. Leung, P. A. Sharp, *Mol. Cell* **40**, 205 (2010).
23. H. Puthalakath *et al.*, *Cell* **129**, 1337 (2007).
24. D. Kieran, I. Woods, A. Villunger, A. Strasser, J. H. Prehn, *Proc. Natl. Acad. Sci. U.S.A.* **104**, 20606 (2007).
25. A. G. Lerner *et al.*, *Cell Metab.* **16**, 250 (2012).

Acknowledgments: We thank R. Kaufman for *Atf6α*$^{-/-}$ MEFs and D. Ron for *Perk*$^{-/-}$ and *Ire1α*$^{-/-}$ MEFs. The work was supported by NIH: DP2OD001925 (F.R.P), R01CA136577 (S.A.O.), R01CA136717 (A.G.), R01DK080955 (F.R.P), R01CA154916 (D.R.), GM080783 (M.T.M.), DK063720 (M.T.M.), and R01CA140456 (D.R.); Leukemia & Lymphoma Society Scholar Award (D.R.); Howard Hughes Medical Institute Physician-Scientist Early Career Award (S.A.O.); American Cancer Society Research Scholar Award (S.A.O.); Burroughs Wellcome Foundation (F.R.P.); Hillblom Foundation (F.R.P.); Juvenile Diabetes Research Foundation (F.R.P); Partnership for Cures (F.R.P); National Science Foundation (E.S.W.); Susan G. Komen Foundation (A.G.); and an A*STAR Fellowship (L.L.). J-P.U., L.W., D.H., E.S.W., N.H., and M.T. designed and performed experiments and contributed to the manuscript. L.L., M.T.M., D.R., and A.G. contributed key ideas, reagents, and data interpretation. F.R.P. and S.A.O. designed the study and wrote the manuscript. There are no conflicts of interest.

Supplementary Materials

www.sciencemag.org/cgi/content/full/science.1226191/DC1
Materials and Methods
Figs. S1 to S15
Reference (*26*)

18 June 2012; accepted 10 September 2012
Published online 4 October 2012;
10.1126/science.1226191

Mitochondrial Network Size Scaling in Budding Yeast

Susanne M. Rafelski,[1,2]*† Matheus P. Viana,[3]† Yi Zhang,[1,4] Yee-Hung M. Chan,[1,2] Kurt S. Thorn,[1] Phoebe Yam,[5] Jennifer C. Fung,[5] Hao Li,[1,2] Luciano da F. Costa,[3] Wallace F. Marshall[1,2]*

Mitochondria must grow with the growing cell to ensure proper cellular physiology and inheritance upon division. We measured the physical size of mitochondrial networks in budding yeast and found that mitochondrial network size increased with increasing cell size and that this scaling relation occurred primarily in the bud. The mitochondria–to–cell size ratio continually decreased in aging mothers over successive generations. However, regardless of the mother's age or mitochondrial content, all buds attained the same average ratio. Thus, yeast populations achieve a stable scaling relation between mitochondrial content and cell size despite asymmetry in inheritance.

The amount of mitochondria in the cell varies in response to metabolic demands (*1*), requiring active size regulation mechanisms. The mitochondrial to cell size ratio is relatively constant in mammalian cells (*2*) and two yeast species (*3*, *4*). We used the budding yeast *Saccharomyces cerevisiae* to study how the relationship between mitochondrial and cell size is achieved in cells growing and dividing asymmetrically (fig. S1). Yeast mitochondria are three-dimensional (3D) networks of dynamic membrane-bound tubules localized at the cell periphery (*5*). To study mitochondrial size scaling, we developed a method to quantify the 3D skeletons of mitochondrial networks (Fig. 1A and fig. S2) using spinning disk confocal z-stacks of live yeast cells expressing mitochondrial matrix-targeted green fluorescent protein (GFP). We converted network length to mitochondrial volume (μm^3), assuming a constant tubule diameter. Absolute network length accuracy was within 85% of manual measurements, with an average reproducibility of 96% (*6*).

We imaged time courses of live yeast cells growing for one to two generations and measured the total cell and mitochondrial volumes for mother and bud compartments. We found a strong correlation between total mitochondrial and cell volumes (Fig. 1B). However, when we compared mother and bud compartments separately, the constant mitochondrial volume ratio found in the population as a whole was dominated by the scaling in the bud (Fig. 1, C and D). Mitochondrial volume ratio in the buds increased and then

[1]Department of Biochemistry and Biophysics, University of California–San Francisco (UCSF), San Francisco, CA, USA. [2]Center for Systems and Synthetic Biology, UCSF, San Francisco, CA, USA. [3]Instituto de Física de São Carlos, Universidade de São Paulo, São Carlos, SP, Brazil. [4]Center for Theoretical Biology and School of Physics, Peking University, Beijing, China. [5]Department of Obstetrics, Gynecology, and Reproductive Sciences, UCSF, San Francisco, CA, USA.

*To whom correspondence should be addressed. E-mail: susanner@uci.edu (S.M.R); wallace.marshall@ucsf.edu (W.F.M)
†Present address: Department of Developmental and Cell Biology, Center for Complex Biological Systems, University of California–Irvine, Irvine, CA, USA.

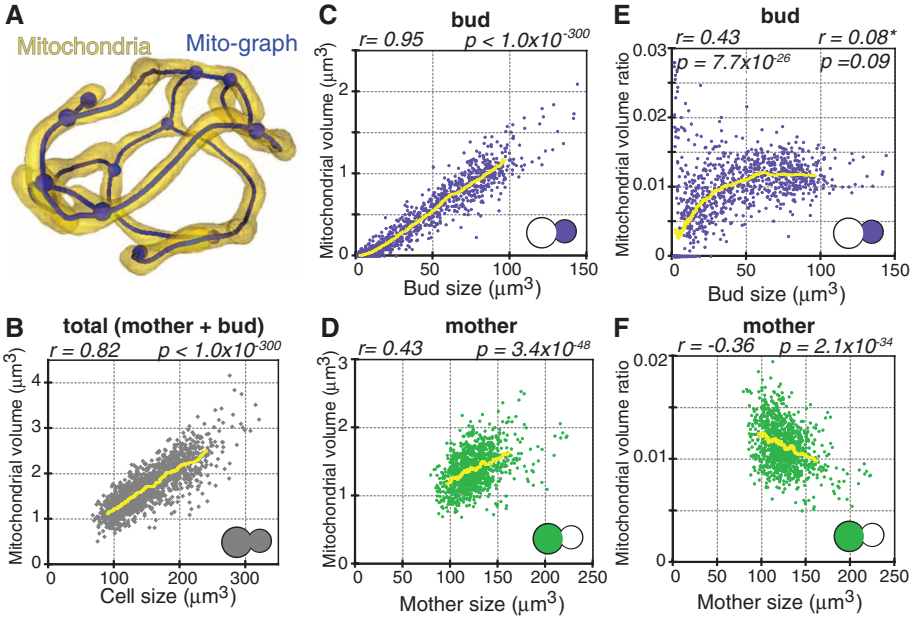


Fig. 1. Mitochondrial-cell size scaling is strongest in the bud. (**A**) Example of a mitochondrial network graph (blue), generated from 3D confocal images of a mitochondrion (yellow), imaged using matrix-targeted GFP in a live yeast cell. (**B**) Mitochondrial volume versus cell size for all cells analyzed in the time-course population (n = 1430 cells), including budding and nonbudding cells. The population maintained a consistent average mitochondrial to cell volume ratio. (**C** and **D**) Mitochondrial volume in the bud or mother and (**E** and **F**) Mitochondrial volume ratio in the bud or mother versus bud or mother size, respectively, for all budding cells (n = 1053 cells). (C and D) Buds displayed a much stronger correlation between mitochondrial and cell volume than mothers. Pearson's correlation coefficient, r, and significance value, P, are shown. Values for r and P on left and right sides in (E) are for the bud population greater/less than 40 μm^3. Yellow lines indicate rolling average.

Downloaded from www.sciencemag.org on November 9, 2012

leveled off when buds were about half their final size (Fig. 1E). Bud size reflects the progression of budding, suggesting that buds accumulate mitochondria until they reach a set point of mitochondrial volume relative to bud size. In contrast, in mothers the mitochondrial volume ratio decreased with increasing cell size (Fig. 1F). Mother size reflects generational age (*7*), suggesting that older mothers do not preserve the mitochondrial volume ratio set point that they inherited when they were buds.

Analysis of the dynamics of cell growth and mitochondrial accumulation during budding time courses revealed dramatic asymmetry in mitochondrial accumulation between mother and bud (Fig. 2). During budding, mothers experienced an overall loss of both mitochondrial volume and the resultant volume ratio, while at the same time mitochondrial content increased in the bud proportional to bud growth (Fig. 2 and figs. S3 and S4). The mitochondrial accumulation rate in mothers was most negative at the moment that it was greatest in the bud (fig. S3B), suggesting that the bud might gain mitochondria at the expense of its mother. Although first and 2+ generation mothers differed significantly in cell size and mitochondrial content at the start of budding, the average kinetics of both bud growth and mitochondrial accumulation in their buds was indistinguishable (Fig. 2C and fig. S3), resulting in the same average volume ratios at division (Fig. 2D). Thus, regardless of the initial size or mitochondrial content of mothers, they generate, on average, identical buds and do so with the same dynamics throughout budding.

Yeast cells displayed "mitochondrial content asymmetry" with a lower mitochondrial volume ratio in the mother than in the bud upon division (Fig. 2D). We asked whether mitochondrial content is replenished during the G1, unbudded, phase of the cell cycle. The mitochondrial volume ratio tended to increase for cells with lower, and decrease for cells with higher, initial volume ratios (Fig. 3A and fig. S5), suggesting a partial homeostatic restoration toward a unique mitochondrial volume ratio set point. We found no evidence that cells delayed G1 exit in response to a decreased volume ratio (fig. S6), but instead that cells may respond to deviations in the appropriate volume ratio by adjusting their rate of mitochondrial biogenesis (Fig. 3B and fig. S7). Analysis of mitochondrial content versus generational age (Fig. 3C) showed that sequential loss during budding and partial regain during G1 resulted in continual loss of mitochondrial volume ratio in aging mother cells (Fig. 3D and figs. S8 and S9). However, these much older mothers still generated buds with the same average volume ratio at division. By generating buds with identical mitochondrial content, the population can renew and maintain a narrow distribution of mitochondrial volume ratios despite asymmetry in the inheritance of mitochondrial content between mother and bud (fig. S10).

There are two possibilities for how proper mitochondrial volume ratio is achieved in the bud: a passive mechanism not modulated as a function of mitochondrial content, where scaling would arise inherently [e.g., allometric growth (*8*)], or an active mechanism capable of sensing and feedback. In the passive case, a delay in mitochondrial inheritance would lead to fewer mitochondria entering the bud and a decreased volume ratio in the newborn mothers. In the active case, cells could sense and compensate for the delay to achieve the target volume ratio in the bud upon division. In Δ*ypt11* mutants, which exhibit delayed appearance of mitochondria in the bud (*6*, *9*, *10*), we found that while buds were delayed in mitochondrial inheritance (figs. S11 and S12), their volume ratio increased rapidly such that volume ratios in Δ*ypt11* and wild-type buds were indistinguishable at division (Fig. 4, A and B), consistent with an active mechanism. Meanwhile,

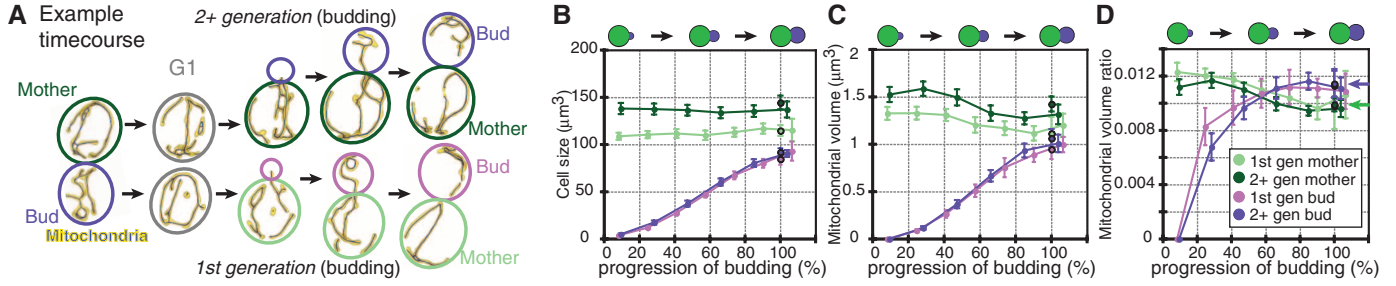


Fig. 2. Mitochondrial accumulation dynamics during progression of budding. (**A**) Overview of time-course experiment. First-generation mothers were considered separately from older, 2+, generation mothers. Yellow and blue represent mitochondria and network graphs. Colors for first generation (1st gen) and older generation (2+ gen) mothers and buds correspond to the colors used in all other figures. (**B**) Average cell size, (**C**) mitochondrial volume, and (**D**) mitochondrial volume ratio for mothers (green) and buds (purple) averaged throughout progression of budding, in percentage units where 100% is the average time until division for that generation. Predivision data points, outlined in black, are included at time = 100%. Error bars: ±95% confidence intervals and numbers of cells in (*6*). (B) As expected, mothers grew very little (*7*), while the buds grew rapidly, with a peak growth rate halfway through budding (fig. S3A). (C) Mothers lost, while their buds gained, mitochondrial volume. (D) The resultant mitochondrial volume ratio in the bud increased and then plateaued (similar to Fig. 1E). At division, mothers had a significantly lower mitochondrial volume ratio than their buds. Arrows in (D) depict mean values; $P = 0.005$ by rank sum; $n = 25$ predivision cells.

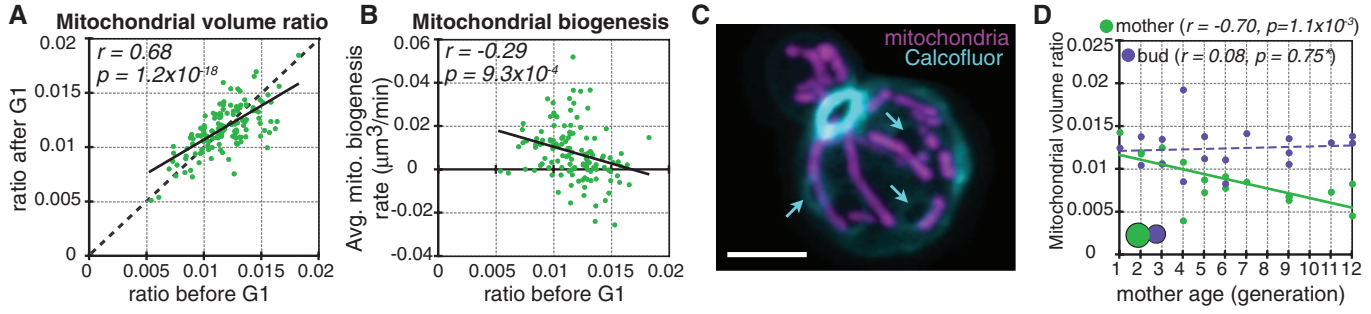


Fig. 3. Homeostatic control of mitochondrial content during cell aging. (**A**) In individual cells, mitochondrial volume ratio is strongly correlated between the start and end of G1 ($n = 130$ cells). Linear regression trendline (black) and line of equal volume ratio at the start and end of G1 (dotted) are shown. (**B**) Average mitochondrial biogenesis rate during G1 is negatively correlated with mitochondrial volume ratio at start of G1 ($n = 129$ cells). (**C**) Example of bud scar staining with Calcofluor (cyan) and mitochondria (magenta) for a mother of generational age 10. Images are maximum intensity projections of a z-stack. Scale bar is 3μm. Arrows point to three example bud scars. (**D**) Predivision mitochondrial volume ratio versus mother's age for Calcofluor-labeled mothers (green) and buds (purple) (*6*). Volume ratio is maintained in buds but decreases in mothers as they age. Solid lines in (A), (B), and (D) represent statistically significant linear regression trendlines; Pearson's correlation coefficient, *r*, and significance value, *P*, are shown. Dotted line in (D) represents the best-fit trendline.

Downloaded from www.sciencemag.org on November 9, 2012

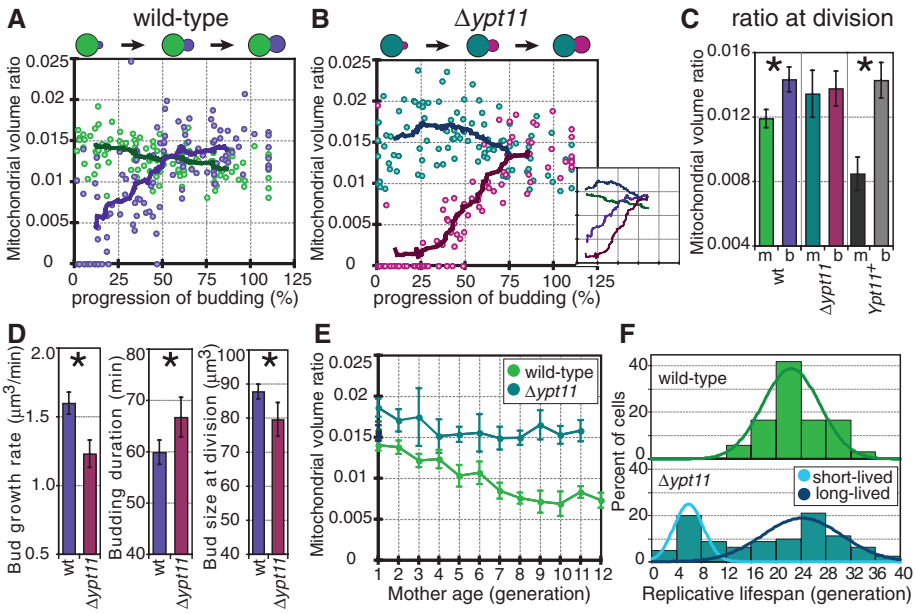


Fig. 4. Mitochondrial accumulation dynamics and aging in Δ*ypt11* mutant. (**A**) Wild-type and (**B**) Δ*ypt11* buds reach the same mitochondrial volume ratio at division despite different accumulation dynamics during budding. Mitochondrial volume ratio of (A) wild-type and (B) Δ*ypt11* mothers (green and turquoise, respectively) and buds (purple and magenta, respectively) as a function of progression of budding. Average time-course behavior was obtained by converting bud sizes from single time-point data into progression of budding (fig. S16). Thick and thin lines indicate the rolling average and 95% confidence interval, respectively. (**C**) Ypt11p is involved in generating mother-daughter mitochondrial content asymmetry. The average mitochondrial volume ratio at division for wild-type (n = 39 cells), Δ*ypt11* (n = 28 cells), and Ypt11p-overexpressing (Ypt11+) (n = 36 cells) (*12*) mothers (m) and buds (b). Asterisks: $P = 1.9 \times 10^{-5}$ and 5.6×10^{-9} by rank sum. (**D**) Average bud growth rate, duration of budding (n = 56 and 24 cells for wild-type and Δ*ypt11* buds, respectively), and bud size at division (n = 106 and 53 cells, respectively) for wild-type (purple) and Δ*ypt11* (magenta) buds during budding. Asterisks: $P = 5.3 \times 10^{-6}$, $<1 \times 10^{-14}$, and 4.6×10^{-4} by rank sum. (**E**) Age-dependent loss of mitochondrial volume ratio from mothers. The average mitochondrial volume ratio for wild-type (green) and Δ*ypt11* (turquoise) mothers of increasing generational age. Darker first-generation data points represent average values of mothers at their "birth" (*6*). Error bars: ±95% confidence intervals and numbers of cells in (*6*). (**F**) Replicative life-span histogram for wild-type (green, n = 36 cells) and Δ*ypt11* (turquoise, n = 80 cells) cells calculated using live-cell imaging in a microfluidic device (*6*). The Δ*ypt11* distribution was found to be bimodal, consisting of two Gaussian-like populations (light and dark turquoise curves), and the maximal life span (cells living beyond 30 generations) (fig. S15) was found to be significantly higher for Δ*ypt11* than for wild-type cells [statistical details in (*6*)].

mother mitochondrial content increased transiently, presumably because mitochondria could not be redistributed into the buds. Mother-daughter mitochondrial content asymmetry was thus eliminated in the absence, and was enhanced with overexpression, of Ypt11p (Fig. 4C), suggesting that Ypt11p contributes to this asymmetry. However, in all three cases, the proper volume ratio was achieved in the bud at division. We thus propose that yeast cells can somehow sense mitochondrial accumulation kinetics in the bud and respond to ensure that the target volume ratio is achieved in time for division. The compensatory behavior observed in Δ*ypt11* mutants likely involves one or both of the remaining mitochondrial inheritance pathways (*6*, *10*), which themselves may also contribute to mother-daughter mitochondrial content asymmetry.

Δ*ypt11* buds could potentially reach the proper mitochondrial volume ratio by slowing their growth and "waiting" for the delayed mitochondrial content to catch up. We analyzed time courses of Δ*ypt11* cells and found that buds indeed grew at slower rates and for a longer time before division (Fig. 4D). Mutants with the longest budding durations exhibited greatly decreased mitochondrial volume ratios at the time when normal Δ*ypt11*cells would divide (fig. S13). However, Δ*ypt11* cells divided with buds of a smaller size than wild-type buds, suggesting, unexpectedly, that cell size may be affected by mitochondrial inheritance kinetics. Yeast cell size is known to respond to changes in metabolism brought about by nutritional environment (*11*), suggesting perhaps that a delay in mitochondrial inheritance somehow altered the cell's metabolic state even though its environment remained unchanged.

We tested whether simply delaying redistribution of mitochondria into the bud could alter the age-dependent loss of volume ratio observed in wild-type mothers (Fig. 3D). Aging Δ*ypt11* mothers lost mitochondrial volume ratio much more slowly than wild-type mothers (Fig. 4E and fig. S14). Replicative life-span distributions of Δ*ypt11* mutants (*6*) were similar to *Δmmr1* mitochondrial inheritance mutants (*12*). The Δ*ypt11* distribution was statistically bimodal (*6*), consisting of a shorter-lived population, not seen in wild type, and a longer-lived population with both a slightly increased average and significantly increased maximum life span compared with wild type (Fig. 4F and fig. S15) (*6*). Because of their decreased life spans, short-lived Δ*ypt11* cells represent a decreasing proportion of the aging Δ*ypt11* population (e.g., 19 and 5% of cells at generations 6 and 10). Thus, the Δ*ypt11* cells with increased mitochondrial volume ratios at later generations consisted almost entirely of the second population with a longer life span than wild-type cells. Thus, in addition to the quality of mitochondria retained in the mother (*12*), their quantity may also contribute to their replicative life spans.

The failure of mother cells to maintain mitochondrial volume ratio suggests that they either cannot sense reduced content or are unable to compensate for the loss. Failing to preserve her own mitochondrial volume ratio could be the cost incurred for generating the healthiest, fittest offspring upon division.

References and Notes

1. A. Devin, M. Rigoulet, *Toxicol. Mech. Methods* **14**, 271 (2004).
2. J. W. Posakony, J. M. England, G. Attardi, *J. Cell Biol.* **74**, 468 (1977).
3. K. Tanaka, T. Kanbe, T. Kuroiwa, *J. Cell Sci.* **73**, 207 (1985).
4. M. Uchida *et al.*, *Yeast* **28**, 227 (2011).
5. J. Nunnari *et al.*, *Mol. Biol. Cell* **8**, 1233 (1997).
6. Materials and methods are available as supplementary materials on *Science* Online.
7. C. L. Woldringh, P. G. Huls, N. O. Vischer, *J. Bacteriol.* **175**, 3174 (1993).
8. J. S. Huxley, G. Teissier, *Nature* **137**, 780 (1936).
9. T. Itoh, A. Watabe, A. Toh-E, Y. Matsui, *Mol. Cell. Biol.* **22**, 7744 (2002).
10. R. L. Frederick, K. Okamoto, J. M. Shaw, *Genetics* **178**, 825 (2008).
11. J. J. Turner, J. C. Ewald, J. M. Skotheim, *Curr. Biol.* **22**, R350 (2012).
12. J. R. McFaline-Figueroa *et al.*, *Aging Cell* **10**, 885 (2011).

Acknowledgments: We thank J. Nunnari, J. Shaw, and A. Lewandowska for plasmids, strains, and discussions; G. Pesce for sharing unpublished results and discussions; and A. Caudy, E. Hong, K. C. Huang, A. Rosebrock, and the Marshall laboratory for reading the manuscript. Microscopy was performed at the UCSF Nikon Imaging Center. This work was supported by Sandler and Boyer Postdoctoral Fellowships (S.M.R.); the Herbert Boyer Junior Faculty Endowed Chair Award and NIH grant R01GM097017 (W.F.M.); an NIH National Research Service Award fellowship (Y.-H.M.C.); Fundação de Amparo à Pesquisa do Estado de São Paulo (05/00587-5, 07/50882-9) and Conselho Nacional de Desenvolvimento Científico e Tecnológico (301303/06-1) grants (L.d.F.C. and M.P.V.); NIH grants R01GM070808, R01GM026259, P50Gm081879, and a Packard Fellowship (Y.Z. and H.L.); a China Scholarship Council (CSC) scholarship (Y.Z.); and NIH grant 5RO1GM097213-02 (P.Y. and J.C.F.). Image analysis algorithms are described in detail in methods (*6*). The data are included in the main and supplementary figures.

Supplementary Materials

www.sciencemag.org/cgi/content/full/338/6108/822/DC1
Materials and Methods
Figs. S1 to S21
References (*13*–*32*)

6 June 2012; accepted 18 September 2012
10.1126/science.1225720

Downloaded from www.sciencemag.org on November 9, 2012

New Products

CHIRAL MEDIA

Lux Cellulose-1 and -2 are unique and complementary chiral stationary phases, which are now available in a 10 µm particle size for batch preparative chromatography. The two cellulose-based phases add to a dependable, high-resolution screening set with a wide range of selectivity. The new 10 µm particles are available both in Axia-packed preparative columns, and in bulk, enabling customers to pack their own columns. Lux chiral phases Cellulose-1, -2, -3, and -4 are already offered in 20 µm bulk media for use in batch preparative and simulated moving bed chromatography. Packing columns with new 10 µm particles delivers increased efficiencies by enabling the use of shorter columns without compromising results. Lux Cellulose phases benefit from Phenomenex's unique manufacturing process and silica coating technology. Lux Cellulose-1 uses cellulose tris (3, 5-dimethylphenylcarbamate) as the chiral selector. Lux Cellulose-2 provides a second chiral selector, cellulose tris (3-chloro-4-methylphenylcarbamate), providing a unique chlorinated stationary phase with complementary selectivity to Lux Cellulose-1.

Phenomenex

For info: 310-212-0555 | www.phenomenex.com



DNA CLONING AND ASSEMBLY KITS

GeneArt Seamless PLUS Cloning and Assembly Kits use a proprietary enzyme mix to recognize and precisely assemble DNA fragments without the need for restriction digestion, ligation, or introduction of extra DNA sequence (seamless). The kits are designed to work with any vector a researcher chooses plus one to four fragments (or more depending on fragment sizes and workflow) in an in vitro, typically ≤30 minute room temperature reaction to create constructs up to 40 kb in size. The GeneArt Seamless Cloning and Assembly Enzyme Mix is the economical choice for creating constructs up to 13 kb with the option for high throughput assembly. The GeneArt Site-Directed Mutagenesis PLUS System can be employed to introduce deletions, insertions, and substitutions ranging from small to large fragment sizes and can facilitate single or multisite mutagenesis. Up to three sites can be edited in a single plasmid at greater than 90% efficiency.

Life Technologies

For info: 800-955-6288 | www.lifetechnologies.com

MODULAR CHROMATOGRAPHY SYSTEM

The ÄKTA pure is a chromatography system for flexible, reliable, and intuitive purification of proteins. ÄKTA pure is an easy-to-use modular system that offers the flexibility to support both routine and challenging purification requirements, as well as being adaptable to changing research needs. In today's research environment, scientists are often expected to undertake all aspects of the protein discovery workflow, from genomics to purification and characterization, and the requirement to isolate specific proteins at high purity in short timelines makes chromatography conditions and methodologies more challenging. ÄKTA pure is specifically designed to enable researchers—from beginners to experts—to easily isolate their target protein, whether under simple or complex conditions. ÄKTA pure eliminates the need for programming skills to control the chromatography run, with the addition of simple drag-and-drop method templates in the UNICORN 6 control software.

GE Healthcare

For info: 800-526-3593 | www.gelifesciences.com/aktapure

UV CROSSLINKER

A high-quality, inexpensive ultraviolet crosslinker that makes it possible to identify and analyze trace amounts of DNA/RNA with far greater sensitivity, accuracy, and speed than with conventional analysis. The Select XLE-Series UV crosslinker covalently binds nucleic acids to membranes in under 30 seconds—240 times faster than vacuum-oven baking. It has a unique true-ultraviolet (UV)-monitoring circuitry that safeguards valuable test results from washouts, even when the tubes age. Researchers also rely on this versatile instrument for eliminating polymerase chain reaction contamination, nicking ethidium-bromide-stained DNA in agarose gels, gene mapping for creating cleavage-inhibiting thymine dimers, RecA mutation screening in *E. coli*, UV sterilization, and miscellaneous UV-dosage applications. The Select Series crosslinker features a "smart" user-friendly, fully programmable microprocessor, built-in "help" messages, and an auto-repeat function that make its operation amazingly fast and simple. It features five 8-watt tubes and is available in a choice of 254 nm, 312 nm, and 365 nm versions.

Spectroline

For info: 800-274-8888 | www.spectroline.com

C-MOUNT SPECTROMETERS

A new series of adapters simplify the integration of c-mount cMOS and CCD cameras with McPherson high-performance spectrometers. Easy and secure c-mount adapters are suitable for cryogenic, TE-cooled, deep depletion, near infrared InGaAs, and sensitive Silicon visible range cameras. They fasten via one-inch, 32-pitch screw thread with 17.526 mm back distance to focal plane. C-mount adapters are widely used for many types of digital cameras. Two dimensional detectors like digital cameras are essential for techniques like spectral imaging and multi-fiber spectroscopy. The new McPherson adapters have a nested design to accommodate the threaded, rotating c-mount. The new adapters allow mounting c-mount detectors firmly, precisely, and in the correct rotational orientation on spectrometers to intercept well focused spectra at the focal plane. A micrometer inside the spectrometer—not a wiggly draw tube—allows precise and reproducible focus trimming (if required). The adapters are available as optional accessories for all new and legacy McPherson instruments.

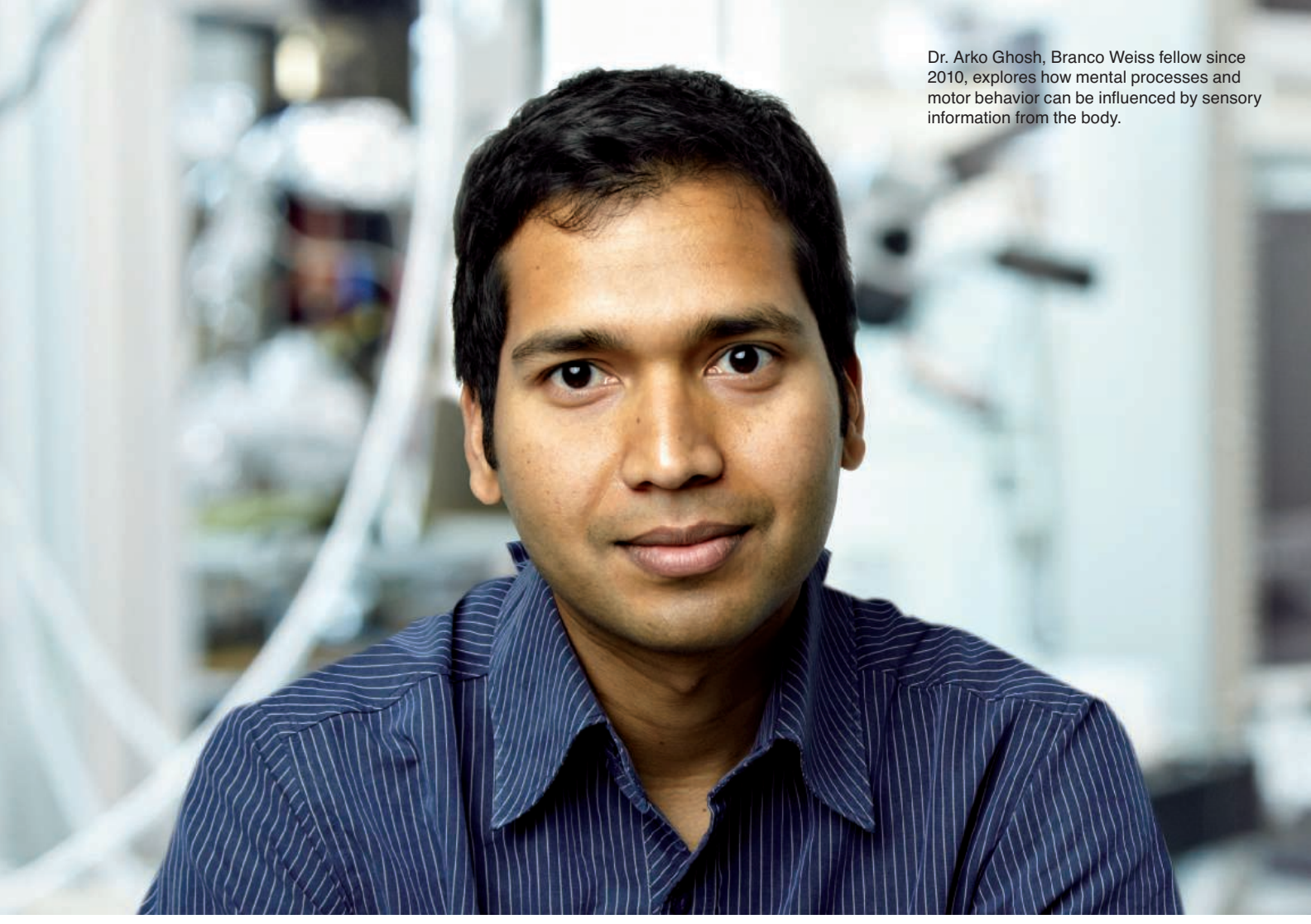
McPherson

For info: 978-256-4512 | www.mcphersoninc.com

Electronically submit your new product description or product literature information! Go to **www.sciencemag.org/products/newproducts.dtl** for more information.

Newly offered instrumentation, apparatus, and laboratory materials of interest to researchers in all disciplines in academic, industrial, and governmental organizations are featured in this space. Emphasis is given to purpose, chief characteristics, and availability of products and materials. Endorsement by *Science* or AAAS of any products or materials mentioned is not implied. Additional information may be obtained from the manufacturer or supplier.

Downloaded from www.sciencemag.org on November 9, 2012



Dr. Arko Ghosh, Branco Weiss fellow since 2010, explores how mental processes and motor behavior can be influenced by sensory information from the body.

Know what science will look like tomorrow?

Apply today.

The magnitude of the challenges we face today requires people with fresh thinking and novel approaches. To help find new ways forward, Society in Science – The Branco Weiss Fellowship gives extraordinary postdocs and engineers a generous grant to pursue an unconventional project for up to five years anywhere in the world. Have an idea that could change tomorrow? Get in touch with us today!

www.society-in-science.org

society in science
The Branco Weiss Fellowship

ETH
Eidgenössische Technische Hochschule Zürich
Swiss Federal Institute of Technology Zurich

cell sciences®

cytokine center

Browse our web site of recombinant proteins, including cytokines, growth factors, chemokines and neurotrophins. Daily shipping and competitive pricing are offered. Bulk quantities of many proteins available. Cell Sciences also carries corresponding antibodies and ELISA kits.



www.cellsciences.com

LIST OF PROTEINS

4-1BBL
4-1BB Receptor
6 Ckine
ACAD8
ACAT2
gAcrp30/Adipolean
Activin A
ACY1
ADAT1
Adiponectin
ADRP
AITRL
Akt1
Alpha-Feto Protein (AFP)
Alpha-Galactosidase A
Angiopoietin-1 (Ang-1)
Angiopoietin-2 (Ang-2)
Angiostatin K1-3
Annexin-V
apo-SAA
Apoliprotein A-1
Apoliprotein E2
Apoliprotein E3
Apoliprotein E4
APRIL
Artemin
ATF2
Aurora A
Aurora B
BAFF
BAFF Receptor
BCA-1 / BLC / CXCL13
BCMA
BD-1
BD-2
BD-3
BDNF
Bivalirudin
BMP-2
BMP-4
BMP-7
BMP-13
sBMPR-1A
Brain Natriuretic Protein
BRAK
Breast Tumor Antigen
C5a
C5L2 Peptide
C-10
C-Reactive Protein
C-Src
Calbindin D-9K
Calbindin D-28K
Calbindin D-29K
Calmodulin
Calcitonin Acetate
Carbonic Anhydrase III
Carcino-embryonic Antigen
Cardiotrophin-1
Caspase-3
Caspase-6
CD4
CD14
CD22
CD40 Ligand / TRAP
CD95 / sFas Ligand
CD105 / Endoglin
CHIPS
CNTF
Collagen
CREB
CTACK/CCL27
CTGF
CTGFL/WISP-2
CTLA-4/Fc
CXCL16
Cytokeratin 8
DEP-1
Desmopressin
Disulfide Oxidoreductase
E-selectin
ECGF
EGF
Elafin/SKALP
EMAP-II
ENA-78
Endostatin
Enteropeptidase
Eotaxin
Eotaxin-2
Eotaxin-3 (TSC)
EPHB2
EPHB4
Eptifbatide
Erk-2
Erythropoietin (EPO)
Exodus-2
Fas Ligand
Fas Receptor
FGF-1 (acidic)
FGF-2 (basic)
FGF-4
FGF-5
FGF-6
FGF-7/ KGF
FGF-8
FGF-9
FGF-10
FGF-16
FGF-17
FGF-18
FGF-19
FGF-20
sFGFR-1 (IIIc) / Fc Chimera
sFGFR-2 (IIIc) / Fc Chimera
sFGFR-3 / Fc Chimera
sFGFR-4 / Fc Chimera
sFlt-1 (native)
sFlt-1 (D3)
sFlt-1 (D4)
sFlt-1 (D5)
sFlt-1 (D7)
Flt3-Ligand
sFlt-4
sFlt-4/ Fc Chimera
Follistatin
FSH
Fractalkine/ CX3C
G-CSF
α-Galactosidase A
Galectin-1
Galectin-3
Gastrointestinal CA
GCP-2
GDF-3
GDF-9
GDF-11
GDNF
GLP-1
Glucagon
Goserelin
GM-CSF
GPBB
GROα
GROβ
GROγ
GRO/MGSA
Growth Hormone
Growth Hormone BP
GST-p21/WAF-1
HB-EGF
HCC-1
HGF
Histdyl-tRNA synthetase
Histrelin
HRG1-β1
I-309
I-TAC
IFN-α
IFN-α A
IFN-α 2a
IFN-α 2b
IFN-β
IFN-γ
IFN-Omega
IGF-I
IGF-II
proIGF-II
IGFBP-1
IGFBP-2
IGFBP-3
IGFBP-4
IGFBP-4
IGFBP-5
IGFBP-6
IGFBP-7
IL-1α
IL-1β
IL-2
IL-3
IL-4
sIL-4 Receptor
IL-5
IL-6
sIL-6 Receptor
IL-7
IL-8 (72 a.a.)
IL-8 (77 a.a.)
IL-9
IL-10
IL-11
IL-12
IL-13
IL-13 analog
IL-15
IL-16 (121 a.a.)
IL-16 (130 a.a.)
IL-17
IL-17B
IL-17D
IL-17E
IL-17F
IL-19
IL-20
IL-22
IL-31
Insulin
IP-10
JE
JNK2a1
JNK2a2
KC / CXCL1
KGF
L-asparaginase
LAG-1
LALF Peptide
LAR-PTP
LC-1
LBP
LD-78β
LDH
LEC/NCC-4
Leptin
LIGHT
LIX
LKM
LL-37
Lymphotactin
sLYVE-1
M-CSF
MCP-1 (MCAF)
MCP-2
MCP-3
MCP-4
MCP-5
MDC (67 a.a.)
MDC (69 a.a.)
MDH
MEC
Mek-1
MIA
Midkine
MIG / CXCL9
MIP-1α / CCL3
MIP-1β / CCL4
MIP-3 / CCL23
MIP-3α / CCL20
MIP-3β / CCL19
MIP-4 (PARC) / CCL18
MIP-5 / CCL15
MMP-3
MMP-7
MMP-13
Myostatin
Nanog
NAP-2
Neurturin
NFAT-1
beta-NGF
NOGGIN
NOV
NP-1
NT-1/BCSF-3
NT-3
NT-4
Ocreotide
Oncostatin M
Osteoprotegerin (OPG)
OTOR
Oxytocin
p38-α
Parathyroid Hormone
PDGF-AA
PDGF-AB
PDGF-BB
Persephin
PF-4
PIGF-1
PIGF-2
PKA α-subunit
PKC-α
PKC-γ
Pleiotrophin
PLGF-1
Polymyxin B (PMB)
PRAS40
PRL-1
PRL-2
PRL-3
Prokineticin-2
Prolactin
Protirelin
PTHrP
PTP1B
PTP-IA2
PTP-MEG2
PTP-PEST
sRANK
sRANKL
RANTES
RELM-α
RELM-β
Resistin
RPTPβ
RPTPγ
RPTPμ
SCF
SCGF-α
SCGF-β
SDF-1α
SDF-1β
Secretin
SF20
SHP-2
STAT1
c-Src
TACI
TARC
TC-PTP
TECK
TFF2
TGF-α
TGF-β1
TGF-β2
TGF-β3
Thymosin α1
sTIE-1/Fc Chimera
sTIE-2/Fc Chimera
TL-1A
TNF-α
TNF-β
sTNFR1
sTNFR2
TPO
TRAIL/Apo2L
sTRAIL R-1 (DR4)
sTRAIL R-2 (DR5)
TSH
TSLP
TWEAK
TWEAK Receptor
Urokinase
VEGF121
VEGF145
VEGF165
VEGF-C
VEGF-C I525
EG-VEGF
VEGF-E
HB-VEGF-E
sVEGFR-1
sVEGFR-2
sVEGFR-3
WISP-1
WISP-2
WISP-3
WNT-1

CELL SCIENCES INC • 480 NEPONSET STREET, BUILDING 12A, CANTON, MA 02021 • INFO@CELLSCIENCES.COM

TOLL FREE: (888) 769-1246 • TEL: (781) 828-0610 • FAX: (781) 828-0542 • WEB: WWW.CELLSCIENCES.COM



MiSeq®: Next-generation sequencing for all you seek.

You want amazing accuracy and performance on your benchtop. Illumina delivers—yet again. The MiSeq personal sequencer is the only fully integrated, truly end-to-end benchtop solution around. It's just one more example of why Illumina solutions generate a remarkable 90% of all the world's sequencing data. Discover what's possible.
www.illumina.com/miseq

illumina®

THE SECOND HOTTEST TOOL IN CHEMISTRY?



If you think Bunsen burners are hot, get to know SciFinder®, the world's hottest chemical information research product. Used by top scientists, SciFinder is the only tool that provides access to the most comprehensive and trustworthy chemistry-related content. And that's why SciFinder is the choice for chemistry research.™

Find out more at www.cas.org.

SciFinder®
The choice for chemistry research.™

New Products

CHIRAL MEDIA

Lux Cellulose-1 and -2 are unique and complementary chiral stationary phases, which are now available in a 10 µm particle size for batch preparative chromatography. The two cellulose-based phases add to a dependable, high-resolution screening set with a wide range of selectivity. The new 10 µm particles are available both in Axia-packed preparative columns, and in bulk, enabling customers to pack their own columns. Lux chiral phases Cellulose-1, -2, -3, and -4 are already offered in 20 µm bulk media for use in batch preparative and simulated moving bed chromatography. Packing columns with new 10 µm particles delivers increased efficiencies by enabling the use of shorter columns without compromising results. Lux Cellulose phases benefit from Phenomenex's unique manufacturing process and silica coating technology. Lux Cellulose-1 uses cellulose tris (3, 5-dimethylphenylcarbamate) as the chiral selector. Lux Cellulose-2 provides a second chiral selector, cellulose tris (3-chloro-4-methylphenylcarbamate), providing a unique chlorinated stationary phase with complementary selectivity to Lux Cellulose-1.



Phenomenex

For info: 310-212-0555 | www.phenomenex.com

DNA CLONING AND ASSEMBLY KITS

GeneArt Seamless PLUS Cloning and Assembly Kits use a proprietary enzyme mix to recognize and precisely assemble DNA fragments without the need for restriction digestion, ligation, or introduction of extra DNA sequence (seamless). The kits are designed to work with any vector a researcher chooses plus one to four fragments (or more depending on fragment sizes and workflow) in an in vitro, typically ≤30 minute room temperature reaction to create constructs up to 40 kb in size. The GeneArt Seamless Cloning and Assembly Enzyme Mix is the economical choice for creating constructs up to 13 kb with the option for high throughput assembly. The GeneArt Site-Directed Mutagenesis PLUS System can be employed to introduce deletions, insertions, and substitutions ranging from small to large fragment sizes and can facilitate single or multisite mutagenesis. Up to three sites can be edited in a single plasmid at greater than 90% efficiency.

Life Technologies

For info: 800-955-6288 | www.lifetechnologies.com

MODULAR CHROMATOGRAPHY SYSTEM

The ÄKTA pure is a chromatography system for flexible, reliable, and intuitive purification of proteins. ÄKTA pure is an easy-to-use modular system that offers the flexibility to support both routine and challenging purification requirements, as well as being adaptable to changing research needs. In today's research environment, scientists are often expected to undertake all aspects of the protein discovery workflow, from genomics to purification and characterization, and the requirement to isolate specific proteins at high purity in short timelines makes chromatography conditions and methodologies more challenging. ÄKTA pure is specifically designed to enable researchers—from beginners to experts—to easily isolate their target protein, whether under simple or complex conditions. ÄKTA pure eliminates the need for programming skills to control the chromatography run, with the addition of simple drag-and-drop method templates in the UNICORN 6 control software.

GE Healthcare

For info: 800-526-3593 | www.gelifesciences.com/aktapure

UV CROSSLINKER

A high-quality, inexpensive ultraviolet crosslinker that makes it possible to identify and analyze trace amounts of DNA/RNA with far greater sensitivity, accuracy, and speed than with conventional analysis. The Select XLE-Series UV crosslinker covalently binds nucleic acids to membranes in under 30 seconds—240 times faster than vacuum-oven baking. It has a unique true-ultraviolet (UV)-monitoring circuitry that safeguards valuable test results from washouts, even when the tubes age. Researchers also rely on this versatile instrument for eliminating polymerase chain reaction contamination, nicking ethidium-bromide-stained DNA in agarose gels, gene mapping for creating cleavage-inhibiting thymine dimers, RecA mutation screening in *E. coli*, UV sterilization, and miscellaneous UV-dosage applications. The Select Series crosslinker features a "smart" user-friendly, fully programmable microprocessor, built-in "help" messages, and an auto-repeat function that make its operation amazingly fast and simple. It features five 8-watt tubes and is available in a choice of 254 nm, 312 nm, and 365 nm versions.

Spectroline

For info: 800-274-8888 | www.spectroline.com

C-MOUNT SPECTROMETERS

A new series of adapters simplify the integration of c-mount cMOS and CCD cameras with McPherson high-performance spectrometers. Easy and secure c-mount adapters are suitable for cryogenic, TE-cooled, deep depletion, near infrared InGaAs, and sensitive Silicon visible range cameras. They fasten via one-inch, 32-pitch screw thread with 17.526 mm back distance to focal plane. C-mount adapters are widely used for many types of digital cameras. Two dimensional detectors like digital cameras are essential for techniques like spectral imaging and multi-fiber spectroscopy. The new McPherson adapters have a nested design to accommodate the threaded, rotating c-mount. The new adapters allow mounting c-mount detectors firmly, precisely, and in the correct rotational orientation on spectrometers to intercept well focused spectra at the focal plane. A micrometer inside the spectrometer—not a wiggly draw tube—allows precise and reproducible focus trimming (if required). The adapters are available as optional accessories for all new and legacy McPherson instruments.

McPherson

For info: 978-256-4512 | www.mcphersoninc.com

Electronically submit your new product description or product literature information! Go to **www.sciencemag.org/products/newproducts.dtl** for more information.

Newly offered instrumentation, apparatus, and laboratory materials of interest to researchers in all disciplines in academic, industrial, and governmental organizations are featured in this space. Emphasis is given to purpose, chief characteristics, and availability of products and materials. Endorsement by *Science* or AAAS of any products or materials mentioned is not implied. Additional information may be obtained from the manufacturer or supplier.

Announcing our new partnership with NASA Federal Credit Union

Dear Member:

AAAS is committed to offering you member benefits that fit your needs and make your membership more valuable.

With that in mind AAAS is embarking on a new partnership with NASA Federal Credit Union that will provide you with access to a wide range of financial tools and products. Like AAAS, NASA Federal Credit Union is dedicated to serving the scientific community. This shared perspective is just one of the many reasons that we are embarking on this partnership.

As you may know, we have recently ended our banking relationship with Bank of America, but we're confident that our new partnership with NASA FCU will provide you with a superior banking experience. NASA FCU offers members better ways to save and smarter ways to borrow with friendly, professional service – along with anytime, anywhere account access.

Moreover, unlike other financial institutions that have public stockholders, NASA FCU is a not-for-profit financial cooperative where being a member means being an owner, too. And as a member/owner, you will enjoy unique benefits like: better loan rates, higher dividends and state-of-the-art products and services.

We'll be sending you more information about this great new benefit over the coming months. In the meantime, be sure to visit **nasafcu.com/AAASpackage** to apply for the new AAAS Platinum Advantage Rewards or Platinum Cash Rewards credit cards. You can also take a sneak peek at the AAAS Check Card and Checks coming soon.

Sincerely,



Ian King
Director of Marketing and Membership, AAAS

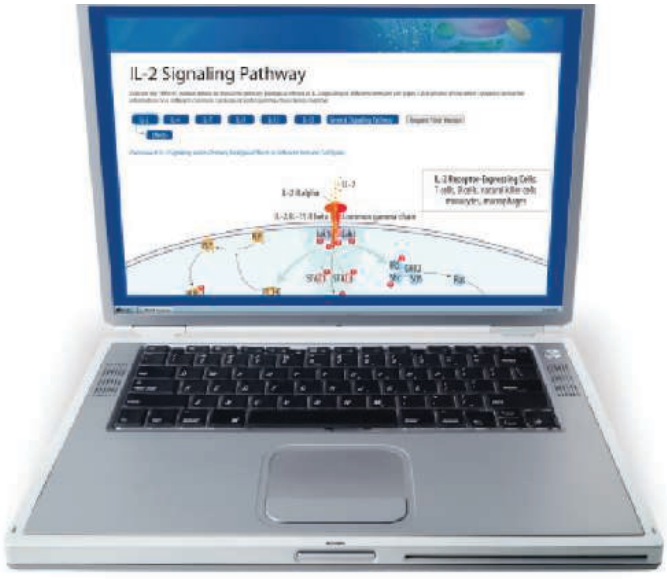
R&D Systems Tools for Cell Biology Research™

NEW Interactive Pathways & Processes

✓ Designed by scientists for scientists

✓ One click to access the widest collection of products

✓ Request a printed copy, which includes additional resources



R&D Systems is excited to announce the addition of Interactive Pathways & Processes to the growing list of reference tools available on our website. These new fully-interactive pathways allow you to explore a variety of biological processes, including Apoptosis, Wnt Signaling, and Th1 Differentiation.

Start exploring today
www.RnDSystems.com/**Pathways**

R&D SYSTEMS®

There's only one Science



Science Careers Advertising

For full advertising details, go to ScienceCareers.org and click For Employers, or call one of our representatives.

Tracy Holmes
Worldwide Associate Director
Science Careers
Phone: +44 (0) 1223 326525

THE AMERICAS

E-mail: advertise@sciencecareers.org
Fax: 202-289-6742

Tina Burks
East Coast/West Coast/South America
Phone: 202-326-6577

Allyson Rosen
Midwest/Canada/Corporate
Phone: 202-326-6578

Marci Gallun
Sales Administrator
Phone: 202-326-6582

Online Job Posting Questions
Phone: 202-312-6375

EUROPE & REST OF WORLD

E-mail: ads@science-int.co.uk
Fax: +44 (0) 1223 326532

Ben Asfaha
Phone: +44 (0)1223 326529

Lucy Nelson
Phone: +44 (0)1223 326527

Kelly Grace
Phone: +44 (0) 1223 326528

JAPAN

Yuri Kobayashi
Phone: +81-50-3696-5100
E-mail: ykobayas@aaas.org

CHINA & TAIWAN

Ruolei Wu
Phone: +86-1367-1015-294
E-mail: rwu@aaas.org

All ads submitted for publication must comply with applicable U.S. and non-U.S. laws. *Science* reserves the right to refuse any advertisement at its sole discretion for any reason, including without limitation for offensive language or inappropriate content, and all advertising is subject to publisher approval. *Science* encourages our readers to alert us to any ads that they feel may be discriminatory or offensive.

Science Careers
From the journal *Science* AAAS

European Commission

'Destination Europe' Conference

San Francisco, California 6-7 December 2012

Registration is open!

'Destination Europe' events showcase the vibrant and exciting research and innovation culture in Europe and the opportunities available to researchers, from anywhere in the world, interested in working in Europe. It is a joint initiative of the European Union and its Member States.

At the San Francisco event you will find:

- Experts from European research organisations, industry, universities, funding agencies and European Commission services who will present programmes, initiatives, excellent institutions and opportunities to develop innovation and technology transfer
- Researchers who have had the experience of moving to Europe temporarily or permanently and who will share their experience with you
- Information about the practicalities of moving to Europe (scientific visa, mobility centres etc.)
- An exhibition space with stands to provide additional information.



Venue: The Renaissance, Stanford Court Hotel, 905 California Street - Nob Hill, San Francisco, USA.
Cost: there will be no charge for participation, but prior registration will be obligatory.
Further Information and **on-line registration** details are available at:
http://destinationeurope.teamwork.fr/en/
http://www.facebook.com/ec.europa.eu

Research and Innovation



AAAS is here – helping scientists achieve career success.

Every month, over 400,000 students and scientists visit ScienceCareers.org in search of the information, advice, and opportunities they need to take the next step in their careers.

A complete career resource, free to the public, *Science* Careers offers a suite of tools and services developed specifically for scientists. With hundreds of career development articles, webinars and downloadable booklets filled with practical advice, a community forum providing answers to career questions, and thousands of job listings in academia, government, and industry, *Science* Careers has helped countless individuals prepare themselves for successful careers.

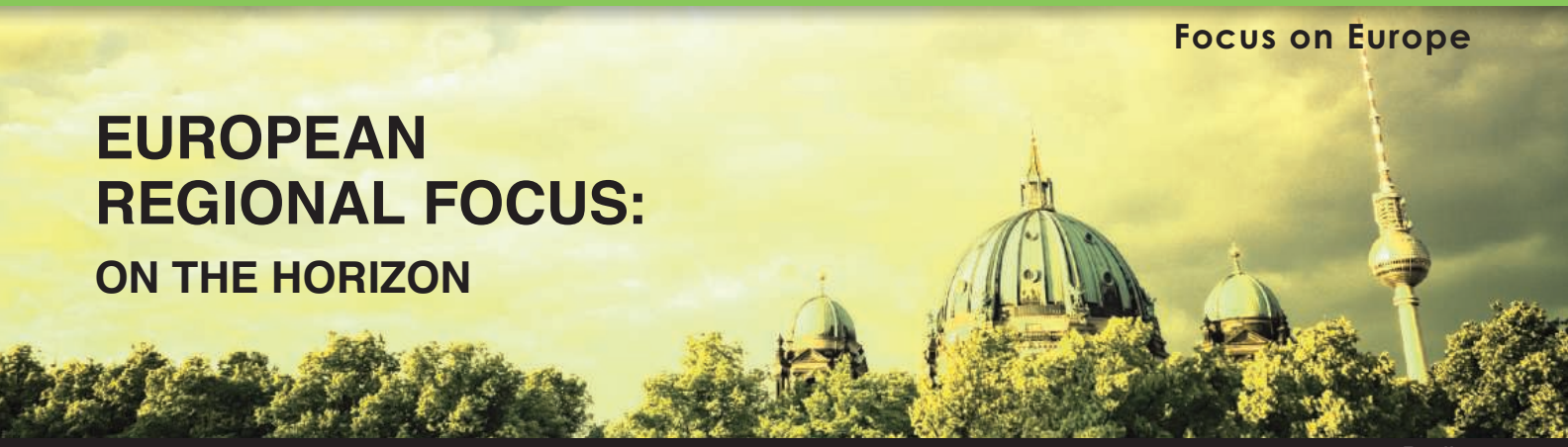
As a AAAS member, your dues help AAAS make this service freely available to the scientific community. If you're not a member, join us. Together we can make a difference.

To learn more, visit
aaas.org/plusyou/sciencecareers

AAAS + U = Δ

EUROPEAN REGIONAL FOCUS:

ON THE HORIZON



Berlin

Across Europe, budgets are tight. But investing in research and development drives economic growth, say scientific advisers. Our knowledge is a resource, they say, and countries with high research spending—Germany and Scandinavian countries such as Sweden—have high GDP growth. European Union politicians are getting the message as they plan Horizon 2020, a €90 billion program to fund European research in 2014–2020. In the meantime, educational and research institutions are preparing for science in an uncertain economy with practical training, applicable results, and networking to join forces with local and global partners. **By Chris Tachibana**

"Humans are meant to explore so we will always find a way to do that."

"All we hear about Europe is gloom and doom and the global economic crisis," says **Anne Glover,** "but we have a fantastic raw resource—our knowledge—so why not talk about that?" In January 2012, Glover became Europe's first chief scientific adviser, a job she previously held for her home country of Scotland. Now, she advises European Commission President José Manuel Barroso on scientific topics from global health to climate change.

Glover's message to European policymakers is that Europe's talent in science, engineering, and technology could boost the economy of the entire region—and she's confident her message is getting through. "Two things that might gladden hearts of young scientists are that in this economic environment, the president of the European Commission appointed a chief scientific adviser, so he regards science as crucial for the future of Europe. Also, even with fiscal constraint in other areas, the proposed budget for Horizon 2020 is a substantial increase from the previous program."

PLANNING FOR 2020

Horizon 2020 is the next European Union (EU) research funding program, running from 2014 to 2020 and taking over from FP7 (Framework Programme 7). Horizon 2020 is still under discussion by the EU governing bodies, so the proposed budget of nearly €90 billion is still uncertain. However, scientists are "reasonably optimistic" about the ongoing negotiations, says **Peter Tindemans,** secretary general of Euroscience, a nonprofit organization that supports and promotes science, similar to the American Association for the Advancement of Science. So far, the funding seems secure.

FP7 funding was under themes such as health, transport, and space. Horizon 2020 organizes activities under three priorities, or pillars: excellent science, competitive industries, and a better society. Don't worry, these changes are largely organizational, say those who are following the development of Horizon 2020. Scientists familiar with FP7 should be able to find opportunities in the new program.

Information and communication technology are priorities in Horizon 2020 under the excellent science and competitive industries pillars. An example is the Future and Emerging Technologies program that funds exploratory research and high-risk proposals. A related field to watch, says Tindemans, is data-driven science. This is emerging as a new scientific discipline as fields such as systems biology generate large amounts of data, driving a demand for facilities and methods for storing, managing, and analyzing large datasets.

Horizon 2020 includes initiatives to promote small and medium-sized enterprises, and public-private partnerships, and applicants will need to describe their potential return on investment. However, this is not new—EU funding programs have long encouraged collaborations between research institutions and industry. continued>

UPCOMING FEATURES

Faculty—February 1, 2013

Regional Focus on India—February 22, 2013

Postdocs—March 8, 2013

CREDIT: © ISTOCKPHOTO.COM/SIMMISIMONS

Focus on Europe

Tindemans says that policymakers and industry leaders continue to feel that basic research is a priority. Successful public-private partnerships work at the interface of basic and applied research, he says, with enough room for both types of science.

Professor **Elena Cattaneo,** School of Pharmacy, University of Milan, agrees but says that academic scientists are feeling a lot of pressure to do translational research, especially in her field of stem cell research. She urges caution, saying "There is nothing worse than clinical trials done too early." Cattaneo hopes funding agencies will remember that science is also about exploring the unknown. "How can we promise we will cure something without knowing precisely how tissue and cells work and how they are affected by a disease? We need the two elements of research—basic and translational—to work tightly together. Otherwise it is like asking to go from here to the moon without acknowledging that in many cases we do not even know where the moon is."



"We must maintain R&D and science education funding, or we'll waste investments over the last decade in infrastructure improvements and efforts to make research careers attractive to young scientists."

—Marja Makarow

ACTING LOCALLY

Many countries are looking for the balance between applied and basic science in their own research and training programs. In these uncertain economic times, practicality is often the strategy, with an emphasis on knowledge and technology transfer, job training, and public-private partnerships.

Practical training and industrial partnerships are actually long-term U.K. initiatives, says **Iain Cameron,** head of research careers for Research Councils UK (RCUK). For example, the country has an engineering Doctorate that is equivalent to a Ph.D. but with training that aligns with business practices. Rather than focusing on a single project, students conduct a series of smaller projects while spending time working in industry.

Cameron says that a specific area of emphasis in the past 10 years has been "training researchers to be aware of the transferable skills they have so they can be prepared for jobs outside of academia." He notes that 50 percent of Ph.D. students in the United Kingdom find work outside of universities, so "we want researchers to think about who will use the research they are doing, and what they will make of it." Thinking about the two-way transfer of knowledge and people that occurs between the research base and industry is a culture change in the educational system, says Cameron. RCUK is now studying the effects of the emphasis on practical training, for example tracking Ph.D. students to see if it helps them be more immediately effective in their jobs.

The United Kingdom, like several other European countries, is imposing strict austerity measures in response to the economic crisis. The RCUK budget is frozen at 2010 levels (about £2.5 billion annually) through 2015. Although this means budget reductions of about nine percent over four years, Cameron says that funding is still available for all research areas. That's good, says **Marja Makarow,** because this is a critical time for countries to continue research funding. Makarow, who was chief executive of the European Science Foundation through 2011 and is now vice president of the Academy of Finland (the Finnish Research Council), says we should remember that only five to seven percent of total European research funding is from the European Commission, with most support coming from individual countries. We must maintain R&D and science education funding, warns Makarow, or we'll waste investments over the last decade in infrastructure improvements and efforts to make research careers attractive to young scientists. "If we miss this opportunity," says Makarow, "we'll miss out on the next generation of researchers."

As we train young scientists to think about the future applications of their work, we also need to train them in knowledge and technology transfer that is smart, deliberate, and effective. This is the realm of **Guy A. Boy,** director of the Human Centered Design Institute of the Florida Institute of Technology, fellow of the Air and Space Academy in Toulouse, France, and author of the book *Orchestrating Human-Centered Design*. "We live in a very short-term-oriented society," says Boy. "Everything has to be effective now." However, fast and cheap rarely succeeds, especially in introducing research results into society, says Boy, who advocates for STEAM education—science, technology, engineering, and math—with art and creativity. Boy calls for a mature approach to introducing new inventions and technologies that considers the impact on society's practices and organizations. Human-centered design can ease the introduction of a new technology or policy, making it acceptable to the public. This approach requires input from the humanities and the arts, and in fact, Horizon 2020 includes funding and opportunities to integrate the humanities and arts into research activities.

LOOKING GLOBALLY

In addition to focusing on technology development and applications, European countries and universities are increasingly seeking to globalize. Spinning an international web with far-flung anchor points can support research by diversifying funding sources, continued>

challenges love solutions

We think there's a solution for every problem. That's why BASF researchers from all disciplines always work on innovations with passion. Help us, in a modern environment, to find not just products but comprehensive solutions for tomorrow's challenges. That's how we create chemistry. At BASF. Find out more now and apply at: **www.basf.com/career**



Visit us on Facebook: www.facebook.com/basfcareer

BASF
The Chemical Company

We proudly announce the foundation of the **German Centre for Integrative Biodiversity Research (iDiv)** which aims to become a world-class research centre in this emerging field. Its central mission is to promote **theory-driven experiments and synthesis** and **data-driven theory.** The concept of iDiv encompasses the detection of biodiversity, understanding its emergence, exploring its consequences for ecosystem functions and services, and developing strategies to safeguard biodiversity under global change.

iDiv
German Centre for Integrative Biodiversity Research

iDiv is a **National Research Centre** funded by the German Research Foundation (DFG). It is located in the city of Leipzig and jointly hosted by the Friedrich Schiller University Jena (FSU), the Martin Luther University Halle-Wittenberg (MLU), the University of Leipzig (UL) and the Helmholtz Centre for Environmental Research – UFZ. It is supported by the Leibniz Association, the Max Planck Society, the Klaus Tschira Foundation and the Free State of Saxony. Under one roof, 85 scientists and 45 support staff will collaborate in a highly integrated environment and benefit from central services (IT, eco- and bioinformatics, mechanics workshop, greenhouses).

The **iDiv founders form a consortium** of internationally renowned labs covering many aspects of biodiversity sciences and leading or co-leading several large-scale biodiversity experiments (e. g. Jena Experiment, BEF-China project, German Biodiversity Exploratories). The UFZ is currently establishing two new platforms: the *Global Change Experimental Facility (GCEF)* on 4 ha and a mesocosm ecotron facility. iDiv founders have initiated biodiversity databases of global relevance and host important biodiversity collections. Several groups work in the field of ecological theory and modeling.

As a unique feature, **a Synthesis Centre for Biodiversity Sciences (sDiv)** is integrated in the research environment of iDiv and offers international workshops, postdoc positions, and a sabbatical program to foster theory and synthesis. The **young biodiversity research training group (yDiv)** creates a new generation of biodiversity scientists with a solid theoretical background combined with diverse experimental and computational skills.

The alliance of the three universities (FSU, MLU, UL) and the UFZ invites applications for eight full professor positions (salary W3):

A professorship in "Theory in Biodiversity Sciences"

will develop comprehensive theories on the emergence and functional role of biodiversity using a synthetic and data-oriented approach (affiliated with FSU).

A professorship in "Experimental Interaction Ecology"

will analyze the role of trophic diversity and the linkage of below and aboveground interaction networks for ecosystem functions under climate change (affiliated with UL).

A professorship in "Molecular Interaction Ecology"

will use "omic" approaches to characterize structural and functional diversity in terrestrial or aquatic interaction networks (affiliated with FSU).

A professorship in "Evolution and Adaptation"

will address accelerated evolution and adaptation in host-pathogen systems and invasive species as well as community evolution under climate change (affiliated with UL).

A professorship in "Physiological Diversity"

will explore the physiological dimension of fundamental functional trade-offs across the plant kingdom using up-to-date analytical methods (affiliated with MLU).

A professorship in "Biodiversity Conservation"

with strong roots in both theoretical and empirical ecology and / or conservation genetics will translate modern biodiversity research into novel conservation concepts (affiliated with MLU).

A professorship in "Ecosystem Services"

will assimilate and analyze experimental and field data to link biodiversity patterns with ecosystem services at different scales (affiliated with FSU).

A professorship in "Biodiversity Synthesis"

will analyze large-scale datasets of biodiversity, ecosystem processes, environmental drivers and land-use as well as data from complex local experiments to test biodiversity theory using advanced computational methods (affiliated with MLU).

WHAT WE OFFER

The iDiv research centre is located on the BIO CITY campus (http://bio-city-leipzig.de) in Leipzig, a city known for its rich culture, excellent schools, and beautiful surroundings. Substantial funds for new personnel as well as start up grants for equipment are provided. Teaching will be at the affiliating university.

APPLICATION

We promote a research environment free of gender bias. Severely disabled persons are encouraged to apply and are preferred in the case of equal suitability. Applicants have an outstanding record in publications and third-party funding, experience in project coordination, and a successful teaching record. All iDiv groups are engaged in cross-disciplinary communication and outreach. Applications are in English with a detailed CV, certificates, complete publication list, description of teaching experience and successful grant applications. The cover letter summarizes past achievements, explains motivation to join iDiv and describes planned research and concepts of cooperation. Further information is given on www.idiv-biodiversity.de.

Applications should be sent before **November 30, 2012** in printed and electronic form (as a single pdf file). A detailed description of each professorship and the respective application address can be found under www.idiv-biodiversity.de.

Please note that although the deadline for these positions has been extended, this is not a new posting and applications already submitted will be considered and do not need to be resubmitted.

UNIVERSITÄT LEIPZIG
Friedrich-Schiller-Universität Jena
HELMHOLTZ ZENTRUM FÜR UMWELTFORSCHUNG UFZ
MARTIN-LUTHER-UNIVERSITÄT HALLE-WITTENBERG



Research is still your favorite?

MAKE GREAT THINGS HAPPEN

Opportunities for research scientists and professionals: You have always strived to sustainably improve the patients' lives. Welcome to Merck. Contribute to exciting research projects in one of our high-growth therapeutic areas – cancer, neurodegenerative as well as autoimmune and inflammatory diseases, infertility and hormone disorders. We offer excellent development perspectives and exceptionally quick decision-making processes you will only find in mid-sized companies like ourselves. Join us and take part in shaping our diversified bio pharma business. Ready to tread new paths?

come2merck.com

Merck Serono
Living science, transforming lives

MERCK

Focus on Europe



"In our world, in the 21st century, scientists are inventing the future. Why not be part of that?"

—Anne Glover

increasing collaborations and business opportunities, and tapping into the global talent pool.

The Freie Universität Berlin has relied on international partnerships since its founding after World War II as an educational institution committed to being free of Soviet political influence. The global perspective has continued throughout the university's history. For universities seeking international research collaborations, President **Peter-André Alt** advises that these types of partnerships are most successful when the universities are matched in their fields of strength, size of faculty, and number of students.

In contrast, study abroad exchanges can focus on complementary, rather than shared strengths, says Alt. For example, Freie Universität Berlin has student exchanges with emerging countries such as Egypt. The university's first exchange students went to Stanford in 1949 and now roughly half of all Freie Universität Berlin undergraduates participate in a study abroad. Universities should encourage this by being flexible in accepting credit for classwork done abroad, says Alt. He hopes that U.S. universities in particular will encourage European partnerships and study abroad programs, noting that the current U.S. focus on Asia is causing his university to work more with Canada, which tends to be more focused on Europe.

Effective globalization relies on creating a solid network and knowing how to use it. **Angie Bukley** is dean and vice president for academic affairs at the International Space University (ISU) in Strasbourg, France. She has experience in the academic and corporate worlds, a job that spans multiple countries, and 500+ LinkedIn connections. Although ISU combines space and education—two areas that are prime targets for financial austerity advocates—75 percent of ISU graduates successfully find jobs in their field. Contacts are the secret, says Bukley. "ISU has more than 3,300 graduates in over 100 countries, many in high-level management positions, so we really leverage that network to help students find internships and jobs."

Bukley takes the long view and has no qualms about promoting space science and engineering careers. "I've been around for a while and seen the economy go up and down," she says. "Humans are meant to explore so we will always find a way to do that." In promoting its programs, ISU can play the technology transfer card, pointing to civilian applications such as weather graphics, remote sensing, and global satellite positioning that have come from government and military research including space science. Bukley is optimistic about the future of European research. Having worked in both the United States and the EU, she says that although the EU is extremely slow in making decisions, once they decide to fund something, "it's pretty solid," unlike funding in the United States, which can involve ongoing negotiations, contingencies, and post-award cuts.

MOVING EAST

To make international exchanges easier, many universities are establishing a physical presence in another country, particularly in Asia. Germany's Max Planck Society has several international partner institutes and centers, including in Shanghai. In 2010, the eight Danish universities and the Graduate University of the Chinese Academy of Sciences created the Sino-Danish Center for Education and Research near Beijing. Work has begun on a new building for the center, which has a goal of 100 researchers, 100 Ph.D. students, and 300 Master's students by the end of 2013. European and Chinese students gain research experience on collaborative projects and take classes together in English, led by Danish and Chinese professors. Currently, students can earn a Master's degree in Neuroscience and Neuroimaging, Water and Environment, Innovation Management, and Public Management and Social Development, with additional Master's programs in Nanoscience and Nanotechnology, Chemical and Biochemical Engineering, and 'Omics starting in 2013.

"Personally, I think it's a great opportunity for students," says **Hans Gregersen**, executive director of the Sino-Danish Center. "They'll get a degree with Danish and Chinese accreditation and multicultural experience. We hope they'll learn the language. About 500 Danish companies are active in China, and we think these and other companies will want to employ our students after they graduate."

Another institution reaching out to the East is ETH continued>

CREDIT: EUROPEAN UNION 2012

ÉCOLE POLYTECHNIQUE
FÉDÉRALE DE LAUSANNE

Assistant Professor of Translational Cancer Science

Swiss Institute for Experimental Cancer Research (ISREC)
at Ecole polytechnique fédérale de Lausanne (EPFL)

We seek to appoint a tenure track assistant professor to develop an innovative research program studying mechanisms of cancer, with a strategic goal to apply unfolding knowledge to better detect, evaluate, and treat human cancers. The successful candidate will join the faculty of ISREC **http://isrec.epfl.ch**, one of the four institutes of the School of Life Sciences at EPFL, the Swiss Federal Institute of Technology Lausanne **http://sv.epfl.ch**. ISREC is based on the shore of Lake Geneva amidst the EPFL campus and its interactive faculty in life sciences, chemistry and physics, computer science, and engineering. ISREC plans to establish a translational cancer research branch proximal to the new Department of Oncology at the University of Lausanne (UNIL), located at its teaching hospital and biomedical research campus (CHUV), positioned to nucleate substantive collaborations with clinical investigators. The successful candidate will participate in a new multi-institutional cancer center – the Swiss Cancer Center Lausanne – involving CHUV, UNIL, and EPFL. Lausanne is centrally located in Europe **http://www.lausanne.ch** amidst a vibrant academic and biopharmaceutical research community spanning from Geneva to Montreux **http://www.bioalps.org** and more broadly to Basel and Zurich.

We are particularly interested in candidates whose research will integrate basic and translational approaches, in areas including: tumor immunology & immunoengineering (e.g. novel strategies for manipulating anti-tumor immunity); functions and regulation of the tumor microenvironment; inflammation & cancer; mechanisms of disease in specific tumor types (e.g. melanoma, brain, gastrointestinal); tumor metabolomics & energetics; cancer stem cells; and systems approaches to cancer genetics and epigenetics.

ISREC faculty members receive generous core support (salary and research funds) with the expectation that their research programs will be similarly complemented by extramural grant support. Participation in undergraduate and graduate teaching is required. ISREC and the School of Life Sciences have an excellent infrastructure, including a number of technology core facilities **http://sv.epfl.ch/platforms**

Competitive applicants for appointment are envisioned to have an exceptional track record of accomplishment, with evident future potential and commitment to translational/applied cancer research, and teaching. Candidates are requested to submit via the website below, in separate PDF files, a curriculum vitae with a list of three-five mentors who can provide letters of recommendation, a list of publications (annotated to indicate the candidate's contributions), a brief statement of teaching interests and experience, and a 2–3 page research synopsis that both summarizes current/past research accomplishments and presents a strategic vision for development of the candidate's research program in the next 5–10 years.

Applications should be uploaded at
http://isrec-search.epfl.ch

The application deadline is **January 7, 2013**, after which there is no guarantee of consideration.

Inquiries may be addressed to:

Professor Douglas Hanahan,
Director, ISREC
School of Life Sciences
EPFL
CH-1015 Lausanne, Switzerland
Email: dh@epfl.ch

EPFL is committed to expanding the ranks of women on its faculty, and qualified women are strongly encouraged to apply.

FOCUS ON EUROPE Science Careers online @sciencecareers.org

Focus on Europe

Featured Participants

Academy of Finland
www.aka.fi/eng

Air and Space Academy
www.academie-air-espace.com

ETH Global
www.global.ethz.ch

European Commission
ec.europa.eu/index_en.htm

European Science Foundation
www.esf.org

Euroscience
www.euroscience.org

Florida Institute of Technology
www.fit.edu

Freie Universität Berlin
www.fu-berlin.de/en

International Space University (ISU)
www.isunet.edu

Research Councils UK
(RCUK) - www.rcuk.ac.uk

Sino-Danish Center for Education and Research
www.sinodanishcenter.com

University of Milan
www.unimi.it/ENG


University of Milan

Zurich, a public Swiss science and technology university. ETH Zurich has had international engagements before, including outreach to China in the 1980s, but marked a new era with ETH Global, a center for international exchange and interdisciplinary projects. The ETH Global perspective is that developing countries are an opportunity and a growing market for smart, clean development. Europe can provide the methods and means for this development, from sustainable city planning and high-precision machinery such as tunnel-boring machines, to personal items such as pharmaceuticals. ETH has decided this strategy requires being on site in regions such as Africa, South America, and Asia.

This is what brought Professor **Gerhard Schmitt,** ETH Zurich chair of information architecture and senior vice president, ETH Global, to Singapore. He is establishing the Singapore-ETH Center (SEC) for global environmental sustainability, currently with 140 faculty and students, funded by both ETH Zurich and the National Research Foundation of Singapore. Long-term goals are attracting the best students and faculty, while training them for international success. "Our first goal is top-quality research and education," says Schmitt, "but we also want to make people around the world more aware of ETH and recruit from the global pool. Intelligence and talent are distributed worldwide, so it doesn't make sense to exclude anyone." The first program of the SEC is the Future Cities Laboratory (FCL). With 31 nationalities in the program, FCL embodies the goals of ETH Global and the charrette approach to science. FCL is a nontraditional, nonsiloed research degree program, in which sociology, physics, architecture, engineering, and simulations contribute to a project, for example in transportation systems.

From its global efforts, ETH hopes to harvest novel education models, cultivate international collaborations, and broaden the institute's knowledge base. Even sabbaticals are a potential resource. Both faculty and academic staff have sabbatical leave opportunities, and are primed before they go to watch for institutional innovations that might improve ETH, and debriefed on their observations when they return. Schmitt says ETH has its own internal LinkedIn-type system: a database of international connections "so the ETH community knows who of our colleagues is interacting with whom around the globe and can connect to them."

INVENTING THE FUTURE

European countries and the EU are hoping that investment in R&D will drive economic growth. This is creating a world of opportunities for young scientists. The trend in globalization expands educational and job possibilities. "We're moving from a linear, local world to a world that is nonlinear and global," says Boy. His advice is to embrace the complexity and connectivity. Incorporate technology, arts, a variety of people and organizations into your work, and take advantage of the symbiosis.

Get connected to the world early, says Freie Universität Berlin President Peter-Andre Alt. "Study abroad is a great experience. It's helpful for communication, learning a different culture and system, and maybe also finding your own way." With companies, universities, and research institutions stressing globalization, it's also an experience that could pay off in the job market. Keep this in mind during your training, says RCUK's Iain Cameron. Think about implications, applications, and dissemination of your research. "Know the research environment and know your skills. Think about how to communicate what you can do to people in other disciplines, in industry, and internationally."

Finally, keep your eyes on the horizon. To young people considering a career in science, Europe's Chief Science Advisor Anne Glover says when you face challenges, remember the rewards of struggling with a concept then celebrating when you figure something out or make a discovery. "In our world, in the 21st century, scientists are inventing the future, says Glover. "Why not be part of that?"

Chris Tachibana is a science writer based in Seattle, USA, and Copenhagen, Denmark.

DOI: 10.1126/science.opms.r1200126

CREDIT: © ISTOCKPHOTO.COM/TELLA_DB

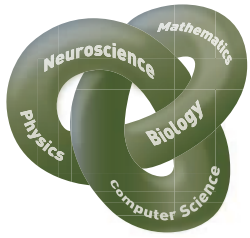


CAMPUS VISIT DAY
November 24, 2012

CALL FOR PhD STUDENTS

The Graduate School at IST Austria invites applicants from all countries to its PhD program. IST Austria is a new institution located on the outskirts of Vienna dedicated to cutting-edge basic research in the natural sciences and related disciplines. The language at the Institute and the Graduate School is English.

The PhD program combines advanced coursework and research, with a focus on Biology, Computer Science, Mathematics, Physics, Neuroscience, and interdisciplinary areas. IST Austria offers internationally competitive PhD salaries supporting 4–5 years of study. Applicants must hold either a BS or MS degree or equivalent.

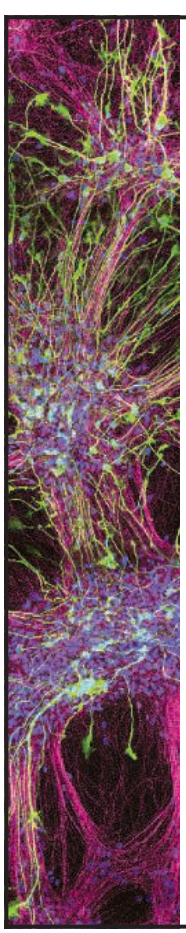


The Institute offers PhD students positions in the following fields:
Biology | Computer Science | Mathematics | Physics | Neuroscience

For a list of faculty members please visit www.ist.ac.at. For further information and access to the online application please consult www.ist.ac.at/gradschool. For inquiries, please contact gradschool@ist.ac.at. For students wishing to enter the program in the fall of 2013, the deadline for applications is January 15, 2013.

IST Austria is committed to Equality and Diversity.

IST AUSTRIA
Institute of Science and Technology



Group Leader(s)

The Wellcome Trust/Cancer Research UK Gurdon Institute, University of Cambridge
Salary to £52,706 (plus start-up package)

The Gurdon Institute is a world-renowned centre in the fields of developmental, cell, and cancer biology, located in the heart of the historic city of Cambridge, and part of the University's School of Biological Sciences. Founded in 1991, its purpose is to provide the best possible environment for research, and to foster interactions and collaborations between scientists with diverse but complementary interests. It is generously supported by core funding from the Wellcome Trust and Cancer Research UK, and benefits from state-of-the art facilities in a friendly, modern, purpose-built environment (see www.gurdon.cam.ac.uk).

We are now seeking to recruit one or more new Group Leaders and are particularly interested in applicants with fewer than seven years postdoctoral experience. This would be an ideal position for a scientist wishing to take up his or her first position as an independent researcher, and offers a world-class platform for career development. Informal enquiries are invited and can be directed to any of the Institute's Group Leaders.

Applicants should send a full Curriculum Vitae and a brief outline of research interests as a single PDF file, as well as a University application form (CHRIS/6 - available from http://www.admin.cam.ac.uk/offices/hr/forms/chris6/) to glsearch@gurdon.cam.ac.uk or to the Administration Secretary at the Wellcome Trust/Cancer Research UK Gurdon Institute, Tennis Court Road, Cambridge CB2 1QN, UK, Tel: +44 1223 334133, Fax: +44 1223 334134. Applicants should also arrange for three letters of reference to be sent to the same email or mailing address. Closing date for applications: 15th December 2012.

UNIVERSITY OF CAMBRIDGE

Gurdon INSTITUTE

UNIVERSITÄT BASEL

Professor in Molecular Stem Cell Biology

The Biozentrum of the University of Basel (Switzerland) invites applications for a Professorship in Molecular Stem Cell Biology at the rank of Assistant (tenure-track), Associate or Full Professor, depending on the qualifications of the applicant.

We are seeking outstanding candidates in basic molecular and cellular stem cell biology. Areas of research interests include, but are not limited to, stem cell-niche interactions, programming/reprogramming, differentiation/dedifferentiation and asymmetric cell division.

The ideal candidate should establish an internationally competitive research program, will complement currently existing strengths of the Biozentrum and will contribute to the Basel Stem Cell network. The successful candidate is expected to actively participate in teaching at the undergraduate and postgraduate level.

The Biozentrum offers an outstanding scientific environment and an attractive research endowment. Basel is the home of a vibrant international life science community and provides a high standard of living and a superb cultural atmosphere.

Applications, including CV, list of publications and a research program summary, should be sent by e-mail (pdf or zip to Prof. Dr. Jörg Schibler, Dean, Faculty of Science, University of Basel, Klingelbergstrasse 50, 4056 Basel, Switzerland, to dekanat-philnat@unibas.ch. For informal inquiries please contact Prof. Dr. Erich A. Nigg (erich.nigg@unibas.ch, phone: +41-61-267 16 56).

The deadline for receipt of applications is December 31, 2012. The University of Basel is an equal opportunity employer and encourages applications from female candidates.

UNI BASEL

New Phytologist
Tansley Medal
for excellence in plant science

Calling all early stage career scientists!
Deadline for submissions for 2013: 15 December 2012

Win £2000 (GBP) and have your work highlighted in *New Phytologist*, one of the world's leading plant science journals (2011 Impact Factor 6.645).

- The New Phytologist Tansley Medal is awarded annually in recognition of an outstanding contribution to research in plant science
- This is a global competition open to all plant scientists in the early stages of their career and includes both student and post-doctoral researchers with up to five years' experience, excluding career breaks, since gaining/defending their PhD
- Selection is based on a two-stage process:
 - **Stage 1)** Submit your CV, a personal statement and reference: Deadline: **15 December 2012**
 - **Stage 2)** Submission of a single-authored minireview intended for publication: **Deadline: 31 March 2013**
- All competition articles that are accepted after peer review will be published in *New Phytologist* and the Tansley medal winner selected by the judges from these final papers

New Phytologist

Full details, terms and conditions at:
www.newphytologist.org

bioss
CENTRE FOR BIOLOGICAL SIGNALLING STUDIES

UNI FREIBURG

The University of Freiburg (Germany) is accepting applications for the faculty position of a

Full Professorship (W3) for Pharmaceutical Technology and Biopharmacy

This chair is established by the Excellence Cluster of the University Freiburg: **BIOSS Centre for Biological Signalling Studies** (www.bioss.uni-freiburg.de) at the **Institute of Pharmaceutical Sciences**. We seek a visionary scientist with strong research credentials in "Molecular dynamics and engineering of membrane systems" or similar areas. Close cooperation within the BIOSS program and projects in pharmacy, biology or medicine are expected. Experience in teaching pharmaceutical technology and in acquisition of research grants is required.

Deadline for applications is **15.12.2012**. Applications including necessary supporting documents should be sent (exclusively in electronic form; email: kontakt@bioss.uni-freiburg.de) to: Dekan der Fakultät für Chemie, Pharmazie und Geowissenschaften, Hebelstraße 27, D-79104 Freiburg.

The University of Freiburg is an equal opportunity employer. Applications of women are strongly encouraged. Handicapped candidates with equivalent qualifications will be given preference. Applicants should ask for an application form for professorship at the Deans office.

Call for Candidates to a chair in Integrative Biology of Infection

The Institut Pasteur announces an international call for a Chair of "Infection Systems Biology" on its Paris campus. The position is open for an outstanding candidate who wishes to develop a cutting-edge research program on microbial pathogenesis (caused by virus, bacteria, fungi or protozoan parasites) with a strong focus/interest on systems-level proteomic approaches on any aspect of infection biology.

The chair holder will join the Laboratory of Excellence (LabEx) program called, "Integrative Biology of Emerging Infectious Diseases" (**IBEID: http://www.pasteur.fr/labex/ibeid**) and will benefit from the cutting edge interdisciplinary environment provided by the Institut Pasteur in Paris and by the LabEx.

The Chair will also benefit from the technical and scientific expertise of the Institut Pasteur proteomics core facility. He/she will have access to state-of-the-art equipment in mass spectrometry (last generation orbitraps equipped with ETD, MALDI-TOF/TOF, triple quadrupole) and separation techniques (nanoLC, UPLC, 2D gel electrophoresis) allowing high throughput data to be obtained. The platform has been completely renovated and is now part of a research unit in structural mass spectrometry and proteomics, with which interactions will be facilitated.

The candidate should have a PhD and/or MD degree, relevant experience as an independent investigator and a demonstrated track record of high productivity.

The deadline for applications is **April 1, 2013**. Short-listed candidates will be called for interview in **May-June 2013**, and decisions will be announced by **October 2013**.

General conditions and applications. The successful candidate will be appointed as Chair of Infection Systems Biology for a period of 8 years and will create an Infection Systems Biology research unit. The budget (up to 3,200,000€ over 8 years) includes a tenured salary for the Chair (if necessary), 3 three-year postdoctoral positions, a technician, half-time secretarial assistance, basic laboratory equipment, a substantial contribution to running costs and essential large equipment, and access to on-campus facilities including state-of-the-art technology platforms.

Candidates should send their formal applications by E-mail to the **Director of Scientific Evaluation, Prof. Alain Israël, at the Institut Pasteur (25, rue du Dr. Roux, 75724 Paris, France; ibeidchair@pasteur.fr)**.

The Application shall comprise the following (in order) in a single pdf file:
1. A brief introductory letter (candidates are encouraged to contact the IBEID coordinators, Pascale Cossart (**pascale.cossart@pasteur.fr**) or Philippe Sansonetti (**philippe.sansonetti@pasteur.fr**))
2. A Curriculum Vitae and a full publication list.
3. A description of past and present research activities (up to 5 pages with 1.5 spacing).
4. The proposed research project (up to 10 pages with 1.5 spacing) and how it would fit in the defined topic.
5. The names of 3 scientists from whom letters of recommendation can be sought, together with the names of scientists with a potential conflict of interest from whom opinions should not be requested.

LMU LUDWIG-MAXIMILIANS-UNIVERSITÄT MÜNCHEN
FACULTY OF PHYSICS

As one of Europe's leading research universities, Ludwig-Maximilians-Universität (LMU) Munich is committed to the highest international standards of excellence in research and teaching. Building on its more than 500-year-long tradition, it offers a broad spectrum of all areas of knowledge within its 18 Faculties, ranging from the humanities, law, economics and social studies, to medicine and the sciences. The **Faculty of Physics** invites applications for a

Professorship (W2) (6 years/tenure track) of Experimental Physics – Physics with Nanosystems

commencing as soon as possible.

The successful candidate is expected to represent the field of Physics with Nanosystems in research and teaching. The LMUinnovativ initiative „Functional Nanosystems" dedicates this position to the area of „Physics with macromolecular/colloidal nanosystems". Possible topics include molecular self-assembly, hybrid materials, energy conversion with hybrid Nano- and Biosystems, Nanoscopy, Nanooptics and Nanoelectronics. The participation in the interdisciplinary activities of the cluster of excellence "Nanosystems Initiative Munich" (NIM) and the "Center for NanoScience" (CeNS) as well as in several local collaborative research centres is possible.

LMU Munich seeks to appoint a highly qualified junior academic to this professorship and, therefore, especially encourages early-career scholars to apply. Prerequisites for this position are a university and a doctoral degree. With an excellent record in research and teaching to date, prospective candidates will have demonstrated the potential for an outstanding academic career.

The initial appointment will be for six years. After a minimum of three years, it can be converted into a permanent position pending a positive evaluation of the candidate's performance in research and teaching as well as his or her personal aptitude and if all legal conditions are met.

Under the terms of the "LMU Academic Career Program", in exceptional cases and subject to outstanding performance in research and teaching, the position may be converted from a W2 into a W3 Full Professorship at a later date.

LMU Munich makes a point of providing newly appointed professors with various types of support, such as welcoming services and assistance for dual career couples.

LMU Munich is an equal opportunity employer. Our success in increasing the number of female faculty members is substantial. To continue this process, applications by female candidates are most important to us. In addition, we aim to further increase the diversity of our faculty members and, therefore, explicitly encourage candidates from specific backgrounds to apply. Disabled candidates with essentially equal qualifications will be given preference.

Please, submit your application comprising a curriculum vitae, academic records, a list of publications, as well as a two-page summary of planned research activities to the **Dekan der Fakultät für Physik der Ludwig-Maximilians-Universität München, Schellingstr. 4, 80799 München, Germany,** not later than **January 15, 2013.**

Science Careers online @sciencecareers.org

Jiangsu Academy of Agricultural Sciences

Open position as Deputy Director and Full Professor in the Institute of Agricultural Facility and Equipment

Jiangsu Academy of Agricultural Sciences (JAAS) is a professional agricultural research and extension institution that has been established since 1932. JAAS ranks at the top of provincial agricultural academies in China in terms of the comprehensive strength in agriculture. JAAS's headquarter and main research facilities are located in Nanjing, Jiangsu,China.

Currently, JAAS is seeking a deputy director with the rank of full professor in the area of agricultural facility and equipment researches. Applicant should have a commitment to scientific excellence and the enthusiasm, energy, and innovative thinking necessary to lead a dynamic institute with a broad and diverse portfolio. Applicant must possess a faculty position already beyond the assistant professor level in a university or the equivalent position in a research institution. In addition, the candidate should demonstrate excellent records of research accomplishment and has a command of bilingual language for English and Chinese, both in spoken and written.

Successful applicant will be offered a competitive package, including sufficient laboratory space, startup funding, relocation fee and competitive salary commensurate with experience, in addition to a housing allowance, and other employee benefits. Applicant can go to **www.jaas.ac.cn** for application details.

In addition, more information for other regular faculty positions from JAAS relevant to a variety of disciplines in agriculture is also available at **www.jaas.ac.cn**.

Contact information
E-mail: **rsc-gbk@jaas.ac.cn**; Tel: **086-25-84390037**

STANFORD SCHOOL OF MEDICINE

Stanford University Medical Center

The Department of Genetics and the Center for Genomics and Personalized Medicine invites applications to fill a **TENURE-TRACK POSITION** at the **ASSISTANT, ASSOCIATE, and/or FULL PROFESSOR** level. Faculty rank will be determined by the qualifications and experience of the successful candidate.

We are interested in outstanding scientists with innovative research programs in any area of genetics and/or genomics. The successful candidate should have a Ph.D. and/or M.D. degree and a clear record of creative achievement. The predominant criteria for appointment in the University Tenure Line are a major commitment to research and to teaching.

Although all areas of genetics and genomics will be considered, we are particularly interested in candidates with an outstanding record of achievement in medical and clinical genetics and/or genomics. Candidates should be highly interactive, are expected to run a successful, independent research program, and to participate in teaching and other activities of the department.

The Department of Genetics and The Center for Genomics and Personalized Medicine at the Stanford University School of Medicine offer a highly collegial and interdisciplinary environment that spans clinical medicine, human genetics, model-organism genetics, and genome-scale approaches. For more information, see **http://genetics.stanford.edu**.

Stanford University is an Equal Opportunity Employer and is committed to increasing the diversity of its faculty. It welcomes nominations of and applications from women and members of minority groups, as well as others who would bring additional dimensions to the University's research, teaching, and clinical missions.

Candidates are encouraged to apply electronically by December 3, 2012 with curriculum vitae, a brief letter, and the names of three references, in one pdf file, with your last name in the subject line, to: search-genetics@stanford.edu. Applicants for the position at the Assistant Professor rank should also arrange to have three letters of evaluation sent to: **Michael Snyder, Chair, Department of Genetics, 300 Pasteur Drive, Alway M344, Stanford, CA 94305-5120; search-genetics@stanford.edu.**

Cornell University
Faculty Position in Molecular Medicine

The Department of Molecular Medicine at Cornell University in Ithaca, NY invites applications for a tenure-track faculty position at the rank of Assistant Professor. Applications from individuals at a more advanced rank may also be considered. We seek candidates dedicated to a mechanistic understanding of cellular function and dysfunction using structural, biochemical, or cell biological approaches. The successful candidate is expected to develop a strong and independent research program and contribute to the teaching activities of the Department.

Molecular Medicine is a basic science department located in the College of Veterinary Medicine and is committed to making discoveries that advance human and animal health. It is part of a vibrant and interdisciplinary Life Sciences community on Cornell's main campus in Ithaca, New York that includes the Weill Center for Cell and Molecular Biology and the Center for Vertebrate Genomics (Visit **http://www.cornell.edu/lifesciences/**).

Qualifications: Candidates should have a Ph.D., D.V.M., M.D, or equivalent degree, postdoctoral experience, a track record of excellence in research, and the potential to develop an outstanding, extramurally funded research program.

We welcome candidates who will create a climate that attracts students of all races, nationalities and genders. Women and minority candidates are strongly encouraged to apply. Cornell seeks to meet the needs of dual-career couples through a Dual Career program and is a member of the Upstate New York Higher Education Recruitment Consortium (**http://www.upstatenyherc.org**).

The application, submitted at **https://academicjobsonline.org/ajo/jobs/2255**, must include a cover letter, curriculum vitae, 2 to 3 page research plan, and email addresses for letter requests from 3 referees who will be invited to upload their letters at this site. The committee will begin considering applications December 10 and will continue until the position is filled.

Diversity and Inclusion have been and continue to be part of our heritage. Cornell University is a recognized EEO/AA employer and educator.

VirginiaTech
Invent the Future

College of Science

Integrated Science Faculty

As part of Virginia Tech's expanding presence in emerging interdisciplinary programs and degrees in nanoscience, neuroscience, and computational science, the College of Science seeks to fill tenure-track or tenured faculty positions to begin Fall 2013 at our Blacksburg, VA campus. These new faculty positions signify a continued University commitment to the importance of interdisciplinary science to help solve major societal challenges in energy, the environment, and health. Appointments at the rank of Assistant, Associate or Full Professor will be made in one of the College's eight departments: biological sciences, chemistry, economics, geosciences, mathematics, physics, psychology, and statistics.

New faculty associated with these interdisciplinary programs and degrees will be expected to participate in the College of Science's recently launched Integrated Science Curriculum (**www.science.vt.edu/isc**) and interdisciplinary courses, which collectively serve to build strong research and educational partnerships across the sciences. The successful candidates will be expected to establish a vigorous research program, teach effectively at the undergraduate and graduate levels, continue development of scholarly activities and professional capabilities, participate in department, college, and university governance, and pass a criminal background check. Occasional travel to attend professional conferences is required.

The positions are likely to be at the Assistant Professor level, but outstanding senior candidates will be considered. Please visit **www.science.vt.edu** and click on the links under Faculty Openings. Consideration of applications will begin as early as **December 1, 2012** and will continue until the positions are filled.

Virginia Tech is an AA/EEO Employer; applications from members of underrepresented groups are especially encouraged.

College of Science
Biological Sciences • Chemistry • Economics • Geosciences
Mathematics • Physics • Psychology • Statistics

Department of Biotechnology
Ministry of Science & Technology
Government of India

RAMALINGASWAMI RE- ENTRY FELLOWSHIP

Applications are solicited from Indian nationals working in overseas research institutions for the "**Ramalingaswami Re-entry Fellowship**", a re-entry scheme of the Department of Biotechnology (DBT), Ministry of Science & Technology, Government of India.

Aim of the Fellowship

The scheme is conceptualized with the aim of attracting highly skilled researchers (Indian nationals) working overseas in various cutting edge disciplines of biotechnology (agriculture, health sciences, bio-engineering, energy, environment, bioinformatics and other related areas), by providing them an attractive avenue to pursue R&D in Indian institutions.

Who is eligible to apply ?

The applicant should possess a Ph.D., M.D., M. Tech, M.VSc. or equivalent degree with an outstanding track record as reflected in publications and other recognitions and with at least three years of post-doctoral research experience in overseas research laboratories. Only candidates (Indian nationals) working overseas are eligible to apply. ***Those who have already returned to India and are currently working in India are not eligible.***

Researcher's upto 55 years of age as determined on closing date of application are eligible to apply.

Incentives of being a Ramalingaswami Fellow

1. This is a senior fellowship programme, and awardees are to be considered synonymous to the faculty/scientists at the level of Scientist-D. They are entitled to take up teaching/research assignments and supervising Doctoral/MS students.

2. The scheme provides a consolidated monthly remuneration of Rs. 75,000/. In addition, a House Rent Allowance of Rs. 7,500/- p.m. is given to fellows. In case where host institute provides accommodation to the fellow, no house rent allowance is admissible.

3. Fellows will receive a research/contingency grant of Rs. 10.00 lakhs for the 1st year, Rs. 7.50 lakhs for the 2nd year and Rs. 5.00 lakhs for the subsequent 3 yrs. for purchase of consumables, minor equipment, international and domestic travel, engaging manpower and other contingent expenditure to be incurred for the implementation of research proposal.

4. DBT encourages host institutions to provide medical benefits, transport allowance, leave travel allowance and other benefits as per their prevailing norms as applicable to their employees of the rank equivalent to Scientist D out of their own resources/ funds.

5. Fellows retain an option for drawing either the fellowship or salary if they are appointed at a suitable permanent scientific position. Fellows opting for salary can continue to avail the research /contingency grant with prior approval of DBT.

6. Ramalingaswami Re-entry Fellows could take up fellowship at any of the scientific institutes/ universities in the country. However, application should be duly forwarded by the competent authority of the host Institute.

7. Awardees are eligible to apply for research grants to any of the funding agencies towards accomplishment of research proposal. However, the Co-PI has to be a permanent employee of the host institution.

Tenure of fellowship

Fellows can draw fellowship for a term of five years. Fellowship is further extendable for another term on a fresh appraisal of performance of the fellow.

How to apply

Applications may be sent as per Proforma downloadable from DBT website (**www.dbtindia.nic.in**) and duly forwarded by the competent authority *to* ***Dr. Meenakshi Munshi , Director, Department of Biotechnology, Block-2, 7th Floor, CGO Complex, Lodhi Road, New Delhi -110 003, Email :- rls fellowship.dbt@nic.in*** latest by **31th December, 2012.**

THE HONG KONG UNIVERSITY OF SCIENCE AND TECHNOLOGY

School of Science
Lecturer I/II

The School of Science has opening(s) of Lecturer I/II in the Environmental Science Programs [ENVS]. The successful candidate is expected to contribute to both undergraduate and postgraduate teaching in the areas of (marine and atmospheric) environmental sciences and assist in curriculum development, student consultation and advising, and promotion of the Environmental Science Programs (at both UG and PG levels).

Successful applicants should have a PhD degree in the areas of marine/ environmental biology, environmental impact/risk assessment, conservation biology, or environmental chemistry with ample teaching experiences and proven ability to teach effectively in English.

The Environmental Science Programs [ENVS] was established in April 2012 under the School of Science. Professors under the Programs have excellent expertise and research experience particularly in atmospheric or marine environmental science. ENVS offers fundamental and research training in environmental field through an integrated undergraduate curriculum (BSc in Environmental Science) and research degree programs (MPhil/PhD in both Atmospheric and Marine Environmental Sciences). In response to the current needs of our society, we are planning to launch an MSc in Environmental Health and Safety Program in September 2013. HKUST is located ideally on the shoreline of Port Shelter which provides direct access to high quality seawater. The Coastal Marine Laboratory on campus is an essential infrastructure supporting our marine researches, while the Environmental Central Facility serves as a platform supporting our atmospheric researches. (Duration: 2 years, renewable)

For further details of the Environmental Science Programs, please visit http://envs.ust.hk/.

Starting salary will be commensurate with qualifications and experience. Fringe benefits including annual leave, medical and dental benefits will be provided. For appointment at Lecturer I rank, housing benefits will also be provided where applicable. A gratuity will be payable upon successful completion of contract.

Application Procedure

Applications including a curriculum vitae, a statement of research interests and teaching goals, and names and addresses of three referees should be sent, preferably by email (envsjob@ust.hk), to the **Environmental Science Programs, School of Science, HKUST, Clear Water Bay, Kowloon, Hong Kong** on or before **31 December 2012**. We thank applicants for their interest, but advise that only shortlisted candidates will be notified of the result of the application. The search will continue until the positions are filled.

(Information provided by applicants will be used for recruitment and other employment-related purposes.)

VANDERBILT UNIVERSITY

FACULTY POSITION IN MICROBIAL PATHOGENESIS
Department of Pathology, Microbiology and Immunology
Program in Microbial Pathogenesis
Vanderbilt University School of Medicine

The Department of Pathology, Microbiology and Immunology at Vanderbilt University School of Medicine invites applications for a tenure-track faculty position in microbial pathogenesis at the Assistant Professor level (PhD, MD, MD/PhD). Successful candidates will be expected to establish and maintain an independent research program and participate in teaching of graduate and medical students. Candidates should have substantial post-graduate training highlighted by peer-reviewed publications that demonstrate research productivity.

Vanderbilt University Medical Center, located on the Vanderbilt University campus, is home to internationally recognized programs in bioinformatics, drug discovery, global health, inflammation, imaging science, pharmacology, proteomics, and vaccine science. The School consistently ranks in the Top 20 US Medical Schools and provides outstanding opportunities for scholarship, collaboration, and teaching.

The Vanderbilt University campus is a National Arboretum located in the heart of Nashville, the capital of Tennessee. Known internationally as "Music City USA", Nashville is also the home to professional sports teams, the Nashville Symphony, the Frist Center for the Visual Arts, and numerous activities for outdoor enthusiasts. Nashville, Tennessee is a wonderful place to live, work, and raise a family.

Applicants should send a *curriculum vitae*, a statement of current and future research interests, and three letters of recommendation to: **Eric Skaar, Ph.D., Director, Program in Microbial Pathogenesis, Department of Pathology, Microbiology and Immunology, Vanderbilt University School of Medicine, Room A-5102, Medical Center North, 1161 21st Ave. S., Nashville, TN 37232**. Inquiries, applications, and recommendation letters can be directed via email to **eric.skaar@vanderbilt.edu**.

Vanderbilt University is an Affirmative Action/Equal Opportunity Employer. Women and minority candidates are encouraged to apply.

Science Careers online @sciencecareers.org

WASHINGTON STATE UNIVERSITY

CHAIRPERSON
DEPARTMENT OF VETERINARY MICROBIOLOGY AND PATHOLOGY
WASHINGTON STATE UNIVERSITY
PULLMAN, WA

The College of Veterinary Medicine at Washington State University seeks a distinguished researcher and academic leader to be Chairperson of the Department of Veterinary Microbiology and Pathology (VMP) (**http://www.vetmed.wsu.edu/depts-vmp/index.aspx**). As one of the foremost pathobiology departments in the nation, VMP's mission is to enhance animal and public health through training veterinary medical students, graduate students and residents, conducting global outreach, and performing biomedical research in immunology, infectious diseases, food safety, genomics, and pathology. VMP's strong, extramurally funded research programs benefit from close collaborative ties with the USDA/ARS Animal Disease Research Unit, and other College of Veterinary Medicine entities including the Washington Animal Disease Diagnostic Laboratory, the newly founded Paul G. Allen School for Global Animal Health, and the School for Molecular Biosciences. VMP excellence in teaching is supported by the first-in-the-nation College Teaching Academy, whose mission is to enhance educational enterprises at all levels. The Chairperson's portfolio includes fiscal management of VMP, participation in and promotion of mentoring and professional development for faculty members, and fostering curricular development and scholarship in teaching. The successful candidate will have a record of academic leadership, productive, sustained, extramurally funded, internationally recognized research, and excellence in graduate education. Applicants must hold an earned doctorate in microbiology, immunology, pathology, veterinary medicine, medicine or a related discipline and be eligible for academic appointment at the level of Professor.

Review of applications will begin **January 7, 2013**. To apply or obtain more detailed information go to **www.wsujobs.com**. For questions or confidential expressions of interest about this position candidates may email or telephone **Ms. Sue Zumwalt** at **szumwalt@vetmed.wsu.edu** or **509.335.6027**.

WSU is an EO/AA Educator Employer.

UK

BIOCHEMISTRY FACULTY POSITION

The Department of Molecular and Cellular Biochemistry invites applications for a tenure track faculty position at the Professor, Associate Professor or Assistant Professor level. We are particularly interested in candidates whose area of research complements departmental programs including, but not limited to the molecular basis of diabetes, cardiovascular disease, neuroscience, and cancer. The successful candidate must possess a Ph.D., M.D. or equivalent degree. Senior applicants must have an active, funded research program and junior applicants must have obtained external funding.

The successful candidate will benefit from a stimulating and collaborative environment within the department, a strong graduate program and state-of-the-art facilities in a new 185,000 ft^2 research building. Competitive start-up funds and appropriate space will be offered.

Evaluation of applicants will begin **December 2012**. Interested applicants should visit **http://medicine.mc.uky.edu/biochemreference/** to access the on-line faculty application. Required application materials include a curriculum vitae, a description of your current and future research program, and the names of three references. Inquiries may also be sent to the Faculty Search Committee at **Biochem@uky.edu**.

For further information about the Department, visit: **www.mc.uky.edu/biochemistry**

The University of Kentucky is an Equal Opportunity Employer and encourages applications from minorities and women.

Georgia Tech College of Engineering

EMORY UNIVERSITY SCHOOL OF MEDICINE

Faculty Position Openings
Atlanta, Georgia
Georgia Tech Campus

The Wallace H. Coulter Department of Biomedical Engineering, a joint department between Georgia Tech's College of Engineering and Emory University's School of Medicine, invites applications for tenure track faculty at the assistant, associate, and full professor levels. Applicant's research should be synergistic with the existing strengths in the department, which are described under Research Overviews on our website, **www.bme.gatech.edu**. We are particularly interested in applicants with expertise in cardiovascular biology/bioengineering, systems biology/synthetic biology, image processing/analysis, and pediatric bioengineering. However, outstanding applicants in other areas of research will also be considered.

Applicants must hold a doctoral degree (PhD, MD or MD/PhD) in engineering, the natural sciences, or medicine. Successful applicants will be expected to develop a funded research program and to participate in teaching and advising undergraduate and graduate students.

Applications with a statement of research and teaching interests, curriculum vitae, and names and complete contact information for three professional references should be sent to: **Amy Tang, Department of Biomedical Engineering, Georgia Tech and Emory University, 313 Ferst Drive, N.W., Atlanta, GA 30332 (Phone: 404-385-7177; e-mail: amy.tang@bme.gatech.edu)**. Applicants may also apply on-line at: **https://www.bme.gatech.edu/jobs/**

Application deadline: January 31, 2013

Applications from women and underrepresented minorities are encouraged. Georgia Institute of Technology and Emory University are AA/EOE Employers.

Boston, MA

Northeastern University

ASSISTANT OR ASSOCIATE PROFESSOR

The Department of Pharmaceutical Sciences at Northeastern University invites applications for a tenure-track or tenured faculty position at the rank of Assistant or Associate Professor. The position is in the area of Pharmaceutics and Drug Delivery and encompasses expertise in nano-biotechnology, nano-medicine, and tissue engineering.

The candidate should have demonstrated research productivity through a focused research program and complement the department's existing strengths in nano-sensors, nano-medicine, and drug delivery, as well as drug discovery/medicinal chemistry, neuropharmacology, inflammation and immunology, and translational imaging. The successful candidate will be expected to establish an extramurally-funded research program, participate in professional (PharmD) and graduate (MS and PhD) teaching, and provide service. Applicants with current transferable funding will be given a priority. The candidate must have experience in, or commitment to working with diverse student populations and/or in a culturally diverse work and educational environments. Interdisciplinary appointments and highly competitive start-up packages are available to qualified applicants.

Applications must be completely submitted on-line at: **http://apptrkr.com/296918** Applicants should submit a formal letter of interest, along with curriculum vitae and the names and addresses of three references. More information regarding this position may be obtained by contacting: S. John Gatley, Ph.D., Professor and Search Committee Chair, at s.gatley@neu.edu.

Northeastern University is an equal opportunity Title IX employer. Women and minority, and persons with disability are strongly encouraged to apply.

University of Southern California
Faculty Positions
Ming Hsieh Department of Electrical Engineering

The Ming Hsieh Department of Electrical Engineering (http://ee.usc.edu) of the USC Viterbi School of Engineering (http://viterbi.usc.edu) seeks outstanding faculty candidates for appointment as tenure-track assistant professor, tenured associate professor, or tenured professor. Specific areas of interest include but may not be limited to:

1. Communications and/or signal processing theory and methods relevant to distributed and collaborative information processing, data driven and adaptive learning methodologies, "big data," distributed storage, cloud computing, sparse representations, and networking.
2. Computer architecture, networks, VLSI and CAD, with emphasis on exascale, heterogeneous and accelerated computing, mission-critical systems, new domains (e.g. smart grid, cyber security, computation-driven science); algorithms and protocols for future wireless networks, interface of social and communication networks; extreme-scale, post-CMOS, bio-inspired, and ubiquitous computing, resilience, 3D VLSI, system-level design and verification, and new applications (e.g., biomimetic systems).
3. Electronic/quantum devices/circuits/systems based on emerging micro and nano science and technologies that will provide the basis for innovations as we transition to a post Moore's law era, and/or will be revolutionary for energy harvesting, micro power sources, ubiquitous health care, wireless communications, environmental monitoring, homeland and border security, etc.
4. Energy/power devices and systems, with possible application to smart grid, energy storage and generation, advanced battery science, low-cost monitoring of the health of electric power grids, advanced high-power electronics, efficient power generation and transmission, etc.

Outstanding senior applicants in the energy/power area who have demonstrated academic excellence and leadership may also be considered for the Lloyd Hunt Endowed Chair.

Faculty members are expected to teach undergraduate and graduate courses, supervise undergraduate, graduate, and post-doctoral researchers, and develop a funded research program. Applicants must have a Ph.D. or the equivalent in electrical engineering or a related field and a strong research and publication record. Applications must include a letter clearly indicating area(s) of specialization, a detailed curriculum vitae, a concise statement of current and future research directions, and contact information for at least four professional references. This material should be submitted electronically at **http://ee.usc.edu/about/2013_faculty_positions.htm**. Early submission is strongly advised and encouraged. The application review process will commence **January 2, 2013**.

The USC Viterbi School of Engineering is among the top tier engineering schools in the world. It counts 174 full-time, tenure-track faculty members, and is home to the Information Sciences Institute (ISI), two National Science Foundation Engineering Research Centers, the Department of Homeland Security's first University Center of Excellence (CREATE), and an Energy Frontiers Research Center (EFRC) supported by the Department of Energy. USC Viterbi faculty conduct research in leading-edge technologies with annual research expenditures typically exceeding $180 million.

We encourage applications from transformative scholars -- distinguished individuals whose accomplishments are transforming the field; and interdisciplinary scholars -- outstanding individuals engaged in research aligned with the interests of the department but whose research also cuts across other departments in the School and University.

USC values diversity and is committed to equal opportunity in employment.
Women and men, and members of all racial and ethnic groups are encouraged to apply.

STANFORD UNIVERSITY SCHOOL OF MEDICINE
DEPARTMENT OF MICROBIOLOGY AND IMMUNOLOGY

invites applications for a **tenure-track** faculty position

at the **Assistant Professor** level. We are looking for highly interactive candidates with outstanding records of research achievement in the area of **innate or acquired immunity, virology, bacteriology or parasitology or susceptibility genetics, with a potential emphasis on quantitative analysis or the molecular mechanisms of pathogenesis and symbiosis**. The predominant criteria for appointment in the University Tenure Line are major commitments to research and teaching.

The Department of Microbiology and Immunology (**http://microimmuno.stanford.edu**) is a collegial, interactive and interdisciplinary environment. Current faculty use classical, contemporary and cutting-edge approaches, enlivened by the entire Stanford research community. Applicants are expected to establish a vigorous and innovative research program that complements and extends the current research of the department and the university. Responsibilities will also include teaching graduate, undergraduate or medical students.

Interested applicants should submit a curriculum vitae, a two-page statement of research objectives and a statement of teaching preferences. Please arrange for three letters of reference to be sent directly to:

David Schneider, Ph.D. and Karla Kirkegaard, Ph.D.
c/o Mayumi Beppu
Department of Microbiology and Immunology
Stanford University School of Medicine
Fairchild Science Building
299 Campus Drive, D338d
Stanford, CA 94305-5124

Applications will be accepted until **December 31, 2012**.

Stanford University is an Equal Opportunity Employer and is committed to increasing the diversity of its faculty. It welcomes nominations of and applications from women and members of minority groups, as well as others who would bring additional dimensions to the university's research, teaching and clinical missions.

WASHINGTON STATE UNIVERSITY

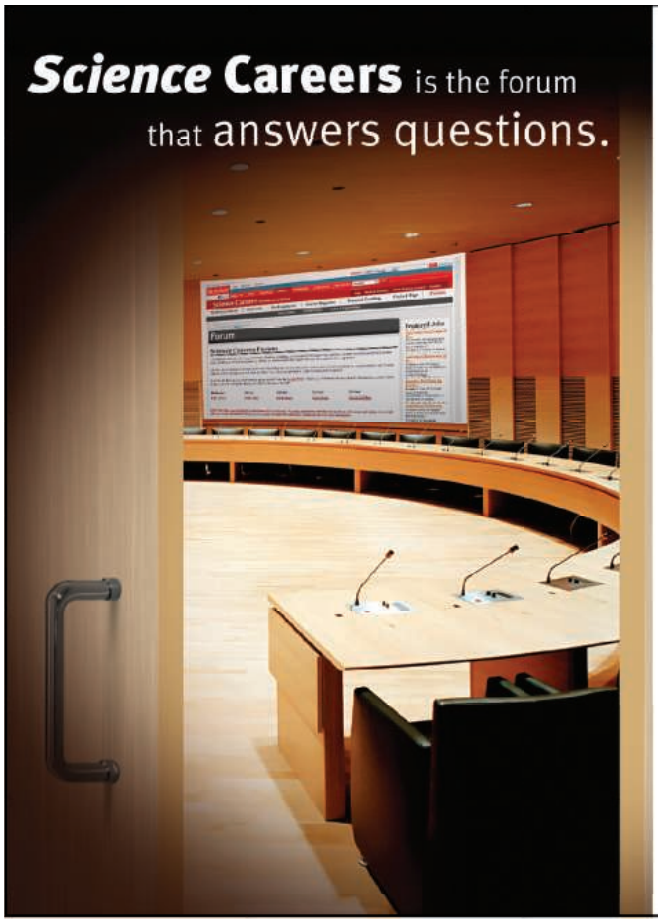
Director
Center for Environmental Research, Education and Outreach (CEREO)

Washington State University is in the process of identifying a new CEREO Director to promote system-wide (multi-campus) interdisciplinary environmental activities integrated across research, education, and outreach efforts that are regional, national, and global in scope. CEREO (**www.cereo.wsu.edu**) is a faculty-led initiative featuring 200+ affiliates from six colleges. It is the premier center of research, teaching and service activity at WSU for collaborative efforts pursuing major environmental initiatives. CEREO advances three principal goals: (a) promotion of broad, multi-investigator interdisciplinary research programs for groundbreaking environmental research and graduate training; (b) facilitation of high quality environmental research, teaching, and institutional outreach supporting the Land Grant mandate across WSU's four campuses and numerous Extension centers; and (c) promotion of productive relationships with diverse stakeholders.

This position is part of WSU's priority to build a diverse faculty and as such female and minority candidates are strongly encouraged to apply. WSU has faculty friendly policies that include partner accommodations and on-site childcare. WSU is an Affirmative Action, Equal Opportunity Employer.

Both *nominations* and *applications* are welcome. All *nominations* should be sent to **Ana Blaisdell** (**ablaisdell@wsu.edu**). For a full position description and details regarding application, please go to **www.cereo.wsu.edu**. All inquiries will be treated confidentially.

Science Careers online @sciencecareers.org



Science Careers is dedicated to opening new doors and answering questions on career topics that matter to you. With timely feedback and a community atmosphere, our careers forum allows you to connect with colleagues and experts to get the advice and guidance you seek as you pursue your career goals.

Science Careers Forum:

- Relevant Career Topics
- Timely Advice and Answers
- Community, Connections, and More!

Visit the forum and join the conversation today!



Your Future Awaits.

Science Careers
From the journal *Science* AAAS
ScienceCareers.org

UC DAVIS

Assistant Professor in Physiology

The University of California at Davis is pleased to announce recruitment for a nine-month tenure-track faculty position in Physiology. The successful candidate will join the Department of Animal Science in the College of Agricultural and Environmental Sciences at the rank of Assistant Professor. Criteria for appointment include: a Ph.D. or equivalent, a strong interest in improving sustainable animal production by understanding how environmental, metabolic, nutritional, or management stressors interact with gene expression including investigation of epigenetic effects, a record of excellence in scholarly research, and demonstrable potential to establish a competitively-funded research program relevant to animal stress in sustainable animal agriculture. The appointee will be responsible for teaching an undergraduate course in physiology and additional contributions to the departmental curriculum, be actively involved in undergraduate advising, curricular development and department and university service. The appointee is also expected to guide and mentor graduate students and participate in the outreach programs of the department and college.

Applicants should submit materials via the following website: **https://recruit.ucdavis.edu/apply/JPF00018**. Additional inquiries can be directed to **Professor Trish Berger**, telephone **(530) 752-1267**, **tberger@ucdavis.edu**. The position will remain open until filled but to ensure consideration, applications should be received by **December 1, 2012**.

UC Davis is an Affirmative Action/Equal Employment Opportunity Employer and is dedicated to recruiting a diverse faculty community. We welcome all qualified applicants to apply, including women, minorities, veterans, and individuals with disabilities.

Yale UNIVERSITY

Tenure-Track Faculty Position in Genomics and Computational Biology Department of Genetics, Yale University School of Medicine

The Department of Genetics at Yale University School of Medicine invites applications for a tenure-track position. The rank of the successful applicant will be commensurate with experience. We seek applicants that aim to develop a strong research program in Genome Informatics and Computational Biology. We are particularly interested in candidates using novel genomics approaches to address fundamental questions in biology including human genetics, developmental biology, gene regulation, cancer biology or systems biology with a focus on computational biology.

The Department of Genetics comprises an exceptional group of 24 primary faculty with research interests including fundamental aspects of genetics, genomics and epigenetics, with investigation of model systems including flies, worms, fish and mouse, as well as humans. To this end, the Department has established a highly productive next generation DNA sequencing center (Yale Center for Genome Analysis) that is producing extremely rich genetic and functional genomic datasets for analysis.

Applications should be received by **December 31, 2012**. Curriculum vitae, a concise statement of research plans (2-3 pages), and three letters of recommendation should be sent electronically to: **genetics.admin@yale.edu** to the attention of **Richard Lifton, Chair, Department of Genetics**.

Yale University is an Equal Opportunity/Affirmative Action Employer and strongly encourages applications from women and minority candidates.

THE UNIVERSITY of TENNESSEE KNOXVILLE

NIMBioS

Director for the National Institute of Mathematical and Biological Synthesis

The University of Tennessee, Knoxville requests nominations and applications of individuals to lead the National Institute for Mathematical and Biological Synthesis (NIMBioS). We seek an internationally-recognized biologist or mathematician with extensive experience working at the interface of these two fields to direct NIMBioS over the next five years of its support from the National Science Foundation and to provide the vision and guidance necessary to aid the University in planning for the longer-term sustainability of NIMBioS beyond the supported renewal period, which ends in 2018.

NIMBioS has been highly successful in responding to the needs for research and education across a diversity of biological disciplines that benefit from collaborative efforts with mathematical and computational scientists. We seek an innovative leader who can guide the current and future activities of this national resource.

Requirements are a Ph.D. and research experience to be appointed to a permanent position as Full Professor in a University Department, demonstrated experience managing federally-funded projects appropriate to lead a unit with approximately 25 full-time staff and researchers, and a recognized record of national and international accomplishment in the biological sciences. The candidate should have experience guiding students and postdoctoral researchers, demonstrated ability to compose effective research proposals for external support, experience developing partnerships, and a commitment to enhancing the diversity of those involved in interdisciplinary research. Departmental affiliation of the successful candidate will be determined based upon input from the candidate, appropriate departments, and the University administration. Nominations and applications from individuals from under-represented groups in biology and mathematics are particularly encouraged. For further information, please contact Prof. Daniel Simberloff at **dsimberloff@utk.edu**.

Applications should include a cover letter detailing your experience and interest in the position, a current CV, and the names and contact information for five individuals who can attest to your abilities to direct NIMBioS. For information about NIMBioS, visit **http://nimbios.org**. Applications should be sent as PDFs to: **Ms. Chandra Eskridge** at **director-search@nimbios.org**. Review of applications will begin **December 9, 2012** and will continue until the position is filled.

The University of Tennessee is an EEO/AA/Title VI/Title IX/Section 504/ADA/ADEA institution in the provision of its education and employment programs and services. All qualified applicants will receive equal consideration for employment without regard to race, color, national origin, religion, sex, pregnancy, marital status, sexual orientation, gender identity, age, physical or mental disability, or covered veteran status.

The Knoxville campus of the University of Tennessee is seeking candidates who have the ability to contribute in meaningful ways to the diversity and intercultural goals of the University.

HSCI HARVARD STEM CELL INSTITUTE

The Center for Translational Regenerative Medicine at Brigham and Women's Hospital invites applications for a tenure-track Assistant Professor position. Outstanding scientists in the field of regenerative biology will be considered. Candidates with a research program focused on the fundamental biology and applications of regenerative medicine and who have a demonstrated interest in human disease are especially welcome. The successful candidate will be a member of the **Harvard Stem Cell Institute** and faculty at **Harvard Medical School**. Candidates must hold an MD and/or PhD and have a strong track record of innovative, interactive research.

Applicants should send an electronic copy of (1) letter of interest, (2) research plan, (3) current curriculum vitae and (4) three letters of recommendation as a single pdf file to **Professor Richard T. Lee, BWH Center for Translational Regenerative Medicine, RLee@Partners.org, 65 Landsdowne St., Cambridge, MA 02139**.

Women and minority candidates are urged to apply. BWH is an Equal Opportunity/ Affirmative Action Employer.

SIU School of Medicine

Department of Medical Microbiology, Immunology, and Cell Biology (MMICB)

Tenure-Track Faculty Position in Bacterial Pathogenesis

Southern Illinois University's School of Medicine at Springfield invites applications for a tenure track faculty position to join a supportive, interactive research environment within MMICB (www.siumed.edu/mmi). The MMICB department has active research programs in areas ranging from virology, neuroscience, reproductive immunology, developmental genetics, host responses to infection, and cancer biology. The Department's integrated graduate program hosts ~40 MS/PhD students. The Department occupies new laboratory space and shares a CDC-certified BSL3 laboratory with the Illinois Department of Public Health.

We seek an energetic scientist with research expertise in molecular and cellular mechanisms of bacterial infectious disease and bacterial-host interactions that control disease outcomes. Successful candidate will demonstrate strong commitments to teaching and research, collaborative potential, and an ability to bring novel expertise to the institution. Appointment is State-supported with competitive salary and start up package. Expectations are to establish and maintain independent, externally funded research programs, and contribute to medical student and graduate education. Excellent written and verbal communication skills are required. Appointment at Associate/Full Professor requires current and sustained extramural funding. Eligible candidates must possess Ph.D. and/or M.D. degrees, and postdoctoral training with a strong publication record.

Applicants should submit a letter of interest, a CV including history of external funding, description of research accomplishments and plans, a statement of teaching experience, and names and email addresses of three professional references in a single PDF to the email address below: **Donald S. Torry, Ph.D., Chair, MMICB Search Committee, P.O. Box 19626, Springfield, IL 62794-9626, Email: tcasson@siumed.edu.** Review of applications will begin on November 1, 2012 and continue until the position is filled.

The Southern Illinois University School of Medicine is an equal opportunity, affirmative action employer. Background investigation required.

Science Careers online @sciencecareers.org

Science Careers online @sciencecareers.org

WEBINAR
Now available on demand.



FACTS & FICTION

Careers in Industry and Academia

Trying to figure out the next step in your career? Join us for a roundtable discussion that will look at facts and fiction surrounding academic and industry career options for PhD-level scientists. Get some nuts and bolts advice on how to research career options, what questions to ask, and how to best prepare for various careers.

- Do industry and academic careers require different skill sets?
- Do industry jobs have better compensation? Less autonomy?
- Do academic scientists have less work/life balance?

For answers view our roundtable discussion for free at:

ScienceCareers.org/webinar

Science Careers
From the journal *Science* AAAS

Produced by the *Science*/AAAS Business Office.

Oregon State University OSU

TWO FACULTY POSITIONS (Assistant or Associate Professor)

Cetacean Ecologist (Telemetry) and Marine Mammal Behavioral Ecologist/ Sea Grant Extension Specialist

The Oregon State University Marine Mammal Institute (**http://mmi.oregonstate.edu/**) seeks two full-time faculty positions:

Cetacean Ecologist (Posting #0009881): We seek an individual with demonstrated potential to develop a strong research program in whale telemetry and to provide continuity with the existing research group.

Marine Mammal Behavioral Ecologist/Sea Grant Extension Specialist (Posting #0009875): We seek an individual with potential to develop a strong research program in the behavioral ecology of marine mammals, as well as strong skills in engaging stakeholders and the public on management issues.

Both positions are 12 month (1.0 FTE), with 0.5 FTE supported by recurring funds (tenurable) and 0.5 FTE provided through grants and contracts secured by the successful candidate. The positions will be based at the Hatfield Marine Science Center in Newport, Oregon. The position ranks (Assistant or Associate Professor) and salaries will be commensurate with experience. Minimum qualifications include a PhD or equivalent advanced degree in a biological discipline, research experience with marine mammals and a strong record of peer-reviewed and refereed publications. Go to **http://oregonstate.edu/jobs** and search for postings 0009881 or 0009875 to access the full position announcements and to submit an application. To ensure full consideration, complete applications should be received by **15 December, 2012**; applications will be accepted until 5 January 2013.

Oregon State University is an Equal Opportunity Affirmative Action Employer.

Southern Illinois University Edwardsville

MOLECULAR GENETICIST/GENOMICIST

DESCRIPTION OF DUTIES: The Department of Biological Sciences, Southern Illinois University Edwardsville invites application for a tenure-track position at the Assistant Professor level. We seek applicants with training in molecular genetics, bioinformatics, and/or comparative genomics. The successful candidate will share responsibility for teaching an introductory genetics course for biology majors, offer upper-division courses in area of expertise, and may also participate in non-majors courses in biology. Candidates should exhibit potential for independent and innovative research involving Master's and undergraduate students.

QUALIFICATIONS: a Ph.D. in the biological sciences with specialization in genetics and/or molecular biology. Post-doctoral teaching and/or research experience preferred. Review of applications will begin December 10, 2012 and continue until position is filled. To apply, send a letter of application, statement of teaching philosophy, statement of research interest, curriculum vitae, copies of representative publications, copies of transcripts, three letters of reference sent by referees directly to the department, and names, phone numbers, addresses, and email addresses of three referees to:

Geneticist Search Committee
Department of Biological Sciences
Southern Illinois University Edwardsville
Box 1651S
Edwardsville, IL 62026

SIUE is a comprehensive regional university located on a 2,660 acre campus in a semi-rual setting 25 minutes from downtown St. Louis, MO.. SIUE is dedicated to excellence in undergraduate education.

SIUE is an Affirmative Action and Equal Opportunity Employer. SIUE is a state university—benefits under state sponsored plans may not be available to holders of F1 or J1 Visas. Applicants may be subject to a background check prior to an offer of employment.

University of California UC Riverside

POSITION ANNOUNCEMENTS
TWO FACULTY POSITIONS- ASSISTANT PROFESSOR
TWO COMMUNITY ECOLOGISTS

1. The Department of Botany and Plant Sciences invites applications for an assistant professor, tenure-track (9-month) position in Plant Community Ecology. Applicants should work at the forefront of the field, with emphasis on a functional approach to understanding community dynamics. We seek a plant ecologist who can interact with programs in conservation biology, invasive species ecology, ecological genomics, ecosystem and landscape ecology, and/or theoretical and computational ecology. Preference will be given to candidates who integrate empirical with statistical, phylogenetic, or modeling approaches, and who can apply advanced techniques such as, but not limited to, GIS/remote sensing, niche modeling, ecophysiological measurements, or stable isotopes. The successful candidate will supervise graduate students, develop a graduate-level community ecology course, and participate in the life science undergraduate teaching program. The position includes a research appointment in the Agricultural Experiment Station with an expectation to develop a nationally competitive program and obtain extramural grant funds. For additional information about the Department and the campus visit **http://cnas.ucr.edu/** and **http://www.plantbiology.ucr.edu/**.

 Applicants must hold a Ph.D. in ecological or environmental sciences or related fields with postdoctoral experience. Evaluation of applications will begin Jan 7, 2013 and continue until the position is filled. The position will be available July 1, 2013. Interested individuals should submit (1) a curriculum vitae, (2) a statement of research and teaching interests, and (3) have three letters of recommendation submitted through **https://academicjobsonline.org/ajo/jobs/2291**.

2. The **Department of Biology** invites applications for a 9-month tenure-track faculty position in the area of **Community Ecology**, starting July 1, 2013. We are searching for an empirical ecologist who studies relationships between interacting species and their environment. Examples of research focus could include (but are not limited to) community assembly, consumer-resource dynamics, evolutionary ecology, including ecological genetics and genomics, interactions between ecology and evolution, and responses of communities to stressors such as climate change and invasive species. The ideal candidate will have a strong field component to their research and expertise in advanced statistical techniques. The successful candidate will join a vibrant community of researchers in the Department of Biology, The Ecology, Evolution and Organismal Biology Graduate Program, the Center for Conservation Biology, the Center for Invasive Species Research, the Institute for Integrative Genome Biology, and have access to modern campus facilities in genomics, proteomics, microscopy, stable isotope analysis, geographic information systems, ecological sensing technologies and field stations and facilities. Consult www.biology.ucr.edu for details about the department. Applicants will be expected to pursue vigorously extramurally-funded research and contribute to undergraduate and graduate teaching. A Ph.D. and demonstrated excellence in research are required.

Applications, including a curriculum vitae, separate statements of research and teaching interests, and up to three selected reprints must be submitted through: **www.academicjobsonline.org/ajo/jobs/2304**. In addition, applicants should request that three letters of recommendation be submitted through this site. Evaluation of applications for this position will begin **January 3, 2013**, but the position will remain open until filled.

The University of California, Riverside is an Affirmative Action Equal Opportunity Employer committed to excellence through diversity.

Science Careers online @sciencecareers.org

POSITIONS OPEN

USDA ARS Agricultural Research Service
www.ars.usda.gov

The U.S. Department of Agriculture (USDA), Agricultural Research Service (ARS), San Joaquin Valley Agricultural Sciences Center (SJVASC) in Parlier, California, is seeking a permanent, full-time **DIRECTOR** and **LOCATION COORDINATOR.** The mission of SJVASC is to develop science-based environmentally acceptable and sustainable agricultural production systems; improve the traits of horticultural crops; control invasive pests and diseases; ensure access and maintenance of the postharvest quality and safety of tree fruits and nuts, and small fruits; and protect natural resources by improved irrigation and drainage water management and water quality. In consultation with other management officials, the Center Director is responsible for formulating and guiding a broad-scale multidisciplinary research program covering the Center's mission research areas, and managing an annual budget of $11.8 million in addition to extramural and in kind resources. Provides supervisory oversight to the Center's workforce of over 120 employees, including 27 research scientists in the disciplines of entomology, plant physiology, plant pathology, plant genetics and breeding, soil and water science, and agricultural engineering. Acts as liaison with other agencies within the Department, industry, and stakeholders. *U.S. Citizenship is required.* Salary will be commensurate with qualifications and experience. GS-15 salary range is $113,735.00 to $147,857.00 per annum (ARS-X13W-0001) and SSTS salary range is $145,700.00 to $199,700.00 per annum (AG-03-2013-0004). A comprehensive Federal benefits package is available. For application instructions, see **website: http://www.usajobs.gov** (**Keyword: ARS-X13W-0001** and/or **AG-03-2013-0004**). Questions about the position may be directed to **Dr. Maureen Whalen, telephone: 510-559-6063; e-mail: maureen.whalen@ars.usda.gov.** Announcements close November 29, 2012.

The USDA/ARS is an Equal Opportunity Employer and Provider.

MOLECULAR BIOLOGIST
Research Investigator

DuPont, a Global Leader in Biotechnology is looking for Molecular Biologists to work in its CR&D Biochemical Sciences & Engineering division to develop biological routes for the production of industrial compounds, small molecules, and macromolecules via metabolic and protein engineering. The successful candidates will have expertise in relevant areas such as molecular biology, genetics, microbial metabolism, and microbial physiology; a Ph.D. in Molecular Biology, Biochemistry, or related field; and at least two years of postdoctoral experience as well as a demonstrated record of productivity through multiple publications or patents. Apply online at **website: http://www.dupont.com/careers.** Search: Ph.D. Early Career Opportunities.

BIOCHEMIST
Research Investigator

DuPont, a Global Leader in Biotechnology is looking for Biochemists to work in its CR&D Biochemical Sciences & Engineering division to develop biocatalytic routes for the production of industrial compounds, small molecules, and macromolecules via metabolic engineering or in vitro biocatalysis and protein engineering. The successful candidates will have expertise in relevant areas such as microbial metabolism, enzymology, or metabolomics; a Ph.D. in Biochemistry, Chemistry, or related field; and at least two years of postdoctoral experience as well as a demonstrated record of productivity through multiple publications or patents. Apply online at **website: http://www.dupont.com/careers.** Search: Ph.D. Early Career Opportunities.

POSITIONS OPEN

THE UNIVERSITY OF CHICAGO

MICROBIOLOGY FACULTY POSITION
Req # 01499

The Department of Microbiology at The University of Chicago invites applications for a tenure-track faculty position at the rank of **ASSISTANT PROFESSOR,** although, depending on qualifications, candidates may be proposed for a senior appointment. Applicants must have a Ph.D. or M.D.-Ph.D. and relevant postdoctoral training. The successful candidate is expected to develop an extramurally supported research program focusing on host-pathogen interactions of viral, parasitic, fungal, or bacterial infectious agents. Candidates are also expected to contribute to departmental teaching. The University of Chicago maintains extensive core facilities in support of microbiological research including facilities for experiments with gnotobiotic animals and risk group one-three infectious agents. A competitive salary and startup package will be provided. Review of applications will begin on January 1, 2013 and continue until the position is filled. Interested applicants should submit a cover letter, curriculum vitae, the names and contact information for at least three references, and a statement of research interests emphasizing career goals addressed to **Professor Howard Shuman** and **Associate Professor Glenn Randall,** Co-Chairs of the Microbiology Search Committee, at the following **website: http://tinyurl.com/9clb75k.**

The University of Chicago is an Affirmative Action/Equal Opportunity Employer.

BIOPROCESS ENGINEER
Research Investigator

DuPont Central Research and Development has an immediate opening for Biochemical Engineers with a strong background in biology enabled process research and development. Successful applicants will have excellent communication, project management, and leadership skills as well as strong theoretical knowledge and hands-on experience in one or more areas including bioreactor design, fermentation optimization, enzymatic transformations, and downstream separations/purification design. The position also requires conceptual design and experimental validation of biology enabled processes from laboratory to pilot scale within a collaborative and multidisciplinary team of biological scientist and engineers. Apply online at **website: http://www.dupont.com/careers.** Search: Ph.D. Early Career Opportunities.

FERMENTATION ENGINEER
Research Investigator

DuPont Central Research and Development has an immediate opening for Biochemical Engineers with a strong background in fermentation based process research and development. Successful applicants will have excellent communication, project management, and leadership skills as well as strong theoretical knowledge and hands-on experience in one or more areas including metabolic engineering, systems biology, bioreactor design, fermentation optimization, and fermentation scale-up. The position also requires conceptual design and experimental validation of fermentation-based processes within a collaborative and multidisciplinary team of molecular biologists, biochemists, and engineers. Apply online at **website: http://www.dupont.com/careers.** Search: Ph.D. Early Career Opportunities.

POSITIONS OPEN

ASSISTANT PROFESSOR
Department of Cell Biology and Anatomy

The Department of Cell Biology and Anatomy of The Chicago Medical School, Rosalind Franklin University of Medicine and Science, invites applications for a tenure-track Assistant Professor faculty position. The successful applicant is expected to establish a strong, extramurally funded research program, and to contribute to medical and graduate teaching. Candidates are particularly encouraged who are applying cellular and molecular approaches to the study of human disease. Clinical populations and physician collaborators are available through affiliations with Advocate Lutheran General Hospital and the Lovell Federal Health Care Center (a veterans administration hospital), and other sites in the Chicago area. Available core resources include confocal, live-cell and electron microscopy facilities, as well as structural biology and proteomics centers. Current areas of research in the Department include the neurobiology of learning and memory, community structure of neural networks, molecular cell biology of muscle development, cellular trafficking and extracellular matrix, RNA biology, RNA processing in human disease, organization of gene expression, and molecular defects underlying muscular dystrophies. Information on the Department may be found at **website: http://www.rosalindfranklin.edu/cms/biology.aspx.** To apply, visit **website: http://rosalindfranklin.peopleadmin.com/postings/3378.** Applicants must submit curriculum vitae, a cover letter containing the names of three references, and a statement of current and future research plans. Review of applications will begin immediately and will continue until the position is filled.

Rosalind Franklin University of Medicine and Science is an Equal Opportunity/Affirmative Action Employer.

TENURE-TRACK FACULTY POSITION
Cell/Molecular Biologist

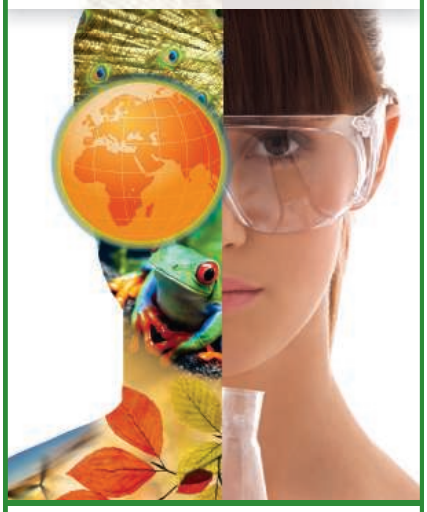
The Department of Biological Sciences at Western Michigan University (WMU) seeks applications for a Cell/Molecular Biologist at the **ASSISTANT PROFESSOR** level beginning in fall 2013, pending budgetary approval. Preference will be given to applicants using molecular approaches in their field and whose research complements existing strengths within the department. A Ph.D. and relevant postdoctoral experience are required. The successful candidate will teach introductory undergraduate and upper level specialty courses in molecular and cellular biology, establish an extramurally funded research program, and serve on Departmental and University committees. A competitive salary and startup funding will be offered.

Information concerning the Biological Sciences Department's programs and faculty can be obtained at **website: http://www.wmich.edu/biology/.** Western Michigan University is a learner centered, discovery driven and globally engaged research institution and a U.S. News and World Report top 100 public university, with a growing graduate program that offers a unique opportunity for individuals seeking a balanced research and teaching career. The Carnegie Foundation for the Advancement of Teaching has placed WMU among the 139 public institutions in the nation designated as research universities with high research activity.

Applicants should visit **website: http://www.wmich.edu/hr/careers-at-wmu.html** to apply. To apply please send letter of application, curriculum vitae, statements of teaching philosophy and research interests, and have three letters of reference sent to: **Todd Barkman, Ph.D., Cell/Molecular Biologist Search Committee, Department of Biological Sciences, Room 3441 Wood Hall, Western Michigan University, Kalamazoo, MI 49008-5410.** Applications are due November 30, 2012, but will be considered until position is filled. *WMU is an Affirmative Action/Equal Opportunity Employer consistent with applicable federal and state law. All qualified applicants are encouraged to apply.*

WOMEN IN SCIENCE

forging new pathways in green science



Read inspiring stories of women working in "Green Science" who are blending a unique combination of enthusiasm for science and concern for others to make the world a better place.

Download this free booklet ScienceCareers.org/LOrealWiS

Science AAAS

FOR WOMEN IN SCIENCE L'ORÉAL

This booklet is brought to you by the AAAS/*Science* Business Office in partnership with the L'Oreal Foundation

Northeastern University

Department of Biology
Professor and Chair

The Department of Biology at Northeastern University (www.northeastern.edu/biology/) has an open search for the Chair of the Department. Candidates who hold a Ph.D. in biology or related field; a record of external funding and research appropriate for the academic rank of Full Professor; demonstrated administrative, leadership, and interpersonal skills; a record of innovative program development and interdisciplinary collaboration; and documented teaching effectiveness are encouraged to apply. The successful candidate will lead and expand a dynamic department that plays a key role in the research and educational missions of the University.

The Biology Department is strongly interdisciplinary, with 15 tenured and tenure track faculty in Biology and an additional 10 faculty with joint appointments in other departments. Approximately 1000 undergraduates are enrolled in the Biology, the Biochemistry, and the Behavioral Neuroscience majors. Our graduate programs serve approximately 60 PhD students, and the Biology department participates in Professional MS programs in Bioinformatics and Biotechnology. We are searching for an educator and scholar who will complement our research programs and foster and expand collaborative research.

Research interests in the department are diverse, including microbiology, cell biology, neurobiology and motor control, and developmental biology, with a significant emphasis on molecular and cellular approaches to problems in basic and translational science. The Department is affiliated with the Antimicrobial Discovery Center, the New England inflammation and Tissue Protection Institute, and the Marine Science Center in Nahant. Northeastern University is in the process of hiring 300 new faculty. The incoming Chair will have an opportunity to contribute to this process.

Northeastern University occupies a vibrant 67-acre campus in the heart of Boston, surrounded by other leading educational, health care, technological, and research institutions, as well as world-renowned venues for art and music. The campus has received an American Institute of Architects award for "most beautiful new or renovated exterior space." Northeastern University is an Equal Opportunity, Affirmative Action Educational Institution and Employer, Title IX University. Northeastern University particularly welcomes applications from minorities, women and persons with disabilities. A competitive salary and startup package will be provided. To apply, visit the College of Science website at: **http://www.northeastern.edu/cos/** and click on the Faculty Positions button at the bottom of the page. Please include a letter of application, curriculum vitae, the names and contact information for five references, and a brief description of research interests. *Candidate must have experience in, or a demonstrated commitment to, working with diverse student populations and/or in a culturally diverse work and educational environment.*

Informal inquiries can be addressed to: **Dr. Kim Lewis, Chair, Biology Chair Search Committee, k.lewis@neu.edu; 617-373-8238**. The earliest anticipated start date is July, 2013. Review of applications will begin in **January, 2013** and continue until the position is filled.

Recruitment: Executive Chief Editor of Journal of Integrative Plant Biology

Journal of Integrative Plant Biology (JIPB; **www.jipb.net**) is a monthly plant biology journal that reports novel scientific discoveries using integrative genetic, chemical, cell and molecular biological approaches. As a leading Wiley-Blackwell journal, JIPB is subscribed to by over 14,200 libraries, and is indexed by 67 databases including SCI, PubMed, and Google Scholar. We are now looking for a highly-motivated Executive Chief Editor to guide the journal's development. Compensation will be 200,000–300,000 RMB, depending on qualifications. The position is available immediately.

Main Responsibilities:

- Assist the Chief Editor to promote JIPB;
- Guide the development of the journal;
- Evaluate manuscript quality, assign manuscripts to editors;
- Write academic news and presentations;
- Aid in manuscript processing.

Qualifications:

- Ph.D. in botany, genetics, or related field;
- More than 2 publications as the 1st or corresponding author in a SCI journal with an impact factor greater than 9;
- 3 years of research experience abroad;
- Professional written & spoken English;
- Enthusiastic, organized, and an interest in academic journals.

To apply, please send your CV and cover letter to **Ping He** at **he1001@ibcas.ac.cn**.

UNIVERSITY OF MIAMI

ASSISTANT PROFESSOR - COMPLEXITY SCIENCE

The College of Arts and Sciences at the University of Miami seeks applicants and nominations for four tenure track appointments in Complexity Science, including complex networks and complex systems, from disciplines across the physical, biological, computational, mathematical, statistical, medical, economic and social sciences. Candidates should have a Ph.D. in a suitable quantitative discipline, and have experience in analyzing real-world data, as well as mathematical and computational modeling. To be considered at Associate or Full Professor level the candidate must have independent teaching and research experience. The successful candidate will be expected to teach at both undergraduate and graduate levels and to develop and maintain internationally recognized research.

Applicants should forward a cover letter, CV, two representative publications, research plan, statement of teaching philosophy and the names of three referees using the application portal at http://www.as.miami.edu/sciencecluster/. Review of applications will begin November 15, 2012 and continue until the positions are filled. Information about the College can be found at http://www.as.miami.edu/.

The University of Miami is an Equal Opportunity/ Affirmative Action Employer.

www.miami.edu

POSITIONS OPEN

UF UNIVERSITY of FLORIDA
The Foundation for The Gator Nation

ASSISTANT, ASSOCIATE, OR FULL PROFESSOR POSITION in Plant Systematics
University of Florida
Department of Biology

We invite applications for an open-rank, nine-month tenure-track faculty position in Plant Systematics, effective fall semester, 2013. We will consider outstanding candidates from all areas of plant systematics, with an emphasis on researchers interested in diversity and natural history; we especially encourage applications from collaborative researchers working in areas that complement existing strengths in molecular systematics and phylogenetics. Both undergraduate and graduate instruction is expected, e.g., courses in plant taxonomy, local flora, and introductory biology. The successful applicant must have a Ph.D. and postdoctoral experience and will be expected to develop a vigorous, externally funded research program. A strong commitment to excellence in teaching and mentoring graduate and undergraduate students is required.

Detailed application instructions are at **website: http://www.biology.ufl.edu/jobs/plsyst.aspx.** Review of applications will begin on January 3, 2013. *Our department is committed to diversity as a component of excellence. Women, minorities and members of other underserved groups are encouraged to apply. The University of Florida is an Equal Opportunity Institution.*

ASSISTANT PROFESSOR
Department of Biological Sciences

Seton Hall University (SHU) is seeking to fill one tenure-tracked Assistant Professor Position in the Department of Biological Sciences starting August 2013. Candidate must have a Ph.D. with at least two years of postdoctoral training. Individuals with expertise in metabolic pathways, metabolomics, virology, mycology, and/or microbiology are invited to apply. The successful applicant will develop a research program that involves both undergraduate and graduate students and can be externally funded. He/She will teach at most a 3/3 course load including graduate courses in his/her area of expertise. Commitment to teaching is important. For consideration, please submit curriculum vitae, statements of teaching philosophy and research interests and three letters of recommendation with cover letter to the address below. Applications are due December 15, 2012.

Seton Hall, the oldest Catholic diocesan university in the United States, is located 14 miles west of Manhattan, in South Orange, New Jersey and an enrollment of approximately 10,000 students. Candidates should be supportive of the Catholic mission of the university. *SHU is committed to programs of Equal Employment Opportunity and Affirmative Action to achieve our objectives of creating and supporting a diverse racial, ethnic, and cultural community.*

Jane L. Ko, Ph.D.
Department of Biological Sciences
Seton Hall University
400 South Orange Avenue
South Orange, NJ 07079-2694
E-mail: jane.ko@shu.edu

Visit our **website: http://www.shu.edu.**

ANIMAL PHYSIOLOGIST/ MORPHOLOGIST

The Department of Biology, California State University Bakersfield invites applicants for a tenure-track position in Animal Physiology/Morphology at the rank of Assistant Professor. The candidate must be capable of developing an externally funded research program that includes both undergraduate and graduate students (M.S. level). Candidates will teach courses in animal biology, their area of specialty, physiology, comparative anatomy, and genetics. Position available 1 September 2013. Application deadline 15 January 2013. See **website: http://www.csub.edu/biology** for full details.

POSITIONS OPEN

UNIVERSITY OF MARYLAND

TENURE-TRACK FACULTY POSITIONS in Biology
University of Maryland, College Park
Department of Biology

The Department of Biology at the University of Maryland, College Park is seeking to hire several exceptional tenure-track faculty members at any professorial rank. Successful candidates will extend, complement, or integrate the Department's existing research strengths in ecology, evolutionary and developmental biology, comparative genomics, sensory neuroscience, and biophysics. Each will be expected to establish a vibrant research program and to be a creative and dedicated teacher at the undergraduate and graduate levels. More information about the Department can be found at **website: http://www.biology.umd.edu.** In certain cases, joint appointments with other campus units may be appropriate.

To apply, please visit **website: http://jobs.umd.edu/applicants/Central?quickFind=55652.** Use this site to submit curriculum vitae, a concise statement of current and future research interests, a description of teaching interests, and contact information for three references. Applications received by December 1, 2012 will receive best consideration, but review will continue until all positions are filled. *The University of Maryland is an Equal Opportunity/Affirmative Action Employer. Applications from women and minority candidates are especially encouraged.*

KUSHLAN CHAIR in Waterbird Biology and Conservation

The Kushlan Endowed Chair's research is to focus on the biology and conservation of waterbirds (including marine birds), primarily at the organismal level. It is desirable that the incumbent use (or use in collaboration) modern integrative approaches such as physiological, genetic, isotopic, or molecular methods. The research program is expected to be extramurally funded and at the cutting edge of important questions on the biology and conservation of waterbirds.

The chosen individual will hold joint appointments at the University of Miami: (1) In the Marine Biology and Fisheries department at the renowned Rosenstiel School of Marine and Atmospheric Sciences which offers a rich variety of research venues. (2) In the Biology department in the College of Arts and Sciences, an integrated biology department in which the Kushlan chair will be the third of four endowed chairs to be held by an ornithologist, creating an outstanding opportunity for synergy.

Ph.D required. Send applications (curriculum vitae, letter of interest, research and teaching statements, and names of references) to **e-mail: kushlanchair@bio.miami.edu.**

Applications received by December 3, 2012 will receive the fullest attention.

The University of Miami is an Affirmative Action/Equal Opportunity University that values diversity and has progressive work-life policies. Women, person with disabilities, and members of other underrepresented groups are encouraged to apply.

☑ More scientists agree—we are the most useful website.
Science Careers
From the journal Science AAAS
www.ScienceCareers.org

POSITIONS OPEN

ASSISTANT PROFESSOR
Environmental Microbiology

The Department of Microbiology and the Institute on Ecosystems at Montana State University Bozeman invites candidates with a Ph.D. in Microbiology or related area to apply for a full-time, nine-month tenure-track position in Environmental Microbiology at the Assistant Professor level beginning August 2013. The successful candidate will have postdoctoral and/or Assistant Professor experience and will be responsible for developing an extramurally funded, nationally recognized research program within the broad field of environmental microbiology. The faculty member will participate in teaching departmental undergraduate and graduate courses in their area of specialization, and will be responsible for providing service to the university and scientific community via integration of research, teaching, and service. A competitive institutional salary, a generous startup package, and a renovated state-of-the-art research facility support this position. Full details about the position and application procedure are available at **website: http://www.montana.edu/jobs/faculty/12245-2.** Potential candidates are encouraged to contact the Search Committee Chairpersons, **Drs. Mark Young** or **Matthew Fields,** (**e-mails: myoung@montana.edu; matthew.fields@biofilm.montana.edu**) for more details. Screening will begin December 1, 2012 and will continue until a suitable applicant is hired. *ADA/Equal Opportunity/Affirmative Action/Veterans Preference Employer.*

MICROBIAL ECOLOGIST

The W.K. Kellogg Biological Station (KBS) of Michigan State University seeks to fill a tenure-track academic year faculty position in microbial ecology. The position is available beginning in fall 2013 and can be filled at either the **ASSISTANT** or **ASSOCIATE PROFESSOR** level. We seek a candidate conducting research that uses microbes to address fundamental ecological and evolutionary questions. While the specific research area of interest is open, the successful candidate should have a demonstrated interest in research involving aquatic systems. The primary appointment for this position will be at the Kellogg Biological Station (**website: http://www.kbs.msu.edu**), an off-campus location rich in lakes and wetlands and ideally suited to a field-focused research program. Joint appointments in the campus departments of Microbiology and Molecular Genetics, Zoology or Plant Biology will be evaluated as part of the search process. Application materials should be submitted to MSU's online application site (**website: https://jobs.msu.edu; position number 30198796, posting number 6950**), including: a letter of interest, curriculum vitae, a statement of research accomplishments and goals, a statement of teaching interests, and contact information for three references. Questions should be addressed to **e-mail: microbialecologysearch@kbs.msu.edu** or **Dr. Steve Hamilton** (**e-mail: hamilton@kbs.msu.edu**), Chair of the Search Committee.

POSTDOCTORAL POSITIONS

We seek two postdoctoral fellows (100%, multiyear) with neuroscience background to study how developmental exposure of alcohol induces epigenetic modification of genes of neuroendocrine-immune system and how it is transmitted through generations. Also, whether stem cell-derived hypothalamic neuron transplants prevent alcohol-induced neuroendocrine-immune dysfunction. Experience in rodent surgery, neuron cultures, ChIP assay, real-time RT-PCR, western blotting, transcriptional and gel-shift assays is strongly preferred. RNA sequencing experience is a plus. Salary depends upon experience (NIH scale). Send curriculum vitae to **e-mail: sarkar@aesop.rutgers.edu.** *Rutgers University is an Affirmative Action/Equal Opportunity Employer.*



AAAS is here – promoting universal science literacy.

In 1985, AAAS founded Project 2061 with the goal of helping all Americans become literate in science, mathematics, and technology. With its landmark publications *Science for All Americans* and *Benchmarks for Science Literacy*, Project 2061 set out recommendations for what all students should know and be able to do in science, mathematics, and technology by the time they graduate from high school. Today, many of the state standards in the United States have drawn their content from Project 2061.

Every day Project 2061 staff use their expertise as teachers, researchers, and scientists to evaluate textbooks and assessments, create conceptual strand maps for educators, produce groundbreaking research and innovative books, CD-ROMs, and professional development workshops for educators, all in the service of achieving our goal of universal science literacy.

As a AAAS member, your dues help support Project 2061 as it works to improve science education. If you are not yet a AAAS member, join us. Together we can make a difference.

To learn more, visit **aaas.org/plusyou/project2061**

AAAS + U = Δ

Download your free copy today.

ScienceCareers.org/booklets



From technology specialists to patent attorneys to policy advisers, learn more about the types of careers that scientists can pursue and the skills needed in order to succeed in nonresearch careers.

Science Careers
From the journal *Science* AAAS

Your career is our cause.

Get help from the experts.

www.sciencecareers.org

- Job Postings
- Job Alerts
- Resume/CV Database
- Career Advice
- Career Forum

Science Careers
From the journal *Science* AAAS

We deliver customized job alerts and more...

Science Careers
From the journal *Science* AAAS

www.ScienceCareers.org

MARKETPLACE

Widely Recognized Original & Guaranteed

KlenTaq 1

8¢/u Truncated Taq DNA Polymerase Withstand 99°C

US Pat #5,436,149 **e-mail:** abpeps@msn.com
Call: AB Bioscience, LLC 1•800•383•3362
Fax: 314•968•8988 **www.abpeps.com**